haematologica
Journal of The Ferrata Storti Foundation

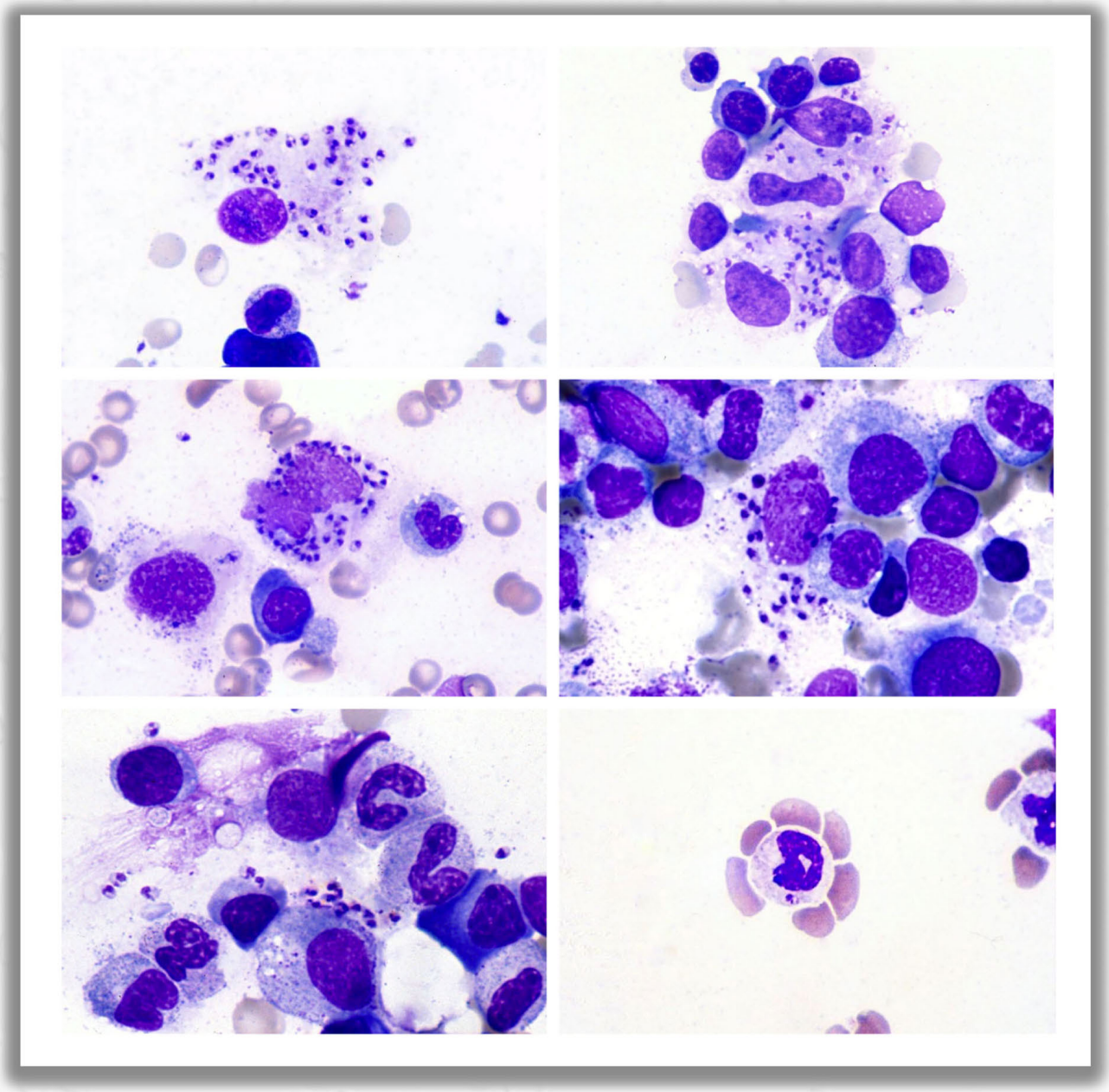

ISSN 0390-6078
Volume 106
AUGUST
2021 - 8
www.haematologica.org

haematologica
Journal of the Ferrata Storti Foundation

haematologica
Journal of the Ferrata Storti Foundation

Information for readers, authors and subscribers

Haematologica (print edition, pISSN 0390-6078, eISSN 1592-8721) publishes peer-reviewed papers on all areas of experimental and clinical hematology. The journal is owned by a non-profit organization, the Ferrata Storti Foundation, and serves the scientific community following the recommendations of the World Association of Medical Editors (www.wame.org) and the International Committee of Medical Journal Editors (www.icmje.org).

Haematologica publishes editorials, research articles, review articles, guideline articles and letters. Manuscripts should be prepared according to our guidelines (www.haematologica.org/information-for-authors), and the Uniform Requirements for Manuscripts Submitted to Biomedical Journals, prepared by the International Committee of Medical Journal Editors (www.icmje.org).

Manuscripts should be submitted online at http://www.haematologica.org/.

Conflict of interests. According to the International Committee of Medical Journal Editors (http://www.icmje.org/#conflicts), "Public trust in the peer review process and the credibility of published articles depend in part on how well conflict of interest is handled during writing, peer review, and editorial decision making". The ad hoc journal's policy is reported in detail online (www.haematologica.org/content/policies).

Transfer of Copyright and Permission to Reproduce Parts of Published Papers. Authors will grant copyright of their articles to the Ferrata Storti Foundation. No formal permission will be required to reproduce parts (tables or illustrations) of published papers, provided the source is quoted appropriately and reproduction has no commercial intent. Reproductions with commercial intent will require written permission and payment of royalties.

Detailed information about subscriptions is available online at www.haematologica.org. Haematologica is an open access journal. Access to the online journal is free.
For subscriptions to the printed issue of the journal, please contact: Haematologica Office, via Giuseppe Belli 4, 27100 Pavia, Italy (phone +39.0382.27129, fax +39.0382.394705, E-mail: info@haematologica.org).

Rates of the International edition for the year 2021 are as following:

	Institutional	*Personal*
Print edition	*Euro 700*	*Euro 170*

Advertisements. Contact the Advertising Manager, Haematologica Office, via Giuseppe Belli 4, 27100 Pavia, Italy (phone +39.0382.27129, fax +39.0382.394705, e-mail: marketing@haematologica.org).

Direttore responsabile: Prof. Carlo Balduini; Autorizzazione del Tribunale di Pavia n. 63 del 5 marzo 1955.
Printing: Press Up, zona Via Cassia Km 36, 300 Zona Ind.le Settevene - 01036 Nepi (VT)

Associated with USPI, Unione Stampa Periodica Italiana.
Premiato per l'alto valore culturale dal Ministero dei Beni Culturali ed Ambientali

TRANSFORM MYELOMA

HELPING PATIENT SUBGROUPS WITH **UNMET NEEDS** IN MULTIPLE MYELOMA

Sanofi Genzyme has focused efforts on multiple myeloma (MM) patient groups that often have unmet needs in clinical trials. The need for the participation of these subgroups in MM clinical trials is vital to help discover new treatment guidelines.

Renal Impairment

of patients with multiple myeloma have **renal impairment** and are often excluded or underrepresented in clinical trials[1,2]

Older Patients

- Multiple myeloma is predominantly a disease of the elderly[3]
- Patients >65 years of age have worse survival rates than younger patients[3]

Cytogenetic Abnormalities

- There remains a detrimental gap between high-risk and standard-risk cytogenetic patients[4,5]

FIND OUT MORE:

Explore Sanofi Genzyme's focus on patient factors and impacts at **TransformMyeloma.com**.

SANOFI GENZYME

References: 1. Richardson PG, San Miguel JF, Moreau P, et al. Interpreting clinical trial data in multiple myeloma: translating findings to the real-world setting. *Blood Cancer J.* 2018;8(11):109. **2.** Faiman B, Doss D, Colson K, Mangan P, King T, Tariman JD. Renal, GI, and peripheral nerves: evidence-based recommendations for the management of symptoms and care for patients with multiple myeloma. *Clin J Oncol Nurs.* 20171;21(5 Suppl):19-36. **3.** National Cancer Institute. Cancer stat facts: myeloma. https://seer.cancer.gov/statfacts/html/mulmy.html. Accessed April 2021. **4.** Lancman G, Tremblay D, Barley K, et al. The effect of novel therapies in high-molecular-risk multiple myeloma. *Clin Adv Hematol Oncol.* 2017;15(11):870-879. **5.** Kumar S, Fonseca R, Ketterling RP, et al. Trisomies in multiple myeloma: impact on survival in patients with high-risk cytogenetics. *Blood.* 2012;119(9):2100-2105.

This advertisement is intended for HCPs only.

MAT-GLB-2102145 (v1) - 05/2021

haematologica
Journal of the Ferrata Storti Foundation

Table of Contents

Volume 106, Issue 8: August 2021

About the Cover

Editorials

Review Articles

Articles

Acute Lymphoblastic Leukemia

Acute Myeloid Leukemia

haematologica
Journal of the Ferrata Storti Foundation

Letters to the Editor

haematologica
Journal of the Ferrata Storti Foundation

Case Reports

Errata Corrige

Images from the Haematologica Atlas of Hematologic Cytology: visceral leishmaniasis

Rosangela Invernizzi[1] and Antonello Malfitano[2]

[1]University of Pavia and [2]IRCCS Policlinico San Matteo Foundation, Pavia, Italy

E-mail: ROSANGELA INVERNIZZI - rosangela.invernizzi@unipv.it

doi:10.3324/haematol.2021.279161

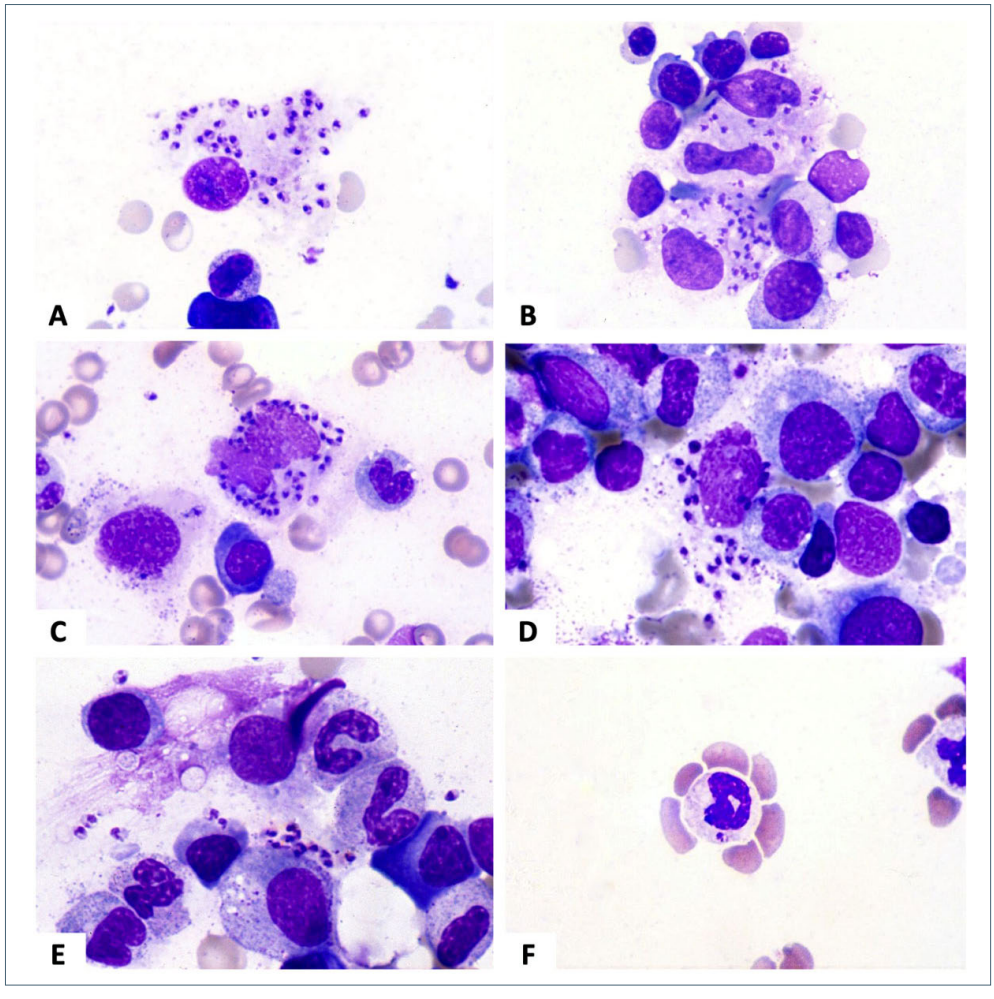

Bone marrow smears remain the diagnostic gold standard for visceral leishmaniasis, although Donovan's bodies, the identifying marker of the disease, may also be found in lymph nodes as well as in spleen fine-needle aspirate smears. These bodies are the asexual form of the parasite, the so-called amastigotes. They are oval, measure 1-5 µm long by 1-2 µm wide, and show a round nucleus and a bar-shaped inclusion, the kinetoplast, which is the remnant of the flagellum of the promastigote. Amastigotes of *Leishmania donovani* may be numerous inside bone marrow macrophages (Figure A-D) or extracellularly as macrophages can be broken during preparation of the smear (Figure E). They may also be observed in the peripheral blood within the cytoplasm of granulocytes, particularly after centrifugation and concentration of white blood cells (Figure F).[1]

Disclosures

No conflicts of interest to disclose.

Contributions

Both authors contributed.

Reference

1. Malfitano A, Invernizzi R. Parasitic and fungal diseases. Haematologica. 2020;105(Suppl 1):29-39.

Is it NICE (nuclear import as a carcinogenic mechanism) to restrict HBZ in the cytoplasm?

Yukata Tagaya

Institute of Human Virology, University of Maryland School of Medicine, Baltimore MD, USA

E-mail: YUKATA TAGAYA - ytagaya@ihv.umaryland.edu

doi:10.3324/haematol.2021.278377

The paper by Forlani *et al.* found in this volume of Haematologica[1] presents an intriguing argument that the control over the subcellular localization of an antisense protein (HBZ, HTLV-1 basic-zipper factor) encoded by the human T-cell leukemia virus-1 (HTLV-1) critically controls its oncogenicity. HTLV-1 was the first human retrovirus identified[2] and is arguably the most carcinogenic agent know to humans.[3] Adult T-cell leukemia (ATL)[4] is a fatal CD4 type T-cell leukemia that occurs in 5% of HTLV-1 carriers. After 40 years of extensive research since the discovery of HTLV-1, the precise mechanism by which HTLV-1 transforms host T cells is not completely understood, and the prevailing paradigm points to two HTLV-1 factors, Tax-1 and HBZ[5] as the cause of T-cell leukemia. HBZ is a multi-functional protein and interacts with many cellular proteins. Not only that, HBZ transcripts have their own function as a cancer-promoting factor.[6] The group led by Roberto Accolla (last author of the paper) has been carefully studying the subcellular distribution of HBZ using a monoclonal antibody that they generated, and they observed that HBZ's localization differs in HTLV-1 infected cells in individuals manifesting different disease status. They found that HBZ exclusively localizes to the cytoplasm[7] in cells from asymptomatic carriers and patients with HAM/TSP (HTLV-1 associated myelopathy/tropical spastic paraparesis), a myelopathy that resembles multiple sclerosis in symptoms and the second major disease manifestation that HTLV-1 causes in humans. In contrast, they report in the current article that HBZ localizes in the nucleus in ATL cell lines. Though not exclusive, the nuclear localization of HBZ was distinct in *ex vivo* leukemic cells from ATL patients. They also showed that the nuclear localization of HBZ may be accompanied by a unidirectional displacement of HBZ from the cytoplasm to the nucleus. With these results, the authors suggest an attractive new hypothesis that the nuclear localization of HBZ is a hallmark of ATL and that the cytoplasmic-to-nuclear translocation of HBZ plays a major role in the leukemogenic mechanism of HTLV-1. These findings may help establish new diagnosis of ATL as well as providing new insights to the research on HTLV-1's oncogenesis. So, can a misguided subcellular localization of a particular protein lead to invoking an oncogenic capacity of the protein?

There are a few other examples that could shed light on this question.

Nucleophosmin (NPM) is an example. NPM shuttles between the nucleus and the cytoplasm and the cytoplasmic localization seems to facilitate its tumor promoting activities.[8] Another example is STAT3 (signal transducer and activator of transcription-3). STAT3 is a transcription factor involved in the signaling of many cytokines. Gain-of-function mutants of STAT3 are often found in many cancers including T-cell malignancies. Mutations of STAT3 that are associated with cancer cases cause a self-dimerization of this molecule, which enhances the nuclear transport and binding of STAT3 to the regulatory region of many target genes. In the case of STAT3, the control of subcellular localization *per se* is not directly connected to the oncogenicity of STAT3, but a mechanism that facilitates the nuclear translocation and DNA binding of STAT3 is likely making STAT3 an oncoprotein.

So how is the subcellular localization of HBZ controlled? It likely involves the interaction of HBZ with other proteins. Other groups have shown that HBZ can be retained in the cytoplasm by a T cell-specific molecule THEMIS,[9] but the Accolla group demonstrated that this does not explain the cytoplasmic distribution of HBZ in HAM/TSP patients.[10] Thus, an involvement of another protein for this observation is suggested. Hopefully, future studies will show the clue and help us know how HTLV-1 transforms host CD4 T cells and how we can control the fatal ATL which do not yet have curative treatment.

Disclosures

No clonflicts of interest to disclose.

References

1. Forlani G, Shallak M, Tedeschi A, et al. Dual cytoplasmic and nuclear localization of HTLV-1-encoded HBZ protein is a unique feature of Adult T cell Leukemia. Haematologica. 2021;106(8):2076-2085.
2. Poiesz BJ, Ruscetti FW, Gazdar AF, Bunn PA, Minna JD, Gallo RC. Detection and isolation of type C retrovirus particles from fresh and cultured lymphocytes of a patient with cutaneous T-cell lymphoma. Proc Natl Acad Sci U S A. 1980;77(12):7415-7419.
3. Tagaya Y, Gallo RC. The exceptional oncogenicity of HTLV-1. Front Microbiol. 2017;8:1425.
4. Takatsuki K. Adult T-cell leukemia. Intern Med. 1995;34(10):947-952.
5. Satou Y, Yasunaga J, Zhao T, et al. HTLV-1 bZIP factor induces T-cell lymphoma and systemic inflammation in vivo. PLoS Pathog. 2011;7(2):e1001274.
6. Satou Y, Yasunaga J, Yoshida M, Matsuoka M. HTLV-1 bZIP Factor (HBZ) gene has a growth-promoting effect on adult T-cell leukemia cells]. Rinsho Ketsueki. 2008;49(11):1525-1529.
7. Baratella M, Forlani G, Raval GU, et al. Cytoplasmic localization of HTLV-1 HBZ protein: a biomarker of HTLV-1-associated myelopathy/tropical spastic paraparesis (HAM/TSP). PLoS Negl Trop Dis. 2017;11(1):e0005285.
8. Lam L, Aktary Z, Bishay M, et al. Regulation of subcellular distribution and oncogenic potential of nucleophosmin by plakoglobin. Oncogenesis. 2012;1:e4.
9. Kinosada H, Yasunaga JI, Shimura K, et al. HTLV-1 bZIP Factor enhances T-Cell proliferation by impeding the suppressive signaling of co-inhibitory receptors. PLoS Pathog. 2017;13(1):e1006120.
10. Forlani G, Baratella M, Tedeschi A, Pique C, Jacobson S, Accolla RS. HTLV-1 HBZ protein resides exclusively in the cytoplasm of infected cells in asymptomatic carriers and HAM/TSP patients. Front Microbiol. 2019;10:819.

The promised land

Eytan M. Stein

Department of Medicine, Memorial Sloan Kettering Cancer Center, New York, NY, USA

E-mail: EYTAN M. STEIN - steine@mskcc.org

doi:10.3324/haematol.2020.276428

In 2021, most, if not all, presentations and publications about the treatment of acute myeloid leukemia (AML) start biblically: hematologists spent 40 years in the desert of "7+3" and in 2017 reached a promised land flowing with Food and Drug Administration approvals. One of the first approvals addressed the vexing problem of *FLT3*-mutant AML. While the *FLT3*-internal tandem duplication (ITD) was discovered over 25 years ago, the success of randomized clinical studies targeting the mutant FLT-3 protein only occurred years later with the RATIFY trial.[1] In this trial, the combination of the multikinase inhibitor midostaurin with induction chemotherapy led to a statistically significant improvement in the 4-year overall survival of patients with newly diagnosed *FLT3*-mutant AML.[2] The approval of single-agent gilteritinib, a second-generation FLT-3 inhibitor for patients with relapsed and refractory AML, based on the randomized phase III ADMIRAL trial, consolidated the role of FLT-3 inhibitors in the treatment of patients with AML.[3]

But while gilteritinib was being approved, a second FLT-3 inhibitor, quizartinib, was axed by the Oncologic Drugs Advisory Committee (ODAC). Quizartinib, a potent inhibitor of *FLT3*-ITD but not *FLT3*-tyrosine kinase domain (TKD) mutations, was studied in a randomized phase III trial, for relapsed and refractory AML. Despite demonstrating a statistically significant overall survival benefit in the company-sponsored analysis of the clinical trial, concerns about dropouts in the standard treatment arm led to a negative vote against quizartinib at an ODAC meeting. Despite this, quizartinib was approved in Japan and is now a standard-of-care therapy in that country.

Building on previous work showing the relative benefit of treating patients with the combination of sorafenib, a weak FLT-3 inhibitor, with azacitidine, in this issue of *Haematologica*, Swaminathan and colleagues[4] report the outcomes of patients with either newly diagnosed or relapsed *FLT3*-ITD AML treated with the combination of azacitidine or low-dose cytarabine with quizartinib. Perhaps the most impressive outcome in this trial is the high rate of composite complete response of 87% with quizartinib/azacitidine and 74% with quizartinib/low-dose cytarabine. These rates of remission are certainly encouraging, although definitive results will need to wait for the time of a randomized, ideally placebo-controlled, study. As a cautionary note, the randomized phase III LACEWING study, in which patients were assigned to treatment with the two-drug combination of gilteritinib/azacitidine or azacitidine monotherapy, failed to meet its primary endpoint of an overall survival benefit in favor of the former despite encouraging results of the "doublet" in a phase II clinical trial.

Concurrent with the development of treatments targeting FLT-3, there has been a dramatic improvement in the outcomes of adults who are not considered good candidates for induction chemotherapy with the use of azacitidine and venetoclax. *FLT3*-mutant patients appear to do as well with azacytidine/venetoclax as patients without *FLT3* mutations, at least when it comes to response. How then, should we think about the doublet of azacitidine/quizartinib? The field of leukemia research is now moving past doublets, and Swaminathan and colleagues have set a firm foundation for thinking about triplets of azacitidine/venetoclax/quizartinib or sequential treatments with azacitidine/venetoclax followed by azacitidine/quizartinib. Studies on these combinations will take time to perform but are worthwhile and will continue to improve the lives of all of our patients with *FLT3*-mutant AML.

Disclosures

No conflicts of interest to disclose.

References

1. Nakao M, Yokota S, Iwai T, et al. Internal tandem duplication of the flt3 gene found in acute myeloid leukemia. Leukemia. 1996;10(12):1911-1918.
2. Stone RM, Mandrekar SJ, Sanford BL, et al. Midostaurin plus chemotherapy for acute myeloid leukemia with a FLT3 mutation. N Engl J Med. 2017;377(5):454-464.
3. Perl AE, Martinelli G, Cortes JE, et al. Gilteritinib or chemotherapy for relapsed or refractory FLT3-mutated AML. N Engl J Med. 2019;381(18):1728-1740.
4. Swaminathan M, Kantarjian HM, Levis M, et al. A phase I/II study of the combination of quizartinib with azacitidine or low-dose cytarabine for the treatment of patients with acute myeloid leukemia and myelodysplastic syndrome. Haematologica. 2021;106(8):2121-2130.

A new enemy is emerging in the fight against the SARS-CoV-2 pandemic

Francesco Rodeghiero[1] and Carlo L. Balduini[2]

[1]Hematology Project Foundation, Vicenza and [2]Fondazione Ferrata-Storti, Pavia, Italy

E-mail: CARLO L. BALDUINI - carlo.balduini@unipv.it

doi:10.3324/haematol.2021.279186

The discovery of a new disease is always big news even more so when a new iatrogenic disorder emerges after the administration of a vaccine to millions of people during a global pandemic. This is precisely the case of vaccine-induced immune thrombotic thrombocytopenia (VITT) reported after vaccination against severe acute respiratory syndrome coronavirus 2 (SARS-CoV-2). VITT was first described in April 2021 by three independent groups in 39 people, 5 to 29 days after the first administration of the vaccine ChAdOx1 nCoV-19 (AstraZeneca), a recombinant chimpanzee adenoviral vector encoding the spike protein of SARS-CoV-2.[1-3] Affected people were young or middle-aged adults, mostly women, who had acute onset of moderate to severe thrombocytopenia and thrombosis, often in unusual localizations such as cerebral venous sinus or portal, splanchnic, or hepatic veins. Other patients presented with venous thromboembolisms or acute arterial thrombosis. The disease was serious, with 40% mortality. Of note, nearly all patients had high levels of antibodies reacting to platelet factor 4 (PF4)-heparin complexes, as in heparin-induced thrombocytopenia, but they had not been previously exposed to this anticoagulant. This finding suggests a close correlation between VITT and autoimmune heparin-induced thrombocytopenia, which occurs in patients never exposed to heparin. The sequence of events leading to thrombosis did not emerge from these three pioneering studies. In particular, the nature of the polyanion macromolecule mimicking heparin remains uncertain. While the intact vaccine did not seem to be implicated, a pathogenic role of some specific components, including the spike protein synthetized by the vaccine, could not be ruled out.

In this issue of *Haematologica*, two papers provide new information on VITT. The article by Althaus *et al.*[4] describes the clinical and laboratory features of eight additional cases and significantly confirms the clinical and laboratory picture that has emerged from previous reports. Furthermore, this study provides new evidence of the pathogenesis of VITT by comparison of platelet activation induced by sera from patients with this condition with sera from subjects vaccinated without any clinical complications, as well as from patients with SARS-CoV-2. Finally, the authors report on the autopsy findings of two deceased VITT patients that revealed multidistrict thrombosis and showed kidney lesions similar to those of thrombotic microangiopathies.

The letter by Pomara *et al.*[5] published in the same issue focuses on the results of a thorough *post-mortem* examination of two patients with typical VITT. The macroscopic picture was impressive revealing the extent of thrombosis which was much more widespread than initially revealed by imagining during life. The authors made extensive use of immunocytochemistry for the characterization of the affected organs and noted, among other interesting findings, platelet aggregates diffusely lining the endothelial layer of small and medium vessels. Pomara's paper, therefore, confirms the observation made by Althaus that VITT has this feature in common with thrombotic microangiopathies, confirming that generalized platelet activation plays a major role in this disorder.

The study of these additional ten new cases advances

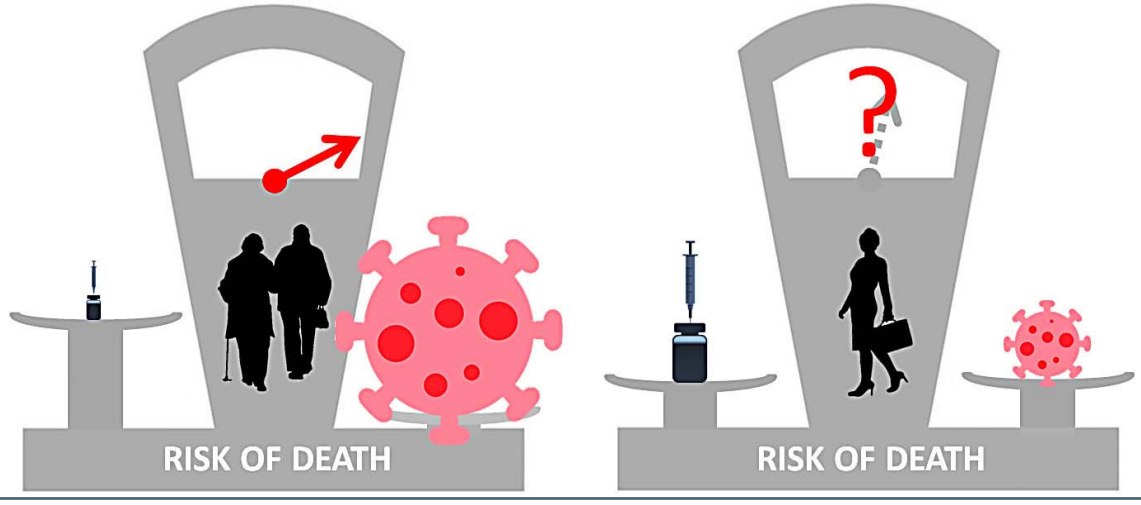

Figure 1. Of the 49 patients with vaccine-induced immune thrombotic thrombocytopenia reported to date, 79% were women and only 4% were over 60 years old. The risk of this disease, therefore, seems to be extremely low in old people who, on the other hand, have a high risk of death from SARS-CoV-2. The administration of adenoviral vaccines against SARS-CoV-2 is therefore highly advantageous in this category of subjects. Conversely, vaccine-induced immune thrombotic thrombocytopenia (VITT) seems to be more common in young or middle-aged adults, especially women, who instead have a risk of death from SARS-CoV-2 much lower and in some age categories even close to zero. Pending new data, these considerations have convinced some countries not to administer adenoviral vaccines to young subjects.

the knowledge of VITT, which, however, still remains poorly defined because many questions await to be answered. First and foremost, how common is this complication after vaccination with ChAdOx1 nCoV-2? At present, a total of only 49 cases have been described and the disease therefore appears exceptionally rare considering that millions of people have received this drug. However, VITT was only identified in April 2021 and, therefore, its diagnosis was impossible prior to this date and, hence, this complication may currently be greatly underreported.

As of 4 April 2021, a total of 169 cases of CVST and 53 cases of splanchnic vein thrombosis were reported to EudraVigilance in around 34 million people vaccinated in the EEA and UK (Europenan Medicine Agency).[6] How many of these patients had VITT? Furthermore, the diagnosis of cerebral venous sinus and splanchnic vein thrombosis is not always easy, and we cannot exclude that their occurrence has so far been underestimated. We fear that the number of cases of VITT reported after the ChAdOx1 nCoV-19 vaccine will augment in the coming months, as specific testing for anti PF4-polyanion complexes will be increasingly applied to clinically suspected cases.

Another important question is whether VITT is caused only by the ChAdOx1 nCoV-19 vaccine or may be triggered by other adenoviral vaccines. The answer to this question was given by a paper[7] published at the end of April 2021 that described 12 patients who developed a disease with the clinical and laboratory characteristics of VITT 5 to 26 days after vaccination with Ad26.COV2.S COVID-19 (Johnson & Johnson/Janssen). This drug, too, uses a human adenoviral vector, which, however, differs in many respects from that used by the ChAdOx1 nCoV-19 vaccine. It is, therefore, possible that the risk of VITT is a common feature of drugs that use adenoviral vectors. It is important at this point to emphasize that adenoviral vectors are presently employed not only for vaccines against SARS-CoV-2 and EBOLA,[8] but they are under investigation for vaccines against other infectious diseases,[8] for cancer immunotherapy[9] and for gene therapy of inherited disorders.[10] Should it be shown that the risk of VITT is intrinsic to different adenovirus-based treatments, the risk-benefit ratio would be completely different if this approach is used to treat cancer or to prevent an infectious disease that has a mortality of about 1-2% (and in some age groups very close to 0%).

A final question is how to treat patients with VITT. Clinicians who have reported their experience in this field have generally suggested avoiding the use of heparin and platelet transfusions, given to correct the profound thrombocytopenia and associated cerebral hemorrhage. Instead, they believe that non-heparin anticoagulants and high-dose intravenous immunoglobulin could have some efficacy. These recommendations are mainly based on previous experience with heparin-induced thrombocytopenia and heparin-induced autoimmune thrombocytopenia, and are currently only anecdotal experiences suggesting their use in VITT. A better understanding of the pathogenic mechanisms of VITT and prospective clinical studies are required to identify the best treatment for VITT, which is a rare or even very rare disease. Only large international collaborations will be able to ensure the provision of credible results in a short time. Furthermore, it has not been established if these treatments are also appropriate for any atypical thrombosis after vaccination, particularly in the absence of the specific laboratory features of VITT. A long way of laboratory and clinical research lies ahead.

Disclosures

No clonflicts of interest to disclose.

References

1. Greinacher A, Thiele T, Warkentin TE, Weisser K, Kyrle PA, Eichinger S. Thrombotic thrombocytopenia after ChAdOx1 nCov-19 Vaccination. N Engl J Med. 2021;384(22):2092-2101.
2. Schultz NH, Sørvoll IH, Michelsen AE, et al. Thrombosis and thrombocytopenia after ChAdOx1 nCoV-19 vaccination. N Engl J Med. 2021;384(22):2124-2130.
3. Scully M, Singh D, Lown R, et al. Pathologic antibodies to platelet factor 4 after ChAdOx1 nCoV-19 vaccination. N Engl J Med. 2021;384(23):2202-2211.
4. Althaus K, Möller P, Uzun G, et al. Antibody-mediated procoagulant platelets in SARS-CoV-2-vaccination associated immune thrombotic thrombocytopenia. Haematologica. 2021;106(8):2170-2179.
5. Pomara C, Sessa F, Ciaccio M, et al. Post-mortem findings in vaccine-induced Thrombotic Thombocytopenia. Haematologica. 2021;106 (8)2291-2293.
6. European Medicines Agency. AstraZeneca's COVID-19 vaccine: EMA finds possible link to very rare cases of unusual blood clots with low blood platelets. https://www.ema.europa.eu/en/news/astrazenecas-covid-19-vaccine-ema-finds-possible-link-very-rare-cases-unusual-blood-clots-low-blood. Accessed 11 May 2021
7. See I, Su JR, Lale A, et al. US Case Reports of Cerebral Venous Sinus Thrombosis With thrombocytopenia after Ad26.COV2.S vaccination, March 2 to April 21, 2021. JAMA. 2021 Jun 22;325(24):2448-2456
8. Tomori O, Kolawole MO. Ebola virus disease: current vaccine solutions. Curr Opin Immunol. 2021;71:27-33.
9. Tessarollo NG, Domingues ACM, Antunes F, et al. Nonreplicating adenoviral vectors: improving tropism and delivery of cancer gene therapy. Cancers (Basel). 2021;13(8):1863.
10. van Haasteren J, Li J, Scheideler OJ, Murthy N, Schaffer DV. The delivery challenge: fulfilling the promise of therapeutic genome editing. Nat Biotechnol. 2020;38(7):845-855.

REVIEW ARTICLE

Ferrata Storti Foundation

The post-hematopoietic cell transplantation microbiome: relationships with transplant outcome and potential therapeutic targets

Yannouck F. van Lier,[1,2] Marcel R.M. van den Brink,[3,4] Mette D. Hazenberg[1,2,5] and Kate A. Markey[3,4]

[1]Department of Hematology, Amsterdam UMC, Amsterdam, the Netherlands; [2]Department of Experimental Immunology, Amsterdam Institute for Infection and Immunity (AII), Cancer Center Amsterdam, Amsterdam UMC, Amsterdam, the Netherlands; [3]Adult Bone Marrow Transplantation Service, Department of Medicine, Memorial Sloan Kettering Cancer Center, New York, NY, USA; [4]Department of Medicine, Weill Cornell Medical College, New York, NY, USA and [5]Department of Hematopoiesis, Sanquin Research, Amsterdam, the Netherlands

Haematologica 2021
Volume 106(8):2042-2053

ABSTRACT

Microbiota injury occurs in many patients undergoing allogeneic hematopoietic cell transplantation, likely as a consequence of conditioning regimens involving chemo- and radiotherapy, the widespread use of both prophylactic and therapeutic antibiotics, and profound dietary changes during the peri-transplant period. Peri-transplant dysbiosis is characterized by a decrease in bacterial diversity, loss of commensal bacteria and single-taxon domination (e.g., with Enterococcal strains). Clinically, deviation of the post-transplant microbiota from a normal, high-diversity, healthy state has been associated with increased risk of bacteremia, development of graft-*versus*-host disease and decreases in overall survival. A number of recent clinical trials have attempted to target the microbiota in allogeneic hematopoietic cell transplantation patients via dietary interventions, selection of therapeutic antibiotics, administration of pre- or pro-biotics, or by performing fecal microbiota transplantation. These strategies have yielded promising results but the mechanisms by which these interventions influence transplant-related complications remain largely unknown. In this review we summarize the current approaches to targeting the microbiota, discuss potential underlying mechanisms and highlight the key outstanding areas that require further investigation in order to advance microbiota-targeting therapies.

Correspondence:

KATE MARKEY
markeyk@mskcc.org

Received: January 11, 2021.

Accepted: April 1, 2021.

Pre-published: April 22, 2021.

https://doi.org/10.3324/haematol.2020.270835

Introduction

Allogeneic hematopoietic cell transplantation (HCT) is the oldest form of cellular therapy for patients with hematologic malignancies, and utilizes stem cell-containing grafts from carefully selected donors to invoke immunological anti-malignancy effects. This procedure remains high risk for patients, as transplantation-related complications, such as infection and graft-*versus*-host disease (GvHD), are causes of high morbidity and mortality among allogeneic HCT recipients.[1,2] The incidence of acute GvHD in human leukocyte antigen-matched donors remains 30-35%.[3] The role of the microbiome in transplant-related complications has been a point of investigation in the field for decades, but advances in sequencing technology and our capacity to study the function of intestinal microbial communities have accelerated this interest in recent years. Approaches to conserve or recover a healthy microbiome in transplant patients are increasingly being used in experimental settings with the goal of improving overall transplant outcome.

Pre-transplant conditioning regimens expose the gastrointestinal tract to high doses of chemo- and radiotherapy, resulting in loss of integrity of the intestinal epithelium and inflammatory damage which often results in mucositis.[4] Clinical manifestations of mucositis include mouth sores, pain during eating or swallowing, nausea, intestinal cramping, bloating and diarrhea, which commonly minimize a patient's oral dietary intake. Mucositis is also thought to increase the risk of micro-

bial translocation from the lumen of the oral cavity or gastrointestinal tract into the systemic circulation, which has led to the widespread use of antibiotic prophylaxis in allogeneic HCT recipients in whom prolonged mucositis and co-incident neutropenia are common. Patients also have high rates of exposure to broad-spectrum empiric antibiotics, which are initiated in response to fever in the neutropenic period. Microbial sources of these neutropenic febrile episodes are rarely proven but the consequences of untreated severe infection in this group of patients are such that it is standard practice to initiate broad-spectrum empiric therapy when a fever occurs.[5]

Acute GvHD is classically described as a three-step process.[6,7] The first step involves host tissue injury, resulting in release of damage-associated patterns (DAMPS; uric acid, ATP, heparin sulfate, HMGB-1, interleukin [IL]-33) and pathogen-associated patterns (PAMPS; lipopolysaccharides [LPS]), which further stimulate the production of inflammatory cytokines such as tumor necrosis factor [TNF]-α, IL-1 and IL-6. The second step comprises priming and expansion of alloreactive donor lymphocytes, predominantly T cells, which are recruited to the host tissues; hematopoietic and non-hematopoietic antigen-presenting cells interact with alloreactive lymphocytes, skewing $CD4^+$ T lymphocytes towards a T-helper (Th1) or Th17 phenotype that produce inflammatory cytokines such as interferon (IFN)-γ and IL-17, activating cytotoxic $CD8^+$ T cells, and stimulating their proliferation. The third step involves recruitment and activation of additional (innate) effector cells, such as macrophages and neutrophils, which amplify the cytokine production ('cytokine storm') and orchestrate further apoptotic tissue damage.

Systemic, high-dose corticosteroids are the first-line treatment for acute GvHD and are successful in about two-thirds of the cases.[8] Patients with severe or steroid-refractory GvHD have a dismal prognosis, with long-term survival rates reported between 5-30%.[9] This has led to persistent efforts to identify new therapies for GvHD.

Our current knowledge of the composition of the intestinal microbial community, in both health and disease, is largely based on the analysis of fecal samples using an amplicon-based sequencing approach that targets the variable regions of the prokaryotic 16S ribosomal RNA gene. 16S rRNA sequencing allows us to measure microbial composition (i.e., the presence of certain taxa) and compute the summary measure α-diversity (commonly measured by the Simpson or Shannon index), which has been used in a large number of transplant studies that have associated microbiota abnormalities with transplant outcome.[10] A second method is metagenomic sequencing, which involves untargeted ('shotgun') metagenomic sequencing of all the genes present in a given sample. Multiple technologies are available for metagenomic sequencing, but they can be broadly grouped into either short-read (e.g., Illumina) or long-read (e.g., PacBio, Nanopore) platforms.[11] Independently of the sequencing method, metagenomic sequencing provides reliable species-level taxonomy, as well as profiling of the functional capacity of the intestinal microbial community as a whole, by identifying genes that confer microbial function (e.g., fatty acid synthesis or degradation). Metagenomic sequencing can thus be a powerful hypothesis-generating tool and can enhance our understanding of potential mechanisms underpinning associations between particular microbial compositions and clinical outcome.

The healthy microbiome and intestinal homeostasis

The human microbiome constitutes a diverse collection of bacteria, viruses, archaea and eukaryotic microbes that inhabit all parts of the body but predominantly reside in the gut.[12] Bacteria represent the largest group within the intestinal microbiome and most species belong to the Firmicutes or Bacteroidetes phyla with smaller contributions from the Proteobacteria, Actinobacteria, Fusobacteria and Verrucomicrobia phyla. The dynamic ecosystem within the intestinal tract is continuously subjected to environmental changes induced by diet, medication and disease of the host, which can dramatically alter microbial composition.[13-15] Factors important in maintaining homeostasis and preventing pathogen outgrowth and translocation include: an intact *gut epithelium* that physically separates the luminal microorganisms from the underlying host tissue; an extra layer of protection, provided by the *mucus layer* that is produced by goblet cells, to hinder bacterial translocation and prevent mucosal barrier injury; the *anaerobic commensals* that predominate in the gut microbiota community of healthy individuals and that provide resistance against colonization by pathogens. The products of anaerobic commensals further prevent pathogen outgrowth; molecules derived from commensal bacteria, which can signal to Paneth cells via toll-like receptors (TLR) 2, 4, 5 and 9, and induce production of *antimicrobial peptides*.[16] Antimicrobial peptides, such as defensins and regenerating gene (REG) III proteins, shape the microbial composition by sequestering essential nutrients and permeabilizing bacterial membranes; the commensals, which in addition to mediating resistance to colonization by potential pathogens, also produce metabolites that are essential *micronutrients for the human host*.

Microbial metabolites include vitamins (K, B_{12}), short-chain fatty acids (SCFA) such as butyrate, propionate and acetate, which are the products of indigestible dietary fiber fermentation, aryl hydrocarbon receptor ligands called indoles generated through tryptophan metabolism and secondary bile acids.[17-20] These microbial metabolites are locally important for maintenance of epithelial integrity and stimulation of the mucosal immune system, but can also exert effects on peripheral organs via secretion into the systemic circulation.[21-24] SCFA act via several pathways to maintain homeostasis: they serve as an energy source for colonocytes, promote mucus secretion, enhance expression of tight junction proteins to improve epithelial integrity, induce anti-inflammatory cytokines such as IL-10 and IL-18, and promote differentiation of anti-inflammatory regulatory T cells via engagement with G-protein coupled receptors (GPR) 43, 41 and 109a on both epithelial cells and immune cells.[25] Indoles also have immune-modulating potential. For example, they can induce IL-22 production by different aryl hydrocarbon receptor-expressing lymphocytes, such as Th17 cells, natural killer T cells, γδ T cells and innate lymphoid cells, which in turn enhances epithelial barrier function and promotes antimicrobial peptide production.[26]

Relationship of the microbiome with transplant-related toxicities

There are many contributors to the disruption of the intestinal microbiota observed in the peri-transplant period, including conditioning, diet changes, and exposure to antibiotics (Figure 1). Early after transplantation, there is a loss of microbial diversity as well as a shift towards a microbiome dominated by *Enterococci*, *Streptococci* or, in fewer cases, *Proteobacteria*, at the expense of anaerobic populations, such as *Bacteroides*, *Clostridium* and *Bifidobacterium*. Intestinal domination, here defined as a relative abundance of ≥30% of a single taxonomic unit, is associated with exposure to certain antibiotics and increases the risk of blood stream infection by the respective dominating taxon.[27,28]

Decreases in fecal α-diversity can be observed even prior to HCT in some patients, but deepens in the days following transplantation, and is associated with the timing and type of antibiotic treatment.[27,29-34] Indeed, clinical studies have shown a reduction of bacterial burden and loss of fecal α-diversity following cancer treatment, e.g., for acute myeloid leukemia, which is consistent with the dysbiosis observed pre-transplant.[27,29,30,35-39] Loss of fecal bacterial diversity is recognized in transplant patients across different geographic locations as was recently documented in a large, observational study that included 8,767 stool samples from 1,362 patients, collected at four different centers in three different continents.[30] This study also reinforced a previously recognized association between intestinal diversity during the peri-engraftment period (days 7-21 post-HCT) and transplant outcome: low microbial diversity is associated with significantly higher transplantation-related mortality, GvHD-related mortality and lower overall survival.[40,41] The prevalence of intestinal domination was high in this cohort: it was detected in more than 75% of the samples collected 1 week after transplantation, with *Enterococcus* domination being most prevalent. In an earlier study, *Enterococcus* domination was associated with lower overall survival and higher GvHD-related mortality.[42] Indeed, perturbations of the microbiome are particularly overt in patients with acute GvHD.[37,42-47] Pre-clinical studies in mice have demonstrated that intestinal microbiota play an important role in the development of acute GvHD and, *vice versa*, acute GvHD itself can aggravate intestinal dysbiosis. A study by Varelias and colleagues found that the dysbiotic microbiome of IL-17-deficient mice induced hyperacute GvHD and that this effect was transferable to wild-type mice during co-housing experiments.[48] A second study showed that increases in major histocompatibility complex class II (MHCII) expression on intestinal epithelial cells was microbiota-dependent, and that this upregulation process, which was essential for the initiation of lethal acute GvHD, could be abrogated by antibiotic-mediated bacterial depletion.[49] After initiation of acute GvHD, GvHD-mediated tissue damage includes the destruction of Paneth cells, which actively shape the microbial community via production of α-defensins.[50] Loss of Paneth cells decreased the expression of α-defensins and propagated expansion of pathogenic bacteria (*Escherichia coli*), which accelerated GvHD. An abundance of *Enterococcus* species has also been associated with acute GvHD severity: mice with an *Enterococcus*-dominated microbiome experienced worse GvHD and had an inferior survival.[42] In contrast, the presence of intestinal *Blautia*, a genus from the butyrate-producing *Lachnospiraceae* family, appeared to have protective capacities against acute GvHD development both in mice and humans.[41]

Changes in gut microbiota composition have not only been associated with the development and severity of acute GvHD, but have also been linked to other transplant-related complications. For example, analysis of the fecal microbiota composition early (day 0 to 21) after allogeneic HCT identified a cluster of bacteria, dominated by *Eubacterium limosum*, which was associated with a decreased risk of relapse or progressive disease.[51]

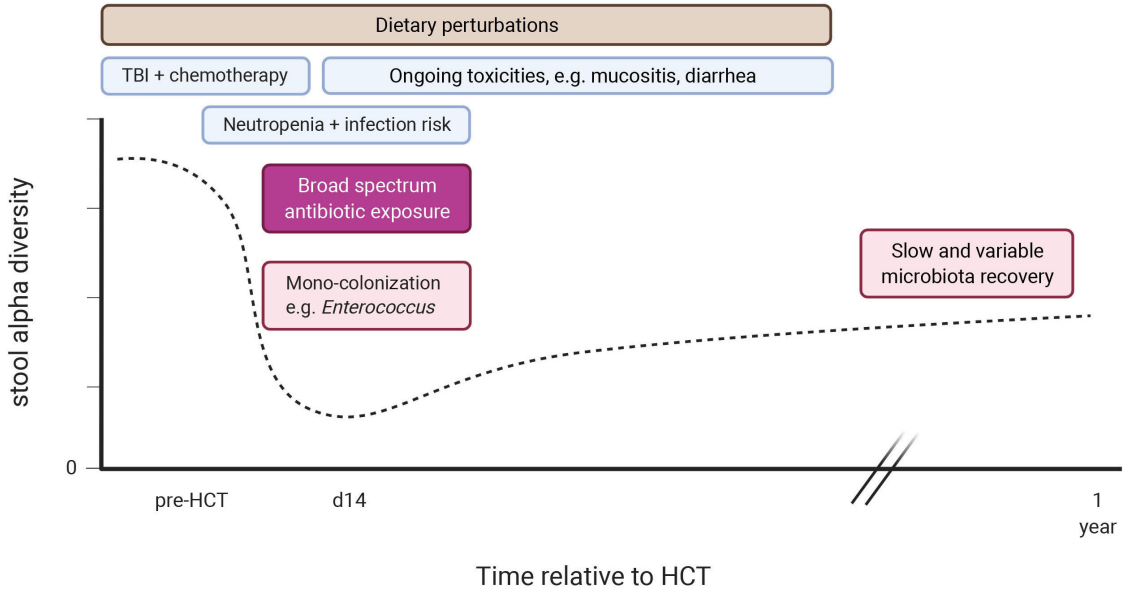

Figure 1. Timeline of potential microbiota perturbations after allogeneic hematopoietic cell transplantation. HCT: hematopoietic cell transplantation; TBI: total body irradiation. Created with BioRender.com

Additionally, features of the intestinal microbiome have been associated with the development of pulmonary infiltrates post-transplant.[52] A further study found that the presence of butyrate-producing bacteria in fecal samples was associated with a lower rate of viral lower respiratory tract infections.[53]

Finally, there is also evidence emerging that early post-HCT microbiome damage may remain for some time, and have consequences for the late complications of transplantation. A recent study by our group showed that dysbiosis can still be observed at 100 days after transplantation and that patients who go on to develop chronic GvHD have lower concentrations of circulating SCFA.[54] As this was a small study of chronic GvHD patients, further work is needed to explore this association.

The studies described above found several links between dysbiotic gut microbiota and transplant-related complications but it remains largely unresolved whether these associations reflect causal relationships. If this is indeed the case, then manipulation of the microbiota – particularly in a fashion that ensures maintenance of anaerobic bacterial taxa and prevents colonization with potential pathogens – could be an effective way to reduce acute transplant-related toxicities and also improve the long-term outcomes for allogeneic HCT recipients. At present, potential strategies for microbiota modification include dietary modification, prebiotics, probiotics or postbiotics and fecal microbiota transplantation (FMT) (Table 1).

Potential mechanisms of microbiome-targeting therapies

Therapies targeting the microbiota could contribute to preserving or restoring intestinal homeostasis by providing resistance to colonization, enhancing mucosal healing, or dampening the inflammatory immune response.

Colonization resistance

As mentioned above, outgrowth of a single taxon, particularly *Enterococcus*, is a common feature of the post-HCT microbiome and is associated with a poor transplant outcome. In addition to *Enterococcus* colonization, intestinal expansion of other pathogenic bacteria, such as the Enterobacterales species *Klebsiella pneumoniae* and *Escherichia coli*, has been observed in patients who subsequently developed bloodstream infections caused by the respective species.[55] Domination may negatively affect intestinal homeostasis: (i) indirectly via loss of beneficial anaerobic bacteria, resulting in a drastic reduction of 'health-promoting' metabolites such as SCFA or, (ii) directly, if the dominating species itself compromises the gut epithelium or invokes an inflammatory response from the mucosal immune system.

Enterococcus faecalis (for example) has the capacity to impair epithelial barrier integrity via matrix metalloproteases and can also induce a strong dose-dependent activation of dendritic cells, resulting in enhanced production of the cytokines IL-6, IL-10, IL-12 and TNF-α.[56,57] A recent mouse study showed that intake of the disaccharide lactose was necessary for *Enterococcus* expansion whereas a lactose-free diet attenuated the emergence of *Enterococcus* and reduced the severity of acute GvHD.[42] These pre-clinical findings need further exploration in clinical trials, for example, of lactose-free diets in the peri-transplant period, or enzymatic supplementation (e.g., with the lactase enzyme (Lactaid), which is cheap and easily available as it is used commonly by individuals with lactose intolerance).

Reintroduction of specific strains via defined bacterial consortia in oral capsule form (commonly known as probiotics) or transfer of a complete (healthy) microbiome via FMT could prevent domination by a single taxon by promoting resistance to colonization. For example, probiotic therapy with *Lactobacillus johnsonii* prevented *Enterococcus* domination after bone marrow transplantation in mice, which coincided with attenuation of acute GvHD.[47] Similarly, FMT effectively eliminated vancomycin-resistant *Enterococcus* from densely colonized mice, which was mediated by anaerobic bacteria.[58] More specifically, recolonization with *Barnesiella* correlated with eradication of vancomycin-resistant *Enterococcus*. In these studies, successful engraftment of donor strains was a key component of successful treatment. Factors that could influence this process include pre-treatment strategy (i.e., antibiotic decontamination or bowel lavage, with the latter appearing to be more effective), taxonomic configuration of both donor and recipient and possibly also genetic host factors.[59-61]

Alternative approaches that bypass the bacterial community itself but may still enhance colonization resistance include supplementation of antimicrobial peptides or administration of specific TLR agonists. For example, TLR7 might be a candidate as activation of TLR7 on dendritic cells induced IL-22 and mediated colonization resistance against vancomycin-resistant *Enterococcus*.[62] Whether targeting this pathway could also be beneficial for transplant outcome needs further investigation.

Healing of the mucosal barrier

The mucosal barrier becomes compromised during the allogeneic HCT process due to the toxic effects of chemo- and radiotherapy and subsequent mucositis, as a result of tissue destruction during acute GvHD, opportunistic

Table 1. Strategies for targeting the microbiome.

Method	Strategy	Goal
Prebiotics (i.e. non-digestible food ingredients)	Supplement essential bacterial nutrients	Preserve protective taxa
Optimizing dietary intake	Stimulate enteral feeding, avoid consumption of certain nutrients	Preserve protective taxa
Antibiotic selection	Reduce exposure to anaerobe-targeting antibiotics	Limit microbial damage
Probiotics/defined consortia (i.e. selected viable microorganisms) or FMT	Actively reintroduce (specific) microbial populations	Recover gut microbial communities
Postbiotics (bioactive metabolic compounds)	Supplement products of bacterial fermentation	Replenish beneficial microbial metabolites

FMT: fecal microbiota transplantation.

infections (e.g., cytomegalovirus) or because of the indirect influence of diminished nutritional intake. Dietary carbohydrates normally serve as the main source of nutrition for the gut microbiota, but in their absence the mucus layer can become an alternative source of energy. As an example, *Akkermansia muciniphila* is thought to have mucolytic capacities and its relative abundance increases in mice with acute GvHD after imipinem/cilastatin treatment.[32,63] Another study showed that a diet lacking fiber resulted in thinning of the mucus layer, which increased proximity of microbes to the epithelium.[64] Enteral feeding (diet or prebiotics) could thus enhance intestinal homeostasis by directly stimulating preservation of commensal populations as well as indirectly by preventing damage to the mucus layer. An alternative way to promote the integrity of the mucus layer is by activating goblet cells which are responsible for the formation of the intestinal mucus layer but are often lost upon development of acute GvHD. It was recently described that stimulation of goblet cells via IL-25 could prevent bacterial translocation and dampened inflammation in an experimental acute GvHD model.[65] Exogenous supplementation of butyrate or indoles was also able to enhance epithelial integrity and mitigate acute GvHD in experimental mouse models whereas deletion of the SCFA receptor GPR43 increased acute GvHD.[66-68] However, butyrate can have opposite effects and may delay mucosal wound repair by inhibiting proliferation of intestinal epithelial stem/progenitor cells in a dose-dependent manner.[69] Whether butyrate has a net-protective or net-pathogenic effect may depend on the time after transplantation, the state of underlying tissue damage, or the activation status of effector T cells and further work is needed to assess the translatability of these preclinical findings to clinical practice and whether they may be targeted for therapeutic benefit.

Another candidate for promoting mucosal repair is IL-22. IL-22, secreted by recipient innate lymphoid cells type 3, protected intestinal stem cells from immune-mediated damage during murine acute GvHD.[70] Similarly, recombinant IL-22 enhanced intestinal stem cell recovery, stimulated epithelial regeneration and reduced intestinal acute GvHD pathology. However, pro-inflammatory and destructive effects of donor-derived Il-22 have also been described, suggesting a dual, context-dependent role for this cytokine, which needs further investigation.[71]

Immune modulation

The cycle of dysbiosis, tissue damage and lymphocyte activation that characterizes the early post-transplant environment and is even more exaggerated when acute GvHD has developed, contains many potential pathways for intervention (Figure 2). Therapies that alter the microbiome and thereby break these feed-forward loops may offer an attractive target in GvHD prevention or treatment.

A number of preclinical studies have determined the immunomodulatory properties of microbiome-targeting or microbiome-adjunct therapies. A prebiotic mixture of glutamine, fiber and oligosaccharides (GFO) as well as FMT lowered colonic expression of IL-1β in dextran sodium sulfate-induced colitis in mice.[72,73] In addition, FMT reduced the MHCII-dependent antigen-presenting capacities of colonic dendritic cells, monocytes and macrophages while simultaneously enhancing IL-10 production by these antigen-presenting cells, as well as in $CD4^+$ T cells and invariant natural killer T cells.[73] FMT also appeared to limit $CD4^+$ T-cell proliferation while increasing the frequency of $FoxP3^+$ regulatory T cells. Induction of regulatory T cells was also accomplished by oral administration of a rationally selected mixture of bacterial strains which mitigated experimental colitis and allergic diarrhea and mainly comprised clusters IV, XIVa and XVIII Clostridia.[74]

While it remains to be clarified whether these mechanisms are also involved in FMT-mediated resolution of steroid-refractory acute GvHD, microbial metabolites might be involved in this process. In addition to SCFA, secondary bile acids, such as lithocholic acid and 3β-hydroxydeoxycholic acid, are other products of microbiota-mediated biotransformation that are thought to have immunomodulatory properties. For example, lithocholic acid, 3β-hydroxydeoxycholic acid and other bile acid metabolites have been implicated in the induction of regulatory T-cell populations.[75,76] A number of studies have shown that bile acid metabolism is altered in patients with acute or chronic GvHD, which might impact disease severity.[77-79] A randomized controlled trial examining the use of the secondary bile acid ursodeoxycholic acid (also known as ursodiol) for prevention of hepatic complications (e.g., veno-occlusive disease) found a lower incidence of severe acute GvHD and intestinal GvHD in the treatment group that used ursodiol from the start of conditioning through 90 days post-transplantation compared with control-treated patients.[80] Furthermore, a study of patients with recurrent *Clostridioides difficile* infections (n=16), which included seven allogeneic HCT recipients, successfully used ursodiol to prevent recurrence of disease.[81] While the effects of ursodiol on the microbiome of allogeneic HCT recipients requires further investigation, these data suggest that therapeutic interventions targeting microbial bile acid metabolism might be worth exploring.

Opportunities for intervention

Therapies aimed at modulating intestinal microbiota function can target bacterial energy sources (prebiotics, diet), the bacterial community itself (antibiotic choice, probiotics, FMT) or its metabolites (postbiotics). Their protective or therapeutic potential has been studied in a number of interventional, predominantly single-arm studies.

Prevention of damage by antimicrobials: making the best antimicrobial choices

Antibiotic stewardship is most commonly considered in terms of its benefits in preventing the emergence of pathogens, but broadly speaking it involves the critical evaluation of antibiotic prescribing and use, to protect patients from all harms (including microbiome disruption) caused by the use of antibiotics, while at the same time effectively treating infections. For example, in a retrospective study, Weber and colleagues observed that rifaximin, a broad-spectrum antibiotic with minimal systemic absorption, was equally effective at preventing infectious complications in allogeneic HCT recipients as ciprofloxacin/metronidazole, while sparing bacterial gut communities.[82] Another retrospective analysis found that treatment of neutropenic fever with broad-spectrum antibiotics, specifically imipenem/cilastatin and

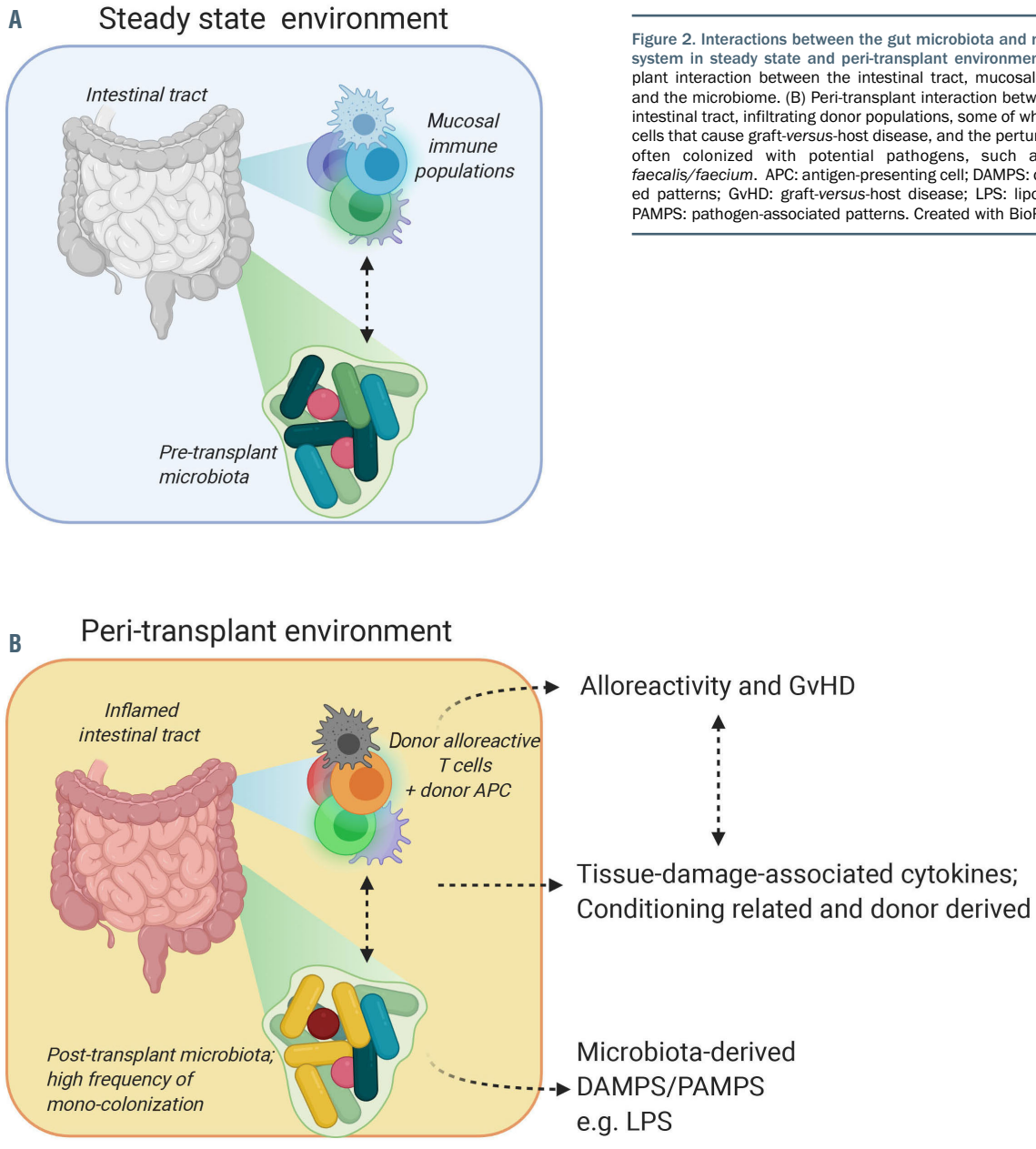

Figure 2. Interactions between the gut microbiota and mucosal immune system in steady state and peri-transplant environments. (A) Pre-transplant interaction between the intestinal tract, mucosal immune system and the microbiome. (B) Peri-transplant interaction between the inflamed intestinal tract, infiltrating donor populations, some of which alloreactive T cells that cause graft-*versus*-host disease, and the perturbed microbiome, often colonized with potential pathogens, such as *Enterococcus faecalis/faecium*. APC: antigen-presenting cell; DAMPS: damage-associated patterns; GvHD: graft-*versus*-host disease; LPS: lipopolysaccharides; PAMPS: pathogen-associated patterns. Created with BioRender.com

piperacillin/tazobactam, was associated with increased GvHD-related mortality while this was not observed when anaerobic-sparing antibiotics, aztreonam and cefepime, were used.[32] Of note, shortening the duration of administration of empiric broad-spectrum antibiotics in patients with febrile neutropenia without an identifiable infectious cause has been studied and appears to be safe; however, it remains unclear whether the shortened exposure also reduced intestinal dysbiosis in these patients.[83] Other strategies that are currently being developed to prevent antibiotic-mediated microbial disruption include molecules that degrade or neutralize antibiotic residues in the intestinal tract.[84,85]

Pre-transplantation optimization of the intestinal microbiome

Since a relatively preserved microbiome prior to allogeneic HCT translates into a higher chance of a favorable outcome,[30] it is worth considering a potential role for pre-emptive microbiota-targeting therapies. Two studies examined the effect of prebiotic supplementation prior to HCT: a prospective study by Yoshifuji and colleagues demonstrated that adequate intake of resistant starch and GFO from day -7 before allogeneic HCT to day +28 after the transplant reduced the incidence of acute GvHD and preserved populations of butyrate-producing bacteria, while fecal butyrate concentration in samples after transplantation did not differ significantly between GFO-treated patients and historical controls.[86] The patients with initial high microbial diversity in this cohort appeared more likely to benefit from prebiotic supplementation (n=14 of 30 in the whole cohort). Remarkably, the incidence of late-onset acute GvHD was higher in the prebiotic group, suggesting that there is only a temporary benefit from prebiotic supplementation and that the benefit subsides after cessation of the treatment. Similarly, a second retrospective study observed that patients who received GFO during the same period had higher survival rates early

after HCT (<day 100) than patients who were not on prebiotic treatment, but this advantage had disappeared 1 year after allogeneic HCT.[87]

A number of small studies have evaluated the safety and feasibility of probiotic use prior to allogeneic HCT but studies evaluating their potency with respect to minimization of transplantation-related complications have not been performed.[88,89] Oral administration of *Lactobacillus rhamnosus GG* in mice, starting from day 7 prior to transplantation and continuing throughout the transplantation period, limited bacterial translocation, mitigated acute GvHD and improved survival.[90] Microbiome analysis was not included in this study, thus further studies are needed to understand the precise mechanism of the observed effects.

Donor FMT effectively reversed antibiotic- and chemotherapy-induced dysbiosis in a murine model, returning the composition of the microbiome to the naïve, pre-treatment configuration within 16 days after FMT.[91] In five allogeneic HCT recipients, donor FMT was successfully used for decolonization of antibiotic-resistant bacteria prior to HCT but the enteric microbiome of these patients was not analyzed.[92,93]

Apart from these studies, data on the impact of microbiota-targeting therapies on the pre-transplant microbiome are scarce. Large, prospective trials are needed to assess to what extent these pre-emptive treatments can overcome treatment-induced microbiota injury and protect against post-transplant complications.

Diet

It is well-established that dietary changes influence the enteric microbiome and thus it is likely that specific alterations in nutritional support could provide an extra stimulus for the growth and activity of anaerobic bacteria in the peri-transplant setting.[94] A recent study in mice showed that administration of a tyrosine-enriched diet prior to HCT positively modulated the gut microbiome and metabolome, which was accompanied by reduced acute GvHD pathology and improved survival.[95] Whether a specific diet could help to preserve a healthy microbiome in allogeneic HCT recipients or improve intestinal health prior to allogeneic HCT remains to be elucidated. A study in pediatric patients (n=20) found that patients receiving enteral nutrition after allogeneic HCT had increased fecal diversity, higher concentrations of fecal SCFA and a higher relative abundance of certain butyrate-producing populations than patients receiving parenteral nutrition.[96] In adult patients (n=23), fecal microbial diversity was similar in groups receiving either enteral or parenteral nutrition. However, minimal oral intake for a prolonged period was associated with less diversity, as well as less abundance of intestinal *Blautia*.[97] Earlier studies had reported the superiority of enteral over parenteral nutrition in terms of transplant-related complications and survival.[98,99]

There remains a gap in our knowledge regarding the impact of diet on the microbiome of allogeneic HCT recipients. It has been described that there is a high interpersonal variability in microbiome response to types of nutrition and it might prove difficult to formulate universal dietary recommendations.[94,100,101] To what extent a specific diet, e.g., devoid of lactose-containing products, could benefit the health of transplant patients needs to be investigated in randomized trials.

Post-transplant recovery of the microbiome

It is likely that even with the best preventive strategies, some abnormalities in the microbiome will remain after the acute post-transplant period. For those patients with extensive microbial damage, probiotics or (donor) FMT might offer a way to directly repair the microbial community itself. Commercially available probiotic formulations contain bacterial strains predominantly belonging to the *Lactobacillus* and *Bifidobacterium* genera. The efficacy of probiotics as a preventive or therapeutic measure has been studied in the context of various disease entities with mixed results.[102] In fact, the use of probiotics after antibiotic therapy delayed recovery of the indigenous microbiota in healthy individuals.[103] As for allogeneic HCT recipients, a number of case reports raised safety concerns after systemic infections developed in immunocompromised patients upon probiotic use, even though the bacterial strains that are commonly incorporated in commercially available probiotics are infrequently the cause of bloodstream infections.[104-109] Probiotic therapy, comprising *Lactobacillus rhamnosus GG* capsules administered from the time of neutrophil engraftment, did not appreciably alter the microbiome or reduce acute GvHD incidence in a randomized trial (n=31) and was therefore prematurely terminated.[110]

A second option for the re-introduction of a whole community of microorganisms is via transfer of a healthy "previous self" or a donor-derived fecal suspension. In a randomized, controlled trial by Taur *et al.*, allogeneic HCT recipients received either an autologous FMT (n=14), using the patient's banked stool sample that was collected prior to transplant conditioning and carried a high microbial diversity but no intestinal pathogens, or no intervention (n=11).[29] Autologous FMT improved microbial diversity and reinstated commensal members of the patient's gut microbiome which had disappeared after allogeneic HCT. While effective, autologous FMT can be logistically challenging, as it requires upfront collection of a patient's healthy stool; for this reason, most current studies have used related or unrelated healthy donors as the source for FMT.

High success rates have been reported for single or repeated donor FMT in patients to restore symbiosis, eradicate antibiotic-resistant bacteria or treat recurrent *Clostridioides difficile* infections, which coincidently also relieved GvHD symptoms in one patient.[92,93,111-118] Resolution of steroid-refractory acute GvHD using donor FMT has been described in a number of case reports.[119-122] Additionally, a pilot study from our group showed that donor FMT alleviated steroid-refractory or steroid-dependent acute GvHD in ten of 15 participants, which was accompanied by an increase of fecal microbial diversity, expansion of butyrate-producing bacteria, and enhanced donor species engraftment.[123] The intrinsic and extrinsic factors that facilitate donor species engraftment remain to be elucidated and blinded, randomized clinical trials are needed to determine the additive value of donor FMT in GvHD treatment.

Safety has been one of the major concerns regarding the use of donor FMT in immunocompromised patients. For this reason, FMT trials have, thus far, largely postponed administration until allogeneic HCT recipients have achieved neutrophil engraftment. The number of reported infection-related adverse events associated with donor FMT administration is low but transmission of

pathogenic microorganisms has been described and can be fatal.[124,125] While there is no debate that potential donors of fecal material should undergo stringent screening, the donor screening protocols have been and, for the foreseeable future, will be subject to change as our experience with FMT therapy increases. International guidelines for donor screening protocols, for example as published by the European FMT working group, may help to reduce the variability of screening protocols used in FMT trials.[126] In addition to donor screening and selection, other steps in the FMT procedure could be reviewed for optimization. For example, potentially beneficial obligate anaerobic organisms may be lost in the process of FMT preparation unless care is taken to process potential donor material in an anaerobic fashion. Additionally, the best route of administration of the FMT product is unknown, with options including capsules, nasoduodenal infusion and enema.

Microbial metabolites

Finally, one could bypass the bacterial community and directly supply microbial metabolites, such as the SCFA, acetate, butyrate or propionate. Fecal SCFA concentrations decrease in patients with acute GvHD in proportion to the severity of their disease.[46] Similarly, the plasma concentrations of butyrate and propionate were reduced in patients who developed chronic GvHD.[54] Exogenous butyrate supplementation as well as administration of a consortium of 17 known butyrate-producing bacterial strains mitigated murine GvHD in a study by Mathewson and colleagues.[66] In contrast, a high relative abundance of butyrogenic bacteria in allogeneic HCT with acute GvHD has been associated with steroid-resistance, although luminal butyrate concentrations were not measured.[127] These contrasting results highlight that we still have more work to do to understand the biology of butyrate signaling in the post-transplant setting, particularly with respect to GvHD.

Outstanding questions and future perspective

Considering that the field of microbiome research in hematologic patients is relatively young, significant advances have been made in recent years. Large cohort studies have robustly shown that microbiota injury during allogeneic HCT is common and associated with adverse outcomes. This has already led to some changes in practice – e.g., the favoring of anaerobe-sparing empiric antibiotics in many centers. Results from the first, predominantly single-arm trials have demonstrated potential for microbiota-modulating therapies to improve transplant outcomes (e.g., our recent study of FMT for steroid-refractory acute GvHD), paving the way for eagerly awaited randomized controlled trials that will confirm the clinical efficacy of these therapies in preventing or treating transplantation-related complications. The accessibility of these biological, often already commercially available treatments has facilitated rapid translation from bench to bedside, with a large number of clinical trials currently being undertaken to target dysbiosis in allogeneic HCT recipients. In order to move the field forward in the coming years, several fundamental questions will need to be addressed (summarized inTable 2).

Several microbiome-targeting approaches have shown promising results in preclinical and clinical studies but the key players that underlie this beneficial effect are yet to be defined. Thus far, *Blautia* as well as butyrate-producing Clostridia appear to be prominent candidates based on fecal microbiome analysis. Still, it is important to keep in mind that there is only partial overlap between the fecal microbiome and the intestinal microbial composition and that the taxa that we have associated with positive transplant outcomes might only be a reflection of a balanced microbiota community.[128] More invasive sampling (e.g., consecutive colon biopsies) will be needed to confirm the taxa present at the most immunologically active sites within the gastrointestinal tract, and access to these samples will also further enhance our understanding of the working mechanisms of these therapies. Apart from the bacterial constituents of the microbiome, it is going to be important to examine other microbial kingdoms present in the enteric flora such as viruses, including bacteriophages, fungi and archaea. A small study demonstrated that a sterile fecal transplant, filtered from bacterial microbiota, was sufficient to cure *Clostridioides difficile* infection, implying that non-bacterial microorganisms and/or microbial metabolites are also capable of disease resolution.[129]

In addition to identifying protective bacterial taxa and their related metabolites, the long-term effects of treatment response warrant further investigation. It is not known whether the different therapies discussed here only induce a local and temporary reset of the microbiome or whether they elicit a systemic and durable response to dampen ongoing inflammatory processes. Yoshifuji and colleagues observed that after termination of prebiotics (at day 28 post-HCT), the incidence of late-onset acute GvHD (>day 100) was higher in the prebiotic group than in historical controls, suggesting that more work is needed to understand the potential mechanisms of prebiotic activity after HCT.[86] The same holds true for FMT in which donor bacterial strains are eventually undermined by environmental and/or host factors in modeling the bacterial composition.[118] This is supported by the finding in our FMT trial that early use of antibiotics after donor FMT appeared to abrogate treatment response. Antibiotic treatment might thus be taken into account in clinical trial design for microbiome-targeting therapies, for example by including an additional/escape intervention in the case of antibiotic treatment. Once intestinal homeostasis is restored, disappearance of donor strains might be less problematic; while taxonomic similarity to the donor's microbiome declined in the study by Moss *et al.*, the functional similarity persisted at a high level. Future studies including long-term follow-up and longitudinal sampling will help to determine the optimal interval for intervention or whether, for example, lifelong dietary restrictions or prebiotic or postbiotic supplementation should be encouraged.

Ideally, in the near future, microbiome analysis should be included in the routine work-up/follow-up for HCT, just as other organ function is measured, since the microbiome can function as a biomarker for transplant-related complications, as well as being potentially modifiable in the pre-transplant period.[130,131] The microbiome is a significant focus of many research groups internationally, and it is likely that the coming years will continue to yield important results in both the pre-clinical and clinical set-

Table 2. Outstanding questions and potential investigational approaches.

Key questions	Potential investigational approach
Bacterial composition-focused	
Which 'protective' taxa from associative studies are truly beneficial as therapeutics?	Transfer defined bacterial consortia in HCT patients + trials with more invasive sampling especially at time of GvHD diagnosis.
What is the best way to collect additional data to support that change in bacterial composition is indeed the mechanism of clinical improvement?	Add important secondary endpoints to initial studies as well as clinical responses (e.g., fecal engraftment of specific taxa, bacterial diversity, active metabolic pathways, serum and fecal SCFA concentrations).
What is the optimal diet for the patient to produce the optimal microbiome?	Start with observational diet studies, move toward interventional randomized trials.
Metabolite-focused	
Which are most important (SCFA, bile acids etc.)? Where do they need to act for maximum benefit?	Mouse studies + trials of 'post-biotic' compounds.
Which patient-intrinsic factors influence therapy efficacy (e.g. baseline diversity, presence of specific taxa, level of epithelial damage, genetic factors)?	Large (interventional) randomized studies of the microbiome-targeting intervention of interest.
What is the optimal timing and interval for intervention?	Small interventional studies + trials with long-term follow-up.

HCT: hematopoietic cell transplantation; GvHD: graft-*versus*-host disease; SCFA: short-chain fatty acids.

ting with regard to how we may target the microbiome for maximal benefit for patients.

Disclosures

MRMvdB has received research support from Seres Therapeutics; has consulted for, received honorarium from or participated in advisory boards for Seres Therapeutics, WindMIL therapeutics, Rheos, Frazier Healthcare Partners, Nektar Therapeutics, Notch Therapeutics, Forty Seven inc., Priothera, Ceramedix, Lygenesis, Pluto Immunotherapeutics, Magenta Therapeutics, Merck & Co, Inc., and DKMS Medical Council (Board); has IP Licensing with Seres Therapeutics, Juno Therapeutics, and stock options from Seres and Notch Therapeutics. None of the other authors has anything to disclose.

Contributions

YvL and KAM wrote the manuscript. MRMvdB and MDH provided critical feedback and edited the manuscript.

References

1. Jagasia M, Arora M, Flowers ME, et al. Risk factors for acute GVHD and survival after hematopoietic cell transplantation. Blood. 2012;119(1):296-307.
2. D'Souza A, Fretham C, Lee SJ, et al. Current use of and trends in hematopoietic cell transplantation in the United States. Biol Blood Marrow Transplant. 2020;26(8):e177-e182.
3. Gooptu M, Koreth J. Translational and clinical advances in acute graft-versus-host disease. Haematologica. 2020;105(11):2550-2560.
4. Sonis ST. The pathobiology of mucositis. Nat Rev Cancer. 2004;4(4):277-284.
5. Bennett JE, Dolin R, Blaser MJ, Mandell GL, Douglas RG. Mandell, Douglas, and Bennett's Principles and Practice of Infectious Diseases. 2015. Eighth edition.
6. Zeiser R, Blazar BR. Acute graft-versus-host disease - biologic process, prevention, and therapy. N Engl J Med. 2017;377(22):2167-2179.
7. Antin JH, Ferrara JL. Cytokine dysregulation and acute graft-versus-host disease. Blood. 1992;80(12):2964-2968.
8. MacMillan ML, Robin M, Harris AC, et al. A refined risk score for acute graft-versus-host disease that predicts response to initial therapy, survival, and transplant-related mortality. Biol Blood Marrow Transplant. 2015;21(4):761-767.
9. Jagasia M, Zeiser R, Arbushites M, Delaite P, Gadbaw B, Bubnoff NV. Ruxolitinib for the treatment of patients with steroid-refractory GVHD: an introduction to the REACH trials. Immunotherapy. 2018;10(5):391-402.
10. Rinninella E, Raoul P, Cintoni M, et al. What is the healthy gut microbiota composition? A changing ecosystem across age, environment, diet, and diseases. Microorganisms. 2019;7(1):14.
11. Amarasinghe SL, Su S, Dong X, Zappia L, Ritchie ME, Gouil Q. Opportunities and challenges in long-read sequencing data analysis. Genome Biol. 2020;21(1):30.
12. Turnbaugh PJ, Ley RE, Hamady M, Fraser-Liggett CM, Knight R, Gordon JI. The human microbiome project. Nature. 2007;449(7164):804-810.
13. Falony G, Joossens M, Vieira-Silva S, et al. Population-level analysis of gut microbiome variation. Science. 2016;352(6285):560-564.
14. Zhernakova A, Kurilshikov A, Bonder MJ, et al. Population-based metagenomics analysis reveals markers for gut microbiome composition and diversity. Science. 2016;352(6285):565-569.
15. Jackson MA, Verdi S, Maxan ME, et al. Gut microbiota associations with common diseases and prescription medications in a population-based cohort. Nat Commun. 2018;9(1):2655.
16. Hooper LV, Macpherson AJ. Immune adaptations that maintain homeostasis with the intestinal microbiota. Nat Rev Immunol. 2010;10(3):159-169.
17. Kamada N, Seo SU, Chen GY, Nunez G. Role of the gut microbiota in immunity and inflammatory disease. Nat Rev Immunol. 2013;13(5):321-335.
18. Yatsunenko T, Rey FE, Manary MJ, et al. Human gut microbiome viewed across age and geography. Nature. 2012;486(7402):222-227.
19. Miller TL, Wolin MJ. Pathways of acetate, propionate, and butyrate formation by the human fecal microbial flora. Appl Environ Microbiol. 1996;62(5):1589-1592.
20. Ridlon JM, Kang DJ, Hylemon PB. Bile salt biotransformations by human intestinal bacteria. J Lipid Res. 2006;47(2):241-259.
21. Correa-Oliveira R, Fachi JL, Vieira A, Sato FT, Vinolo MA. Regulation of immune cell function by short-chain fatty acids. Clin Transl Immunology. 2016;5(4):e73.
22. Tan J, McKenzie C, Potamitis M, Thorburn AN, Mackay CR, Macia L. The role of short-chain fatty acids in health and disease. Adv Immunol. 2014;121:91-119.
23. Smith T. A modification of the method for determining the production of indol by bacteria. J Exp Med. 1897;2(5):543-547.
24. Ridlon JM, Harris SC, Bhowmik S, Kang DJ, Hylemon PB. Consequences of bile salt biotransformations by intestinal bacteria. Gut Microbes. 2016;7(1):22-39.
25. Sun M, Wu W, Chen L, et al. Microbiota-derived short-chain fatty acids promote Th1 cell IL-10 production to maintain intestinal homeostasis. Nat Commun. 2018;9(1):3555.
26. Dudakov JA, Hanash AM, van den Brink MR. Interleukin-22: immunobiology and pathology. Annu Rev Immunol. 2015;33:747-785.
27. Taur Y, Xavier JB, Lipuma L, et al. Intestinal domination and the risk of bacteremia in patients undergoing allogeneic hematopoi-

etic stem cell transplantation. Clin Infect Dis. 2012;55(7):905-914.
28. Ubeda C, Taur Y, Jenq RR, et al. Vancomycin-resistant Enterococcus domination of intestinal microbiota is enabled by antibiotic treatment in mice and precedes bloodstream invasion in humans. J Clin Invest. 2010;120(12):4332-4341.
29. Taur Y, Coyte K, Schluter J, et al. Reconstitution of the gut microbiota of antibiotic-treated patients by autologous fecal microbiota transplant. Sci Transl Med. 2018;10(460):eaa9489.
30. Peled JU, Gomes ALC, Devlin SM, et al. Microbiota as predictor of mortality in allogeneic hematopoietic-cell transplantation. N Engl J Med. 2020;382(9):822-834.
31. Weber D, Jenq RR, Peled JU, et al. Microbiota disruption induced by early use of broad-spectrum antibiotics is an independent risk factor of outcome after allogeneic stem cell transplantation. Biol Blood Marrow Transplant. 2017;23(5):845-852.
32. Shono Y, Docampo MD, Peled JU, et al. Increased GVHD-related mortality with broad-spectrum antibiotic use after allogeneic hematopoietic stem cell transplantation in human patients and mice. Sci Transl Med. 2016;8(339):339ra371.
33. Simms-Waldrip TR, Sunkersett G, Coughlin LA, et al. Antibiotic-induced depletion of anti-inflammatory clostridia is associated with the development of graft-versus-host disease in pediatric stem cell transplantation patients. Biol Blood Marrow Transplant. 2017;23(5):820-829.
34. Lee SE, Lim JY, Ryu DB, et al. Alteration of the intestinal microbiota by broad-spectrum antibiotic use correlates with the occurrence of intestinal graft-versus-host disease. Biol Blood Marrow Transplant. 2019;25(10):1933-1943.
35. van Vliet MJ, Tissing WJ, Dun CA, et al. Chemotherapy treatment in pediatric patients with acute myeloid leukemia receiving antimicrobial prophylaxis leads to a relative increase of colonization with potentially pathogenic bacteria in the gut. Clin Infect Dis. 2009;49(2):262-270.
36. Zwielehner J, Lassl C, Hippe B, et al. Changes in human fecal microbiota due to chemotherapy analyzed by TaqMan-PCR, 454 sequencing and PCR-DGGE fingerprinting. PLoS One. 2011;6(12):e28654.
37. Biagi E, Zama D, Nastasi C, et al. Gut microbiota trajectory in pediatric patients undergoing hematopoietic SCT. Bone Marrow Transplant. 2015;50(7):992-998.
38. Galloway-Pena JR, Shi Y, Peterson CB, et al. Gut microbiome signatures are predictive of infectious risk following induction therapy for acute myeloid leukemia. Clin Infect Dis. 2020;71(1):63-71.
39. Montassier E, Gastinne T, Vangay P, et al. Chemotherapy-driven dysbiosis in the intestinal microbiome. Aliment Pharmacol Ther. 2015;42(5):515-528.
40. Taur Y, Jenq RR, Perales MA, et al. The effects of intestinal tract bacterial diversity on mortality following allogeneic hematopoietic stem cell transplantation. Blood. 2014;124(7):1174-1182.
41. Jenq RR, Taur Y, Devlin SM, et al. Intestinal blautia is associated with reduced death from graft-versus-host disease. Biol Blood Marrow Transplant. 2015;21(8):1373-1383.
42. Stein-Thoeringer CK, Nichols KB, Lazrak A, et al. Lactose drives Enterococcus expansion to promote graft-versus-host disease. Science. 2019;366(6469):1143-1149.
43. Holler E, Butzhammer P, Schmid K, et al. Metagenomic analysis of the stool microbiome in patients receiving allogeneic stem cell transplantation: loss of diversity is associated with use of systemic antibiotics and more pronounced in gastrointestinal graft-versus-host disease. Biol Blood Marrow Transplant. 2014;20(5):640-645.
44. Biagi E, Zama D, Rampelli S, et al. Early gut microbiota signature of aGvHD in children given allogeneic hematopoietic cell transplantation for hematological disorders. BMC Med Genomics. 2019;12(1):49.
45. Ilett EE, Jorgensen M, Noguera-Julian M, et al. Associations of the gut microbiome and clinical factors with acute GVHD in allogeneic HSCT recipients. Blood Adv. 2020;4(22):5797-5809.
46. Payen M, Nicolis I, Robin M, et al. Functional and phylogenetic alterations in gut microbiome are linked to graft-versus-host disease severity. Blood Adv. 2020;4(9):1824-1832.
47. Jenq RR, Ubeda C, Taur Y, et al. Regulation of intestinal inflammation by microbiota following allogeneic bone marrow transplantation. J Exp Med. 2012;209(5):902-910.
48. Varelias A, Ormerod KL, Bunting MD, et al. Acute graft-versus-host disease is regulated by an IL-17-sensitive microbiome. Blood. 2017;129(15):2172-2185.
49. Koyama M, Mukhopadhyay P, Schuster IS, et al. MHC class II antigen presentation by the intestinal epithelium initiates graft-versus-host disease and is influenced by the microbiota. Immunity. 2019;51(5):885-898.
50. Eriguchi Y, Takashima S, Oka H, et al. Graft-versus-host disease disrupts intestinal microbial ecology by inhibiting Paneth cell production of alpha-defensins. Blood. 2012;120(1):223-231.
51. Peled JU, Devlin SM, Staffas A, et al. Intestinal microbiota and relapse after hematopoietic-cell transplantation. J Clin Oncol. 2017;35(15):1650-1659.
52. Harris B, Morjaria SM, Littmann ER, et al. Gut microbiota predict pulmonary infiltrates after allogeneic hematopoietic cell transplantation. Am J Respir Crit Care Med. 2016;194(4):450-463.
53. Haak BW, Littmann ER, Chaubard JL, et al. Impact of gut colonization with butyrate-producing microbiota on respiratory viral infection following allo-HCT. Blood. 2018;131(26):2978-2986.
54. Markey KA, Schluter J, Gomes ALC, et al. The microbe-derived short-chain fatty acids butyrate and propionate are associated with protection from chronic GVHD. Blood. 2020;136(1):130-136.
55. Tamburini FB, Andermann TM, Tkachenko E, Senchyna F, Banaei N, Bhatt AS. Precision identification of diverse bloodstream pathogens in the gut microbiome. Nat Med. 2018;24(12):1809-1814.
56. Steck N, Hoffmann M, Sava IG, et al. Enterococcus faecalis metalloprotease compromises epithelial barrier and contributes to intestinal inflammation. Gastroenterology. 2011;141(3):959-971.
57. Molina MA, Diaz AM, Hesse C, et al. Immunostimulatory effects triggered by Enterococcus faecalis CECT7121 probiotic strain involve activation of dendritic cells and interferon-gamma production. PLoS One. 2015;10(5):e0127262.
58. Ubeda C, Bucci V, Caballero S, et al. Intestinal microbiota containing Barnesiella species cures vancomycin-resistant Enterococcus faecium colonization. Infect Immun. 2013;81(3):965-973.
59. Le Roy T, Debedat J, Marquet F, et al. Comparative evaluation of microbiota engraftment following fecal microbiota transfer in mice models: age, kinetic and microbial status matter. Front Microbiol. 2018;9:3289.
60. Smillie CS, Sauk J, Gevers D, et al. Strain tracking reveals the determinants of bacterial engraftment in the human gut following fecal microbiota transplantation. Cell Host Microbe. 2018;23(2):229-240.
61. Hall AB, Tolonen AC, Xavier RJ. Human genetic variation and the gut microbiome in disease. Nat Rev Genet. 2017;18(11):690-699.
62. Abt MC, Buffie CG, Susac B, et al. TLR-7 activation enhances IL-22-mediated colonization resistance against vancomycin-resistant enterococcus. Sci Transl Med. 2016;8(327):327ra325.
63. Derrien M, Van Baarlen P, Hooiveld G, Norin E, Muller M, de Vos WM. Modulation of mucosal immune response, tolerance, and proliferation in mice colonized by the mucin-degrader Akkermansia muciniphila. Front Microbiol. 2011;2:166.
64. Earle KA, Billings G, Sigal M, et al. Quantitative imaging of gut microbiota spatial organization. Cell Host Microbe. 2015;18(4):478-488.
65. Ara T, Hashimoto D, Hayase E, et al. Intestinal goblet cells protect against GVHD after allogeneic stem cell transplantation via Lypd8. Sci Transl Med. 2020;12(550):eaaw0720.
66. Mathewson ND, Jenq R, Mathew AV, et al. Gut microbiome-derived metabolites modulate intestinal epithelial cell damage and mitigate graft-versus-host disease. Nat Immunol. 2016;17(5):505-513.
67. Swimm A, Giver CR, DeFilipp Z, et al. Indoles derived from intestinal microbiota act via type I interferon signaling to limit graft-versus-host disease. Blood. 2018;132(23):2506-2519.
68. Fujiwara H, Docampo MD, Riwes M, et al. Microbial metabolite sensor GPR43 controls severity of experimental GVHD. Nat Commun. 2018;9(1):3674.
69. Kaiko GE, Ryu SH, Koues OI, et al. The Colonic Crypt Protects Stem Cells from Microbiota-Derived Metabolites. Cell. 2016;165(7):1708-1720.
70. Hanash AM, Dudakov JA, Hua G, et al. Interleukin-22 protects intestinal stem cells from immune-mediated tissue damage and regulates sensitivity to graft versus host disease. Immunity. 2012;37(2):339-350.
71. Couturier M, Lamarthee B, Arbez J, et al. IL-22 deficiency in donor T cells attenuates murine acute graft-versus-host disease mortality while sparing the graft-versus-leukemia effect. Leukemia. 2013;27(7):1527-1537.
72. Joo E, Yamane S, Hamasaki A, et al. Enteral supplement enriched with glutamine, fiber, and oligosaccharide attenuates experimental colitis in mice. Nutrition. 2013;29(3):549-555.
73. Burrello C, Garavaglia F, Cribiu FM, et al. Therapeutic faecal microbiota transplantation controls intestinal inflammation through IL10 secretion by immune cells. Nat Commun. 2018;9(1):5184.
74. Atarashi K, Tanoue T, Oshima K, et al. Treg induction by a rationally selected mixture of Clostridia strains from the human microbiota. Nature. 2013;500(7461):232-236.
75. Campbell C, McKenney PT, Konstantinovsky D, et al. Bacterial metabolism of bile acids promotes generation of peripheral regulatory T cells. Nature.

2020;581(7809):475-479.
76. Hang S, Paik D, Yao L, et al. Bile acid metabolites control TH17 and Treg cell differentiation. Nature. 2019;576(7785):143-148.
77. Reikvam H, Gronningsaeter IS, Mosevoll KA, Lindas R, Hatfield K, Bruserud O. Patients with treatment-requiring chronic graft versus host disease after allogeneic stem cell transplantation have altered metabolic profiles due to the disease and immunosuppressive therapy: potential implication for biomarkers. Front Immunol. 2017;8:1979.
78. Michonneau D, Latis E, Curis E, et al. Metabolomics analysis of human acute graft-versus-host disease reveals changes in host and microbiota-derived metabolites. Nat Commun. 2019;10(1):5695.
79. Joshi NM, Hassan S, Jasani P, et al. Bile acid malabsorption in patients with graft-versus-host disease of the gastrointestinal tract. Br J Haematol. 2012;157(3):403-407.
80. Ruutu T, Juvonen E, Remberger M, et al. Improved survival with ursodeoxycholic acid prophylaxis in allogeneic stem cell transplantation: long-term follow-up of a randomized study. Biol Blood Marrow Transplant. 2014;20(1):135-138.
81. Webb BJ, Brunner A, Lewis J, Ford CD, Lopansri BK. Repurposing an old drug for a new epidemic: ursodeoxycholic acid to prevent recurrent Clostridioides difficile infection. Clin Infect Dis. 2019;68(3):498-500.
82. Weber D, Oefner PJ, Dettmer K, et al. Rifaximin preserves intestinal microbiota balance in patients undergoing allogeneic stem cell transplantation. Bone Marrow Transplant. 2016;51(8):1087-1092.
83. Rearigh L, Stohs E, Freifeld A, Zimmer A. De-escalation of empiric broad spectrum antibiotics in hematopoietic stem cell transplant recipients with febrile neutropenia. Ann Hematol. 2020;99(8):1917-1924.
84. Kaleko M, Bristol JA, Hubert S, et al. Development of SYN-004, an oral beta-lactamase treatment to protect the gut microbiome from antibiotic-mediated damage and prevent Clostridium difficile infection. Anaerobe. 2016;41:58-67.
85. de Gunzburg J, Ghozlane A, Ducher A, et al. Protection of the human gut microbiome from antibiotics. J Infect Dis. 2018;217(4):628-636.
86. Yoshifuji K, Inamoto K, Kiridoshi Y, et al. Prebiotics protect against acute graft-versus-host disease and preserve the gut microbiota in stem cell transplantation. Blood Adv. 2020;4(19):4607-4617.
87. Iyama S, Sato T, Tatsumi H, et al. Efficacy of enteral supplementation enriched with glutamine, fiber, and oligosaccharide on mucosal injury following hematopoietic stem cell transplantation. Case Rep Oncol. 2014;7(3):692-699.
88. Ladas EJ, Bhatia M, Chen L, et al. The safety and feasibility of probiotics in children and adolescents undergoing hematopoietic cell transplantation. Bone Marrow Transplant. 2016;51(2):262-266.
89. Sadanand A, Newland JG, Bednarski JJ. Safety of probiotics among high-risk pediatric hematopoietic stem cell transplant recipients. Infect Dis Ther. 2019;8(2):301-306.
90. Gerbitz A, Schultz M, Wilke A, et al. Probiotic effects on experimental graft-versus-host disease: let them eat yogurt. Blood. 2004;103(11):4365-4367.
91. Le Bastard Q, Ward T, Sidiropoulos D, et al. Fecal microbiota transplantation reverses antibiotic and chemotherapy-induced gut dysbiosis in mice. Sci Rep. 2018;8(1):6219.
92. Battipaglia G, Malard F, Rubio MT, et al. Fecal microbiota transplantation before or after allogeneic hematopoietic transplantation in patients with hematologic malignancies carrying multidrug-resistance bacteria. Haematologica. 2019;104(8):1682-1688.
93. Innes AJ, Mullish BH, Fernando F, et al. Faecal microbiota transplant: a novel biological approach to extensively drug-resistant organism-related non-relapse mortality. Bone Marrow Transplant. 2017;52(10):1452-1454.
94. Kolodziejczyk AA, Zheng D, Elinav E. Diet-microbiota interactions and personalized nutrition. Nat Rev Microbiol. 2019;17(12):742-753.
95. Li X, Lin Y, Li X, et al. Tyrosine supplement ameliorates murine aGVHD by modulation of gut microbiome and metabolome. EBioMedicine. 2020;61:103048.
96. D'Amico F, Biagi E, Rampelli S, et al. Enteral nutrition in pediatric patients undergoing hematopoietic SCT promotes the recovery of gut microbiome homeostasis. Nutrients. 2019;11(12):2958.
97. Andersen S, Staudacher H, Weber N, et al. Pilot study investigating the effect of enteral and parenteral nutrition on the gastrointestinal microbiome post-allogeneic transplantation. Br J Haematol. 2020;188(4):570-581.
98. Gonzales F, Bruno B, Alarcon Fuentes M, et al. Better early outcome with enteral rather than parenteral nutrition in children undergoing MAC allo-SCT. Clin Nutr. 2018;37(6 Pt A):2113-2121.
99. Beckerson J, Szydlo RM, Hickson M, et al. Impact of route and adequacy of nutritional intake on outcomes of allogeneic haematopoietic cell transplantation for haematologic malignancies. Clin Nutr. 2019;38(2):738-744.
100. Segal L, Opie RS. A nutrition strategy to reduce the burden of diet related disease: access to dietician services must complement population health approaches. Front Pharmacol. 2015;6:160.
101. Johnson AJ, Vangay P, Al-Ghalith GA, et al. Daily sampling reveals personalized diet-microbiome associations in humans. Cell Host Microbe. 2019;25(6):789-802.
102. McFarland LV. Use of probiotics to correct dysbiosis of normal microbiota following disease or disruptive events: a systematic review. BMJ Open. 2014;4(8):e005047.
103. Suez J, Zmora N, Zilberman-Schapira G, et al. Post-antibiotic gut mucosal microbiome reconstitution Is impaired by probiotics and improved by autologous FMT. Cell. 2018;174(6):1406-1423.
104. Cohen SA, Woodfield MC, Boyle N, Stednick Z, Boeckh M, Pergam SA. Incidence and outcomes of bloodstream infections among hematopoietic cell transplant recipients from species commonly reported to be in over-the-counter probiotic formulations. Transpl Infect Dis. 2016;18(5):699-705.
105. Ambesh P, Stroud S, Franzova E, et al. Recurrent Lactobacillus bacteremia in a patient with leukemia. J Investig Med High Impact Case Rep. 2017;5(4):2324709617744233.
106. Mehta A, Rangarajan S, Borate U. A cautionary tale for probiotic use in hematopoietic SCT patients-Lactobacillus acidophilus sepsis in a patient with mantle cell lymphoma undergoing hematopoietic SCT. Bone Marrow Transplant. 2013;48(3):461-462.
107. Salminen MK, Rautelin H, Tynkkynen S, et al. Lactobacillus bacteremia, clinical significance, and patient outcome, with special focus on probiotic L. rhamnosus GG. Clin Infect Dis. 2004;38(1):62-69.
108. Vahabnezhad E, Mochon AB, Wozniak LJ, Ziring DA. Lactobacillus bacteremia associated with probiotic use in a pediatric patient with ulcerative colitis. J Clin Gastroenterol. 2013;47(5):437-439.
109. Robin F, Paillard C, Marchandin H, Demeocq F, Bonnet R, Hennequin C. Lactobacillus rhamnosus meningitis following recurrent episodes of bacteremia in a child undergoing allogeneic hematopoietic stem cell transplantation. J Clin Microbiol. 2010;48(11):4317-4319.
110. Gorshein E, Wei C, Ambrosy S, et al. Lactobacillus rhamnosus GG probiotic enteric regimen does not appreciably alter the gut microbiome or provide protection against GVHD after allogeneic hematopoietic stem cell transplantation. Clin Transplant. 2017;31(5).
111. DeFilipp Z, Peled JU, Li S, et al. Third-party fecal microbiota transplantation following allo-HCT reconstitutes microbiome diversity. Blood Adv. 2018;2(7):745-753.
112. Bilinski J, Grzesiowski P, Sorensen N, et al. Fecal microbiota transplantation in patients with blood disorders inhibits gut colonization with antibiotic-resistant bacteria: results of a prospective, single-center study. Clin Infect Dis. 2017;65(3):364-370.
113. Neemann K, Eichele DD, Smith PW, Bociek R, Akhtari M, Freifeld A. Fecal microbiota transplantation for fulminant Clostridium difficile infection in an allogeneic stem cell transplant patient. Transpl Infect Dis. 2012;14(6):E161-165.
114. de Castro CG Jr, Ganc AJ, Ganc RL, Petrolli MS, Hamerschlack N. Fecal microbiota transplant after hematopoietic SCT: report of a successful case. Bone Marrow Transplant. 2015;50(1):145.
115. Mittal C, Miller N, Meighani A, Hart BR, John A, Ramesh M. Fecal microbiota transplant for recurrent Clostridium difficile infection after peripheral autologous stem cell transplant for diffuse large B-cell lymphoma. Bone Marrow Transplant. 2015;50(7):1010.
116. Webb BJ, Brunner A, Ford CD, Gazdik MA, Petersen FB, Hoda D. Fecal microbiota transplantation for recurrent Clostridium difficile infection in hematopoietic stem cell transplant recipients. Transpl Infect Dis. 2016;18(4):628-633.
117. Bluestone H, Kronman MP, Suskind DL. Fecal microbiota transplantation for recurrent Clostridium difficile infections in pediatric hematopoietic stem cell transplant recipients. J Pediatric Infect Dis Soc. 2018;7(1):e6-e8.
118. Moss EL, Falconer SB, Tkachenko E, et al. Long-term taxonomic and functional divergence from donor bacterial strains following fecal microbiota transplantation in immunocompromised patients. PLoS One. 2017;12(8):e0182585.
119. Kakihana K, Fujioka Y, Suda W, et al. Fecal microbiota transplantation for patients with steroid-resistant acute graft-versus-host disease of the gut. Blood. 2016;128(16):2083-2088.
120. Spindelboeck W, Schulz E, Uhl B, et al. Repeated fecal microbiota transplantations attenuate diarrhea and lead to sustained changes in the fecal microbiota in acute, refractory gastrointestinal graft-versus-host-disease. Haematologica. 2017;102(5):e210-e213.
121. Qi X, Li X, Zhao Y, et al. Treating steroid

refractory intestinal acute graft-vs.-host disease with fecal microbiota transplantation: a pilot study. Front Immunol. 2018;9:2195.
122. Kaito S, Toya T, Yoshifuji K, et al. Fecal microbiota transplantation with frozen capsules for a patient with refractory acute gut graft-versus-host disease. Blood Adv. 2018;2(22):3097-3101.
123. van Lier YF, Davids M, Haverkate NJE, et al. Donor fecal microbiota transplantation ameliorates intestinal graft-versus-host disease in allogeneic hematopoietic cell transplant recipients. Sci Transl Med. 2020;12(556): eaaz8926.
124. DeFilipp Z, Bloom PP, Torres Soto M, et al. Drug-Resistant E. coli bacteremia transmitted by fecal microbiota transplant. N Engl J Med. 2019;381(21):2043-2050.
125. Bilinski J, Lis K, Tomaszewska A, et al. Eosinophilic gastroenteritis and graft-versus-host disease induced by transmission of Norovirus with fecal microbiota transplant. Transpl Infect Dis. 2021;23(1):e13386.
126. Cammarota G, Ianiro G, Tilg H, et al. European consensus conference on faecal microbiota transplantation in clinical practice. Gut. 2017;66(4):569-580.
127. Golob JL, DeMeules MM, Loeffelholz T, et al. Butyrogenic bacteria after acute graft-versus-host disease (GVHD) are associated with the development of steroid-refractory GVHD. Blood Adv. 2019;3(19):2866-2869.
128. Zmora N, Zilberman-Schapira G, Suez J, et al. Personalized gut mucosal colonization resistance to empiric probiotics is associated with unique host and microbiome features. Cell. 2018;174(6):1388-1405.e21.
129. Ott SJ, Waetzig GH, Rehman A, et al. Efficacy of sterile fecal filtrate transfer for treating patients with Clostridium difficile infection. Gastroenterology. 2017;152(4): 799-811.
130. Han L, Zhang H, Chen S, et al. Intestinal microbiota can predict acute graft-versus-host disease following allogeneic hematopoietic stem cell transplantation. Biol Blood Marrow Transplant. 2019;25(10): 1944-1955.
131. Kusakabe S, Fukushima K, Maeda T, et al. Pre- and post-serial metagenomic analysis of gut microbiota as a prognostic factor in patients undergoing haematopoietic stem cell transplantation. Br J Haematol. 2020;188 (3):438-449.

REVIEW ARTICLE

Ferrata Storti Foundation

European Myeloma Network perspective on CAR T-cell therapies for multiple myeloma

Benedetto Bruno,[1,2*] Ralph Wäsch,[3] Monika Engelhardt,[3] Francesca Gay,[1] Luisa Giaccone,[1] Mattia D'Agostino,[1] Luis-Gerardo Rodríguez-Lobato,[4,5] Sophia Danhof,[5] Nico Gagelmann,[6] Nicolaus Kröger,[6] Rakesh Popat,[7] Niels W C J van de Donk,[8] Evangelos Terpos,[9] Meletios A Dimopoulos,[9] Pieter Sonneveld,[10] Hermann Einsele[5] and Mario Boccadoro[1]

[1]Department of Molecular Biotechnology and Health Sciences, University of Torino and Department of Oncology, Division of Hematology, A.O.U. Città della Salute e della Scienza di Torino, Presidio Molinette, Torino, Italy; [2]Division of Hematology and Medical Oncology, Perlmutter Cancer Center, Grossman School of Medicine, NYU Langone Health, New York, NY, USA; ; [3]Department of Hematology, Oncology and Stem Cell Transplantation, University Medical Center, Faculty of Medicine, University of Freiburg, Freiburg, Germany; [4]Unit of Amyloidosis and Multiple Myeloma, Department of Hematology, Hospital Clínic of Barcelona, Institut d'Investigacions Biomèdiques August Pi i Sunyer (IDIBAPS), Barcelona, Spain; [5]Division of Medicine II, University Hospital Würzburg, Würzburg, Germany; [6]Department of Stem Cell Transplantation, University Medical Center Hamburg-Eppendorf, Hamburg, Germany; [7]Department of Hematology, University College London Hospitals, London, UK; [8]Department of Hematology, Amsterdam University Medical Centers, Cancer Center Amsterdam, Location VUmc, Amsterdam, the Netherlands; [9]Stem Cell Transplantation Unit, Plasma Cell Dyscrasias Unit, Department of Clinical Therapeutics, School of Medicine, National and Kapodistrian University of Athens, Athens, Greece and [10]Erasmus MC Cancer Institute, Rotterdam, the Netherlands.

[*]Current address: Division of Hematology and Medical Oncology, Perlmutter Cancer Center, Grossman School of Medicine, NYU Langone Health, New York, NY, USA.

Haematologica 2021
Volume 106(8):2054-2065

ABSTRACT

Chimeric antigen receptor (CAR) T cells (CAR-T) have dramatically changed the treatment landscape of B-cell malignancies, providing a potential cure for relapsed/refractory patients. Long-term responses in patients with acute lymphoblastic leukemia and non Hodgkin lymphomas have encouraged further development in myeloma. In particular, B-cell maturation antigen (BCMA)-targeted CAR-T have established very promising results in heavily pre-treated patients. Moreover, CAR-T targeting other antigens (*i.e.*, SLAMF7 and CD44v6) are currently under investigation. However, none of these current autologous therapies have been approved, and despite high overall response rates across studies, main issues such as long-term outcome, toxicities, treatment resistance, and management of complications limit as yet their widespread use. Here, we critically review the most important pre-clinical and clinical findings, recent advances in CAR-T against myeloma, as well as discoveries in the biology of a still incurable disease, that, all together, will further improve safety and efficacy in relapsed/refractory patients, urgently in need of novel treatment options.

Correspondence:

BENEDETTO BRUNO
benedetto.bruno@unito.it

Received: December 7, 2020.

Accepted: March 11, 2021.

Pre-published: April 1, 2021.

https://doi.org/10.3324/haematol.2020.276402

Introduction

Recently engineered chimeric antigen receptors (CAR) have greatly increased anti-tumor effects of CAR T cells (CAR-T). Impressive results have been observed with CD19-directed CAR-T in B-cell lymphoproliferative disorders.[1-3] In addition, several CAR-T products have been developed for the treatment of multiple myeloma (MM). None has yet been approved, and, despite high overall response (OR) across studies, main issues such as long-term outcomes, toxicities and complications need to be solved to allow their widespread clinical use. In this review, the European Myeloma Network (EMN) group aimed to describe the most important pre-clinical and clinical findings, and recent advances in CAR-T technology against MM that may improve their safety and efficacy. Contents, comments and sugges-

tions have been incorporated in the manuscript after at least three rounds of discussion resulting in the final unanimously approved version.

Target antigens

CAR are artificial fusion proteins with a modular design that confer antigen-specificity to T cells in an human leukocyte antigen (HLA)-independent manner providing intracellular stimulatory signals to enhance survival, proliferation, cytolytic capacity and cytokine production of T cells.[4] Figure 1 illustrates the components of CAR constructs.[5-8] For successful CAR-T therapy, identification of suitable tumor antigens is crucial, since it requires a delicate balance between effectiveness and safety considerations. Ideal antigens should be: (i) highly and homogeneously expressed on tumor cell surface, (ii) expressed at different disease stages, (iii) pivotal in disease pathophysiology, (iv) limited or not shed into the bloodstream, (v) not affected by selective treatment pressure that may cause down-regulation or elimination, and (vi) not expressed on normal tissues.[9-10] Great progress has been made to identify potential molecules as CAR targets in MM. In this section, we summarize pre-clinical data on the most relevant MM-associated antigens, while a comprehensive overview is provided in Table 1.

B-cell maturation antigen

The B-cell maturation antigen (*BCMA*) gene is located on chromosome 16 and the BCMA (aliases: CD269, TNFRSF17) protein, a transmembrane glycoprotein member of the tumor necrosis factor receptor (TNFR) superfamily, is expressed on subsets of B cells (plasmablasts and plasma cells) and up-regulated during B-cell differentiation. It is not expressed on solid organ tissues, hematopoietic cells or naïve B cells.[11-12] Along with two associated receptors (calcium modulator and cyclophilin ligand interactor [TACI] and B-cell activation factor receptor [BAFF-R]) and its ligands (a proliferation inducing ligand [APRIL] and B-cell activating factor [BAFF]) BMCA regulates maturation, differentiation, and promotes B-cell survival.[13-15]

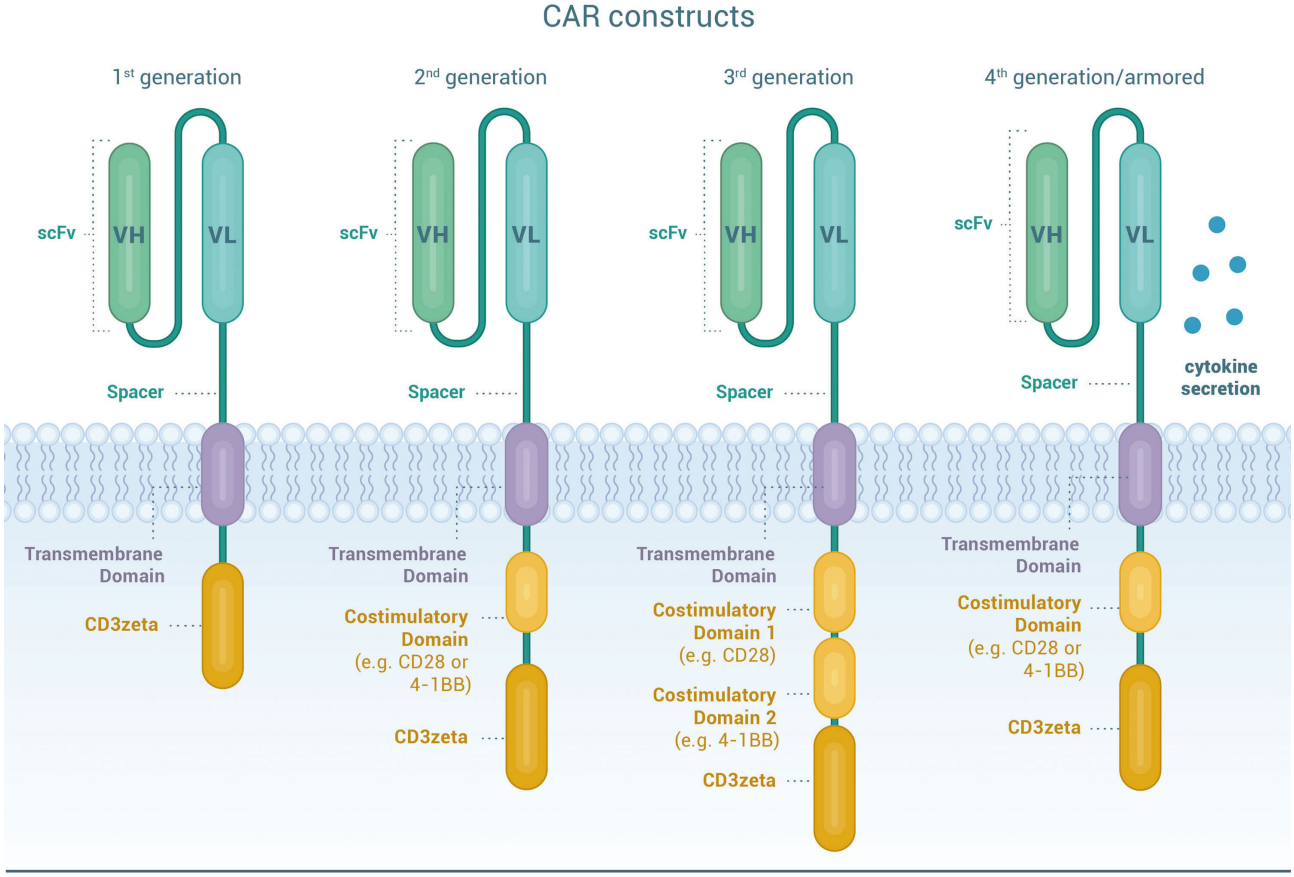

Figure 1. Chimeric antigen receptor T cells. Chimeric antigen receptors (CAR) are designer proteins that redirect T cells towards a defined surface antigen on tumor cells. The CAR construct contains four essential components. The extracellular antigen recognition domain consists of a single chain variable fragment (scFv) commonly derived from the variable domains of the heavy and light chains (VH and VL) of monoclonal antibodies joined by a linker to provide flexibility and solubility and therefore improve antigen recognition and binding capacity. The hinge or spacer moiety based on Ig- (IgG1 or IgG4), CD8- or CD28-derived domains, provides flexibility, stability and the suitable length for optimal access to the target antigen. The transmembrane domain links the extracellular and intracellular domains of the CAR. It is based on CD3ζ, CD4, CD8α, CD28 or ICOS moieties, influences CAR stability and signaling and may also be involved in immune synapse arrangement. The last components of the CAR construct are the intracellular signaling domains. The activation domain is typically derived from the CD3ζ moiety of the T-cell receptor (first generation CAR), whereas co-stimulatory domains are derived from CD28, 4-1BB, OX40, CD27, or ICOS (second and third generation CAR). Co-stimulation results in intracellular signals that further optimize T-cell function, persistence and proliferation. Through additional genetic modifications, so called "armored" CAR T cells (CAR-T) (fourth generation CAR) secrete cytokines or express ligands to bolster CAR-T function or to overcome the immunosuppressive tumor microenvironment. Taken together, the molecular fine-tuning of pre-existing CAR components can greatly improve cellular migration, foster expansion and persistence of the CAR-T and decrease toxicity.

Expression of BCMA in malignant plasma cells is enhanced compared to non-malignant cells, though levels are not homogeneous. Its expression is associated with proliferation and survival of tumor cells and contributes to the immunosuppressive bone marrow (BM) microenvironment.[15-17] BCMA cleavage by γ-secretase sheds soluble BCMA (sBCMA) into the bloodstream.[18] sBCMA may play a role in myeloma pathogenesis, and high sBCMA levels have been associated to worse prognosis.[19] BCMA is currently considered the most compelling antigen for targeted immunotherapy. Carpenter *et al.* reported on the first proof-of-concept using a second generation, CD28 co-stimulated CAR against BCMA in the preclinical setting. BCMA CAR-T specifically recognized the antigen, eradicated *in vivo* tumors and killed primary myeloma cells,[11] setting the cornerstone for the first-in-human phase I clinical trial evaluating BCMA CAR-T in MM.[20]

Transmembrane activator, calcium modulator, and cyclophilin ligand interactor

TACI (TNFRSF13B) is a transmembrane protein that recognizes ligands APRIL, BAFF and calcium modulator and cyclophilin ligand (CAML). It is expressed on subsets of naïve and memory B cells, plasma cells, non-germinal center cells, monocytes and dendritic cells. TACI supports growth and survival in myeloma cells, though its expression is lower compared to BCMA.[21-23] A third-generation APRIL-based CAR recognizing both BCMA and TACI antigens has been engineered. Though this construct demonstrated tumor control in an *in vivo* model of tumor escape with $BCMA^-$ $TACI^+$ cells,[22] the AUTO2 trial (clinicaltrials.gov. Identifier: NCT03287804) was, however terminated because of lack of efficacy.[24]

CD19

In most B-cell malignancies, CD19 is highly and uniformly expressed.[25-29] MM was traditionally considered mostly CD19 negative with low level CD19 expression attributed to a putative "myeloma stem cell". However, highly sensitive direct stochastic optical reconstruction microscopy (*d*STORM) unveiled expression of CD19 on a considerable subset (10–80%) of myeloma cells in more than two thirds of patients, of whom only one fifth was considered CD19 positive by conventional flow cytome-

Table 1. Potential target antigens for CAR-T therapy for mutiple myeloma.

Antigen	Expression in MM	Expression in normal hematopoietic cells	Expression in healthy solid organ tissues	Development state
BCMA	60-100%	Late memory B cells, plasma cells	No	Clinical trial
TACI	78%	Naïve and memory B cells, plasma cells, monocytes and dendritic cells	No	Clinical trial
CD19	10-80%	B-cells, plasma cells	No	Clinical trial
SLAMF7 (CD319)	High and uniform expression	NK-cells, monocytes, macrophages, dendritic cells, T cells, B cells, plasma cells	No	Clinical trial
CD38	High and uniform expression	Lymphoid and myeloid cells, hematopoietic precursors, thymocytes	Prostatic epithelium, pancreatic islet cells, cerebellar Purkinje cells	Clinical trial
CD44v6	43% in advanced stage	Activated T cells, monocytes	Keratinocytes	Clinical trial
GPRC5D	≥50% in 65% of patients	B-cells, plasma cells	Hair follicles	Clinical trial
CD138	High expression	Plasma cells	Epithelial cells, gastrointestinal tract and hepatocytes	Clinical trial
NKG2D	Heterogenous	NK, T and γδ T cells	No	Clinical trial
κ light chain	κ-restricted myeloma cells	Mature B cells	No	Clinical trial
CD56	High expression, decreased in extramedullary disease	T and NK cells	Central and peripheral nervous system	Clinical trial
Lewis Y	50%	No	Epithelial cells	Clinical trial
NY-ESO-1	60-100%	No	No	Clinical trial
CD229 (SLAMF3)	High and homogeneous expression, probably in myeloma stem cell	T, NK and B cells	No	Preclinical investigation
Integrin β7	High expression	High expression in B cells and low to moderate expression in $CD34^+$ hematopoietic cells	No	Preclinical investigation
CD70	0.2-42%	Activated T and B cells, dendritic cells and plasma cells	No	Preclinical investigation
CD1d	High expression	Antigen-presenting cells, thymocytes, B cells, and hematopoietic stem cells	Epithelial cells	Preclinical investigation

BCMA: B-cell maturation antigen; GPRC5D: G protein-coupled receptor class C group 5 member D; NKG2D: Natural Killer Group 2 member D; NY-ESO-1: New York Esophageal Squamous Cell Carcinoma 1; SLAMF3 and SLAMF7: signaling lymphocytic activation molecules family member 3 and 7; TACI: Transmembrane activator, calcium modulator, and cyclophilin ligand interactor.

try. As CAR-T can eliminate cells expressing less than 100 target antigens/cell, CD19 has become a relevant CAR target antigen. In preclinical models, BCMA-CD19 bispecific CAR-T eliminated myeloma cell lines more potently than BCMA- or CD19-directed CAR-T alone.[30] Due to an off-target expression limited to B cells, toxicity concerns of (co-)targeting CD19 are limited and clinical evaluation of bispecific CAR-T is ongoing (clinicaltrials gov. Identifier: NCT03455972, NCT03549442).

SLAMF7

The elotuzumab target antigen signaling lymphocytic activation molecule (SLAM) family member 7 (SLAMF7, aliases: CD319, CS-1, CRACC) is an immunomodulatory transmembrane receptor, initially identified on the surface of natural killer (NK) cells.[31] It is expressed on a variety of other innate immune cells,[32] but also T cells, B cells and plasma cells.[31-33] Importantly, SLAMF7 is expressed on aberrant plasma cells and its precursor[34] and confers homing of the myeloma cells to the BM niche. While redirecting T cells against a self-antigen may appear difficult, preclinical experiments demonstrated that it is feasible to generate clinically relevant doses of SLAMF7-directed CAR-T, with or without additional inactivation of the endogenous *SLAMF7* gene.[33-35] In preclinical models, potent anti-myeloma activity was demonstrated, resulting in rapid, comprehensive and sustained cell depletion.[33] SLAMF7-directed CAR-T eliminated SLAMF7 positive lymphocytes *in vitro*, while SLAMF7 negative lymphocytes were spared and retained their functions.[33] Clinical evaluation of SLAMF7 CAR-T with functional safety switches is currently ongoing (clinicaltrials gov. Identifier: NCT03958656, EudraCT Nr.2019-001264-30).

CD38

Successfully targeting CD38 (cyclic ADP ribose hydrolase, ADPRC1) with daratumumab and isatuximab has led to the development of anti-CD38 CAR-T. CD38 is a transmembrane glycoprotein that functions as an ectoenzyme, adhesion molecule and regulator of migration and signaling. It is expressed on malignant plasma cells,[36] but low expression can be found on lymphoid and myeloid cells, hematopoietic precursors,[37] thymocytes, cerebellar Purkinje cells and other tissues. CD38 is an activation marker of T cells at intermediate or late activation stages. As CD38-directed CAR-T demonstrated great antigen-specific efficacy in preclinical myeloma models,[38] affinity modification of the CAR was developed as an approach to mitigate on-target, off-tumor toxicity towards other CD38 positive hematopoietic cells. Affinity reduction of the antigen binding domain by a factor of 1,000 enabled selective elimination of myeloma cells with high CD38 expression while sparing normal cells with less pronounced CD38 expression. However, it has been reported that levels of CD38 expression on myeloma cells can decline over the disease course.[39] In this regard, agents that induce selective modulation of CD38 expression levels, such as all-trans retinoic acid (ATRA) or histone deacetylase (HDAC) inhibitors,[40] represent a promising group for combination therapy with CD38-directed CAR-T. In order to address the issue of antigen reduction by increasing the potency of the cell product, a novel construct termed "dimeric antigen receptor" (DAR) was developed. In fact, the DAR T cells that incorporate a fragment antigen-binding (Fab) moiety instead of the single chain variable fragment (scFv), demonstrated superior preclinical activity. However, their clinical relevance, and the risk of on-target, off-tumor effects, remains to be determined.

CD44v6

CD44 glycoproteins are encoded by a highly conserved gene,[41] but are nevertheless characterized by considerable protein heterogeneity due to post-transcriptional modifications or splicing variants. While CD44 plays a role in physiological processes and is expressed on healthy tissues,[42] the isoform variant 6 is relatively restricted to malignant cells[43,44] including plasma cells. In healthy tissues, CD44v6 expression is limited to skin keratinocytes. It is absent on hematopoietic precursor cells, but low level expression can be found on activated T cells and monocytes. While the development of an anti-CD44v6 immunoconjugate was discontinued due to severe skin toxicities,[45] preclinical investigation of CD44v6-directed CAR-T showed promising efficacy with no impact on keratinocytes that represent potentially immune-privileged sites.[46] The clinical relevance of the observed monocyte depletion remains unclear. However, as monocyte-derived cytokines play a relevant role for the pathogenesis of cytokine release syndrome (CRS) and immune effector cell-associated neurotoxicity syndrome (ICANS), a beneficial effect is possible and clinical evaluation is ongoing (clinicaltrials gov. Identifier: NCT04097301).

GPRC5D

The orphan G protein–coupled receptor, class C group 5 member D (GPRC5D), is expressed ubiquitously in malignant bone marrow plasma cells (500 to 1,000 times higher expression than on normal cells), hair follicles, and in the lung. CAR-T targeting GPRC5D have demonstrated promising preclinical activity, and a phase I clinical trial is ongoing (clinicaltrials gov. Identifier: NCT04555551).

CD229

CD229, a SLAM family receptor ("SALM3"), is generally expressed on myeloma cells and "precursor" myeloma cells. Its high expression suggests a potential as a target for CAR-T studies have shown that this newly designed CD229 CAR-T has high activity against MM cells, memory B cells and MM stem cells *in vitro* and *in vivo*.[47]

Clinical studies

B-cell maturation antigen-specific chimeric antigen receptor T cells

The National Cancer Institute group performed the first study with BCMA-specific CAR-T with a CD28 costimulatory domain (murine scFv) in heavily pretreated patients.[20] At the highest CAR-T dose ($9x10^6$ cells/kg), 13 of 16 patients (81%) achieved at least partial response (PR) with a median event-free survival of 31 weeks. Other studies confirmed high activity of BCMA CAR-T in this patient subset.[48-50] Advanced clinical findings have been reported with ide-cel[50,51] and cilta-cel.[48] Both therapies received Food and Drug Administration breakthrough designation. In this section, we will discuss these two CAR-T products. CAR-T constructs and main clinical characteristics are summarized in Table 2.

Ide-cel (bb2121)

The first-in-man study with ide-cel (CRB-401) evaluated escalating doses of CAR-T ($50x10^6$, $150x10^6$, $450x10^6$, or $800x10^6$ in the dose-escalation phase, and $150x10^6$-$450x10^6$ in the expansion phase) in extensively pretreated MM (median of six prior therapy lines; 69% triple-class refractory).[51] Sixty-two patients were enrolled. At least PR was achieved by 76% of patients including complete response (CR) in 39%. All 15 patients with ≥CR who had an assessment for minimal residual disease (MRD) were MRD-negative at the level of 10^{-5}. Baseline BCMA expression or sBMCA levels did not affect response. There was a trend towards lower response in patients who received ≤$150x10^6$ CAR-T, in those with less *in vivo* CAR-T expansion, and in those with high-risk cytogenetic abnormalities. Median progression free survival (PFS) was 8.8 months for all patients, and 9.0 months for those who received $450x10^6$ CAR-T. Median overall survival (OS) was 34.2 months. Based on these promising results of the phase I trial, a second trial (KarMMa, phase II study) was initiated to evaluate the value of ide-cel in larger numbers of patients who were previously exposed to immunomodulatory drugs (IMiD), a proteasome inhibitor, and a CD38 antibody.[50] In this study 140 patients were enrolled with a manufacturing success of 99%; 128 of 140 (91%) received CAR-T, whereby 88% received bridging therapy prior to

Table 2. Ide-cel and Cilta-cel: CAR-T and clinical characteristics

	Ide-cel (bb2121) / KarMMa (phase II)	Cilta-cel (JNJ-4528) / CARTITUDE-1 (phase IB/ II)
Antigen-binding domain	scFv (murine)	Bispecific variable fragments of llama heavy-chain antibodies; two distinct BCMA epitopes are targeted
Signaling domains	CD3ζ/4-1BB	CD3ζ/4-1BB
Vector	Lentiviral	Lentiviral
Other features	Bb21217 uses the same CAR construct as used for ide-cel. During *ex vivo* culture a PI3K inhibitor is added to enrich for CAR-T with memory-like phenotype	Bi-epitope BCMA binding confers high avidity binding
Lymphodepletion	Flu/Cy	Flu/Cy
CAR-T dose	$150\text{-}450x10^6$	Median dose: $0.71x10^6$/kg
Number of patients	128 (140 patients underwent leukapheresis)	Data presented for first 97 (113 patients were enrolled/apheresed
Bridging therapy (%)	88	65
Number of prior therapies (median)	6	6
Triple-class refractory (%)	84	88
High-risk cytogenetics (del(17p), t(4;14), or t(14;16) (%)		35 24
Extramedullary disease (%)	39	13
≥PR	$150\text{-}450x10^6$: 73% $150x10^6$: 50% $300x10^6$: 69% $450x10^6$: 82%	97%
≥CR	$150\text{-}450x10^6$: 33% $150x10^6$: 25% $300x10^6$: 29% $450x10^6$: 39%	67%
Median PFS	$150\text{-}450x10^6$: 8.8 months $150x10^6$: 2.8 months $300x10^6$: 5.8 months $450x10^6$: 12.1 months	Median PFS: Not reached; 12-month PFS rate: 77%
CRS (all grades) (%)	84	95
CRS (grade ≥3) (%)	5	4
Median time to CRS onset (any grade) (days)	1	7
Median duration of CRS (any grade) (days)	5	4
Neurotoxicity (all grades) (%)	18	21 (ICANS: 17%; other neurotoxicity*: 12%)
Neurotoxicity (grade ≥3) (%)	3	10 (ICANS: 2%; other neurotoxicity: 9%)
Median time to neurotoxicity onset (any grade) (days)	2	ICANS: 8 days; other neurotoxicities*: 27 days
Median duration of neurotoxicity (any grade) (days)	3	ICANS: 4 days; other neurotoxicities: 75 days
Time to peak CAR-T expansion (days)	11	13
CAR-T persistence 6 months, %	59	42

*Other neurotoxicities are defined as neurotoxicities occurring after resolution of cytokine release syndrome (CRS) and/or immune effector cell-associated neurotoxicity syndrome (ICANS). PR: partial response; CR: complete response; PFS: progression free survival.

CAR-T. Patients were highly pretreated with a median of six prior therapy lines and 84% had triple-class refractory disease (refractory to one protease inhibitor [PI], one IMiD, and a CD38 antibody). At least PR was achieved by 73% including ≥CR in 33%. MRD-negative CR was achieved in 26%. Median time to response was 1 month. Fifty-four patients, who received 450x10^6 CAR-T, had superior response (≥PR: 82%; ≥CR: 39%; MRD-negative CR: 28%) when compared to lower doses. Revised Multiple Myeloma International Staging System (R-ISS) stage 3 disease at enrollment had inferior response, compared to R-ISS stage 1 or 2. As in the phase I trial, baseline BCMA expression did not affect response to ide-cel. With median follow-up of 13.3 months, overall median PFS was 8.8 months. Median PFS increased with higher CAR-T dose with a median PFS of 12.1 months for patients who received 450x10^6 CAR-T. Patients, who achieved at least CR, also experienced better PFS (≥CR: median PFS of 20.2 months; very good partial response [VGPR]: median PFS of 11.3 months; PR: median PFS of 5.4 months; no-response: 1.8 months). Median OS was 19.4 months. Durable CAR-T persistence was observed up to 1 year: CAR-T were detected at 1, 3, 6, 9, and 12 months in 99%, 75%, 59%, 37%, and 46% respectively. CAR-T expansion was increased at higher doses. In an ongoing phase III study, ide-cel is compared with standard-of-care regimens in patients with 2-4 prior regimens, including IMiD, PI, and CD38 antibody (KarMMa-3). Ide-cel is also evaluated in the multi-cohort KarMMa-2 study, in patients with early relapse after first-line therapy or patients with sub-optimal response after autografting (<VGPR).

Cilta-cel (JNJ-4528)

The CARTITUDE-1 study evaluates cilta-cel (target dose: 0.75x10^6 CAR^+ T /kg) in patients exposed to PI, IMiD and CD38 antibody. Preliminary results were presented at the 2020 ASH conference. Sixteen of 113 patients, who underwent apheresis, were not dosed because of consent withdrawal (n=5), progressive disease (n=2) or death (n=9). The remaining 97 patients had received a median of six prior lines of therapy. Ninety-seven percent of patients achieved at least PR with stringent CR in 67%. Fourty-eight of the 57 patients evaluable for MRD, 93% were MRD-negative at the level of 10^{-5}. Response was independent of baseline BCMA expression. Median time to first response was 1 month. At a median follow-up of 12.4 months, 12-month PFS was 77%. Peak CAR-T expansion was observed around day 10-14, and CAR-T were observed in 36% of patients at 3 months of follow-up.[52] Interestingly, response to cilta-cel was independent of CAR-T expansion and persistence.[52] In the Chinese LEGEND-2 trial, different conditioning regimens were used, as well as variable CAR-T infusion methods (split *vs*. single infusion). The Xi'an site, which used cyclophosphamide lymphodepletion therapy and three CAR-T cell infusions (dose: 0.07-2.1x10^6/kg; median dose: 0.50x10^6/kg), enrolled 57 out of 74 patients.[53] These patients had received a median of three prior lines of therapy (prior PI and IMiD: 60%). Overall response rate (ORR) was 88% with CR in 74% (median time to response: 1 month). MRD-negative CR was achieved in 68%. At a median follow-up of 25 months, median PFS was 19.9 months for all patients, while it was 28.2 months for those in CR. Median OS was 36.1 months (not reached for patients in CR). Cilta-cel is also being evaluated in a phase III study (CARTITUDE-4), which compares CAR-T *versus* pomalidomide, bortezomib and dexamethasone or daratumumab, pomalidomide and dexamethasone in relapsed and lenalidomide-refractory MM. In addition, the ongoing CARTITUDE-2 study is evaluating cilta-cel in different patient populations, including those with early relapse after frontline therapy, prior exposure to a BCMA-targeting drug, and those with <CR post-auto-SCT.

Other B-cell maturation antigen-specific chimeric antigen receptor T cells

In order to further improve the activity and/or persistence of CAR-T, several studies are evaluating novel BCMA-targeting CAR-T. Studies include CAR constructs containing a fully human BCMA-specific binding domain to reduce development of humoral and/or cellular immune responses against CAR-T, which may impair CAR-T persistence.[49,54-56] One of these products with a fully human antigen-binding domain is orva-cel (orvacabtagene autoleucel), which is currently evaluated in the phase I/II EVOLVE study. This study shows promising efficacy of orva-cel in heavily pretreated MM (median of six prior lines of therapy; 94% triple-class refractory). At least PR was achieved in 92% of 62 patients treated at higher dose levels (300-600x10^6 CAR-T), with CR in 36%. Follow-up is ongoing. Treatment was associated with a low incidence of grade ≥3 cytokine release syndrome (3%) and grade ≥3 neurotoxicity (3%). Following CAR-T, there was robust expansion and durable persistence (69% of patients had detectable CAR-T at 6 months). Moreover, preclinical studies have shown that enrichment for BCMA-targeting CAR-T displaying a memory-like phenotype leads to improved persistence in mouse models,[57] which may result in more durable disease control. Bb21217 uses the same CAR molecule as ide-cel, but bb21217 is cultured in the presence of a PI3 kinase inhibitor, which leads to enrichment for CAR-T with a memory-like phenotype. Preliminary results showed efficacy in 69 heavily pretreated patients (64% triple-class refractory) with an ORR of 68% (CR of 29%; median response duration: 17.0 months). Interestingly, a high memory-like T-cell count in the drug product was associated with superior CAR-T expansion and less progression at 6 months. The manufacturing process for orva-cel is also designed to produce CAR-T enriched for central memory T-cell phenotype.[56] Other trials are evaluating combinations of CAR-T with other drugs to improve activity and durability of response. Based on preclinical data showing that the T-cell stimulatory effects of IMiD enhance the efficacy of CAR-T,[58-60] several ongoing clinical studies are evaluating the combination of lenalidomide and CAR-T. The combination of BCMA CAR-T with γ-secretase inhibitors is also investigated, because *in vitro* studies show that γ-secretase inhibitors block BCMA cleavage and increase BCMA cell surface expression levels.[54,61] These results are confirmed in an ongoing clinical study, which shows that gamma secretase inhibition enhances BCMA surface expression on MM cells and reduces soluble BCMA levels.[54]

CD19-specific CAR-T

Recent studies showed that MM cells express ultra-low levels of CD19,[30] moreover MM cells with disease-propagating properties also express CD19. This formed the rationale for the evaluation of CD19-specific CAR-T in

MM.[62] One study evaluated CD19 CAR-T following salvage high-dose therapy and autologous transplantation. All ten patients had shown a PFS shorter than 1 year from a previous transplant. Two experienced a longer PFS after transplant plus CD19 CAR-T therapy, compared with first autologous stem-cell transplantation. Only one patient experienced CRS (grade 1).[63]

Chimeric antigen receptor T-cell toxicity in multiple myeloma

CAR-T may induce several life-threatening side effects such as CRS and ICANS.[64] Hemophagocytosis and prolonged cytopenias may also occur. CRS mainly consists of fever, hypotension, hypoxia and organ toxicity, which may result in organ failure. ICANS may include several symptoms: impaired concentration, cognitive disorders, confusion, agitation, tremor, lethargy, aphasia, delirium, somnolence, seizures, motor weakness, paresis or signs of intracerebral pressure. ICANS usually occurs during or after CRS and may manifest a biphasic course, in about 10% of cases up to 4 weeks after CAR-T infusion. A ten-point neurologic assessment, at least twice a day, using the ICE screening tool is recommended for early detection.[64] Reported toxicity rates of hallmark studies are illustrated in Table 3. Importantly, a broad consensus statement offering updated comprehensive recommendations for the treatment of toxicities associated with immunotherapies has been recently published.[65] Though many aspects remain unknown, mechanisms underlying CRS and ICANS have become clearer. Several factors contribute to different toxicity rates.[65] Moreover, incidence and severity of adverse effects vary between diseases. While the incidence of any grade CRS is comparable between diseases, CRS severity (≥grade 3) is highest in patients with ALL and lowest in MM. This may partly be explained by disease burden and aggressiveness. In addition, earlier treatment of CAR-T side effects with more experience in recent trials may have contributed to reduce progression to higher grades of toxicity. Unlike CRS, incidence of ICANS is higher in ALL or lymphoma and appears lower in MM patients. Other factors such as tumor burden, prior treatment, CAR-T constructs and dose administered have been described. Several grading systems have been proposed to assess CRS and ICANS. Recently, the American Society for Transplantation and Cellular Therapy grading system was compared to other grading scores in two adult populations.[66] Interestingly, incidence of CRS and ICANS were similar in all grading systems. By contrast, only 25% and 54% of patients were however assigned to the same severity grade given the discrepancies in scoring adverse symptoms. These differences may also easily lead to inconsistent management guidelines among studies. Overall, efforts should be made to unify grading systems be used across clinical trials.

Improving chimeric antigen receptor T-cell therapies in multiple myeloma

Despite numerous autologous CAR-T products under development[67,68] and encouraging high response rates,[69] none have yet been approved, with BCMA remaining the best evaluated target.[49,51,69] Other limitations are toxicities, resistance mechanisms, availability, and patient management (Table 4). Here we highlight possible strategies for improvement.[70,71]

Safety

Preventing cytokine release

The pro-inflammatory interleukin-6 (IL-6) is increasingly acknowledged to play a central role in the pathogenesis of CRS.[47] A recent study designed a nonsignaling membrane-bound IL-6 receptor (mbaIL6) which was constituted by a scFv derived from an antibody against IL-6, and linked to a transmembrane anchoring peptide. The study identified expression of mbaIL6 on the surface of T cells

Table 3. Toxicity of CAR-T cell treatment in multiple myeloma

CAR-T	Construct	Cell dose	Trial	Sponsor	N	Cytopenia 3/4	CRS 3/4	ICANS 3/4	Ref
BCMA/CD28		$9x10^6$ cells / kg bw	First-in-humans	NIH	16	leucopenia 94% neutropenia 88% thrombopenia 63% prolonged 13%	38%	6%	30
BCMA/4-1BB		C1: $1-5x10^8$ total cells C2: Cy+$1-5x10^7$ total cells C3: Cy+$1-5x10^8$ total cells	Phase I	UPenn	25	leucopenia 44% neutropenia 44% thrombopenia 28% prolonged n.r.	32%	12%	49
BCMA/4-1BB	LCAR-B38M (JNJ-4528)	med. $0.5x10^6$ cells / kg bw	LEGEND-2	China (Phase 1)	57	leucopenia 30% neutropenia n.r. thrombopenia 23% prolonged 16%	7%	0%	53
BCMA/4-1BB	JNJ-4528	med. $0.73x10^6$ cells / kg bw	CARTITUDE-1 (Phase I/II)	Janssen	29	leucopenia 59% neutropenia 100% thrombopenia 69% prolonged n.r.	7%	3%	48 68
BCMA/CD28	bb2121	50-800 x 10^6 total cells	CRB-401 (Phase I)	BMS / Celgene	33	leucopenia 58% neutropenia 85% thrombopenia 45% prolonged n 3% t 35%	6%	3%	51

CRS: cytokine-release syndrome; ICANS: immune effector cell-associated neurotoxicity syndrome; Ref.: references; bw: body weight; C: cohort; Cy: cyclophosphamide; n.r.: not reported; n: number of patients.

which was associated with rapid removal of IL-6 from the culture supernatant. Furthermore, T-cell proliferation increased while the signaling and function of IL-6 was neutralized. T cells co-expressing mbaIL6 and anti-CD19 CAR, neutralized IL-6 derived from macrophages while maintaining antitumor activity *in vitro* and in a xenograft model.[72] Thus, CAR-T incorporating the capacity to remove IL-6 may provide new strategies for preventing CRS. Another strategy is the incorporation of "suicide" switches, such as constructs containing a CAR and inducible caspase 9. Administration of a small molecule causing dimerization of inducible caspase 9 resulted in apoptosis and CAR-T-specific depletion.[73]

Reducing off-tumor on-target toxicity

In order to avoid adverse off-tumor effects, spatial and temporal activity of CAR-T need to be limited. Under this hypothesis, GPRC5D has been proposed as a novel target antigen, expressed on almost all CD138+ cells.[74] Like BCMA, its expression is restricted to plasma cells, except for hair follicles. Preliminary results of anti-GPRC5D CAR-T showed potent anti-MM efficacy *in vitro* and in a mouse model, with the encouraging finding that these cells also effectively eradicated MM after treatment with anti-BCMA CAR-T. Most recently, it was demonstrated that simultaneous targeting of GPRC5D and BCMA could prevent relapse mediated by BCMA escape. Several multi-target constructs were compared and in BCMA-negative disease, dual-target (bicistronic) and pooled approaches exhibited the highest efficacy, whereas for GPRC5D/BCMA-expressing disease, the dual-target appeared to be more efficacious. Mechanistically, expressing two CAR on one cell enhanced the strength of CAR-T/target interactions.

Reducing immunogenicity and simplifying structures

In order to reduce the immunogenicity of the CAR binding domain, human or humanized scFv have been used more frequently in recent studies, instead of murine sequences.[68,75] Furthermore, a reduction of immunogenicity might be achieved by the incorporation of heavy-chain-only binding domains, which subsequently simplify the structure of the CAR antigen-binding domain without having a light-chain domain.[76] In general, simplified structures may facilitate better gene expression by transduced T cells.[76,77] Moreover, limiting the size of expressed genes is important for the potential expression of >1 protein.[78,79] A recent study demonstrated that CAR with antigen-recognition domains consisting of only a fully human heavy-chain variable domain (FHVH33) in addition to 4-1BB and CD3ζ domains mediated comparable cytokine release, reduction in tumor burden, and degranulation in mice when compared to an identical CAR with a conventional scFv.[76,80] Further investigations identified a crucial contribution of 4-1BB in reducing activation-induced cell death, enabling survival of T cells expressing FHVH33-CAR.[76]

Efficacy

Understanding antigen loss

Some relapses are either antigen-negative or antigen-low.[80] One study in leukemia mouse models could dissect evidence for CAR promoting reversible antigen loss through a mechanism called trogocytosis.[81] This mechanism defines an active process of rapid intercellular transfer of membrane fragments and related molecules. The specific target antigen is transferred to T cells resulting in decreased density on tumor cells, leading to declined T-cell activity by boosting fratricide T-cell killing and exhaustion.[81] These cascades affected CAR constructs that included different costimulatory domains (CD28 or 4-1BB), and the effect was dependent on antigen density. Thus, it was hypothesized that multi-target CAR-T could overcome these limitations.[81]

Multi-targeting

T-cells expressing single-chain bispecific CAR are able to prevent antigen escape.[68,82] Moreover, CAR pools combining two single-input CAR-T products have been proposed (Figure 2). Pooling a humanized anti-CD19 and a

Table 4. Limitations and ways to improve CAR-T therapy in multiple myeloma.

	What may limit CAR-T therapy?	How to improve CAR-T therapy?
Toxicity	On-target, on-tumor	Anti-IL6 treatment and prevention Safeguard designs incorporating drugs such as rituximab/cetuximab
	On-target, off-tumor	Tackling immunogenicity Simplified CAR structures (*e.g.,* heavy-chain-only binding domains)
Resistance	Impaired CAR-T expansion/persistence	Multi-targting therapy (dual-target, OR-target, CARpool) More accurate measurement of expansion/persistence "Suicide switches"
	Immunosuppression induced by BM microenvironment	Combination of immunomodulatory modulation and CAR-T Senolytic CAR-T (?)
	Antigen loss or downregulation	Address trogocytosis Increase antigen density (*e.g.* γ-secretase-inhibition for anti-BCMA therapy)
Management	Suboptimal recognition and treatment of severe events	Increase comparability and knowledge sharing of intensive care unit management and other care settings Outcome prediction
Availability	Lack of scale-up High costs No stockpiling Time	Allogeneic CAR-T Optimize supply chain models (*e.g.,* intermediate players for cryopreservation)

BCMA: B-cell maturation antigen; IL6: interleukin-6; BM: bone marrow.

murine anti-BCMA CAR-T was investigated in 22 patients.[63] The study had a median follow-up of 6 months and reported a high ORR of 95%, with CR of 57%, and relatively low CRS of grades ≥3 (4%).[63] Preliminary results of two other CD19/BCMA studies showed similar ORR but lower CR (22% and 16%).[83,84] One study investigated dual-target CAR-T co-expressing two full-length receptors, namely CD38 and BCMA.[85] Median follow-up was 9 months and the ORR was 88%. PFS was 75% and higher CRS of grades ≥3 were noted compared with tandem CAR (25%). OR-gate tandem CAR consist of a single CAR structure targeting two antigens with two distinct antigen recognition domains (scFv) linked consecutively with a single signal transducing intracellular domain.[82-86] A recent study using CS1/BCMA tandem CAR-T showed superior CAR expression and function in comparison with T cells co-expressing individual CS1 and BCMA CAR. When compared to the OR-gate (tandem) CAR, dual-target CAR require a much larger genetic payload, leading to poorer transduction efficiency and reduced proliferation. A recent Chinese study using BCMA-CD19 dual FasT CAR-T showed an overall response rate of 93.8% with median duration of follow up of 7.3 months at cutoff. Importantly, most patients showed high-risk features.[87] A much more compact genetic footprint may greatly support viral integration, thus product manufacturing, suggesting an advantage for single-chain tandem CAR in relation to dual-targeting. With respect to CARpools, this strategy could avoid poor transduction efficiency. Among these three approaches, mechanistically, CAR pool may be the least effective.[80]

Targeting the tumor microenvironment

The BM milieu is heavily involved in MM pathogenesis and resistance to treatment. Conflicting data exist on whether monoclonal antibodies against CD38 are effective in the BM microenvironment,[88] whereas immunomodulatory agents may be able to overcome these inhibitory effects.[89] Accordingly, combining these drugs with CAR-T therapy may provide synergistic effects.[59] Conversely, tissue microenvironment itself is modulated by secretory programs and stable cell-cycle arrest, defined as cellular senescence, which is a tumor-suppressive mechanism. Accumulating aberrant senescent cells create an inflammatory milieu resulting in tissue damage and fibrosis. In order to eliminate these senescent cells, "senolytic" CAR-T have been proposed.[90] One study discovered the cell-surface protein urokinase-type plasminogen activator receptor (uPAR) being broadly induced during senescence,[88] and further dissected that anti-uPAR CAR-T efficiently ablated senescent cells *in vitro* and *in vivo*, restoring tissue homeostasis in mice with liver fibrosis.[90] In MM, it has been shown that u-PAR contributes to the functioning of cancer-associated fibroblasts during MM progression,[91] and that higher expression of u-PAR was associated with disease progression, worse survival and early extramedullary spread of MM cells. Although it has to be noted that a caveat of senolytic CAR-T are the potential off-target toxicities,[92] these results may encourage the incorporation of cellular strategies specifically addressing the MM microenvironment.

Availability and management

Allogeneic chimeric antigen receptor T cells

Allogeneic CAR-T may decrease cost and enable broader availability.[93] Notwithstanding, allogeneic CAR-T bare the risk for graft-*versus*-host disease (GvHD). For this reason, TALEN- and CRISPR-based gene editing has been introduced to produce allogeneic CAR-T with off-the-shelf availability.[68,93,94] One recent study on allogeneic anti-BCMA CAR-T used gene editing, namely TALEN, to confer resistance to lymphodepletion and to reduce GvHD risk.[95] By further incorporating a CD20 mimotope-based switch-off within the CAR, rituximab could be given to eliminate the CAR-T in case of adverse events. Another preclinical approach using similar safety features but anti-CS1 CAR-T (UCARTCS1),[35] specifically degranulated and proliferated in response to MM cells, supporting further evaluation and testing of this universal therapy. Current investigational studies also include (i) the non-viral piggyBac system, aimed at transposing stem cell memory T cells together with (ii) the Cas-CLOVER™ gene editing

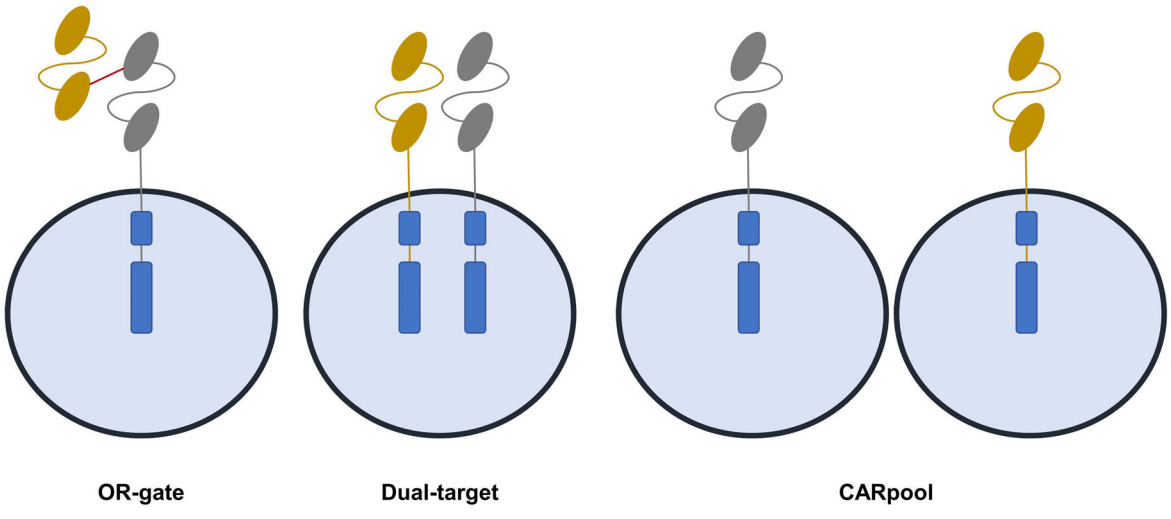

Figure 2. Overview of current multi-targeted chimeric antigen receptor T-cell approaches. Multi-targeting may be a mean to improve efficacy of CAR-T. Three major methods could be exploited: OR-gate (tandem) CAR-T: consist of the expression of two different CAR on the same T cell; dual-target CAR-T: consist of encoding two different target specific single-chain variable fragment antibodies on same CAR protein using a single vector; CARpool: involves production of two separate single target CAR-T products infused together or sequentially.

system consisting of CRISPR guide-RNA and dead Cas9 fused to Clo51 nuclease, and (iii) a nano-particle delivery system carrying the gene for an anti-BCMA Centyrin-based CAR with a fully human binding domain. Rimiducid, a lipid-permeable tacrolimus analogue and protein dimerizer, may be administered for safety switch activation.[96] Two phase I dose escalation and cohort expansion studies have recently been initiated. The CTX120 (clinicaltrials gov. Identifier: NCT04244656) is using anti-BCMA allogeneic CRISPR-Cas9-engineered T cells and the PBCAR269A (clinicaltrials gov. Identifier: NCT04171843) which applies its own gene editing tool (ARCUS) for GvHD risk reduction.

Integration of chimeric antigen receptor T cells into clinical routine - FACT-JACIE* standards and EBMT** guidelines

Since 2018, with version 7.0, the *Joint Accreditation Committee of ISCT and the **European Bone Marrow Transplantation Group (EBMT) (JACIE) prerequisites for cell therapy accreditation have included standards for infusions of immune-effector cells and CAR-T. The current recommendation is that CAR-T should be administered within the framework of an accredited allogeneic transplant program. The Foundation for the Accreditation of Cellular Therapy (FACT)-JACIE do not cover the manufacturing of CAR-T but do include supply chain and handover of responsibilities when the product is provided by third party. Overall, JACIE standards are structured on the basis of three major functional areas in cellular therapy: cell collection, laboratory processing, and clinical program. All areas required dedicated and highly qualified personnel. Accredited programs for cell therapy must implement a product labeling system that guarantees identification and traceability from collection to manufacturing site and return to clinical units. EBMT recommendations further stress the importance of staff training[97] and of multidisciplinary approaches with teams who include transplant physicians along with qualified internal medicine sub-specialists after a specific education program. Importantly, CAR-T infusions should be coordinated with intensive care specialists. All accredited centers must implement a policy for rapid escalation of care for critically ill patients including availability of specific drugs (*i.e.*, tocilizumab). Though complications may vary among CAR-T products, they tend to follow a predictable timeline contributing to bed-planning decisions. Recent reports allow designing protocols for anti-infective prophylaxis and common post-infusion complications such as infections and tumor lysis syndrome.[98] Inevitably, the unfortunate COVID-19 pandemic stresses the importance of scrupulous adherence to recommended hygiene procedures.[99] Importantly, an EBMT registry, for all transplant centers accredited for cell therapies, has been created to collect date on efficacy, side effects and clinical outcomes for post-marketing surveillance.

Conclusions

The clinical role of CAR-T in the current armamentarium of MM treatments remains as yet to be fully determined. Moreover, other promising forms of antibody-based immunotherapies have been added. Despite some limitations of CAR-T therapy experienced in early studies in MM, one advantage of this cellular therapy is the inherent potential to finetune its design. Simpler structures and multi-target approaches may significantly improve efficacy and safety. Constant learning to handle CAR-T therapy may also enable better patient-centered management. Last, long-term outcome studies and specific detection and analysis of CAR-T dynamics *in vivo* are essential to allow deeper understanding of their inherent functions which will facilitate future designs of improved CAR-T products. However, selecting patients who may most benefit from CAR-T and best timing of their administration still require rather lengthy and thorough clinical investigations. One more challenge that lies ahead will be the cost effectiveness of future commercial products. This issue has already been addressed in patients with lymphoma where cost reductions will be inevitable to make CAR-T sustainable therapies for health care systems.[100] Despite all remaining open questions and issues that still need to be addressed, and hopefully answered and resolved within the next years, we are now, without any doubt, at the dawn of a new era that will significantly improve patient outcome.

Disclosures

No conflicts of interest to disclose.

Contributions

BB, ME, NWCJD designed the review and wrote the manuscript; LG, MD, FG, ET, LGRL, SD, NG, NK, RP and ET provided data and interpretation; MAD, PS, HE and MB reviewed the manuscript.

Funding

LGRL as BITRECS fellow has received funding from the European Union's Horizon 2020 research and innovation programme under the Marie Sklodowska-Curie grant agreement No 754550 and from "La Caixa" Foundation. SD has received funding from the Mildred Scheel Early Career Center funded by the German Cancer Aid.

References

1. Maude SL, Laetsch TW, Buechner J, et al. Tisagenlecleucel in children and young adults with B-cell lymphoblastic leukemia. N Engl J Med. 2018;378(5):439-448.
2. Neelapu SS, Locke FL, Bartlett NL, et al. Axicabtagene ciloleucel CAR T-cell therapy in refractory large B-cell lymphoma. N Engl J Med. 2017;377(26):2531-2544.
3. Cerrano M, Ruella M, Perales MA, et al. The advent of CAR T-cell therapy for lymphoproliferative neoplasms: integrating research into clinical practice. Front Immunol. 2020;11:888.
4. Sadelain M, Brentjens R, Riviere I. The basic principles of chimeric antigen receptor design. Cancer Discov. 2013;3(4):388-398.
5. Hudecek M, Lupo-Stanghellini MT, Kosasih PL, et al. Receptor affinity and extracellular domain modifications affect tumor recognition by ROR1-specific chimeric antigen receptor T cells. Clin Cancer Res. 2013;19(12):3153-3164.
6. Jonnalagadda M, Mardiros A, Urak R, et al. Chimeric antigen receptors with mutated IgG4 Fc spacer avoid fc receptor binding and improve T cell persistence and antitumor efficacy. Mol Ther. 2015;23(4):757-768.
7. Kawalekar OU, RS OC, Fraietta JA, et al. Distinct signaling of coreceptors regulates specific metabolism pathways and impacts memory development in CAR T cells.

Immunity. 2016;44(3):712.
8. Sadelain M, Riviere I, Riddell S. Therapeutic T cell engineering. Nature. 2017;545(7655):423-431.
9. Abbott RC, Cross RS, Jenkins MR. Finding the Keys to the CAR: identifying novel target antigens for T cell redirection immunotherapies. Int J Mol Sci. 2020;21 (2):515.
10. Maude S, Barrett DM. Current status of chimeric antigen receptor therapy for haematological malignancies. Br J Haematol. 2016;172(1):11-22.
11. Carpenter RO, Evbuomwan MO, Pittaluga S, et al. B-cell maturation antigen is a promising target for adoptive T-cell therapy of multiple myeloma. Clinical Cancer Res. 2013;19(8):2048-2060.
12. O'Connor BP, Raman VS, Erickson LD, et al. BCMA is essential for the survival of long-lived bone marrow plasma cells. J Exp Med. 2004;199(1):91-98.
13. Mackay F, Tangye SG. The role of the BAFF/APRIL system in B cell homeostasis and lymphoid cancers. Curr Opin Pharmacol. 2004;4(4):347-354.
14. Ng LG, Mackay CR, Mackay F. The BAFF/APRIL system: life beyond B lymphocytes. Mol Immunol. 2005;42(7):763-772.
15. Claudio JO, Masih-Khan E, Tang H, et al. A molecular compendium of genes expressed in multiple myeloma. Blood. 2002;100(6): 2175-2186.
16. Novak AJ, Darce JR, Arendt BK, et al. Expression of BCMA, TACI, and BAFF-R in multiple myeloma: a mechanism for growth and survival. Blood. 2004;103(2): 689-694.
17. Moreaux J, Legouffe E, Jourdan E, et al. BAFF and APRIL protect myeloma cells from apoptosis induced by interleukin 6 deprivation and dexamethasone. Blood. 2004;103(8):3148-3157.
18. Laurent SA, Hoffmann FS, Kuhn PH, et al. gamma-Secretase directly sheds the survival receptor BCMA from plasma cells. Nat Commun. 2015;6:7333.
19. Ghermezi M, Li M, Vardanyan S, et al. Serum B-cell maturation antigen: a novel biomarker to predict outcomes for multiple myeloma patients. Haematologica. 2017; 102(4):785-795.
20. Ali SA, Shi V, Maric I, et al. T cells expressing an anti-B-cell maturation antigen chimeric antigen receptor cause remissions of multiple myeloma. Blood. 2016;128(13): 1688-1700.
21. Mackay F, Schneider P. TACI, an enigmatic BAFF/APRIL receptor, with new unappreciated biochemical and biological properties. Cytokine Growth Factor Rev. 2008;19(3-4):263-276.
22. Lee L, Draper B, Chaplin N, et al. An APRIL-based chimeric antigen receptor for dual targeting of BCMA and TACI in multiple myeloma. Blood. 2018;131(7):746-758.
23. Quinn J, Glassford J, Percy L, et al. APRIL promotes cell-cycle progression in primary multiple myeloma cells: influence of D-type cyclin group and translocation status. Blood. 2011;117(3):890-901.
24. Popat R, Zweegman S, Cavet J, et al. Phase 1 first-in-human study of AUTO2, the first chimeric antigen receptor (CAR) T cell targeting APRIL for patients with relapsed/refractory multiple myeloma (RRMM). Blood. 2019;134(Suppl 1):S3112.
25. Poe JC, Minard-Colin V, Kountikov EI, Haas KM, Tedder TF. A c-Myc and surface CD19 signaling amplification loop promotes B cell lymphoma development and progression in mice. J Immunol. 2012;189 (5):2318-2325.
26. Ali S, Moreau A, Melchiorri D, et al. Blinatumomab for acute lymphoblastic leukemia: the first bispecific T-cell engager antibody to be approved by the EMA for minimal residual disease. Oncologist. 2020;25(4):e709-e715.
27. Loffler A, Kufer P, Lutterbuse R, et al. A recombinant bispecific single-chain antibody, CD19 x CD3, induces rapid and high lymphoma-directed cytotoxicity by unstimulated T lymphocytes. Blood. 2000;95(6):2098-2103.
28. Porter DL, Levine BL, Kalos M, Bagg A, June CH. Chimeric antigen receptor-modified T cells in chronic lymphoid leukemia. N Engl J Med. 2011;365(8):725-733.
29. Schuster SJ, Svoboda J, Chong EA, et al. Chimeric antigen receptor T cells in refractory B-cell lymphomas. N Engl J Med. 2017;377(26):2545-2554.
30. Nerreter T, Letschert S, Götz R, et al. Super-resolution microscopy reveals ultra-low CD19 expression on myeloma cells that triggers elimination by CD19 CAR-T. Nat Commun. 2019;10(1):3137.
31. Boles KS, Stepp SE, Bennett M, Kumar V, Mathew PA. 2B4 (CD244) and CS1: novel members of the CD2 subset of the immunoglobulin superfamily molecules expressed on natural killer cells and other leukocytes. Immunol Rev. 2001;181:234-249.
32. Chen J, Zhong MC, Guo H, et al. SLAMF7 is critical for phagocytosis of haematopoietic tumour cells via Mac-1 integrin. Nature. 2017;544(7651):493-497.
33. Gogishvili T, Danhof S, Prommersberger S, et al. SLAMF7-CAR T cells eliminate myeloma and confer selective fratricide of SLAMF7(+) normal lymphocytes. Blood. 2017;130(26):2838-2847.
34. De Salort J, Sintes J, Llinas L, Matesanz-Isabel J, Engel P. Expression of SLAM (CD150) cell-surface receptors on human B-cell subsets: from pro-B to plasma cells. Immunol Lett. 2011;134(2):129-136.
35. Mahtur R, Zhang Z, He J, et al. Universal SLAMF7-specific CAR T-cells as treatment or multiple myeloma Blood. 2017;130 (Suppl 1):S502.
36. Harada H, Kawano MM, Huang N, et al. Phenotypic difference of normal plasma cells from mature myeloma cells. Blood. 1993;81(10):2658-2663.
37. von Laer D, Corovic A, Vogt B, et al. Loss of CD38 antigen on CD34+CD38+ cells during short-term culture. Leukemia. 2000;14(5):947-948.
38. Drent E, Groen RW, Noort WA, et al. Pre-clinical evaluation of CD38 chimeric antigen receptor engineered T cells for the treatment of multiple myeloma. Haematologica. 2016;101(5):616-625.
39. Nijhof IS, Casneuf T, van Velzen J, et al. CD38 expression and complement inhibitors affect response and resistance to daratumumab therapy in myeloma. Blood. 2016;128(7):959-970.
40. Garcia-Guerrero E, Gotz R, Doose S, et al. Upregulation of CD38 expression on multiple myeloma cells by novel HDAC6 inhibitors is a class effect and augments the efficacy of daratumumab. Leukemia. 2021;35(1):201-214.
41. Ponta H, Sherman L, Herrlich PA. CD44: from adhesion molecules to signalling regulators. Nat Rev Mol Cell Biol. 2003;4(1):33-45.
42. Zoller M. CD44: can a cancer-initiating cell profit from an abundantly expressed molecule? Nat Rev Cancer. 2011;11(4):254-267.
43. Gunthert U, Hofmann M, Rudy W, et al. A new variant of glycoprotein CD44 confers metastatic potential to rat carcinoma cells. Cell. 1991;65(1):13-24.
44. Legras S, Gunthert U, Stauder R, et al. A strong expression of CD44-6v correlates with shorter survival of patients with acute myeloid leukemia. Blood. 1998;91(9):3401-3413.
45. Tijink BM, Buter J, de Bree R, et al. A phase I dose escalation study with anti-CD44v6 bivatuzumab mertansine in patients with incurable squamous cell carcinoma of the head and neck or esophagus. Clin Cancer Res. 2006;12(20 Pt 1):6064-6072.
46. Casucci M, Nicolis di Robilant B, Falcone L, et al. CD44v6-targeted T cells mediate potent antitumor effects against acute myeloid leukemia and multiple myeloma. Blood. 2013;122(20):3461-3472.
47. Radhakrishnan SV, Luetkens T, Scherer SD, et al. CD229 CAR T cells eliminate multiple myeloma and tumor propagating cells without fratricide. Nat Commun. 2020;11 (1):798.
48. Madduri D, Berdeja JG, Usmani SZ, et al. CARTITUDE-1: phase 1b/2 study of ciltacabtagene autoleucel, a B-cell maturation antigen-directed chimeric antigen receptor T cell therapy, in relapsed/refractory multiple myeloma. Blood. 2020;136 (Suppl 1):S22-25.
49. Cohen AD, Garfall AL, Stadtmauer EA, et al. B cell maturation antigen-specific CAR T cells are clinically active in multiple myeloma. J Clin Invest. 2019;129(6):2210-2221.
50. Munshi N, Anderson LD, Jr., Shah N, et al. Idecabtagene vicleucel (ide-cel; bb2121), a BCMA-targeted CAR T-cell therapy, in patients with relapsed and refractory multiple myeloma (RRMM): initial KarMMa results. J Clin Oncol. 2020;38(Suppl):S8503.
51. Yi Lin, Raje NS, Berdeja JG, et al. Idecabtagene vicleucel (ide-cel, bb2121), a BCMA-directed CAR T cell therapy, in patients with relapsed and refractory multiple myeloma: updated results from phase 1 CRB-401 study. Blood. 2020;136(Suppl 1):S26-27.
52. Zudaire E, Madduri D, Usmani S, et al. Translational analysis from CARTITUDE-1, an ongoing phase 1b/2 study of JNJ-4528 BCMA-targeted CAR-T cell therapy in relapsed and/or refractory multiple myeloma (R/R MM), indicates preferential expansion of CD8+ T cell central memory cell subset. Blood. 2019;134(Suppl 1):S928.
53. Wang B, Zhao W, Liu J, et al. Long-term follow-up of a phase 1, first-in-human open-label study of LCAR-B38M, a structurally differentiated chimeric antigen receptor T (CAR-T) cell therapy targeting B-cell maturation antigen (BCMA), in patients (pts) with relapsed/refractory multiple myeloma (RRMM). Blood. 2019;134(Suppl 1):S579.
54. Cowan A, Pont M, Sather B, et al. Efficacy and safety of fully human Bcma CAR T cells in combination with a gamma secretase inhibitor to increase Bcma surface expression in patients with relapsed or refractory multiple myeloma. Blood. 2019;134(Suppl 1):S204.
55. Li C, Wang J, Wang D, et al. Efficacy and safety of fully human BCMA targeting CAR T-cell therapy in relapsed/refractory MM. Blood. 2019;134(Suppl 1):S929.
56. Mailankody S, Jakubowiak A, Htut M, et al. Orvacabtagene autoleucel (orva-cel), a B-cell maturation antigen (BCMA)-directed CAR T cell therapy for patients (pts) with relapsed/refractory multiple myeloma

(RRMM): update of the phase 1/2 EVOLVE study (NCT03430011). J Clin Oncol. 2020;38(15_suppl):8504.
57. Alsina M, Shah N, Raje NS, et al. Updated results from the phase I CRB-402 study of anti-Bcma CAR-T cell therapy bb21217 in patients with relapsed and refractory multiple myeloma: correlation of expansion and duration of response with T cell phenotypes. Blood. 2020;136 (Suppl 1):S25-26.
58. Kuramitsu S, Ohno M, Ohka F, et al. Lenalidomide enhances the function of chimeric antigen receptor T cells against the epidermal growth factor receptor variant III by enhancing immune synapses. Cancer Gene Ther. 2015;22(10):487-495.
59. Wang X, Walter M, Urak R, et al. Lenalidomide enhances the function of CS1 chimeric antigen receptor-redirected T cells against multiple myeloma. Clin Cancer Res. 2018;24(1):106-119.
60. Works M, Soni N, Hauskins C, et al. Anti-B-cell maturation antigen chimeric antigen receptor T cell function against multiple myeloma is enhanced in the presence of lenalidomide. Mol Cancer Ther. 2019;18(12):2246-2257.
61. Pont MJ, Hill T, Cole GO, et al. γ-Secretase inhibition increases efficacy of BCMA-specific chimeric antigen receptor T cells in multiple myeloma. Blood. 2019;134(19): 1585-1597.
62. Garfall AL, Maus MV, Hwang WT, et al. Chimeric antigen receptor T cells against CD19 for multiple myeloma. N Engl J Med. 2015;373(11):1040-1047.
63. Yan Z, Cao J, Cheng H, et al. A combination of humanised anti-CD19 and anti-BCMA CAR T cells in patients with relapsed or refractory multiple myeloma: a single-arm, phase 2 trial. Lancet Haematol. 2019;6(10):e521-e529
64. Lee DW, Santomasso BD, Locke FL, et al. ASTCT consensus grading for cytokine release syndrome and neurologic toxicity associated with immune effector cells. Biol Blood Marrow Transplant. 2019;25(4):625-638.
65. Ragoonanan D, Khazal SJ, Abdel-Azim H, et al. Diagnosis, grading and management of toxicities from immunotherapies in children, adolescents and young adults with cancer. Nat Rev Clin Oncol. 2021;18(7): 435-453.
66. Pennisi M, Jain T, Santomasso BD, et al. Comparing CAR T-cell toxicity grading systems: application of the ASTCT grading system and implications for management. Blood Adv. 2020;4(4):676-686.
67. Wäsch R, Munder M, Marks R. Teaming up for CAR-T cell therapy. Haematologica. 2019;104(12):2335-2336.
68. Gagelmann N, Riecken K, Wolschke C, et al. Development of CAR-T cell therapies for multiple myeloma. Leukemia. 2020;34 (9):2317-2332.
69. Mikkilineni L, Kochenderfer JN. Chimeric antigen receptor T-cell therapies for multiple myeloma. Blood. 2017;130(24):2594-2602.
70. García-Guerrero E, Sierro-Martínez B, Pérez-Simón JA. Overcoming chimeric antigen receptor (CAR) modified T-cell therapy limitations in multiple myeloma. Front Immunol. 2020;11:1128.
71. Rafiq S, Hackett CS, Brentjens RJ. Engineering strategies to overcome the current roadblocks in CAR T cell therapy. Nat Rev Clin Oncol. 2020;17(3):147-167.
72. Tan AHJ, Vinanica N, Campana D. Chimeric antigen receptor-T cells with cytokine neutralizing capacity. Blood Adv. 2020;4(7):1419-1431.
73. Gargett T, Brown MP.The inducible caspase-9 suicide gene system as a "safety switch" to limit on-target, off-tumor toxicities of chimeric antigen receptor T cells. Front Pharmacol. 2014;5:235.
74. Smith EL, Harrington K, Staehr M, et al. GPRC5D is a target for the immunotherapy of multiple myeloma with rationally designed CAR T cells. Sci Transl Med. 2019;11(485):eaau7746.
75. Holliger P, Hudson PJ. Engineered antibody fragments and the rise of single domains. Nat Biotechnol. 2005;23(9):1126-1136.
76. Lam N, Trinklein ND, Buelow B, Patterson GH, Ojha N, Kochenderfer JN. Anti-BCMA chimeric antigen receptors with fully human heavy-chain-only antigen recognition domains. Nat Commun. 2020;11(1): 283.
77. Kumar M, Keller B, Makalou N, Sutton RE. Systematic determination of the packaging limit of lentiviral vectors. Hum Gene Ther. 2001;12(15):1893-1905.
78. De Munter S, Ingels J, Goetgeluk G, et al. Nanobody based dual specific CARs. Int J Mol Sci. 2018;19(2):403.
79. Martyniszyn A, Krahl AC, Andre MC, Hombach AA, Abken H. CD20-CD19 bispecific CAR T cells for the treatment of B-cell malignancies. Hum Gene Ther. 2017;28(12):1147-1157.
80. Majzner RG, Mackall CL. Tumor antigen escape from CAR T-cell therapy. Cancer Discov. 2018;8(10):1219-1226.
81. Hamieh M, Dobrin A, Cabriolu A, et al. CAR T cell trogocytosis and cooperative killing regulate tumour antigen escape. Nature. 2019;568(7750):112-116.
82. Hegde M, Mukherjee M, Grada Z, et al. Tandem CAR T cells targeting HER2 and IL13Ralpha2 mitigate tumor antigen escape. J Clin Invest. 2016;126(8):3036-3052.
83. Garfall AL, Cohen AD, Lacey SF, et al. Combination anti-Bcma and anti-CD19 CAR T cells as consolidation of response to prior therapy in multiple myeloma. Blood. 2019;134(supplement 1):1863.
84. Shi X, Yan L, Shang J, et al. Tandom autologous transplantation and combined infusion of CD19 and Bcma-specific chimeric antigen receptor T cells for high risk MM: initial safety and efficacy report from a clinical pilot study. Blood. 2018;132(Suppl 1):S1009.
85. Li C, Mei H, Hu Y, Guo T, Liu L, Jiang H. A bispecific CAR-T cell therapy targeting Bcma and CD38 for relapsed/refractory multiple myeloma: updated results from a phase 1 dose-climbing trial. Blood. 2019;134(supplement 1):930.
86. Zah E, Lin MY, Silva-Benedict A, Jensen MC, Chen YY. T cells expressing CD19/CD20 bispecific chimeric antigen receptors prevent antigen escape by malignant B cells. Cancer Immunol Res. 2016;4 (6):498-508.
87. Jiang H, Dong B, Gao L, et al. Clinical results of a multicenter study of the first-in-human dual BCMA and CD19 targeted novel platform fast CAR-T cell therapy for patients with relapsed/refractory multiple myeloma. Blood. 2020;136(Suppl 1):S25-26.
88. Chari A, Suvannasankha A, Fay JW, et al. Daratumumab plus pomalidomide and dexamethasone in relapsed and/or refractory multiple myeloma. Blood. 2017;130 (8):974-981.
89. Wang X, Walter M, Urak R, et al. Lenalidomide enhances the function of CS1 chimeric antigen receptor-redirected T cells against multiple myeloma. Clin Cancer Res 2018;24(1):106–119.
90. Amor C, Feucht J, Leibold J, et al. Senolytic CAR T cells reverse senescence-associated pathologies. Nature. 2020;583(7814):127-132.
91. Ciavarella S, Laurenzana A, De Summa S, et al. u-PAR expression in cancer associated fibroblast: new acquisitions in multiple myeloma progression. BMC Cancer. 2017; 17(1):215.
92. Wagner V, Gil J. T cells engineered to target senescence. Nature. 2020;583(7814):37-38.
93. Depil S, Duchateau P, Grupp SA, Mufti G, Poirot L. 'Off-the-shelf' allogeneic CAR T cells: development and challenges. Nat Rev Drug Discov. 2020;19(3):185-199.
94. Cong L, Ran FA, Cox D, et al. Multiplex genome engineering using CRISPR/Cas systems. Science. 2013;339(6121):819-823.
95. Sommer C, Boldajipour B, Kuo TC, et al. Preclinical evaluation of allogeneic CAR T cells targeting BCMA for the treatment of multiple myeloma. Mol Ther. 2019;27(6): 1126-1138.
96. Zhou X, Dotti G, Krance RA, et al. Inducible caspase-9 suicide gene controls adverse effects from alloreplete T cells after haploidentical stem cell transplantation. Blood. 2015;125(26):4103-4113.
97. Yakoub-Agha I, Chabannon C, Bader P, et al. Management of adults and children undergoing chimeric antigen receptor T-cell therapy: best practice recommendations of the European Society for Blood and Marrow Transplantation (EBMT) and the Joint Accreditation Committee of ISCT and EBMT (JACIE). Haematologica. 2020;105 (2):297-316.
98. Hill JA, Li D, Hay KA, et al. Infectious complications of CD19-targeted chimeric antigen receptor-modified T-cell immunotherapy. Blood. 2018;131(1):121-130.
99. Ljungman P, Mikulska M, de la Camara R, et al. The challenge of COVID-19 and hematopoietic cell transplantation; EBMT recommendations for management of hematopoietic cell transplant recipients, their donors, and patients undergoing CAR T-cell therapy. Bone Marrow Transplant. 2020;55(11):2071-2076
100. Cher BP, Gan KY, Aziz MIA, et al. Cost utility analysis of tisagenlecleucel vs salvage chemotherapy in the treatment of relapsed/refractory diffuse large B-cell lymphoma from Singapore's healthcare system perspective. J Med Econ. 2020;23(11):1321-1329.

Ferrata Storti Foundation

Haematologica 2021
Volume 106(8):2066-2075

DUX4r, *ZNF384r* and *PAX5*-P80R mutated B-cell precursor acute lymphoblastic leukemia frequently undergo monocytic switch

Michaela Novakova,[1,2,3*] Marketa Zaliova,[1,2,3*] Karel Fiser,[1,2*] Barbora Vakrmanova,[1,2] Lucie Slamova,[1,2,3] Alena Musilova,[1,2] Monika Brüggemann,[4] Matthias Ritgen,[4] Eva Fronkova,[1,2,3] Tomas Kalina,[1,2,3] Jan Stary,[2,3] Lucie Winkowska,[1,2] Peter Svec,[5] Alexandra Kolenova,[5] Jan Stuchly,[1,2] Jan Zuna,[1,2,3] Jan Trka,[1,2,3] Ondrej Hrusak[1,2,3#] and Ester Mejstrikova[1,2,3#]

[1]CLIP - Childhood Leukemia Investigation Prague, Czech Republic; [2]Department of Paediatric Hematology and Oncology, Second Faculty of Medicine, Charles University, Prague, Czech Republic; [3]University Hospital Motol, Prague, Czech Republic; [4]Department of Internal Medicine II, University Hospital Schleswig-Holstein, Kiel, Germany and [5]Comenius University, National Institute of Children's Diseases, Bratislava, Slovakia

*MN, MZ and KF contributed equally as co-first authors.

#OH and EM contributed equally as co-senior authors.

ABSTRACT

Recently, we described B-cell precursor acute lymphoblastic leukemia (BCP-ALL) subtype with an early switch to the monocytic lineage and the loss of the B-cell immunophenotype, including CD19 expression. Thus far, the genetic background has remained unknown. Among 726 children consecutively diagnosed with BCP-ALL, 8% patients experienced a switch detectable by flow cytometry (FC). Using exome and RNA sequencing, the switch was found to positively correlate with three different genetic subtypes: *PAX5*-P80R mutation (five cases with switch of five), rearranged (*DUX4r*) (30 cases of 41) and rearranged (*ZNF384r*) (four cases of ten). Expression profiles or phenotypic patterns correlated with genotypes, but within each genotype no cases who subsequently switched could be indentified. If switching was not taken into account, the B-cell-oriented FC assessment underestimated the minimal residual disease level. For patients with *PAX5*-P80R, a discordance between FC-determined and polymerase chain reaction-determined minimal residual disease was found on day 15, resulting from a rapid loss of the B-cell phenotype. Discordance on day 33 was observed in all the *DUX4r*, *PAX5*-P80R and *ZNF384r* subtypes. Importantly, despite the substantial phenotypic changes, possibly even challenging the appropriateness of BCP-ALL therapy, the monocytic switch was not associated with a higher incidence of relapse and poorer prognosis in patients undergoing standard ALL treatment.

Correspondence:

ESTER MEJSTRIKOVA
ester.mejstrikova@lfmotol.cuni.cz

Received: February 18, 2020.

Accepted: June 25, 2020.

Pre-published: July 9, 2020.

https://doi.org/10.3324/haematol.2020.250423

Introduction

We recently described a pediatric B-cell precursor acute lymphoblastic leukemia (BCP-ALL) subtype with an early switch towards the monocytic lineage.[1] Such a monocytic switch leads to a variable degree of monocytosis in the early phase of treatment. The switched monocytic cells ("monocytoids") have significantly diminished expression of immature or lymphoid markers (*i.e.*, CD19 and CD34) and upregulated myeloid markers (*i.e.*, CD33 and CD14) while keeping shared immunoglobulin/T-cell receptor (IG/TR) rearrangements with malignant B lymphoblasts. The increase in monocytoid cells was most prominent at days 8 and 15 after the start of therapy, although the proportion differed between the patients. We reported frequent expression of CD2 and a higher prevalence of *ERG* deletions and *IKZF1* gene alterations in this leukemia subtype than in other subtypes.[1] However, at that time, we

were unable to uncover the genetic background. In our previous work, we observed a slower response to initial treatment in patients with a monocytic switch than in patients without it. Despite significant changes in the phenotype towards the monocytic lineage in some of the patients, risk-based ALL treatment remained the treatment of choice.[1]

Recently, new genetic subtypes of ALL, particularly within the "B-other" group, were discovered using RNA sequencing (RNA-seq).[2,3] We investigated whether any of the newly defined subsets had a higher tendency to undergo monocytic switch.

Monocytic switch is accompanied by the gradual loss of CD19. As the determination of minimal residual disease (MRD) by flow cytometry (FC) relies on B-cell markers, switching leads to MRD underestimation. The FC MRD value on day 15 is used for patient stratification in the current pediatric Berlin-Frankfurt-Münster (BFM) BCP-ALL treatment protocols. It is an open question whether FC monitoring of MRD should be adapted for patients with switch.

Recently, anti-CD19 therapy, namely, blinatumomab, was added to pediatric ALL frontline treatment protocols, and a larger proportion of patients will be treated with it in the near future. As patients with switch that includes CD19 loss may be selected for anti-CD19 treatment, knowledge about subtypes prone to switch will be of interest. Moreover, anti-CD19 therapy may result in monocytic switch, as was repeatedly reported, especially for cases of *KMT2A* rearrangement.[4-9]

The aim of this study is to describe the molecular landscape of ALL with monocytic switch in the context of newly discovered genetic subtypes. We aim to describe the switching behavior in distinct genetic subtypes and to analyze the extent of its influence on the FC assessment of MRD. In addition, we analyzed the impact of switching phenomenon on relapse risk.

Methods

This study was approved by the Institutional Review board of the University Hospital Motol and the Second Faculty of Medicine and informed consent was obtained from all patients and their guardians in accordance with the Declaration of Helsinki.

We included 726 BCP-ALL patients (age, 0-18 years) diagnosed in the Czech Republic between 09/2007 and 02/2019. Patients were treated according to the following BFM protocols: ALL-IC-BFM-2002 (n=17); ALL BFM 2000 (n=177); ALL BFM 2009 (n=483); the Interfant 2006 protocol (for children younger than 12 months; n=30); the EsPhALL protocol (for *BCR-ABL1*-positive patients; n=16); and other protocols (n=3; one patient was treated by a modified protocol, one Down syndrome patient with significant comorbidities was treated with a reduced ALL BFM 2009 protocol, and one patient moved abroad after induction therapy). Some of the 726 patients (179 of 726) diagnosed between 09/2007 and 05/2010 were included in a previous study.[1] For selected analyses, we expanded this consecutive cohort with additional 19 patients who were diagnosed before 09/2007 and for whom the switching phenomenon was identified and described retrospectively (n=16)[1] or who were diagnosed abroad (Germany, n=2; and Slovakia, n=1) (*Online Supplementary Figure S1*). All patients were screened for the presence of recurrent fusion genes (*BCR-ABL1*, *KMT2A-AFF1*, *ETV6-RUNX1* and *TCF3-PBX1*). In all patients, standard cytogenetic evaluation and assessment of the DNA index were performed as published previously.[1,10] The B-other subset was defined as BCP-ALL by the absence of all routinely investigated classifying aberrations (*ETV6-RUNX1*, hyperdiploidy, hypodiploidy, *BCR-ABL1*, *KMT2A* rearrangements and *TCF3-PBX1*).

Flow cytometry

The diagnostic phenotype was determined through standard protocols.[11–13] Ambiguous lineage acute leukemia (ALAL) diagnosis was based on the European Group for the Immunological Characterization of Leukemias (EGIL) criteria[11,12,14,15] and/or the World Health Organization[16] classification. A summary of the antibody clones and vendors is presented in the *Online Supplementary Table S1*. In addition, the percentage of the B-monocytoid population defined as $CD19^{pos}CD14^{pos}$ was determined with an eight-color combination of antibodies against CD45, CD14, CD34, CD19, CD33, CD20, CD10 and CD3 at diagnosis (day zero [d0]), day 8 [d+8], day 15 [d+15], and day 33 [d+33] in the bone marrow (BM) and/or peripheral blood (PB) as shown previously.[1] FC-assessed MRD was evaluated using three- or four-color monoclonal antibody combinations in the period between 1998 and 2007[17] and using eight-color combinations starting in 2007.[18,19] The sensitivity (level of quantification and level of detection, LoQ and LoD, respectively) of the FC-assessed MRD was defined by the number of nucleated cells measured in an MRD-specific tube (for a sensitivity of 10^{-3} and 10^{-4}, 20,000 and 200,000 nucleated cells were measured, respectively). Only samples with an appropriate FC MRD sensitivity were included in the analysis: generally, a sensitivity of 10^{-4} was required; for cases with polymerase chain reaction (PCR)-determined MRD $\geq 10^{-2}$, measures of sensitivity that were at least one log value lower than that of the actual PCR-determined MRD value were sufficient. The sample was assessed as FC MRD positive when a cluster of at least 20 events with an aberrant B-cell phenotype was detected.

Definition of the switching phenomenon

Based on our previous work,[1] we defined the switching phenomenon as the presence of an intermediate B-monocytoid population, *i.e.*, BCP-ALL blasts with a gradual decrease in CD19 expression accompanied by a gradual increase in the expression of at least one monocytic marker (CD14, CD33, or higher side scatter, SSC) (*Online Supplementary Figure S2*) at any time point between d0 and d+33. We used fluorescence-activated cell sorting (FACS) of the intermediate B-monocytoid ($CD19^{pos}CD14^{pos}$) and monocytoid ($CD19^{neg}CD14^{pos}$) populations to show that the IG/TR rearrangements were identical to those in B lymphoblasts when enough material was available (patients n =37; samples n=70) between d0 and d+33.

Immunoglobulin/T-cell receptor polymerase chain reaction-assessed minimal residual disease

Patient-specific IG/TR assays were developed as described previously.[1,20,21] In patients with two independent IG/TR targets, the higher value was reported. Sensitivity (LoD) and quantitative range (LoQ) for each assay was defined according to the European Study Group on MRD guidelines.[22] A minimum LoD of 10^{-4} was achieved in all patients/timepoints.

Statistics

Fisher's exact test was used for comparing categorical variables, and the Mann-Whitney test was used for continuous variables. Other tests used are explicitly indicated in the text. The results were considered significant when *P*-values were less than 0.05. Statistical analyses were performed using GraphPad software (GraphPad Software, Inc., La Jolla, CA, USA), R[23] and StatView version 5.0 (StatView Software, Cary, NC, USA).

Data analysis of genetic and immunophenotypic data

RNA-seq data (patients with switch, n=73; patients without switch, n=124), whole-exome sequencing (WES) data (patients with switch, n=30; patients without switch, n=70), single-nucleotide polymorphism (SNP) data (patients with switch, n=59; patients without switch, n=108) and ERG deletion data were analyzed in diagnostic samples as published previously.[24–26] Diagnostic samples were sorted if blasts comprised fewer than 80% of mononuclear cells. Purity of sorted populations was at least 90%. Patients in the B-other group without the following aberrations were assigned to the B-other rest subgroup: *DUX4*, *ZNF384*, *MEF2D* and *NUTM1* rearrangements; *BCR-ABL1*-like and *ETV6-RUNX1*-like expression profiles; and iAMP21, *PAX5*-P80R and *IKZF1*-N159Y mutations.

In order to analyze RNA-seq and immunophenotypic data, uniform manifold approximation and projection (UMAP)[27] was used as the dimensionality reduction algorithm. Hierarchical clustering analysis (HCA) was performed using Euclidean distance and Ward's linkage.

Results

Incidence and features of patients with monocytic switch

Prospectively, we identified 61 patients with monocytic switch using the criteria described above (Table 1), which corresponded to 8% of patients.

No sex difference occurred in the monocytic switch (69% females *vs*. 56% males, not significant [n.s.]) but the monocytic switch was associated with older age at diagnosis (median 7.8 *vs*. 4.5 years, respectively, *P*<0.001) and a higher initial white blood cell (WBC) count (median 10,750/μL *vs*. 6,670/μL, *P*=0.038), lower hemoglobin level (median 7.8 g/dL *vs*. 8.8 g/dL, *P*=0.0046), higher platelet count (median 74,000/μL vs. 58,000/μL, *P*=0.048) and a higher proportion of blasts in PB (59% *vs*. 32%, *P*=0.0039), while the proportion in BM did not differ (91.2% *vs*. 90%, n.s.).

We confirmed the presence of patient-specific IG/TR rearrangements in the sorted monocytoid cells in 33 of 37 patients in whom the sorting was successful at various time points between d0 and d+33 (16 of 19 positive at d0; 23 of 27 positive between d+1 and d+14; 14 of 15 positive at d+15; eight of nine positive between d+16 and d+33). In the morphological examination of some patients, an increase in monocytic cells with variable morphology (monoblasts, promonocytes, and mature monocytes) was very clear. In three patients, at d+8 (DUX4r, n=2; and ZNF384r, n=1), we observed over 10,000 monocytes/μL in the PB samples (*Online Supplementary Figure S3A* and *B*).

Monocytic switch is most frequent in the *PAX5*-P80R, *DUX4r*, and *ZNF384r* genetic subtypes

In order to study the relationship between monocytic switch and genetic background, routine (cyto)genetic investigations were supplemented with a retrospective analysis using RNA-seq data, enabling a more detailed genomic characterization of the ALL patients. Patients with monocytic switch were unequally distributed across the ALL subtypes in the unselected consecutive cohort (chi square test *P*<0.0001; Table 1); they were significantly enriched in the *PAX5*-P80R-, *DUX4r*- and *ZNF384r*- -positive ALL subtypes

Table 1. Distribution of cases with monocytic switch in an unselected cohort of B-cell precursor acute lymphoblastic leukemia patients (n=726) stratified into genetic/biological subtypes.

BCP-ALL subtypes		Monocytic switch		*P*
		No n (%)	Yes n (%)	
HHD[1]		266 (97)	8 (3)	*P*<0.0001
ETV6-RUNX1		180 (99)	1 (1)	*P*<0.0001
KMT2Ar		29 (88)	4 (12)	ns
TCF3-PBX1		27 (100)	0 (0)	ns
BCR-ABL1		13 (76)	4 (24)	ns
Hypodiploidy[2]		8 (89)	1 (11)	ns
B-other[3]	B-other rest[4]	49 (94)	3 (6)	ns
	DUX4r	11 (27)	30 (73)	*P*<0.0001
	BCR-ABL1-like	18 (95)	1 (5)	ns
	ZNF384r	6 (60)	4 (40)	*P*=0.0022
	ETV6-RUNX1-like	10 (100)	0 (0)	ns
	iAMP21	6 (100)	0 (0)	ns
	PAX5-P80R	0 (0)	5 (100)	*P*<0.0001
	NUTM1r	4 (100)	0 (0)	ns
	MEF2Dr	3 (100)	0 (0)	ns
	IKZF1-N159Y	1 (100)	0 (0)	ns
	Unknown[5]	34 (100)	0 (0)	ns
Total		665 (92)	61 (8)	

[1]High hyperdiploidy with >50 chromosomes; [2]<44 chromosomes; [3]BCP-ALL negative for high hyperdiploid cases (*HHD*), *ETV6-RUNX1*, *KMT2Ar*, *TCF3-PBX1*, *BCR-ABL1* and hypodiploidy; [4]B-other analyzed by RNA sequencing (RNA-seq) and not belonging to any of the established subtypes; [5]B-other not analyzed by RNA-seq (this subset is biased towards nonswitching cases because RNA-seq was performed in samples from all patients with monocytic switch, without identified genetic aberrations using polymerase chain reaction [PCR] and/or cytogenetics); [6]*P*-value of the Fisher's exact test on a comparison of the frequency of cases with monocytic switch in individual subsets vs. the frequency of switch among all the remaining cases. Multiple testing correction was done using Benjamini-Hochberg procedure. ns: no statistically significant difference; BCP-ALL: B-cell precursor acute lymphoblastic leukemia.

but were significantly less frequent among high-hyperdiploid subtypes and extremely rare in *ETV6*-RUNX1-positive ALL. In addition to 61 patients with monocytic switch in the consecutive cohort, we identified another 19 patients with monocytic switch who belonged to the *DUX4r* (n=15), *PAX5*-P80R (n=2), *ZNF384r* (n=1) and high-hyperdiploid (n=1) ALL subtypes. Nevertheless, except for the *DUX4r* ALL subtype (representing the subgroup with the highest prevalence of switch, with nearly half of all patients having monocytic switch [30 of 61]), the number of patients was too low (and/or the genomic data were too limited) to study the impact of the broader genomic context on monocytic switch occurrence within the individual subtypes. In the *DUX4r* ALL subtype group, we did not find any association between monocytic switch and the most frequent secondary genetic aberrations (deletions of *ERG*, *CDKN2A/B*, *IKZF1* or *PAX5* or mutations in the *NRAS* or *KMT2D* genes; *Online Supplementary Table S2*).

The pattern of monocytic switch correlated with the genotype (Figure 1). Patients with the *DUX4r* ALL subtype presented with predominant CD19 positive ($CD19^{pos}$) B-precursor blasts at diagnosis and typically maintained these cells, while the phenotype gradually became more monocytic on d+8 and d+15. Among the 25 patients with switching phenomenon identified already at diagnosis, only two patients were of the *DUX4r* subtype (Fisher's exact test P=0.0002). Patients with the *PAX5*-P80R mutation also presented with $CD19^{pos}$ B precursor blasts, but after d+8, the B-cell markers had typically disappeared concomitantly during the switch. Patients with the *ZNF384* fusion often co-expressed B-precursor and monocytic markers at diagnosis or presented with bilineal disease with separate monocytoid population of blasts, and the monocytoid population often became more prominent during chemotherapy.

The amplitude of monocytic switch (determined as the maximum number of intermediate B-monocytoid cells) did not differ among the different genetic subtypes (*Online Supplementary Figure S3C*, Kruskal-Wallis test, n.s.).

Differences in the diagnostic gene expression signature associated with a subsequent monocytic switch are driven by genotype

We used RNA-seq to assess changes in gene expression that were related to monocytic switch at the time of diagnosis. We analyzed 197 diagnostic transcriptomes and determined the genes that were differentially expressed among patients with (n=73) and without monocytic switch (n=124). Among the 50 top-ranking genes (only protein-encoding genes with absolute fold changes ≥2.5 were considered; *Online Supplementary Table S3*), we found the pro-

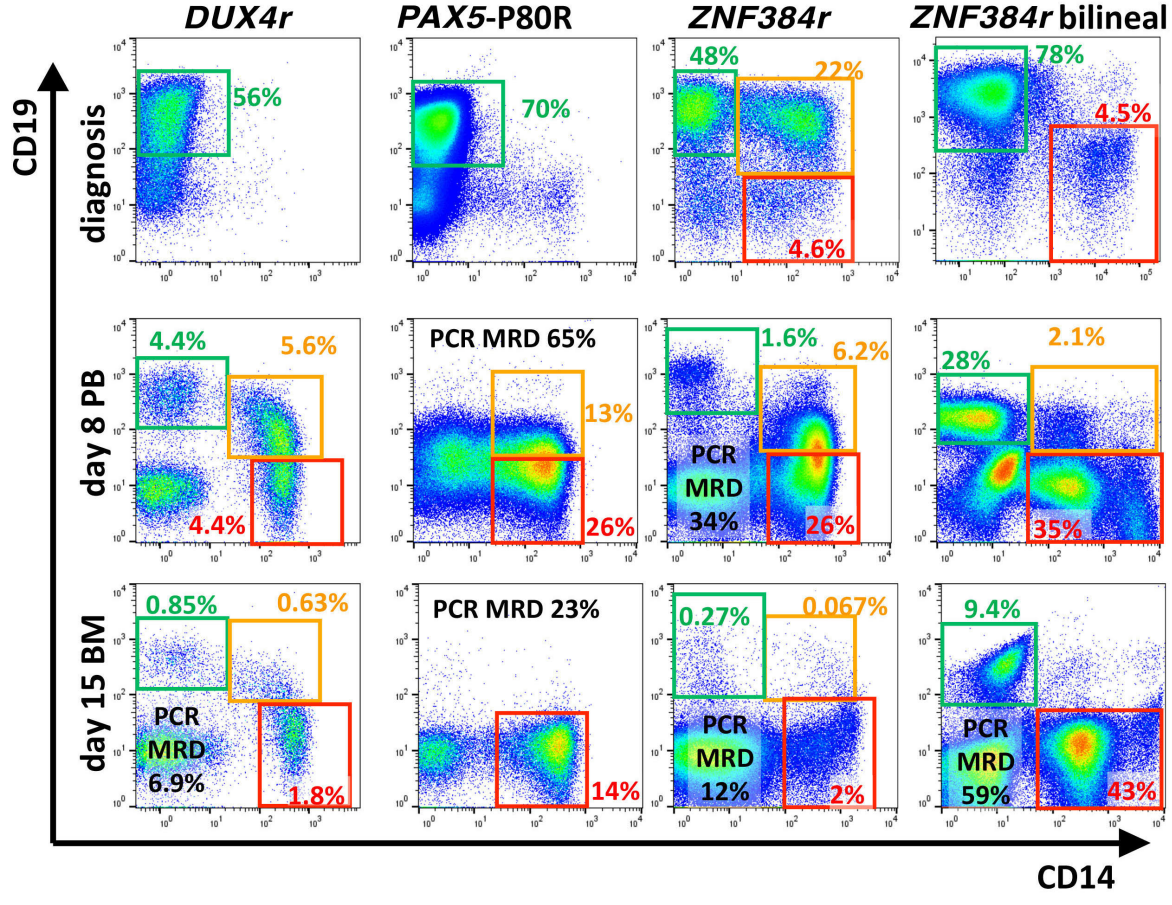

Figure 1. Monocytic switch appearance. In cytometric plots, mononuclear cells after exclusion of doublets and nonmalignant T cells and B cells (if available) are shown. Green, orange and red rectangles highlight the preswitched B-precursor blasts, B-monocytoid intermediate cells and fully switched monocytoids, respectively. Examples of patients with the respective genotypes are shown at day zero (d0) (bone marrow [BM]), d+8 (peripheral blood [PB]) and d+15 (BM). The percentage of each population is shown (of all nuclear cells) in the corresponding color. Polymerase chain reaction (PCR)-determined minimal residual disease (MRD) values in percentages are shown in black. We observed *DUX4r* monocytic switch pattern in 43 of 45 patients, *PAX5*-P80R pattern in seven of seven patients and *ZNF384r* pattern in three of five patients within the respective genotypes in all patients analyzed (n=745).

liferation-activating gene *CRLF2* (lower in patients with monocytic switch than in those without monocytic switch), the cell cycle regulator *CCNA1* (cyclin A1, higher in patients with monocytic switch) and androgen receptor (AR, higher in patients with monocytic switch), as well as six genes with a CD marker designation: *CD371*, *CD301*, *CD1E*, *CD125* (all higher in patients with monocytic switch), *CD158K* and *CD20* (both lower in patients with monocytic switch). Consistent with our previously published data, patients with switch had increased *CEBPA* expression ($P<0.0001$), which was also the case when only *DUX4r* patients were analyzed ($P<0.0001$).

We asked whether these changes were primarily driven by monocytic switch itself or by the underlying genotype. Both the unsupervised hierarchical clustering and the UMAP analyses showed that the patients primarily clustered according to genotype, including the *DUX4r*, *PAX5*-P80R and *ZNF384r* subtypes, which were enriched for monocytic switch, and whether the patients eventually experienced monocytic switch seemed to be secondary (Figure 2A; *Online Supplementary Figure S4*).

As genotype-associated transcriptome differences may override monocytic switch-associated differences, we repeated the analysis in the most prevalent (accounting for >60% of the patients with switch) genotypic subset (*DUX4r*). The *Online Supplementary Figure S5* shows that the clustering of the switching patients was not clear. Among the top-ranking most differentially expressed genes between switching (n=44) and nonswitching (n=11) patients were the previously described *CEBPA*,[1] hematopoietic regulator *FLT3* and Toll-like receptor *TLR10*, which were all higher in patients with the *DUX4r* subtype with switch than in patients with *DUX4r* without switch (*Online Supplementary Table S4*).

Genotype also influences immunophenotype associated with subsequent monocytic switch

We next sought to determine whether the diagnostic immunophenotype predicts, similarly to transcriptome, monocytic switch behavior and whether it can be associated with underlying genetic aberrations.

For these purposes we analyzed the diagnostic immunophenotype of the blast population in 745 patients.

The overall picture appeared to be analogous to that of the transcriptome data: diagnostic immunophenotypes were grouped based on the genetic subtype as seen in the UMAP analysis rather than by the monocytic switch status (Figure 2B).

In our previous study all patients with monocytic switch harbored CD2 expression, although belonging to different genetic subtypes. As we have shown recently,[28] CD2 is expressed in approximately 75% of *DUX4r* patients whereas a newly described marker CD371 (CLL-1) is found in all patients with *DUX4r* (*Online Supplementary Figure S8*).

We also observed the expression of CD2 and CD371 in five of seven and two of five patients with *PAX5*-P80R, respectively. Interestingly, all seven patients with *PAX5*-P80R had homogeneous expression of CD66c. Expression of CD4, a rare aberrant marker in BCP-ALL, was present in four of seven *PAX5*-P80R patients, all of which had cells with a phenotype of $CD34^{neg}33^{pos}$ (in contrast to the other three of seven $CD4^{neg}CD34^{pos}$ patients). Interestingly, CD66c expression was retained on switched monocytoid cells on d+15 in all six patients with available data.

Patients with the *ZNF384r* subtype were often classified as having acute leukemia of ambiguous lineage (ALAL) using the EGIL classification (six of 11 patients).

The typical immunophenotypes of the main three subtypes with switch (*DUX4r*: $CD10^{pos}CD20^{neg}CD34^{pos}CD2^{pos}CD371^{pos}$; *PAX5*-P80R: $CD10^{neg/pos}CD66c^{>75\%}CD2^{<50\%}CD4^{neg}CD34^{pos}CD33^{<50\%}$ or $CD10^{neg/pos}CD66c^{>75\%}CD2^{pos}CD4^{pos}CD34^{neg}CD33^{pos}$; ZNF384r: $CD10^{<50\%}CD13^{pos}CD66c^{neg}CD34^{pos}CD135^{pos}CD24^{<60\%}$), are shown in the *Online Supplementary Figure S8*.

Discordance between flow cytometry- and polymerase chain reaction-determined minimal residual disease reflects different switching dynamics in individual genetic subtypes

Loss of B-cell markers during monocytic switch interferes with B-cell-oriented MRD analysis by FC. As we showed previously in our pilot study[1] and now in a significant cohort of patients, switched monocytoid blasts maintain leukemic IG/TR rearrangements despite completely losing the B-cell phenotype. We thus analyzed the influence of switch on MRD detection by comparing FC and PCR MRD quantitation results in the genotype subsets most prone to switch.

We had only limited data for d+8 PB samples from *PAX5*-P80R (n=3) and *ZNF384r* patients (n=2). Spearman R for *DUX4r* (n=31) and patients with monocytic switch outside these three genetic subtypes (n=11) was 0.7 and 0.72, respectively (*Online Supplementary Figures S6* and *S7*).

But, as shown in Figure 3, FC underestimation of MRD led to pronounced discordance at d+15 in the *PAX5*-P80R patients. The concordance of the FC and PCR MRD positivity/negativity at the 10^{-3} level was 91% for the *DUX4r* subtype and 82% for the *ZNF384r* subtype but only 17% for the *PAX5*-P80R subtype. Concordance at the 10^{-1} level, which was determined at this time point as the FC cut-off value for stratifying patients for undergoing high-risk treatment according to the BFM protocols, was 78% for the *DUX4r* subtype and 78% for the *ZNF384r* subtype but only 43% for the *PAX5*-P80R subtype.

At d+33, all three subtype groups showed poor correlation between the FC and PCR MRD values (Figure 3) compared to previously published data.[18,29] The concordance of the FC- and PCR-determined MRD at the level of 10^{-3} was 55% for the *DUX4r* subtype, 56% for the *ZNF384r* subtype and 33% for the *PAX5*-P80R subtype.

Monocytic switch rarely caused MRD discrepancies in the other genetic subtypes. When analyzed separately, among 23 patients in the $DUX4r^{neg}$*PAX5*-P80R^{neg}*ZNF384r*^{neg} subset and in which monocytic switch was observed, FC MRD at the appropriate level of sensitivity (defined in the Methods) was measured in 21 and 16 patients on d+15 and d+33, respectively (*Online Supplementary Figure S7*). The concordance at d+15 for the 10^{-1} and 10^{-3} levels was 86% and 90%, respectively. The concordance at d+33 at the 10^{-3} level was 76%.

At week plus 12 majority of samples were PCR (86%) and FC (97%) MRD negative. Concordance for *DUX4r* (n=44), *PAX5*-P80R (n=5), *ZNF384r* (n=8) and cases with switch outside these subtypes (n=21) was 82%, 80%, 100% and 90%, respectively (*Online Supplementary Figures S6* and *S7*).

Prognostic relevance of monocytic switch

From a clinical perspective, it is important to know whether monocytic switch is of prognostic relevance and whether the phenotype changes during relapse. All but one

patient with monocytic switch was treated according to standard BCP-ALL frontline protocols. In the whole study cohort, eight of 80 patients with monocytic switch relapsed. Of the eight relapsed patients, six patients relapsed with an identical BCP-ALL subtype to the subtype at diagnosis (two had the *BCR-ABL1* subtype, one had the *DUX4r* subtype, one had the HHD subtype, one had the *ZNF384r* subtype, and one had the B-other rest subtype). Interestingly, only one of those patients (*ZNF384r*) developed monocytic switch during induction therapy for relapse. Two patients (one with the *DUX4r* subtype and one with the *KMT2Ar* subtype) relapsed with monocytic AML. In all three patients with the presence of monocytoid blasts at relapse, we proved IG/TR rearrangements in the

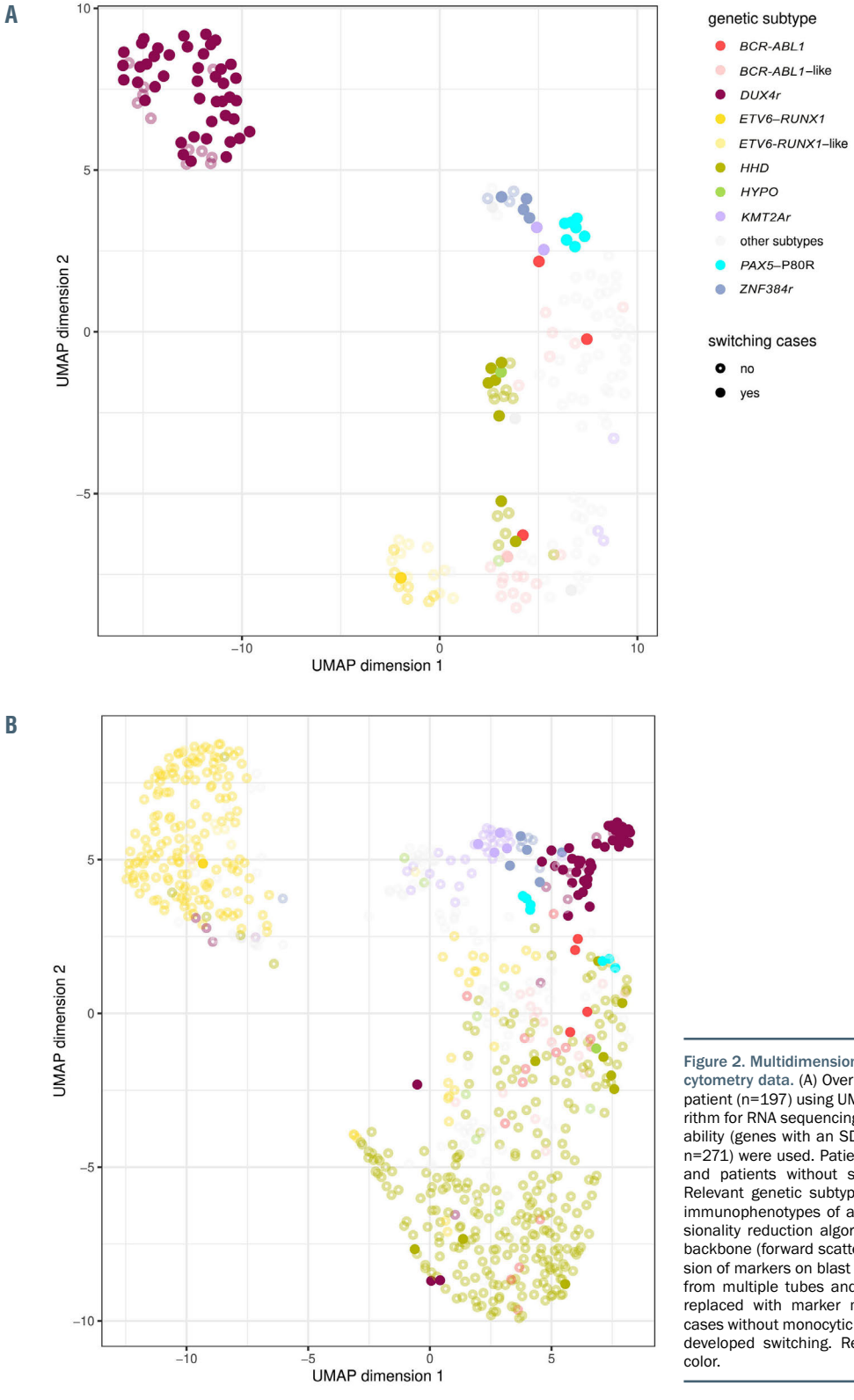

Figure 2. Multidimensional analysis of RNA sequencing and flow cytometry data. (A) Overview of the gene expression found for all patient (n=197) using UMAP as the dimensionality reduction algorithm for RNA sequencing data. Only the genes with the most variability (genes with an SD 0.4-fold higher than the maximum SD, n=271) were used. Patients with switch are shown as full circles, and patients without switching are shown as empty circles. Relevant genetic subtypes are shown in color. (B) Overview of immunophenotypes of all cases (n=745) using UMAP as dimensionality reduction algorithm. Blasts were gated using common backbone (forward scatter, side scatter, CD45). The data (expression of markers on blast population in percentage) were prepared from multiple tubes and merged together. Missing values were replaced with marker median values. Open circles represent cases without monocytic switch, full circles represent cases which developed switching. Relevant genetic subtypes are shown in color.

monocytoid cells identical to those in the original BCP-ALL clone. There was no difference in the event-free survival (EFS) between the prospective patients with or without monocytic switch (5-year EFS, 82±5.5% and 86±1.6% , respectively, Figure 4) also when only patients in the high risk/slow early response group were considered (*Online Supplementary Figure S9*).

Discussion

Monocytic switch provides evidence for the relationship between the monocytic and lymphoid lineages. Rigid models of hematopoiesis assume early separation of the monocytic and lymphoid lineages, but there is increasing evidence of innate immune functions in lymphoid lineages, including phagocytosis.[30] The biological origin of the phenomenon remains to be clarified. Rarely B-cell malignancies of various stages of differentiation under unknown circumstances can undergo transdifferentiation into myeloid/histiocytic malignancies.[31,32] An interesting area for future investigation is the relationship between of monocytic cells to their CD14^{pos} dendritic cells counterparts. CD2, a frequent aberrant marker of BCP ALL blasts prior to monocytic switching, does not clarify their fate as it is known to be expressed in subsets of both dendritic cells[33] and monocytic AML.[34] The constant role of the transcription factor C/EBPα seems to play a role in the process. In our previous work, we found higher expression of *CEBPA* in patients with monocytic switching, which was also true in this extended cohort. C/EBPα directly represses B-cell genes. DiStefano *et al.* reported that C/EBPα can enforce B-cell transcription factor silencing by increasing the expression of the histone demethylase Lsd1 (Kdm1a) and the histone deacetylase Hdac1 at the protein level and that these enzymes are required for the downregulation of B-cell enhancers and the silencing of the B-cell program.[35] *In vitro* models demonstrate that C/EBPα induces the repression of key B-cell regulators such as Foxo1, Ebf1 and Pax5[36].

In our study we show that monocytic switch behavior is not limited to a single genotypic subset and that various leukemia genotypes show different propensities to switch to monocytic cells. In agreement with our previous report, in this study, the majority of patients whose blasts switched to monocytoids were categorized in the B-other subset (70% of patients with monocytic switch compared to 21% of patients without switch; Fisher's exact test P<0.00001). New genomic methods – namely, RNA-seq – were recently used to discover new recurring genetic subtypes within the mixture of the genotypes thus far labeled B-other.[2,3,24,25,37–40] Three of these subsets, *DUX4r*, *PAX5*-P80R, and *ZNF384r*, were frequently associated with switch, constituting the majority of the patients with switch in this study. We did not identify a known subtype-defining genetic aberration (B-other rest) in only 3.8% of the patients with monocytic switch (Table 1). Interestingly, all patients with *PAX5*-P80R presented with monocytic switch.

Although it did not reach statistical significance (probably due to the low number of patients), a switching phenomenon was observed in 24% of cases with *BCR-ABL1*. McClellan *et al.* found that primary *BCR-ABL1*-positive BCP-ALL cells could be reprogrammed into macrophage-like cells through exposure to cytokines in vitro or by transient expression of the transcription factor C/EBPα or PU.1.[41] Surprisingly, monocytic switch was not significantly more frequent in the *KMT2Ar* subtype than in other sub-

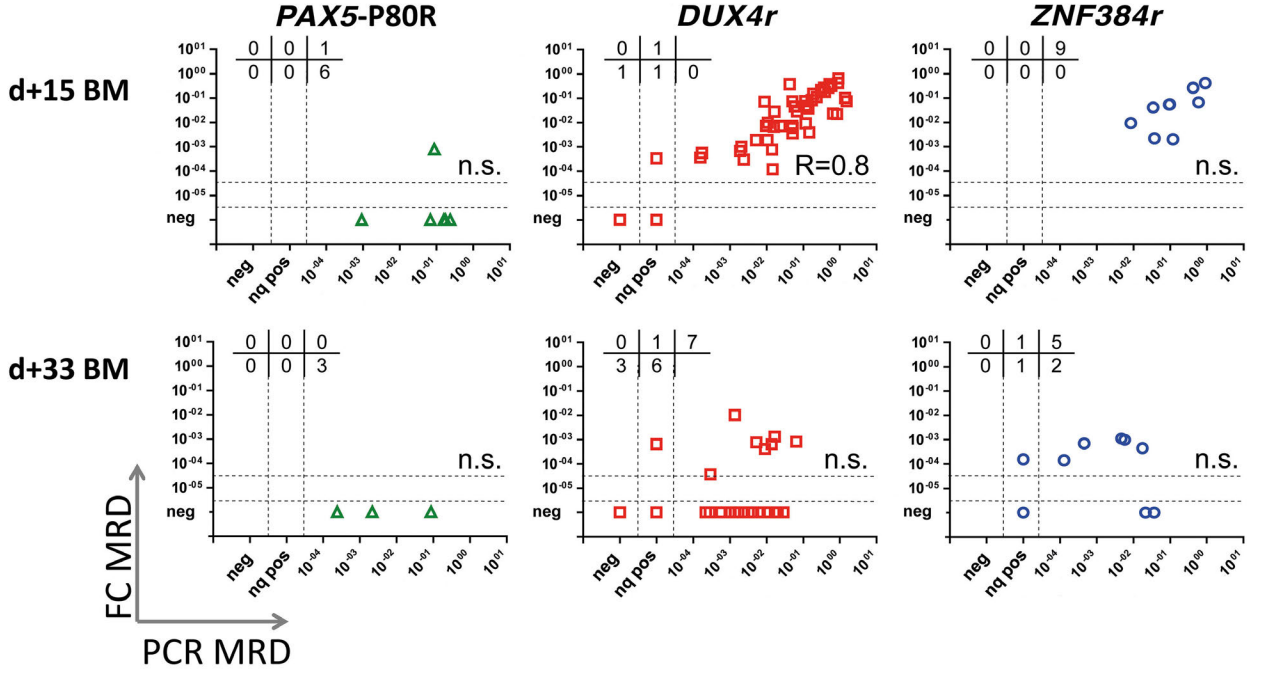

Figure 3. Correlation of the mimal reidual disease results obtained by flow cytometry and polymerase chain reaction in selected patient groups. Only samples with appropriate measured sensitivity are shown (the flow cytometry [FC] sensitivity is 0.0001 if the polymerase chain reaction [PCR]-determined minimal residual disease [MRD] <0.01; for samples with PCR-determined MRD ≥0.01, the FC measurement sensitivity is at least one log value lower than the actual PCR-determined MRD log value). In the upper part of each graph, the number of patients with MRD values FC^{pos}/PCR^{neg}, FC^{pos}/PCR$^{nq\ pos}$, and FC^{pos}/PCR^{pos} (upper lane); and FC^{neg}/PCR^{neg}, FC^{neg}/PCR$^{nq\ pos}$, and FC^{neg}/PCR^{pos} (bottom lane) are indicated. Spearman's rank correlation coefficient indicated if the P-value was <0.05. Nq pos: nonquantifiable positivepositive; BM: bone marrow.

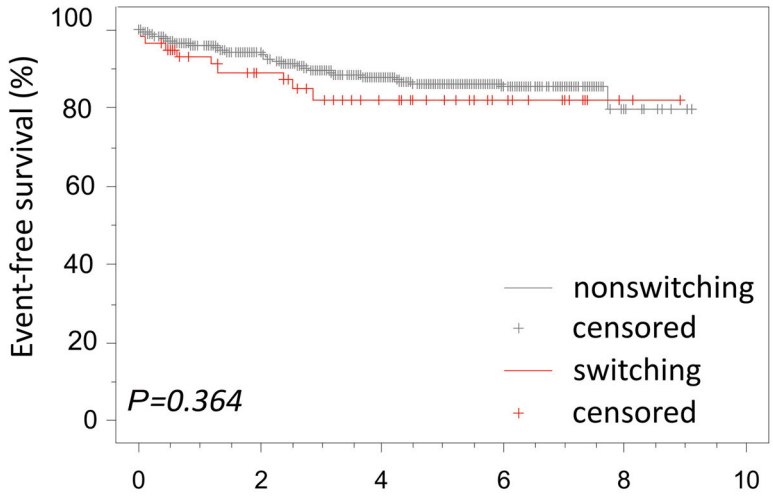

Figure 4. Event-free survival of B-cell precursor acute lymphoblastic leukemia patients with and without switch. The prospective cohort (n=725) is shown. One patient was lost to follow-up.

types, although *KMT2Ar* leukemias can present with a mixed phenotype. However, due to the heterogeneity of *KMT2Ar* leukemias and the limitations of our cohort, the correlation of monocytic switch with specific *KMT2Ar* subtypes should be verified in larger cohorts.

The results from the multidimensional analyses of the gene expression profiles (GEP) and immunophenotypes showed that the patients with monocytic switch coclustered based on genotype. Similarly, Alexander *et al.*[42] recently showed that gene expression-based clustering primarily distinguished genetic subtypes irrespective of MPAL (mixed phenotype acute leukemia) status. Together, these findings show that monocytic switch is a behavior with varying propensity across BCP-ALL genotypes rather than being exclusive to a distinct genetic subtype of leukemia.

Similarly, switching cannot be predicted using a diagnostic immunophenotype according to our data. Nevertheless, immunophenotype can help to predict genotype, as was shown previously and extended in this study.[39,40,43,44]

Monocytic switch may lead to uncertainty about the continuation of ALL-type therapy. In some patients the phenomenon was very discreet and might be overlooked using routine examination. On the contrary, we observed monocytosis at d+8 of as high as 20,804/μL, 3,969/μL and 15,544/μL for the *DUX4r*, *PAX5*-P80R and *ZNF384r* subtypes, respectively. Although such findings may trigger thoughts of changing to the AML type of treatment, all but one patient with detected monocytic switch achieved complete remission on an ALL type of treatment. One patient died during induction therapy. The EFS for an ALL type of therapy was identical among patients with and without monocytic switch. However, we did observe two patients (one with the *DUX4r* subtype and one with the *KMT2Ar* subtype) who relapsed with monocytic AML, showing that the optimal treatment of such rare patients has yet to be determined. Of note, the majority of the published cases of monocytic relapse after primary BCP-ALL had the *KMT2Ar* genotype.[45] In addition to these AML relapses, we discovered that six patients with detectable monocytic switch relapsed later with BCP-ALL. According to published data, the prognosis of patients with the *DUX4r* or the *PAX5*-P80R subtype does not seem to be unfavorable.[3,38]

The clinical significance of switched monocytoids, *per se*, remains unknown. To date, we have limited evidence about their potential to initiate relapse. Functional tests of those switched cells so far have not been performed. Interestingly, we observed a rapidly enlarging spleen in one patient and progressive liver failure in another patient, most likely caused by infiltrating macrophages, which had identical IG/TR rearrangements as the original malignant B precursors.

Despite several observed features of switched monocytoids in *DUX4r*- and *PAX5*-P80R-mutated patients (*e.g.*, CD45RA and CD2 positivity in *DUX4r*, CD13 negativity and CD66c positivity in *PAX5*-P80R), their interpretation (especially at time points with myeloid regeneration, including time point d+33) is challenging.

Monocytic switch not only creates discordance between MRD levels determined by FC and MRD levels determined by PCR but also affects the availability of CD19 as a therapeutic target. In some current pediatric treatment protocols, these patients can be stratified for anti-CD19 treatment regardless of their CD19 expression levels. Thus far, data are limited regarding the efficacy of such treatment in patients with monocytic switch. Recently, the first case report of myeloid relapse in BCP-ALL patients with a *ZNF384r* subtype after CAR-T therapy was published.[46] However, myeloid relapse in *ZNF384r* patients without targeted therapy has also been described.[47]

In conclusion, we report the frequency of monocytic switch in novel genetic subtypes of BCP-ALL and highlight the discordance between MRD levels determined by FC and PCR during the switch. New markers for discriminating switched monocytoid blasts from nonmalignant monocytes are needed to overcome FC underestimation of MRD levels, which is becoming more relevant with the use of targeted anti-CD19 therapy.

Disclosures

No conflicts of interest to disclose

Contributions

MN analyzed immunophenotypic data, evaluated FC MRD and wrote the manuscript; MZ was responsible for whole-exome and RNA-seq data and wrote the manuscript; KF analyzed RNA-seq data and wrote the manuscript; BV analyzed immunophenotypic data and evaluated FC MRD; LS performed PCR MRD on sorted samples, evaluated PCR MRD levels and analyzed immunophenotypic data; AM analyzed RNA-seq and immunophenotypic data; MB and MR performed the investigation in German patients; EF was responsible for PCR MRD

analysis; TK analyzed the flow cytometry data and designed the sorting; JStu managed the patients and contributed to data collection; LW analyzed whole-exome and RNA-seq data; PS and AK performed the investigation in Slovak patients; JSta performed statistical analyses; JZ and TK supervised the molecular genetic data analysis; OH wrote and reviewed the manuscript; EM designed the research, analyzed the data and wrote the manuscript. All authors have read and approved the final submission of the manuscript.

Acknowledgments

The authors would like to thank Iveta Janotova for data management, Alena Houdkova for the morphological review, and Pavel Semerak, Pavla Luknarova, Katerina Rejlova, Marketa Musilova and Daniel Thurner for processing the flow cytometry samples. We thank the Czech Pediatric Hematology Group for collaboration (Doctors Sterba, Timr, Pospisilova, Votava, Prochazkova, Blazek and Hak).

Funding

This project is the main output of grant number NV18-03-00343. EF was supported by Primus/17/MED/11. MZ was supported by Primus/MED/28. BV was supported by GAUK number 364119. The FACS Aria instrument was provided by EU-Prague project CZ.2.16/3.1.00/24022. Infrastructure was supported by CZ.2.16/3.1.00/21540 and by CZ.2.16/3.1.00/24505.

References

1. Slamova L, Starkova J, Fronkova E, et al. CD2-positive B-cell precursor acute lymphoblastic leukemia with an early switch to the monocytic lineage. Leukemia. 2014;28(3):609-620.
2. Lilljebjörn H, Fioretos T. New oncogenic subtypes in pediatric B-cell precursor acute lymphoblastic leukemia. Blood. 2017;130 (12):1395-1401.
3. Passet M, Boissel N, Sigaux F, et al. PAX5 P80R mutation identifies a novel subtype of B-cell precursor acute lymphoblastic leukemia with favorable outcome. Blood. 2019;133(3):280-284.
4. Rayes A, McMasters RL, O'Brien MM. Lineage switch in MLL-rearranged infant leukemia following CD19-directed therapy. Pediatr Blood Cancer. 2016;63(6):1113-1115.
5. Zoghbi A, zur Stadt U, Winkler B, Müller I, Escherich G. Lineage switch under blinatumomab treatment of relapsed common acute lymphoblastic leukemia without MLL rearrangement. Pediatr Blood Cancer. 2017;64(11):e26594.
6. Wölfl M, Rasche M, Eyrich M, Schmid R, Reinhardt D, Schlegel PG. Spontaneous reversion of a lineage switch following an initial blinatumomab-induced ALL-to-AML switch in MLL -rearranged infant ALL. Blood Adv. 2018;2(12):1382-1385.
7. Aldoss I, Song JY. Extramedullary relapse of KMT2A (MLL)-rearranged acute lymphoblastic leukemia with lineage switch following blinatumomab. Blood. 2018;131(22): 2507-2507.
8. Haddox CL, Mangaonkar AA, Chen D, et al. Blinatumomab-induced lineage switch of B-ALL with t(4:11)(q21;q23) KMT2A/AFF1 into an aggressive AML: pre- and post-switch phenotypic, cytogenetic and molecular analysis. Blood Cancer J. 2017;7(9):e607.
9. Jacoby E, Nguyen SM, Fountaine TJ, et al. CD19 CAR immune pressure induces B-precursor acute lymphoblastic leukaemia lineage switch exposing inherent leukaemic plasticity. Nat. Commun. 2016; 7(1):12320.
10. Zaliova M, Hovorkova L, Vaskova M, Hrusak O, Stary J, Zuna J. Slower early response to treatment and distinct expression profile of childhood high hyperdiploid acute lymphoblastic leukaemia with DNA index <1.16. Genes Chromosom Cancer. 2016;55(9):727-737.
11. Dworzak MN, Buldini B, Gaipa G, et al. AIEOP-BFM Consensus Guidelines 2016 for flow cytometric immunophenotyping of pediatric acute lymphoblastic leukemia. Cytometry B Clin Cytom. 2018;94(1):82-93.
12. Mejstrikova E, Volejnikova J, Fronkova E, et al. Prognosis of children with mixed phenotype acute leukemia treated on the basis of consistent immunophenotypic criteria. Haematologica. 2010;95(6):928-935.
13. Vaskova M, Mejstrikova E, Kalina T, et al. Transfer of genomics information to flow cytometry: expression of CD27 and CD44 discriminates subtypes of acute lymphoblastic leukemia. Leukemia. 2005;19(5):876-878.
14. Bene MC, Castoldi G, Knapp W, et al. Proposals for the immunological classification of acute leukemias. European Group for the Immunological Characterization of Leukemias (EGIL). Leukemia. 1995;9(10): 1783-1786.
15. Hrusak O, de Haas V, Stancikova J, et al. International cooperative study identifies treatment strategy in childhood ambiguous lineage leukemia. Blood. 2018;132(3):264-276.
16. Arber DA, Orazi A, Hasserjian R, et al. The 2016 revision to the World Health Organization classification of myeloid neoplasms and acute leukemia. Blood. 2016;127(20):2391-405.
17. Mejstříková E, Froňková E, Kalina T, et al. Detection of residual B precursor lymphoblastic leukemia by uniform gating flow cytometry. Pediatr Blood Cancer. 2010;54(1): 62-70.
18. Theunissen P, Mejstrikova E, Sedek L, et al. Standardized flow cytometry for highly sensitive MRD measurements in B-cell acute lymphoblastic leukemia. Blood. 2017;129(3): 347-357.
19. Mejstríková E, Hrusak O, Borowitz MJ, et al. CD19-negative relapse of pediatric B-cell precursor acute lymphoblastic leukemia following blinatumomab treatment. Blood Cancer J. 2017;7(12):659.
20. van der Velden VHJ, van Dongen JJM. MRD detection in acute lymphoblastic leukemia patients using Ig/TCR gene rearrangements as targets for real-time quantitative PCR. Methods Mol Biol. 2009;538:115-150.
21. Kotrova M, van der Velden VHJ, van Dongen JJM, et al. Next-generation sequencing indicates false-positive MRD results and better predicts prognosis after SCT in patients with childhood ALL. Bone Marrow Transplant. 2017;52(7):962-968.
22. van der Velden VHJ, Cazzaniga G, Schrauder A, et al. Analysis of minimal residual disease by Ig/TCR gene rearrangements: guidelines for interpretation of real-time quantitative PCR data. Leukemia. 2007;21(4):604-611.
23. R Core Team. R: a language and environment for statistical computing. R Found Stat Comput. Vienna, Austria. 2014.
24. Zaliova M, Stuchly J, Winkowska L, et al. Genomic landscape of pediatric B-other acute lymphoblastic leukemia in a consecutive European cohort. Haematologica. 2019;104(7):1396-1406.
25. Zaliova M, Kotrova M, Bresolin S, et al. ETV6/RUNX1 -like acute lymphoblastic leukemia: a novel B-cell precursor leukemia subtype associated with the CD27/CD44 immunophenotype. Genes Chromosom Cancer. 2017;56(8):608-616.
26. Zaliova M, Potuckova E, Hovorkova L, et al. ERG deletions in childhood acute lymphoblastic leukemia with DUX4 rearrangements are mostly polyclonal, prognostically relevant and their detection rate strongly depends on screening method sensitivity. Haematologica. 2019;104(7):1407-1416.
27. McInnes L, Healy J, Melville J. UMAP: uniform manifold approximation and projection for dimension reduction. ArXiv e-prints 1802.03426. 2018.
28. Schinnerl D, Mejstrikova E, Schumich A, et al. CD371 cell surface expression: A unique feature of DUX4 -rearranged acute lymphoblastic leukemia. Haematologica. 2019;104(8):e352-e355.
29. Gaipa G, Cazzaniga G, Valsecchi MG, et al. Time point-dependent concordance of flow cytometry and real-time quantitative polymerase chain reaction for minimal residual disease detection in childhood acute lymphoblastic leukemia. Haematologica. 2012; 97(10):1582-1593.
30. Černý J, Stříž I. Adaptive innate immunity or innate adaptive immunity? Clin Sci (Lond). 2019;133(14):1549-1565.
31. Pagni F, Fazio G, Zannella S, et al. The role of PAX5 and C/EBP α/β in atypical non-Langerhans cell histiocytic tumor post acute lymphoblastic leukemia. Leukemia. 2014;28 (6):1377-1379.
32. Waanders E, Hebeda KM, Kamping EJ, et al. Independent development of lymphoid and histiocytic malignancies from a shared early precursor. Leukemia. 2016;30(4):955-958.
33. Crawford K, Gabuzda D, Pantazopoulos V, et al. Circulating CD2+ monocytes are dendritic cells. J Immunol. 1999;163(11):5920-5928.
34. Creutzig U, Harbott J, Sperling C, et al. Clinical significance of surface antigen expression in children with acute myeloid leukemia: results of study AML-BFM-87. Blood. 1995;86(8):3097-3108.
35. Di Stefano B, Collombet S, Jakobsen JS, et al. C/EBPα creates elite cells for iPSC reprogramming by upregulating Klf4 and increasing the levels of Lsd1 and Brd4. Nat Cell Biol. 2016;18(4):371-381.
36. Collombet S, Van Oevelen C, Ortega JLS, et al. Logical modeling of lymphoid and myeloid cell specification and transdifferentiation. Proc Natl Acad Sci U S A. 2017;114

(23):5792-5799.
37. Zhang J, McCastlain K, Yoshihara H, et al. Deregulation of DUX4 and ERG in acute lymphoblastic leukemia. Nat Genet. 2016;48(12):1481-1489.
38. Yasuda T, Tsuzuki S, Kawazu M, et al. Recurrent DUX4 fusions in B cell acute lymphoblastic leukemia of adolescents and young adults. Nat Genet. 2016;48(5):569-574.
39. Gu Z, Churchman ML, Roberts KG, et al. PAX5-driven subtypes of B-progenitor acute lymphoblastic leukemia. Nat Genet. 2019;51(2):296-307.
40. Bastian L, Schroeder MP, Eckert C, et al. PAX5 biallelic genomic alterations define a novel subgroup of B-cell precursor acute lymphoblastic leukemia. Leukemia. 2019;33 (8):1895-1909.
41. McClellan JS, Dove C, Gentles AJ, Ryan CE, Majeti R. Reprogramming of primary human Philadelphia chromosome-positive B cell acute lymphoblastic leukemia cells into nonleukemic macrophages. Proc Natl Acad Sci U S A. 2015;112(13):4074-4079.
42. Alexander TB, Gu Z, Iacobucci I, et al. The genetic basis and cell of origin of mixed phenotype acute leukaemia. Nature. 2018;562 (7727):373-379.
43. Hirabayashi S, Ohki K, Nakabayashi K, et al. ZNF384-related fusion genes define a subgroup of childhood B-cell precursor acute lymphoblastic leukemia with a characteristic immunotype. Haematologica. 2017;102 (1):118-129.
44. Griffith M, Griffith OL, Krysiak K, et al. Comprehensive genomic analysis reveals FLT3 activation and a therapeutic strategy for a patient with relapsed adult B-lymphoblastic leukemia. Exp Hematol. 2016;44 (7):603–613.
45. Rossi JG, Bernasconi AR, Alonso CN, et al. Lineage switch in childhood acute leukemia: An unusual event with poor outcome. Am J Hematol. 2012;87(9):890-897.
46. Oberley MJ, Gaynon PS, Bhojwani D, et al. Myeloid lineage switch following chimeric antigen receptor T-cell therapy in a patient with TCF3-ZNF384 fusion-positive B-lymphoblastic leukemia. Pediatr Blood Cancer. 2018;65(9):e27265.
47. Grammatico S, Vitale A, La Starza R, et al. Lineage switch from pro-B acute lymphoid leukemia to acute myeloid leukemia in a case with t(12;17)(p13;q11)/ TAF15–ZNF384 rearrangement. Leuk Lymphoma. 2013;54 (8):1802-1805.

Ferrata Storti Foundation

Dual cytoplasmic and nuclear localization of HTLV-1-encoded HBZ protein is a unique feature of adult T-cell leukemia

Greta Forlani,[1] Mariam Shallak,[1] Alessandra Tedeschi,[1] Ilaria Cavallari,[2] Ambroise Marçais,[3] Olivier Hermine[3] and Roberto S. Accolla[1]

[1]Laboratories of General Pathology and Immunology "Giovanna Tosi", Department of Medicine and Surgery, University of Insubria, Varese, Italy; [2]Istituto Oncologico Veneto IOV - IRCCS, Padua, Italy and [3]Department of Hematology, Necker-Enfants Malades, University Hospital, Assistance Publique Hopitaux de Paris, Paris Descartes University, Paris, France

Haematologica 2021
Volume 106(8):2076-2085

ABSTRACT

Adult T-cell leukemia-lymphoma (ATL), is a highly malignant T-cell neoplasm caused by human T-cell leukemia virus type 1 (HTLV-1), characterized by poor prognosis. Two viral proteins, Tax-1 and HTLV-1 basic-zipper factor (HBZ) play important roles in the pathogenesis of ATL. While Tax-1 can be found in both the cytoplasm and nucleus of HTLV-1 infected patients, HBZ is exclusively localized in the cytoplasm of HTLV-1 asymptomatic carriers and in patients with the chronic neurologic disease HTLV-I-associated myelopathy/tropical spastic paraparesis (HAM/TSP). HBZ is only localized in the nucleus of ATL cell lines, suggesting that the nuclear localization of HBZ can be a hallmark of neoplastic transformation. In order to clarify this crucial point, we investigated in detail the pattern of HBZ expression in ATL patients. We made use of our monoclonal antibody 4D4-F3, that at present is the only reported reagent, among the few described, able to detect endogenous HBZ by immunofluorescence and confocal microscopy in cells from asymptomatic carriers, HAM/TSP and ATL patients. We found that HBZ is localized both in the cytoplasm and nucleus of cells of ATL patients irrespective of their clinical status, with a strong preference for the cytoplasmic localization. Also Tax-1 is localized in both compartments. As HBZ is exclusively localized in the cytoplasm in asymptomatic carriers and in non-neoplastic pathologies, this finding shows that neoplastic transformation consequent to HTLV-1 infection is accompanied and associated with the capacity of HBZ to translocate to the nucleus, which suggests a role of cytoplasmic-to-nuclear translocation in HTLV-1-mediated oncogenesis.

Correspondence:

ROBERTO S. ACCOLLA
roberto.accolla@uninsubria.it

Received: September 16, 2020.

Accepted: January 19, 2021.

Pre-published: February 25, 2021.

https://doi.org/10.3324/haematol.2020.272468

Introduction

Human T-cell leukemia virus type 1 (HTLV-1), the first identified human oncogenic retrovirus, is the etiological agent of a severe form of adult T-cell leukemia/lymphoma (ATL)[1] and of HTLV-associated myelopathy/tropical spastic paraparesis (HAM/TSP), a progressive neurological disease.[2,3] 10-20 million people are infected by HTLV-1 worldwide with a preferential localization in the Southwestern region of Japan, Australasia region, North and Central Africa, the Middle East, Central and South America and the Caribbean.[4] Virus transmission occurs via cell-to-cell contact through breastfeeding, sexual intercourse, blood transfusions, and drug use with contaminated needles.[5]

Pathologies associated to HTLV-1 infections usually manifest after a long period of incubation that, in the case of ATL, may be of decades.[6] ATL are divided into four clinical subtypes: acute, lymphoma, chronic, and smoldering, depending upon the relative lymphocytosis and lymphocyte abnormalities,[7] the presence or absence of hypercalcemia, lactate dehydrogenase (LDH) serum concentration, and involvement of other organs.[8]

Although progress has been made in the pathophysiology and clinical treatment

of the disease, prognosis of ATL remains poor.[9,10] It is generally accepted that the oncogenic process leading to overt ATL proceeds through a multistep mode in which additional mutations are accumulated in the neoplastic clones.[6,11,12] However, due to the specificity of ATL phenotype in comparison to other T- cell neoplasias, it is likely that virus infection and viral protein expression play a role in oncogenesis.[13]

Two viral proteins, the viral transactivator Tax-1 and the HTLV-1 basic-zipper factor (HBZ), have shown oncogenic activities *in vitro* and *in vivo* in experimental animal models.[14,15] Tax-1 seems to be crucial in the onset of the oncogenic process mostly by disarranging several cellular activation pathways and particularly the NF-κB pathway.[16-18] However, Tax-1 expression is lost in most of ATL cases suggesting that it might be dispensable for maintaining the neoplastic state. Loss of Tax-1 expression can be generated by both genetic lesions and epigenetic mechanisms.[19,20]

Onset of ATL clones with defects in Tax-1 expression are probably favored by immunological selection. Indeed, Tax-1 is strongly immunogenic and a preferential target of cytotoxic T cells (CTL).[21,22] In contrast to Tax-1, the negative strand-encoded HBZ,[23] is expressed at all stages of infection and neoplastic transformation,[24] suggesting that it may be required for the maintenance of the oncogenic process. Interestingly, it has been shown that not only HBZ protein but also *HBZ* mRNA may be involved in the HTLV-1-mediated oncogenesis.[25] Nevertheless, the intimate mechanism by which HBZ participates to the HTLV-1-mediated neoplastic transformation still remains elusive. The subcellular distribution of HBZ in the various phases of the disease may be relevant as recent studies of our group demonstrated a peculiar and exclusive cytoplasmic distribution of HBZ protein in peripheral blood mononuclear cells (PBMC) of both asymptomatic carriers (AC)[26] and HAM/TSP patients[27,28] compared to a preferential nuclear localization in a small sample of ATL cells.[29]

These findings were unprecedented and rather unexpected as previous studies, mostly performed in HBZ transfected cells, showed an exclusively nuclear distribution of the protein.[30,31]

Our studies, thus suggested that neoplastic transformation of HTLV-1-infected cells may be accompanied by a unidirectional displacement of HBZ from the cytoplasm to the nucleus.

Thus, we analyzed HBZ localization in fresh leukemic cells of ATL patients, representative of distinct clinical forms of the disease, to investigate potential HBZ transition from the cytoplasm to the nucleus and, in case of transition, to correlate it with distinct ATL clinical entities.

Here we show that leukemic cells from eight ATL patients can express HBZ not only in the nucleus but also in the cytoplasm. Neoplastic transformation is, thus accompanied by a dichotomy of HBZ localization and the exclusively cytoplasmic localization, as observed in AC and in HAM/TSP patients, is progressively modified to include nuclear localization of the protein.

Methods

Cells and ethics statement

This study was approved by the Ethical Committee (CPP Ile de FranceII, CNIL: number 1692254, registration number 000001072) and all surviving patients gave written informed consent. The study had a retrospective observational design. Patients with acute or chronic ATL at diagnosis were analyzed. See the *Online Supplementary Appendix* for further details.

HTLV-1 proviral load measurement and determination of unspliced *versus* spliced *HBZ* mRNA

Specific information on proviral load measurement and detection of unspliced *versus* spliced HBZ RNA is provided in the *Online Supplementary Appendix*.

Cell treatments

See the *Online Supplementary Appendix* for details.

Immunofluorescence, flow cytometry and confocal microscopy

Frozen vials containing PBMC were thawed by immediate passage from liquid nitrogen to a water bath set at 37°C. Cells were washed with warm RPMI medium and immediately processed for immunofluorescence and flow cytometry analysis or for confocal microscopy as previsouly described.[26,32,33] Additional information on antibodies used for detection of specific markers is reported in the *Online Supplementary Appendix*.

Results

Cell surface phenotype and HBZ subcellular localization in acute adult T-cell leukemia-lymphoma patients: HBZ can reside in the cytoplasm

We first investigated a group of four clinically defined acute ATL patients (namely PH131213, PH140126, PH160822 and PH1612N07).

Preliminary cell surface phenotype of PBMC from these patients showed that $CD4^+$ T cells were the predominant, if not the total, cell subpopulation present in peripheral blood (*Online Supplementary Figure S1*). Interestingly, expression of the CD4 marker varied in the analyzed ATL patients, with strong (PH140126), moderate (PH131213 and PH1612N07) and low (PH160822) expression. This, however, did not correlate with expression of the CD3 marker which was either very low or absent in PBMC of these patients, a result reminiscent of previous findings reported by our group and others.[27,29,34,35] The T-cell activation marker CD25 was expressed in two (PH131213 and PH140126) of four patients' ATL cells, however, without correlation with the other T-cell activation marker, HLA class II. Expression and subcellular localization of HBZ was then analyzed by immunofluorescence and confocal microscopy Surprisingly, in contrast to what has been reported to date, in all four patients HBZ was predominantly found in the cytoplasm where it appeared as large dots (PH1612N07 and PH160822) with the tendency to converge in diffuse areas (PH131213 and PH140126) around the nucleus (Figure 1A). Interestingly, in PH1612N07 HBZ-positive cells showed the typical flower-like phenotype described in acute ATL. HBZ cytoplasmic localization was confirmed by co-staining with the cytoplasmic marker vimentin and the nuclear marker DRAQ5 (Figure 1B).

Of note, a wide variation in the percentage of HBZ positive cells was found in the four acute ATL patients, ranging from as low as 8.5% (PH131213) to as high as 83% (PH140126) of PBMC leukemic cells (*Online Supplementary Table S1*). When present, HBZ nuclear localization was

found in a minority of the HBZ-positive cells with the exception of patient PH140126 in which all HBZ-positive cells expressed the viral protein in both cellular compartments. Nevertheless, even in the case of PH140126, the nuclear localization was clearly under-represented with respect to the cytoplasmic localization (Figure 1A). In acute ATL, the proviral load (PVL) was generally higher than chronic ATL and did not strictly correlate with the percentage of HBZ-positive cells (*Online Supplementary Table S1*), even though the limited number of patients analyzed does not allow to draw a conclusion in terms of statistical significance. Interestingly, PVL values exceeded one copy of viral genome per cell in three of four patients, suggesting multiple integrations per single cell, as also demonstrated by recent molecular studies at a clonal level.[36]

In order to compare expression and subcellular localization of HBZ with those of Tax-1, a similar analysis was performed. Three of four acute ATL, namely PH140126, PH1612N07 and PH160822 showed expression of Tax-1 in 65%, 8,5% and 43% of cells, respectively, while PH131213 ATL were negative for Tax-1 (*Online Supplementary Table S1*). It is interesting to note that the two patients expressing the highest number of Tax-1 positive cells (PH140126 and PH160822), were the same expressing the highest number of HBZ-positive cells.

As found for HBZ, Tax-1 subcellular localization was predominantly seen in the cytoplasmic compartment (Figure 2A and B; *Online Supplementary Table S1*). In assessable samples, most, but not all, Tax-1 positive cells were positive also for HBZ (*Online Supplementary Table S1*); in these cases HBZ and Tax-1 were mainly co-localized in the cytoplasmic compartment (Figure 2C).

HBZ cytoplasmic localization is found also in chronic adult T-cell leukemia-lymphoma

Four patients, clinically defined as chronic ATL, were analyzed. We first assessed the PBMC cell surface phenotype of these patients; as expected it was quite distinct from the phenotype observed in acute ATL. CD3 marker identifying all T cells, was clearly assessable in the majority of the cells in all patients analyzed with a noticeable

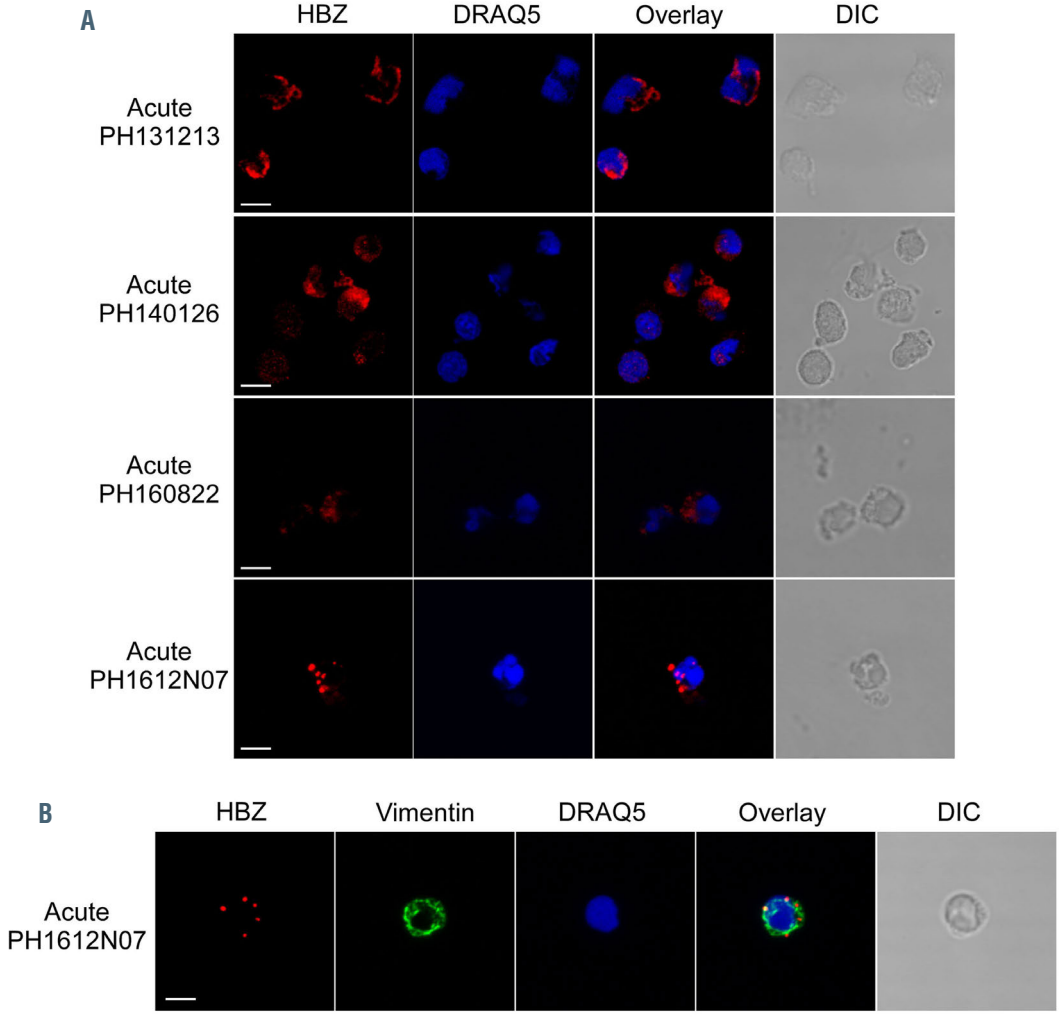

Figure 1. HBZ subcellular localization in peripheral blood mononuclear cells of patients with acute adult T-cell leukemia-lymphoma. (A) Peripheral blood mononuclear cells (PBMC) from PH131213, PH1401263, PH160822 and PH1612N07 patients were stained with the 4D4-F3 anti-HBZ monoclonal antibody (mAb) followed by Alexa Fluor 546-conjugated goat anti-mouse IgG1 antibody (red) and analyzed by confocal microscopy; DRAQ5 was used to detect the nucleus. (B). Specific counterstaining of cytoplasmic compartment in PH1612N07 patient's PBMC was performed by using anti-vimentin rabbit polyclonal antibody followed by goat anti-rabbit IgG conjugated to Alexa Fluor 488 (green). DIC represents the differential interference contrast image. At least 200 cells were analyzed. A representative image of HBZ staining is shown of each patient. All scale bars are 5μm.

distinction in patient PH171206 where only 20% of the cells were CD3-positive (*Online Supplementary Figure S2*). Moreover, the CD4 T-cell marker identifying the T-helper subpopulation of CD3-positive T cells, although strongly expressed, was not present in the entire population (*e.g.*, see patients PH170706 and PH150610). Here, at variance with acute ATL, the observed phenotype was more similar to the CD4 phenotype observed in healthy donors PBMC. In chronic ATL patients the CD8 marker was expressed in a variable proportion of PBMC (*Online Supplementary Figure S2*), again mirroring the CD8 phenotype of normal PBMC more than the phenotype of acute ATL. The CD25 T-cell activation marker was not expressed, while HLA-DR was variably expressed, but always in a minor proportion of cells again mimicking the phenotype of normal PBMC.

Expression and subcellular localization of HBZ were then analyzed. As for acute ATL cases, HBZ was expressed in all cases ranging from 9.7% in patient PH171206 to 12.0%, 38.0% and 97.5% in patients PH170706, 150610 and PH170918, respectively (*Online Supplementary Table S1*), demonstrating that the variability in the percentage of HBZ-positive cells was similar in chronic and acute ATL. Thus, at least in the small number of cases analyzed, expression of HBZ may be not correlated with the clinical stage of the disease. Importantly, as observed in acute ATL, in all four chronic ATL cases HBZ was localized mostly in the cytoplasm (Figure 3A), with no cells expressing HBZ exclusively in the nucleus (*Online Supplementary Table S1*). Cells expressing nuclear HBZ were a minority as compared to the cells expressing HBZ only in the cytoplasm (29% *vs.* 68% in PH170918, and 2.1% *vs.* 7.5% in PH171206). Moreover, PBMC of two chronic ATL patients, PH150610 and PH170706, did not show detectable nuclear HBZ expression at all (Figure 3A; *Online Supplementary Table S1*). HBZ appeared as distinctive dots, smaller in the nucleus when present as compared to the cytoplasm (Figure 3A, PH170918 and PH171206) where the dots were often confluent creating a sort of ring around the nucleus (Figure 3A, PH170706 and PH150610).

Interestingly Tax-1 was found expressed only in two of four chronic ATL patients, namely, PH170706 and PH171206, with a relative percentage of 6.4% and 1.0%, respectively (*Online Supplementary Table S1*). Tax-1-positve cells of patients PH170706 expressed the viral marker only in the cytoplasm (Figure 3B; *Online Supplementary Table S1*)

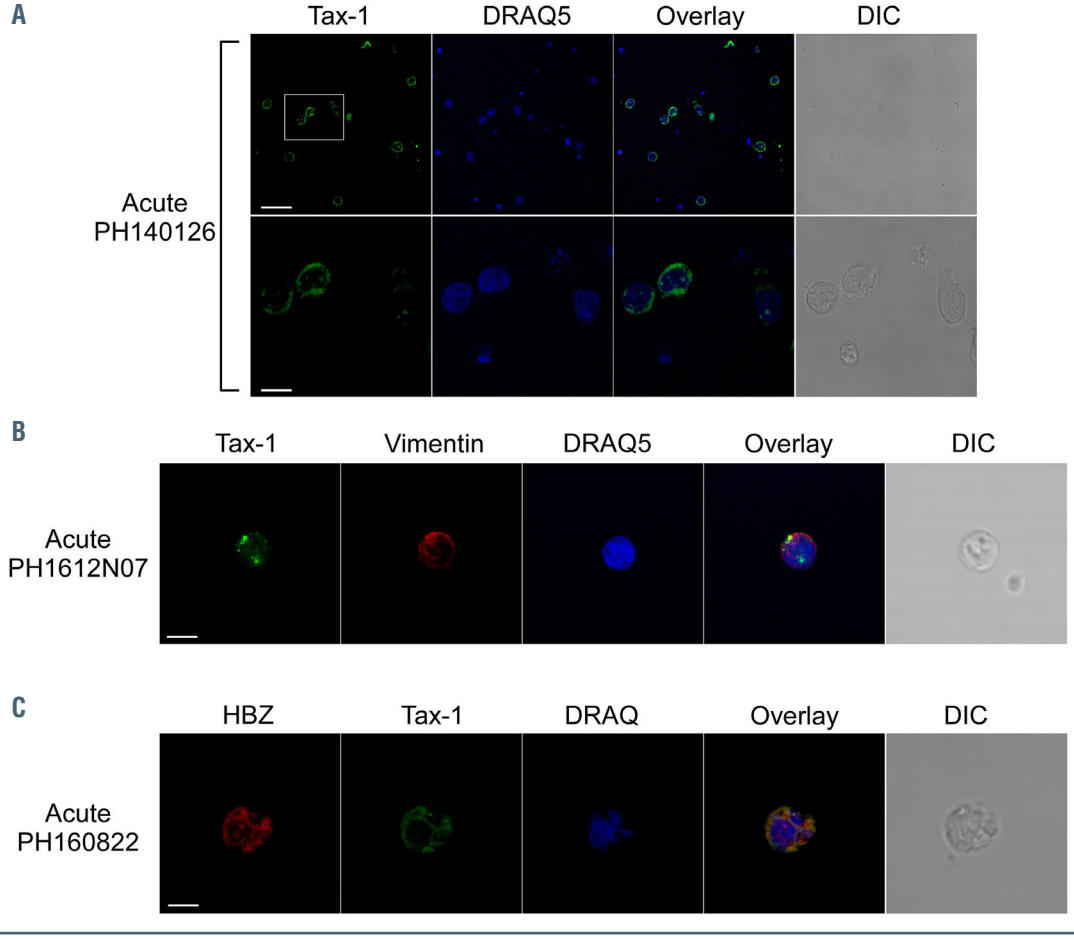

Figure 2. Tax-1 subcellular localization in peripheral blood mononuclear cells of patients with acute adult T-cell leukemia-lymphoma. (A) Peripheral blood mononuclear cells (PBMC) of representative acute adult T-cell leukemia-lymphoma patients PH40126 (A) and PH1612N07 (B) were stained with the A51-2 anti-Tax-1 monoclonal antibody (mAb) followed by Alexa Fluor 488-conjugated goat-anti-mouse IgG2a antibody (green) and analyzed by confocal microscopy. Counterstaining of the nuclear or cytoplasmic compartments was performed by using DRAQ5 fluorescence probe to detect the nucleus (blue) and anti-vimentin rabbit polyclonal antibody followed by goat anti-rabbit IgG conjugated to Alexa Fluor 546 (B, red) to stain the cytoplasmic compartment. (C) PBMC of representative acute ATL patient PH160822 were costained with the 4D4-F3 anti-HBZ mAb followed by Alexa Fluor 546-conjugated goat anti-mouse IgG1 antibody (red) and with the A51-2 anti-Tax-1 mAb followed by Alexa Fluor 488-conjugated goat-anti-mouse IgG2a antibody (green) and analyzed by confocal microscopy. DRAQ5 fluorescence probe was used to detect the nucleus (blue). DIC represents the differential interference contrast image. At least 300 cells were analyzed. All scale bars are 5μm.

with a confluent dot-like fashion evenly distributed throughout this compartment; conversely Tax-1-positve cells of patients PH171206 expressed the viral marker both in the cytoplasm and the nucleus (*Online Supplementary Table S1*). Of note, Tax-1 was expressed in those two chronic ATL patients, PH170706 and PH171206, which expressed the lower percentage of HBZ positive cells. Moreover, as observed in acute ATL patients, not all Tax-1-positive cells were also HBZ-positive, as observed in PH170706 in which only 1% out of 6.4% of cells co-expressed the two viral proteins (*Online Supplementary Table S1*). As previously reported,[26,27] HBZ was expressed mostly in CD4-positive cells (Figure 4A). However in PBMC of those patients with a distinctive and relatively normal proportion of CD8-positive cells, such as PH170918 (see the *Online Supplementary Figure S1*), HBZ expression could also be found in few CD8-positive cells (Figure 4B).

Predominance of spliced *versus* unspliced form of *HBZ* mRNA in adult T-cell leukemia-lymphoma

Then we verified whether predominant HBZ cytoplasmic localization in leukemic cells correlated with preferential expression of one of the two described forms of *HBZ* mRNA, spliced *versus* unspliced.[37,38] We found a clear predominance of the spliced *versus* unspliced *HBZ* form in our leukemic samples without appreciable differences between acute and chronic ATL (*Online Supplementary Figure S3*). This was in line with the results obtained in HAM/TSP patients and asymptomatic carriers, which expressed HBZ exclusively in the cytoplasm (*Online Supplementary Figure S3*),[26,27] but at variance with the ATL-2 leukemic cell line and with PH1505 patient leukemic cells, which expressed mostly nuclear HBZ.[27] Here the unpliced form was predominant (ATL-2) or similar (PH1504) to spliced form.

Cytoplasmic HBZ protein does not shuttle between the cytoplasm and nucleus

We have previously shown that in PBMC from both asymptomatic carriers and HAM/TSP patients the exclusive cytoplasmic localization of HBZ could not be modified by treatment with Leptomycin B (LMB), a specific inhibitor of CRM1/exportin-mediated nuclear export,[39] strongly suggesting that in AC and HAM/TSP, HBZ does

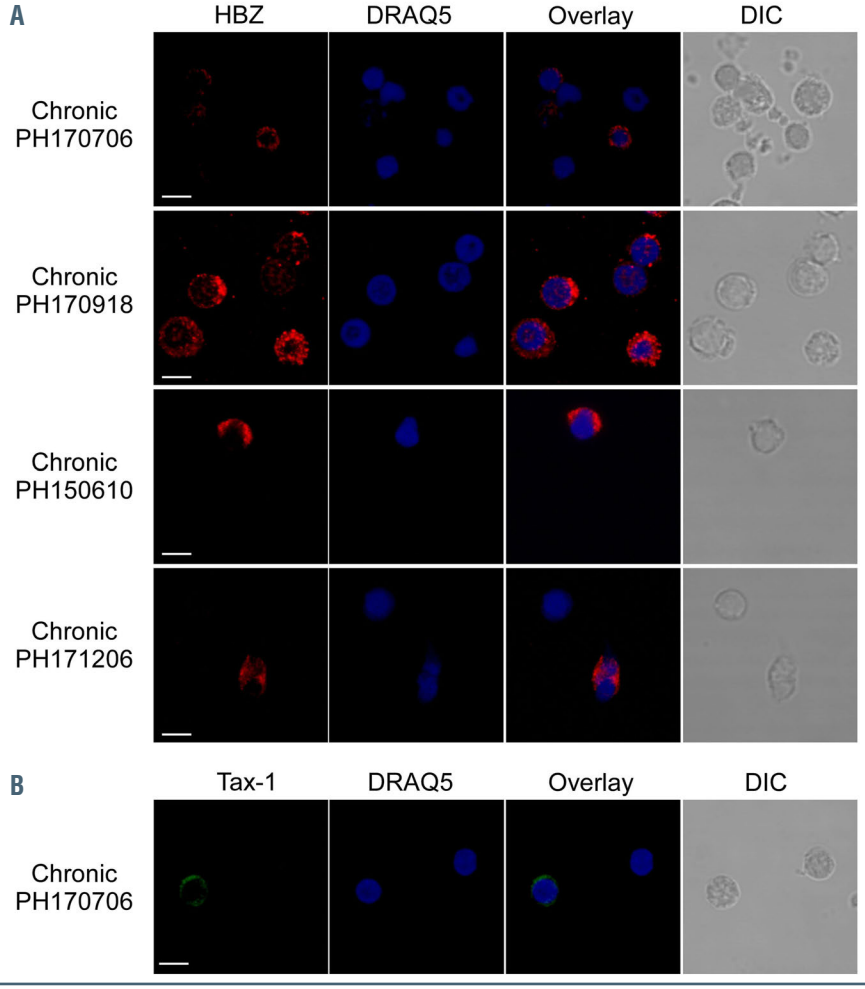

Figure 3. HBZ subcellular localization in peripheral blood mononuclear cells of patients with chronic adult T-cell leukemia-lymphoma. (A) Peripheral blood mononuclear cells (PBMC) of representative chromic leukemia patients PH150610, PH170706, PH170918 and PH171206 were stained with the 4D4-F3 anti-HBZ monoclonal antibody (mAb) followed by Alexa Fluor 546-conjugated goat anti-mouse IgG1 antibody (red) and analyzed by confocal microscopy. DRAQ5 fluorescence probe was used to detect the nucleus. (B) PBMC of representative chronic leukemia patient PH170706 was stained with the A51-2 anti-Tax-1 mAb followed by Alexa Fluor 488-conjugated goat-anti-mouse IgG2a antibody (green) and analyzed by confocal microscopy. Nucleus was stained with DRAQ5. DIC represents the differential interference contrast image. At least 300 cells were analyzed. One representative image of HBZ staining derived from PBMC samples of each patient is shown. At least 300 cells were analyzed. All scale bars are 5μm.

not shuttle between the cytoplasm and nucleus.[27] Since in acute and chronic ATL, HBZ could be localized in both compartments, with a clear preference for the cytoplasm, it was important to assess whether the entire pool of cytoplasmic HBZ could indeed shuttle between cytoplasm and nucleus. Cells were treated with LMB and analyzed by immunofluorescence and confocal microscopy. Results presented in Figure 5A show that this was not the case because LMB treatment did not result in the accumulation of HBZ protein in the nucleus in either acute (PH140126) or chronic (PH170918) ATL cells (Figure 5A).

As a control, LMB treatment of normal PHA-treated PBMC was instead capable to significantly retain the p65/RelA component of the NF-κB complex in the nucleus (Figure 5B). Taken together, these results strongly suggest that the cytoplasmic component of HBZ protein in both acute and chronic ATL does not ostensibly shuttle between the cytoplasm and nucleus through CRM1/exportin regulated mechanism.

Calreticulin may regulate Tax-1 nuclear export by interacting with, and retaining the viral protein in the cytoplasm in a concentration dependent fashion.[40] In order to verify whether calreticulin might contribute to the cytoplasmic localization of HBZ, we costained PBMC from both acute and chronic patients with HBZ and calreticulin specific antibodies. Cytoplasmic HBZ did not colocalize with calreticulin. Moreover, we could not detect a significant increased expression of calreticulin in HBZ-positive cells, compared to HBZ-negative cells (*Online Supplementary Figure S4A*). Cytoplasmic Tax-1 instead partially colocalized with calreticulin in acute ATL patient PH160822, although also in this case we could not observe a clear different level of calreticulin expression in Tax-1 positive cells compared to Tax-1-negative cells (*Online Supplementary Figure S4B*)

The cytoplasmic localization of HBZ in adult T-cell leukemia-lymphoma patients may partially affect p65/RelA but not JunD subcellular distribution

Previous studies have shown that HBZ inhibits Tax-1-mediated NF-κB activation and consequent transcription of various NF-κB target genes by targeting p65/RelA suggesting that this can contribute to the attenuation of viral replication and persistence of infection.[41,42] Here we analyzed the subcellular localization of p65/RelA in PBMC isolated from both acute and chronic ATL subjects. Interestingly, we found p65/RelA in the cytoplasm of HBZ-positive cells of both acute and chronic patients, partially colocalizing with HBZ (*Online Supplementary Figure S5A*, PH160822 and PH170706, respectively). This suggests that a possible, although limited, HBZ-p65/RelA cytoplasmic interaction may limit p65/RelA transition into the nucleus and the activation of the NF-κB target genes.

In order to evaluate the impact of the observed cytoplasmic localization of HBZ on other cellular pathways targeted by the viral protein, we analyzed the subcellular distribution of the transcription factor JunD, previously shown to weakly interact and partially colocalize with HBZ in an ATL patient expressing HBZ in the nucleus.[29] When HBZ was expressed in the cytoplasm, JunD was still localized

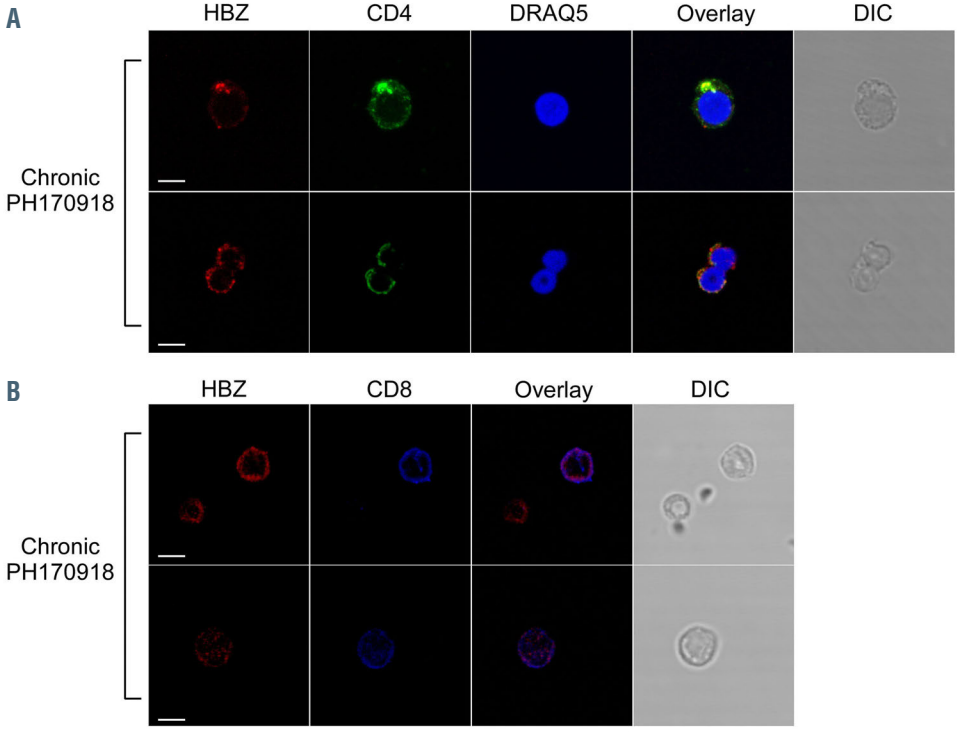

Figure 4. HBZ expression in T-cell subpopulations of chronic adult T-cell leukemia-lymphoma. Confocal microscopy analysis of peripheral blood mononuclear cells (PBMC) from representative chronic (CH) leukemic PH170918. (A) Upper panels: PBMC of patient CH PH170918 were costained with the 4D4-F3 anti-HBZ monoclonal anitbody (mAb) followed by Alexa Fluor 546-conjugated goat anti-mouse IgG1 antibody (red) and with the anti-CD4 rabbit mAb (RabmAb) followed by Alexa Fluor 488-conjugated goat-anti-rabbit IgG antibody (green). Nucleus was stained with DRAQ5. (B) PBMC of CH patient PH170918 were costained with the 4D4-F3 anti-HBZ mAb followed by Alexa Fluor 546-conjugated goat anti-mouse IgG1 antibody (red) and with the anti-CD8 RabmAb directly conjugated to Alexa Fluor 647 (blue). At least 200 cells were analyzed; DIC represents the differential interference contrast image. representative images derived from each sample are shown. All scale bars are 5μm.

in the nucleus (*Online Supplementary Figure S5B*, PH160822 and PH170706).

Discussion

The nuclear localization of HBZ in ATL has been largely inferred from studies describing the many functions that this protein exerts directly on cellular gene promoters of infected cells or by interacting with a large number of host transcription factors in the nucleus.[6,43-46] Recent investigations conducted by confocal microscopy and biochemical approaches focused on endogenous HBZ protein were consistent with the idea that leukemic cells from HTLV-1-infected ATL patients express the viral protein in the nucleus.[29] These findings, in association with elegant studies in *HBZ*-transgenic animal models,[15] gave strong support to the idea that HBZ nuclear localization is instrumental for, or at least strongly associated with, the maintenance of the leukemic state. On the other hand, more recent and precise immune localization studies have clearly indicated that HBZ expression is always and only confined to the cytoplasm in HTLV-1 AC and in HAM/TSP patients in contrast to Tax-1 localization that can be found in both compartments.[26,27] Since AC and more rarely HAM/TSP states may evolve to the leukemic state, it could be, thus, realistic to think that HBZ translocation from the cytoplasm to the nucleus is associated with the genesis of the neoplastic process leading to ATL. In order to verify this hypothesis it was instrumental to demonstrate that stages of leukemic transformation could indeed show evidence of cytoplasmic-only or cytoplasmic-nuclear localization of endogenous HBZ protein. In this study, we have demonstrated that indeed leukemic cells from ATL patients could be found that express HBZ in the cytoplasm with high frequency. Apparently, therefore, we filled the gap with previous studies and showed the unidirectional subcellular translocation from the cytoplasm to the nucleus of HBZ during oncogenic transformation. Moreover, HBZ was expressed not only in $CD4^+$ T cells, the preferential target of the HTLV-1 retrovirus, but also in a very small percentage of $CD8^+$ T cells indicating that $CD8^+$ T cells can be infected by HTLV-1, confirming our previous observations,[26,27] and persist in ATL patients.

Several findings reported in this study require further investiagtions to be framed in the context of unidirectional cytoplasm-to-nucleus localization of HBZ in ATL.

A rather unexpected and important finding was that none of the eight patients, either acute or chronic ATL, analyzed in this study had cells expressing HBZ exclusively in the nucleus. As a partial explanation, we can adduce that most of the previous studies describing endogenous HBZ localization were carried out in leukemic cell lines possibly representative of highly selected phenotypes in culture, while only three patients were described with an exclusive nuclear localization by a similar confocal microscopy approach.[27,29] In this context, it is important to stress that previously analyzed ATL patients and those described in this study did not differ in terms of geographic origin or ethnic group being all afro caribbeans but one (PH150610).

A second important finding relates to the evidence, again common to both acute and chronic ATL, that in cells expressing HBZ in both the cytoplasm and nucleus, the cytoplasmic fraction was always consistently higher than the nuclear fraction. Actually, in two ATL chronic patient (PH150610 and PH170706), HBZ was only observed in the cytoplasm. A relative exception was represented by the acute ATL patient PH140126 displaying the highest percentage of HBZ-positive cells (83%) all of which were positive for both cytoplasmic and nuclear localization. The unprecedented HBZ cytoplasmic localization in leukemic patients found in this study was paralleled by the known more abundant expression of the spliced *versus*

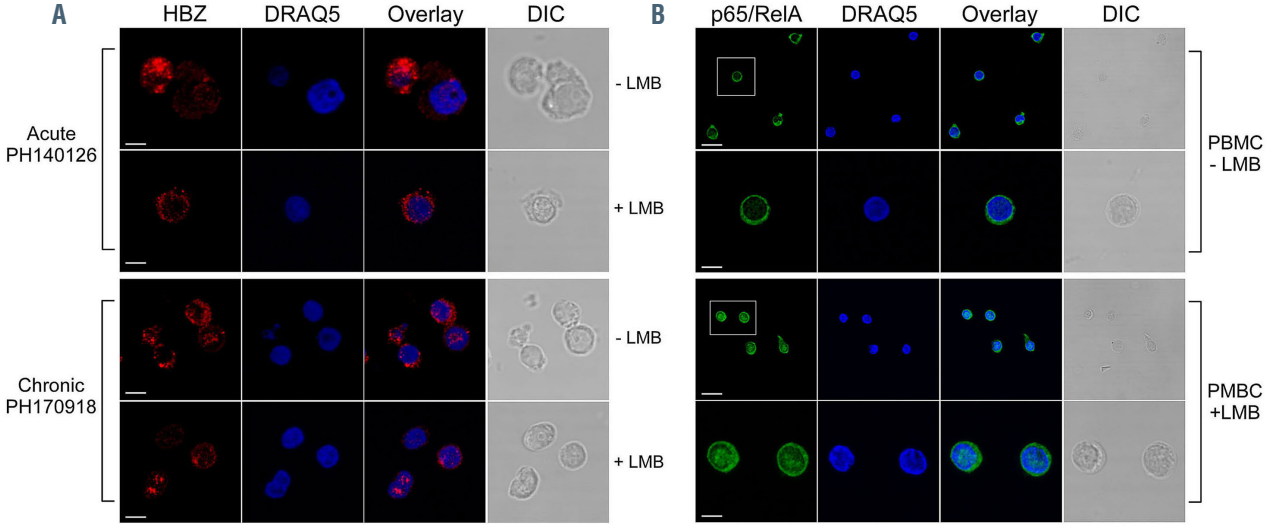

Figure 5. Cytoplasmic HBZ is retained in this compartment and does not shuttle to the nucleus. (A) Peripheral blood mononuclear cells (PBMC) of representative acute PH140126 and chronic PH170918, were either treated (+LMB, bottom panels) or not treated (-LMB, top panels) with Leptomycin B (LMB), an inhibitor CRM1/exportin-mediated nuclear export, before fixing and stained with the anti-HBZ 4D4-F3 monoclonal antibody (mAb) followed by Alexa Fluor 546-conjugated goat anti-mouse IgG1 antibody (red) and analyzed by confocal microscopy. (B) As control of inhibition of nuclear export by LMB, treated (+LMB) and untreated (-LMB) cells were fixed and stained with antibodies against p65/RelA followed by Alexa Fluor 546-conjugated goat-anti-rabbit secondary antibody (red) and analyzed by confocal microscopy. One representative image on the field and an enlargement of this are shown. Nucleus was stained with DRAQ5 (blue). DIC represents the differential interference contrast image. One representative image is shown for each sample. At least 300 cells were analyzed. All scale bars are 5μm.

unspliced form of *HBZ* mRNA,[25] corroborated also in HAM/TSP patients and in AC that have exclusive HBZ protein cytoplasmic localization.[26,27] Conversely, the ATL-2 leukemic cell line and leukemic cells of a previously described patient (PH1505), displaying a predominant HBZ nuclear localization, showed a more abundant or similar unspliced *versus* spliced *HBZ*, suggesting a correlation between subcellular protein localization and distinct forms of alternatively spliced *HBZ* mRNA.

Taken together, these results show for the first time that the dual cytoplasmic/nuclear localization of HBZ is an exclusive feature of ATL, giving further credit to the hypothesis of subcellular re-localization of HBZ in leukemogenesis (Figure 6).

The high percentage of HBZ-positive cells observed in chronic ATL, a situation usually characterized by a low number of leukemic cells,[47] as well as the exclusive cytoplasmic localization of HBZ found in two chronic ATL patients, remain to be clarified. Are the described conditions the mirror of a specific step of the neoplastic process such as the anticipation of an acute phase of the disease or a phase in which HBZ is progressively relocated into the nucleus without any modification of the clinical status, or, provocatively, the manifestation of novel disease subgroups? The first hypothesis seems unlikely as clinical follow-up suggests that these patients have not evolved toward an aggressive phenotype, indicating that other factors, possibly involved in the cytoplasmic dislocation of HBZ, are needed to mark the transition *versus* a different clinical state of ATL.

Previous studies of our group have clearly demonstrated that both in asymptomatic carriers and HAM/TSP patients the exclusive HBZ cytoplasmic localization was due to a retention in this subcellular compartment, as inhibition of CRM-1 dependent nuclear export by LMB did not result in nuclear retention of the viral protein.[26,27] It was therefore important to assess whether in cells of ATL patients showing both cytoplasmic and nuclear localization, HBZ could freely shuttle between the two subcellular compartments. This was neither the case in acute nor chronic ATL, suggesting, besides the above described association of spliced-cytoplasmic *versus* unspliced-nucleus, the existence of an active mechanism of cytoplasmic HBZ retention even in presence of a quota of nuclear protein, and irrespective of the clinical form of the disease (Figure 6). One possible candidate for the cytoplasmic retention of HBZ could be calreticulin previously shown to regulate Tax-1 nuclear export.[40] However, at least for the patients analyzed, HBZ was not clearly confined in a calreticulin subcellular compartment, while Tax-1 partially colocalized with calreticulin. A more in-depth analysis with an increased number of acute and chronic ATL subjects might further clarify this aspect.

Recent results have suggested that HBZ can be retained in the cytoplasm by interacting with the T cell-specific molecule THEMIS.[48] Conversely, we showed that this did not explain the cytoplasmic retention of HBZ in cells of HAM/TSP patients.[26] Thus, although in ATL a partial involvement of THEMIS in the retention of HBZ in the cytoplasm cannot be excluded, it is certainly important to further investigate the possibility that different cytoplasmic anchoring molecules or molecular complexes may also be involved in the cytoplasmic localization of HBZ in ATL. Whatever the mechanism, it is

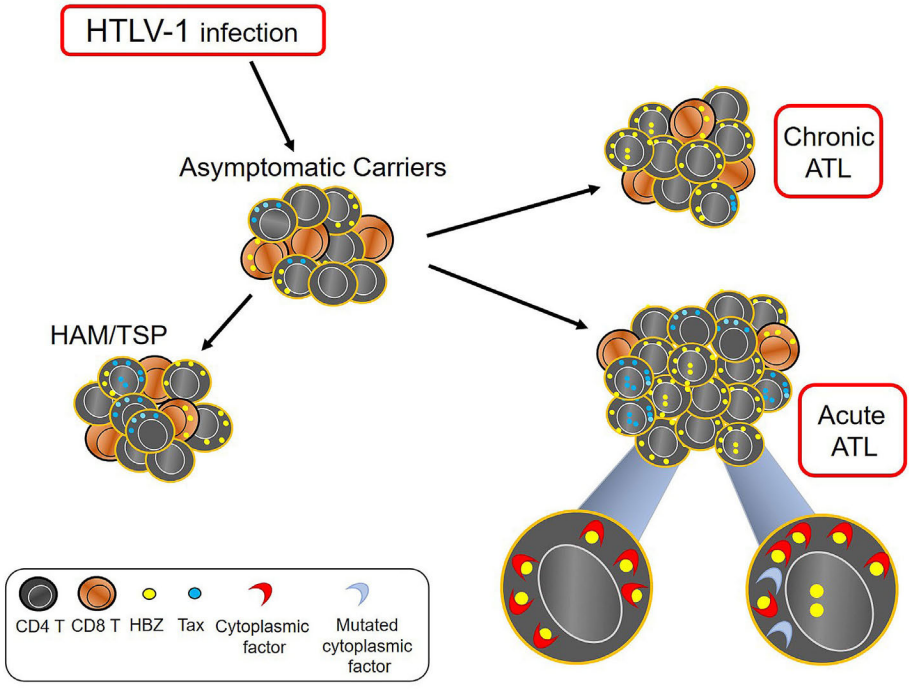

Figure 6. Subcellular localization of HTLV-1 HBZ protein during adult T-cell leukemia-lymphoma progression. Primary infection of T cells by HTLV-1 is characterized by the expression and localization of HBZ protein exclusively in the cytoplasm, at variance with Tax-1 that can be found both in the cytoplasm and nucleus. This feature is conserved during the progression to chronic neurologic inflammatory HTLV-I-associated myelopathy/tropical spastic paraparesis (HAM/TSP) disease possibly due to retention by a cytoplasmic factor present in both asymptomatic carriers and HAM/TSP patients. Leukemogenesis, instead, is marked by the progressive translocation of HBZ from the cytoplasm to the nucleus, both in chronic and in acute adult T-cell leukemia-lymphoma (ATL). On the basis of our results presented here, it is likely that HBZ cytoplasmic localization in ATL is mediated by the same retention factor/mechanism present in asymptomatic carriers and HAM/TSP, that is gradually lost during neoplastic transformation allowing HBZ protein to dislocate into the nucleus.

clear that a quota of the HBZ molecular pool can translocate into the nucleus and can be retained there to functionally participate in the maintenance of the leukemic phenotype. The molecular basis of this nuclear retention remains to be investigated.

An additional relevant aspect of the present study was the expression and subcellular localization of Tax-1 protein. Tax-1 was not expressed in three of eight patients analyzed in this study, confirming previous findings on the silencing of the viral oncogene in ATL.[19] Interestingly, however, a clear difference was observed between acute and chronic ATL, as Tax-1 was expressed in three of four acute ATL in a relevant proportion of cells, ranging from 8.4% to 65.0% of PBMC, and only in two of four chronic ATL but in a considerably low proportion of cells, namely 1.0% and 6.4 % of PBMC. This finding correlated quite well with the cell surface phenotype of leukemic cells in that PBMC of chronic ATL patients resembled more closely the phenotype observed in healthy individuals.

An exclusive Tax-1 nuclear localization was found in very few cases and only in acute ATL, whereas the vast majority of the Tax-1-positive cells expressed the viral protein both in the cytoplasm and nucleus. The fact that in acute ATL cases analyzed in this study Tax-1 was expressed in a considerable proportion of cells, although unexpected, may indeed support the idea that increased and/or sustained cell proliferation observed in the acute leukemic state is associated with a burst of Tax-1 expression, as recently proposed.[49,50] Furthermore, both in acute and in chronic ATL most of Tax-1-positive cells were also HBZ-positive suggesting a distinct behaviour with respect to what has been recently found in asymptomatic carriers and HAM/TSP patients in which HBZ and Tax-1 were very rarely found co-expressed in the same cells.[26,27] As stressed above, this may be correlated with the distinct replicative state of the cells in asymptomatic carriers and HAM/TSP patients as compared to leukemic patients.

In conclusion, the results presented in this study establish for the first time a correlation between modification of the subcellular localization of HBZ and acquisition of neoplastic state in subjects infected by HTLV-1. Future studies will be devoted to the clarification of the intimate molecular mechanisms that are at the basis of the cytoplasmic and nuclear retention of HBZ in HTLV-1-mediated leukemogenesis.

Disclosures

No conlicts of interest to disclose.

Contributions

GF and RSA conceived the experiments, performed data analysis, wrote and revised the manuscript; GF, MS, AT and IC performed the experiments; AM and OH provided ATL samples and reviewed the manuscript.

Funding

This study was supported by the University of Insubria "FAR 2018 and 2019" (to RSA and GF); by The Institutional Grant 2017, University of Insubria (to RSA); in part by the European Community FP7 Grant no. 602893 "Cancer Vaccine Development for Hepatocellular Carcinoma-HepaVAC" http://www.hepavac.eu (to RSA, and GF); by grants from the Institut National du Cancer (INCA), France (to OH and FM).

References

1. Poiesz BJ, Ruscetti FW, Gazdar AF, Bunn PA, Minna JD, Gallo RC. Detection and isolation of type C retrovirus particles from fresh and cultured lymphocytes of a patient with cutaneous T-cell lymphoma. Proc Natl Acad Sci U S A. 1980;77(12):7415-7419.
2. Gessain A, Vernant JC, Maurs L, et al. Antibodies to human T-lymphotropic virus type-1 in patients with tropical spastic paraparesis Lancet. 1985;326(8452):407-410.
3. Osame M, Usuku K, Izumo S, et al. HTLV-I associated myelopathy, a new clinical entity. Lancet. 1986;327(8488):1031-1032.
4. Gessain A, Cassar O. Epidemiological aspects and world distribution of HTLV-1 infection. Front Microbiol. 2012;3:388-388.
5. Pique C, Jones KS. Pathways of cell-cell transmission of HTLV-1. Front Microbiol. 2012;3:378.
6. Watanabe T. Adult T-cell leukemia: molecular basis for clonal expansion and transformation of HTLV-1-infected T cells. Blood. 2017;129(9):1071-1081.
7. Uchiyama T, Yodoi J, Sagawa K, Takatsuki K, Uchino H. Adult T-cell leukemia: clinical and hematologic features of 16 cases. Blood. 1977;50(3):481-492.
8. Shimoyama M, Group moTLS. Diagnostic criteria and classification of clinical subtypes of adult T-cell leukaemia-lymphoma. Br J Haematol. 1991;79(3):428-437.
9. Hermine O, Ramos JC, Tobinai K. A review of new findings in adult T-cell leukemia-lymphoma: a focus on current and emerging treatment strategies. Adv Ther. 2018;35(2):135-152.
10. Cook LB, Fuji S, Hermine O, et al. Revised Adult T-cell Leukemia-Lymphoma International Consensus Meeting Report. J Clin Oncol. 2019;37(8):677-687.
11. Kataoka K, Nagata Y, Kitanaka A, et al. Integrated molecular analysis of adult T cell leukemia/lymphoma. Nat Genet. 2015;47(11):1304-1315.
12. Rosewick N, Durkin K, Artesi M, et al. Cis-perturbation of cancer drivers by the HTLV-1/BLV proviruses is an early determinant of leukemogenesis. Nat Commun. 2017;8:15264.
13. Matsuoka M, Jeang K-T. Human T-cell leukaemia virus type 1 (HTLV-1) infectivity and cellular transformation. Nat Rev Cancer. 2007;7(4):270-280.
14. Hasegawa H, Sawa H, Lewis MJ, et al. Thymus-derived leukemia-lymphoma in mice transgenic for the Tax gene of human T-lymphotropic virus type I. Nat Med. 2006;12(4):466-472.
15. Satou Y, Yasunaga J-i, Zhao T, et al. HTLV-1 bZIP factor induces T-cell lymphoma and systemic inflammation in vivo. PLoS Pathog. 2011;7(2):e1001274.
16. Tanaka A, Takahashi C, Yamaoka S, Nosaka T, Maki M, Hatanaka M. Oncogenic transformation by the tax gene of human T-cell leukemia virus type I in vitro. Proc Natl Acad Sci U S A. 1990;87(3):1071-1075.
17. Grassmann R, Berchtold S, Radant I, et al. Role of human T-cell leukemia virus type 1 X region proteins in immortalization of primary human lymphocytes in culture. J Virol. 1992;66(7):4570-4575.
18. Grassmann R, Aboud M, Jeang K-T. Molecular mechanisms of cellular transformation by HTLV-1 Tax. Oncogene. 2005;24(39):5976-5985.
19. Takeda S, Maeda M, Morikawa S, et al. Genetic and epigenetic inactivation of tax gene in adult T-cell leukemia cells. Int J Cancer. 2004;109(4):559-567.
20. Taniguchi Y, Nosaka K, Yasunaga J-i, et al. Silencing of human T-cell leukemia virus type I gene transcription by epigenetic mechanisms. Retrovirology. 2005;2:64.
21. Jacobson S, Shida H, McFarlin DE, Fauci AS, Koenig S. Circulating CD8+ cytotoxic T lymphocytes specific for HTLV-I pX in patients with HTLV-I associated neurological disease. Nature. 1990;348(6298):245-248.
22. Kannagi M, Harada S, Maruyama I, et al. Predominant recognition of human T cell leukemia virus type I (HTLV-I) pX gene products by human CD8+ cytotoxic T cells directed against HTLV-I-infected cells. Int Immunol. 1991;3(8):761-767.
23. Gaudray G, Gachon F, Basbous J, Biard-Piechaczyk M, Devaux C, Mesnard J-M. The complementary strand of the human T-cell leukemia virus type 1 RNA genome encodes a bZIP transcription factor that down-regulates viral transcription. J Virol. 2002;76(24):12813-12822.
24. Usui T, Yanagihara K, Tsukasaki K, et al. Characteristic expression of HTLV-1 basic zipper factor (HBZ) transcripts in HTLV-1 provirus-positive cells. Retrovirology. 2008;5:34.
25. Satou Y, Yasunaga J-i, Yoshida M, Matsuoka M. HTLV-I basic leucine zipper factor gene mRNA supports proliferation of adult T cell leukemia cells. Proc Natl Acad Sci U S A. 2006;103(3):720-725.
26. Forlani G, Baratella M, Tedeschi A, Pique C,

Jacobson S, Accolla RS. HTLV-1 HBZ protein resides exclusively in the cytoplasm of infected cells in asymptomatic carriers and HAM/TSP patients. Front Microbiol. 2019;10:819.
27. Baratella M, Forlani G, Raval GU, et al. Cytoplasmic localization of HTLV-1 HBZ protein: a biomarker of HTLV-1-associated myelopathy/tropical spastic paraparesis (HAM/TSP). PLoS Negl Trop Dis. 2017;11(1):e0005285.
28. Baratella M, Forlani G, Accolla RS. HTLV-1 HBZ viral protein: a key player in HTLV-1 mediated diseases. Front Microbiol. 2017;8:2615.
29. Raval GU, Bidoia C, Forlani G, Tosi G, Gessain A, Accolla RS. Localization, quantification and interaction with host factors of endogenous HTLV-1 HBZ protein in infected cells and ATL. Retrovirology. 2015;12:59.
30. Hivin P, Frédéric M, Arpin-André C, et al. Nuclear localization of HTLV-I bZIP factor (HBZ) is mediated by three distinct motifs. J Cell Sci. 2005;118(7):1355-1362.
31. Hivin P, Basbous J, Raymond F, et al. The HBZ-SP1 isoform of human T-cell leukemia virus type I represses JunB activity by sequestration into nuclear bodies. Retrovirology. 2007;4:14.
32. Tosi G, Forlani G, Andresen V, et al. Major histocompatibility complex class II transactivator CIITA is a viral restriction factor that targets human T-cell lymphotropic virus type 1 Tax-1 function and inhibits viral replication. J Virol. 2011;85(20):10719-10729.
33. Forlani G, Abdallah R, Accolla RS, Tosi G. The major histocompatibility complex class II transactivator CIITA inhibits the persistent activation of NF-κB by the human T cell lymphotropic virus type 1 Tax-1 oncoprotein. J Virol. 2016;90(7):3708-3721.
34. Shirono K, Hattori T, Matsuoka M, Matsushita S, Asou N, Takatsuki K. Adult T cell leukemia cell lines that originated from primary leukemic clones also had a defect of expression of CD3-T cell receptor complex. Leukemia. 1988;2(11):728-733.
35. Suzushima H, Asou N, Hattori T, Takatsuki K. Adult T-cell leukemia derived from S100 beta positive double-negative (CD4- CD8-) T cells. Leuk Lymphoma. 1994;13(3-4):257-262.
36. Artesi M, Marçais A, Durkin K, et al. Monitoring molecular response in adult T-cell leukemia by high-throughput sequencing analysis of HTLV-1 clonality. Leukemia. 2017;31(11):2532-2535.
37. Cavanagh MH, Landry S, Audet B, et al. HTLV-I antisense transcripts initiating in the 3'LTR are alternatively spliced and polyadenylated. Retrovirology. 2006;3:15.
38. Murata K, Hayashibara T, Sugahara K, et al. A novel alternative splicing isoform of human T-cell leukemia virus type 1 bZIP factor (HBZ-SI) targets distinct subnuclear localization. J Virol. 2006;80(5):2495-2505.
39. Ossareh-Nazari B, Bachelerie F, Dargemont C. Evidence for a role of CRM1 in signal-mediated nuclear protein export. Science. 1997;278(5335):141-144.
40. Alefantis T, Flaig KE, Wigdahl B, Jain P. Interaction of HTLV-1 Tax protein with calreticulin: implications for Tax nuclear export and secretion. Biomed Pharmacother. 2007;61(4):194-200.
41. Zhao T, Yasunaga J, Satou Y, et al. Human T-cell leukemia virus type 1 bZIP factor selectively suppresses the classical pathway of NF-kappaB. Blood. 2009;113(12):2755-2764.
42. Zhi H, Yang L, Kuo YL, Ho YK, Shih HM, Giam CZ. NF-κB hyper-activation by HTLV-1 tax induces cellular senescence, but can be alleviated by the viral anti-sense protein HBZ. PLoS Pathog. 2011;7(4):e1002025.
43. Yamagishi M, Fujikawa D, Watanabe T, Uchimaru K. HTLV-1-mediated epigenetic pathway to adult T-cell leukemia–lymphoma. Front Microbiol. 2018;9:1686.
44. Ma G, Yasunaga J-I, Matsuoka M. Multifaceted functions and roles of HBZ in HTLV-1 pathogenesis. Retrovirology. 2016;13:16.
45. Giam C-Z, Semmes OJ. HTLV-1 Infection and adult T-cell leukemia/lymphoma - a tale of two proteins: Tax and HBZ. Viruses. 2016;8(6):161.
46. Matsuoka M, Mesnard J-M. HTLV-1 bZIP factor: the key viral gene for pathogenesis. Retrovirology. 2020;17(1):2.
47. Bazarbachi A, Suarez F, Fields P, Hermine O. How I treat adult T-cell leukemia/lymphoma. Blood. 2011;118(7):1736-1745.
48. Kinosada H, Yasunaga J-I, Shimura K, et al. HTLV-1 bZIP factor enhances T-cell proliferation by impeding the suppressive signaling of co-inhibitory receptors. PLoS Pathog. 2017;13(1):e1006120.
49. Mahgoub M, Yasunaga J-I, Iwami S, et al. Sporadic on/off switching of HTLV-1 Tax expression is crucial to maintain the whole population of virus-induced leukemic cells. Proc Natl Acad Sci U S A. 2018;115(6):e1269-e1278.
50. Billman MR, Rueda D, Bangham CRM. Single-cell heterogeneity and cell-cycle-related viral gene bursts in the human leukaemia virus HTLV-1. Wellcome Open Res. 2017;2:87.

Ferrata Storti Foundation

Haematologica 2021
Volume 106(8):2086-2094

Pediatric-inspired chemotherapy incorporating pegaspargase is safe and results in high rates of minimal residual disease negativity in adults up to the age of 60 years with Philadelphia chromosome-negative acute lymphoblastic leukemia

Mark B. Geyer,[1,2] Ellen K. Ritchie,[3] Arati V. Rao,[4] Shreya Vemuri,[5] Jessica Flynn,[6] Meier Hsu6, Sean M. Devlin,[6] Mikhail Roshal,[7] Qi Gao,[7] Madhulika Shukla,[1] Jose M. Salcedo,[1] Peter Maslak,[1] Martin S. Tallman,[1] Dan Douer[1] and Jae H. Park[1,2]

[1]Leukemia Service, Department of Medicine, Memorial Sloan Kettering Cancer Center, New York, NY; [2]Center for Cell Engineering, Department of Medicine, Memorial Sloan Kettering Cancer Center, New York, NY; [3]Weill Cornell Medical College, Hematology and Medical Oncology, Joan and Sanford I. Weill Department of Medicine, New York, NY; [4]Kite-A Gilead Company, Foster City, CA; [5]Sloan Kettering Institute, New York, NY; [6]Department of Epidemiology and Biostatistics, Memorial Sloan Kettering Cancer Center, New York, NY and [7]Department of Pathology, Memorial Sloan Kettering Cancer Center, New York, NY, USA

ABSTRACT

Administration of pediatric-inspired chemotherapy to adults up to age 60 with acute lymphoblastic leukemia (ALL) is challenging in part due to toxicities of asparaginase as well as myelosuppression. We conducted a multi-center phase II clinical trial (clinicaltrials gov. Identifier: NCT01920737) investigating a pediatric-inspired regimen, based on the augmented arm of the Children's Cancer Group 1882 protocol, incorporating six doses of pegaspargase 2,000 IU/m^2, rationally synchronized to avoid overlapping toxicity with other agents. We treated 39 adults aged 20-60 years (median age 38 years) with newly-diagnosed ALL (n=31) or lymphoblastic lymphoma (n=8). Grade 3-4 hyperbilirubinemia occurred frequently and at higher rates in patients aged 40-60 years (n=18) *versus* 18-39 years (n=21) (44% *vs*. 10%, *P*=0.025). However, eight of nine patients rechallenged with pegaspargase did not experience recurrent grade 3-4 hyperbilirubinemia. Grade 3-4 hypertriglyceridemia and hypofibrinogenemia were common (each 59%). Asparaginase activity at 7 days post-infusion reflected levels associated with adequate asparagine depletion, even among those with antibodies to pegaspargase. Complete response (CR)/CR with incomplete hematologic recovery was observed post-induction in 38 of 39 (97%) patients. Among patients with ALL, rates of minimal residual disease negativity by multi-parameter flow cytometry were 33% and 83% following induction phase I and phase II, respectively. Event-free and overall survival at 3 years (67.8% and 76.4%) compare favorably to outcomes observed in other series. These results demonstrate pegaspargase can be administered in the context of intensive multi-agent chemotherapy to adults aged ≤60 years with manageable toxicity. This regimen may serve as an effective backbone into which novel agents may be incorporated in future frontline studies. Trial registration: https://clinicaltrials.gov/ct2/show/NCT01920737

Correspondence:

JAE H. PARK
parkj6@mskcc.org

Received: March 23 2020.

Accepted: September 25, 2020.

Pre-published: October 13, 2020.

https://doi.org/10.3324/haematol.2020.251686

Introduction

Treatment of acute lymphoblastic leukemia (ALL) and lymphoblastic lymphoma (LBL) in children represents one of the greatest success stories in hematologic oncology and >85% of pediatric patients with ALL are ultimately cured.[1]

However, outcomes in adults have been less encouraging, with historical 5-year relative survival <45% and 5-year overall survival <50% among adults under the age of 60.[2,3] Several retrospective studies have suggested superior outcomes among adolescents and younger adults (AYA) treated on pediatric *versus* adult cooperative group studies[4-6] We and others have consequently investigated adapting pediatric ALL regimens for use in younger adults.[7-12] One large, prospective US intergroup phase II clinical trial (Cancer and Leukemia Group B [CALGB] 10403, in collaboration with the Eastern Cooperative Oncology Group and SWOG), treated 295 AYA aged 17-39 years with a true pediatric ALL regimen and observed 3-year event-free survival (EFS) of 59%, promising compared with historical controls.[13] However, successfully adapting pediatric ALL therapy for adults over the age of 40 presents additional challenges and the upper age limit for safe administration of pegaspargase is not clearly defined, due in part to increasing risk of asparaginase-related toxicities with increasing age.[8]

L-asparaginase, a bacterial enzyme depleting serum asparagine, was historically a standard component of ALL therapy in children and AYA. In contrast to most healthy cells, ALL/LBL cells lack asparagine synthetase and are thus dependent on exogenous asparagine and uniquely sensitive to asparaginase.[14] Randomized studies have demonstrated a survival benefit in pediatric patients treated with asparaginase-containing regimens.[15,16] However, asparaginase is associated with a host of toxicities, in part related to the above effects on protein synthesis, including hepatotoxicity, hypertriglyceridemia, hyperglycemia, hypofibrinogenemia, and thrombosis, as well as risks of hypersensitivity.[17] Pegaspargase consists of polyethylene glycol covalently bound to the enzyme and may be associated with decreased immunogenicity and rates of hypersensitivity reactions compared with native *E. coli* asparaginase, and has a considerably longer half-life.[18-20] Pegaspargase has been successfully incorporated into frontline treatment of pediatric patients and younger adults with ALL.[7,19,21,22]

We previously reported our experience utilizing a regimen incorporating two courses of induction chemotherapy and six doses of pegaspargase 2,000 IU/m^2 at ≥4-week intervals, sequenced to avoid overlapping hepatotoxicity with other agents in adults with newly-diagnosed ALL/LBL.[7] We subsequently modified this regimen to exclude two myelosuppressive courses of consolidation and incorporated serial monitoring of minimal residual disease (also known as "measurable residual disease," MRD). Additional changes herein included higher doses of methotrexate (MTX, 3.5 g/m^2 *vs.* 1 g/m^2 for B-ALL/LBL; 5 g/m^2 *vs*. 2.5 g/m^2 for T-ALL/LBL) to reflect institutional experience that MTX doses ≥3.5 g/m^2 are sufficient to treat lymphomatous leptomeningeal and brain involvement independent of intrathecal MTX, and as T lymphoblasts require a higher MTX dose to achieve optimal MTX/MTX-polyglutamate concentrations.[23-25] Maintenance chemotherapy was extended from 2 to 3 years for all patients, as 3-year maintenance is commonly used for boys treated on pediatric protocols and adults broadly exhibit higher rates of relapse than children.[26,27] Pegaspargase dose was uncapped, consistent with the prior study although capping at 3,750 IU/m^2 was reported by others in an attempt to reduce toxicity.[7,28] Herein, we present results of a phase II multi-center trial investigating this approach in adults up to the age of 60 years with newly-diagnosed Philadelphia chromosome-negative (Ph-negative) ALL/LBL.

Methods

Clinical trial

From August 2014 to July 2017, patients with newly-diagnosed, previously untreated Ph-negative precursor B-cell or T-cell ALL/LBL, aged 18-60 years, were enrolled at participating centers (see the *Online Supplementary Methods* for eligibility criteria and study design). Forty-three patients signed informed consent; four were determined ineligible prior to beginning treatment (Ph-positive, n=2; mixed phenotype acute leukemia, n=2) and 39 patients received treatment on protocol.

The primary objective of the study was to determine rates of MRD negativity following induction phase I (Table 1). Secondary objectives including assessing rates of MRD negativity following induction phase II, rates of complete response (CR), overall survival (OS), event-free survival (EFS), disease-free survival (DFS), and pegaspargase toxicities.

Toxicities were graded using National Cancer Institute Common Terminology Criteria for Adverse Events (CTCAE) v4.03.

Regimen design

Study regimen details are summarized in Table 1. Treatment was adapted from the augmented arm of the Children's Cancer Group 1882 protocol, with substitution of pegaspargase for native *E. coli* asparaginase and use of high-dose MTX (HD-MTX) intensification *versus* escalating (Capizzi) MTX,[27] as previously reported.[7] Pegaspargase was given after the second dose of HD-MTX in intensification I/II, and only after leucovorin rescue began. The protocol was approved by the Institutional Review Boards of all participating institutions.

Pegaspargase 2,000 IU/m^2 IV (not capped) was administered over 1-2 hours at ≥4-week intervals. Hydrocortisone 100 mg intravenous (IV) was given prior to each dose and 1-2 weeks of corticosteroids followed each dose for hypersensitivity prophylaxis (Table 1). A specific pegaspargase toxicity management guideline was adopted; asparaginase enzyme activity and anti-asparaginase antibodies were measured at pre-specified time points (see the *Online Supplementary Methods* and the *Online Supplementary Table S1*).

Minimal residual disease assessment

MRD was assessed centrally in bone marrow (BM) aspirate samples using multiparameter flow cytometry (FACS) with sensitivity of at least 10^{-4}. Any unequivocal evidence of residual ALL by FACS was considered as MRD positivity, even if <0.01% of BM mononuclear cells (see the Online Supplementary Methods; *Online Supplementary Table S2*; *Online Supplementary Figure S1*).

Statistical analyses

Incidence of grade 3-4 toxicities was compared between groups by age, sex, and BMI using Fisher's exact test. OS, EFS, and DFS were computed using the Kaplan-Meier method and compared between groups using log-rank tests. EFS was defined as time from initiation of protocol therapy until date of morphologic relapse, confirmed refractory disease, or death from any cause; patients not known to have any of these events were censored on date of last follow-up. OS was defined as time from start of protocol therapy to death from any cause, with surviving patients censored at last follow-up. Among patients achieving CR/CRi,

DFS was defined as time from post-induction I or II disease assessment until morphologic relapse or death; patients without any of these events were censored on date of last follow-up. In order to compare OS between patients undergoing *versus* not undergoing allogeneic hematopoietic cell transplantation (alloHCT) in CR1, OS was measured from date of first confirmed CR. Statistical analyses were performed in R v3.5.0. A 2-sided *P*-value <0.05 was considered significant.

Results

Patients characteristics

Demographic and clinical characteristics of treated patients are summarized in Table 2. Of the 39 patients, 30 (77%) were men. Median age at the start of treatment was 38.7 years (range, 20.2-60.4 years); 18 (46%) patients were 40-60 years old. Lineage was B cell in 27 (69%) patients (ALL, n=24; LBL, n=3) and T cell in 12 patients (ALL, n=7; LBL, n=5). Three patients had central nervous system (CNS)-2/3 cerebrospinal fluid (n=2) or parenchymal brain involvement (n=1) and 16 had extramedullary disease at diagnosis. Five of 12 patients with T-cell ALL/LBL demonstrated early T-precursor phenotype as previously defined.[29] Cytogenetic findings associated with unfavorable risk (per classification used in the CALGB 19802 study; *Online Supplementary Table S3*) were observed in five patients (11q23 rearrangement, n=2; trisomy 8, n=2; monosomy 7, n=1). Among 11 patients with B-ALL/LBL who underwent evaluation for fusions/re-arrangements characteristic of Philadelphia chromosome-like ("Ph-like") ALL (see the *Online Supplementary Methods*), only one case was identified (FIP1L1-PDGFRA fusion).

Clinical responses

Thirty-eight of 39 (97%) patients achieved CR or CR with incomplete hematologic recovery (CRi) by the conclusion of induction II. Following induction I, 36 of 38 (95%) of evaluable patients were in CR/CRi. Of the two patients who were not in CR/CRi, both had T-cell ALL;

Table 1. Treatment regimen.

Regimen Block	Agent	Dose	Route	Days
Induction Phase I	Daunorubicin	60 mg/m^2	IV push	1,2,3
	Vincristine	1.4 mg/m^2 (cap 2 mg)	IVPB/IV push	1,8,15,22
	Pegaspargase	2,000 U/m^2	IVPB over 1-2h	15
	Prednisone	60 mg/m^2	PO	1-28
	Methotrexate	12 mg	IT	8,15
	Hydrocortisone	25 mg	IT	8.15
Induction Phase II	Cyclophosphamide	1 g/m	IVPB	1,29
	Cytarabine	75 mg/m^2	IVPB	1-4,8-11,29-32,36-39
	Mercaptopurine	60 mg/m^2	PO	1-14,29-42
	Vincristine	1.4 mg/m^2 (cap 2 mg)	IVPB/IV push	1,15,29,43
	Pegaspargase	2,000 U/m^2	IVPB over 1-2h	15
	Prednisone	20 mg	PO	15-22
	Methotrexate	12 mg	IT	1,15,29,43
	Hydrocortisone2	25 mg	IT	1,15,29,43
Intensification I	Methotrexate	3.5 g/m^2 (B-cell)	IVPB over 3h	1,15
		5 g/m^2 (T-cell)	IVPB over 3h	1,15
	Leucovorin*	25 mg	IVPB q6h	24h from start of MTX
	Pegaspargase	2,000 U/m^2	IVPB over 1-2h	16 or 17
	Prednisone	20 mg	PO	15-22
Re-induction I	Daunorubicin	25 mg/m^2	IV push	1,8,15
	Vincristine	1.4 mg/m^2 (cap 2 mg)	IVPB/IV push	1,8,15,29,43
	Pegaspargase	2,000 U/m^2	IVPB over 1-2h	15
	Dexamethasone	10 mg/m^2	PO	15-22,29-36
	Methotrexate	12 mg	IT	1,8,29
	Hydrocortisone	25 mg	IT	1,8,29
	Cyclophosphamide	1 g/m^2	IVPB	29
	Cytarabine	75 mg/m^2	IVPB	29-32,36-39
	Thioguanine	60 mg/m^2	PO	29-42
Intensification II	Same as intensification I			
Re-induction II	Same as re-induction I			
Maintenance (Monthly for 36 months total)	Prednisone	60 mg/m^2	PO	1-5 (q mon, mon. 1-12; q2 mon, mon. 13-24)
	Vincristine	1.4 mg/m^2 (cap 2 mg)	IV	1 (q mon, mon. 1-12; q2 mon, mon. 13-36)
	Methotrexate	10 mg/m^2	PO	1,8,15,22 (held on days of IT MTX)
	Mercaptopurine	60 mg/m^2	PO	1-28, daily
	Methotrexate	12 mg	IT	1 (q3 mon, mon. 1-12)
	Hydrocortisone	25 mg	IT	1 (q3 mon, mon. 1-12)

*Leucovorin rescue following the day 15 dose of high-dose methotrexate was started prior to administration of pegaspargase. IVPB: intravenous piggy back; PO: by mouth; IT: intrathecal; MTX: methotrexate, mon: month; cap: capped; q2: calender quarter 2 (April, May, and June); q3: calender quarter 3 (July, August, and Septembe).

one continued protocol therapy and achieved CR following induction II and the other was removed from study after induction I at the discretion of the investigator to pursue alternative therapy (representing the single patient who did not achieve CR/CRi on study). One patient was not evaluable for response post-induction I due to incomplete restaging; this patient continued protocol therapy and was confirmed to be in CR following induction II. No patients died during induction I or II.

Central evaluation for MRD in BM was performed in 26 of 31 patients with ALL (i.e., not LBL) on day 15 of induction I; at that time, five of 26 (19%) of patients had achieved MRD negativity. The proportion of patients with ALL exhibiting BM MRD negativity on central review increased following induction I (nine of 27, 33%) and induction II (20 of 24, 83%). Patients with LBL and low-level BM involvement at diagnosis are not included in the aforementioned analysis. However, four of four patients with low-level BM involvement by LBL exhibited MRD negativity in the BM on day 15 of induction I. Local MRD data are summarized in the *Online Supplementary Results*.

Table 2. Patient demographics and clinical characteristics.

Characteristic	All Patients (N=39)		Aged 40-60 years (N=18)	
	N	%	N	%
Age at start of induction, years				
Median	38.7	50.9		
Range	20.2-60.4	43.6-60.4		
Sex				
Male	30	77	14	78
Female	9	23	4	22
Lineage and presentation				
B cell	27	69	12	67
B-cell ALL	24	62	12	67
B-cell LBL	3	8	0	0
T cell	12	31	6	33
T-cell ALL	7	18	3	17
T-cell LBL	5	13	3	17
ETP immunophenotype	5	13	2	11
Non-ETP	6	15	4	22
ETP status indeterminate	1	3	0	0
Cytogenetics				
Unfavorable	5	13	3	17
Intermediate	9	23	3	17
Favorable	2	5	0	0
Not prognostically classified	8	21	4	22
Not evaluable	15	38	8	44
ALL subgroup only				
Unfavorable	5	13	3	17
Intermediate	4	10	1	6
Favorable	2	5	0	0
Not prognostically classified	7	18	4	22
Not evaluable	13	33	7	39
CNS disease (CNS-2/3 CSF or parenchymal brain involvement) at diagnosis				
Yes	3	8	0	0
No	36	92	18	100
Unequivocal extramedullary disease at diagnosis				
Yes	16	41	7	39
No	23	59	11	61
Pegaspargase doses received				
Median	3		2	
Range	1-6		1-6	
AlloHCT in CR1*				
Yes	11	28	3	17
No	28	72	15	83

*Includes patients known to have undergone allogeneic hematopoietic cell transplantation (alloHCT) in first complete response. ALL: acute lymphoblastic leukemia; LBL: lymphoblastic lymphoma; ETP: early T-precursor phenotype (CD1a-, CD8-, CD5dim/-, with expression of one or more stem cell or myeloid antigens, e.g., CD11b, CD13, CD33, CD34, CD117, HLA-DR); cytogenetic risk group classification per criteria used in the CALGB 19802 study, are summarized in the *Online Supplementary Table S3*; CNS: central nervous system; CSF: cerebrospinal fluid.

Pegaspargase administration, enzymatic activity, and immunogenicity

All treated patients received at least one dose of pegaspargase, and the median number of doses received was three (range, 1-6). Reasons for receipt of <6 total doses of pegaspargase are summarized in the *Online Supplementary Table S4*. Asparaginase enzymatic activity as measured 7 days post-pegaspargase is summarized in *Online Supplementary Table S3*. All activity levels obtained 7 days following a full dose of pegaspargase (i.e., excluding those with immediate hypersensitivity) were >0.1 IU/mL (minimum observed level 0.34 IU/mL). In two patients with immediate hypersensitivity to pegaspargase who received 5 and 15 minutes of the infusion, activity levels 7 days post-pegaspargase were <0.013 and 0.028 IU/mL, respectively. Enzymatic activity appeared similar in patients ageg 40-60 years *versus* 18-39 years (*Online Supplementary Table S5*).

In 19 patients, 75 plasma samples were screened for antibodies specific to Oncaspar® and polyethylene glycol (PEG; see the *Online Supplementary Methods*). Inhibition with Oncaspar® showed ten confirmed positive samples and specific inhibition with 5 kDa PEG showed six confirmed positive samples; these confirmed results were from four patients and are summarized in the *Online Supplementary Table S6*. Despite the presence of antibodies, asparaginase activity levels were >0.1 IU/mL (minimum 0.34 IU/mL) 7 days post-pegaspargase in all instances in which the full dose of pegaspargase was administered (i.e., not terminated early due to hypersensitivity).

Pegaspargase toxicity

Selected grade 3-4 toxicities of pegaspargase in all patients and in those aged 40-60 years at treatment initiation are summarized in the *Online Supplementary Table S4*. Grade 3-4 hypofibrinogenemia and hypertriglyc-

Table 3. Serum asparaginase enzymatic activity post-polyethylene glycol.

Time point in treatment	Samples (N)	Serum asparaginase enzymatic activity 7 days post-PEG (IU/mL)	
		Mean	SD
Induction I	15	0.787	0.238
Induction Phase II	14	0.881	0.234
Intensification I	6	0.989	0.149
Re-induction I	7	0.852	0.238
Intensification II	10	1.057	0.190
Re-induction II	7	1.087	0.145
All Phases	59	0.919	0.233

PEG: polyethylene glycol; SD: standard deviation.

eridemia were common (each observed in 59% of patients). Grade 3-4 hyperbilirubinemia was significantly more common in patients aged 40-60 years *versus* 18-39 years (44% *vs*. 10%, *P*=0.025); a non-significant trend toward greater risk of grade 3-4 hyperbilirubinemia was observed in patients with body mass index (BMI) ≥30 *versus* <30 kg/m^2 at treatment initiation (50% *vs.* 17%, *P*=0.087). Incidence of grade 3-4 transaminitis, hypertriglyceridemia, hyperglycemia, hypofibrinogenemia, pancreatitis, and thromboembolic events otherwise did not significantly differ by age (18-39 years *vs*. 40-60 years), BMI (≥30 kg/m^2 *vs.* <30 kg/m^2), or sex.

Nine of the ten patients experiencing grade 3-4 hyperbilirubinemia following pegaspargase during induction I resumed pegaspargase at the dose and schedule per protocol; eight of nine patients resuming pegaspargase did not experience recurrent grade 3-4 hyperbilirubinemia. In four patients, *Erwinia* asparaginase was substituted for pegaspargase due to hypersensitivity associated with pegaspargase infusion.

Other non-hematologic adverse events and febrile neutropenia definitely, probably, or possibly related to protocol therapy are detailed in the *Online Supplementary Table S7*. Association of pegaspargase with treatment delays is summarized in the *Online Supplementary Results*.

Subsequent therapy and relapse

The patient with T-ALL who was withdrawn from study after exhibiting persistent disease following induction I received second-line chemotherapy off-protocol with nelarabine, etoposide, and cyclophosphamide, and subsequently underwent alloHCT. Ten additional patients receiving protocol therapy underwent alloHCT in CR1. Rationale for alloHCT in CR1 was as follows: persistent MRD following course II of induction (n=3), Ph-like ALL (n=1), unfavorable cytogenetic features including t(4;11) (n=1) or evidence of clonal evolution (n=1), or physician preference (n=4).

Of 38 patients achieving CR/CRi on protocol, ten subsequently experienced relapse (BM, n=4; CNS only, n=2; combined BM and CNS, n=1; combined BM and other extramedullary sites, n=1; testis, n=1; cortical bone, n=1); median time to relapse from start of therapy was 15.4 months (range, 5.4-40.4) in these ten patients. Six patients underwent alloHCT following relapse, including one patient who had relapsed following first alloHCT in CR1.

Survival outcomes

Two patients died in CR1 during re-induction I due to complications of sepsis (n=1) or multi-organ system failure (n=1), aged 55 and 47 years, respectively, at the time of death. At median follow-up of 38.6 months among surviving patients (range, 1.8-57.8), 3-year OS is 76.4% (95% Confidence Interval [CI]: 63.3-92.3) and 3-year EFS is 67.8% (95% CI: 53.4-86.0), as summarized in Figure 1A and B. Three-year cumulative incidence of relapse (CIR, with death in CR as competing event) is 25.3% (95% CI: 11.4-42.0). Superior OS and EFS were observed among patients aged 18-39 years *versus* 40-60 years at the start of therapy (3-year OS: 88.2 *vs*. 61.9%, *P*=0.03 and 3-year EFS: 85.0% *vs*. 48.6%, *P*=0.05, respectively, Figure 1C and D). OS and EFS did not differ significantly with respect to B-cell *versus* T-cell lineage (3-year OS: 78.7% *vs.* 71.6%, *P*=0.8, and 3-year EFS: 71.8% *vs*. 58.7%, *P*=0.7, respectively). In this small study, significant differences were not observed in OS, DFS, or CIR between the 10 patients undergoing alloHCT after achieving CR1 with protocol therapy and the 27 evaluable patients not undergoing alloHCT in CR1 (3-year OS: 100% *vs*. 70.7%, *P*=0.3; 3-year DFS: 88.9% *vs*. 62.5%, *P*=0.09; 3-year CIR: 11.1% *vs*. 29.8%, *P*=0.197).

Among the patients with ALL achieving MRD-negative CR *versus* MRD-positive CR/CRi (central review) following induction 1, there was no difference in OS or DFS measured from time of post-induction I disease assessment (3-year OS: 75.0% *vs*. 80.8%, *P*=0.8, and 3-year DFS: 75.0% *vs*. 68.8%, *P*=0.5). Twelve patients with ALL who were in MRD-positive CR/CRi following induction I subsequently achieved MRD negativity following induction II (MRD converter group) and seven patients with ALL were confirmed to be in MRD-negative CR following both induction I and induction II (early MRD negativity group). The MRD converter and early MRD negativity groups achieved 3-year DFS 56.2% and 71.4%, respectively, *P*=0.7, and 3-year OS 90.9% and 71.4%, *P*=0.5, respectively, as measured from time of post-induction II disease assessment. The small number of patients with MRD positivity post-induction II (n=4) also precludes meaningful comparison of this group with those exhibiting MRD negativity post-induction II; these patients are described in the *Online Supplementary Table S8*. All patients with MRD positivity post-induction II underwent alloHCT (CR1, n=3; CR2, n=1) following subsequent therapy and three are in ongoing CR.

Table 4. Selected grade 3-4 toxicities possibly, probably, or definitely attributed to pegaspargase.

Toxicity	All patients (N=39)						Patients aged 40-60 years (N=18)					
	Grade 3		Grade 4		Total Grade 3-4		Grade 3		Grade 4		Total Grade 3-4	
	N	%	N	%	N	%	N	%	N	%	N	%
Hypofibrinogenemia	21	54	2	5	23	59	10	56	0	0	10	56
Hypertriglyceridemia	11	28	12	31	23	59	4	22	6	33	10	56
Transaminitis	15	38	1	3	16	41	9	50	1	6	10	56
Hyperglycemia	8	21	4	10	12	31	4	22	2	11	6	33
Hyperbilirubinemia	5	13	5	13	10	26	3	17	5	28	8	44
Pancreatitis	1	3	0	0	1	3	0	0	0	0	0	0
Thromboembolic events	1	3	0	0	1	3	1	6	0	0	1	6

ALL: acute lymphoblastic leukemia.

Discussion

In this phase II study, we sought to improve the toxicity profile of the regimen investigated at the University of Southern California (USC) and previously reported by members of our group, and to define rates of MRD negativity associated with this approach.[7] Specifically, we omitted two intensely myelosuppressive courses of consolidation (cytarabine/teniposide) and incorporated standardized post-pegaspargase laboratory monitoring to enhance the safety of this regimen, particularly for adults over the age of 40 years. We observed no deaths during induction chemotherapy and toxicities of pegaspargase were manageable, albeit common, in patients up to the age of 60 years as subsequently discussed. Removal of the cytarabine/teniposide consolidation blocks did not appear to result in inferior outcomes compared with our prior experience.[7] However, two patients died during post-remission therapy, underscoring the Re-induction blocks' associated risks of myelosuppression. Incidence of febrile neutropenia (ten patients, 26%) herein was comparable to other pediatric regimens[10,13] though not reported directly with the USC regimen. Further follow-up will be needed to assess whether longer duration of maintenance chemotherapy will be associated with lower risk of late relapse. Despite incorporation of higher-dose MTX in the updated regimen and 16 doses of intrathecal MTX given throughout treatment in both regimens, three patients experienced CNS relapse (isolated or with marrow relapse). Neither this regimen nor its USC predecessor incorporated cranial radiation; further follow-up and clinical experience will clarify long-term rates of CNS relapse associated with this regimen. This study also provides further data on kinetics of MRD clearance in adults over the age of 40 treated with a pediatric-inspired regimen, whereas much of the existing MRD data utilizing similar regimens reflects treatment of children, adolescents, and younger adults. OS and EFS compare favorably to outcomes historically observed in adults with ALL/LBL.

Others have also investigated incorporation of pegaspargase into frontline treatment paradigms for adults with ALL. The UK National Cancer Research Institute UKALL14 trial evaluated pegaspargase 1,000 IU/m^2 given on days 4 and 18 in combination with daunorubicin, vincristine, and dexamethasone, ± rituximab (B-cell ALL) and imatinib (Ph-positive), in patients aged 25-65 years with newly-diagnosed ALL.[8] However, 16 of 90 patients succumbed to treatment-related mortality during induction, with 11 deaths related to hepatotoxicity ± infection and associated with grade 3-4 hyperbilirubinemia in nine patients. However, while patients with Ph+ ALL accounted for only 29% of study participants, those with Ph+ ALL accounted for 11 of 16 deaths during induction and

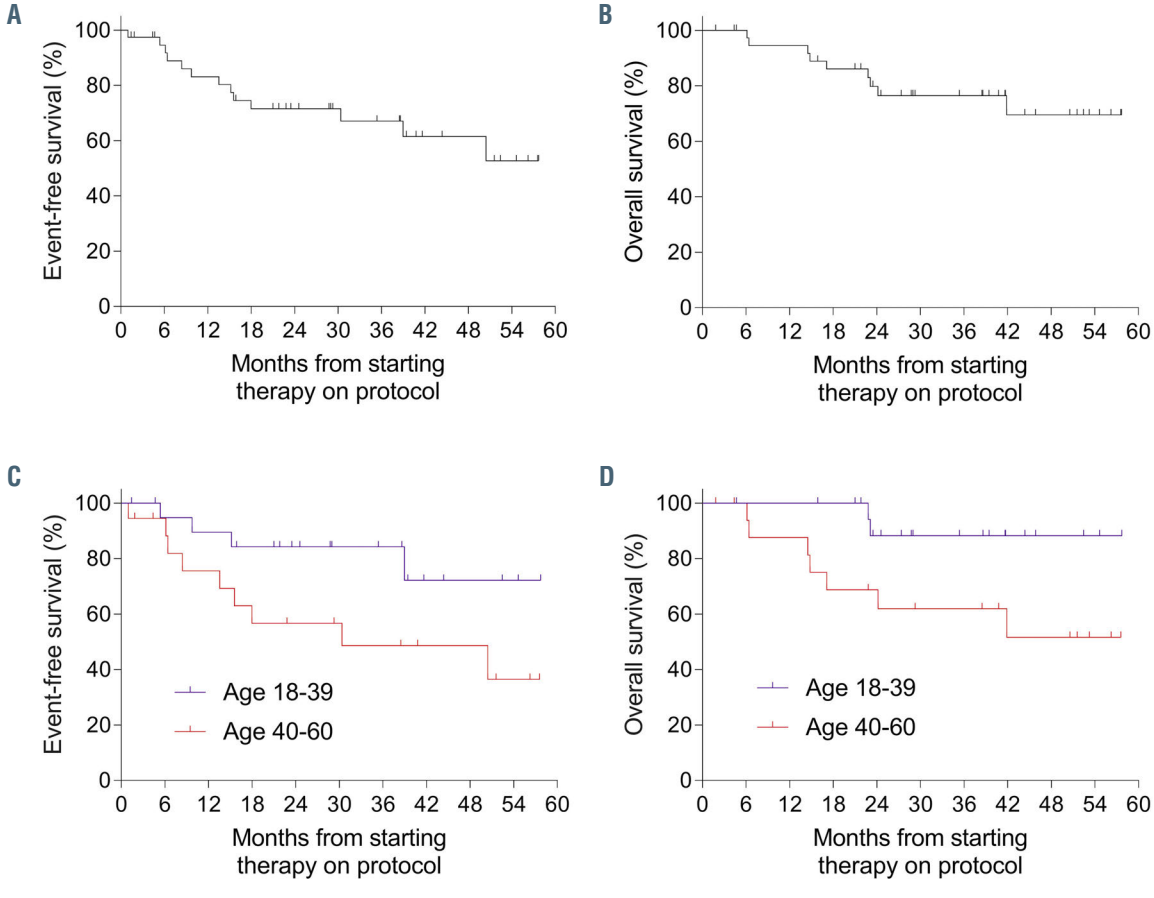

Figure 1. Survival outcomes among treated patients. (A) Event-free survival (EFS) (freedom from morphologic relapse, removal from study for refractory disease, or death) and (B) overall survival (OS) among all treated patients. (C) EFS and (D) OS among patients aged 18-39 years *vs*. 40-60 years at initiation of therapy (P=0.06 and P=0.03, respectively).

seven of 11 hepatotoxicity-associated deaths (OR 8.65, $P<0.001$). UKALL14 data suggest the combination of imatinib and pegaspargase may have been particularly toxic, though similarly severe toxicity was not observed in patients with Ph+ ALL receiving imatinib in combination with the USC regimen.[7] In contrast, our study did not include patients with Ph+ ALL. Additionally, use of pegaspargase 1,000 IU/m^2 on days 4 and 18 of induction (*vs*. 2,000 IU/m^2 on day 15 in this regimen) may have resulted in different duration of asparagine depletion, and in the context of the UKALL14 regimen, weekly dosing of daunorubicin 60 mg/m^2 (*vs*. 60 mg/m^2 days 1-3 in this regimen) may have led to greater overlap of hepatoxicity from pegaspargase and intense myelosuppression from the anthracycline. Similarly, patients aged 46-60 years *versus* 15-45 years treated on the GRAALL-2003 study tended to have higher rates of grade 3-4 hepatotoxicity during induction (28% *vs.* 18%), received significantly lower median cumulative dose of L-asparaginase during induction (36,000 IU/m^2 *vs.* 48,000 IU/m^2) and post-remission (29,000 IU/m^2 *vs*. 81,000 IU/m^2), experienced delays in consolidation initiation, and exhibited significantly increased risk of death during induction (13% *vs.* 4%) and cumulative incidence of death in first CR (15% *vs*. 2%).[9] Administration of cyclophosphamide and daunorubicin in proximity to L-asparaginase during induction with the GRAALL-2003 regimen may also have contributed to toxicity. Like other series, toxicities associated with pegaspargase were common in our study, and grade 3-4 hyperbilirubinemia was observed more commonly in patients aged 40-60 years *versus* 18-39 years, albeit without evidence of acute liver failure or long-term hepatic morbidity. Notably, nearly all patients experiencing grade 3-4 hyperbilirubinemia were able to be re-challenged with the drug without recurrent severe toxicity, suggesting that a single episode of grade 3-4 hyperbilirubinemia does not necessitate pegaspargase discontinuation in adults with ALL, even in patients aged 40-60 years. We observed no deaths during induction chemotherapy, though two patients aged 40-60 years ultimately died in CR1 during post-remission therapy. The rate of thrombosis was low (3%), perhaps due in part to chance as routine antithrombotic prophylaxis was not used (*Online Supplementary Table S1*); the USC regimen was associated with a 16% incidence of deep vein thrombosis, similar to other pediatric regimens studied in this age group.[7,10] Our restrictive approach to fibrinogen repletion (<50 mg/dL or bleeding) may have limited thrombotic risk as well, consistent with other recent reports.[30] This regimen may serve as an effective option for patients aged 40-60 years, particularly for patients for whom an asparaginase-containing regimen may be especially desirable (e.g. T-ALL/LBL).[15,31,32]

Asparaginase activity levels measured at 7 days following a full dose of pegaspargase were uniformly in the range associated with asparagine depletion (>0.1 IU/mL, with minimum observed level 0.34 IU/mL herein) across all age groups. Mean asparaginase activity at 7 days post-dose was 0.601 IU/mL in our prior pharmacokinetic study of pegaspargase 2,000 IU/m^2 during remission induction for younger adults with ALL, and in that series, 12 of 12 and nine of 11 patients exhibited asparagine depletion at 14 and 20 of 21 days post-pegaspargase, respectively.[33] In this study, mean asparaginase activity at 7 days was 0.919 IU/mL (Table 3), suggesting at least similarly robust asparagine depletion, though activity levels were not directly measured at 14 and 21 days post-dose. Of note, even in patients developing antibodies to pegaspargase, there was no evidence of silent inactivation, providing some reassurance against this phenomenon as a major mechanism of therapeutic resistance in the enrolled patients, despite prophylactic administration of hydrocortisone to all patients. Absence of silent inactivation further suggests routine monitoring of asparaginase activity following each pegaspargase may not be essential. Whether pegaspargase doses <2,000 IU/m^2 might achieve similar enzymatic activity levels and asparagine depletion within the context of this regimen, while leading to lower rates of severe toxicity, remains unclear. However, among patients treated on the GMALL07/2003 protocol, pegaspargase doses of 1,000 IU/m^2 or 2,000 IU/m^2 resulted in asparaginase activity targets achieved in 96% and 98% of patients in the second week post-dose, and 73 and 89% in the third week post-dose, respectively.[34]

As noted previously, CALGB 10403 demonstrated the safety and efficacy of a true pediatric regimen in patients up to the age of 39 years and is currently considered one of several standard-of-care options for AYAs with newly-diagnosed ALL/LBL.[13] The regimen herein differs from the CALGB 10403 treatment plan in incorporating a two-phase induction (with induction II bearing similarities to the consolidation phase of CALGB 10403), HD-MTX *versus* standard escalating ("Capizzi") MTX, two sequential intensification/re-induction blocks of therapy (*vs*. one block of interim maintenance and one block of delayed re-induction), 3-years of maintenance chemotherapy for all patients (*vs*. a shorter 2-year maintenance period for women), a pegaspargase dose of 2,000 IU/m^2 *versus* 2,500 IU/m2, and six total doses *versus* seven total doses of pegaspargase. While it is challenging to compare clinical results directly given differences in trial size, follow-up time, ages of patients enrolled (17-39 years *vs*. 18-60 years) and period during which patients were enrolled (2007-2012, CALGB 10403 *vs.* 2014-2017, study herein), the 3-year EFS observed herein (68% among all patients and 85% among patients aged 18-39 years *vs*. 59% on CALGB 10403) is encouraging. Long-term follow-up to assess durability of responses observed in this study will further inform interpretation of these results.

Most patients with ALL (83%) treated on this study exhibited MRD negativity by FACS following induction II. While achievement of MRD negativity following induction I herein did not predict superior long-term DFS and OS among patients with ALL, this study was not powered to perform such a comparison. Other studies have reported a significant difference in DFS/OS among patients achieving MRD negativity by one of several methods at the conclusion of induction phase I.[13,35] The small number of patients with MRD positivity post-induction II does not allow for formal comparison of this group of patients with those who exhibited MRD negativity post-induction II, and alloHCT was favored for patients with MRD positivity post-induction II. It remains unclear whether those patients achieving MRD negativity following two courses (*vs*. one course) of induction therapy using this approach have inferior long-term disease control or would benefit from earlier introduction of novel agents (e.g., blinatumomab for B-cell ALL), intensified chemotherapy (high-dose cytarabine, nelarabine), or alloHCT in CR1. Inotuzumab ozogamicin and blinatumomab are actively being investigated as

components of frontline therapy for B-cell ALL/LBL and may facilitate faster achievement of MRD negativity.[36,37] Incorporating other new agents, such as venetoclax, into this therapeutic backbone may further enhance efficacy and increase rates of MRD negativity post-induction I.

This study has several limitations, foremost being its small size. Samples for central MRD review were available for most, but not all patients, and local MRD was not considered in the primary analysis herein. While standardized criteria for pegaspargase toxicity monitoring and management were provided, institutional practices in this multi-center study likely varied slightly nonetheless. During the conduct of this study, comprehensive genomic profiling of ALL at time of diagnosis, including assessment for targetable alterations characteristic of "Ph-like" ALL, became more common practice.[38] Such profiling was performed inconsistently in the course of this study, limiting our ability to define the incidence of Ph-like ALL or overall mutational landscape in this cohort. While FACS is a powerful tool for MRD assessment with rapid results, monitoring for the malignant clonal T-cell receptor or immunoglobulin heavy chain re-arrangement by next-generation sequencing may have provided even more sensitive detection of MRD. Finally, long-term follow-up remains limited.

In summary, a pediatric-inspired regimen including pegaspargase 2,000 IU/m^2 in each of six blocks of intensive therapy, timed to avoid overlapping toxicities, and omitting two myelosuppressive courses of consolidation, resulted in manageable toxicity, high rates of MRD negativity following two-phase induction, and promising long-term efficacy in adults up to aged 60 years with newly-diagnosed ALL/LBL. The addition of active novel agents to such a regimen may increase rates of early MRD negativity and reduce rates of relapse.

Disclosures

MBG has received research support from Amgen; EKR sits on the advisory board of Agios, Celegne, Genetech, Pfizer and Tolero, has received travel support from Celgene, Novartis and Pfizer, has received research funding from Bristol-Myers Squibb, NS Pharma, Jazz Pharmaceuticals, Novartis, Astellas and Pfizer, consults for Celgene, Novartis, Pfizer and Incyte, is part of the speakers' bureau of Pfizer, Novartis, Incyte and Ariad; AVR is employed by Kite; DD consults for Servier Pharmaceuticals and Amgen, is part of the speakers' bureau of Servier Pharmaceuticals, Amgen and Adaptive Biotech, and consults for Servier Pharmaceuticals and Amgen; MST sits on the advisory board of Daiichi, Oncolyze, Tetraphase, Jazz Pharmaceuticals, Rigel, KAHR, Abbvie, Nohla, Orsenix, Delta Fly Pharma, BioLineRx and Roche, has received research funding from Cellerant, Biosight, ADC Therapeutics and Abbvie, has patents and royalties at UpToDate, and consults for Daiichi-Sankyo, Oncolyze, Tetraphase, Jazz Pharmaceuticals, Rigel, KAHR, Abbvie, Nohla, Orsenix, Delta Fly Pharma and BioLineRx; JHP has received research funding from Juno Therapeutics and Genentech/Roche, has a consultancy advisory role at Amgen and Juno Therapeutics, and consults for Kite, Incyte, GSK, Autolus, AstraZeneca, Allogene, Novartis, Takeda, Servier and Intellia.

Contributions

MBG performed the research, including providing care for patients enrolled to the study, analyzed the results, and wrote the paper; EKR, AVR and PM performed the research, including providing care for patients enrolled to the study; SV, MS, and JMS gathered and managed the data; MR and QG performed the research and analyzed the results; JF, MH and SMD analyzed the results; MST, DD and JHP designed and performed the research, including providing care for patients enrolled to the study, analyzed the results, and wrote the paper. All authors critically reviewed the paper.

Acknowledgments

The authors thank Jessica Wardrope for assistance with organizing and compiling the centralized flow cytometric minimal residual disease analysis reports and thank Dr. Michael Borowitz for providing details of the Johns Hopkins University flow cytometric minimal residual disease analysis methods.

Funding

Research support was provided by Servier Pharmaceuticals. MBG received funding from Lymphoma Research Foundation, American Society of Hematology, MSK Comedy versus Cancer Grant, Nancy and Jeffrey Heller Giving Fund; JHP received funding from Conquer Cancer Foundation of ASCO, Leukemia and Lymphoma Society Career Development Grant, The Geoffrey Beene Cancer Foundation, National Comprehensive Cancer Center Young Investigator Award, and American Society of Hematology Scholar Junior Faculty Award.

References

1. Hunger SP, Mullighan CG. Acute lymphoblastic leukemia in children. N Engl J Med. 2015;373(16):1541-1552.
2. Pulte D, Gondos A, Brenner H. Improvement in survival in younger patients with acute lymphoblastic leukemia from the 1980s to the early 21st century. Blood. 2009;113(7):1408-1411.
3. Rowe JM, Buck G, Burnett AK, et al. Induction therapy for adults with acute lymphoblastic leukemia: results of more than 1500 patients from the international ALL trial: MRC UKALL XII/ECOG E2993. Blood. 2005;106(12):3760-3767.
4. Boissel N, Auclerc MF, Lheritier V, et al. Should adolescents with acute lymphoblastic leukemia be treated as old children or young adults? Comparison of the French FRALLE-93 and LALA-94 trials. J Clin Oncol. 2003;21(5):774-780.
5. Stock W, La M, Sanford B, et al. What determines the outcomes for adolescents and young adults with acute lymphoblastic leukemia treated on cooperative group protocols? A comparison of Children's Cancer Group and Cancer and Leukemia Group B studies. Blood. 2008;112(5):1646-1654.
6. de Bont JM, Holt B, Dekker AW, et al. Significant difference in outcome for adolescents with acute lymphoblastic leukemia treated on pediatric vs adult protocols in the Netherlands. Leukemia. 2004;18(12):2032-2035.
7. Douer D, Aldoss I, Lunning MA, et al. Pharmacokinetics-based integration of multiple doses of intravenous pegaspargase in a pediatric regimen for adults with newly diagnosed acute lymphoblastic leukemia. J Clin Oncol. 2014;32(9):905-911.
8. Patel B, Kirkwood AA, Dey A, et al. Pegylated-asparaginase during induction therapy for adult acute lymphoblastic leukaemia: toxicity data from the UKALL14 trial. Leukemia. 2017;31(1):58-64.
9. Huguet F, Leguay T, Raffoux E, et al. Pediatric-inspired therapy in adults with Philadelphia chromosome-negative acute lymphoblastic leukemia: the GRAALL-2003 study. J Clin Oncol. 2009;27(6):911-918.
10. DeAngelo DJ, Stevenson KE, Dahlberg SE, et al. Long-term outcome of a pediatric-inspired regimen used for adults aged 18-50 years with newly diagnosed acute lymphoblastic leukemia. Leukemia. 2015;29(3):526-534.
11. Huguet F, Chevret S, Leguay T, et al. Intensified therapy of acute lymphoblastic leukemia in adults: report of the randomized GRAALL-2005 Clinical Trial. J Clin Oncol. 2018;36(24):2514-2523.
12. Gökbuget N, Beck J, Brandt K, et al.

Significant improvement of outcome In adolescents and young adults (AYAs) aged 15-35 Years with acute lymphoblastic leukemia (ALL) with a pediatric derived adult ALL protocol; results Of 1529 AYAs in 2 consecutive trials of The German Multicenter Study Group For Adult ALL (GMALL). Blood. 2013;122(21):839-839.
13. Stock W, Luger SM, Advani AS, et al. A pediatric regimen for older adolescents and young adults with acute lymphoblastic leukemia: results of CALGB 10403. Blood. 2019;133(14):1548-1559.
14. Earl M. Incidence and management of asparaginase-associated adverse events in patients with acute lymphoblastic leukemia. Clin Adv Hematol Oncol. 2009;7(9):600-606.
15. Amylon MD, Shuster J, Pullen J, et al. Intensive high-dose asparaginase consolidation improves survival for pediatric patients with T cell acute lymphoblastic leukemia and advanced stage lymphoblastic lymphoma: a Pediatric Oncology Group study. Leukemia. 1999;13(3):335-342.
16. Sallan SE, Hitchcock-Bryan S, Gelber R, et al. Influence of intensive asparaginase in the treatment of childhood non-T-cell acute lymphoblastic leukemia. Cancer Res. 1983;43(11):5601-5607.
17. Stock W, Douer D, DeAngelo DJ, et al. Prevention and management of asparaginase/pegasparaginase-associated toxicities in adults and older adolescents: recommendations of an expert panel. Leuk Lymphoma. 2011;52(12):2237-2253.
18. Asselin BL, Whitin JC, Coppola DJ, et al. Comparative pharmacokinetic studies of three asparaginase preparations. J Clin Oncol. 1993;11(9):1780-1786.
19. Avramis VI, Sencer S, Periclou AP, et al. A randomized comparison of native Escherichia coli asparaginase and polyethylene glycol conjugated asparaginase for treatment of children with newly diagnosed standard-risk acute lymphoblastic leukemia: a Children's Cancer Group study. Blood. 2002;99(6):1986-1994.
20. Muller HJ, Loning L, Horn A, et al. Pegylated asparaginase (Oncaspar) in children with ALL: drug monitoring in reinduction according to the ALL/NHL-BFM 95 protocols. Br J Haematol. 2000;110(2):379-384.
21. Larsen EC, Devidas M, Chen S, et al. Dexamethasone and high-dose methotrexate improve outcome for children and young adults with high-risk B-acute lymphoblastic leukemia: a report from Children's Oncology Group Study AALL0232. J Clin Oncol. 2016;34(20):2380-2388.
22. Wetzler M, Sanford BL, Kurtzberg J, et al. Effective asparagine depletion with pegylated asparaginase results in improved outcomes in adult acute lymphoblastic leukemia: Cancer and Leukemia Group B Study 9511. Blood. 2007;109(10):4164-4167.
23. Rubenstein JL, Gupta NK, Mannis GN, et al. How I treat CNS lymphomas. Blood. 2013;122(14):2318-2330.
24. Khan RB, Shi W, Thaler HT, et al. Is intrathecal methotrexate necessary in the treatment of primary CNS lymphoma? J Neurooncol. 2002;58(2):175-178.
25. Synold TW, Relling MV, Boyett JM, et al. Blast cell methotrexate-polyglutamate accumulation in vivo differs by lineage, ploidy, and methotrexate dose in acute lymphoblastic leukemia. J Clin Invest. 1994;94(5):1996-2001.
26. Seibel NL, Steinherz PG, Sather HN, et al. Early postinduction intensification therapy improves survival for children and adolescents with high-risk acute lymphoblastic leukemia: a report from the Children's Oncology Group. Blood. 2008;111(5):2548-2555.
27. Nachman JB, Sather HN, Sensel MG, et al. Augmented post-induction therapy for children with high-risk acute lymphoblastic leukemia and a slow response to initial therapy. N Engl J Med. 1998;338(23):1663-1671.
28. Christ TN, Stock W, Knoebel RW. Incidence of asparaginase-related hepatotoxicity, pancreatitis, and thrombotic events in adults with acute lymphoblastic leukemia treated with a pediatric-inspired regimen. J Oncol Pharm Pract. 2018;24(4):299-308.
29. Coustan-Smith E, Mullighan CG, Onciu M, et al. Early T-cell precursor leukaemia: a subtype of very high-risk acute lymphoblastic leukaemia. Lancet Oncol. 2009;10(2):147-156.
30. Orvain C, Balsat M, Tavernier E, et al. Thromboembolism prophylaxis in adult patients with acute lymphoblastic leukemia treated in the GRAALL-2005 study. Blood. 2020;136(3):328-338.
31. Quist-Paulsen P, Toft N, Heyman M, et al. T-cell acute lymphoblastic leukemia in patients 1-45 years treated with the pediatric NOPHO ALL2008 protocol. Leukemia. 2020;34(2):347-357.
32. Luskin MR, DeAngelo DJ. T-cell acute lymphoblastic leukemia: Current approach and future directions. Adv Cell Gene Ther. 2019;2(4):e70.
33. Douer D, Yampolsky H, Cohen LJ, et al. Pharmacodynamics and safety of intravenous pegaspargase during remission induction in adults aged 55 years or younger with newly diagnosed acute lymphoblastic leukemia. Blood. 2007;109(7):2744-2750.
34. Lanvers-Kaminsky C, Niemann A, Eveslage M, et al. Asparaginase activities during intensified treatment with pegylated E. coli asparaginase in adults with newly-diagnosed acute lymphoblastic leukemia. Leuk Lymphoma. 2020;61(1):138-145.
35. Patel B, Rai L, Buck G, et al. Minimal residual disease is a significant predictor of treatment failure in non T-lineage adult acute lymphoblastic leukaemia: final results of the international trial UKALL XII/ECOG2993. Br J Haematol. 2010;148(1):80-89.
36. Inotuzumab Ozogamicin and Blinatumomab in treating patients with newly diagnosed, recurrent, or refractory CD22-positive B-lineage acute lymphoblastic leukemia. [cited; available from: https://clinicaltrials.gov/ct2/show/NCT03739814
37. Combination chemotherapy with or without blinatumomab in treating patients with newly diagnosed BCR-ABL-negative B lineage acute lymphoblastic leukemia. https://clinicaltrials.gov/ct2/show/NCT02003222
38. Roberts KG, Li Y, Payne-Turner D, et al. Targetable kinase-activating lesions in Ph-like acute lymphoblastic leukemia. N Engl J Med. 2014;371(11):1005-1015.

ARTICLE

Fenofibrate reduces osteonecrosis without affecting antileukemic efficacy in dexamethasone-treated mice

Emily R. Finch,[1] Monique A. Payton,[1] David A. Jenkins,[1] Xiangjun Cai,[1] Lie Li,[1] Seth E. Karol,[2] Mary V. Relling[1] and Laura J. Janke[3]

[1]Department of Pharmaceutical Sciences, St. Jude Children's Research Hospital; [2]Department of Oncology, St. Jude Children's Research Hospital and [3]Department of Pathology, Division of Comparative Pathology, St. Jude Children's Research Hospital, Memphis, TN, USA

Ferrata Storti Foundation

Haematologica 2021
Volume 106(8):2095-2101

ABSTRACT

Recent clinical trials in children with acute lymphoblastic leukemia (ALL) indicate that severe hypertriglyceridemia (>1000 mg/dL) during therapy is associated with an increased frequency of symptomatic osteonecrosis. Interventions to lower triglycerides have been considered, but there have been no preclinical studies investigating the impact of lowering triglycerides on osteonecrosis risk, nor whether such interventions interfere with the antileukemic efficacy of ALL treatment. We utilized our clinically relevant mouse model of dexamethasone-induced osteonecrosis to determine whether fenofibrate decreased osteonecrosis. To test whether fenofibrate affected the antileukemic efficacy of dexamethasone, we utilized a BCR-ABL$^+$ model of ALL. Serum triglycerides were reduced by fenofibrate throughout the period of treatment, with the most pronounced, 4.5-fold, decrease at week 3 ($P<1x10^{-6}$). Both frequency (33% *vs.* 74%, $P=0.006$) and severity (median necrosis score of 0 *vs.* 75; $P=6x10^{-5}$) of osteonecrosis were reduced with fenofibrate. Fenofibrate had no impact on BCR-ABL$^+$ ALL survival ($P=0.65$) nor on the antileukemic properties of dexamethasone ($P=0.49$). These data suggest that lowering triglycerides with fenofibrate reduces dexamethasone-induced osteonecrosis while maintaining antileukemic efficacy, and thus may be considered for clinical trials.

Introduction

Hypertriglyceridemia occurs in 4-19% of children treated with glucocorticoids and/or asparaginase during therapy for acute lymphoblastic leukemia (ALL).[1-7] Although hypertriglyceridemia has been thought to be transient and relatively benign,[1,2] recent studies suggest that patients with severe hypertriglyceridemia (>1000 mg/dL) during ALL therapy may be at increased risk of long-term complications, including symptomatic osteonecrosis.[3,7,8]

Recent recommendations for pharmaceutical management of severe hypertriglyceridemia include the use of fibrates, specifically fenofibrate.[9] In addition to being associated with fewer drug-drug interactions than statins,[10-12] fenofibrate specifically reduces serum triglycerides by as much as 50%, with minimal adverse reactions,[13-15] whereas the main effect of statins is the decrease of serum low-density lipoprotein cholesterol.[9,16,17] The active metabolite of fenofibrate, fenofibric acid, targets peroxisome proliferator activated receptor-α, leading to activation of lipoprotein lipase which increases lipolysis and elimination of triglyceride-rich particles,[18] resulting in reduction of circulating serum triglycerides.[19,20] Therefore, it has been suggested that fenofibrate could be useful in the management of acute hypertriglyceridemia, such as that observed during ALL therapy. However, there is no evidence that lowering triglyceride levels with fenofibrate can reduce risk of osteonecrosis. Moreover, with very effective ALL therapy, caution must be exercised before adding any new agents to treatment regimens, to avoid untoward drug interactions.

In these proof-of-principle experiments, we tested the hypothesis that lowering serum triglyceride levels with fenofibrate in dexamethasone-treated mice would

Correspondence:

LAURA JANKE
laura.janke@stjude.org

Received: March 18, 2020.
Accepted: July 6, 2020.
Pre-published: July 16, 2020.

https://doi.org/10.3324/haematol.2020.252767

result in decreased osteonecrosis and would not interfere with the efficacy of antileukemic therapy.

Methods

Treatment

Experiments were approved by the Institutional Animal Care and Use Committee of St. Jude Children's Research Hospital (SJCRH; Memphis, TN, USA): protocol numbers 423-100428 and 465-100549.

All mice received prophylactic antibiotics in drinking water (herein referred to as "base-water"): continuous tetracycline (1 g/L; Sigma-Aldrich, St. Louis, MO, USA) and intermittent sulfamethoxazole/trimethoprim oral suspension (600/120 mg/L for 3.5 days/week; Aurobindo Pharma, USA, Inc., Dayton, NJ, USA). Mice were randomized to receive continuous dexamethasone (0.4 mg/mL sodium phosphate solution; Fresenius Kabi, Lake Zurich, IL, USA) in drinking water, herein referred to as "dexamethasone water" (3 mg/L in the osteonecrosis model and 4 mg/L in the BCR-ABL$^+$ ALL model).[21-23]

The folic acid-deficient diet (0.2 ppm folic acid; TestDiet, Richmond, IN, USA) was the "base-diet".[21] Fenofibrate (Sigma Aldrich, St. Louis, MO, USA) was added to the base-diet for a final concentration of 0.2% fenofibrate (w/w) to make the "fenofibrate-supplemented diet" (TestDiet, Richmond, IN, USA). This dose had been used in prior experimental rodent models.[24-26]

Serum triglycerides were measured with an ABX Penta 400 instrument (Horiba, Montpellier, France) after the animals had fasted for 12 to 16 h (food was withheld; mice had free access to water).

Mice were randomized to one of four treatment groups: control (base-water and base-diet); fenofibrate-only (base-water and fenofibrate-supplemented diet); dexamethasone-only (dexamethasone-water and base-diet); or dexamethasone + fenofibrate (dexamethasone-water and fenofibrate-supplemented diet).

Osteonecrosis model

The protocol was modified from that previously described.[21,22,27-29] At postnatal days 26 to 28, male Balb/cJ mice (bred in-house at SJCRH) were randomized by body weight (13.5 g, 95% confidence interval [95% CI]: 13.0- 14.7) to 6 weeks of treatment. Fasting serum triglycerides were measured after 1, 3, and 6 weeks of treatment. At the end of treatment, white adipose tissue; and plasma dexamethasone and fenofibric acid levels were measured. Osteonecrosis and epiphyseal arteriopathy were evaluated and scored in both distal femora, by a board-certified veterinary pathologist (LJJ), as described previously[21,22,27-29] Details are provided in the *Online Supplementary Methods*.

BCR-ABL$^+$ acute lymphoblastic leukemia model

The BCR-ABL (p185$^+$, *Arf*$^{-/-}$) luciferase-positive cell line (BCR-ABL$^+$) was generated.[23,30-32] Female 8-week-old matched syngeneic mice (C57Bl/6J, *Arf*-wildtype; Jackson Laboratory, Bar Harbor, ME, USA) received intravenous injections of 2,000 BCR-ABL$^+$ cells. Bioluminescent imaging was performed weekly,[23] to monitor leukemic burden. At day 3, mice were stratified by luminescent signal and body weight to treatment (n=10/treatment group). Fasting serum triglycerides were measured at day 24. Treatment ended at day 28: mice were maintained on base-diet/base-water until a humane endpoint or the end of study at day 63. Details are given in the *Online Supplementary Methods*.

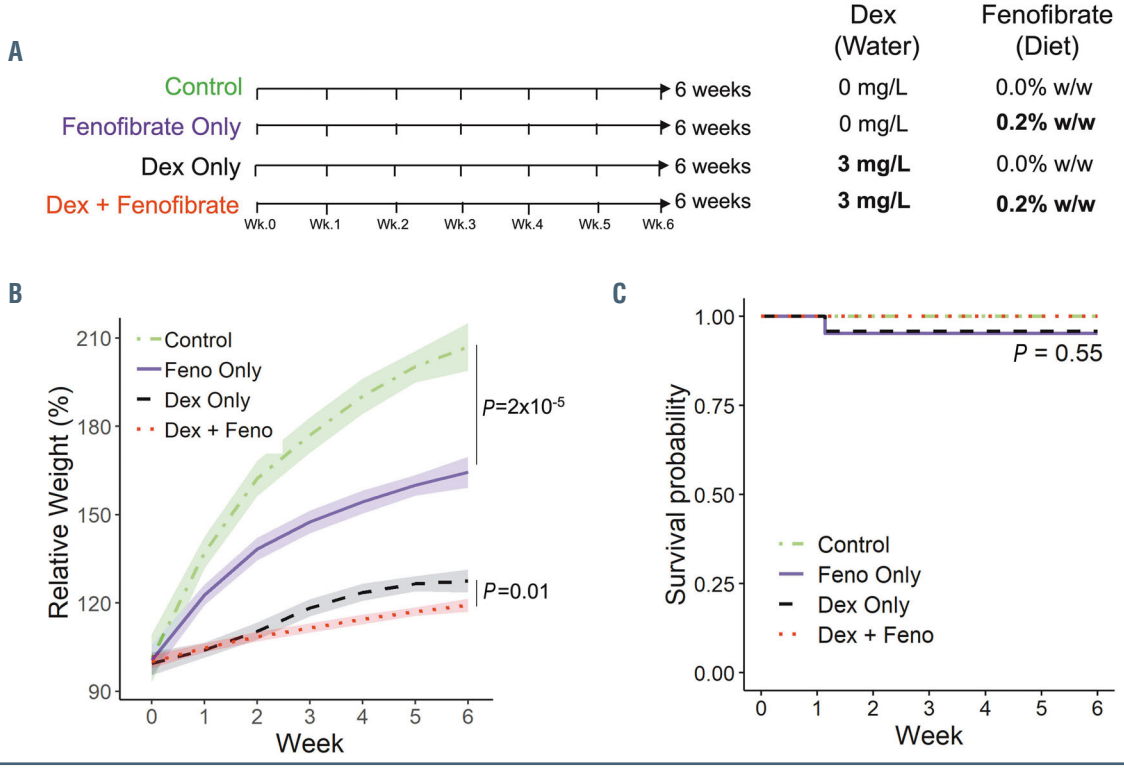

Figure 1. Experimental design, body weight, and survival in dexamethasone-induced osteonecrosis. (A) Experimental design: male Balb/cJ mice were placed on 6 weeks of continuous treatment with dexamethasone, fenofibrate, or both. (B) Body weight relative to week 0 is shown as a median with 95% confidence interval (95% CI). Control mice and mice treated with fenofibrate (Feno) only weighed more than those treated with dexamethasone (Dex) only or Dex + Feno from weeks 1-6 of treatment ($P<1x10^{-6}$). (C) Survival did not differ by treatment group. The survival rate was 100% in the control group (12/12) and the group treated with Dex + Feno (33/33), whereas it was 98% in both the Dex Only (23/24) and Feno Only (20/21) groups ($P=0.55$).

Statistical analysis

The frequency of osteonecrosis/arteriopathy was compared using the χ^2 test. Log-rank testing was used for survival comparisons. For continuous variables, the two-tailed Mann-Whitney test was used (two groups); the Kruskal-Wallis test with Dunn correction was used for multiple comparisons (three or more groups). All continuous statistics are expressed as the median with 95% confidence interval. The R program (version 3.5.1)[33] or GraphPad Prism[34] was used for the statistical analyses and visual representation. *P* values <0.05 were considered statistically significant for all analyses.

Results

Fenofibrate in experimental osteonecrosis

Consistent with previous observations,[21,22,28,29] mice that received dexamethasone (i.e., animals in the dexamethasone-only and dexamethasone + fenofibrate treatment groups) gained less weight over time compared to those not treated with dexamethasone (control and fenofibrate-only treatment groups) (Figure 1B). Fenofibrate supplementation suppressed weight gain over the course of treatment. By week 6 of treatment, control mice had gained 50% more weight than mice treated with fenofibrate only ($P=2x10^{-5}$) and mice treated with dexamethasone only had gained 10% more weight than those treated with dexamethasone + fenofibrate ($P=0.01$) (Figure 1B). There was no difference in survival between groups ($P=0.55$) (Figure 1C).

In mice treated with dexamethasone, fenofibrate significantly reduced serum triglyceride levels as early as week 1, from 130.1 mg/dL (95% CI: 85.2- 201.1) to 37.4 mg/dL (95% CI: 17.1- 60.3), a 3.5-fold decrease ($P=0.0004$). Fenofibrate supplementation continued to suppress dexamethasone-induced hypertriglyceridemia at week 3 (4.5-fold decrease, $P<1x10^{-6}$) through to the end of treatment at week 6 (3.5-fold decrease, $P=5x10^{-6}$). There was no difference in triglyceride levels at weeks 1 and 3 between mice treated with fenofibrate only and those treated with

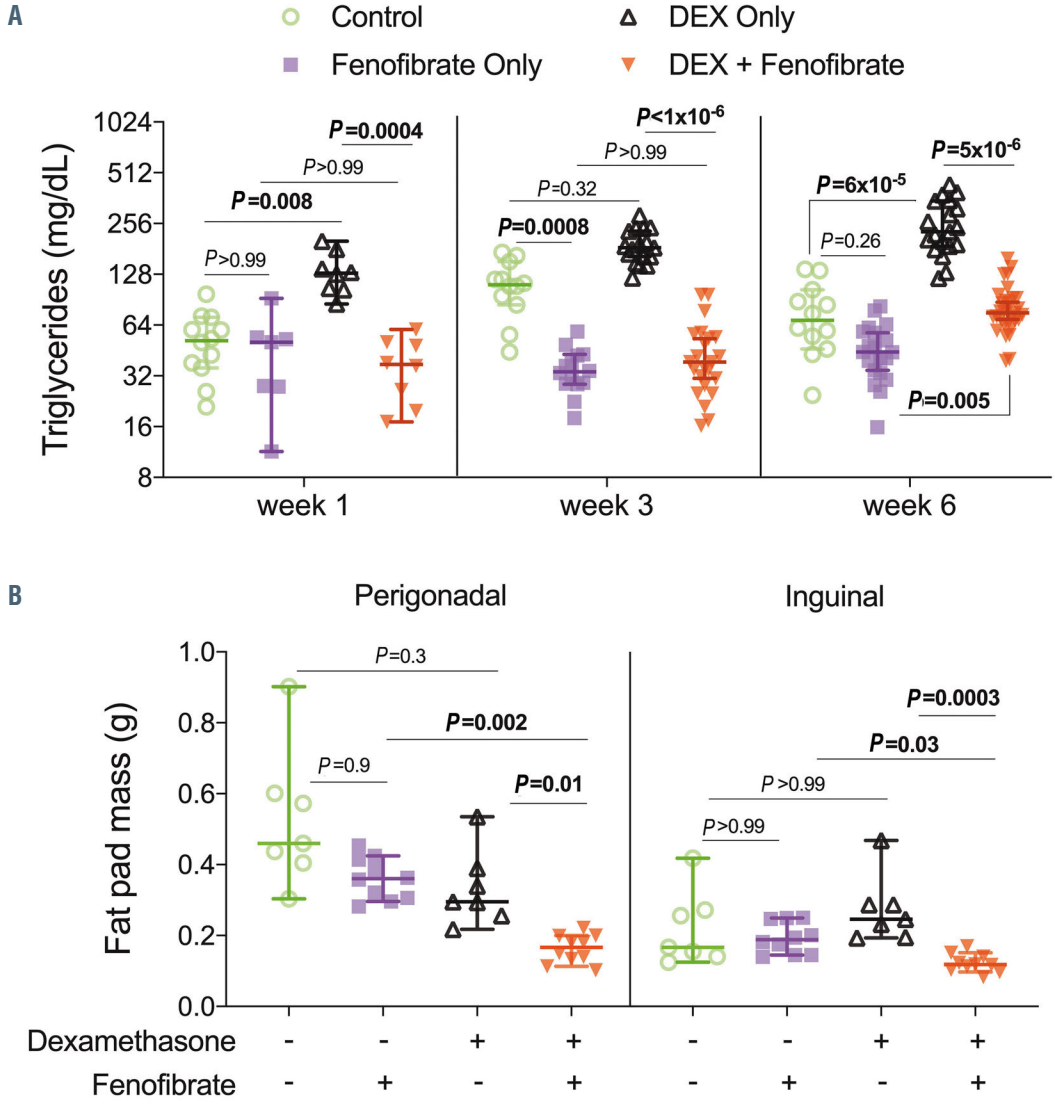

Figure 2. Fenofibrate reduces serum lipids and fat depots in dexamethasone-treated mice. (A) Median (with 95% confidence interval) fasting serum triglyceride levels at weeks 1, 3, and 6 of treatment. Week 1, n=8-12/group; week 3, n=12-27/group; week 6, n=12-31/group. (B) Perigonadal and inguinal fat pads at week 6; n=8-10/group. *P*-values shown between relevant groups: control *versus* fenofibrate only; control *versus* dexamethasone (DEX) only; fenofibrate only *versus* DEX + fenofibrate; DEX only *versus* DEX + fenofibrate.

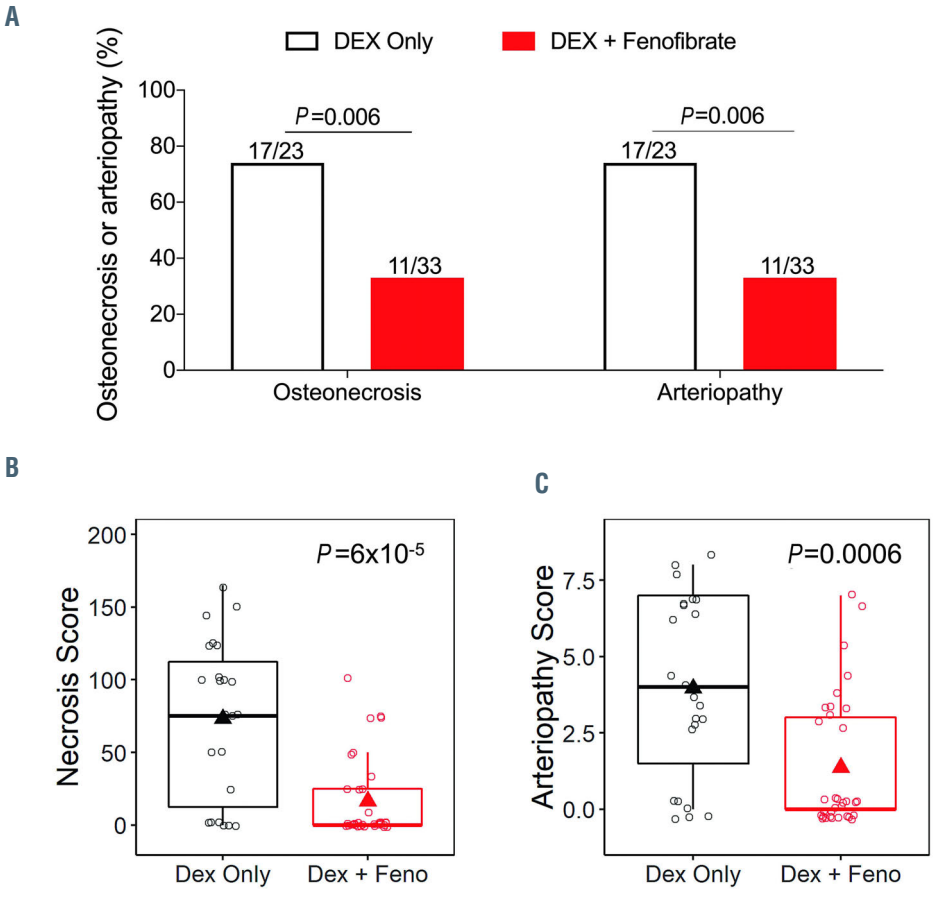

Figure 3. Fenofibrate reduces the frequency and severity of osteonecrosis and arteriopathy in dexamethasone-treated mice. (A) Frequency of osteonecrosis or arteriopathy, compared with the χ^2 test. (B) Necrosis scores (possible range of 0 [no osteonecrosis] to 200 [equivalent to 100% necrosis in both hind limbs]) and (C) arteriopathy scores (possible range of 0 [no arteriopathy] to 8 [thrombotic arteriopathy in both limbs]) were reduced with fenofibrate. Median with 95% confidence interval (box and whiskers) and mean (triangle). Note that no control mice or mice treated with fenofibrate only developed osteonecrosis or arteriopathy. Dex: dexamethasone; Feno: fenofibrate.

fenofibrate + dexamethasone (P>0.99 at each time point). By week 6, triglycerides were higher in the mice treated with fenofibrate + dexamethasone than in those treated with fenofibrate only (P=0.005): however, levels were comparable to those in control mice (P>0.99) (Figure 2A).

In dexamethasone-treated mice, fenofibrate reduced white adipose tissue: perigonadal fat (representative of visceral fat) was reduced from 0.30 g (95% CI: 0.22- 0.54) to 0.17 g (95% CI: 0.11- 0.20; P=0.01) and inguinal fat (representative of posterior subcutaneous fat) was reduced from 0.25 g (95% CI: 0.19- 0.47) to 0.12 g (95% CI: 0.10- 0.15; P=0.0003) (Figure 2B).

As expected, only mice that received dexamethasone developed osteonecrosis and/or arteriopathy (Figure 3). The frequency of both osteonecrosis and arteriopathy was 74% in mice treated with dexamethasone only *versus* 33% in those treated with dexamethasone + fenofibrate (P=0.006) (Figure 3A). Not only was the frequency of osteonecrosis and arteriopathy reduced over 2-fold with fenofibrate, but the severity of these conditions was significantly reduced. In the mice treated with dexamethasone only, the necrosis score was reduced from 75 to 0 with fenofibrate supplementation (P=6x10^{-5}) (Figure 3B) and the arteriopathy score was reduced from 4 to 0 (P=0.0006) (Figure 3C).

In mice treated with dexamethasone + fenofibrate, there was a correlation between the triglyceride level at week 3 and osteonecrosis: mice that developed osteonecrosis had a median triglyceride concentration of 67.5 mg/dL (95% CI: 21.1-96.9) *versus* 37.2 mg/dL (95% CI: 30.9-53.1) in osteonecrosis-negative mice (P=0.03) (*Online Supplementary Figure S1A*). By the end of treatment, there was no difference in triglyceride levels by osteonecrosis status (P>0.99) (*Online Supplementary Figure S1B*).

At the end of treatment, there was no difference in plasma dexamethasone levels between mice treated with dexamethasone only (26.6 nM, 95% CI: 20.0-58.3 nM) and those treated with dexamethasone + fenofibrate (20.5 nM, 95% CI: 16.7- 25.9 nM; P=0.1) (*Online Supplementary Figure S2A*). The levels of fenofibric acid were significantly lower in animals treated with dexamethasone + fenofibrate (1.9 μg/mL, 95% CI: 1.6-2.4 μg/mL) than in those treated with fenofibrate only (6.7 μg/mL, 95% CI: 6.1-8 μg/mL, P<1x10^{-6}) (*Online Supplementary Figure S2B*).

Fenofibrate in experimental BCR-ABL$^+$ acute lymphoblastic leukemia

In a BCR-ABL$^+$ dexamethasone-sensitive model of murine ALL, (Figure 4A), all mice that did not receive dexamethasone succumbed to disease by day 35 (Figure 4C), and animals in both the groups treated with dexamethasone only and dexamethasone + fenofibrate lived longer than those that did not receive dexamethasone (P<1x10^{-6}). Mice were monitored for relapse until the end of follow-up at day 63. There was no difference in disease burden between the dexamethasone-only *versus* dexamethasone + fenofibrate treatment groups, as indicated by survival (P=0.49) (Figure 4C), spleen weight (P>0.99) (*Online Supplementary Figure S3A*), and white blood cell count (P>0.99) (*Online Supplementary Figure S3B*). Among the dexamethasone-treated mice, fenofibrate decreased triglyceride levels from 89.9 mg/dL to 29.0 mg/dL (P=0.001) (Figure 4D).

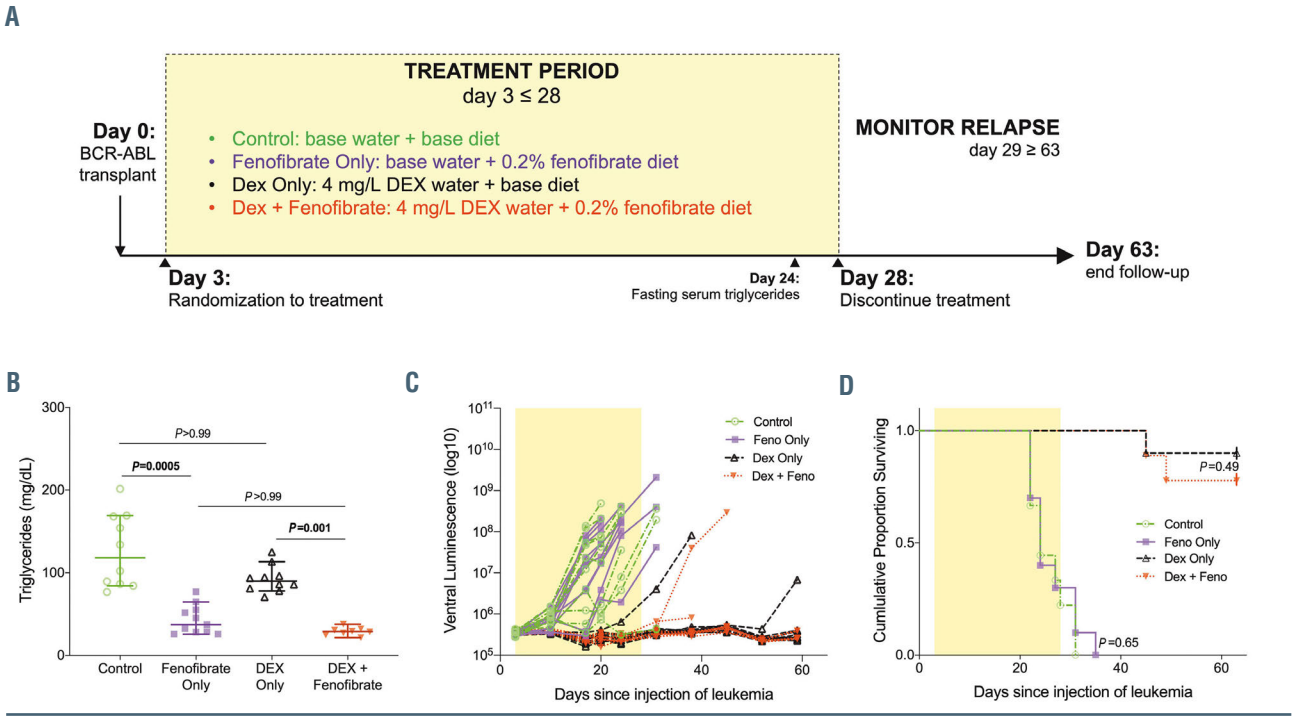

Figure 4. Fenofibrate does not affect efficacy of dexamethasone in BCR-ABL⁺ acute lymphoblastic leukemia. (A) Experimental design. DEX water: continuous dexamethasone in drinking water; base-water: drinking water; base-diet: folic acid-deficient diet. (B) Ventral luminescence was measured weekly. (C) A log-rank test of survival data shows *P*-values for the comparisons between the various groups: control mice, mice treated with fenofibrate only, dexamethasone (DEX) only and DEX + fenofibrate. $P<1x10^6$ between DEX-treated groups (DEX only and DEX + fenofibrate) *versus* no DEX treatment (control and fenofibrate only). The shaded yellow area indicates time on therapy. (D) Fasting serum triglyceride levels at day 24 (3 weeks after BCR-ABL transplant). N=9-10/group.

Discussion

Although the etiology of osteonecrosis is not completely understood, the involvement of lipid metabolism has been well documented.[35-37] However, there have been few studies investigating whether pharmacologically lowering triglycerides prevents osteonecrosis.[38]

We found that fenofibrate supplementation successfully managed dexamethasone-induced hypertriglyceridemia (Figure 2) and was associated with reductions in the frequency and severity of osteonecrosis (Figure 3). The correlation between week 3, but not week 6 triglyceride levels (*Online Supplementary Figure S1*), and osteonecrosis suggest that management of triglycerides is especially important early in the progression of the disease. Although there was an increase in triglyceride levels between mice treated with fenofibrate + dexamethasone and those treated with fenofibrate only by week 6 (Figure 2A), fenofibrate was able to maintain triglyceride levels comparable to those in control mice, even with prolonged continuous exposure to dexamethasone.

Any addition to ALL therapy must be thoroughly assessed to ensure that it does not interfere with the highly effective modern drug regimens. For our purposes, we utilized a model of BCR-ABL⁺ ALL known to be sensitive to dexamethasone treatment. Fenofibrate supplementation did not cause observable differences in the efficacy of dexamethasone in the treatment of experimental BCR-ABL⁺ ALL (Figure 4).

In our experimental models, the dosage of both dexamethasone and fenofibrate were well tolerated (Figure 1C) and resulted in plasma levels of the drug/metabolites in the clinical range.[13,39,40] Although the plasma concentration of fenofibric acid was lower in mice treated with dexamethasone + fenofibrate than in those treated with fenofibrate only (*Online Supplementary Figure S2B*), it was still effective in reducing dexamethasone-induced hypertriglyceridemia (Figure 2A) and osteonecrosis (Figure 3), while not affecting BCR-ABL⁺ ALL treatment (Figure 4). Statins have been suggested as possible agents to reduce osteonecrosis[41-43] but because they have potent interactions with CYP3A and with SLCO1B1 (enzymes involved in the metabolism and disposition of multiple ALL drugs), their likelihood of drug interactions makes them less desirable agents to use in patients with ALL.

Dexamethasone treatment is associated with hypertriglyceridemia.[1,3,44] It has been shown that elevated levels of serum triglyceride-rich lipoproteins contribute to endothelial dysfunction and subsequent atherosclerosis.[45] We hypothesized that dexamethasone-induced arteriopathy and subsequent osteonecrosis are related to hypertension caused by endothelial dysfunction.[27,46] We therefore suspect that the mechanism by which fenofibrate reduced the incidence of osteonecrosis and arteriopathy was by lowering the dexamethasone-induced elevation of triglyceride-rich lipoproteins and thereby mitigating the effects of endothelial dysfunction.

In children with ALL, there are no specific guidelines for managing triglyceride levels during glucocorticoid and/or asparaginase treatment. However, conservative use of fibrates has been successful in managing triglycerides in specific cases, with no reported adverse events.[3,5,47] In general, the use of fibrates in children is limited to cases of extreme hypertriglyceridemia to prevent pancreatitis, pri-

marily in individuals with familial lipid disorders.[20,48-50] Fibrates have been shown to reduce triglycerides effectively in children, by between 39% and 54%.[49,51] As seen in adults, data suggest that fibrates are well tolerated in children, with the most frequently reported adverse reactions being gastrointestinal disturbances and muscle cramps.[13,14,20,49] However, transient increases in liver function tests have been reported in a small number of cases,[48,51] indicating a potential for hepatotoxicity when used in combination with other hepatotoxic chemotherapeutic agents.

Although fibrates have been included in a case-by-case basis to manage hypertriglyceridemia during ALL therapy[3,5,47] there has been no systematic analysis of the effect of lipid-lowering interventions and long-term outcomes in ALL survivors. Our proof-of-principle preclinical experiments show that fenofibrate treatment is a potential intervention to reduce dexamethasone-induced osteonecrosis in ALL, without carrying the risk of substantial drug interactions and without any untoward effect on the efficacy of ALL therapy. Our findings support the rationale for controlled clinical trials with fenofibrate in chemotherapy-related hypertriglyceridemia.

Disclosures

No conflicts of interest to disclose.

Contributions

ERF: conceptualization of experiments; ERF, MAP, DAJ, XC, LL, SEK, MVR and LJJ: methodology and data collection; ERF, MVR and LJJ: formal analysis; ERF, MVR and LJJ wrote the original manuscript. All authors reviewed and approved the manuscript.

Acknowledgments

We are grateful to St. Jude's Animal Resource Center and Veterinary Pathology Core for technical assistance.

Funding

This research was supported by the National Institutes of Health (CA142665, CA21765, and GM115279) and ALSAC. The content is solely the responsibility of the authors and does not necessarily represent the official views of the National Institutes of Health.

References

1. Steinherz PG. Transient, severe hyperlipidemia in patients with acute lymphoblastic leukemia treated with prednisone and asparaginase. Cancer. 1994;74(12):3234-3239.
2. Parsons SK, Skapek SX, Neufeld EJ, et al. Asparaginase-associated lipid abnormalities in children with acute lymphoblastic leukemia. Blood. 1997;89(6):1886-1895.
3. Bhojwani D, Darbandi R, Pei D, et al. Severe hypertriglyceridaemia during therapy for childhood acute lymphoblastic leukaemia. Eur J Cancer. 2014;50(15):2685-2694.
4. Place AE, Stevenson KE, Vrooman LM, et al. Intravenous pegylated asparaginase versus intramuscular native Escherichia coli L-asparaginase in newly diagnosed childhood acute lymphoblastic leukaemia (DFCI 05-001): a randomised, open-label phase 3 trial. Lancet Oncol. 2015;16(16):1677-1690.
5. Cohen H, Bielorai B, Harats D, Toren A, Pinhas-Hamiel O. Conservative treatment of L-asparaginase-associated lipid abnormalities in children with acute lymphoblastic leukemia. Pediatr Blood Cancer. 2010;54(5):703-706.
6. Salvador C, Entenmann A, Salvador R, Niederwanger A, Crazzolara R, Kropshofer G. Combination therapy of omega-3 fatty acids and acipimox for children with hypertriglyceridemia and acute lymphoblastic leukemia. J Clin Lipidol. 2018;12(5):1260-1266.
7. Finch ER, Smith CA, Yang W, et al. Asparaginase formulation impacts hypertriglyceridemia during therapy for acute lymphoblastic leukemia. Pediatr Blood Cancer. 2020;67(1):e28040.
8. Mogensen SS, Schmiegelow K, Grell K, et al. Hyperlipidemia is a risk factor for osteonecrosis in children and young adults with acute lymphoblastic leukemia. Haematologica. 2017;102(5):e175-e178.
9. Grundy SM, Stone NJ, Bailey AL, et al. 2018 AHA/ACC/AACVPR/AAPA/ABC/ACPM/ADA/AGS/APhA/ASPC/NLA/PCNA guideline on the management of blood cholesterol: a report of the American College of Cardiology/American Heart Association Task Force on Clinical Practice Guidelines. Circulation. 2019;139(25):e1082-e1143.
10. Bellosta S, Corsini A. Statin drug interactions and related adverse reactions. Expert Opin Drug Saf. 2012;11(6):933-946.
11. Wiggins BS, Saseen JJ, Page RL 2nd, et al. Recommendations for management of clinically significant drug-drug interactions with statins and select agents used in patients with cardiovascular disease: a scientific statement from the American Heart Association. Circulation. 2016;134(21):e468-e495.
12. Bellosta S, Corsini A. Statin drug interactions and related adverse reactions: an update. Expert Opin Drug Saf. 2018;17(1):25-37.
13. Balfour JA, McTavish D, Heel RC. Fenofibrate. A review of its pharmacodynamic and pharmacokinetic properties and therapeutic use in dyslipidaemia. Drugs. 1990;40(2):260-290.
14. Davidson MH, Armani A, McKenney JM, Jacobson TA. Safety considerations with fibrate therapy. Am J Cardiol. 2007;99(6A):3C-18C.
15. McKeage K, Keating GM. Fenofibrate: a review of its use in dyslipidaemia. Drugs. 2011;71(14):1917-1946.
16. Branchi A, Fiorenza AM, Rovellini A, et al. Lowering effects of four different statins on serum triglyceride level. Eur J Clin Pharmacol. 1999;55(7):499-502.
17. Besseling J, Hovingh GK, Huijgen R, Kastelein JJP, Hutten BA. Statins in familial hypercholesterolemia: consequences for coronary artery disease and all-cause mortality. J Am Coll Cardiol. 2016;68(3):252-260.
18. Staels B, Dallongeville J, Auwerx J, Schoonjans K, Leitersdorf E, Fruchart JC. Mechanism of action of fibrates on lipid and lipoprotein metabolism. Circulation. 1998;98(19):2088-2093.
19. Sirtori CR, Montanari G, Gianfranceschi G, Sirtori M, Galli G, Bosisio E. Correlation between plasma levels of fenofibrate and lipoprotein changes in hyperlipidaemic patients. Eur J Clin Pharmacol. 1985;28(6):619-624.
20. Kennedy MJ, Jellerson KD, Snow MZ, Zacchetti ML. Challenges in the pharmacologic management of obesity and secondary dyslipidemia in children and adolescents. Paediatr Drugs. 2013;15(5):335-342.
21. Yang L, Boyd K, Kaste SC, Kamdem Kamdem L, Rahija RJ, Relling MV. A mouse model for glucocorticoid-induced osteonecrosis: effect of a steroid holiday. J Orthop Res. 2009;27(2):169-175.
22. Kawedia JD, Janke L, Funk AJ, et al. Substrain-specific differences in survival and osteonecrosis incidence in a mouse model. Comp Med. 2012;62(6):466-471.
23. Ramsey LB, Janke LJ, Payton MA, et al. Antileukemic efficacy of continuous vs discontinuous dexamethasone in murine models of acute lymphoblastic leukemia. PLoS One. 2015;10(8):e0135134.
24. Murai T, Yamada T, Miida T, Arai K, Endo N, Hanyu T. Fenofibrate inhibits reactive amyloidosis in mice. Arthritis Rheum. 2002;46(6):1683-1688.
25. Oosterveer MH, Grefhorst A, van Dijk TH, et al. Fenofibrate simultaneously induces hepatic fatty acid oxidation, synthesis, and elongation in mice. J Biol Chem. 2009;284(49):34036-34044.
26. Huang J, Das SK, Jha P, et al. The PPARalpha agonist fenofibrate suppresses B-cell lymphoma in mice by modulating lipid metabolism. Biochim Biophys Acta. 2013;1831(10):1555-1565.
27. Janke LJ, Liu C, Vogel P, et al. Primary epiphyseal arteriopathy in a mouse model of steroid-induced osteonecrosis. Am J Pathol. 2013;183(1):19-25.
28. Liu C, Janke LJ, Kawedia JD, et al. Asparaginase potentiates glucocorticoid-induced osteonecrosis in a mouse model. PLoS One. 2016;11(3):e0151433.
29. Finch ER, Janke LJ, Smith CA, et al. Bloodstream infections exacerbate incidence and severity of symptomatic glucocorticoid-induced osteonecrosis. Pediatr Blood Cancer. 2019;66(6):e27669.
30. Williams RT, Roussel MF, Sherr CJ. Arf gene loss enhances oncogenicity and limits imatinib response in mouse models of Bcr-Abl-induced acute lymphoblastic leukemia. Proc Natl Acad Sci U S A. 2006;103(17):6688-6693.
31. Boulos N, Mulder HL, Calabrese CR, et al. Chemotherapeutic agents circumvent emer-

gence of dasatinib-resistant BCR-ABL kinase mutations in a precise mouse model of Philadelphia chromosome-positive acute lymphoblastic leukemia. Blood. 2011;117 (13):3585-3595.
32. Ramsey LB, Janke LJ, Edick MJ, et al. Host thiopurine methyltransferase status affects mercaptopurine antileukemic effectiveness in a murine model. Pharmacogenet Genomics. 2014;24(5):263-271.
33. Team RDC. R: A Language and Environment for Statistical Computing. R Foundation for Statistical Computing, Vienna, Austria. 2006.
34. Prism. GraphPad Software, version 8.2.1. La Jolla, CA, USA.
35. Kuroda T, Tanabe N, Wakamatsu A, et al. High triglyceride is a risk factor for silent osteonecrosis of the femoral head in systemic lupus erythematosus. Clin Rheumatol. 2015;34(12):2071-2077.
36. Mankin HJ. Nontraumatic necrosis of bone (osteonecrosis). N Engl J Med. 1992;326(22): 1473-1479.
37. Sakamoto Y, Yamamoto T, Sugano N, et al. Genome-wide association study of idiopathic osteonecrosis of the femoral head. Sci Rep. 2017;7(1):15035.
38. Lee YJ, Cui Q, Koo KH. Is there a role of pharmacological treatments in the prevention or treatment of osteonecrosis of the femoral head? A systematic review. J Bone Metab. 2019;26(1):13-18.
39. Ito C, Evans WE, McNinch L, et al. Comparative cytotoxicity of dexamethasone and prednisolone in childhood acute lymphoblastic leukemia. J Clin Oncol. 1996;14(8):2370-2376.
40. Kawedia JD, Liu C, Pei D, et al. Dexamethasone exposure and asparaginase antibodies affect relapse risk in acute lymphoblastic leukemia. Blood. 2012;119(7): 1658-1664.
41. Pritchett JW. Statin therapy decreases the risk of osteonecrosis in patients receiving steroids. Clin Orthop Relat Res. 2001;(386): 173-178.
42. Pengde K, Fuxing P, Bin S, Jing Y, Jingqiu C. Lovastatin inhibits adipogenesis and prevents osteonecrosis in steroid-treated rabbits. Joint Bone Spine. 2008;75(6):696-701.
43. Ajmal M, Matas AJ, Kuskowski M, Cheng EY. Does statin usage reduce the risk of corticosteroid-related osteonecrosis in renal transplant population? Orthop Clin North Am. 2009;40(2):235-239.
44. Peckett AJ, Wright DC, Riddell MC. The effects of glucocorticoids on adipose tissue lipid metabolism. Metabolism. 2011;60(11): 1500-1510.
45. Peng J, Luo F, Ruan G, Peng R, Li X. Hypertriglyceridemia and atherosclerosis. Lipids Health Dis. 2017;16(1):233.
46. Janke LJ, Van Driest SL, Portera MV, et al. Hypertension is a modifiable risk factor for osteonecrosis in acute lymphoblastic leukemia. Blood. 2019;134(12):983-986.
47. Therrien R, Barret P, Robitaille M, Moghrabi A. Use of fenofibrate in asparaginase-induced hypertriglyceridemia in children with ALL: a case series. http://wwwindicibleca/urpp/20130516_FENOFIBRATE_Annalespdf. 2013
48. Wheeler KA, West RJ, Lloyd JK, Barley J. Double blind trial of bezafibrate in familial hypercholesterolaemia. Arch Dis Child. 1985;60(1):34-37.
49. Smalley CM, Goldberg SJ. A pilot study in the efficacy and safety of gemfibrozil in a pediatric population. J Clin Lipidol. 2008;2(2):106-111.
50. Expert Panel on Integrated Guidelines for Cardiovascular Health and Risk Reduction in Children and Adolescents: National Heart, Lung and Blood Institute. Expert panel on integrated guidelines for cardiovascular health and risk reduction in children and adolescents: summary report. Pediatrics. 2011;128(Suppl 5):S213-56.
51. Steinmetz J, Morin C, Panek E, Siest G, Drouin P. Biological variations in hyperlipidemic children and adolescents treated with fenofibrate. Cli Chim Acta. 1981;112(1):43-53.

Ferrata Storti Foundation

Haematologica 2021
Volume 106(8):2102-2113

CD44 engagement enhances acute myeloid leukemia cell adhesion to the bone marrow microenvironment by increasing VLA-4 avidity

Julia C. Gutjahr,[1,2*] Elisabeth Bayer,[1*] Xiaobing Yu,[3] Julia M. Laufer[4], Jan P. Höpner,[1] Suzana Tesanovic,[5] Andrea Härzschel,[6] Georg Auer,[1] Tanja Rieß,[1] Astrid Salmhofer,[1] Eva Szenes,[1] Theresa Haslauer,[1] Valerie Durand-Onayli,[1] Andrea Ramspacher,[5] Sandra P. Pennisi,[6] Marc Artinger,[4] Nadja Zaborsky,[1] Alexandre Chigaev,[7] Fritz Aberger,[5] Daniel Neureiter,[8] Lisa Pleyer,[1] Daniel F. Legler,[4,9] Veronique Orian-Rousseau,[3] Richard Greil[1] and Tanja N. Hartmann[1,6]

[1]Department of Internal Medicine III with Hematology, Medical Oncology, Hemostaseology, Infectiology and Rheumatology, Oncologic Center, Salzburg Cancer Research Institute - Laboratory for Immunological and Molecular Cancer Research (SCRI-LIMCR), Paracelsus Medical University, Cancer Cluster Salzburg, Salzburg, Austria; [2]Centre for Microvascular Research, William Harvey Research Institute, Barts and The London School of Medicine and Dentistry, Queen Mary University of London, London, UK; [3]Karlsruhe Institute of Technology, Institute of Toxicology and Genetics, Karlsruhe, Germany; [4]Biotechnology Institute Thurgau (BITg) at the University of Konstanz, Kreuzlingen, Switzerland; [5]Department Biosciences, Paris-Lodron University of Salzburg, Cancer Cluster Salzburg, Salzburg, Austria; [6]Department of Internal Medicine I, Medical Center and Faculty of Medicine, University of Freiburg, Freiburg, Germany; [7]Department of Pathology and Cancer Center, University of New Mexico, Albuquerque, NM, USA; [8]Institute of Pathology, Paracelsus Medical University Salzburg, Salzburg, Austria and [9]Theodor Kocher Institute, University of Bern, Bern, Switzerland

**JCG and EB contributed equally as co-first authors.*

ABSTRACT

Adhesive properties of leukemia cells shape the degree of organ infiltration and the extent of leukocytosis. CD44 and the integrin VLA-4, a CD49d/CD29 heterodimer, are important factors in progenitor cell adhesion in bone marrow. Here, we report their cooperation in acute myeloid leukemia (AML) by a novel non-classical CD44-mediated way of inside-out VLA-4 activation. In primary AML bone marrow samples from patients and the OCI-AML3 cell line, CD44 engagement by hyaluronan induced inside-out activation of VLA-4 resulting in enhanced leukemia cell adhesion on VCAM-1. This was independent of VLA-4 affinity regulation but based on ligand-induced integrin clustering on the cell surface. CD44-induced VLA-4 activation could be inhibited by the Src family kinase inhibitor PP2 and the multikinase inhibitor midostaurin. As a further consequence, the increased adhesion on VCAM-1 allowed AML cells to bind stromal cells strongly. Thereby, the VLA-4/VCAM-1 interaction promoted activation of Akt, MAPK, NF-κB and mTOR signaling and decreased AML cell apoptosis. Collectively, our investigations provide a mechanistic description of an unusual CD44 function in regulating VLA-4 avidity in AML, enhancing AML cell retention in the supportive bone marrow microenvironment.

Correspondence:

TANJA N. HARTMANN
tanjanhartmann@gmail.com

Received: July 12, 2019.

Accepted: June 26, 2020.

Pre-published: July 2, 2020.

https://doi.org/10.3324/haematol.2019.231944

Introduction

Acute myeloid leukemia (AML) is an aggressive and difficult-to-treat hematologic malignancy, characterized by the accumulation of immature myeloid blasts. Within the bone marrow (BM), AML cells interact and communicate with stromal and immune cells and reprogram mesenchymal stromal cells to selectively support leukemic cells, while simultaneously suppressing normal hematopoiesis.[1] These microenvironmental interactions contribute to protect leukemic stem cells from chemotherapeutic drugs, thus allowing residual disease after therapy, ultimately causing relapses.[1] A better understanding of the adhesive mechanisms that facilitate

the interactions between AML cells and the supportive microenvironment may pave the way for novel combination therapies antagonizing residual disease.

The glycoprotein CD44 functions by binding to its major ligand hyaluronic acid (HA), which is expressed by BM stromal cells and endothelial cells.[2] In AML, targeting CD44 reduced leukemic repopulation in serial transplantations by eradication of leukemic stem cells.[3]

A second key orchestrator of leukemic cell-BM microenvironment interactions is the integrin VLA-4, a CD49d/CD29 heterodimer. The binding of VLA-4 to its ligand VCAM-1 is strengthened by inside-out signaling. This means that external stimuli mediate intracellular signaling triggered by other cell surface receptors, resulting in a change of either the avidity or the affinity of the integrin for its ligands.[4] Avidity changes occur due to cluster formation of the integrin, whereas affinity is increased by conformational changes.[5] Cooperativity of CD44 and VLA-4 has previously been suggested, but little is known about the mechanism.[6-8] To elucidate the mechanistic crosstalk between the two key homing factors, CD44 and VLA-4, to the BM in AML cell lines and primary AML cells, we used adoptive transplantations as well as static and shear flow adhesion assays in combination with immunofluorescence microscopy approaches. We uncovered a novel HA/CD44-induced inside-out activation of the integrin VLA-4. This activation leads to increased avidity due to VLA-4 clusters but no alterations in affinity between VLA-4 and its ligand VCAM-1. This elevated adhesion is important for AML cell retention in the stromal niche.

Methods

Study approvals and processing of patients' samples

Following written informed consent, BM aspirates from patients with newly diagnosed AML were collected at the Third Medical Department, Paracelsus Medical University Salzburg, Austria (Salzburg ethics committee approval number: 415-E/2009/2-2016). Normal CD34$^+$ progenitor cells from patients with myeloma or non-Hodgkin lymphoma who underwent hematopoietic stem/progenitor cell mobilization were used as non-myeloid controls (Salzburg ethics committee approval number: 415-E/1177/8-2010). Mononuclear cells were isolated using density gradient centrifugation and the viable cells were frozen until further usage. The patients' characteristics are shown in *Online Supplementary Table S1*.

The approval number for the animal experiments is BMWF-66.012/0032-WF/V/3b/2017.

Adoptive transfers

For blocking experiments, primary AML cells or OCI-AML3 cells were pretreated with αCD44 Fab fragments (clone 515, 5 μg/mL) or αCD49d (clone HP2/1, 5 μg/mL) antibodies for 15 min at 37°C, where indicated. The specificity of the blockade was confirmed by isotype control experiments in representative experiments. For homing *versus* engraftment assays (3 h and 3 days), cells were stained using the CellTrace™ Violet Cell Proliferation Kit (Thermo Fisher). Cells (0.3-1.3x10^6) were injected intravenously into NOD *scid* gamma (NSG) mice. After 3 h or 3 days, the mice were sacrificed, and the number of human cells that had homed to BM, spleen and peripheral blood was determined using αCD44 (clone J.173)- and αCD49d (clone 9F10)-specific antibodies. Homing rate was calculated as the number of CD44 and CD49d double-positive cells divided by the number of total measured cells divided by the number of injected AML cells.[9,10] Proliferation after 3 days was determined on the basis of CellTrace™ dye dilution rates.[10] For long-term engraftment (28 days) shCont or shCD49d OCI-AML3 cells were injected intravenously into NSGS mice. After 28 days, the mice were sacrificed, and the number of human CD15 and CD45 double-positive cells per million measured BM cells, spleen cells or per microliter of blood was determined.

Clustering assay

VLA-4 clustering assays were performed as described elsewhere,[11] using 7.5 μg/mL VCAM-1/Fc. AML cells were pretreated for 10 min with 10 μg/mL HA, 60 min with 1 μM midostaurin, 30 min with 10 μM PP2 and 30 min with 10 μM cobimetinib (APExBIO, Houston, USA), where indicated. Cells were allowed to adhere for 30 min at 37°C before fixation with 4% paraformaldehyde. Slides were stained with αCD49d (clone AHP1225), αCD29 (clone 12G10) primary antibodies or isotype control (not shown) followed by a secondary antibody. For CD49d cluster analysis of normal progenitor cells from patients with non-myeloid malignancies, cells were additionally stained with αCD34 antibody (clone QBEND-10). For quantification, high-resolution images were acquired on a Leica TCS SP5 II laser-scanning microscope using a 63×/1.4-NA oil-immersion objective (Leica, Wetzlar, Germany). The number of clusters was analyzed using ImageJ software by particle analysis setting the size of the particle at >2 pixels.[12]

Stroma binding

Falcon culture slides were left either uncoated or coated with 20 μg/mL fibronectin for 1 h at 37°C and then 70,000 M2 stromal cells were seeded and cultured overnight. Primary AML (1x10^6 cells) or OCI-AML3 cells (0.5x10^6 cells) were seeded on M2 stromal cells and co-cultured for 30 min at 37°C. Cells were washed, fixed with 4% paraformaldehyde, and stained using DAPI Antifade Reagent. Images were taken with an Olympus IX81 microscope (UPLSAPO 20xO/0.85 objective). Numbers of cells were determined in 12 pictures for each treatment with ImageJ software.

Additional experimental procedures are described in the *Online Supplementary Methods*.

Results

CD44 reflects and mediates leukemic infiltration of bone marrow

We measured CD44 and CD49d surface expression of BM-derived primary AML patients' samples and the AML cell line OCI-AML3 by flow cytometry. All AML patient-derived blasts, identified via CD45/side scatter gating,[13] and OCI-AML3 cells, expressed CD44 and CD49d (Figure 1A). We also screened various other AML cell lines, which cover most of the AML subtypes, i.e., MV4-11, KG-1a, HL-60, MOLM-13 and MOLM-14, and found a similar expression pattern (*Online Supplementary Figure S1A*).

We next determined the *in vivo* contribution of CD44 and CD49d to homing of AML cells by performing short-term adoptive transfer experiments of primary human AML cells as well as OCI-AML3 cells in immunodeficient NSG mice. In five independent experiments, total mononuclear cells from BM aspirates of five different AML patients (2 with wild-type *FLT3*, 3 with *FLT3*-ITD mutations) with a blast content of over 75% were either left untreated or treated with αCD44 Fab fragment (clone 515) or αCD49d antibody

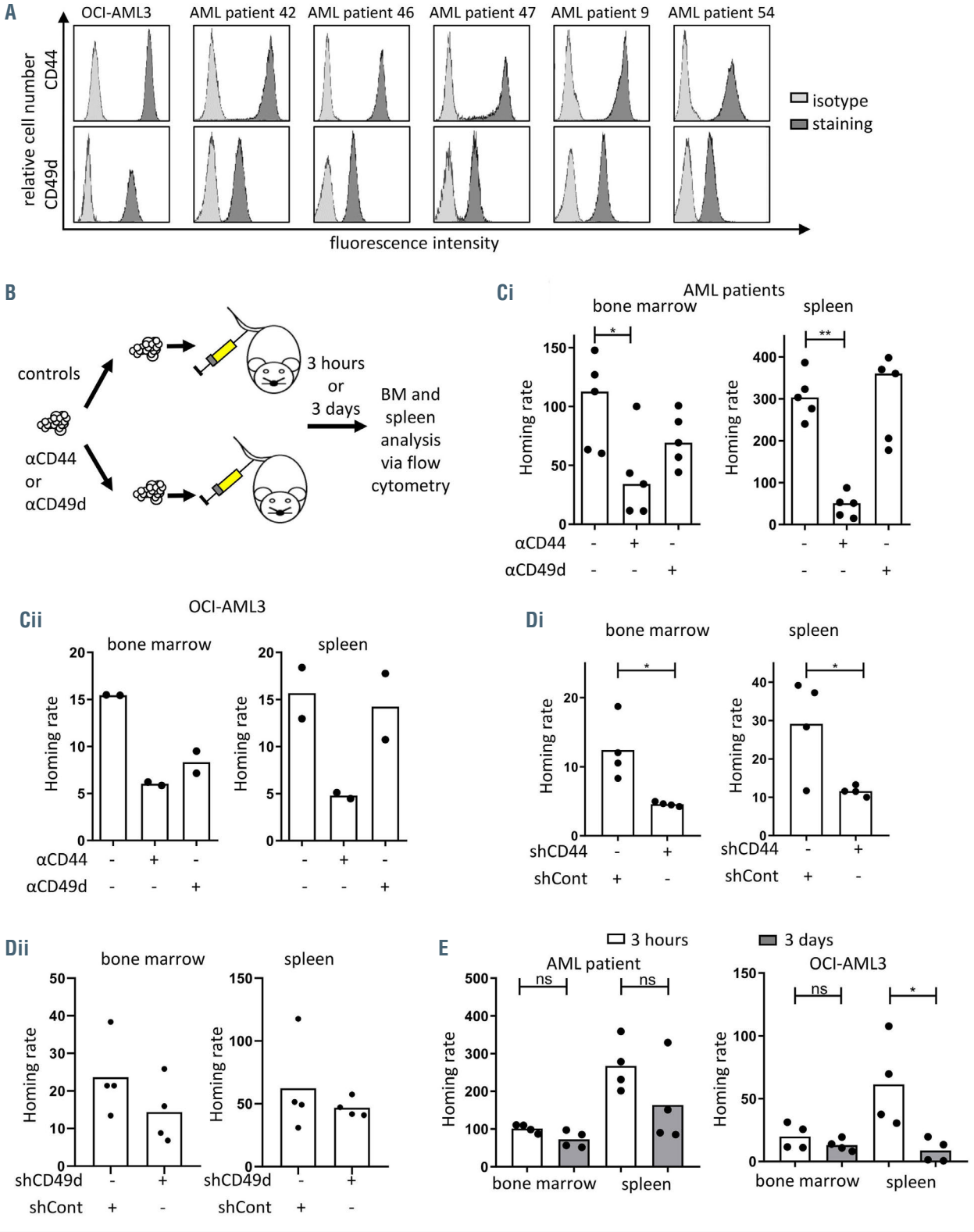

Figure 1. CD44 and CD49d are both expressed on acute myeloid leukemia cells; CD44 has a predominant role in homing. (A) Representative histograms of CD44 and CD49d surface expression of primary acute myeloid leukemia (AML) cells and the AML cell line OCI-AML3. (B) Mononuclear cells from bone marrow (BM) aspirates of AML patients pretreated or not with αCD44 antibody clone 515 (αCD44) or αCD49d clone HP2/1 (αCD49d) were injected into the tail veins of NSG mice. After 3 h the number of AML cells that had homed to BM and spleen of the recipients was determined by flow cytometry using human-specific αCD44 and αCD49d antibodies. The homing rate was defined as the number of measured leukemic cells per 10^6 measured cells per 10^6 injected cells. (Ci) Homing rate to BM and spleen 3 h after injection was measured in five independent experiments using samples from five different AML patients. In each experiment, technical duplicates were performed and they were averaged for the analysis. (Cii) Homing rate to BM and spleen was measured 3 h after injection of OCI-AML3 (n=2). (Di + ii) Homing rate to BM and spleen was measured 3 h after injection of OCI-AML3 cells transduced with shCD44 or shCD49d or control shRNA (shCont) (n=4, unpaired *t*-test). (E) Mononuclear cells from the BM aspirate of one AML patient and OCI-AML3 cells were injected into the tail veins of NSG mice. After 3 h and 3 days the number of AML cells that had homed or engrafted to BM and spleen of the recipient mice was determined by flow cytometry using human-specific αCD44 and αCD49d antibodies (n=4, unpaired *t*-test). **P*<0.05; ***P*<0.01; ns: not significant.

(clone HP2/1) and intravenously injected into NSG mice. Mice were sacrificed after 3 h (short-term homing, allowing leukemia cell entry into organs but no proliferation), and transplanted cells were flow cytometrically identified in the spleen and BM by human-specific antibodies (Figure 1B). Cells that had been treated with the blocking αCD44 Fab fragment had a lower capacity to home to BM within 3 h compared to untreated cells. The homing of primary human AML cells to the spleen was strongly diminished upon CD44 blockade. In contrast, αCD49d antibody treatment only slightly reduced BM homing of AML blasts and had no effect on their spleen homing (Figure 1Ci). In four of the five homing experiments we combined αCD44/αCD49d treatment, but additional CD49d blockade did not further increase the inhibitory effect above the level achieved by treatment with αCD44 alone (*Online Supplementary Figure S1B*). Comparable effects were observed when using OCI-AML3 cells (Figure 1Cii). The significantly reduced recovery of αCD44-treated cells was not due to toxicity of the antibody, as *in vitro* treatment for 3 h had no effect on cell viability (*Online Supplementary Figure S2A*). Neither the functional inhibition of CD44 nor the inhibition of CD49d affected the general CD44 and CD49d expression of the cells (*Online Supplementary Figure S2B*). Anti-CD44 antibody treatment did not affect CD44/E-selectin-mediated cell arrest (*Online Supplementary Figure S2C*). We genetically confirmed the contribution of CD44 to homing by CD44 knockdown in OCI-AML3 cells (*Online Supplementary Figure S2Dii*), observing a significant reduction in homing of $CD44^{low}$ cells (Figure 1Di). These cells also showed reduced rolling on HA substrates under shear flow (*Online Supplementary Figure S2Di*). CD49d knockdown, which was confirmed via quantitative polymerase chain reaction (PCR), did slightly reduce homing and arrests of CD49d knockdown OCI-AML3 on VCAM-1 substrate were diminished (Figure 1Dii, *Online Supplementary Figure S2Ei+ii*). Concurrent analysis 3 days after transplantation allowed us to investigate not only homing but also early engraftment, which includes the first proliferation events.[14] We noted equal numbers of primary AML cells and OCI-AML3 cells at 3 h and 3 days in BM while leukemic recovery in spleen was diminished after 3 days (Figure 1E). In concordance, recovered AML cells had undergone more cell divisions in BM than in spleen at this time (*Online Supplementary Figure S2Fi+ii*), indicating that the BM rather than the spleen microenvironment provides supportive signals for leukemic engraftment. Furthermore, when NSGS mice were engrafted with human AML cells and afterwards treated with an αCD44 antibody, the AML pool shifted from BM to spleen 1 day after treatment, suggesting that CD44 is a BM retention factor (*Online Supplementary Figure S2G*). In summary, we found that CD44 plays a key role in homing of AML cells to murine BM and spleen, with the BM providing a favorable environment for early engraftment of AML.

An interaction between hyaluronic acid and CD44 triggers inside-out activation of VLA-4 in acute myeloid leukemia

To dissect the AML homing process in a mechanistic manner, we used *in vitro* flow chamber assays, as described elsewhere.[15] These assays allowed us to study the individual and combined interactions of CD44 and VLA-4 expressed on AML cells with the respective ligands HA and VCAM-1. First, we perfused OCI-AML3 cells over an immobilized HA substrate under shear stress. We found that the cells had a strong capacity to tether to and roll on this substrate: this capacity was completely abolished upon

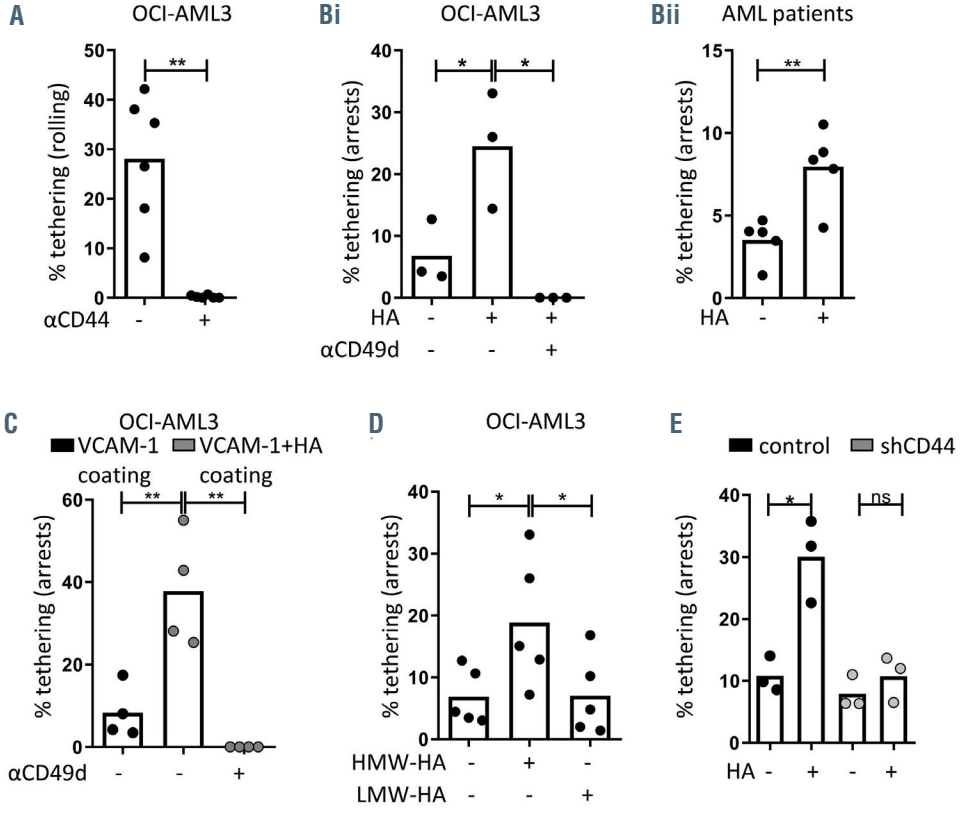

Figure 2. Hyaluronic acid treatment increases acute myeloid leukemia cell arrests on VCAM-1 under shear flow. (A) OCI-AML3 cells were perfused over hyaluronic acid (HA). Where indicated, cells were pretreated with blocking αCD44 antibody (clone 515). (B) OCI-AML3 (i) or primary acute myeloid leukemia (AML) cells from five different patients (ii) were perfused over VCAM-1. Where indicated, cells were pretreated with soluble HA or αCD49d antibody (clone HP2/1) (abrogating VLA-4-mediated interactions). (C) OCI-AML3 cells were perfused over a VCAM-1 or VCAM-1/HA substrate upon pretreatment with αCD49d antibody (clone HP2/1), where indicated. (D) OCI-AML3 cells were perfused over VCAM-1. Where indicated, cells were pretreated with low molecular weight HA (LMW-HA) or high molecular weight HA (HMW-HA). (E) OCI-AML3 cells transduced with shCD44 or control shRNA were perfused over VCAM-1; cells were pretreated with soluble HA, where indicated. Categories of interaction (tethers) are expressed as frequencies of cells in direct contact with the substrate. Two groups were compared with a paired *t*-test, three groups were compared with one-way analysis of variance with multiple comparisons. **P*<0.05; ***P*<0.01; ns: not significant.

treatment with αCD44 blocking antibody (clone 515) (Figure 2A). We further confirmed this HA-binding capacity by flow cytometry using fluorescein-labeled HA (HA-FITC) (*Online Supplementary Figure S3A*). Next, we tested whether AML cells were capable of tethering to the VLA-4 ligand VCAM-1 under shear flow conditions. Unstimulated OCI-AML3 and primary AML cells from five different patients bound immobilized VCAM-1 at low adhesive strength, which was evident by the low frequency of firm adhesion on this substrate (Figure 2Bi+ii). Treatment with a blocking αCD49d antibody abrogated all interactions of the OCI-AML3 and primary cells with the immobilized VCAM-1, confirming the VLA-4 dependency of this process (Figure 2Bi, *Online Supplementary Figure S3B*). Notably, pre-treating AML cells with the CD44 ligand HA and then perfusing the cells over a VCAM-1 substrate increased adhesion, without changing CD44 or CD49d surface expression (Figure 2Bi+ii, *Online Supplementary Figure S3C*), which suggests HA/CD44-induced inside-out VLA-4 activation. Co-immobilization of both ligands HA and VCAM-1 resulted in strong CD49d-dependent adhesive capacity of the leukemia cells, suggesting inside-out activation rather than mere additive effects in adhesion (Figure 2C). CD44-mediated inside-out signaling is well known to vary depending on the molecular weight of the HA trigger.[16] Indeed, CD44-induced VLA-4 activation was only achieved by high molecular weight HA, but not by low molecular weight HA (Figure 2D). Using shCD44-transduced OCI-AML3 cells confirmed that the increased VLA-4/VCAM-1 binding upon HA treatment is CD44-dependent (Figure 2E). These data indicated an unusual integrin activation, different from the well-described, classical CXCL12/CXCR4-induced VLA-4 activation,[17] which led us to investigate the nature of this molecular crosstalk .

Hyaluronic acid-induced inside-out signaling to VLA-4 results in CD49d cluster formation but not in VLA-4 affinity modulation

VLA-4-dependent adhesion is controlled by either affinity changes, gained by several conformational states of the integrin,[18] or avidity changes due to clustering of the molecule on the cell surface[19] (*Online Supplementary Figure S4A*). To investigate the alterations in VLA-4 conformational states upon HA treatment, we used the αCD29 antibody (clone HUTS-21) that binds solely to the ligand-occupied state of VLA-4.[20] To mimic VLA-4 ligand binding, we used a probe containing the conserved Leu-Asp-Val (LDV) sequence, specific for the VLA-4 binding site. Manganese was used as a positive control as it induces the maximal extent of VLA-4 activation, which is not achieved under physiological conditions.[20] Surprisingly, OCI-AML3 cells expressed VLA-4 in an inactive conformation irrespectively of whether the cells were treated with HA or not and bound its ligand with comparable affinity (*Online Supplementary Figure S4B*).[15,20] This unexpected finding prompted us to elucidate whether the HA-induced AML cell arrests on the substrate are based on increased avidity rather than affinity of VLA-4 to VCAM-1. We performed immunofluorescence microscopy and found increased CD49d cluster formation on AML cells upon treatment with HA. This was quantified by counting the number of the clusters on the individual OCI-AML3 and patient AML cells (1 representative of 6 patients shown) (Figure 3Ai+ii). The mean number of clusters per cell was compared between untreated and HA-treated cells from all six patients (Figure 3Aiii). HA treatment also induced clustering of the VLA-4 β subunit CD29 (*Online Supplementary Figure S4C*). Pretreatment with blocking αCD44 (clone 515) inhibited cluster formation on OCI-AML3 as well as primary AML cells (Figure 3B). Using CD44 knockdown and control transduced OCI-AML3 cells, we confirmed that HA-induced CD49d clustering only occurred in cells that expressed CD44 (Figure 3C). This cluster formation translated into enhanced adhesive capacity, as we confirmed in an additional static cell adhesion assay, using an alternative colorimetric method for cell counting (*Online Supplementary Figure S4D*). We also performed an avidity-detecting shear flow assay, as described by Alon *et al.*,[21] by perfusing OCI-AML3 cells and primary cells over an αCD49d (clone HP2/1) substrate, further confirming our observations (Figure 3D, *Online Supplementary Figure S4E*). To get an insight into the lateral organization of the VLA-4 clusters on the membrane, we used methyl-beta-cyclodextrin (MßcD), which interferes with lipid structures. Although MßcD did not significantly reduce the number of HA-induced VLA-4 clusters, it abrogated their function to support cell tethering to VCAM-1 (*Online Supplementary Figure S4F*).

Next, we studied whether CD44-mediated inside-out activation is a general mechanism that also occurs in non-transformed progenitor cells. Using $CD34^+$ cells from four different patients harboring a non-myeloid, i.e. lymphoid malignancy occurring at later differentiation states (non-Hodgkin-lymphoma [n=3] and multiple myeloma [n=1]), we did not find HA-induced CD49d clustering, suggesting that induced cluster formation is a specific feature of transformed myeloid progenitor cells (Figure 3E).

Transformed myeloid progenitors may differ in their CD44variant (CD44v) composition, with an impact on the clinical outcome of AML patients.[22] We have analyzed the CD44v composition of several cell lines as well as primary AML samples and normal $CD34^+$ cells by reverse transcription PCR and found differences in the length of CD44v6 containing transcripts among the different primary samples (*Online Supplementary Figure S5A*). Interestingly, in OCI-AML3 CD44v6 cells, co-immunoprecipitated with CD49d, with a slight pull down increase when cells were preincubated with HA (*Online Supplementary Figure S5B*). In conclusion, our data demonstrate that HA/CD44 binding induces CD49d cluster formation in AML, but not normal $CD34^+$ progenitor cells, without changing the conformation of the VLA-4 heterodimer.

Src family kinase inhibition and midostaurin treatment interfere with the CD44-VLA-4 activation axis

Src family kinases (SFK) are important downstream molecules of HA/CD44[23] and likely candidates for integrin activation.[24] To confirm Src and PI3K activation upon HA treatment, we analyzed Src and Akt phosphorylation by western blot in native, control and shCD44-transduced OCI-AML3 cells (*Online Supplementary Figure S6A*). Remarkably, treating cells with the pan-SFK inhibitor PP2 abrogated the formation of HA-induced CD49d clusters on the surface of OCI-AML3 cells (Figure 4Ai) and six different AML patients' samples (Figure 4Aii + Ci), providing evidence that CD49d clustering was Src family-dependent. To start from broad but therapeutically relevant kinase inhibition, we used the multikinase inhibitor midostaurin, approved for the treatment of *FLT3*-mutated AML. We found that midostaurin is highly potent in antagonizing HA-induced CD49d cluster formation of OCI-AML3 cells (Figure 4Bi)

and six different AML patients' samples independently of their *FLT3* mutation status (*FLT3* wild-type [n=3], *FLT3*-ITD [n=3]) (Figure 4Bii + Cii).

Additional experiments, using the MEK inhibitor cobimetinib and the PI3Kδ inhibitor idelalisib, further suggested that PI3K, but not MAPK pathways are involved in CD44-triggered inside-out CD49d cluster formation (*Online Supplementary Figure S6B*). We next confirmed that PP2, midostaurin and idelalisib treatment not only inhibited cluster formation, but also reduced the binding of primary

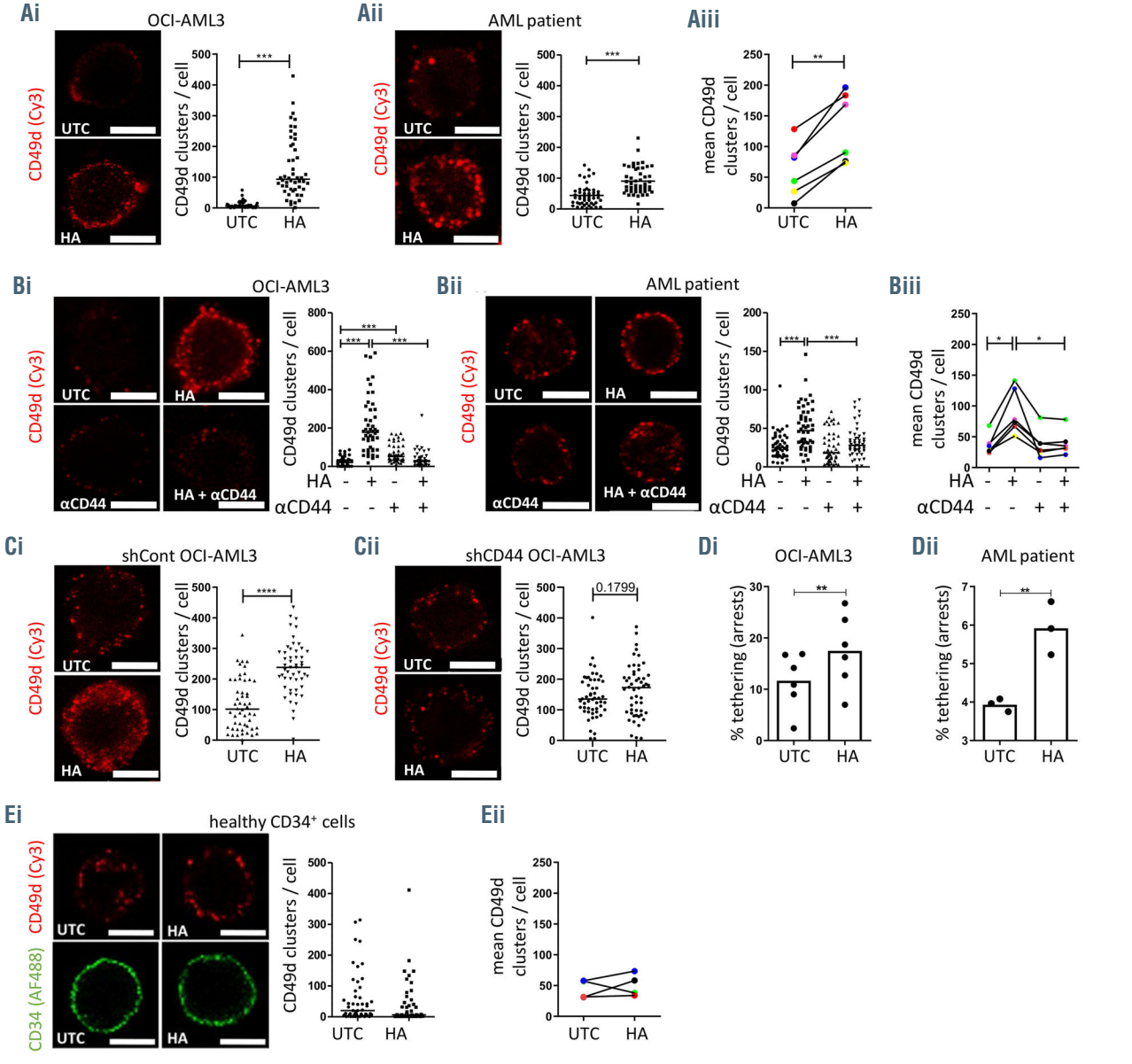

Figure 3. Hyaluronic acid treatment induces CD49d cluster formation on acute myeloid leukemia cells. (A) Confocal images and CD49d cluster analysis of OCI-AML3 (i) or primary acute myeloid leukemia (AML) cells from bone marrow (BM) aspirates (ii). Cells were untreated (UTC) or pretreated with hyaluronic acid (HA) and then settled on immobilized VCAM-1, followed by fixation and staining with αCD49d (red) monoclonal antibody (AHP1225), where indicated (1 representative of 6 different patients is shown). CD49d clusters for each treatment were quantified using ImageJ software (n=50 cells, unpaired *t*-test). Mean numbers of CD49d clusters per cell were compared from six different patients' samples with/without HA treatment (iii, paired *t*-test). (B) Confocal images and CD49d cluster analysis of OCI-AML3 (i) and primary AML cells (ii). Cells were pretreated with/without αCD44 antibody (clone 515) before treatment or not with HA and then settled on immobilized VCAM-1, followed by fixation and staining with αCD49d (red) monoclonal antibody. CD49d clusters were quantified for each treatment using ImageJ software (n=50 cells, one-way analysis of variance [ANOVA] with multiple comparisons). Mean numbers of CD49d clusters per cell were compared from six different patients' samples with/without HA treatment and with/without αCD44 treatment (iii, one-way ANOVA with multiple comparisons). (C) Confocal images and CD49d cluster analysis of control shRNA (shCont) (i) or shCD44-transduced OCI-AML3 (ii). Cells were pretreated with/without HA and then settled on immobilized VCAM-1, followed by fixation and staining with αCD49d (red) monoclonal antibody, where indicated (1 of 2 replicates is shown). CD49d clusters for each treatment were quantified using ImageJ software (n=50 cells, unpaired *t*-test). (D) OCI-AML3 (i) or primary cells (ii) were perfused over an αCD49d (clone HP2/1) substrate for 1 min at 0.5 dyn/cm^2 with/without HA pretreatment. Categories of interaction (tethers) are expressed as frequencies of cells in direct contact with the substrate (6 replicates were performed with OCI-AML3, 3 replicates were performed with a sample from 1 AML patient). (E) Primary CD34$^+$ cells from four different patients (3 with non-Hodgkin-lymphoma and 1 with multiple myeloma) were pretreated with/without HA and then settled on immobilized VCAM-1, followed by fixation and staining with αCD49d (red) and αCD34 (green, clone QBEND-10) monoclonal antibodies (1 representative patient's sample is shown). CD49d clusters were quantified for each treatment using ImageJ software (n=50 cells, unpaired *t*-test). (ii) Mean numbers of CD49d clusters per cell were compared from four different patients' samples with/without HA treatment (paired *t*-test). Bars, 5 μm. **P*<0.05; ***P*<0.01; ****P*<0.001; *****P*<0.0001.

AML cells (Figure 4D) and OCI-AML3 cells (*Online Supplementary Figure S6C*) to VCAM-1 under shear flow conditions. Collectively, our findings point to a Src family- and PI3K-dependent signaling pathway that is initiated upon HA/CD44 engagement, leading to CD49d cluster formation.

The hyaluronic acid-induced VLA-4/VCAM-1 interaction promotes an acute myeloid leukemia cell-stromal cell interaction leading to Akt, MAPK and NF-κB pathway activation

To further identify the impact of the CD44-mediated VLA-4 activation on pathophysiologically relevant processes in the BM microenvironment, we used a static adhesion assay combined with microscopy of AML cells on a stromal cell layer. Untreated or HA-pretreated OCI-AML3 cells or primary AML cells from four different patients were co-cultured with stromal cells for 30 min. After extensive washing, cell nuclei were visualized via DAPI staining. We found that HA-pretreated cells had a much higher ability to adhere firmly to stromal cells. We confirmed that this adhesion was dependent on the HA-induced interaction of VLA-4 expressed by the AML cells and the VCAM-1 expressed by the stromal cell, as additional pretreatment with the αCD44 antibody as well as pretreatment with the αCD49d antibody inhibited the HA-induced adhesion of OCI-AML3 cells on stromal cells (Figure 5A, B). Additional controls using CD44 knockdown and control transduced OCI-AML3 cells (*Online Supplementary Figure S7A*) as well as native OCI-AML3 on αVCAM-1-antibody-treated stromal

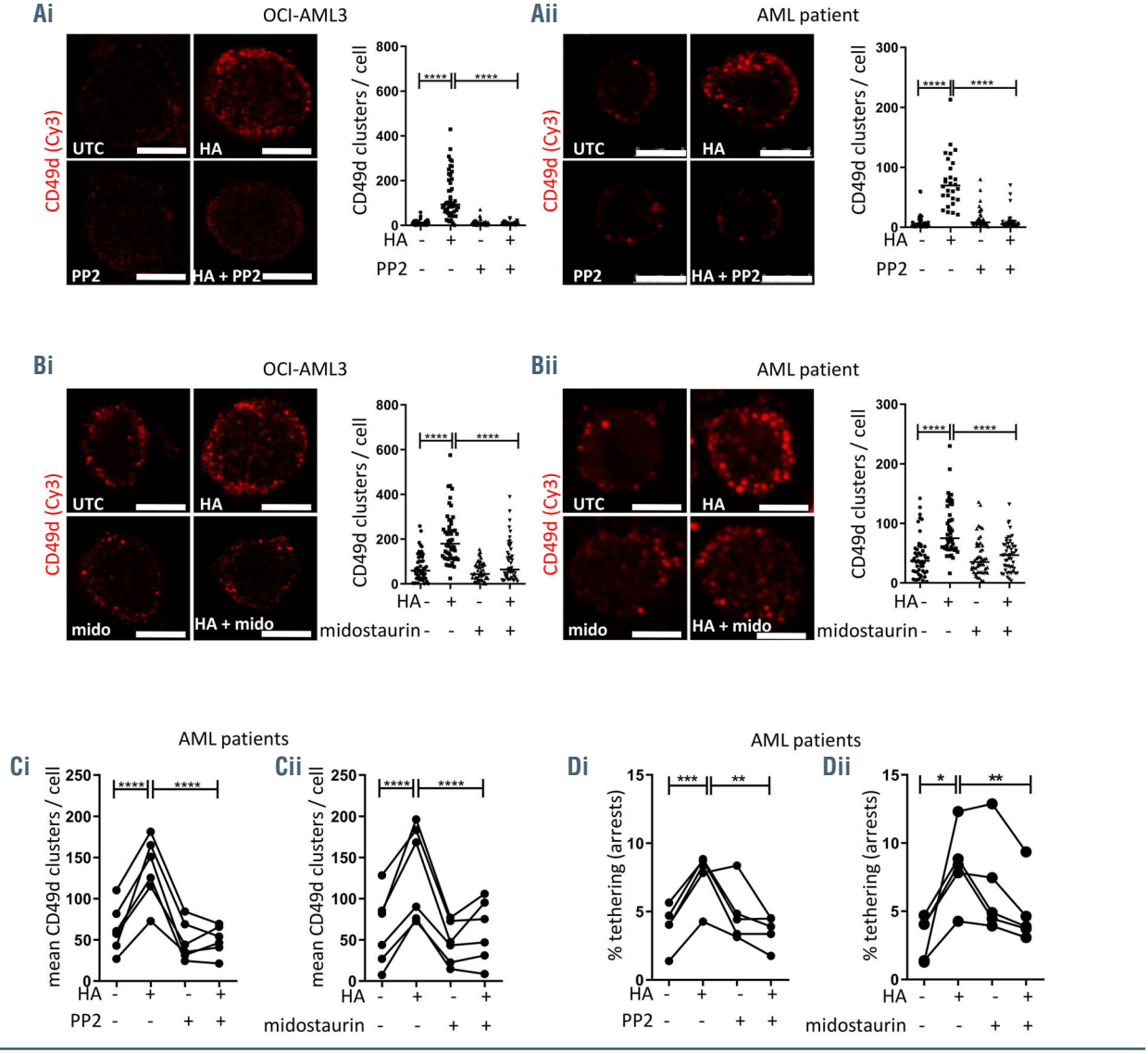

Figure 4. Src family kinase inhibition and midostaurin treatment of acute myeloid leukemia cells inhibit hyaluronic acid-induced cluster formation. (A) Confocal images of OCI-AML3 (i) or primary acute myeloid leukemia (AML) cells from bone marrow (BM) aspirates (ii) that were or were not pretreated with HA and/or the Src family kinase (SFK) inhibitor PP2. Cells were stained with αCD49d (red) monoclonal antibody (clone AHP1225). For OCI-AML3, one representative experiment of three is shown; for primary samples, one representative experiment of six is shown (n=50 cells). (B) Confocal images of OCI-AML3 (i) or primary AML cells from BM aspirates (ii). Cells were pretreated or not with HA and/or the multikinase inhibitor midostaurin. Cells were stained with αCD49d (red) monoclonal antibody. For OCI-AML3, one representative experiment of three is shown; for primary samples, one representative experiment of six is shown (n=50 cells). (C) Mean numbers of CD49d clusters per cell were compared from six different patients' samples with/without HA treatment and with/without PP2 treatment (i) or with/without midostaurin (ii). (D) Primary AML cells from five different patients with/without HA treatment and with/without PP2 treatment (i) or with/without midostaurin (ii) were subjected to shear flow analyses over VCAM-1. One-way analyses of variance with multiple comparisons were used. Bars, 5 μm. **P*<0.05; ***P*<0.01; ****P*<0.001; *****P*<0.0001; ns: not significant.

cells confirmed the specificity of the HA-CD44 interactions in triggering adhesion on VCAM-1 expressed by stromal cells (*Online Supplementary Figure S7B*).

We next investigated downstream signaling of this VLA-4/VCAM-1 interaction in AML cells by western blotting and quantified phosphorylation levels of previously shown signaling molecules that are important for AML cell survival, namely Akt, ERK, IκB and mTOR.[1] Primary cells from five different AML patients were treated with HA and/or with VCAM-1-coated beads, where indicated. In contrast to brief HA treatment, VCAM-1-coated beads alone were sufficient to increase phosphorylation of Akt, ERK, IκB and mTOR in primary AML cells (Figure 6A, B). This can be attributed to the experimental three-dimensional nature of this system, which allows a lot more cells to bind to the VCAM-1-coated beads than immobilized VCAM-1 used for microscopy (*Online Supplementary Figure S8A*). In line with this, VCAM-1 also triggered phosphorylation of ERK, IkB, FAK and paxillin (Pax) in OCI-AML3 cells (*Online Supplementary Figure S8B*).

In light of the key role of active Akt, MAPK, and NF-κB signaling in leukocyte survival, we next tested the protective effect of the CD44-VLA-4-dependent cell adhesion in the context of chemotherapy. We found that OCI-AML3 cells adherent to a co-immobilized substrate of HA and VCAM-1 underwent less doxorubicin-induced apoptosis than cells lacking such a substrate. CD49d expression was mandatory for the protective effect as CD49d knockdown cells were not protected by HA/VCAM-1 (Figure 6C). The importance of CD49d in leukemic progression was also confirmed by long-term *in vivo* engraftment experiments in NSGS mice. AML progression was decelerated upon engraftment of CD49d knockdown (shCD49d) OCI-AML3 cells as compared to engraftment of control cells (shCont) (Figure 6D). In a xenotransplant model anti-CD49d antibody treatment altered the organ-specific localization of engrafted MOLM-13 cells, but did not significantly prolong the overall survival of mice undergoing cytarabine (AraC) treatment (*Online Supplementary Figure S9*). At this point we were not successful in establishing a model for testing standard induction therapy (combined AraC-doxorubicin) and anti-CD49d treatment in immunodeficient mice, as doxorubicin requires careful further dosing studies to avoid severe toxicities.

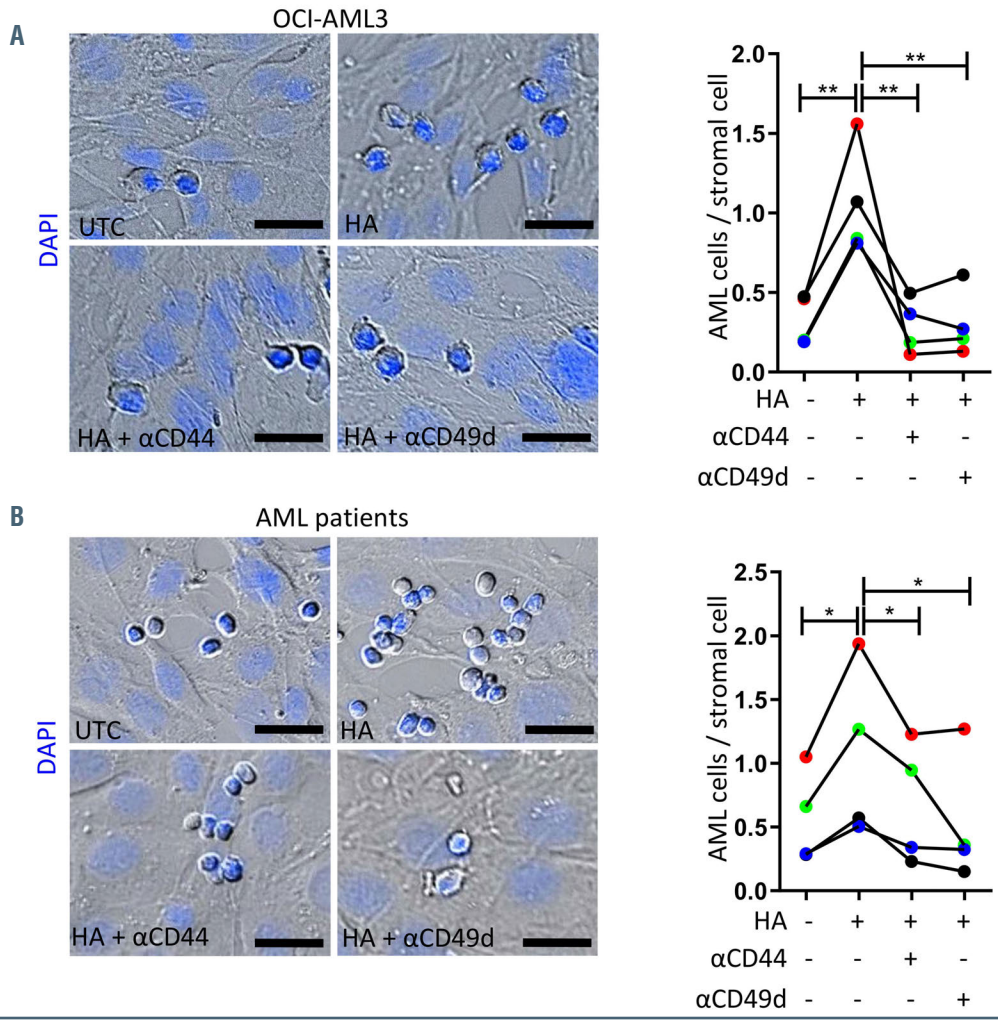

Figure 5. Hyaluronic acid treatment leads to strong interaction between acute myeloid leukemia cells and stromal cells. OCI-AML3 cells (n=4) (A) or primary cells from bone marrow (BM) aspirates from four different patients with acute myeloid leukemia (AML) (B) were pretreated or not with HA and/or αCD44 (clone 515) or αCD49d (clone HP2/1) and allowed to adhere to M2 stromal cells for 30 min. The number of AML cells that bound to the stromal cells was counted on bright field images with additional DAPI staining by fluorescence microscopy. One-way analyses of variance with multiple comparisons were used. Images were taken at 20x magnification. Bars, 20 μm. *P<0.05; **P<0.01.

In conclusion, we demonstrate that HA-induced VLA-4 cluster formation is critical for direct cell-cell contact of human AML cells with stromal cells, thereby contributing to supportive signaling pathways in AML cells (Figure 7).

Discussion

The BM microenvironment plays a decisive role in the evolution and persistence of AML.[1] Adhesive processes are mandatory to signal perception and leukemia cell-microenvironment communication by facilitating the retention of the tumor cells to protective cues. Moreover, CD44 has been reported to be a marker of primary human AML cancer stem cells and its blockade revealed a potential for differentiation in human AML cell lines.[3,25,26] Here, we identified a novel non-classical HA/CD44-triggered way of inside-out activation of the integrin VLA-4, leading to VLA-4 cluster formation and increased adhesive strength on VCAM-1, important for the direct interaction of AML cells with supportive stromal cells.

In short-term adoptive transfers of human primary AML cells to immunodeficient mice, we observed that CD44 had a key function in rapid tumor cell homing to BM and spleen, reflecting the biology of normal cellular counterparts as well as malignant cells, e.g. chronic myeloid leukemia-initiating cells.[27,28] However, BM engraftment of malignant cells is dependent not only on homing events but even more on retention of the cells in distinct supportive zones of this organ.[1] The VLA-4 integrin is known for being key for the retention of progenitor cells in BM.[29] The strength of binding of the integrin to its ligand VCAM-1,

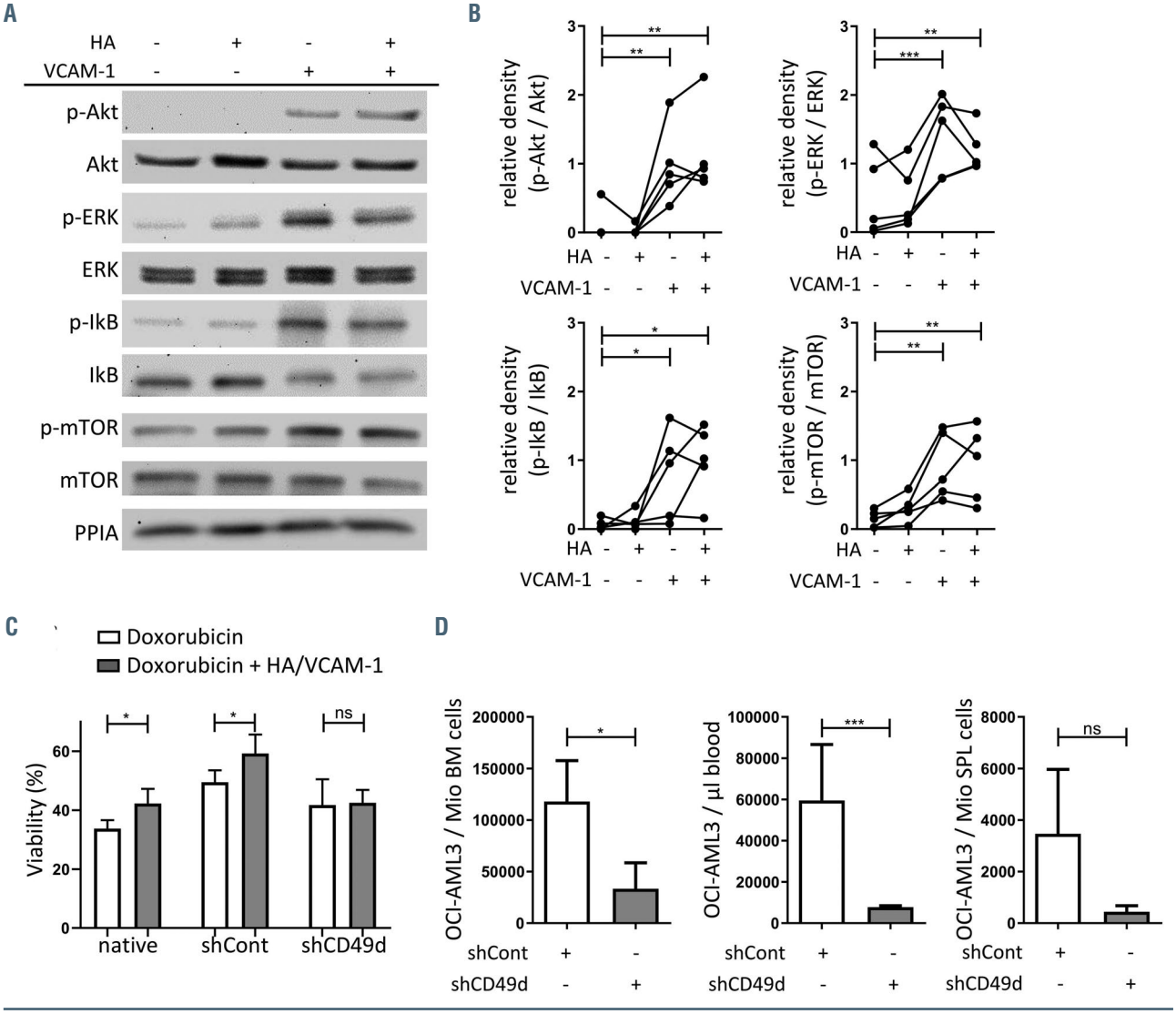

Figure 6. VLA-4 engagement triggers the phosphorylation of Akt, ERK, IκB and mTOR and contributes to acute myeloid leukemia progression. (A) Protein lysates of primary acute myeloid leukemia (AML) cells from bone marrow (BM) aspirates were treated or not with hyaluronic acid (HA) and/or VCAM-1-coated beads and tested for their ERK, phospho-ERK, Akt, phospho-Akt, IκBα, phospho-IκBα, mTOR and phospho-mTOR content by western blot. One representative experiment of five is shown. (B) Five independent experiments with five different AML patients' samples were quantified. Expression intensities were quantified with ImageJ software and phosphorylation was normalized to total protein content. One-way analyses of variance with multiple comparisons were used. (C) Apoptosis of native, shCont or shCD49d OCI-AML3 cells was induced with 0.5 µM of doxorubicin; additionally, cells were treated with immobilized HA and VCAM-1, where indicated. Cell viability was determined using trypan blue. Four replicates of one representative experiment of two independent experiments are shown. (D) Number of shCont or shCD49d OCI-AML3 cells in BM, blood, and spleen (SPL) of NSG mice, 28 days after intravenous injection (n=7 per group). *P<0.05; **P<0.01; ***P<0.001; ns: not significant.

which is presented by stromal cells, is thereby regulated by signaling cascades inducing increased affinity due to conformational changes of the integrin, the so-called inside-out signaling.[30] In contrast to the well-described, classical, chemokine-induced VLA-4 inside-out activation by conformational affinity alterations, less is known about chemokine-independent alternative integrin activation.[14,31] We have previously observed that in B-cell malignancies, signals via the B-cell receptor can induce changes not only in the affinity but also the avidity of the VLA-4 receptor.[11] Here, we identified an AML-specific HA/CD44-mediated VLA-4 activation via integrin cluster formation without obvious conformational modulation, further promoting strong VLA-4/VCAM-1 binding. This chemokine bypass from CD44 towards VLA-4 is somewhat reminiscent of the previously observed E-selectin/HCELL-VLA-4 interaction in mesenchymal stem cells,[32] but it clearly differs in the receptor-ligand couple (HA-CD44) and is observed for the first time in a leukocyte. Nevertheless, the reminiscence may point to a more general mechanism and is also interesting in light of the relevant role of E-selectin in AML and other hematologic malignancies.[33-38] Notably, we did not observe CD44-VLA-4 inside-out activation in normal CD34$^+$ mobilized progenitors, suggesting this is a transformation-related and tumor-acquired feature for increasing integrin-mediated retention of AML cells.

SFK are crucial downstream signaling molecules of CD44 in hematopoietic cells of healthy and sick individuals.[39-41] They can contribute to enrichment of CD44/β1 integrin complexes in lipid rafts[42] and also function immediately downstream of integrins, in concert with focal adhesion kinases.[43] Employing the SFK inhibitor PP2, we identified SFK within the CD44-mediated VLA-4 inside-out activation cascade, and propose that a further stabilization of VLA-4 clusters involves Src-FAK signaling. This could have therapeutic relevance as PP2 administration was reported to attenuate progression of a *FLT3*-mutated AML model.[44] However, in the light of the complexity of the Src kinase family, the particular kinase responsible for the HA/CD44-mediated inside-out signaling needs to be elucidated by a genetic screening approach.

We investigated the therapeutically relevant drug midostaurin, which is approved for treatment of FLT3-mutant AML,[45] and currently under clinical investigations in non-FLT3-mutated AML cases (NCT03512197). Midostaurin is a broad multikinase inhibitor, and more selective inhibitors, such as gilteritinib and quizartinib for FLT3 and dasatinib for Src kinases, recently entered the clinical stage.[46-48] Notably, kinase signals via *FLT3*-ITD can increase the affinity of VLA-4 to soluble VCAM-1.[49] Thus, the here reported CD44-dependent mechanism of VLA-4 activation may be an alternative pathway used by *FLT3* wild-type AML cells to increase their adhesion to protective stromal cells. As *FLT3* mutation status is an important prognostic marker in AML, it is interesting that the observed CD44/VLA-4 crosstalk was independent from the patients' *FLT3* mutation status, suggesting involvement of alternative compensatory kinases.

Further downstream of SFK, we supposed PI3K to mediate signaling[50-52] and indeed observed diminished HA-induced CD49d cluster formation in the presence of the PI3Kδ inhibitor idelalisib. PI3K has been described to promote human AML survival and BM stromal cell-mediated protection,[53] giving a rationale to investigate PI3K inhibitors further in AML. As another functional consequence, the VLA-4-mediated AML adhesion triggered activation of Akt, MAPK, mTOR and NF-κB pathways, which are known important mediators of AML survival.[53,54] However, in a first

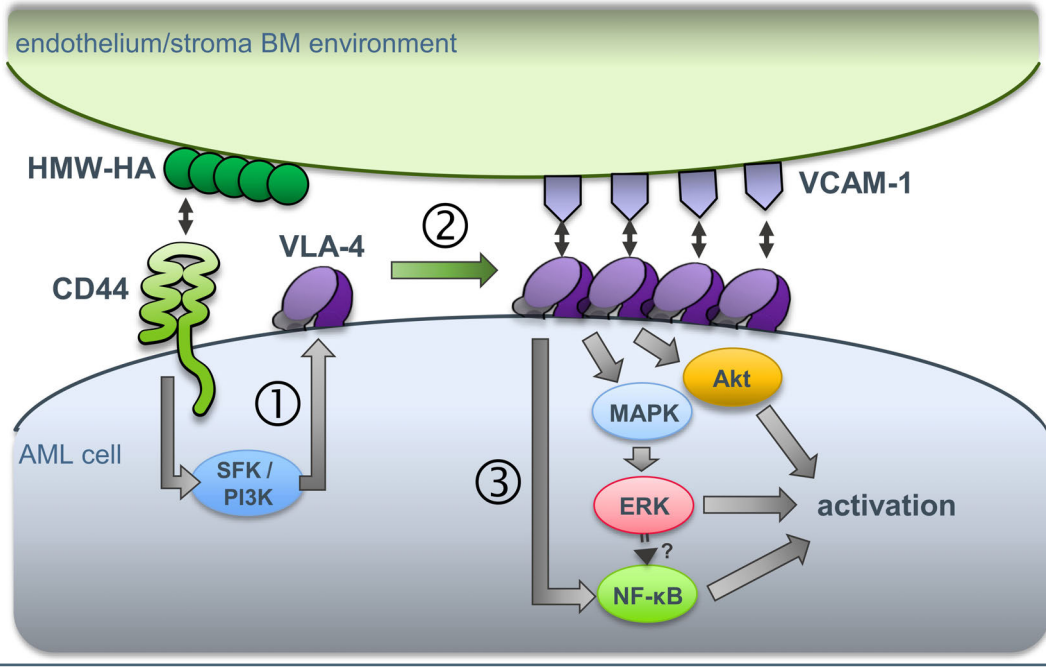

Figure 7. Schematic overview of the suggested CD44-VLA-4 activation axis and downstream consequences. Binding of acute myeloid leukemia (AML) cells to the bone marrow (BM) stromal component hyaluronic acid (HA) is dependent on CD44 and enhances adhesion of AML cells to the VLA-4 substrate VCAM-1, a second important adhesion factor displayed on stromal cells. Mechanistically, this enhanced adhesion is based on inside-out activation of VLA-4, without altering the conformation of the integrin. The signaling downstream of CD44 involves several kinases (e.g. Src family kinases [SFK]) causing clustering of the integrin, thereby stabilizing adhesion strength that facilitates direct interaction with stromal cells. This AML cell-stromal cell interaction leads to survival signaling involving activation of the Akt, MAPK and NF-κB pathways.

xenograft model we could not establish a treatment regime of combined VLA-4 inhibition and induction chemotherapy with a survival benefit for the mice. While this argues for kinase inhibition as the preferential cytarabine combination partner, it does not exclude a role of VLA-4 inhibition in other treatment schedules or at other disease points, e.g. during graft-*versus*-host management.

Taking all our data together, we suggest that HA binding to CD44 triggers a signaling axis via SFK and PI3K to rapidly trigger VLA-4 avidity and hence support the retention of AML cells in their preferential niches (Figure 7). Compensatory survival mechanisms of malignant cells still comprise a major challenge in current AML therapy which may be tackled by the use of combinatorial therapies, administering kinase inhibitors that may help to interfere with cellular position as well as growth signaling accompanied by drugs inducing apoptosis, as a step forward in improving current treatment modalities.

Disclosures

No conflicts of interest to disclose.

Contributions

JCG and TNH conceived and designed the study and wrote the manuscript. JCG, EB, XY, JML, AR, AC and DN developed the methodology. JCG, EB, XY, JML, JPH, GA, TR, AS, ES, TH, AH, ST, SP, AR, MA, AC and DN acquired data. JCG, EB, XY, JML, GA, TR, AS, AH, AC, DN, DFL; VO-R, RG and TNH analyzed and interpreted the data. JCG, EB, XY, JML,, JPH, GA, ST, TR, AS, ES, VD-O, AR, AH, NZ, AC, FA, DN and DFL reviewed and/or revised the manuscript. RG, LP, DN, DFL, VO-R. FA and TNH provided administrative, technical, or material support. TNH supervised the study.

Acknowledgments

We thank all patients for their participation in this study. We also thank the staff from Charles River Research Services Germany GmbH for excellent technical support. We thank Christoph Ratswohl for helpful revision of the manuscript and Alexandra Hödlmoser for support with handling the mice.

Funding

This work was supported by the SCRI-LIMCR GmbH, the province of Salzburg as support to the Cancer Cluster Salzburg work package 2, the Austrian Science Fund (FWF) 25015-B13 (to TNH), the PhD program Immunity in Cancer and Allergy (W1213, Austrian Science Fund) (to TNH, FA and RG), the Paracelsus Medical University PMU-FFF E-15/22/114-HAR (to TNH), the Wilhelm-Seiter Stiftung Freiburg (to TNH), the Deutsche Forschungsgemeinschaft (DFG, German Research Foundation) – 419090910 (to TNH) and the Swiss National Science Foundation (169936 & 189144) (to DFL). This work was also supported by the National Institutes of Health (USA) grant: UNM Comprehensive Cancer Center CCSG P30 CA118100 (to AC).

References

1. Zhou HS, Carter BZ, Andreeff M. Bone marrow niche-mediated survival of leukemia stem cells in acute myeloid leukemia: yin and yang. Cancer Biol Med. 2016;13(2):248-259.
2. Naor D, Nedvetzki S, Golan I, Melnik L, Faitelson Y. CD44 in cancer. Crit Rev Clin Lab Sci. 2002;39(6):527-579.
3. Jin L, Hope KJ, Zhai Q, Smadja-Joffe F, Dick JE. Targeting of CD44 eradicates human acute myeloid leukemic stem cells. Nat Med. 2006;12(10):1167-1174.
4. Alon R, Dustin ML. Force as a facilitator of integrin conformational changes during leukocyte arrest on blood vessels and antigen-presenting cells. Immunity. 2007;26(1):17-27.
5. Dustin ML, Bivona TG, Philips MR. Membranes as messengers in T cell adhesion signaling. Nat Immunol. 2004;5(4):363-372.
6. Lundell BI, McCarthy JB, Kovach NL, Verfaillie CM. Activation of beta1 integrins on CML progenitors reveals cooperation between beta1 integrins and CD44 in the regulation of adhesion and proliferation. Leukemia. 1997;11(6):822-829.
7. Verfaillie CM, Benis A, Iida J, McGlave PB, McCarthy JB. Adhesion of committed human hematopoietic progenitors to synthetic peptides from the C-terminal heparin-binding domain of fibronectin: cooperation between the integrin alpha 4 beta 1 and the CD44 adhesion receptor. Blood. 1994;84(6):1802-1811.
8. Singh V, Erb U, Zoller M. Cooperativity of CD44 and CD49d in leukemia cell homing, migration, and survival offers a means for therapeutic attack. J Immunol. 2013;191(10):5304-5316.
9. Brachtl G, Sahakyan K, Denk U et al. Differential bone marrow homing capacity of VLA-4 and CD38 high expressing chronic lymphocytic leukemia cells. PLoS One. 2011;6(8):e23758.
10. Gutjahr JC, Szenes E, Tschech L, et al. Microenvironment-induced CD44v6 promotes early disease progression in chronic lymphocytic leukemia. Blood. 2018;131(12):1337-1349.
11. Tissino E, Benedetti D, Herman SEM, et al. Functional and clinical relevance of VLA-4 (CD49d/CD29) in ibrutinib-treated chronic lymphocytic leukemia. J Exp Med. 2018;215(2): 681-697
12. Laufer JM, Lyck R, Legler DF. ZAP70 expression enhances chemokine-driven chronic lymphocytic leukemia cell migration and arrest by valency regulation of integrins. FASEB J. 2018;32(9):4824-4835.
13. Lacombe F, Durrieu F, Briais A, et al. Flow cytometry CD45 gating for immunophenotyping of acute myeloid leukemia. Leukemia. 1997;11(11):1878-1886.
14. Lapidot T, Dar A, Kollet O. How do stem cells find their way home? Blood. 2005;106(6):1901-1910.
15. Ganghammer S, Hutterer E, Hinterseer E, et al. CXCL12-induced VLA-4 activation is impaired in trisomy 12 chronic lymphocytic leukemia cells: a role for CCL21. Oncotarget. 2015;6(14):12048-12060.
16. Tavianatou AG, Caon I, Franchi M, Piperigkou Z, Galesso D, Karamanos NK. Hyaluronan: molecular size-dependent signaling and biological functions in inflammation and cancer. FEBS J. 2019;286(15):2883-2908.
17. Peled A, Kollet O, Ponomaryov T, et al. The chemokine SDF-1 activates the integrins LFA-1, VLA-4, and VLA-5 on immature human CD34(+) cells: role in transendothelial/stromal migration and engraftment of NOD/SCID mice. Blood. 2000;95(11):3289-3296.
18. Chigaev A, Zwartz GJ, Buranda T, Edwards BS, Prossnitz ER, Sklar LA. Conformational regulation of alpha 4 beta 1-integrin affinity by reducing agents. "Inside-out" signaling is independent of and additive to reduction-regulated integrin activation. J Biol Chem. 2004;279(31):32435-32443.
19. Kim M, Carman CV, Yang W, Salas A, Springer TA. The primacy of affinity over clustering in regulation of adhesiveness of the integrin {alpha}L{beta}2. J Cell Biol. 2004;167(6):1241-1253.
20. Chigaev A, Waller A, Amit O, Halip L, Bologa CG, Sklar LA. Real-time analysis of conformation-sensitive antibody binding provides new insights into integrin conformational regulation. J Biol Chem. 2009;284(21):14337-14346.
21. Alon R, Feigelson SW, Manevich E, et al. Alpha4beta1-dependent adhesion strengthening under mechanical strain is regulated by paxillin association with the alpha4-cytoplasmic domain. J Cell Biol. 2005;171(6):1073-1084.
22. Legras S, Gunthert U, Stauder R, et al. A strong expression of CD44-6v correlates with shorter survival of patients with acute myeloid leukemia. Blood. 1998;91(9):3401-3413.
23. Ponta H, Sherman L, Herrlich PA. CD44: from adhesion molecules to signalling regulators. Nat Rev Mol Cell Biol. 2003;4(1):33-45.
24. Bouaouina M, Blouin E, Halbwachs-Mecarelli L, Lesavre P, Rieu P. TNF-induced beta2 integrin activation involves Src kinases and a redox-regulated activation of p38 MAPK. J Immunol. 2004;173(2):1313-1320.
25. Gadhoum SZ, Madhoun NY, Abuelela AF, Merzaban JS. Anti-CD44 antibodies inhibit both mTORC1 and mTORC2: a new

rationale supporting CD44-induced AML differentiation therapy. Leukemia. 2016;30 (12):2397-2401.
26. Charrad RS, Gadhoum Z, Qi JY, et al. Effects of anti-CD44 monoclonal antibodies on differentiation and apoptosis of human myeloid leukemia cell lines. Blood. 2002;99(1):290-299.
27. Avigdor A, Goichberg P, Shivtiel S, et al. CD44 and hyaluronic acid cooperate with SDF-1 in the trafficking of human CD34+ stem/progenitor cells to bone marrow. Blood. 2004;103(8):2981-2989.
28. Krause DS, Lazarides K, von Andrian UH, Van Etten RA. Requirement for CD44 in homing and engraftment of BCR-ABL-expressing leukemic stem cells. Nat Med. 2006;12(10):1175-1180.
29. Bendall LJ, Kortlepel K, Gottlieb DJ. Human acute myeloid leukemia cells bind to bone marrow stroma via a combination of beta-1 and beta-2 integrin mechanisms. Blood. 1993;82(10):3125-3132.
30. Chigaev A, Blenc AM, Braaten JV, et al. Real time analysis of the affinity regulation of alpha 4-integrin. The physiologically activated receptor is intermediate in affinity between resting and Mn(2+) or antibody activation. J Biol Chem. 2001;276(52):48670-48678.
31. Laufer JM, Legler DF. Beyond migration-Chemokines in lymphocyte priming, differentiation, and modulating effector functions. J Leukoc Biol. 2018;104(2):301-312.
32. Thankamony SP, Sackstein R. Enforced hematopoietic cell E- and L-selectin ligand (HCELL) expression primes transendothelial migration of human mesenchymal stem cells. Proc Natl Acad Sci U S A. 2011;108 (6):2258-2263.
33. Chien S, Haq SU, Pawlus M, et al. Adhesion of acute myeloid leukemia blasts to E-selectin in the vascular niche enhances their survival by mechanisms such as Wnt activation. Blood. 2013;122(21):61.
34. Rashidi A, Uy GL. Targeting the microenvironment in acute myeloid leukemia. Curr Hematol Malig Rep. 2015;10(2):126-131.
35. Morita K, Tokushige C, Maeda S, et al. RUNX transcription factors potentially control E-selectin expression in the bone marrow vascular niche in mice. Blood Adv. 2018;2(5):509-515.
36. Barbier V, Erbani J, Fiveash C, et al. Endothelial E-selectin inhibition improves acute myeloid leukaemia therapy by disrupting vascular niche-mediated chemoresistance. Nat Commun. 2020;11(1):2042.
37. Krause DS, Lazarides K, Lewis JB, et al. Selectins and their ligands are required for homing and engraftment of BCR-ABL1+ leukemic stem cells in the bone marrow niche. Blood. 2014;123(9):1361-1371.
38. Godavarthy PS, Kumar R, Herkt SC, et al. The vascular bone marrow niche influences outcome in chronic myeloid leukemia via the E-selectin - SCL/TAL1 - CD44 axis. Haematologica. 2020;105(1):136-147.
39. Malfuson JV, Boutin L, Clay D, et al. SP/drug efflux functionality of hematopoietic progenitors is controlled by mesenchymal niche through VLA-4/CD44 axis. Leukemia. 2014;28(4):853-864.
40. Yago T, Shao B, Miner JJ, et al. E-selectin engages PSGL-1 and CD44 through a common signaling pathway to induce integrin alphaLbeta2-mediated slow leukocyte rolling. Blood. 2010;116(3):485-494.
41. Ilangumaran S, Briol A, Hoessli DC. CD44 selectively associates with active Src family protein tyrosine kinases Lck and Fyn in glycosphingolipid-rich plasma membrane domains of human peripheral blood lymphocytes. Blood. 1998;91(10):3901-3908.
42. Lee JL, Wang MJ, Sudhir PR, Chen JY. CD44 engagement promotes matrix-derived survival through the CD44-SRC-integrin axis in lipid rafts. Mol Cell Biol. 2008;28(18):5710-5723.
43. Huveneers S, Danen EH. Adhesion signaling - crosstalk between integrins, Src and Rho. J Cell Sci. 2009;122(Pt 8):1059-1069.
44. Okamoto M, Hayakawa F, Miyata Y, et al. Lyn is an important component of the signal transduction pathway specific to FLT3/ITD and can be a therapeutic target in the treatment of AML with FLT3/ITD. Leukemia. 2007;21(3):403-410.
45. Levis M. Midostaurin approved for FLT3-mutated AML. Blood. 2017;129(26):3403-3406.
46. Cortes JE, Tallman MS, Schiller GJ, et al. Phase 2b study of two dosing regimens of quizartinib monotherapy in FLT3-ITD mutated, relapsed or refractory AML. Blood. 2018;132(6):598-607.
47. Perl AE, Altman JK, Cortes J, et al. Selective inhibition of FLT3 by gilteritinib in relapsed or refractory acute myeloid leukaemia: a multicentre, first-in-human, open-label, phase 1-2 study. Lancet Oncol. 2017;18 (8):1061-1075.
48. Paschka P, Schlenk RF, Weber D, et al. Adding dasatinib to intensive treatment in core-binding factor acute myeloid leukemia-results of the AMLSG 11-08 trial. Leukemia. 2018;32(7):1621-1630.
49. Katsumi A, Kiyoi H, Abe A, et al. FLT3/ ITD regulates leukaemia cell adhesion through alpha4beta1 integrin and Pyk2 signalling. Eur J Haematol. 2011;86(3):191-198.
50. Lu Y, Yu Q, Liu JH, et al. Src family protein-tyrosine kinases alter the function of PTEN to regulate phosphatidylinositol 3-kinase/AKT cascades. J Biol Chem. 2003;278(41):40057-40066.
51. Roversi FM, Pericole FV, Machado-Neto JA, et al. Hematopoietic cell kinase (HCK) is a potential therapeutic target for dysplastic and leukemic cells due to integration of erythropoietin/PI3K pathway and regulation of erythropoiesis: HCK in erythropoietin/PI3K pathway. Biochim Biophys Acta. 2017;1863 (2):450-461.
52. Zhu QS, Xia L, Mills GB, Lowell CA, Touw IP, Corey SJ. G-CSF induced reactive oxygen species involves Lyn-PI3-kinase-Akt and contributes to myeloid cell growth. Blood. 2006;107(5):1847-1856.
53. Pillinger G, Loughran NV, Piddock RE, et al. Targeting PI3Kdelta and PI3Kgamma signalling disrupts human AML survival and bone marrow stromal cell mediated protection. Oncotarget. 2016;7(26):39784-39795.
54. Su Y, Li X, Ma J, et al. Targeting PI3K, mTOR, ERK, and Bcl-2 signaling network shows superior antileukemic activity against AML ex vivo. Biochem Pharmacol. 2018; 148:13-26.

Ferrata Storti Foundation

Haematologica 2021
Volume 106(8):2114-2120

Survival of patients with newly diagnosed high-grade myeloid neoplasms who do not meet standard trial eligibility

Mary-Elizabeth M. Percival,[1,2] Megan Othus,[3] Sarah Mirahsani,[1] Kelda M. Gardner,[1] Carole Shaw,[2] Anna B. Halpern,[1,2] Pamela S. Becker,[1,2] Paul C. Hendrie,[1] Mohamed L. Sorror,[2,4] Roland B. Walter[1,2] and Elihu H. Estey[1,2]

[1]Division of Hematology, Department of Medicine, University of Washington; [2]Clinical Research Division, Fred Hutchinson Cancer Research Center; [3]Public Health Sciences, Fred Hutchinson Cancer Research Center and [4]Division of Medical Oncology, Department of Medicine, University of Washington, Seattle, WA, USA

ABSTRACT

Few patients with cancer, including those with acute myeloid leukemia and high-grade myeloid neoplasms, participate in clinical trials. Broadening standard eligibility criteria may increase clinical trial participation. In this retrospective single-center analysis, we identified 442 consecutive newly diagnosed patients from 2014 to 2016. Patients were considered "eligible" if they had a performance status 0-2, normal renal and hepatic function, no recent solid tumor, left ventricular ejection fraction (EF) ≥50%, and no history of congestive heart failure (CHF) or myocardial infarction (MI); "ineligible" patients failed to meet one or more of these criteria. We included 372 patients who received chemotherapy. Ineligible patients represented 40% of the population and had a 1.79-fold greater risk of death (95% Confidence Interval [CI]: 1.37-2.33) than eligible patients. Very few patients had cardiac comorbidities, including 2% with low EF, 4% with prior CHF, and 5% with prior MI. In multivariable analysis, ineligibility was associated with decreased survival (Hazard ratio [HR] 1.44; 95% CI: 1.07-1.93). Allogeneic transplantation, performed in 150 patients (40%), was associated with improved survival (HR 0.66, 95% CI: 0.48-0.91). Therefore, standard eligibility characteristics identify a patient population with improved survival. Further treatment options are needed for patients considered ineligible for clinical trials.

Correspondence:

MARY-ELIZABETH M. PERCIVAL
mperciva@uw.edu

Received: April 6, 2020.

Accepted: July 6, 2020.

Pre-published: July 9, 2020.

https://doi.org/10.3324/haematol.2020.254938

Introduction

National Comprehensive Cancer Network guidelines state "the best management of any patient with cancer is in a clinical trial." Nonetheless, relatively few adults with cancer participate in clinical trials.[1] Preferences of patients and physicians, and the distances separating patients from an academic center, undoubtedly contribute and are probably not amenable to change. In contrast, protocol eligibility criteria may be more flexible. These are often stereotypical, ignoring the complexity and individualized nature of clinical care. Oncology clinical trials, particularly those sponsored by industry, are generally written with standard eligibility (and ineligibility) criteria which if anything are becoming more stringent over time.[2] The American Society of Clinical Oncology (ASCO) and similar groups have encouraged broader eligibility criteria, thus increasing the relevance of clinical trial results for the great majority of patients who do not participate in trials.[3]

An analysis by Lichtman *et al.*, published simultaneously with the ASCO recommendations, found 50-85% of over 10,000 patients with breast, colorectal, lung, or bladder cancer seen in 2013 and 2014 at Kaiser Permanente Northern California would not meet standard clinical trial eligibility criteria.[4] This analysis defined eligibility as meeting the requirements of younger age, relatively normal heart, kidney, and liver function, and no recent solid tumor. While some investigational

agents may have only theoretical organ toxicity, the organ function parameters are infrequently adjusted or waived.

Clinical trial participation by patients with hematologic malignancies has received less attention. Statler *et al.* found patients retrospectively determined to be ineligible for Soutwest Oncology Group (SWOG) leukemia studies had similar outcomes as eligible patients treated on the same studies. However, many patients were found to be ineligible solely because of such administrative reasons as missing documentation or laboratory values drawn at the wrong time.[5] A more recent single-center analysis examining the effect of comorbidities and organ dysfunction found that a very high proportion of acute myeloid leukemia (AML) patients (88%) would have been excluded from many clinical trials, but that outcomes did not differ significantly between eligible and ineligible patients.[6] The authors therefore suggested that clinical trial eligibility criteria should be liberalized for AML patients.

In this single-center retrospective analysis, we examined the proportion of patients at our center with newly-diagnosed AML or high-grade myeloid neoplasms who would have met standard clinical trial eligibility criteria. We also compared outcome in patients according to whether they met these criteria.

Methods

Patient population

Consecutive patients diagnosed with AML or high-grade myeloid neoplasms (10-19% blasts) at the University of Washington (UW)/Fred Hutchinson Cancer Research Center (FHCRC) between January 1, 2014 and December 31, 2016 were identified through our institutional database. The study was approved by the UW Institutional Review Board.

We identified 442 patients approximately equally divided between 2014, 2015, and 2016. Data on age, sex, performance status (PS), SWOG cytogenetic risk,[7] treatment related mortality (TRM) score,[8] induction treatment and intensity, and baseline values for glomerular filtration rate (GFR), creatinine, bilirubin, and alanine aminotransferase (ALT) were collected using the institional database. The TRM score uses pre-treatment patient and disease characteristics to estimate the probability of death within the first 28 days after induction. In a few patients, a single component for TRM calculation was missing so median values from the database as a whole were used. Patients were classified as having secondary disease if they had an antecedent hematologic disorder or previous exposure to chemotherapy. Induction treatment intensity was divided into three categories: high (containing cytarabine at 1g/m^2/dose or more); intermediate (including 7+3, CPX-351, or similar); and low (hypomethylating agents, low-dose cytarabine, or similar). We excluded patients from subsequent analysis who received either palliative care alone or unknown treatment in the community (n=70; 16% of the entire population). Additional information regarding prior malignancy (excluding prior AML, myelodysplastic syndrome, myeloproliferative neoplasms, and non-melanoma skin cancer), cardiac disease and/or low ejection fraction (EF) within 3 months of planned treatment, were collected from review of medical charts (performed by MEP). Response to induction chemotherapy was defined as complete remission (CR; absolute neutrophil count [ANC] >1,000/μL and platelet count <100,000/μL), CR with incomplete count recovery (CRi; ANC <1,000/μL), or CR with incomplete platelet recovery (CRp; platelet count <100,000/μL). Measurable residual disease (MRD) was assessed using multiparameter flow cytometry.

Definition of eligibility for clinical trials

Patients were considered "eligible" for the purposes of our retrospective analysis had PS 0-2, GFR ≥60 ml/min, ALT ≤ twice the upper limit of normal (ULN), bilirubin ≤1.5 mg/dL, no solid tumor diagnosed within 2 years preceding the diagnosis of AML, left ventricular ejection fraction (EF) ≥50%, and no history of congestive heart failure (CHF) or myocardial infarction (MI). The criteria are similar to those in a previous analysis of solid tumor patients and mimic standard trial eligibility criteria.[4] Patients were classified as "ineligible" if they failed to meet at least one of these eligibility criteria. Unknown values were not considered to make a patient ineligible. Though some trials exclude patients with older age, we did not use age as a criterion in light of the recent drug approvals in AML.[9,10]

Statistical analysis

Overall survival (OS) was measured from date of first evaluation to date of death, with patients last known to be alive censored at the date of last contact. Fisher's exact tests and Wilcoxon rank-sum tests were used to compare eligible and ineligible patients. Fisher's exact test was used to evaluate 28-day mortality; patients censored before day 28 were excluded from the analysis. Fisher's exact test was used to evaluate response; response was not available on 29 patients. Cox regression models and log-rank tests were used to evaluate associations with OS. All statistical analyses were performed using R.[11]

Results

Baseline characteristics

We identified 372 patients; 272 patients received intermediate or high intensity induction and 100 low intensity induction (Table 1). Of these, 207 patients (56%) received treatment on a clinical trial at UW/FHCRC.

Using the above-noted criteria (performance status, GFR, ALT, bilirubin, prior solid tumor within 2 years, EF, and history of CHF or MI), 220 patients (60%) would have been considered eligible. The reasons for ineligibility are shown in Table 1. Typically, for a given eligibility criterion <10% of patients were ineligible. For example, only 2% of patients would have been ineligible based on the usual requirement for EF ≥50%, only 4% because of prior CHF, only 5% because of prior MI, only 5% because of elevated ALT, and only 5% because of abnormal bilirubin. Only 3% of patients would have been ineligible because they had a solid tumor in the last 2 years, which is probably the most common solid-tumor free interval included in clinical trial eligibility criteria.

Relationship between ineligibility and survival

Univariate analyses showed strong associations between risk of death and ineligibility criteria including PS 3-4, GFR < 60 mL/min, and prior CHF or MI (Table 1). Associations between survival and abnormal ALT, abnormal bilirubin, or decreased EF were not noted, but there were relatively few patients in these categories. Patients with one or more ineligibility characteristics represented approximately 40% of the study population and had a 1.79-fold greater risk of death (95% Confidence Interval

Table 1. **Univariate associations between baseline characteristics and overall survival. Median overall survival (OS) (years) based on Kaplan-Meier estimates, and hazard ratios (HR), 95% Confidence Intervals (CI), and *P*-values from univariate Cox regression models reported. Median OS for treatment related mortality (TRM) is reported for all patients.**

Factor	Summary	Median OS (95% CI) (years)	HR (95% CI)	*P*
2014	114 (31)	1.5 (1.1, 3.0)	Reference	–
2015	133 (36)	1.2 (1.0, 2.0)	1.23 (0.9, 1.68)	0.2
2016	125 (34)	1.8 (1.1, 2.5)	1.05 (0.75, 1.47)	0.78
Female	154 (42)	2.2 (1.5, 2.8)	Reference	–
Male	216 (58)	1.2 (1.0, 1.5)	1.31 (1, 1.71)	0.049
AML	264 (71%)	1.5 (1.1, 2.2)	Reference	
High grade myeloid neoplasm (<20% blasts)	107 (29%)	1.4 (1.1, 2.1)	0.94 (0.71, 1.24)	0.64
PS 0-1	300 (81)	1.8 (1.4, 2.4)	Reference	–
PS 2	53 (14)	0.7 (0.6, 1.4)	1.77 (1.25, 2.5)	0.0011
PS 3-4	19 (5)	0.2 (0.1, inf)	2.73 (1.61, 4.63)	<0.001
De novo	181 (49)	2.0 (1.3, 3.0)	Reference	–
Secondary	191 (51)	1.2 (1.0, 1.8)	1.41 (1.08, 1.83)	0.01
Favorable cytogenetic risk	19 (5)	NR (1.6, inf)	Reference	–
Intermediate cytogenetic risk	226 (61)	1.8 (1.3, 2.4)	2.17 (0.96, 4.93)	0.063
Adverse cytogenetic risk	114 (31)	0.9 (0.6, 1.4)	3.4 (1.48, 7.8)	0.0038
Unknown cytogenetic risk	13 (3)	0.4 (0.1, inf)	2.62 (0.88, 7.8)	0.083
TRM score (per 1 point increase in score)	4.59 (0, 73.25)	1.4 (1.2, 2.0)	1.05 (1.04, 1.05)	<0.001
On study	207 (56)	1.4 (1.1, 2.3)	Reference	–
Not on study	165 (44)	1.4 (1.0, 2.0)	1.1 (0.85, 1.43)	0.47
High intensity therapy	212 (57)	2.4 (1.8, 3.5)	Reference	-
Intermediate intensity therapy	60 (16)	0.7 (0.4, 1.6)	2.29 (1.61, 3.26)	<0.001
Low intensity therapy	100 (27)	1.1 (0.9, 1.4)	1.93 (1.44, 2.59)	<0.001
Age ≤ 75	319 (86)	1.9 (1.4, 2.4)	Reference	–
Age > 75	53 (14)	0.7 (0.5, 1.0)	2.38 (1.72, 3.3)	<0.001
ALT ≤ 2x ULN	349 (95)	1.4 (1.2, 2.0)	Reference	–
ALT > 2x ULN	17 (5)	0.7 (0.6, inf)	1.11 (0.59, 2.09)	0.75
GFR ≥ 60 ml/min	319 (87)	1.8 (1.3, 2.3)	Reference	–
GFR < 60 ml/min	46 (13)	0.8 (0.5, 1.8)	1.73 (1.2, 2.49)	0.0035
Bilirubin ≤ 1.5 mg/dL	347 (95)	1.5 (1.2, 2.1)	Reference	–
Bilirubin > 1.5 mg/dL	20 (5)	0.7 (0.1, inf)	1.49 (0.87, 2.56)	0.15
No solid tumor in prior 2 years	353 (97)	1.4 (1.2, 2.1)	Reference	–
Solid tumor within prior 2 years	10 (3)	2.0 (1.3, inf)	0.84 (0.35, 2.05)	0.7
EF ≥ 50%	275 (98)	1.8 (1.2, 2.4)	Reference	–
EF < 50%	5 (2)	3.5 (0.0, inf)	1 (0.32, 3.15)	1
No prior CHF	359 (96)	1.5 (1.2, 2.1)	Reference	–
Prior CHF	14 (4)	0.6 (0.2, inf)	1.9 (1.04, 3.49)	0.037
No prior MI	353 (95)	1.6 (1.2, 2.2)	Reference	-
Prior MI	19 (5)	1.0 (0.5, 0.6)	1.93 (1.18, 3.18)	0.0091

PS: performance status; AML: acute myeloid leukemia; OS: overall survival; TRM: treatment-related mortality; ALT: alanine aminotransferase; ULN: upper limit of normal; GFR: glomerular filtration rate; EF: ejection fraction; CHF: congestive heart failure; MI: myocardial infarction; HR: hazard ratio; CI: Confidence Interval; inf: infinity; NR: not reached.

[CI]: 1.37-2.33) than patients who had no ineligibility characteristics (Table 2; Figure 1). Of the 144 ineligible patients, 73% (106) failed to meet only a single eligibility criterion, 26% did not meet two eligibility criteria, while 5% did not meet three criteria (Table 2).

Relationship between ineligibility and baseline characteristics (Table 3)

Although we did not regard secondary AML as a criterion of ineligibility *per se*, patients with secondary AML were more likely to be ineligible (*P*<0.001). This is likely because many of the secondary AML patients were classified as such due to receipt of chemotherapy for a prior malignancy, which in itself is a common reason for exclusion from trials. As expected, there were strong associations between ineligibility and higher TRM scores (*P*<0.001). Nonetheless, rate of 28-day mortality was similar between eligible and ineligible patients (4% *vs.* 8%, *P*=0.06). Also as expected, ineligible patients were more likely to receive intermediate and less intense induction therapy, rather than more intense induction (*P*=0.006). Although we observed no association between eligibility

Table 2. Univariate associations between ineligibility and overall survival.

Factor	N (%)	HR (95% CI)	P
No ineligible characteristic	220 (60)	Reference	–
1 ineligible characteristic	106 (29)	1.68 (1.26, 2.25)	<0.001
2 ineligible characterisics	31 (9)	2.12 (1.34, 3.34)	0.0013
3 ineligible characteristics	7 (2)	2.26 (1, 5.14)	0.051
No ineligible characteristic	220 (60)	Reference	–
1 or more ineligible characteristic	144 (40)	1.79 (1.37, 2.33)	<0.001

HR: Hazard ratio; CI: Confidence Interval.

and cytogenetic risk, the rate of CR without MRD was significantly higher in eligible patients (55% vs. 38%). Partly as a consequence, although eligible patients comprised 60% of our population, they comprised 74% of the 140 patients who received allogeneic hematopoietic cell transplantation (HCT) (*P*=0.004). It is interesting to observe that 39 "ineligible" patients went on to allogeneic HCT, but notably 30 met only one ineligibility criterion at diagnosis.

Ineligibility is associated with decreased survival (Table 4)

A multivariable Cox regression model indicated that the presence of one more ineligible factors was associated with decreased overall survival (HR 1.45, 95% CI: 1.08-1.93) (Table 4), even after accounting for known prognostic factors. Considered as a time-dependent variable, HCT was associated with improved survival (HR 0.67, 95% CI: 0.49-0.93). Tests of interaction between HCT and ineligibility indicated no evidence of a difference in the association between transplant and outcome between eligible and ineligible patients (HR 0.99, *P*=0.99).

We also examined the effect of participation in clinical trials in our cohort. Many of the clinical trials on which our patients were enrolled were investigator-initiated trials which commonly had more lenient inclusion criteria than the "standard" eligibility criteria defined for the current analysis, perhaps leading our trial patients to have worse prognoses than those more typically enrolled. Examples of clinical trials enrolling during this time period that targeted patients with a high treatment-related mortality include reduced-dose CPX-351[12] and a randomized trial for reduced *versus* full-dose CLAG-M.[13] In fact, despite the relation between shorter survival and ineligibility for clinical trials, participation in a clinical trial (207 patients, 56% of the cohort) was not associated with improvement in survival (HR 1.01, 95% CI: 0.76-1.33). Furthermore, of the 207 patients treated on study, 74 (36%) were ineligible by at least one criterion, and the effect of eligibility on overall survival was similar in patients treated on or off a trial (interaction *P*=0.15).

Discussion

Because overly strict eligibility criteria for clinical trials may lead to unrepresentative study populations, we set out to examine the frequency of characteristics associated with ineligibility. We observed a high percentage of patients with at least one ineligible characteristic (40%), though this finding is somewhat less than the 50-85% ineligible patients identified in the Lichtman analysis of solid tumor trial candidates and less than the 88% ineligible identified in the Statler analysis of AML patients treated with chemotherapy.[4,6] Our analysis excluded a subset of patients who received palliative care alone or unknown treatment in the community. Because of the nature of oncology trials, the Lichtman analysis notably also included age over 75 as an exclusion criterion, which was a characteristic of 14% of our final cohort.

Cardiac disease was uncommon in our cohort, at least based on history of CHF (4%) or MI (5%) and decreased EF within 3 months of leukemia diagnosis (2%). The Lichtman analysis was comparable, with CHF/cardiomyopathy observed in 5-11% of patients and prior MI in 1-5%, depending on cancer type.[4] In our analysis, EF assessment was done on a routine basis for most patients prior to planned receipt of an anthracycline during induction chemotherapy, even though most cardiac toxicity is only seen after high cumulative anthracycline doses.[14] EF evaluation can be expensive and can delay the initiation of life-saving chemotherapy, and these results suggest that it is unnecessary more often than not.[15] In contrast, a previous analysis of 97 randomized controlled trials in hematologic malignancies, not limited to AML and MDS, determined that cardiac eligibility criteria were significantly associated with observed adverse events in a way that hepatic and renal eligibility criteria were not.[16]

Table 3. Univariate associations between baseline characteristics and ineligibility. Median (range) or numbers (N) (%) reported for summary.

Factor	No ineligible characteristic (n=220)	1 or more ineligible characteristics (n=144)	P
2014	68 (31)	42 (29)	0.77
2015	76 (35)	55 (38)	
2016	76 (35)	47 (33)	
Female	98 (45)	52 (36)	0.13
Male	121 (55)	91 (64)	
De novo	135 (61)	45 (31)	<0.001
Secondary	85 (39)	99 (69)	
Favorable cytogenetic risk	12 (5)	7 (5)	0.96
Intermediate cytogenetic risk	134 (61)	86 (60)	
Adverse cytogenetic risk	67 (30)	45 (31)	
Unknown cytogenetic risk	7 (3)	6 (4)	
TRM score	4 (0, 73)	6 (0, 73)	<0.001
High intensity therapy	143 (65)	69 (48)	0.0035
Intermediate intensity therapy	31 (14)	28 (19)	
Low intensity therapy	46 (21)	47 (33)	
Alive past day 28	209 (96)	130 (92)	0.06
Died on or before day 28	8 (4)	12 (8)	
CR without MRD	121 (55)	54 (38)	0.014
CR with MRD	24 (11)	17 (12)	
CRi/CRp with or without MRD	28 (13)	23 (16)	
Refractory	34 (15)	35 (24)	
Missing	13 (6)	15 (10)	

TRM: treatment-related mortality; CR: complete remission; CRi: CR with incomplete neutrophil recovery; CRp: CR with incomplete platelet recovery; MRD: measurable residual disease, as detected by multiparameter flow cytometry.

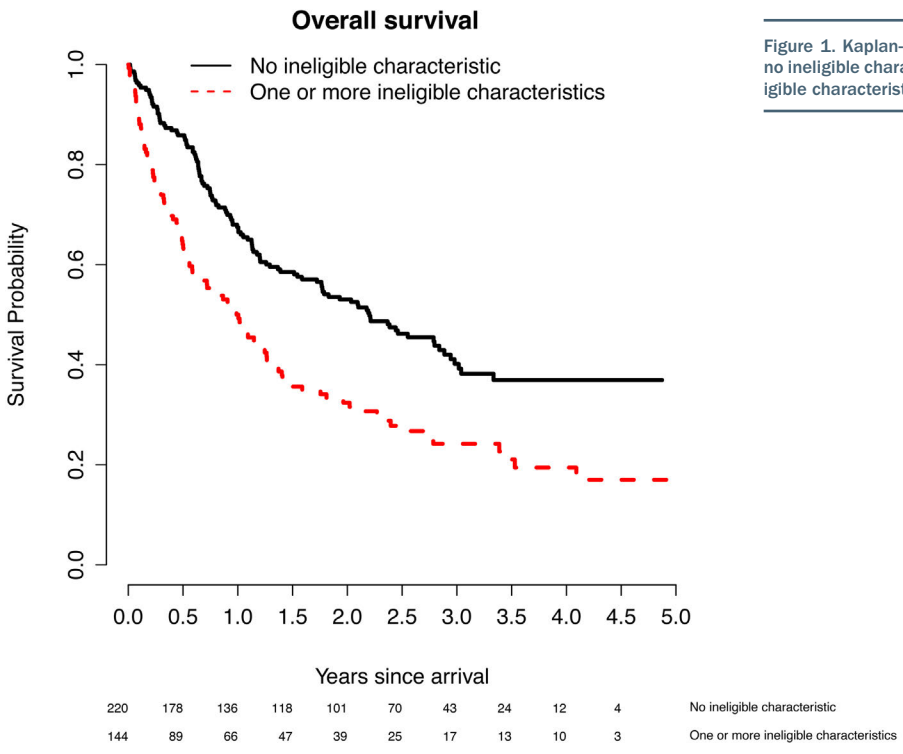

Figure 1. Kaplan-Meier plot for survival comparing patients with no ineligible characteristic (n=220) to those with one or more ineligible characteristics (n=144).

Table 4. **Multivariable Cox regression model with time-dependent transplant variable.**

Covariate	HR	95% CI	*P*
Transplant (ref = no transplant)	0.67	(0.49, 0.93)	0.016
Male (ref = female)	1.15	(0.87, 1.15)	0.33
Secondary AML (ref = *de novo*)	1	(0.75, 1.32)	1
Intermediate cytogenetic risk (ref = favorable)	1.97	(0.86, 4.52)	0.11
Adverse risk (ref = favorable)	3.29	(1.4, 7.73)	0.0063
Unknown risk (ref = favorable)	2.97	(0.99, 8.95)	0.052
Age (years)	1.02	(1.01, 1.04)	<0.001
Intermediate intensity therapy (ref = high intensity)	2.08	(1.44, 3)	<0.001
Low intensity (ref = high intensity)	1.09	(0.77, 1.54)	0.63
Not on study (ref = on study)	1.13	(0.86, 1.49)	0.37
One or more ineligible factors (ref = no ineligible factors)	1.45	(1.08, 1.93)	0.012

AML: acute myeloid leukemia; TRM: treatment-related mortality; HR: hazard ratio; CI: Confidence Interval; ref: reference.

Cardiac eligibility criteria may act as a surrogate for other co-morbidities and may predict toxicity, but the authors of that study conclude that exclusion criteria are often too broad and not applicable.

In our analysis, patients with at least one ineligible characteristic had significantly worse survival than patients with no ineligible characteristic (HR 1.79, 95% CI: 1.37-2.33; Table 4). It is likely that all the criteria used to determine ineligibility are not equally unfavorable. Optimally, our models would analyze each criterion separately, rather than combining them together as in this study. However, estimating the contribution of individual ineligibility characteristics would require a larger patient cohort. Our finding that ineligibility is associated with decreased survival suggests that standard clinical trial criteria may identify a population of patients with better outcomes following treatment; improved responses and survival have also been demonstrated in an "on study" population when the same induction regimen was administered to patients both on and off clinical trial at our center and in a national population-based cohort study from Denmark.[17,18] These findings contrast some with the Statler analysis of AML patients, which did not identify significant differences in response or survival based on comorbidities other than liver disease and organ dysfunction.[6] In the future, evaluation of other factors including travel distance, social support, and frailty level could provide a more nuanced picture of eligibility.

Before performing our analysis, we believed ineligibility would be associated with worse outcomes largely because of its association with early death, or 28-day TRM, based on the sharp decline in death rate after this 28-day period.[8] However, though ineligible patients had higher TRM scores and would be more likely to incur

TRM,[8] the difference in TRM between eligible and ineligible patients was small when contrasted with the much greater differences in survival. This suggests much of the survival difference reflected the considerably higher rate of CR without MRD in eligible patients (55% *vs.* 38%), since achievement of CR without MRD is associated with longer survival.[19] Since cytogenetic risk was similar in eligible and ineligible patients and since none of our ineligibility criteria are known to be associated with resistance to therapy, another explanation is needed for this higher CR without MRD rate. One possibility is the much less frequent use of intense induction in ineligible patients. Ineligible patients were also much less likely to receive allogeneic HCT. Hence while electing not to give ineligible patients intense induction may reduce TRM, this effect may be considerably less than the entailed loss of efficacy (*e.g.*, decreased rate of CR without MRD) and resultant loss of ability to receive HCT.

Most patients with AML are given standard treatment (off trial) in community centers. An important question is whether the effect of "ineligibility" is the same in community and academic centers. Patients treated in community centers are older, have more comorbidities, and travel less distance for treatment than those at academic centers.[20] Although after accounting for these factors survival remained better in academic centers, the negative effect of covariates such as comorbidities and shorter distance traveled was similar in both settings, suggesting that the effect of ineligibility is similar in community and academic centers. Nonetheless, the pre-selection of patients inherent in a retrospective study from an academic medical center undoubtedly adds to the effect of ineligibility in evaluating the relevance of clinical trial outcomes.

As noted in the results, many of the patients entered on trials at our center would have been ineligible for typical trials. The lack of a linkage between participation in a trial and fulfillment of standard eligibility criteria may partially explain the failure of our trials to improve survival, although the trials themselves may have been at fault. Though participation in clinical trials is encouraged, it is also true that not all trials lead to improved outcomes for patients. Patients with characteristics that make them ineligible for most trials may be the very population who would benefit most from novel therapies that are available only within the context of a trial. Additionally, improvements in supportive care over time will benefit all patients, regardless of eligibility. Investigators at MD Anderson Cancer Center published the results of a clinical trial for patients with AML and MDS who were by definition not eligible for standard clinical trials,[21] but we are not aware of any other similar studies either completed or enrolling. Future studies with broader inclusion criteria could also include a "correction factor" to help compensate for the expected worse outcomes of patients who would not meet standard eligibility. The recent Food and Drug Admistration approvals in the AML arena have changed the landscape of treatment options, but the real world use of these drugs may not mimic the cohort studied in the clinical trials leading to approval.

Even the possibility of less benefit for "ineligible" patients may not be sufficient justification for their continued exclusion from trials. For many patients with AML, standard treatment is unsatisfactory. Hence, once properly informed, many patients would prefer to enroll on trials rather than receive standard therapy. Extended to many cancers, this fact underlies the "right-to-try" movement. We understand patients are often ineligible for trials because the trials' sponsors realize inclusion would lead to less encouraging results, harming chances for regulatory approval. A possible means to reconcile the interests of patients and of sponsors would be to make regulatory approval of new drugs might be made conditional on subsequent conduct of trials in patients underrepresented in the trials prompting initial approval, thus potentially increasing the applicability of results to the substantial numbers of patients currently considered "ineligible."

Disclosures

This study was presented, in part, at the American Society of Hematology 2019 annual meeting in Orlando, FL, USA.

Contributions

MEMP and EHE: conceived and designed the study; data collection was performed by MEMP, SM, KMG, and CS; statistical analysis was performed by MO. The remaining authors enrolled patients and provided feedback and revisions. The final manuscript was approved by all authors.

Funding

The study was supported in part by a Cancer Consortium Grant from the National Institutes of Health (P30 CA015704).

References

1. Network NCC. Acute Myeloid Leukemia (version 2.2019). https://www.nccn.org/professionals/physician_gls/pdf/aml.pdf. Accessed April 12, 2019.
2. Srikanthan A, Vera-Badillo F, Ethier J, et al. Evolution in the eligibility criteria of randomized controlled trials for systemic cancer therapies. Cancer Treat Rev. 2016; 43:67-73.
3. Kim ES, Bruinooge SS, Roberts S, et al. Broadening eligibility criteria to make clinical trials more representative: American Society of Clinical Oncology and Friends of Cancer Research Joint Research Statement. J Clin Oncol. 2017;35(33):3737-3744.
4. Lichtman SM, Harvey RD, Damiette Smit MA, et al. Modernizing clinical trial eligibility criteria: recommendations of the American Society of Clinical Oncology-Friends of Cancer Research Organ Dysfunction, Prior or Concurrent Malignancy, and Comorbidities Working Group. J Clin Oncol. 2017;35(33):3753-3759.
5. Statler A, Othus M, Erba HP, et al. Comparable outcomes of patients eligible vs ineligible for SWOG leukemia studies. Blood. 2018;131(25):2782-2788.
6. Statler A, Hobbs BP, Radivoyevitch T, et al. The impact of comorbidities and organ dysfunction commonly used for clinical trial eligibility criteria on outcome in acute myeloid leukemia (AML) patients receiving induction chemotherapy. Blood. 2019; 134(Suppl 1):S16.
7. Slovak ML, Kopecky KJ, Cassileth PA, et al. Karyotypic analysis predicts outcome of preremission and postremission therapy in adult acute myeloid leukemia: a Southwest Oncology Group/Eastern Cooperative Oncology Group Study. Blood. 2000; 96(13):4075-4083.
8. Walter RB, Othus M, Borthakur G, et al. Prediction of early death after induction therapy for newly diagnosed acute myeloid leukemia with pretreatment risk scores: a novel paradigm for treatment assignment. J Clin Oncol. 2011;29(33):4417-4423.
9. Cortes JE, Heidel FH, Hellmann A, et al. Randomized comparison of low dose cytarabine with or without glasdegib in patients with newly diagnosed acute myeloid leukemia or high-risk myelodysplastic syndrome. Leukemia. 2019; 33(2):379-389.
10. DiNardo CD, Pratz K, Pullarkat V, et al. Venetoclax combined with decitabine or azacitidine in treatment-naive, elderly patients with acute myeloid leukemia. Blood. 2019;133(1):7-17.
11. R: A language and environment for statistical computing. R Foundation for Statistical Computing [computer program]. R Foundation for Statistical Computing,

Vienna, Austria; 2017.
12. Walter RB, Othus M, Orlowski KF, et al. Unsatisfactory efficacy in randomized study of reduced-dose CPX-351 for medically less fit adults with newly diagnosed acute myeloid leukemia or other high-grade myeloid neoplasm. Haematologica. 2018;103(3):e106-e109.
13. Halpern AB, Othus M, Gardner KM, et al. Mini- Vs. Regular-dose CLAG-M (Cladribine, Cytarabine, G-CSF, and Mitoxantrone) in medically less fit adults with newly-diagnosed acute myeloid leukemia (AML) and other high-grade myeloid neoplasms. Blood. 2019;134(Suppl 1):S1364.
14. Anderlini P, Benjamin RS, Wong FC, et al. Idarubicin cardiotoxicity: a retrospective study in acute myeloid leukemia and myelodysplasia. J Clin Oncol. 1995;13(11): 2827-2834.
15. Khan HM, Gardner KM, Shaw C, et al. Need for routine examination of left ventricular ejection fraction in patients with AML. Leukemia. 2020;34(4):1169-1171.
16. Statler A, Radivoyevitch T, Siebenaller C, et al. The relationship between eligibility criteria and adverse events in randomized controlled trials of hematologic malignancies. Leukemia. 2017;31(8):1808-1815.
17. Buckley SA, Percival ME, Othus M, et al. A comparison of patients with acute myeloid leukemia and high-risk myelodysplastic syndrome treated on versus off study. Leuk Lymphoma. 2019;60 (4):1023-1029.
18. Ostgard LS, Norgaard M, Sengelov H, et al. Improved outcome in acute myeloid leukemia patients enrolled in clinical trials: a national population-based cohort study of Danish intensive chemotherapy patients. Oncotarget. 2016;7(44):72044-72056.
19. Chen X, Xie H, Wood BL, et al. Relation of clinical response and minimal residual disease and their prognostic impact on outcome in acute myeloid leukemia. J Clin Oncol. 2015;33(11):1258-1264.
20. Bhatt VR, Shostrom V, Giri S, et al. Early mortality and overall survival of acute myeloid leukemia based on facility type. Am J Hematol. 2017;92(8):764-771.
21. Montalban-Bravo G, Huang X, Naqvi K, et al. A clinical trial for patients with acute myeloid leukemia or myelodysplastic syndromes not eligible for standard clinical trials. Leukemia. 2017;31(2):318-324.

ARTICLE

A phase I/II study of the combination of quizartinib with azacitidine or low-dose cytarabine for the treatment of patients with acute myeloid leukemia or myelodysplastic syndrome

Mahesh Swaminathan,[1,2] Hagop M. Kantarjian,[1] Mark Levis,[3] Veronica Guerra,[1] Gautam Borthakur,[1] Yesid Alvarado,[1] Courtney D. DiNardo,[1] Tapan Kadia,[1] Guillermo Garcia-Manero,[1] Maro Ohanian,[1] Naval Daver,[1] Marina Konopleva,[1] Naveen Pemmaraju,[1] Alessandra Ferrajol,[1] Michael Andreeff,[1] Nitin Jain,[1] Zeev Estrov,[1] Elias J. Jabbour,[1] William G. Wierda,[1] Sherry Pierce,[1] Maria Rhona Pinsoy,[1] Lianchun Xiao,[4] Farhad Ravandi[1] and Jorge E. Cortes[1,5]

[1]Department of Leukemia, University of Texas MD Anderson Cancer Center, Houston, TX; [2]Department of Medicine, Roswell Park Comprehensive Cancer Center, Buffalo, NY; [3]Department of Hematological Malignancies, Johns Hopkins Sidney Kimmel Comprehensive Cancer Center, Baltimore, MD; [4]Department of Biostatistics, University of Texas MD Anderson Cancer Center, Houston, TX and [5]Georgia Cancer Center at Augusta University, Augusta, GA, USA

Ferrata Storti Foundation

Haematologica 2021
Volume 106(8):2121-2130

ABSTRACT

The FMS-like tyrosine kinase 3-internal tandem duplication (*FLT3*-ITD) mutation in acute myeloid leukemia (AML) is associated with poor prognosis. We hypothesized that quizartinib, a selective and potent FLT3 inhibitor, with azacitidine (AZA) or low-dose cytarabine (LDAC) might improve the outcomes in patients with *FLT3*-ITD-mutated AML. In this open-label phase I/II trial, patients of any age receiving first-salvage treatment for *FLT3*-ITD AML or age >60 years with untreated myelodysplastic syndrome or AML were treated with quizartinib plus AZA or LDAC. Seventy-three patients were treated (34 frontline, 39 first salvage). With regard to previously untreated patients, the composite response (CRc) rate was 87% (n=13/15: 8 complete responses [CR], 4 CR with incomplete hematologic recovery [CRi], 1 CR without platelet recovery [CRp]) among the patients treated with quizartinib/AZA and 74% (n=14/19: 1 CR, 8 CRi, 5 CRp) among those treated with quizartinib/LDAC. The median overall survival was 19.2 months for the cohort treated with quizartinib/AZA cohort and 8.5 months for the patients treated with quizartinib/LDAC; the corresponding relapse-free survival figures were 10.5 and 6.4 months, respectively. With regard to previously treated patients, the CRc rate was 64% (n=16/25 in the quizartinib/AZA cohort and 29% (n=4/14)) in the quizartinib/LDAC cohort. The median overall survival for patients treated with quizartinib/AZA and quizartinib/LDAC was 12.8 *versus* 4 months, respectively. QTc prolongation grade 3 occurred in only one patient in each cohort. Quizartinib-based combinations, particularly with AZA, appear effective in both frontline and first salvage therapy for patients with *FLT3*-ITD-mutated AML and are well tolerated. ClinicalTrials.gov identifier: NCT01892371.

Introduction

One of the most common types of genetic alterations in acute myeloid leukemia (AML) are mutations in the FMS-like tyrosine kinase 3 (*FLT3*) gene, which occurs in approximately 30% of all newly diagnosed AML cases.[1] Internal tandem duplications (ITD) are the most frequent *FLT3* mutations, occurring in about 20% to 30% of patients with AML.[2,3] *FLT3*-ITD mutations confer an adverse prognosis in patients

Correspondence:

JORGE CORTES
jorge.cortes@augusta.edu

Received: June 15, 2020.
Accepted: December 11, 2020.
Pre-published: April 15, 2021.

https://doi.org/10.3324/haematol.2020.263392

treated with standard chemotherapy.[4-6] Several tyrosine kinase inhibitors, such as lestaurtinib, sunitinib, sorafenib, and midostaurin, have been investigated in patients with *FLT3*-ITD-mutated AML.[2,7-10] Of them, the Food and Drug Administration (FDA) has approved only midostaurin in combination with standard chemotherapy for the treatment of patients with *FLT3*-mutated AML.[11] Next-generation tyrosine kinase inhibitors, such as gilteritinib and quizartinib, used as single agents have greater antileukemic activity because of their complete FLT3 kinase inhibition.[2,12]

Quizartinib is a type II inhibitor that specifically targets the inactive conformation of the *FLT3* kinase domain.[13] This selective affinity makes it active only against *FLT3*-ITD mutations, whereas type I inhibitors are active against both *FLT3*-ITD and tyrosine kinase domain mutations. Quizartinib and gilteritinib have been reported to have significant clinical activity in patients with *FLT3*-mutated refractory/relapsed (R/R) AML.[14,15] The QuANTUM-R trial showed a significant improvement in survival of patients with *FLT3*-ITD AML who received first salvage therapy with quizartinib compared to the survival of those given standard chemotherapy.[16] The FDA recently approved gilteritinib for the treatment of patients with *FLT3*-mutated R/R AML.[17] Azacitidine (AZA), a hypomethylating agent, and cytarabine are standard agents for the treatment of AML in patients not eligible for standard chemotherapy. It has been suggested that combinations of AZA with FLT3 inhibitors (sorafenib, midostaurin) produce higher response rates compared to those expected with FLT3 inhibitors given as single agents.[18-21]

Here we describe the results of a phase I/II, open-label, single-institution study that assessed the efficacy and safety of quizartinib plus AZA (quizartinib/AZA) and quizartinib plus low-dose cytarabine (LDAC, quizartinib/LDAC) in previously untreated elderly patients with AML, or patients with R/R AML at first salvage.

Methods

Study design

This was a single-institution phase I/II, two-arm, open-label study. The primary objective of the phase I part of this study was to assess the safety and determine the dose-limiting toxicity and maximum-tolerated dose of these combinations. The primary objective of the phase II portion of the study was to determine the efficacy of the combination of quizartinib with either AZA or LDAC in patients with AML or high-risk myelodysplastic syndrome. Secondary objectives of phase I included assessment of the efficacy of the treatment regimens. Secondary objectives of phase II included a determination of the safety of the quizartinib-based combinations. All patients signed an informed consent form approved by the Institutional Review Board. The study was conducted in accordance with the Declaration of Helsinki and registered with the. ClinicalTrials.gov identifier, NCT01892371.

AZA (75 mg/m^2/day) was administered subcutaneously or intravenously once daily, and LDAC (20 mg flat dose) was administered subcutaneously twice daily for the first 7 days and 10 days of every 28-day cycle, respectively. The decision of whether to use AZA or LDAC was based on the treating physician's choice. In both regimens quizartinib was administered orally daily for 28 days of every cycle except for the first cycle, in which it was started on day 5 of the cycle. The first six patients in both the AZA and LDAC cohorts received quizartinib at the target dose of 60 mg/day to determine tolerability (i.e., run-in phase). According to the study design, if one or no patient experienced dose-limiting toxicity at this dose, this would be used as the recommended phase II dose. There were no attempts to explore higher doses of quizartinib. If two or more patients experienced dose-limiting toxicity at this dose, a reduced dose level of 30 mg/day was to be explored. Dose-limiting toxicity, defined as any grade ≥3 non-hematologic toxicity at least possibly related to quizartinib or prolonged myelosuppression for ≥6 weeks without evidence of leukemia, was not identified in any of the first six patients treated with each combination. Thus 60 mg/day was used in all patients in the phase II part of the study. The use of hydroxyurea was allowed during the first cycle only. Intrathecal chemotherapy was allowed if clinically indicated.

For the phase I part of the study (run-in phase) only, patients with wild-type (WT)-*FLT3* were eligible. All patients with *FLT3*-WT were to receive quizartinib/AZA. However, one patient with a history of *FLT3*-ITD was enrolled in the quizartinib/LDAC cohort, although *FLT3*-ITD was not detected at the time of enrollment. Only patients with *FLT3*-ITD were eligible for the phase II part of the study.

Patients

Patients with myelodysplastic syndrome, or AML (excluding acute promyelocytic leukemia) meeting at least one of the following criteria were eligible: age ≥18 years with R/R disease who had received no more than one prior treatment regimen; or age ≥60 years with previously untreated disease considered not suitable for intensive chemotherapy. Eastern Cooperative Oncology Group Performance Status ≤2 and adequate organ function were required.

Exclusion criteria included other malignancies concurrent or in remission for <6 months prior to enrollment, or clinically active central nervous system leukemia. Patients whose QTc interval, calculated using the Fridericia correction factor (QTCF), was >450 ms at screening were excluded.

Tolerability and safety assessments

All patients who received at least one dose of any of the treatment were evaluable for toxicity. Physical examination, complete blood count, and biochemical analyses were performed at baseline and throughout the study. Electrocardiograms were recorded at screening and on days 1, 5, 8, and 12 (before treatment on days 1, 5, and 8; 2-6 hours after treatment on days 5 and 12). Triplicate electrocardiograms were obtained for the first three cycles.

Response to treatment

Bone marrow aspirations and/or biopsies were performed between days 21 and 35 of cycle 1, and every one to three cycles thereafter (monthly until remission, then no later than every 3 months). All patients who received at least one dose of therapy were included in the intention-to-treat (ITT) analysis for response to therapy; patients who completed a full course of treatment (AZA for 7 days or LDAC for 10 days, and quizartinib for 24 days in cycle 1) were evaluable for response in the per-protocol analysis. Responses were defined according to the International Working Group 2003 criteria.[22] The composite response (CRc) rate was determined based on the sum of the complete responses (CR), CR with incomplete hematologic recovery (CRi), CR without platelet recovery (CRp) and CR with partial hematologic recovery (CRh). Measurable residual disease (MRD) was assessed by multicolor flow cytometry with a sensitivity of 0.01%.

Statistical analyses

Safety was monitored closely using the method of Thall *et al.*[23]

Categorical variables were tabulated with their frequencies, and continuous variables were summarized with descriptive statistics. The Fisher exact test, Wilcoxon rank-sum test, and logistic regression model were applied to evaluate the association of response and covariates. The log-rank test and Cox proportional hazards models were used to evaluate the association between overall survival or relapse-free survival with covariates. Survival probabilities were calculated by the Kaplan-Meier method. Comparisons of survival endpoints between the two treatment cohorts are descriptive in nature only as the study was not powered to identify statistical significance. The statistical computations were performed using SAS 9.4 (SAS Institute Inc., Cary NC, USA), S-Plus software v8.2 (TIBCO, Palo Alto, CA, USA), and GraphPad Prism 7 (GraphPad Software, Inc., La Jolla, CA, USA).

Results

Patients' characteristics

A total of 73 patients were treated (Figure 1); 34 patients were treated frontline and 39 in a first salvage setting. Fifteen patients received quizartinib/AZA, and 19 received quizartinib/LDAC as frontline treatment. The median age was 75 years (range, 64-82 years) and 70 years (range, 58-80 years), respectively (Table 1). Most patients in both cohorts had adverse-risk genetics according to the European LeukemiaNet 2017 classification. All patients were assessed for mutations, using an 81-gene panel, before the start of treatment. The most frequent co-existing mutations were *DNMT3A* (32%), *RUNX1* (29%), *NPM1* (27%), *TET2* (18%), and *TP53* (6%).

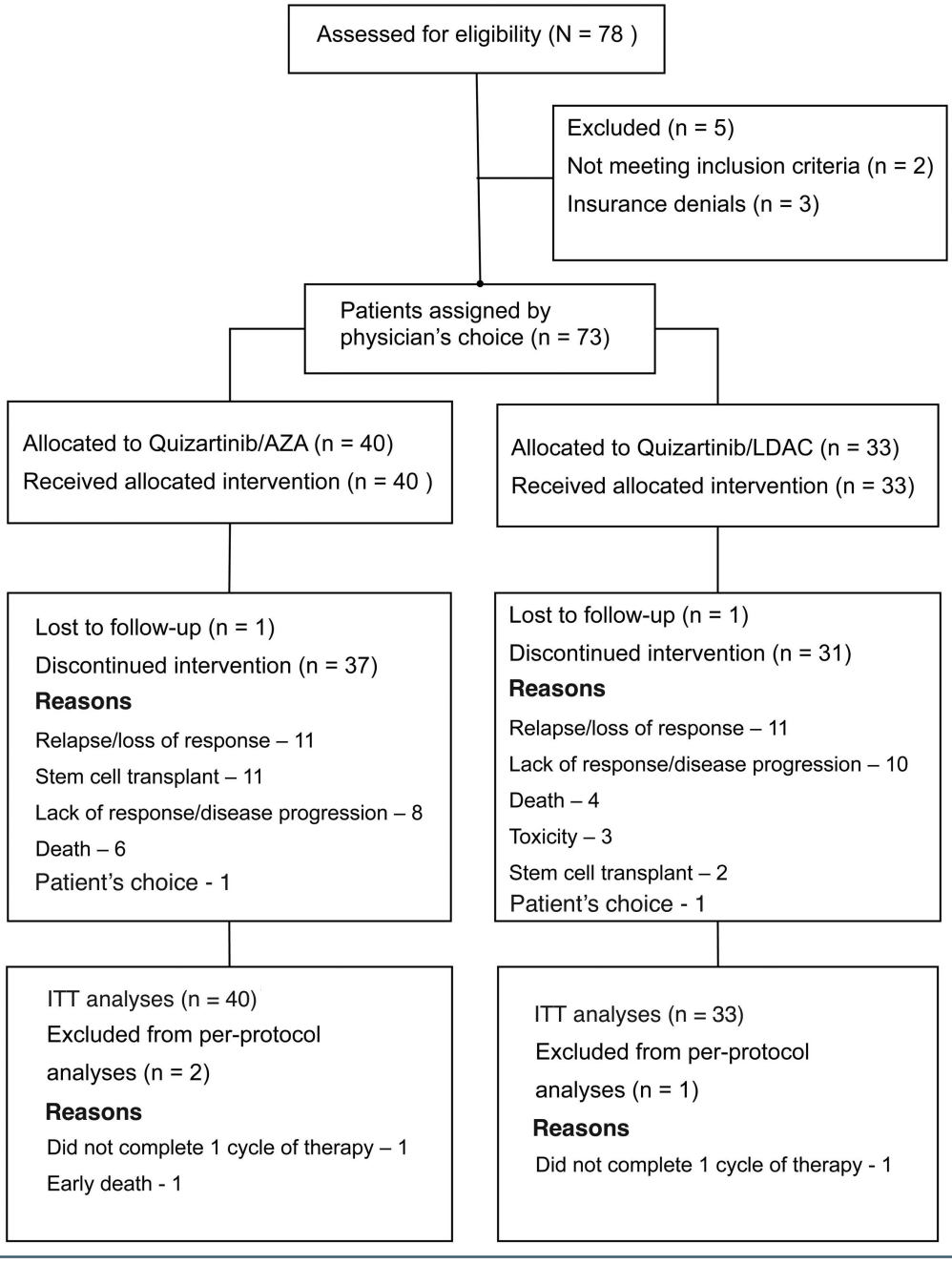

Figure 1. CONSORT flow diagram. AZA: azacitidine; LDAC: low-dose cytarabine; ITT: intention-to-treat.

Table 1. Baseline characteristics of all study patients (n=73).

Patients' characteristics	Frontline			Relapsed/Refractory		
	Overall (n=34)	Quizartinib/AZA (n=15)	Quizartinib/LDAC (n=19)	Overall (n=39)	Quizartinib/AZA (n=25)	Quizartinib/LDAC (n=14)
	N (%) or [range]					
Median age, years	72 [58-82]	75 [64-82]	70 [58-80]	65 [24-84]	59 [24-76]	70 [54-84]
Male	20 (59)	9 (60)	11 (58)	21 (54)	13 (52)	8 (57)
ECOG-PS						
0-1	27 (79)	13 (87)	14 (74)	29 (74)	20 (80)	9 (64)
2	7 (21)	2 (13)	5 (26)	10 (26)	5 (20)	5 (36)
AML[a]	33 (97)	14 (93)	19 (100)	39 (100)	25 (100)	14 (100)
MDS	1 (3)	1 (7)	0	0	0	0
Prior FLT3 inhibitors						
Sorafenib	0	0	0	7 (18)	3 (12)	4 (29)
Midostaurin	0	0	0	2 (5)	0	2[b] (14)
Crenolanib	0	0	0	1 (3)	0	1 (7)
ELN risk stratification group[c]						
Favorable	2 (6)	0	2 (11)	2 (5)	1 (4)	1 (7)
Intermediate	11 (32)	4 (27)	7 (37)	25 (64)	17 (68)	8 (57)
Adverse	21 (62)	11 (73)	10 (53)	12 (31)	7 (28)	5 (36)
FLT3 status						
FLT3-WT	0	0	0	3 (8)	2 (8)	1[d] (7)
FLT3-ITD$^+$	34 (100)	15 (100)	19 (100)	35 (90)	22 (88)	13 (93)
Ratio < 0.5	12 (35)	5 (33)	7 (37)	16 (41)	10 (40)	6 (43)
≥ 0.5	22 (65)	10 (67)	12 (63)	19 (49)	12 (48)	7 (50)
Median *FLT3*-ITD allelic ratio	0.71 [0.01-5.4]	0.86 [0.02-5.4]	0.62 [0.01-2.4]	0.69 [0.01-3.7]	0.72 [0.01-3.7]	0.69 [0.07-1.2]
FLT3-TKD$^+$ only				1 (3)	1 (4)	0
Both *FLT3*-ITD$^+$ & TKD$^+$	2 (6)	1 (7)	1 (5)	3 (8)	1 (4)	2 (14)
Other frequent mutations[e]						
DNMT3A	11 (32)	7 (47)	4 (21)	12 (36)	9 (43)	3 (25)
RUNX1	10 (29)	5 (33)	5 (26)	4 (12)	1 (4)	3 (25)
NPM1	9 (27)	2 (13)	7 (37)	12 (36)	10 (48)	2 (17)
TET2	6 (18)	2 (13)	4 (21)	7 (21)	3 (14)	4 (33)
TP53	2 (6)	0	2 (11)	2 (6)	1 (4)	1 (7)
Laboratory values, median						
Bone marrow blasts, %	56 [15-97]	56 [15-84]	60[f] [17-97]	65 [6-98]	70 [6-98]	49 [21-86]
WBC, 10^9/L	6.1 [1.1-42]	8 [1.2-42]	3.3 [1.1-21]	5.3 [0.5-61]	5.2 [0.5-53.4]	5.4 [0.9-61]
Hemoglobin, g/dL	9.1 [7-11.4]	9.1 [7.7-10]	9 [7-11.4]	9.4 [7.6-12.8]	9.5 [7.6-12.7]	9.2 [7.7-12.8]
Platelets, 10^9/L	34 [7-377]	54 [14-377]	31 [7-75]	25 [4-454]	22 [4-99]	25 [12-454]

AZA: azacitidine; LDAC: low-dose cytarabine; ECOG-PS: Eastern Cooperative Oncology Group-Performance Status; AML: acute myeloid leukemia; MDS: myelodysplastic syndromes; ELN: European LeukemiaNet; ITD: internal tandem duplication; TKD: tyrosine kinase domain; WBC: white blood cells. [a]Six patients in the AZA and 12 in the LDAC cohort treated frontline had secondary AML. Three patients each in both the AZA and LDAC cohorts given with first salvage therapy had secondary AML. [b]One patient who received LDAC was treated with both sorafenib and midostaurin prior to quizartinib. [c]Classified according to the European LeukemiaNet 2017. [d]One patient had a prior *FLT3*-TKD mutation that was negative at the time of starting treatment. [e]The 81-gene panel was not used for mutational analysis prior to starting treatment in four patients given first salvage treatment with AZA and two given LDAC. [f]Two patients were diagnosed based on circulating blast percentages of 22% and 25%.

Of the 39 patients with R/R AML, 25 patients (64%) were treated with quizartinib/AZA and 14 (36%) with quizartinib/LDAC. Their median age was 59 years (range, 24-76 years) and 70 years (range, 54-84 years), respectively. Prior to receiving quizartinib, three (12%) patients in the quizartinib/AZA cohort and seven (50%) in the quizartinib/LDAC cohort had received other FLT3 inhibitors, including sorafenib (n=7), crenolanib (n=2), and midostaurin (n=1). Similarly, five (13%) patients had received prior therapy with AZA for AML and four (10%) for the treatment of a prior myelodysplastic syndrome. Mutation data (from the 81-gene panel) were not available for four patients in the quizartinib/AZA cohort and two in the quizartinib/LDAC cohort. Among the 33 patients with available molecular information, the most common co-existing mutations were *NPM1* (36%), *DNMT3A* (36%), *TET2* (21%), *WT1* (15%), *IDH2* (15%), *IDH1* (12%), and *TP53* (6%).

Response to therapy

All 73 patients received at least one dose of study treatment and were included in the ITT analysis. Among them,

Table 2. Summary of responses in the intention-to-treat population (n=73).

Responses	Overall (n=34)	Frontline Quizartinib/AZA (n=15)	Quizartinib/LDAC (n=19)	Overall (n=39)	Relapsed/Refractory Quizartinib/AZA (n=25)	Quizartinib/LDAC (n=14)
			N (%)			
CR	9 (26)	8 (53)	1 (5)	3 (8)	2 (8)	1 (7)
CRi	12 (35)	4 (27)	8 (42)	14 (36)	12 (48)	2 (14)
CRp	6 (18)	1 (7)	5 (26)	3 (8)	2 (8)	1 (7)
CRc	27 (79)	13 (87)	14 (74)	20 (51)	16 (64)	4 (29)
PR	0	0	0	2 (5)	0	2 (14)
ORR	27 (79)	13 (87)	14 (74)	22 (56)	16 (64)	6 (43)
NR	5 (15)	1 (7)	4 (21)	16 (41)	8 (32)	8 (57)

AZA: azacitidine; LDAC: low-dose cytarabine; CR: complete response; CRi: CR with incomplete hematologic recovery; CRp: CR without platelet recovery; CRh: CR with partial hematologic recovery; CRc: composite response rate (CR+CRi+CRp); PR: partial response; ORR: overall response rate (CRc+PR); NR:, no response.

Table 3. Summary of responses in evaluable patients*(n=70).

Responses	Frontline Quizartinib/AZA (n=14)	Quizartinib/LDAC (n=18)	Relapsed/Refractory Quizartinib/AZA (n=24)	Quizartinib/LDAC (n=14)
		N (%) or [range]		
CR	8 (57)	1 (6)	2 (8)	1 (7)
CRi	4 (29)	8 (44)	12 (50)	2 (14)
CRp	1 (7)	5 (28)	2 (8)	1 (7)
CRh	0	0	0	0
CRc	13 (93)	14 (78)	16 (67)	4 (29)
PR	0	0	0	2 (14)
ORR	13 (93)	14 (78)	16 (67)	6 (43)
NR	1 (7)	4 (22)	8 (33)	8 (57)
Time to best response, months	3.2 [0.9-6.3]	1.5 [0.9-3]	1 [0.9-4.8]	1 [0.9-8.7]
Duration of response[b], months	4.2 [0.2-30]	3.7 [0.2-17]	2.5 [0.1-19.4]	2.4 [0.5-7.2]
MRD[c]				
MRD assessed in responders	11 (85)	12 (86)	13 (81)	3 (50)
MRD negative[d]	5 (45)	3 (25)	6 (46)	2 (67)
CR	4 (80)	1 (33)	1 (17)	1 (50)
CRi	1 (20)	1 (33)	5 (83)	1 (50)
CRp	0	1 (33)	0	0
Time to MRD negativity prior to SCT, months	4.7 [1-5.9]	0.9 [0.9-3]	2 [0.9-4.8]	1.4 [0.9-1.9]

AZA: azacitidine; LDAC: low-dose cytarabine; CR: complete response; CRi: CR with incomplete hematologic recovery; CRp: CR without platelet recovery; CRh: CR with partial hematologic recovery; CRc: composite response rate (CR+CRi+CRp+CRh); PR: partial response; ORR: overall response rate (CRc+PR); NR:, no response; MRD: minimal residual disease; SCT: stem cell transplantation. [a]Only patients who completed at least one course of study treatment were included in the per-protocol response assessment (1 patient in the AZA cohort died early and 1 in each cohort did not complete a course of study treatment due to SCT in 1 case and atrial fibrillation in the other). [b]Patients proceeded to SCT were censored at the date of SCT. One patient treated frontline in quizartinib/LDAC and as first salvage in quizartinib/AZA cohort has an ongoing response. [c]MRD was assessed by multicolor flow cytometry. [d]Censored patients who achieved MRD negativity after SCT in the group treated frontline (n=4; AZA – 3, LDAC -1) and in those with relapsed/refractory disease (AZA – 3).

70 (38 in the quizartinib/AZA cohort, 32 in the quizartinib/LDAC cohort) completed at least one cycle of study treatment and were included for per-protocol response assessment. Three patients were not evaluable for per-protocol response: one proceeded to a stem-cell transplant (SCT) after 14 days of treatment, one developed atrial fibrillation on day 4 (prior to receiving quizartinib), and one died early on day 7 of multi-organ failure secondary to sepsis from an unknown organism. Among the ITT population treated frontline, the CRc rate (CR + CRi + CRp + CRh) was 87% (n=13/15 patients: 8 CR, 4 CRi, 1 CRp) (Table 2) in those treated with quizartinib/AZA and 74% (n=14/19 patients: 1 CR, 8 CRi, 5 CRp) in those treated with quizartinib/LDAC. The per-protocol response data are shown in Table 3. The median duration of response (time from best response to death/disease progression/date of SCT or last follow-up/off treatment) was 4.2 months (range, 0.2 - 30 months) among patients treated with quizartinib/AZA and 3.7 months (range, 0.2 - 17 months) among those treated with quizartinib/LDAC. Among responders, MRD was assessed in 11 patients (85%) in the quizartinib/AZA cohort and 12 (86%) in the quizartinib/LDAC cohort. MRD was undetectable in five (45%) patients treated with quizartinib/AZA and three (25%) with quizartinib/LDAC (excluding patients who achieved MRD-negative status following SCT). Four patients (29%) treated with quizartinib/AZA and one (6%) with quizartinib/LDAC proceeded to SCT after achieving CRc. MRD was assessed in all responders before SCT, and only one of them (treated with quizartinib/AZA) was MRD-negative before undergoing the transplant. With regard to the ITT population with R/R

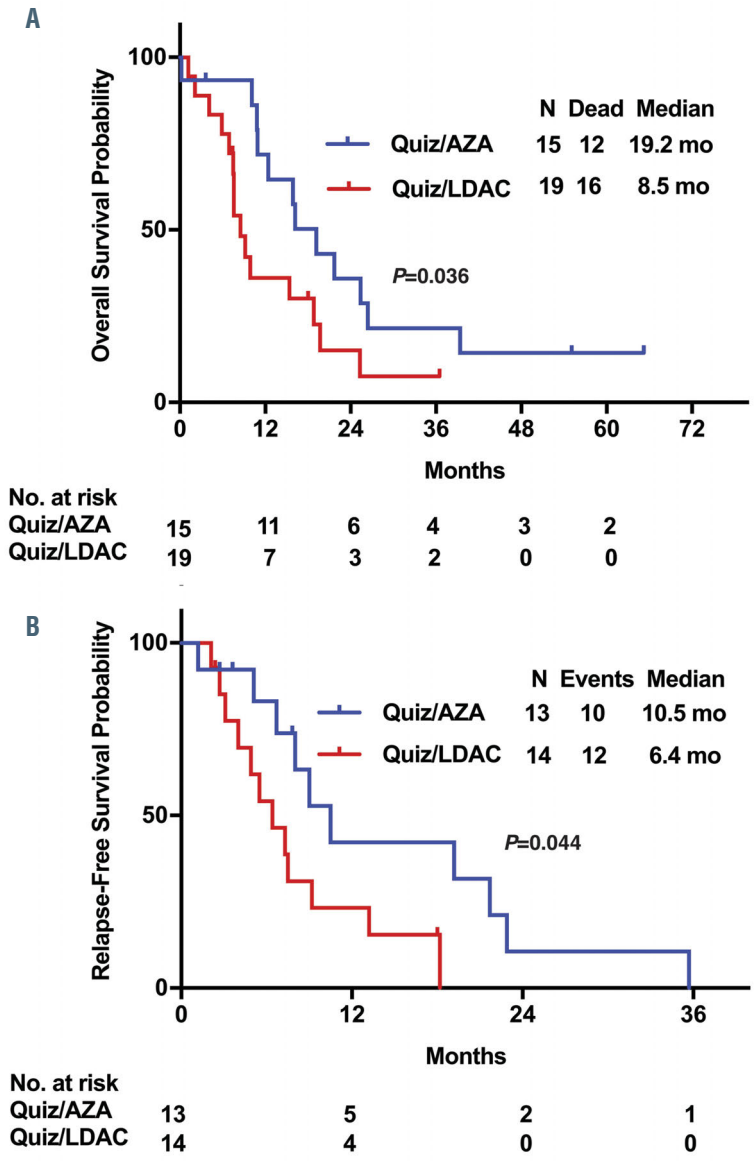

Figure 2. Survival of patients with *FLT3*-ITD$^+$ acute myeloid leukemia treated frontline with quizartinib in combination with azacitidine or low-dose cytarabine. (A) Overall survival. (B) Relapse-free survival. Quiz: quizartinib; AZA: azacitidine; LDAC: low-dose cytarabine; mo: months.

AML, CRc was observed in 64% (n=16 patients: 2 CR, 12 CRi, 2 CRp) of the quizartinib/AZA cohort and 29% (n=4 patients: 1 CR, 2 CRi, 1 CRp) in the quizartinib/LDAC cohort (Table 2). The per-protocol response data are shown in Table 3. The median duration of response was 2.5 months (range, 0.1 - 19.4 months) among the patients treated with quizartinib/AZA and 2.4 months (range, 0.5 - 7.2 months) among those treated with quizartinib/LDAC. Six patients (25%) in the quizartinib/AZA cohort and one (7%) in the quizartinib/LDAC cohort received SCT after achieving CRc. Among the three patients previously exposed to FLT3 inhibitors and treated with quizartinib/AZA, two achieved a CRi and one a CRp (prior sorafenib). Similarly, two of seven (29%) such patients treated with quizartinib/LDAC had responses: one achieved a CRi and one had a PR (prior sorafenib). One of the four patients with prior exposure to AZA for AML achieved a CR with quizartinib/AZA.

Survival

At a median follow-up of 55.1 months (range, 0.2 - 65.2 months), 12 (16%) patients remain alive (8 [20%] in the quizartinib/AZA cohort and 4 [12%] in the quizartinib/LDAC cohort). The median overall survival for all patients treated frontline was 12.4 months. With the caveat that the study was not powered to determine a survival benefit, the median overall survival was longer in patients treated frontline with quizartinib/AZA than in those treated with quizartinib/LDAC (19.2 *vs.* 8.5 months, respectively; *P*=0.036) (Figure 2). The median relapse-free survival for all patients treated frontline in this trial was 8 months: it was longer for patients treated with quizartinib/AZA compared to those treated with quizartinib/LDAC (10.5 *vs.* 6.4 months, respectively; *P*=0.044) (Figure 2). Patients with R/R AML had a median overall survival of 6.2 months, with a trend to longer overall survival for those treated with quizartinib/AZA (12.8 *vs.* 4 months, *P*=0.053). There was no difference in the median relapse-free survival between the two treatment groups (overall, 5.8 months; 5.8 *vs.* 6.2 months by treatment arm, respectively; *P*=0.804) (Figure 3). We did not find any specific factors that significantly influenced CRc or survival in either the frontline or R/R treatment settings in the two cohorts (*Online Supplementary Figures S1* and S2,

Online Supplementary Tables S1-S4). *TET2* mutation was found to have a negative impact on CRc, but only 13/73 patients had a *TET2* mutation (*Online Supplementary Tables S5* and *S6*).

At the last follow-up of all patients, two (5%) in the quizartinib/AZA cohort and one (3%) in the quizartinib/LDAC cohort continued to receive study treatment (Table 4). Disease relapse or loss of response was the most common reason for study discontinuation in both cohorts. Molecular data at the end of treatment were available for 41 patients (including data collected using an 81-gene panel in 9 patients). New mutations identified at the end of treatment included *FLT3*-D835 (11/41, 27%), *IDH1* (2/9, 22%), *RAS* (2/11, 18%), and *KIT* (1/9, 11%) (*Online Supplementary Figure S3*). Eleven (28%) patients in the quizartinib/AZA cohort and two (6%) in the quizartinib/LDAC cohort proceeded to SCT. Three patients (23%) treated with quizartinib/AZA relapsed after a median time of 3.2 months (range, 2.7 - 18 months) following SCT. Seven patients (54%) are alive after SCT without any evidence of disease (5 treated with quizartinib/AZA and 2 treated with quizartinib/LDAC). Of the six patients who died after SCT, three died in CR/CRi/CRp from multi-organ failure secondary to *Klebsiella pneumoniae* bacteremia, late gastrointestinal graft-*versus*-host disease, and an unknown cause, respectively. The three other patients had relapsed disease and died, one each, from multi-organ failure secondary to enteroviral pneumonia, intracerebral hemorrhage, and renal failure.

Table 4. Summary of disposition of all study patients (n=73).

Reasons	Quizartinib/AZA (n=40)	Quizartinib/LDAC (n=33)
	N (%)	
Relapse/loss of response	11 (28)	11 (33)
Stem cell transplant	11 (28)	2 (6)
Lack of response/disease progression	8 (20)	10 (30)
Death[a]	6 (15)	4 (12)
Continuing treatment	2 (5)	1 (3)
Patient's choice[b]	1 (3)	1 (3)
Lost to follow-up	1 (3)	1 (3)
Infection/toxicity[c]	0	3 (9)

AZA: azacitidine; LDAC: low-dose cytarabine. [a]Of six patients in the AZA cohort who died, one died early, two died in complete response with incomplete hematologic recovery (CRi), two in complete response (CR) and one without response. In the LDAC cohort, four patients died: one in CR without platelet recovery, one in CRi, one with a partial response and one with no response. [b]One patient in the AZA cohort chose to be treated at a different institution and one in the LDAC cohort chose to discontinue treatment for financial reasons. [c]One patient each discontinued treatment due to atrial fibrillation and meningitis. One additional patient developed atrial fibrillation prior to receiving quizartinib and was taken off study.

Safety and dose reduction

The most common treatment-emergent adverse events are listed in Table 5. Among grade ≥3 adverse events, febrile neutropenia and pneumonia were frequently reported in both cohorts. Other common grade ≥3 adverse events that occurred in the cohort of patients treated with quizartinib/AZA were hypokalemia (33%), hypotension (24%), and hypophosphatemia (18%). The median time to absolute neutrophil count recovery (neutrophils >1 x 10^9/L) for all cycles in patients treated frontline was 32 days (range, 8 - 125 days): it was 35 days (range, 9 - 125 days in the quizartinib/AZA cohort and 27 days (range, 8 - 68 days in the quizartinib/LDAC cohort. Similarly, the median time to platelet recovery (platelets >100 x 10^9/L) for all cycles was 29 days (range, 7 - 125 days), 30 days (range, 7 - 125 days) in the quizartinib/AZA cohort and 29 days (range, 25 - 60 days) in the quizartinib/LDAC cohort. The median times to recovery of absolute neutrophil count and platelet count were similar in R/R patients.

QTc prolongation was observed infrequently. Only one (3%) patient had grade 3, and three (9%) patients had grade 1-2 QTc prolongation in the quizartinib/AZA cohort, and one (3%) had grade 3 prolongation in the quizartinib/LDAC cohort (*Online Supplementary Figures S4* and *S5*). One (3%) patient who received quizartinib/AZA as frontline treatment died early (day 7 of treatment) due to multi-organ failure secondary to sepsis from an unknown organism.

A total of nine (23%) patients required a dose modification in the quizartinib/AZA cohort. Of them, three patients received quizartinib for only 7 days, 14 days, and 16 days in the first cycle due to the development of multi-organ failure, SCT, and febrile neutropenia, respectively. The quizartinib dose was decreased to 30 mg in six patients (4 due to grade 3 myelosuppression, 1 due to grade 2 supraventricular tachycardia, and 1 due to grade 3 QTc prolongation). Similarly, the quizartinib dose was decreased to 30 mg in three patients (9%) in the quizartinib/LDAC cohort: in two cases due to grade 3 myelosuppression and in one case due to grade 3 QTc prolongation.

Discussion

With the limitations of comparisons across studies, the CRc rates and the median overall survival observed in patients treated frontline with quizartinib/AZA in this study seem to compare favorably to what has been reported for similar combinations using other FLT3 inhibitors. With midostaurin plus AZA, the reported CRc and median overall survival were 31% and 9 months, respectively.[20] Similarly, with sorafenib plus AZA, the CRc and median overall survival were 70% and 8.3 months, respectively.[21] The results with quizartinib/AZA also appear comparable to the results reported with a hypomethylating agent/venetoclax[24] (CR/Cri: 72% in *FLT3*-mutated cases; median overall survival not reached). Although patients with *FLT3* mutations had good responses to hypomethylating agents/venetoclax, mutations in *FLT3*-ITD constitute one of the mechanisms of acquired resistance to venetoclax in preclinical models,[25,26] and have been reported to emerge in some patients as they develop resistance to therapy with venetoclax.[27] Ongoing clinical studies are trying to overcome this resistance by adding FLT3 inhibitors to venetoclax (gilteritinib - NCT03625505 and quizartinib - NCT03735875).

Quizartinib, as a single agent, was found to produce a CRc of 48% in patients with R/R AML, who achieved a median overall survival of 6.2 months.[16] Similarly, AZA monotherapy in R/R AML produced CR/CRi in 16% of patients, who had a median overall survival of 6.8 months.[28] The combination of quizartinib/AZA in our study produced a CRc of 67% with a median overall survival of 12.8 months in patients with R/R AML. Although no comparisons could be made between different studies, higher response rates and longer survival observed with the combination could perhaps be attributed to a possible synergy

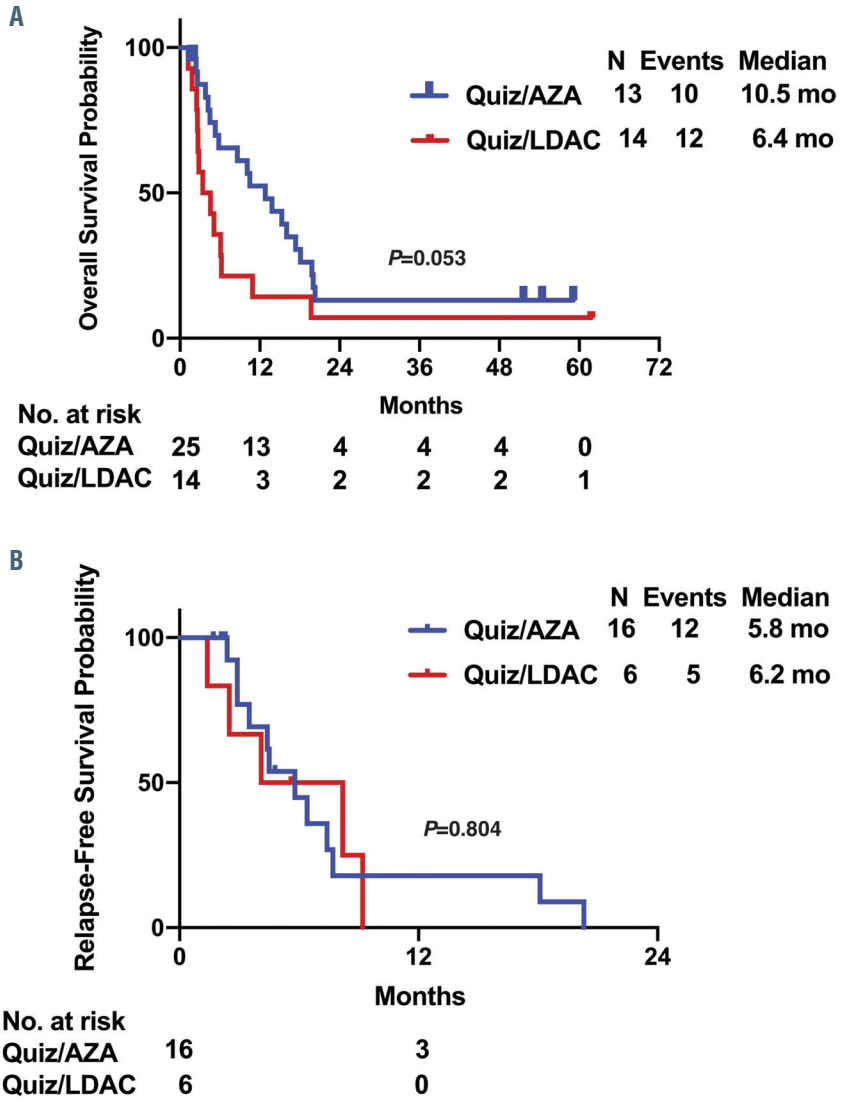

Figure 3. Survival of patients with *FLT3*-ITD$^+$ relapsed/refractory acute myeloid leukemia given first salvage treatment with quizartinib in combination with azacitidine or low-dose cytarabine. (A) Overall survival. (B) Relapse-free survival. Quiz: quizartinib; AZA: azacitidine; LDAC: low-dose cytarabine; mo: months.

between quizartinib and AZA. Similarly, in phase II studies, quizartinib monotherapy showed some activity in patients with *FLT3*-WT AML with a CRc rate of 32%.[29] Our study included only three patients with *FLT3*-WT, who received quizartinib-based combinations as first salvage treatment but had no response. Because of the paucity of patients, no conclusion could be made on the clinical activity of quizartinib in combination with AZA or LDAC in patients with *FLT3*-WT AML. However, based on the reported CRc rate of 32% with quizartinib monotherapy,[14] this approach deserves further investigation in this subset of patients.

Prior studies found that point mutations and gatekeeper mutations (F691L) were the common resistant mutations that were acquired following quizartinib therapy.[30-32] In this series, *FLT3*-D835 was acquired at the time of progression in 27% of patients. This is equivalent to what we had reported previously with single-agent FLT3 inhibitors, mostly sorafenib.[33] Other mutations encountered at the time of progression included *EZH2* and *CREBBP* mutations. However, the mutation analysis was somewhat limited in this study, since mutation data at the time of treatment discontinuation were available for only 41/70 (59%) patients (*Online Supplementary Figure S3*). Similarly, after treatment with gilteritinib, resistance is associated with the emergence of additional mutations, frequently *RAS*. This may represent a selection of clones, often pre-existing, which emerge as clones with sensitive *FLT3* mutations are suppressed by potent FLT3 inhibitors. This suggests that combination therapy would be required to further improve the outcome of patients treated with FLT3 inhibitors. The higher rate of response and more durable responses seen in the present study compared to what has been reported with quizartinib monotherapy are encouraging and merit further investigation.

Like quizartinib monotherapy, quizartinib at a dose of 60 mg in combination with AZA or LDAC was very well tolerated. QTc prolongation was infrequent with only two patients developing grade 3 prolongation and requiring a decrease in quizartinib dose to 30 mg. Overall, therapy was well tolerated by our patients in both the cohorts.

As previously reported, a higher *FLT3*-ITD allelic ratio was found to correlate with the rate of CRc in patients receiving frontline therapy, although the optimal cut point for the ratio was at 0.5 rather than the 0.7 that had been previously proposed. However, no such correlation could be identified for survival. There were no significant correlations between allelic ratio and responses or survival in the salvage cohort (*Online Supplementary Figure S6* and

Table 5. **Incidence of common treatment-emergent adverse events in all patients.**

Adverse events	Quizartinib/AZA (n=40)			Quizartinib/LDAC (n=33)		
	Total	Grade 1-2 N (%)	Grade 3-5	Total	Grade 1-2 N (%)	Grade 3-5
Non-hematologic toxicities						
Hypomagnesemia	27 (68)	26 (65)	1 (3)	10 (30)	10 (30)	0
Hyperbilirubinemia	25 (63)	19 (48)	6 (15)	9 (27)	8 (24)	1 (3)
Hypokalemia	24 (60)	11 (28)	13 (33)	9 (27)	6 (18)	3 (9)
Hypocalcemia	23 (58)	16 (40)	7 (18)	9 (27)	9 (27)	0
Increased ALT	23 (58)	19 (48)	4 (10)	15 (45)	13 (39)	2 (6)
Hyponatremia	17 (43)	12 (30)	5 (13)	8 (24)	5 (15)	3 (9)
Febrile neutropenia	16 (40)	0	16 (40)	12 (36)	0	12 (36)
Elevated creatinine	13 (33)	13 (33)	0	7 (21)	7 (21)	0
Hypophosphatemia	12 (30)	5 (13)	7 (18)	3 (9)	2 (6)	1 (3)
Pneumonia	11 (28)	0	11 (28)	19 (58)	3 (9)	16 (48)
Nausea	10 (25)	9 (23)	1 (3)	14 (42)	12 (36)	2 (6)
Fatigue	9 (23)	8 (20)	1 (3)	10 (30)	7 (21)	3 (9)
Diarrhea	8 (20)	5 (13)	3 (8)	13 (39)	10 (30)	3 (9)
Hypoalbuminemia	8 (20)	6 (15)	2 (5)	7 (21)	7 (21)	0
Vomiting	6 (15)	6 (15)	0	10 (30)	8 (24)	2 (6)
Rash	6 (15)	4 (10)	2 (5)	9 (27)	8 (24)	1 (3)
Hyperkalemia	5 (13)	3 (8)	2 (5)	4 (12)	4 (12)	0
Lower limb edema	5 (13)	5 (13)	0	4 (12)	4 (12)	0
Generalized weakness	5 (13)	4 (10)	1 (3)	5 (15)	3 (9)	2 (6)
Oral mucositis	5 (13)	4 (10)	1 (3)	8 (24)	7 (21)	1 (3)
Anorexia	4 (10)	3 (8)	1 (3)	5 (15)	5 (15)	0
Constipation	4 (10)	4 (10)	0	5 (15)	5 (15)	0
Dizziness	4 (10)	4 (10)	0	6 (18)	5 (15)	1 (3)
Abdominal pain	4 (10)	1 (3)	3 (8)	8 (24)	7 (21)	1 (3)
Hypotension	4 (10)	1 (3)	3 (8)	12 (36)	4 (12)	8 (24)
Atrial fibrillation	2 (5)	0	2 (5)	3 (9)	2 (6)	1 (3)
Headache	1 (3)	1 (3)	0	6 (18)	3 (9)	3 (9)
Pleural effusion	1 (3)	1 (3)	0	5 (15)	4 (12)	1 (3)
Back pain	1 (3)	1 (3)	0	10 (30)	9 (27)	1 (3)
QTc prolongation	1 (3)	0	1 (3)	4 (12)	3 (9)	1 (3)
Sinus tachycardia	1 (3)	0	1 (3)	2 (6)	2 (6)	0
Sinus bradycardia	0	0	0	3 (9)	3 (9)	0
Hematologic toxicities						
Thrombocytopenia	6 (15)	1 (3)	5 (13)	10 (30)	0	10 (30)
Leukopenia	3 (8)	1 (3)	2 (5)	14 (42)	0	14 (42)
Neutropenia	3 (8)	1 (3)	2 (5)	14 (42)	0	14 (42)
Anemia	1 (3)	1 (3)	0	5 (15)	0	5 (15)
Leukocytosis	0	0	0	2 (6)	0	2 (6)

AZA: azacitidine; LDAC, low-dose cytarabine; ALT: alanine transaminase.

Online Supplementary Table S5). Recently, Levis and his colleagues showed that among patients with *FLT3*-mutated R/R AML treated with gilteritinib monotherapy, patients with *NPM1* co-mutation had significantly better survival outcomes.[34] Similarly, *NPM1* co-mutation was associated with non-significantly better CRc rates and longer overall survival in our R/R patients (*Online Supplementary Figure S2* and *Online Supplementary Table S4*). In general, these associations follow the same direction as those found in our series, but the small number of patients preclude firm conclusions. These possible interactions remain to be confirmed in larger series.

In conclusion, our study demonstrated that quizartinib, in combination with AZA or LDAC, can be administered safely to patients with *FLT3*-mutated AML, whether as initial therapy or as first salvage treatment. Our preliminary observations suggest that the combination therapy, particularly with AZA, might improve the probability of response and the response duration in these patients. Prospective randomized studies are warranted to validate our results.

Disclosures

No conflicts of interest to disclose.

Contributions

JC and HK designed the study; MS, JC, VG, SP, MRP and LX collected and analyzed the data, and performed the statistical analysis; MS and JC wrote the manuscript. All the authors reviewed the manuscript and approved the version for submission.

Funding

The study was supported in part by a Cancer Center Support Grant (NCI grant P30 CA016672).

References

1. Gilliland DG, Griffin JD. The roles of FLT3 in hematopoiesis and leukemia. Blood. 2002;100(5):1532-1542.
2. Daver N, Schlenk RF, Russell NH, Levis MJ. Targeting FLT3 mutations in AML: review of current knowledge and evidence. Leukemia. 2019;33(2):299-312.
3. Nagel G, Weber D, Fromm E, et al. Epidemiological, genetic, and clinical characterization by age of newly diagnosed acute myeloid leukemia based on an academic population-based registry study (AMLSG BiO). Ann Hematol. 2017; 96(12):1993-2003.
4. Frohling S, Schlenk RF, Breitruck J, et al. Prognostic significance of activating FLT3 mutations in younger adults (16 to 60 years) with acute myeloid leukemia and normal cytogenetics: a study of the AML Study Group Ulm. Blood. 2002;100(13): 4372-4380.
5. Kottaridis PD, Gale RE, Frew ME, et al. The presence of a FLT3 internal tandem duplication in patients with acute myeloid leukemia (AML) adds important prognostic information to cytogenetic risk group and response to the first cycle of chemotherapy: analysis of 854 patients from the United Kingdom Medical Research Council AML 10 and 12 trials. Blood. 2001;98(6):1752-1759.
6. Schnittger S, Schoch C, Dugas M, et al. Analysis of FLT3 length mutations in 1003 patients with acute myeloid leukemia: correlation to cytogenetics, FAB subtype, and prognosis in the AMLCG study and usefulness as a marker for the detection of minimal residual disease. Blood. 2002;100(1):59-66.
7. Fiedler W, Kayser S, Kebenko M, et al. A phase I/II study of sunitinib and intensive chemotherapy in patients over 60 years of age with acute myeloid leukaemia and activating FLT3 mutations. Br J Haematol. 2015;169(5):694-700.
8. Pratz KW, Cortes J, Roboz GJ, et al. A pharmacodynamic study of the FLT3 inhibitor KW-2449 yields insight into the basis for clinical response. Blood. 2009;113(17): 3938-3946.
9. Smith BD, Levis M, Beran M, et al. Single-agent CEP-701, a novel FLT3 inhibitor, shows biologic and clinical activity in patients with relapsed or refractory acute myeloid leukemia. Blood. 2004; 103(10): 3669-3676.
10. Stone RM, DeAngelo DJ, Klimek V, et al. Patients with acute myeloid leukemia and an activating mutation in FLT3 respond to a small-molecule FLT3 tyrosine kinase inhibitor, PKC412. Blood. 2005;105(1):54-60.
11. Stone RM, Mandrekar SJ, Sanford BL, et al. Midostaurin plus chemotherapy for acute myeloid leukemia with a FLT3 mutation. N Engl J Med. 2017;377(5):454-464.
12. Wander SA, Levis MJ, Fathi AT. The evolving role of FLT3 inhibitors in acute myeloid leukemia: quizartinib and beyond. Ther Adv Hematol. 2014;5(3):65-77.
13. Daver N, Cortes J, Ravandi F, et al. Secondary mutations as mediators of resistance to targeted therapy in leukemia. Blood. 2015;125(21):3236-3245.
14. Cortes J, Perl AE, Dohner H, et al. Quizartinib, an FLT3 inhibitor, as monotherapy in patients with relapsed or refractory acute myeloid leukaemia: an open-label, multicentre, single-arm, phase 2 trial. Lancet Oncol. 2018;19(7):889-903.
15. Perl AE, Altman JK, Cortes J, et al. Selective inhibition of FLT3 by gilteritinib in relapsed or refractory acute myeloid leukaemia: a multicentre, first-in-human, open-label, phase 1-2 study. Lancet Oncol. 2017; 18(8):1061-1075.
16. Cortes JE, Khaled S, Martinelli G, et al. Quizartinib versus salvage chemotherapy in relapsed or refractory FLT3-ITD acute myeloid leukaemia (QuANTUM-R): a multicentre, randomised, controlled, open-label, phase 3 trial. Lancet Oncol. 2019; 20(7):984-997.
17. Perl AE, Martinelli G, Cortes JE, et al. Gilteritinib or chemotherapy for relapsed or refractory FLT3-mutated AML. N Engl J Med. 2019;381(18):1728-1740.
18. Ravandi F, Alattar ML, Grunwald MR, et al. Phase 2 study of azacytidine plus sorafenib in patients with acute myeloid leukemia and FLT-3 internal tandem duplication mutation. Blood. 2013;121(23):4655-4662.
19. Strati P, Kantarjian H, Ravandi F, et al. Phase I/II trial of the combination of midostaurin (PKC412) and 5-azacytidine for patients with acute myeloid leukemia and myelodysplastic syndrome. Am J Hematol. 2015;90(4):276-281.
20. Gallogly MM, Tomlinson BK, Bunner P, et al. A phase II study of midostaurin and 5-azacitidine for elderly patients with acute myeloid leukemia. Blood. 2017;130(Suppl 1):1332.
21. Ohanian M, Garcia-Manero G, Levis M, et al. Sorafenib combined with 5-azacytidine in older patients with untreated FLT3-ITD mutated acute myeloid leukemia. Am J Hematol. 2018;93(9):1136-1141.
22. Cheson BD, Bennett JM, Kopecky KJ, et al. Revised recommendations of the International Working Group for Diagnosis, Standardization of Response Criteria, Treatment Outcomes, and Reporting Standards for Therapeutic Trials in Acute Myeloid Leukemia. J Clin Oncol. 2003;21(24):4642-4649.
23. Thall PF, Simon RM, Estey EH. Bayesian sequential monitoring designs for single-arm clinical trials with multiple outcomes. Stat Med. 1995;14(4):357-379.
24. DiNardo CD, Pratz K, Pullarkat V, et al. Venetoclax combined with decitabine or azacitidine in treatment-naive, elderly patients with acute myeloid leukemia. Blood. 2019;133(1):7-17.
25. Mali RS, Lasater EA, Doyle K, et al. FLT3-ITD activation mediates resistance to the BCL-2 selective antagonist, venetoclax, in FLT3-ITD mutant AML models. Blood. 2017;130(Suppl 1):1348.
26. Zhang Q, Pan R, Han L, et al. Mechanisms of acquired resistance to venetoclax in preclinical AML models. Blood. 2015; 126(23):328-328.
27. Chyla B, Daver N, Doyle K, et al. Genetic biomarkers of sensitivity and resistance to venetoclax monotherapy in patients with relapsed acute myeloid leukemia. Am J Hematol. 2018;93(8):E202-E205.
28. Stahl M, DeVeaux M, Montesinos P, et al. Hypomethylating agents in relapsed and refractory AML: outcomes and their predictors in a large international patient cohort. Blood Adv. 2018;2(8):923-932.
29. Cortes JE, Perl AE, Dombret H, et al. Final results of a phase 2 open-label, monotherapy efficacy and safety study of quizartinib (AC220) in patients ≥ 60 years of age with FLT3 ITD positive or negative relapsed/refractory acute myeloid leukemia. Blood. 2012;120(21):48-48.
30. Albers C, Leischner H, Verbeek M, et al. The secondary FLT3-ITD F691L mutation induces resistance to AC220 in FLT3-ITD+ AML but retains in vitro sensitivity to PKC412 and sunitinib. Leukemia. 2013; 27(6):1416-1418.
31. Smith CC, Lin K, Stecula A, Sali A, Shah NP. FLT3 D835 mutations confer differential resistance to type II FLT3 inhibitors. Leukemia. 2015;29(12):2390-2392.
32. Smith CC, Paguirigan A, Jeschke GR, et al. Heterogeneous resistance to quizartinib in acute myeloid leukemia revealed by single-cell analysis. Blood. 2017;130(1):48-58.
33. Alvarado Y, Kantarjian HM, Luthra R, et al. Treatment with FLT3 inhibitor in patients with FLT3-mutated acute myeloid leukemia is associated with development of secondary FLT3-tyrosine kinase domain mutations. Cancer. 2014;120(14):2142-2149.
34. Levis MJ, Perl AE, Martinelli G, et al. Effect of gilteritinib on survival in patients with FLT3-mutated (FLT3mut+) relapsed/refractory (R/R) AML who have common AML co-mutations or a high FLT3-ITD allelic ratio. J Clin Oncol. 2019;37(15_suppl):7000.

ARTICLE

Bile acids regulate intestinal antigen presentation and reduce graft-*versus*-host disease without impairing the graft-*versus*-leukemia effect

Eileen Haring,[1,2*] Franziska M. Uhl,[1,2*] Geoffroy Andrieux,[3,4] Michele Proietti,[5] Alla Bulashevska,[5] Barbara Sauer,[1] Lukas M. Braun,[1,2] Enrique de Vega Gomez,[1] Philipp R. Esser,[6] Stefan F. Martin,[6] Dietmar Pfeifer,[1] Marie Follo,[1] Annette Schmitt-Graeff,[7] Joerg Buescher,[8] Justus Duyster,[1] Bodo Grimbacher,[5,9,10,11] Melanie Boerries,[3,4,12] Erika L. Pearce,[8] Robert Zeiser[1,4,9] and Petya Apostolova[1]

[1]Department of Medicine I, Medical Center – University of Freiburg, Faculty of Medicine, University of Freiburg; [2]Faculty of Biology, Albert-Ludwigs-University, Freiburg; [3]Institute of Medical Bioinformatics and Systems Medicine, Medical Center - University of Freiburg, Faculty of Medicine, University of Freiburg, Freiburg; [4]German Cancer Consortium (DKTK), partner site Freiburg; and German Cancer Research Center (DKFZ), Heidelberg; [5]Institute for Immunodeficiency, Center for Chronic Immunodeficiency (CCI), Medical Center, Faculty of Medicine, Albert-Ludwigs-University, Freiburg; [6]Allergy Research Group, Department of Dermatology, Medical Center - University of Freiburg, Faculty of Medicine, University of Freiburg; [7]University of Freiburg; [8]Max-Planck Institute of Immunobiology and Epigenetics, Freiburg; [9]CIBSS – Centre for Integrative Biological Signalling Studies, University of Freiburg, Freiburg; [10]DZIF – German Center for Infection Research, Satellite Center Freiburg; [11]RESIST – Cluster of Excellence 2155 to Hanover Medical School, Satellite Center Freiburg and [12]Comprehensive Cancer Centre Freiburg (CCCF), University Medical Center Freiburg, Faculty of Medicine, University of Freiburg, Freiburg, Germany

**EH and FMU contributed equally as co-first authors.*

Ferrata Storti Foundation

Haematologica 2021
Volume 106(8):2131-2146

ABSTRACT

Acute graft-*versus*-host disease (GvHD) causes significant mortality in patients undergoing allogeneic hematopoietic cell transplantation. Immunosuppressive treatment for GvHD can impair the beneficial graft-*versus*-leukemia effect and facilitate malignancy relapse. Therefore, novel approaches that protect and regenerate injured tissues without impeding the donor immune system are needed. Bile acids regulate multiple cellular processes and are in close contact with the intestinal epithelium, a major target of acute GvHD. Here, we found that the bile acid pool is reduced following GvHD induction in a preclinical model. We evaluated the efficacy of bile acids to protect the intestinal epithelium without reducing anti-tumor immunity. We observed that application of bile acids decreased cytokine-induced cell death in intestinal organoids and cell lines. Systemic prophylactic administration of tauroursodeoxycholic acid (TUDCA), the most potent compound in our *in vitro* studies, reduced GvHD severity in three different murine transplantation models. This effect was mediated by decreased activity of the antigen presentation machinery and subsequent prevention of apoptosis of the intestinal epithelium. Moreover, bile acid administration did not alter the bacterial composition in the intestine suggesting that its effects are cell-specific and independent of the microbiome. Treatment of human and murine leukemic cell lines with TUDCA did not interfere with the expression of antigen presentation-related molecules. Systemic T-cell expansion and especially their cytotoxic capacity against leukemic cells remained intact. This study establishes a role for bile acids in the prevention of acute GvHD without impairing the graft-*versus*-leukemia effect. In particular, we provide a scientific rationale for the systematic use of TUDCA in patients undergoing allogeneic hematopoietic cell transplantation.

Correspondence:

PETYA APOSTOLOVA
petya.apostolova@uniklinik-freiburg.de

Received: November 15, 2019.

Accepted: July 7, 2020.

Pre-published: July 16, 2020.

https://doi.org/10.3324/haematol.2019.242990

Introduction

Allogeneic hematopoietic cell transplantation (allo-HCT) is a potentially curative treatment for leukemia and lymphoma. However, approximately 50% of acute myeloid leukemia patients develop a malignancy relapse after allo-HCT.[1] One contributing factor is the administration of immunosuppression as a prophylaxis or treatment for acute graft-*versus*-host disease (aGvHD). aGvHD is a severe transplant-associated complication which affects half of all allo-HCT recipients.[2] Compared to other clinical manifestations of aGvHD, intestinal GvHD causes the highest mortality, especially if it is refractory to corticosteroid treatment.[3] The pathogenesis of aGvHD is marked by activation of donor T cells and their expansion and migration to the target organs liver, skin and gastrointestinal tract where they cause tissue damage either by direct cytotoxicity or via cytokine secretion. A hallmark of intestinal aGvHD is the damage of intestinal stem cells (ISC) and Paneth cells.[4,5] Recent work has shown that interferon γ (IFNγ), a cytokine commonly increased in aGvHD, is responsible for intestinal tissue damage.[6,7] Current approved GvHD prophylaxis strategies are based on immunosuppressive drugs that deplete T cells or modulate their activity and cytokine signaling. Novel developments aiming at regenerating the intestinal epithelium would allow a reduction of broad-spectrum immunosuppression and potentially decrease the relapse rates after allo-HCT.

There are two main classes of bile acids. Primary bile acids are generated in the liver via cholesterol catabolism. In the final step of their synthesis, they are conjugated to the amino acids glycine and taurine. This step stabilizes their amphipathic structure that is necessary to keep their full emulsifying activity in the intestine. After fulfilling their digestive role, most bile acids (appoximately 90-95%) are actively taken up by the intestinal epithelial cells and transported back to the liver.[8] Primary bile acids, which are not re-absorbed, can be converted into secondary bile acids via modification and metabolization by microbial enzymatic activity thereby influencing the microbiome composition.[9] Bile acids have cytoprotective and anti-apoptotic properties for hepatocytes[10,11] via the preservation of mitochondrial glutathione.[12] Moreover, they modulate the translocation of apoptosis-regulating proteins BCL-2-associated X protein (BAX) and BCL-2-antagonist-of-cell-death (BAD) from the cytosol to the mitochondria and *vice versa*.[13,14] Also immunomodulatory effects of bile acids and their receptors have been described. The two most prominent bile acid receptors are the Farnesoid X receptor (FXR) and the transmembrane G protein-coupled bile acid receptor 5 (TGR5). FXR is expressed in both liver and intestine and was shown that mice lacking FXR were more prone to development of acute and chronic colitis.[15] Intestinal damage during GvHD has been previously linked with bile acid malabsorption.[16] In a recent study, metabolomic analysis of serum samples from allo-HCT recipients showed alterations in bile acid levels among other metabolites.[17] So far, no data on bile acid levels in liver, intestines or in intestinal content in the context of GvHD have been available.

The aim of this study was to investigate whether allo-HCT causes alterations in the bile acid composition and whether exogenous bile acid application can positively influence aGvHD development. We show that the bile acid pool was depleted after allo-HCT. Administration of tauroursodeoxycholic acid (TUDCA) improved aGvHD outcome by direct protection of the intestinal epithelium from cytokine damage and by lowering antigen presentation by non-hematopoietic cells. This makes it an attractive compound for combination therapy with already clinically available immunosuppressive strategies.

Methods

Mice

BALB/c (H-2K^{d}) and C57BL/6 (H-2K^{b}) mice were purchased from the animal facility at Freiburg University Medical Center or from Janvier Labs (Le Genest-Saint-Isle, France). Luciferase-transgenic C57BL/6 mice (H-2K^{b}) were bred in the animal facility of the Center for Clinical Research at Freiburg University Medical Center (Freiburg i.Br., Germany). B6.129P2-*Lgr5*$^{tm1(cre/ERT2)Cle/J}$ mice on the C57BL/6 background (H-2K^{b}) were a kind gift from Prof. Roland Schüle (Center for Clinical Research, Freiburg i.Br.). All animals were housed under specific pathogen-free conditions at the animal facility of the Center for Clinical Research (ZKF, Freiburg i.Br., Germany). All animal protocols (G-13/045, G-16/018, G-17/063; X-13/07J; X-15/10A) were approved by the Federal Ministry for Nature, Environment and Consumer Protection of the state of Baden-Württemberg, Germany.

All other materials and methods are provided in the *Online Supplementary Appendix*.

Results

Allogeneic hematopoietic cell transplantation alters the levels of bile acids and the expression of bile acid receptors

We first investigated how allo-HCT influences the enterohepatic circulation (Figure 1A) and the bile acid pool. We extracted metabolites from liver, ileum, ileal contents and serum of untreated mice and mice developing aGvHD (Figure 1B). We measured the levels of eight major bile acid metabolites by liquid chromatography - mass spectrometry (LC-MS) (Figure 1C) and observed that taurocholic acid (TCA) was the predominant bile acid in all four compartments. Induction of aGvHD resulted in reduced bile acid pools. While the levels of most bile acids significantly decreased, the absolute amount of ursodeoxycholic acid (UDCA) increased (Figure 1D; *Online Supplementary Figure S1A* to *C*).

Another important determinant of bile acid signaling is the expression of bile acid receptors. We found that intestinal *Nr1h4* mRNA levels (encoding for FXR) increased and *Gpbar1* levels (encoding for TGR5) decreased with a peak on day 4 after bone marrow transplantation (BMT) (Figure 1E; *Online Supplementary Figure S1D*). Collectively, our results show that allo-HCT causes a reduction of the bile acid pool in liver, intestine and intestinal content as well as a deviation in bile acid receptor expression.

Treatment with bile acids prevents cell death of intestinal organoids and cell lines

Small intestinal organoids mimic the structure of the intestine.[18] We used this *in vitro* system to test the impact of different bile acids on the viability and morphology of the intestinal epithelium. We selected bile acids belonging to different groups for our analysis: chenodeoxycholic acid (CDCA) as a primary bile acid, UDCA as a secondary unconjugated bile acid, TUDCA as a secondary conjugated

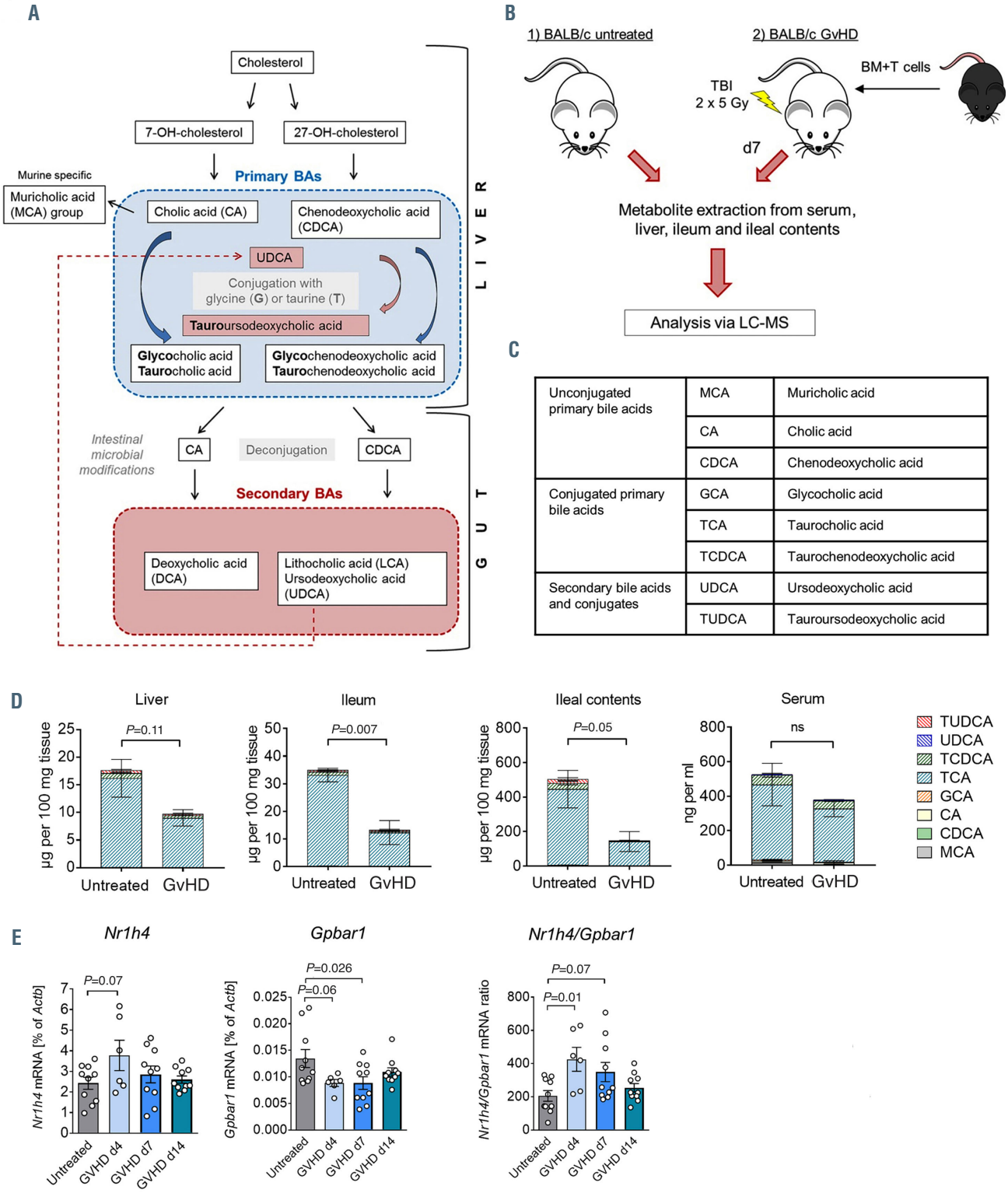

Figure 1. Allogeneic hematopoietic cell transplantation induces changes in bile acid levels and bile acid receptor expression. (A) Simplified schematic overview of bile acid metabolism and the enterohepatic circulation. (B) Experimental flow for metabolomic profiling of the bile acid pool from untreated BALB/c mice and mice developing graft-*versus*-host disease (GvHD). (C) Overview of the bile acids quantified by liquid chromatography - mass spectrometry. (D) Quantification of the bile acid composition in liver, ileum, ileal contents and serum of untreated mice and on day 7 after bone marrow transplantation (BMT). Data were pooled from five individual mice per group and are presented as mean ± standard error of the mean for each metabolite. *P*-values were calculated for the total bile acid pool using the two-tailed unpaired Student's *t*-test; ns: not significant. (E) Quantitative real-time polymerase chain reaction analysis of the mRNA expression of the bile acid receptors *Nr1h4* (encodes for the FXR protein) and *Gpbar1* (encodes for the TGR5 protein) in the small intestine of untreated mice and mice developing GvHD. Data are pooled from n=10 mice in the untreated, GvHD d7 and GvHD d14 groups and n=5 mice in the GvHD day 4 group. The *P*-values were calculated using the ordinary one-way ANOVA test with correction for multiple comparisons.

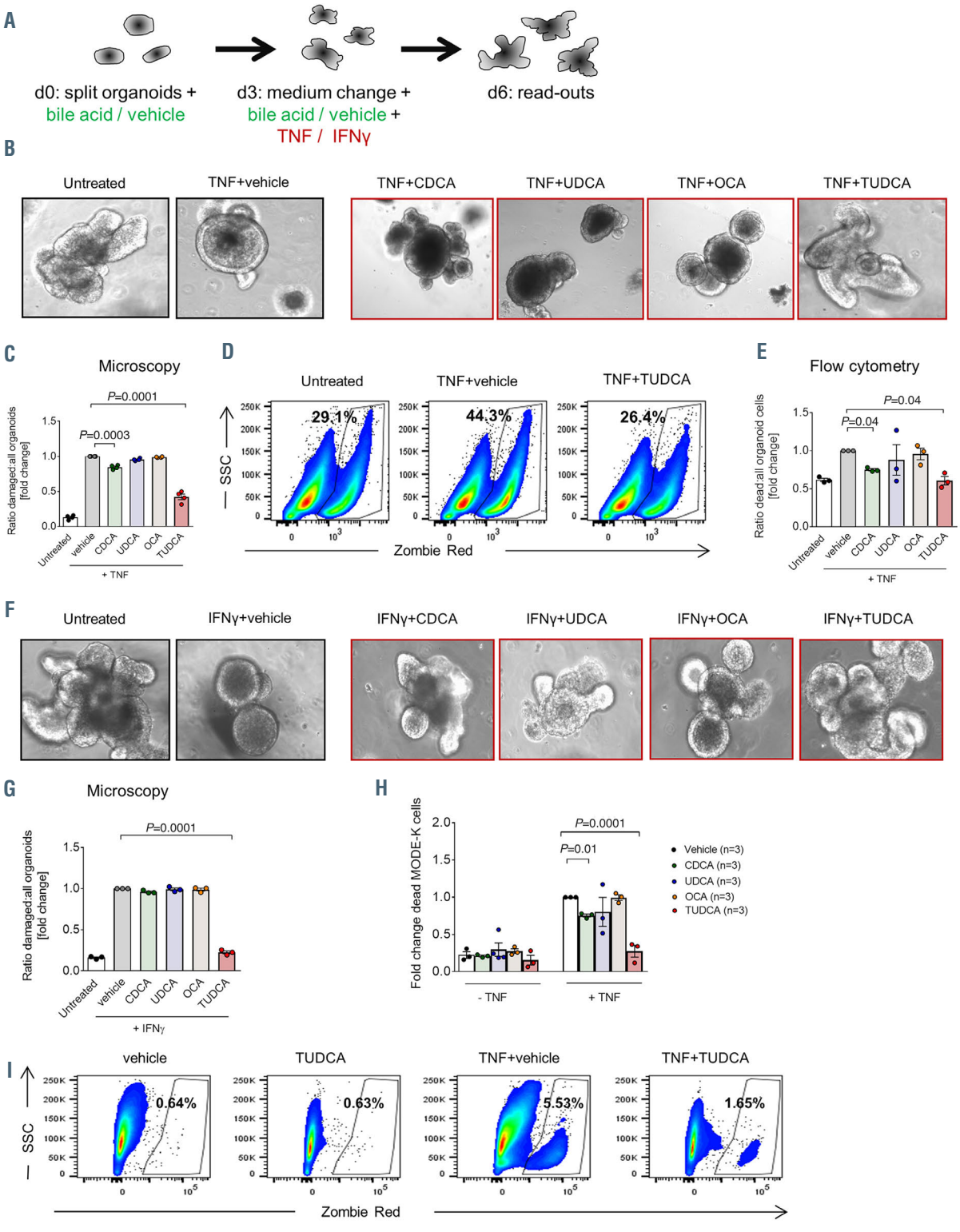

Figure 2. Treatment with bile acids reduces cell death in small intestinal organoids and MODE-K cells. (A) Experimental setting for the treatment of organoids with tumor necrosis factor (TNF) (20 ng/mL), interferon γ (IFNγ) (2.5 ng/mL) and the respective bile acids. (B) Representative images of BALB/c intestinal organoids treated with TNF as described in (A). (C) Quantification of damaged organoids treated with TNF as in (A) performed by manual microscope counting. Data were normalized to the TNF plus (TNF+)vehicle group. Statistical analysis of n=4 biologically independent experiments. The *P*-value was calculated using an ordinary one-way ANOVA test with correction for multiple comparisons. (D and E) Intestinal organoids were cultured as described in (A). Organoids were digested and the proportion of dead cells was determined by flow cytometry. (D) Representative flow cytometry dot plots. (E) Quantification of the percentages of dead cells. Data were normalized to the TNF+vehicle group. Statistical analysis of n=3 biologically independent experiments. The *P*-value was calculated using the ordinary one-way ANOVA test with correction for multiple comparisons. (F) Representative images of BALB/c intestinal organoids treated with IFNγ as described in (A). (G) Quantification of damaged organoids treated with IFNγ as in (A) performed by manual microscope counting. Data were normalized to the IFNγ+vehicle group. Statistical analysis of n=3 biologically independent experiments. The *P*-value was calculated using an ordinary one-way ANOVA test with correction for multiple comparisons. (H and I) Analysis of MODE-K cell viability after treatment with TNF ± chenodeoxycholic acid (CDCA), ursodeoxycholic acid (UDCA), 6-ethylchenodeoxycholic acid (OCA) or tauroursodeoxycholic acid (TUDCA) for 48 hours performed by flow cytometry. (H) Quantification of the percentages of dead cells. Data were normalized to the TNF+vehicle group. Statistical analysis of n=3 biologically independent experiments performed in technical duplicates or triplicates. The *P*-values were calculated using the ordinary one-way ANOVA test with correction for multiple comparisons. (I) Representative flow cytometry dot plots.

bile acid and 6-ethylchenodeoxycholic acid (obeticholic acid, OCA) as a synthetic compound and the strongest agonist of the FXR receptor. We evaluated the toxicity of these bile acids on organoids and the intestinal cell line MODE-K to select non-toxic doses for further experiments (*Online Supplementary Figure S2A* and *B*). Organoids were treated with tumor necrosis factor (TNF) or IFNγ in combination with or without bile acids (Figure 2A). We observed that TNF treatment, performed to induce cellular damage, reduced organoid viability as shown by changes in cell morphology and organoid structure. This effect was partially reversed by addition of CDCA and more significantly of TUDCA (Figure 2B to E). We confirmed the beneficial effect of TUDCA on organoid viability using IFNγ to induce organoid damage (Figure 2F and G). As TUDCA was the most potent bile acid to protect intestinal organoids from cytokine-induced cell death, we performed quantitative polymerase chain reaction (qPCR) analysis from organoids treated with TNF ± TUDCA in order to evaluate which cell types were particularly preserved. We observed a strong upregulation of the anti-microbial peptides defensin α1 and 4 (*Defa1* and *Defa4*) which are produced by Paneth cells (*Online Supplementary Figure S2C*). Additionally, we identified an elevated expression of the intestinal stem cell (ISC) marker leucine-rich repeat-containing G-protein coupled receptor 5 (*Lgr5*). Although there was a trend towards an increase in the goblet cell marker mucin 2 (*Muc2*) and the enteroendocrine cell marker chromogranine A (*Chga*), these changes were not significant (*Online Supplementary Figure S2C*). We confirmed the hypothesis that bile acids protect intestinal cells from cell death via performing additional experiments using the murine small intestine cell line MODE-K. TNF treatment reduced the viability of MODE-K cells. This was reversed partly by CDCA and even more by TUDCA (Figure 2H and I). Together, these data indicate that exposure to bile acids reduces intestinal cell damage induced by pro-inflammatory cytokines.

Prophylactic administration of bile acids reduces acute graft-*versus*-host disease severity in mice through a cell-intrinsic effect independent of the microbiome

Our *in vitro* studies provided evidence that bile acids protect the intestinal epithelium. Since TUDCA showed the strongest effects, we used this compound for further studies in a murine *in vivo* BMT model (Figure 3A and C). We determined bile acid concentrations and confirmed an increase of TUDCA levels after exogenous administration. Levels increased from 0.5% to 35% of the measured bile acids in the serum and from 3.2% to 57% in the ileal content reaching a concentration of almost 1 mg per 100 mg (*Online Supplementary Figure S3A* and *B*). Survival was significantly improved in animals treated with TUDCA in two different transplantation models using total body irradiation (TBI) as the conditioning treatment (Figure 3B and D). As a confirmation, histopathological analysis of the liver, small intestine and colon of recipient mice demonstrated significantly reduced aGvHD scores in the TUDCA-treated group (Figure 3E). This was further validated in an irradiation-free model with chemotherapy conditioning (*Online Supplementary Figure S3C* and *D*). Pro-inflammatory cytokines contribute to tissue damage and T-cell activation during aGvHD. We observed reduced serum cytokine levels in the treatment group with significant differences for TNF and a trend towards lower levels of IFNγ (Figure 3F). These data demonstrate a protective effect of TUDCA in the prophylactic setting with improved survival rates, reduced histological aGvHD scores and lower concentrations of pro-inflammatory cytokines.

Since we found in our *in vitro* system an effect on intestinal cell viability by other bile acids as well, we assessed the impact of CDCA and UDCA as a prophylaxis for aGvHD (*Online Supplementary Figure S3E*). Histopathological analysis revealed a slight improvement upon CDCA administration (*Online Supplementary Figure S3F*) and a more pronounced effect after treatment with UDCA (*Online Supplementary Figure S3G*).

Intestinal bacteria play an essential role in bile acid metabolism. They generate secondary bile acids by removing glycine or taurine residues from primary bile acids, which were not reabsorbed from intestinal epithelial cells and recycled in the enterohepatic circle.[19,20] The microbiome composition and the bile acid pool influence each other.[21] Recent data show that aGvHD is associated with changes in the microbiome including a diminished microbial diversity.[22-24] We therefore investigated whether TUDCA potentially mediates its protective effects by acting directly on the intestinal cells or by modifying the intestinal microbiome composition. Microbiome analysis was conducted in mice developing aGvHD. We could detect the expected reduction in microbial diversity in both groups compared to untreated mice. This reduction was independent of TUDCA treatment as depicted by similar Shannon indices and inversed Simpson indices (Figure 3G and H). Detailed analysis of the relative abundance of different species confirmed that the microbiome is altered during aGvHD development. In line with previous reports, *Lactobacillus* numbers increased and certain anaerobic species (in our case *Muribaculum* and *Sporobacter*) decreased. TUDCA- and vehicle-treated mice exhibited similar relative abundance profiles suggesting that TUDCA protects the intestinal epithelium by directly affecting the intestinal cells and not by changing the microbial composition (Figure 3I). Supporting this concept, TUDCA preserved its beneficial effects on the survival of mice developing aGvHD even after decontaminating antibiotic treatment that was administered prior to BMT (Figure 3J and K). Of note, antibiotic treatment did not lead to the general reduction in the bile acid pool of the ileal content seen as a result from GvHD induction (*Online Supplementary Figure SH3*). Together, these data suggest that although bile acids and the microbiome are closely connected in the intestinal tract, the beneficial effect of TUDCA on GvHD outcome is not mainly mediated by regulation of the intestinal bacteria.

Bile acid treatment decreases intestinal antigen presentation

In order to better understand the mechanism by which bile acid administration protects the intestine from aGvHD-induced damage, we performed gene expression analysis of small intestinal samples on day 14 after BMT. Using samples from TUDCA-treated animals and controls, we performed a hypergeometric test of significant regulated genes (q-value <0.05) to find differentially regulated terms from the Gene Ontology database. The most significantly downregulated pathways upon TUDCA treatment included pathways related to immune activation, among others the gene set 'antigen processing and presentation' (Figure 4A). Expression analysis in a second independent cohort confirmed the data on the mRNA and protein level (Figure 4B

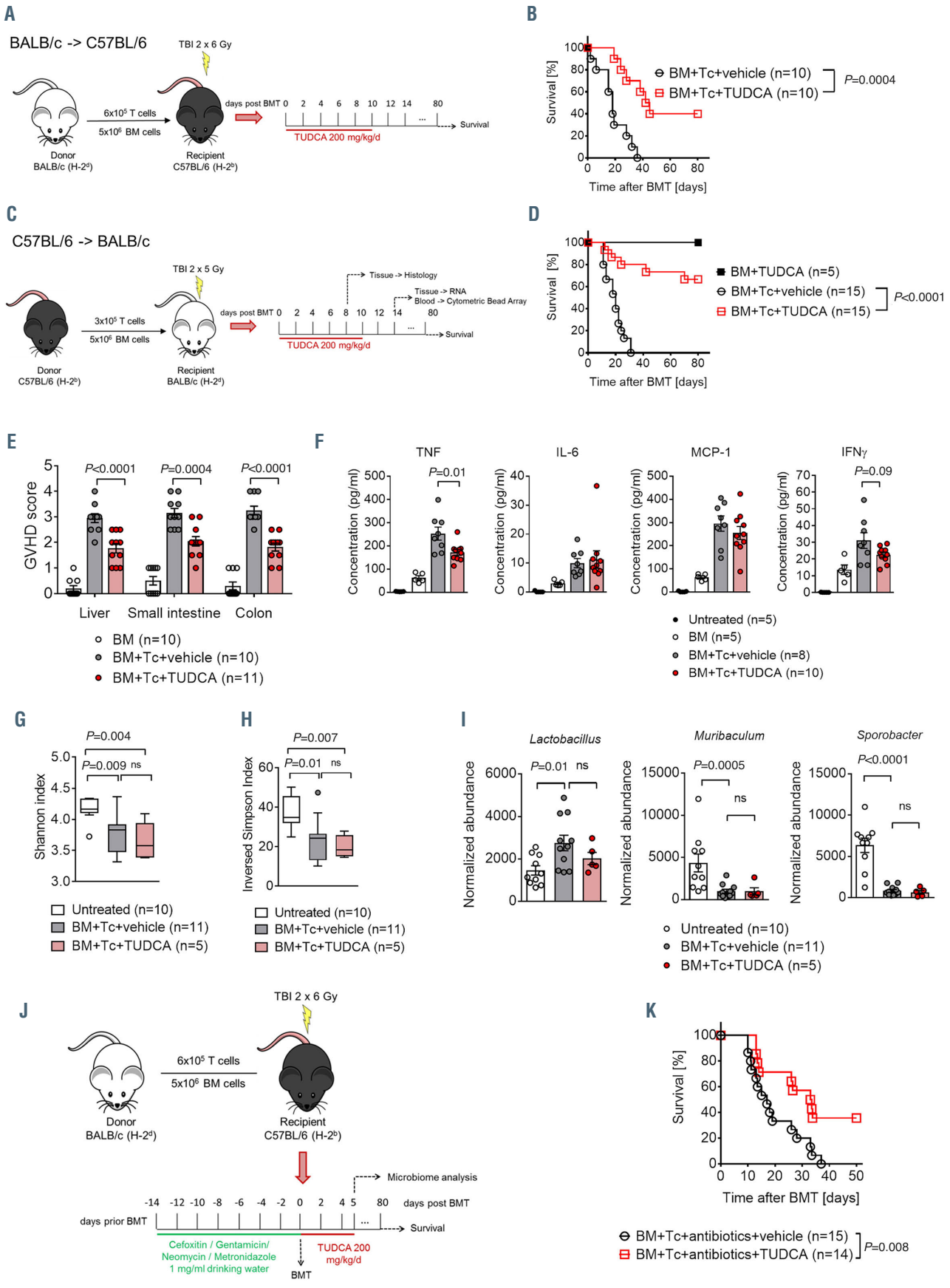

Figure 3. Legend on following page.

Figure 3. Bile acid treatment improves acute graft-*versus*-host disease outcome in mice. (A) Transplantation model with BALB/c (H-2kd) as donor and C57BL/6 (H-2kb) as recipient. Recipient animals were treated with 200 mg/kg body weight tauroursodeoxycholic acid (TUDCA) or an equal volume of vehicle from day 0 until day 10 after bone marrow transplantation (BMT) by a daily intraperitoneal injection. (B) Survival of C57BL/6 mice transplanted as shown in (A). Numbers (N) represent individual mice, the *P*-value was calculated using the two-sided Mantel-Cox test. (C) Transplantation model with C57BL/6 (H-2kb) as donor and BALB/c (H-2kd) as recipient. Recipient animals were treated with 200 mg/kg body weight TUDCA or an equal volume of vehicle from day 0 until day 10 after BMT by a daily intraperitoneal injection. (D) Survival of BALB/c mice transplanted as described in (C). Data were pooled from three independent experiments, numbers (N) represent individual mice. The *P*-value was calculated using the two-sided Mantel-Cox test. (E) Graft-*versus*-host disease (GvHD) histopathology scores of liver, small intestine and colon assessed on day 7 after BMT (C57BL/6 in BALB/c model). Data were pooled from two independent experiments, numbers (N) represent individual mice. *P*-values were calculated using the ordinary one-way ANOVA test with correction for multiple comparisons. (F) Serum cytokine concentrations in untreated mice and transplanted mice determined on day 14 after BMT (C57BL/6 in BALB/c model). Numbers (N) represent individual mice. *P*-values were calculated using the ordinary one-way ANOVA test with correction for multiple comparisons. (G and I) Fecal samples were collected for microbial analysis on day 5 after BMT. Numbers (N) represent individual mice. Data were pooled from two independent experiments. *P*-values were calculated using the ordinary one-way ANOVA test with correction for multiple comparisons; ns: not significant. (G) The Shannon index as a surrogate parameter for microbial diversity. (H) The reversed Simpson index as a surrogate parameter for microbial diversity. (I) Relative abundance of specified bacterial genera. (J) C57BL/6 mice were treated with an antibiotic cocktail comprising 1 mg/mL cefoxitin, metronidazole, neomycin and gentamycin for 2 weeks before they underwent BMT as described in (A). (K) Survival of C57BL/6 mice transplanted and treated as described in (J). Numbers (N) represent individual mice. Data were pooled from two independent experiments. Statistical analysis was performed using the two-sided Mantel-Cox test.

to E). Downregulated genes included transporter associated with antigen processing 1 and 2 (*Tap1* and *Tap2*) (Figure 4B to E), which are involved in the translocation of degraded cytosolic peptides across the endoplasmatic reticulum membrane for antigen-major histocompatibility complex (MHC) class I molecule assembly, as well as TAP binding protein (*Tapbp*) and Tapasin-related protein (*Tapbpl*) which mediate the association between TAP proteins and newly assembled MHC class I complexes. Furthermore, lower transcription of class II MHC complex transactivator (*Ciita*) was observed suggesting decreased MHC class II-related antigen presentation in the intestines of TUDCA-treated animals (Figure 4B and C). Confirming the hypothesis that the antigen presentation machinery in the intestine is reduced, we found decreased levels of MHC class I and MHC class II expression on non-hematopoietic cells in the intestine of TUDCA-treated animals (Figure 4F). In line with data obtained from the organoid culture system, multiple genes associated with the GO term 'Response to IFNγ' were significantly downregulated (Figure 4G). Interestingly, the numbers of $CD11c^+$ MHC class II^+ professional antigen-presenting cells (APC) in ileum and colon were identical between both groups (*Online Supplementary Figure S4A*). There was a slight reduction in TNF expression, whereas costimulatory molecules and other cytokines remained unchanged (*Online Supplementary Figure S4B* and *C*). The migration capacity of bone marrow-derived dendritic cells (BM-DC) was not impaired by TUDCA treatment either (*Online Supplementary Figure S4D*). These data support the hypothesis that antigen presentation by non-hematopoietic cells is reduced by TUDCA treatment. In line with this model, treatment with TNF elevated the expression of *Tap1* and *Tap2* in MODE-K cells which could be reversed by addition of TUDCA (Figure 4H and I). Notably, the effect on *Tap1/2* expression was most evident for TUDCA but occurred upon treatment with CDCA and UDCA as well (Figure 4H and I).

Bile acid administration changes the transcriptional signature of T cells in the intestine but preserves their systemic expansion

Antigen presentation is important for the recognition of malignant cells by alloreactive T cells. Since TUDCA reduces antigen presentation in the intestine, we asked whether its application has an immediate impact on T-cell activation. T-cell numbers in the lamina propria of the small intestine and production of IFNγ, interleukin-6 (IL-6) and TNF were not altered upon TUDCA administration (Figure 5A; *Online Supplementary Figure S5A* and *B*). However, we discovered a transcriptional signature suggesting downregulation of immune cell activation. We observed that the transcriptional levels of many genes associated with the GO term 'T-cell activation' were significantly reduced in GvHD developing mice, treated with TUDCA (Figure 5C). Among these genes were the CD3 subunits Cd3e and Cd3g, the transcription factor interferon regulatory factor 1 (*Irf1*), as well as many genes encoding for proteins that play an important role for signaling pathways downstream of the T-cell receptor (Figure 5D). Among these were lymphocyte-specific protein tyrosine kinase (*Lck*) and linker for activation of T cells (*Lat*). Lck is a tyrosine kinase that phosphorylates the tails of the CD3 chains of the T-cell receptor complex upon antigen recognition via MHC. This allows ZAP70 binding and activation. Lat is phosphorylated by ZAP70/Syk kinases upon T-cell receptor activation and recruits adapter proteins which are important for further signaling. This altered transcriptional signature suggests that multiple events in the downstream signaling of the CD3/T-cell receptor complex are reduced upon treatment with TUDCA.

We then investigated whether TUDCA administration could decrease the general alloreactive T-cell expansion. Bioluminescence-based trafficking analysis revealed that T-cell expansion was similar in vehicle- and TUDCA-treated animals (Figure 5E to G). Flow cytometry confirmed that there were no differences in T-cell numbers in the spleen between both groups (*Online Supplementary Figure S5C* to *F*). T-cell differentiation, migration and TNF production after *in vitro* stimulation and TUDCA treatment were comparable (*Online Supplementary Figure S5G* to *I*). Collectively, our results support the hypothesis that bile acid application is also associated with a transcriptional signature of reduced local T-cell activation without having a negative impact on systemic T-cell expansion.

Tauroursodeoxycholic acid decreases apoptosis in the intestine

We observed that bile acids prevent intestinal cell death *in vitro*. Further analysis of the microarray data obtained from the *in vivo* allo-HCT model revealed a significant downregulation of apoptosis-related genes in mice treated with TUDCA (Figure 6A). Confirming this, we performed an immunofluorescent TdT-mediated dUTP-biotin nick end labeling (TUNEL) staining which marks apoptotic nuclei. While aGvHD induction significantly increased intestinal apoptosis, TUDCA administration reduced it to almost the baseline level in both the small intestine and the colon (Figure 6B and C). The application of TUDCA increased the

expression of the ISC marker genes *Lgr5* and Pleckstrin homology-like domain family A member 1 (*Phlda1*) and of the goblet cell marker *Muc2* (Figure 6D). In contrast, no changes in the expression of *Defa1* and *Defa4* or *Chga* could be identified (*Online Supplementary Figure S6A* and *B*). In order to confirm the protection of ISC upon administration of TUDCA, we utilized B6.129P2-*Lgr5*$^{tm1(cre/ERT2)Cle/J}$ mice which express green fluorescent protein (GFP) under control of the *Lgr5* gene promoter. On day 14 after transplantation, we detected increased numbers of GFP^{+} cells in the small intestine of TUDCA-treated animals compared to vehicle-treated controls (Figure 6E and F). Previous studies

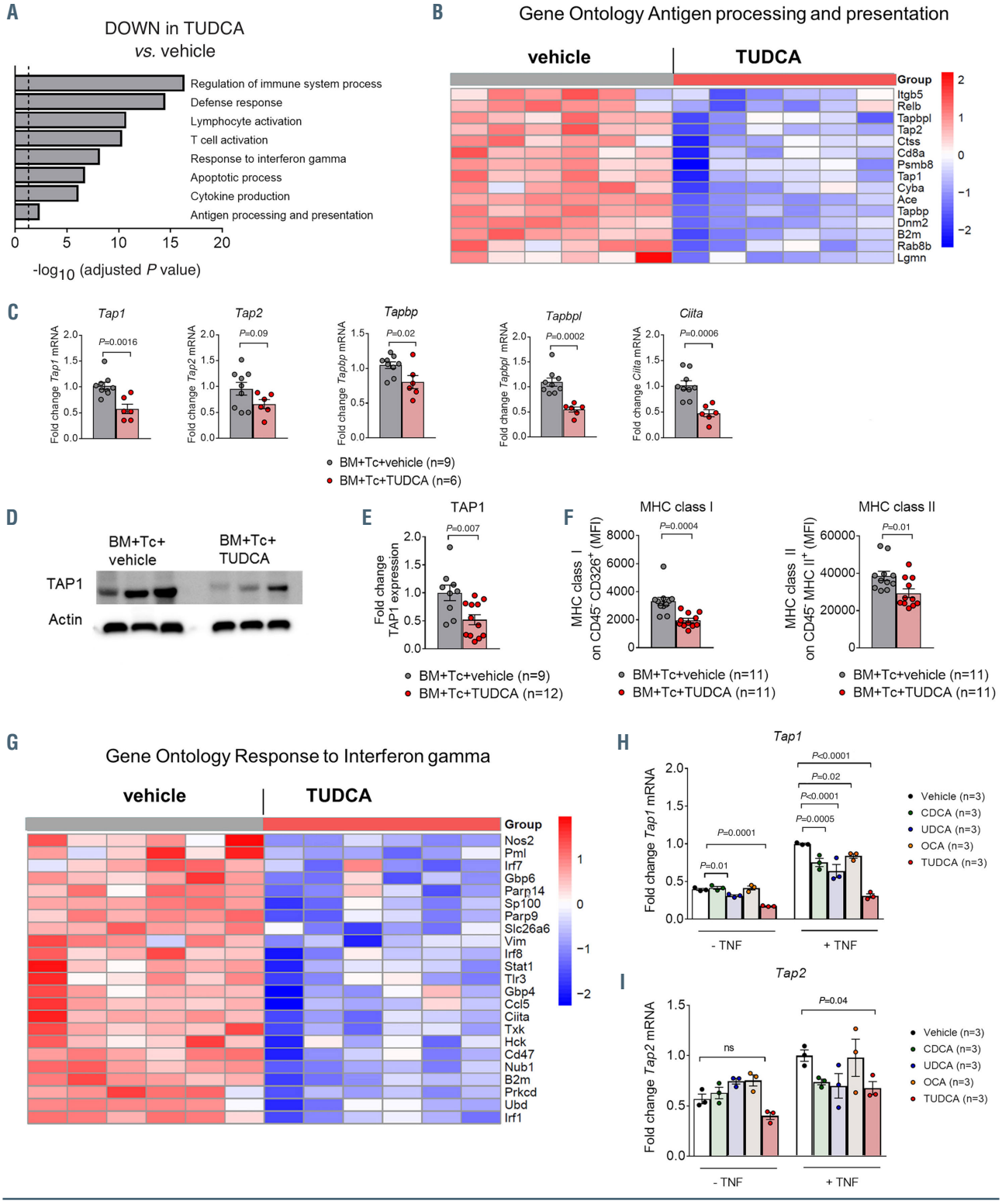

Figure 4. Legend on next page.

Figure 4. Tauroursodeoxycholic acid reduces intestinal antigen presentation. (A to G) Small intestinal samples were isolated from recipient mice treated with vehicle or tauroursodeoxycholic acid (TUDCA), on day 14 after bone marrow transplantation (BMT) (C57BL/6 to BALB/c model). (A) Identification of significantly downregulated Gene Ontology terms in animals treated with TUDCA. The dotted line corresponds to *P*=0.05 (log -0.05=1.29). (B) Heat map based on microarray analysis showing the differentially regulated genes (q-value<0.05) that belong to the term 'antigen processing and presentation' from the Gene Ontology database. Data were pooled from two independent experiments, n=6 mice per group, *P*=0.004. The color code represents the Z-score $\log_2$ intensity. (C) Quantitative real-time polymerase chain reaction (PCR) analysis of the mRNA expression of selected genes with *Actb* as a reference gene. Data were pooled from two independent experiments, numbers (N) represent individual mice. *P*-values were calculated using the unpaired two-tailed Student's *t*-test. (D) Expression of TAP1 protein quantified by western blot. Representative western blot from n=3 mice per group. (E) Quantification of TAP1 protein expression. Data were pooled from two independent experiments, numbers (N) represent individual mice. *P*-values were calculated using the unpaired two-tailed Student's *t*-test. (F) Flow cytometric quantification of major histocompatibility complex (MHC) class I expression on $CD326^+$ ($EpCAM^+$) cells (left panel) and MHC class II expression on $CD45^-$ MHC class II^+ cells (right panel). Data were pooled from two independent experiments, numbers (N) represent individual mice. *P*-values were calculated using the unpaired two-tailed Student's *t*-test. (G) Heat map based on microarray analysis showing the differentially regulated genes (q-value<0.05) that belong to the term 'Response to interferon γ' from the Gene Ontology database. Data were pooled from two independent experiments, n=6 mice per group, $P=6.49 \times 10^{-9}$. The color code represents the Z-score $\log_2$ intensity. (H and I) Quantitative real-time PCR analysis of the mRNA expression of *Tap1* (panel H) and *Tap2* (panel I) with *Actb* as a reference gene in MODE-K cells treated with TNF ± chenodeoxycholic acid (CDCA), ursodeoxycholic acid (UDCA), 6-ethylchenodeoxycholic acid (obeticholic acid, OCA) and TUDCA for 48 hours. Representative data from one of two independent experiments with n=3 replicates/group are presented. *P*-values were calculated using the ordinary one-way ANOVA test with correction for multiple comparisons; ns: not significant.

had shown a role for TUDCA and its chaperone activity for reducing ER stress, a cellular stress response to critical conditions that can potentially lead to apoptosis. We found no changes of ER stress marker expression in the intestine of mice developing aGvHD when treated with TUDCA (*Online Supplementary Figure S6C* and *D*). Altogether, these data demonstrate that TUDCA protects the intestinal tract from apoptosis and particularly preserves ISC and goblet cells from aGvHD-related damage.

Tauroursodeoxycholic acid treatment does not abrogate the graft-*versus*-leukemia activity or hematopoietic regeneration

We next assessed the impact of TUDCA directly on the graft-*versus*-leukemia (GvL) effect. Reduced antigen presentation and human leukocyte antigen (HLA) loss contribute to immune escape of acute myeloid leukemia (AML) cells after allo-HCT.[25] In order to test whether bile acid treatment alters the MHC/TAP antigen presentation in leukemic cells, we treated four human and murine leukemia cell lines with TUDCA. HLA-A, B, C and MHC class I expression were not altered (Figure 7A, B, D and E; *Online Supplementary Figure S7*). Also *Tap1* and *Tap2* gene expression remained unchanged, suggesting that bile acid application does not impair the GvL activity by reducing the expression of MHC/TAP molecules on malignant cells (Figure 7C and F; *Online Supplementary Figure S7*).

We then activated $CD8^+$ T cells by co-incubation with allogeneic dendritic cells and treated them with TUDCA prior to incubation with the A20 lymphoma cell line. T cells were capable of inducing cell death in the leukemic cells which remained stable in the case of TUDCA addition (Figure 7G). We tested *in vivo* T-cell priming by re-isolating T cells from the spleens of vehicle- and TUDCA-treated animals 14 days after BMT (Figure 7H). These *in vivo* activated T cells had a comparable killing capacity when incubated with A20 cells (Figure 7I). Finally, we studied the GvL effect *in vivo* by injecting Ba/F3 cells containing the FLT3-ITD translocation (Ba/F3-ITD) (Figure 7J). Additional transfer of alloreactive T cells reduced the expansion of the malignant cells in the bone marrow and the spleen. This effect persisted in the mice upon TUDCA treatment (Figure 7K). These data indicate that TUDCA affects specifically the intestine and does not impede cytotoxic lymphocyte activity against malignant cells.

Since immune reconstitution is critical for a favorable outcome after allo-HCT, we investigated whether TUDCA might have a negative impact on the peripheral blood cell reconstitution. Mice developing aGvHD treated with TUDCA and vehicle displayed the expected decrease in hemoglobin, hematocrit, platelets and white blood cells (WBC) in comparison to untreated mice (*Online Supplementary Figure S8A*). TUDCA did not enhance cytopenia as treated animals exhibited the same blood counts as vehicle controls. WBC subpopulation analysis by flow cytometry revealed similar proportions of T cells, B cells, granulocytes and monocytes in the peripheral blood (*Online Supplementary Figure S8B*). Analysis of mice with aGvHD at a later time point was not possible due to GvHD-induced mortality in the vehicle group. In order to segregate aGvHD from immune reconstitution, we analyzed animals transplanted only with BM without a GvHD-inducing transfer of T cells. TUDCA treatment did not compromise hematopoietic regeneration (*Online Supplementary Figure S8C* and *D*). These results underline the observation that TUDCA treatment does not prolong the time period necessary for immune reconstitution and suggest that this compound would not impair immune responses to pathogens or the GvL response in allo-HCT patients.

Discussion

Frequency of allo-HCT is rising worldwide since improved conditioning protocols and supportive care allow older patients to undergo this potentially curative leukemia treatment. However, efficient GvHD prophylaxis remains a challenge in the clinical routine with a significant impact on the long-term outcome of allo-HCT.

Here, we observed a depletion of the bile acid pool after allo-HCT. We hypothesized that loss of bile acids might be one of the factors contributing to loss of homeostasis in the intestinal tissue during GvHD (Figure 8). In agreement with recently published data,[6,7] we observed that exposure to pro-inflammatory cytokines caused intestinal tissue damage in an organoid culture model. Treatment with bile acids improved the viability of intestinal organoids and cell lines when cell death was induced by application of TNF or IFNγ. The role of bile acids in the regulation of cell death has been controversially discussed.[26] Depending on their concentration, they can have cytotoxic properties and are able to induce apoptosis either by direct activation of death receptors, for example FAS, or by inducing oxidative damage and mitochondrial dysfunction.[27-29] Other studies indicate that there is a fine balance in bile acid composition in order for their toxic and protective properties to antagonize one another.[30,31] The secondary hydrophilic bile acid UDCA has

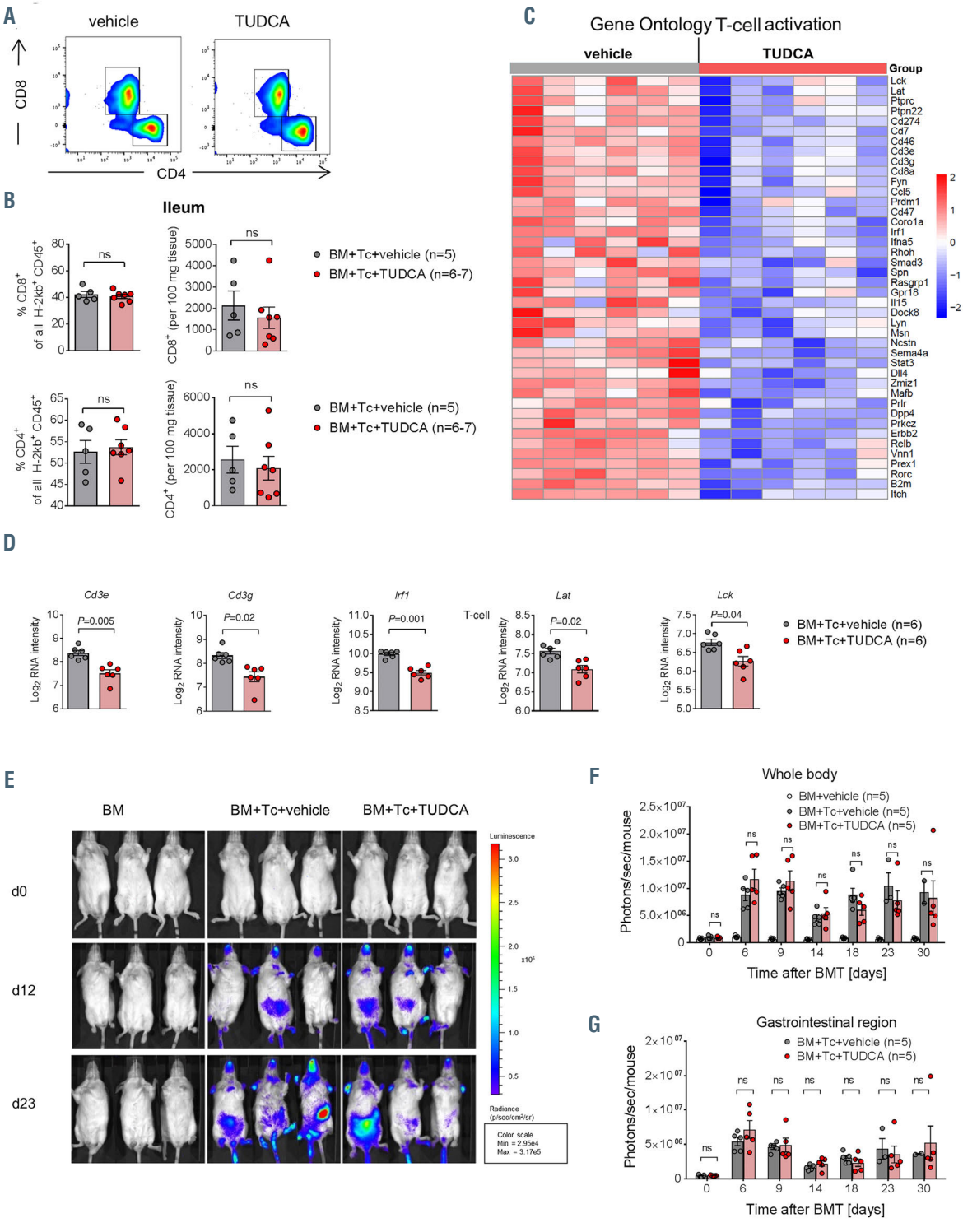

Figure 5. Tauroursodeoxycholic acid administration changes the transcriptional signature of T cells in the intestine but preserves their systemic expansion. (A and B) Flow cytometric analysis of T cells isolated from the small intestinal lamina propria of recipient animals on day 14 after bone marrow transplantation (BMT) (C57BL/6 in BALB/c model). (A) Representative flow cytometry dot plots. (B) Relative (left panel) and absolute (right panel) quantification of $CD8^+$ and $CD4^+$ T cells. Representative data from one of two biologically independent experiments, numbers (N) represent individual mice. *P*-values were calculated using the two-tailed unpaired Student's *t*-test; ns: not significant. (C) Heat map based on microarray analysis (performed as in Figure 4) showing the differentially regulated genes (q-value<0.05) that belong to the term 'T-cell activation' from the Gene Ontology database. Data were pooled from two independent experiments, n=6 mice per group, $P=4.6x10^{-11}$. The color code represents the Z-score log_2 intensity. (D) Log_2 RNA intensity values for selected genes belonging to the GO term "T-cell activation". Data were pooled from two independent experiments, numbers (N) indicate individual mice. An adjusted *P*-value calculated as described in the Methods is presented. (E) BALB/c mice underwent transplantation as described in Figure 3C using luciferase-transgenic T cells. Representative bioluminescence images for T-cell trafficking on different time points after transplantation. (F and G) Quantification of the bioluminescence measurement performed as described in (D). Signal was quantified either from the whole body (F) or from the gastrointestinal region only (G). One of three independent experiments with n=5 mice per group is shown. *P*-values were calculated using the ordinary one-way ANOVA test with correction for multiple comparisons.

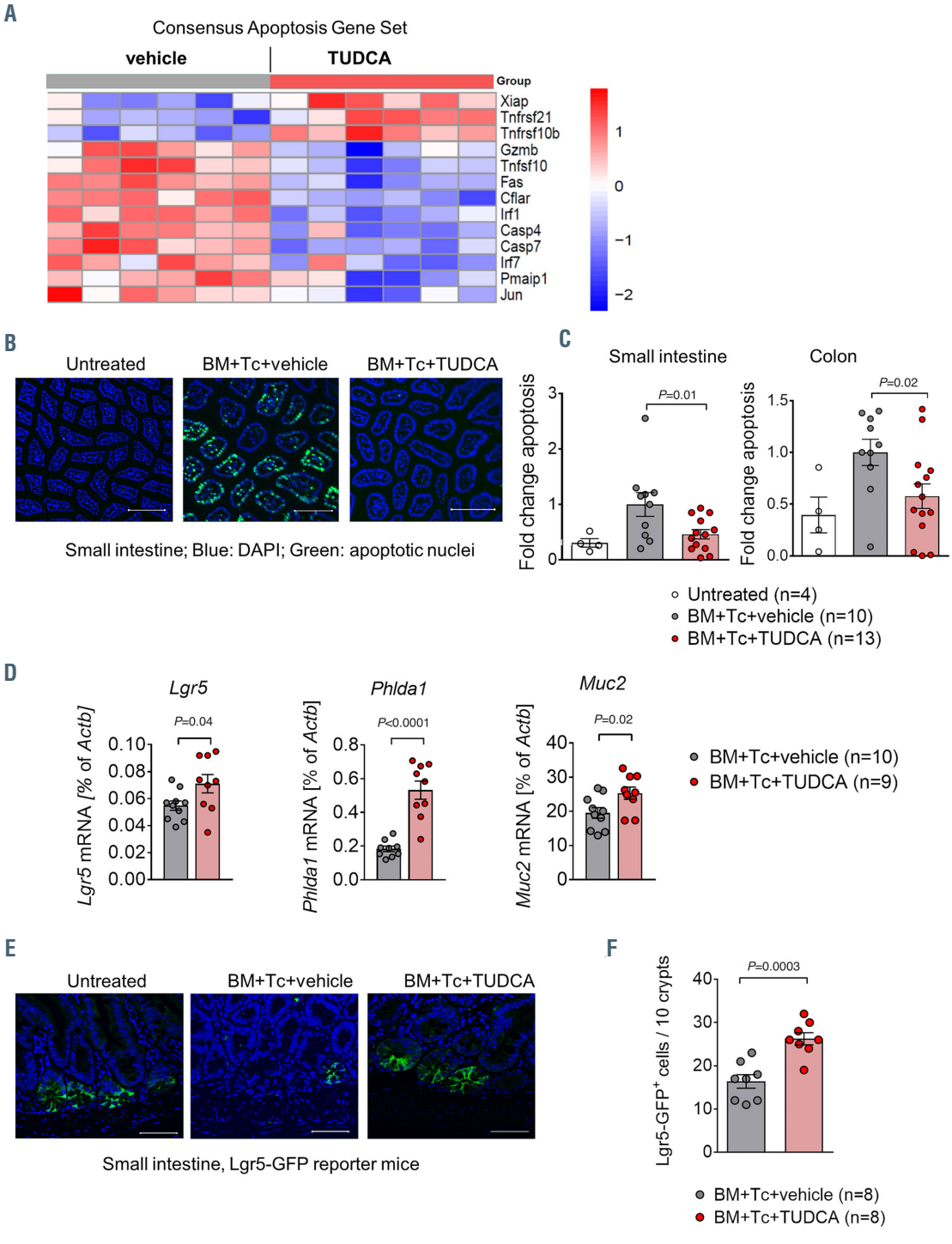

Figure 6. Tauroursodeoxycholic acid decreases intestinal apoptosis. (A to D) Small intestinal samples were isolated from recipient mice which were treated with vehicle or tauroursodeoxycholic acid (TUDCA), on day 14 after bone marrow transplantation (BMT) (C57BL/6 to BALB/c model). (A) Heat map based on microarray analysis showing the differentially regulated genes (q-value<0.05) from the gene set 'apoptosis' from the CONSENSUS database (small intestine, day 14 after BMT). Data were pooled from two independent experiments, n=6 mice per group, *P*=0.001. The color code represents the Z-score $\log_2$ intensity. (B) Representative immunofluorescence images of TUNEL-stained paraffin sections from the small intestine (day 14 after BMT, blue: DAPI, green: apoptotic TUNEL staining). Scale bars 200 μm. (C) Quantification of apoptotic nuclei in the small intestine and the colon was obtained using the Olympus ScanR analysis software (day 14 after BMT). Data were pooled from two independent experiments, numbers (N) indicate individual mice. *P*-values were calculated using the ordinary one-way ANOVA test with correction for multiple comparisons. (D) Quantitative real-time polymerase chain reaction (PCR) analysis of the mRNA expression of the intestinal stem cell markers *Lgr5* and *Phlda1* and the goblet cell marker *Muc2* with *Actb* as a reference gene (small intestine, day 14 after BMT). Data were pooled from two independent experiments, numbers (N) indicate individual mice. *P*-values were calculated using the unpaired two-tailed Student's *t*-test. (E and F) B6.129P2-*Lgr5*$^{tm1(cre/ERT2)Cle/J}$ mice (H-2k^{b}) were transplanted and treated with TUDCA as described in Figure 3A. On day 14 after BMT, the small intestine was analyzed by immunofluorescence for the number of green fluorescent protein positive (GFP^{+}) intestinal stem cells. (E) Representative images obtained using confocal microscopy (blue: DAPI, green: GFP). Scale bars 50 μm. (F) Quantification of data pooled from two independent experiments, N numbers represent individual mice. The *P*-value was calculated using the unpaired two-tailed Student's *t*-test.

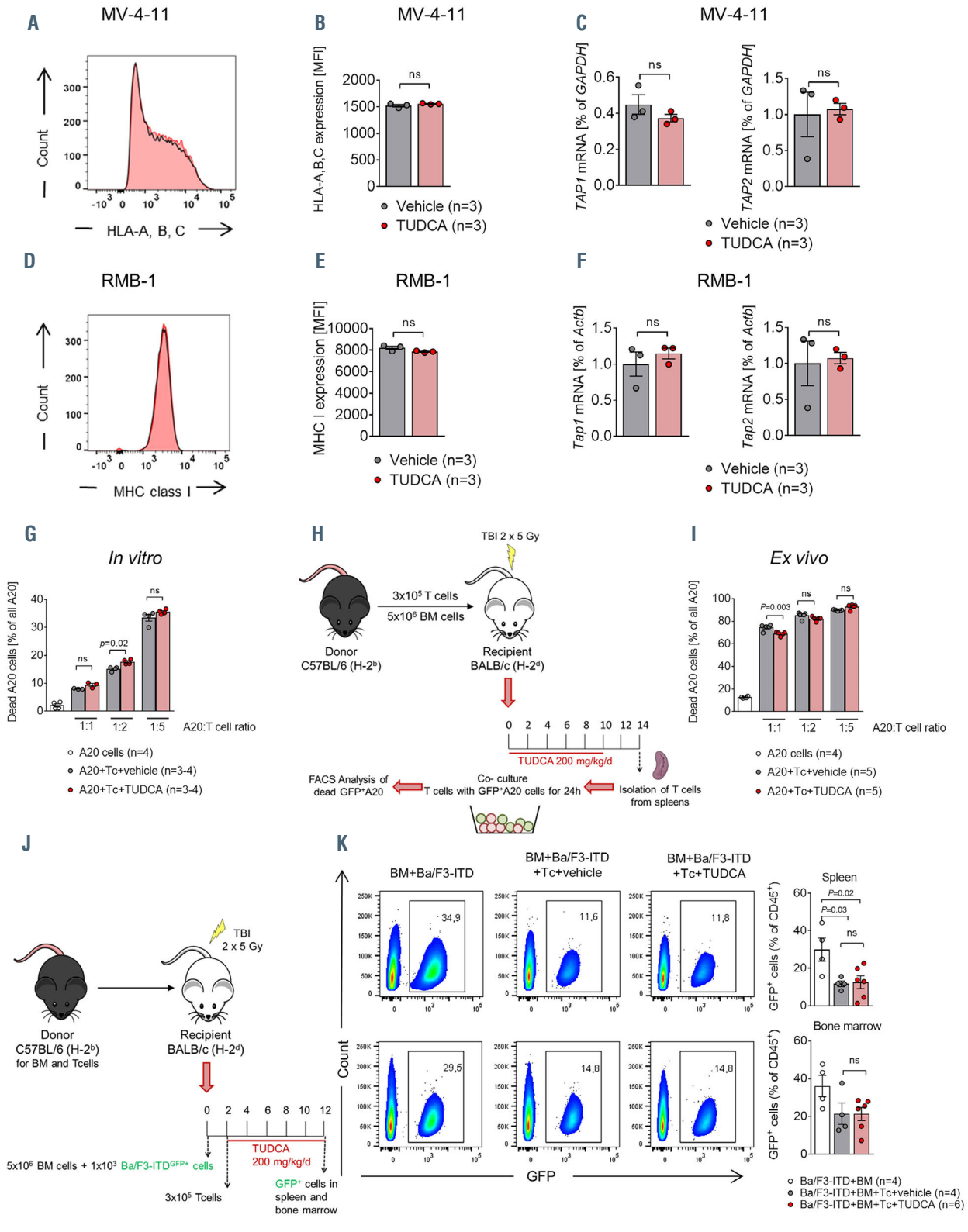

Figure 7. The graft-*versus*-leukemia/lyphoma effect is preserved despite tauroursodeoxycholic acid administration. (A to F) MV-4-11 and RMB-1 cells were cultured for 72 hours (h) with or without addition of tauroursodeoxycholic acid (TUDCA). One representative result from three independent experiments performed in technical triplicates is shown for panel (A) and (D). In panels (B), (C), (E) and (F) data were pooled from three independent experiments performed in technical duplicates or triplicates. *P*-values were calculated using the two-tailed unpaired Student's *t*-test; ns: not significant. (A) Representative histograms from flow cytometric analysis of human leukocyte antigen (HLA) A, B, C expression on MV-4-11 cells. (B) Quantification of HLA A, B and C expression on MV-4-11 cells. (C) Quantitative polymerase chain reaction (PCR) analysis of the expression of the antigen presentation-related genes *TAP1* and *TAP2* in MV-4-11 cells with glyceraldehyde 3-phosphate dehydrogenase (*GAPDH*) as reference gene. (D) Representative histograms from a flow cytometric analysis of major histocompatibility complex (MHC) class I expression on RMB-1 cells. (E) Quantification of MHC class I expression on RMB-1 cells. (F) Quantitative PCR analysis of the expression of the antigen presentation-related genes *Tap1* and *Tap2* in RMB-1 cells with *Actb* as reference gene. (G) C57BL/6 $CD8^+$ T cells were activated with allogeneic (BALB/c) dendritic cells for 72 h and treated with 500 μM TUDCA or vehicle prior to incubation with A20 lymphoma cells. The percentage of dead A20 cells after 24 h of incubation was analyzed by flow cytometry.

Representative data from one of two biologically independent experiments performed with three to four technical replicates respectively. (H) Experimental model for assessing the graft-*versus*-ligand (GvL) response of allogeneic T cells *ex vivo*. BALB/c mice underwent bone marrow transplantation (BMT) as described in Figure 3C and T cells from spleens were isolated for subsequent co-culture with A20 cells on day 14 after BMT. (I) Flow cytometric quantification of dead A20 lymphoma cells co-cultured with $CD4^+$ and $CD8^+$ T cells re-isolated from the spleens of recipient mice on day 14 after BMT as described in (H). Representative data from one of two biologically independent experiments performed with four to five technical replicates respectively. *P*-values were calculated using the ordinary one-way ANOVA test with correction for multiple comparisons, ns: not significant. (J) Experimental model for assessing the GvL response *in vivo*. BALB/c mice underwent BMT with additional injection of green fluorescent protein positive (GFP^+) Ba/F3-ITD leukemia cells. Allogeneic T cells were transferred two days later and animals were treated with 200 mg/kg body weight TUDCA or vehicle for another 10 days. (K) Flow cytometric analysis of spleen and bone marrow for the percentage of GFP^+ cells on day 12 after tumor injection. N numbers represent individual mice. Left panel: representative flow cytometry plots. Right panel: quantification, numbers (N) represent individual mice. *P*-values were calculated using the ordinary one-way ANOVA test with correction for multiple comparisons, ns: not significant.

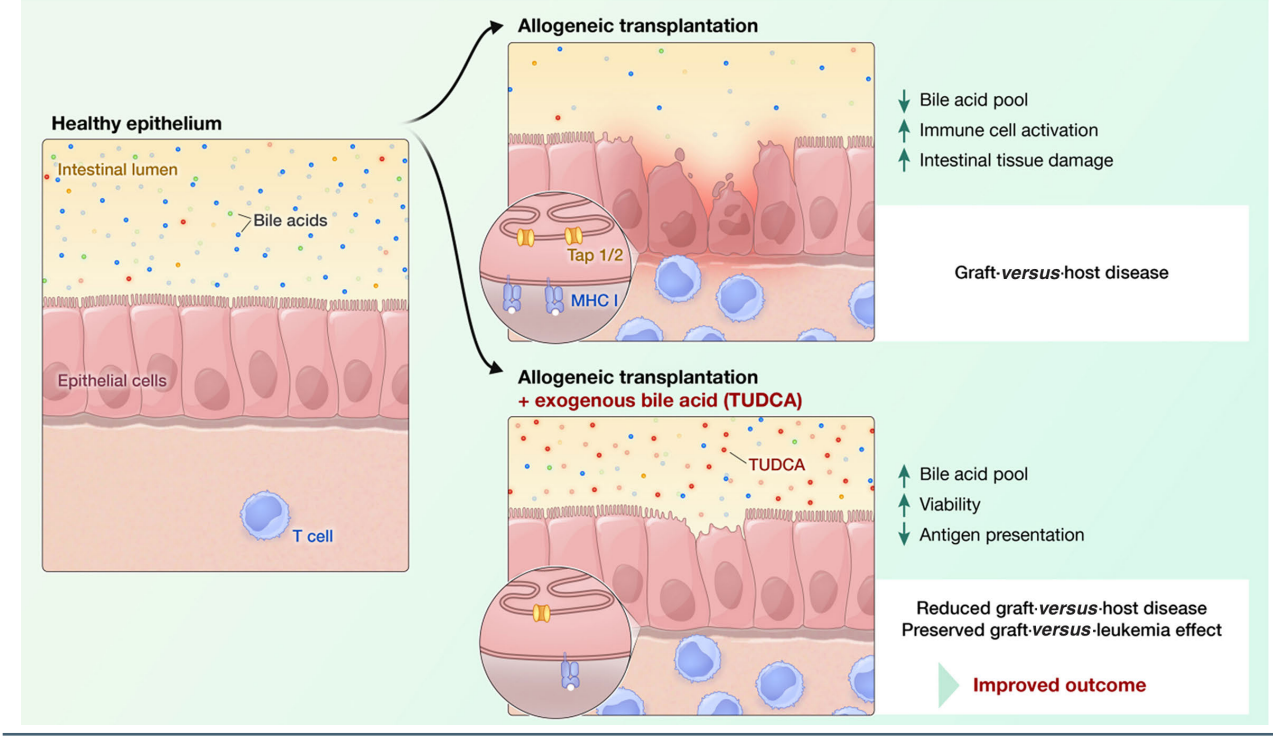

Figure 8. Tauroursodeoxycholic acid leads to a reduction of acute graft-*versus*-host disease. A model, in which this positive effect is achieved by two distinct mechanisms: enhancing the viability during exposure to pro-inflammatory cytokines and reduction of antigen presentation in the intestine with a consequent decrease in apoptosis.

cytoprotective functions. UDCA is approved for the treatment of patients with cholestatic liver diseases based on inhibition of hepatocyte apoptosis and protection from toxic hydrophobic bile acids.[26,32] These effects are linked to a stabilization of the mitochondria, reduced BAX translocation and decreased cytochrome C release and subsequent apoptosis.[32,33] Furthermore, the administration of TUDCA led to the inhibition of cellular damage introduced by the bile acid glycochenodeoxycholic acid (GCDCA) by preventing GCDCA-induced caspase-9 activation and subsequent mitochondrial damage. Therefore, such bile acids can enable survival via protection against more hydrophobic and potentially more toxic bile acid variants.[34,35] Also a protection of hepatocytes from carcinogen-induced apoptosis[36] and of renal tubular cells against contrast media-induced apoptosis[37] has been described.

Translating these data into a preclinical BMT model, we observed that application of the bile acid TUDCA, the most potent agent in our *in vitro* studies, prolonged the survival of mice with aGvHD. Exogenous bile acid application was able to substantially modulate the bile acid pool. TUDCA increased to 35% of all measured bile acids in the serum and almost 60% of the bile acids measured in the ileal content. These data suggest that exogenous application is effective in changing the bile acid pool and therefore probably counteracts the depletion of bile acids observed upon GvHD induction. The prophylactic use of UDCA has been previously proposed in a study which demonstrated a reduction in aGvHD incidence as well as non-relapse mortality with a benefit in overall survival.[38] However, other studies failed to confirm this.[39,40] Overall, a meta-analysis including four prospective trials and two historical analyses of prophylactic UDCA use in allo-HCT recipients showed a reduction in the levels of hepatic veno-occlusive disease and transplant-related mortality, with no statistically significant difference in the incidence of acute hepatic GvHD or overall survival.[41] The impact on intestinal aGvHD incidence was not evaluated. Our observations prompted us to search for a mechanism by which bile acids and TUDCA in particular might protect the intestinal epithelium from an alloimmunity-mediated damage. Administration of TUDCA led to reduced expression of antigen presentation-related genes and to reduced expression of MHC class I and II on subpopulations of non-hematopoietic cells in the intestine. It has recently been shown that MHC class II-expressing intestinal epithelial cells are able to present anti-

gen and activate T cells in the context of GvHD.[42] Little is known about the connection of bile acids and their effect on antigen-presentation, especially in non-hematopoietic cells. In a model of *Schistosoma mansoni* infection, 24-nor-UDCA but not UDCA itself reduced surface MHC class II expression on macrophages and dendritic cells and the activation as well as proliferation of T lymphocytes *in vitro*.[43] Microbial diversity is a key factor in regulating the homeostasis of the intestine. GvHD has been previously linked to alterations in the microbiome with loss of bacterial diversity. In order to prove that TUDCA regulates aGvHD severity by acting directly on the intestinal epithelium and not by changing the microbiome,[44] we analyzed fecal samples of TUDCA-treated animals developing aGvHD. Diversity and abundancy analyses showed comparable results between vehicle- and TUDCA-treated mice underlining the hypothesis that TUDCA protects the intestinal epithelium in a cell-specific manner.

Current GvHD prophylaxis and treatment mostly rely on suppression of T-cell activation and cytokine release which on the downside increases the risk of malignancy relapse. While TUDCA treatment resulted in a decreased expression of genes related to T-cell activation in the intestine, it did not impair systemic T-cell proliferation or the activity against tumor cells. This difference might be explained by the fact that bile acid levels are much more abundant in the intestine than in the systemic blood circulation (0.5 μg/mL in the serum *vs.* 1,000 μg/100 mg ileal content). Furthermore, the expression of antigen presentation-related proteins on leukemic cells was not reduced showing that the recognition of malignant cells by the immune system remains intact upon bile acid administration. In line with this concept, we showed preserved GvL activity in *in vitro*, *ex vivo* and *in vivo* models.

One potential explanation for the divergent effects of bile acids on intestinal and leukemic cells is the differential expression of bile acid receptors and their affinities to different species of bile acids. Intestinal epithelial cells are equipped with various bile acid receptors, FXR and TGR5 amongst others.[45] We show that mRNA expression of both receptors changes upon GvHD induction with an increase of FXR and decrease of TGR5. One could speculate that these alterations in receptor expression make bile acid signaling a potential target for regulating intestinal homeostasis. Both bile acid receptors are able to bind bile acids with a high affinity and subsequently induce different signaling pathways including inflammation and apoptosis signaling. Other receptors of bile acids are more likely to be acknowledged as bile acid "sensors" which rather chemically convert bile acids and can act on bile acid transporters.[46] FXR activation in the intestine has several anti-inflammatory properties. OCA, as a strong semi-synthetic FXR agonist, was shown to ameliorate intestinal mucosal inflammation in several mouse colitis models via induction of antimicrobial peptide production and reinforcement of epithelial barrier function in intestinal epithelial cells.[47] Since OCA and CDCA, the bile acids with the highest affinity to FXR, showed only minor protective effects compared to TUDCA on intestinal epithelium in our experiments, we hypothesize that there must be other underlying mechanisms than the engagement of FXR signaling. One other candidate is the high affinity receptor TGR5 which also induces anti-inflammatory responses similar to FXR[48] but has the highest affinity to secondary bile acids such as UDCA and its taurine conjugate TUDCA and is expressed in the liver and intestine.[49,50]

Amongst our tested bile acids, TUDCA was the one with the strongest anti-apoptotic effects both *in vitro* as and *in vivo*. Active re-absorption of bile acids occurs in the terminal ileum and is dependent on their conjugation status. During this process, bile acids come in contact and modulate the mucosal immune system.[19,20] Our results indicate that for GvHD prevention, bile acids have to be conjugated in order to fulfill their cytoprotective properties.

In summary, we show that allo-HCT induces a depletion of the bile acid pool. Exogenous application of bile acids and in particular TUDCA reduces aGvHD. We propose a model, in which this positive effect is achieved by two distinct mechanisms: enhancing the viability during exposure to pro-inflammatory cytokines and reduction of antigen presentation in the intestine with a consequent decrease in apoptosis (Figure 8). A major advantage of TUDCA is that it is already approved by the Food and Drug Administration and that it possesses a good safety profile. These findings pave the way for a prospective clinical trial using TUDCA to improve the outcome of allo-HCT recipients by preventing aGvHD and preserving the GvL effect.

Disclosures

ELP is the founder of Rheos Medicines and is a SAB member of Immunomet.

Contributions

EH and FMU helped to develop the concept, performed experiments, analyzed data and helped to write the manuscript; GA analyzed microarray data; MP and AB performed the microbiome experiments and analysis; BS performed experiments and analyzed data; LMB and EVG performed research; PRE and SFM helped to develop the overall concept and to write the manuscript; DP performed and analyzed microarray experiments; MF helped with microscopy experiments, imaging and data analysis; ASG performed histopathological analysis; JB and ELP performed metabolomics experiments and helped with data analysis; JD and BG helped to design the study and analyze the data; MB analyzed microarray data and helped to write the manuscript; RZ and PA designed the study, planned the experiments and analyzed data; PA also performed experiments and wrote the manuscript.

Acknowledgments

The authors would like to acknowledge Dr. D. Kaiserlian (INSERM, France) who kindly provided the MODE-K cells. The authors would further like to acknowledge Michal Rössler for designing the graphical abstract.

Funding

This study was supported by the Else Kröner-Fresenius-Stiftung (EKFS 2015_A147 to PA), the INTERREG V European regional development fund (European Union) program (project 3.2 TRIDI-AG to RZ), Wilhelm Sander Stiftung (grant 2008.046.5 to RZ), Deutsche Forschungsgemeinschaft, Germany, SFB1160 (RZ) and SFB850 (MB), ERC Consolidator grant (681012 GvHDCure European Union, to RZ and by the Excellence Strategy of the German Federal and State Governments (CIBSS - EXC 2189). PA is supported by a scholarship from the Berta Ottenstein Program for Physician Scientists, Faculty of Medicine, Medical Center – University of Freiburg, Germany. MB is supported by the German Federal Ministry of Education and Research (BMBF) within the framework of the e:Med research and funding concept

(CoNfirm, FKZ 01ZX1708F) and within the Medical Informatics Funding Scheme (MIRACUM, FKZ 01ZZ1606A-H). BG receives support through the Deutsche Forschungsgemeinschaft (DFG) SFB1160/2_B5, under Germany's Excellence Strategy (CIBSS – EXC-2189 – Project ID 390939984, and RESIST – EXC 2155 – Project ID 39087428); through the E-rare program of the EU, managed by the DFG, grant code GR1617/14-1/iPAD; and through the „Netzwerke Seltener Erkrankungen" of the German Ministry of Education and Research (BMBF), grant code: GAIN_01GM1910A.

References

1. de Lima M, Porter DL, Battiwalla M, et al. Proceedings from the National Cancer Institute's Second International Workshop on the biology, prevention, and treatment of relapse after hematopoietic stem cell transplantation: part III. Prevention and treatment of relapse after allogeneic transplantation. Biol Blood Marrow Transplant. 2014;20(1):4-13.
2. Zeiser R, Blazar BR. Acute Graft-versus-Host Disease - Biologic Process, Prevention, and Therapy. N Engl J Med. 2017; 377(22):2167-2179.
3. McDonald GB. How I treat acute graft-versus-host disease of the gastrointestinal tract and the liver. Blood. 2016;127(12):1544-1550.
4. Takashima S, Kadowaki M, Aoyama K, et al. The Wnt agonist R-spondin1 regulates systemic graft-versus-host disease by protecting intestinal stem cells. J Exp Med. 2011;208(2):285-294.
5. Eriguchi Y, Takashima S, Oka H, et al. Graft-versus-host disease disrupts intestinal microbial ecology by inhibiting Paneth cell production of alpha-defensins. Blood. 2012;120(1):223-231.
6. Eriguchi Y, Nakamura K, Yokoi Y, et al. Essential role of IFN-gamma in T cell-associated intestinal inflammation. JCI Insight. 2018;3(18):e121886.
7. Takashima S, Martin ML, Jansen SA, et al. T cell-derived interferon-gamma programs stem cell death in immune-mediated intestinal damage. Sci Immunol. 2019;4 (42):eaay8556.
8. Monte MJ, Marin JJ, Antelo A, Vazquez-Tato J. Bile acids: chemistry, physiology, and pathophysiology. World J Gastroenterol. 2009;15(7):804-816.
9. Russell DW. The enzymes, regulation, and genetics of bile acid synthesis. Annu Rev Biochem. 2003;72:137-174.
10. Benz C, Angermuller S, Tox U, et al. Effect of tauroursodeoxycholic acid on bile-acid-induced apoptosis and cytolysis in rat hepatocytes. J Hepatol. 1998;28(1):99-106.
11. Sola S, Aranha MM, Steer CJ, Rodrigues CM. Game and players: mitochondrial apoptosis and the therapeutic potential of ursodeoxycholic acid. Curr Issues Mol Biol. 2007;9(2):123-138.
12. Colell A, Coll O, Garcia-Ruiz C, et al. Tauroursodeoxycholic acid protects hepatocytes from ethanol-fed rats against tumor necrosis factor-induced cell death by replenishing mitochondrial glutathione. Hepatology. 2001;34(5):964-971.
13. Castro RE, Sola S, Ramalho RM, Steer CJ, Rodrigues CM. The bile acid tauroursodeoxycholic acid modulates phosphorylation and translocation of bad via phosphatidylinositol 3-kinase in glutamate-induced apoptosis of rat cortical neurons. J Pharmacol Exp Ther. 2004;311(2):845-852.
14. Ishigami F, Naka S, Takeshita K, Kurumi Y, Hanasawa K, Tani T. Bile salt tauroursodeoxycholic acid modulation of Bax translocation to mitochondria protects the liver from warm ischemia-reperfusion injury in the rat. Transplantation. 2001;72 (11):1803-1807.
15. Vavassori P, Mencarelli A, Renga B, Distrutti E, Fiorucci S. The bile acid receptor FXR is a modulator of intestinal innate immunity. J Immunol. 2009;183(10):6251-6261.
16. Joshi NM, Hassan S, Jasani P, et al. Bile acid malabsorption in patients with graft-versus-host disease of the gastrointestinal tract. Br J Haematol. 2012;157(3):403-407.
17. Michonneau D, Latis E, Curis E, et al. Metabolomics analysis of human acute graft-versus-host disease reveals changes in host and microbiota-derived metabolites. Nat Commun. 2019;10(1):5695.
18. Sato T, Clevers H. Primary mouse small intestinal epithelial cell cultures. Methods Mol Biol. 2013;945:319-328.
19. Ridlon JM, Kang DJ, Hylemon PB. Bile salt biotransformations by human intestinal bacteria. J Lipid Res. 2006;47(2):241-259.
20. Camilleri M. Bile Acid diarrhea: prevalence, pathogenesis, and therapy. Gut Liver. 2015;9(3):332-339.
21. Swann JR, Want EJ, Geier FM, et al. Systemic gut microbial modulation of bile acid metabolism in host tissue compartments. Proc Natl Acad Sci U S A. 2011;108 Suppl 1:4523-4530.
22. Jenq RR, Ubeda C, Taur Y, et al. Regulation of intestinal inflammation by microbiota following allogeneic bone marrow transplantation. J Exp Med. 2012;209(5):903-911.
23. Holler E, Butzhammer P, Schmid K, et al. Metagenomic analysis of the stool microbiome in patients receiving allogeneic stem cell transplantation: loss of diversity is associated with use of systemic antibiotics and more pronounced in gastrointestinal graft-versus-host disease. Biol Blood Marrow Transplantat. 2014;20(5):640-645.
24. Staffas A, Burgos da Silva M, van den Brink MR. The intestinal microbiota in allogeneic hematopoietic cell transplant and graft-versus-host disease. Blood. 2017;129(8):927-933.
25. Zeiser R, Vago L. Mechanisms of immune escape after allogeneic hematopoietic cell transplantation. Blood. 2019;133(12):1290-1297.
26. Amaral JD, Viana RJ, Ramalho RM, Steer CJ, Rodrigues CM. Bile acids: regulation of apoptosis by ursodeoxycholic acid. J Lipid Res. 2009;50(9):1721-1734.
27. Rodrigues CM, Fan G, Wong PY, Kren BT, Steer CJ. Ursodeoxycholic acid may inhibit deoxycholic acid-induced apoptosis by modulating mitochondrial transmembrane potential and reactive oxygen species production. Mol Med. 1998;4(3):165-178.
28. Faubion WA, Guicciardi ME, Miyoshi H, et al. Toxic bile salts induce rodent hepatocyte apoptosis via direct activation of Fas. J Clin Invest. 1999;103(1):137-145.
29. Yerushalmi B, Dahl R, Devereaux MW, Gumpricht E, Sokol RJ. Bile acid-induced rat hepatocyte apoptosis is inhibited by antioxidants and blockers of the mitochondrial permeability transition. Hepatology. 2001;33(3):616-626.
30. Rust C, Karnitz LM, Paya CV, Moscat J, Simari RD, Gores GJ. The bile acid taurochenodeoxycholate activates a phosphatidylinositol 3-kinase-dependent survival signaling cascade. J Biol Chem. 2000; 275(26):20210-20216.
31. Torchia EC, Stolz A, Agellon LB. Differential modulation of cellular death and survival pathways by conjugated bile acids. BMC Biochem. 2001;2:11.
32. Rodrigues CM, Fan G, Ma X, Kren BT, Steer CJ. A novel role for ursodeoxycholic acid in inhibiting apoptosis by modulating mitochondrial membrane perturbation. J Clin Invest. 1998;101(12):2790-2799.
33. Rodrigues CM, Ma X, Linehan-Stieers C, Fan G, Kren BT, Steer CJ. Ursodeoxycholic acid prevents cytochrome c release in apoptosis by inhibiting mitochondrial membrane depolarization and channel formation. Cell Death Differ. 1999;6(9):842-854.
34. Schoemaker MH, Conde de la Rosa L, Buist-Homan M, et al. Tauroursodeoxycholic acid protects rat hepatocytes from bile acid-induced apoptosis via activation of survival pathways. Hepatology. 2004;39(6):1563-1573.
35. Im E, Martinez JD. Ursodeoxycholic acid (UDCA) can inhibit deoxycholic acid (DCA)-induced apoptosis via modulation of EGFR/Raf-1/ERK signaling in human colon cancer cells. J Nutr. 2004;134(2):483-486.
36. Vandewynckel YP, Laukens D, Devisscher L, et al. Tauroursodeoxycholic acid dampens oncogenic apoptosis induced by endoplasmic reticulum stress during hepatocarcinogen exposure. Oncotarget. 2015; 6(29):28011-28025.
37. Peng P, Ma Q, Wang L, et al. Preconditioning with tauroursodeoxycholic acid protects against contrast-induced HK-2 cell apoptosis by inhibiting endoplasmic reticulum stress. Angiology. 2015; 66(10): 941-949.
38. Ruutu T, Juvonen E, Remberger M, et al. Improved survival with ursodeoxycholic acid prophylaxis in allogeneic stem cell transplantation: long-term follow-up of a randomized study. Biol Blood Marrow Transplant. 2014;20(1):135-138.
39. Essell JH, Thompson JM, Harman GS, et al. Pilot trial of prophylactic ursodiol to decrease the incidence of veno-occlusive disease of the liver in allogeneic bone marrow transplant patients. Bone Marrow Transplant. 1992;10(4):367-372.
40. Thornley I, Lehmann LE, Sung L, et al. A multiagent strategy to decrease regimen-related toxicity in children undergoing allogeneic hematopoietic stem cell transplantation. Biol Blood Marrow Transplant. 2004; 10(9):635-644.
41. Tay J, Tinmouth A, Fergusson D, Huebsch L, Allan DS. Systematic review of controlled clinical trials on the use of ursodeoxycholic acid for the prevention of hepatic veno-occlusive disease in hematopoietic stem cell transplantation. Biol Blood Marrow Transplant. 2007; 13(2):206-217.
42. Koyama M, Mukhopadhyay P, Schuster IS,

et al. MHC class II antigen presentation by the intestinal epithelium initiates graft-versus-host disease and is influenced by the microbiota. Immunity. 2019;51(5):885-898 e887.
43. Sombetzki M, Fuchs CD, Fickert P, et al. 24-nor-ursodeoxycholic acid ameliorates inflammatory response and liver fibrosis in a murine model of hepatic schistosomiasis. J Hepatol. 2015;62(4):871-878.
44. Ridlon JM, Kang DJ, Hylemon PB, Bajaj JS. Bile acids and the gut microbiome. Curr Opin Gastroenterol. 2014;30(3):332-338.
45. Distrutti E, Santucci L, Cipriani S, et al. Bile acid activated receptors are targets for regulation of integrity of gastrointestinal mucosa. J Gastroenterol. 2015;50(7):707-719.
46. Han S, Li T, Ellis E, Strom S, Chiang JY. A novel bile acid-activated vitamin D receptor signaling in human hepatocytes. Mol Endocrinol. 2010;24(6):1151-1164.
47. Gadaleta RM, van Erpecum KJ, Oldenburg B, et al. Farnesoid X receptor activation inhibits inflammation and preserves the intestinal barrier in inflammatory bowel disease. Gut. 2011;60(4):463-472.
48. Biagioli M, Carino A, Cipriani S, et al. The bile acid receptor GPBAR1 regulates the M1/M2 phenotype of intestinal macrophages and activation of GPBAR1 rescues mice from murine colitis. J Immunol. 2017;199(2):718-733.
49. Maruyama T, Miyamoto Y, Nakamura T, et al. Identification of membrane-type receptor for bile acids (M-BAR). Biochem Biophys Res Commun. 2002;298(5):714-719.
50. Duboc H, Tache Y, Hofmann AF. The bile acid TGR5 membrane receptor: from basic research to clinical application. Dig Liver Dis. 2014;46(4):302-312.

ARTICLE

Endothelial damage and dysfunction in acute graft-*versus*-host disease

Steffen Cordes,[1] Zeinab Mokhtari,[2] Maria Bartosova,[3] Sarah Mertlitz,[1] Katarina Riesner,[1] Yu Shi,[1] Jörg Mengwasser,[1,4] Martina Kalupa,[1] Aleixandria McGeary,[1] Johanna Schleifenbaum,[5,6] Jens Schrezenmeier,[1] Lars Bullinger,[1] Maribel Diaz-Ricart,[7] Marta Palomo,[7,8] Enric Carreras,[8] Gernot Beutel,[9] Claus Peter Schmitt,[3] Andreas Beilhack[2] and Olaf Penack[1]

[1]Department of Hematology, Oncology and Tumor Immunology, Charité Universitätsmedizin Berlin, Campus Virchow Clinic, Berlin, Germany; [2]Department of Medicine II, Würzburg University Hospital, Interdisciplinary Center for Clinical Research (IZKF), Laboratory for Experimental Stem Cell Transplantation, Würzburg, Germany; [3]Pediatric Nephrology, Center for Pediatric and Adolescent Medicine, University Hospital Heidelberg, Heidelberg, Germany; [4]Department of Surgery, Charité Universitätsmedizin Berlin, Campus Charité Mitte/Campus Virchow Clinic, Berlin, Germany; [5]Experimental and Clinical Research Center (ECRC) - a joint cooperation between the Charité Medical Faculty and the Max Delbrück Center for Molecular Medicine (MDC), Berlin, Germany; [6]Charité Universitätsmedizin Berlin, Institute of Vegetative Physiology, Berlin, Germany; [7]Department of Hematopathology, Hospital Clinic of Barcelona, Biomedical Diagnosis Centre (CDB), Institute of Biomedical Research August Pi i Sunyer (IDIBAPS), University of Barcelona, Barcelona, Spain; [8]Josep Carreras Leukemia Research Institute, Hospital Clinic/University of Barcelona Campus, Barcelona, Spain and [9]Department of Hematology, Hemostasis, Oncology and Stem Cell Transplantation, Hannover Medical School, Hannover, Germany

Ferrata Storti Foundation

Haematologica 2021
Volume 106(8):2147-2160

ABSTRACT

Clinical studies have suggested a potential involvement of endothelial dysfunction and damage in the development and severity of acute graft-*versus*-host disease (aGvHD). Accordingly, we found an increased percentage of apoptotic caspase 3 positive blood vessels in duodenal and colonic mucosa biopsies of patients with severe aGvHD. In murine experimental aGvHD, we detected severe microstructural endothelial damage and reduced endothelial pericyte coverage accompanied by reduced expression of endothelial tight junction proteins leading to increased endothelial leakage in aGvHD target organs. During intestinal aGvHD, colonic vasculature structurally changed, reflected by increased vessel branching and vessel diameter. As recent data demonstrated an association of endothelium-related factors and steroid refractory aGvHD (SR-aGvHD), we analyzed human biopsies and murine tissues from SR-aGvHD. We found extensive tissue damage but low levels of alloreactive T-cell infiltration in target organs, providing the rationale for T-cell independent SR-aGvHD treatment strategies. Consequently, we tested the endothelium-protective PDE5 inhibitor sildenafil, which reduced apoptosis and improved metabolic activity of endothelial cells *in vitro*. Accordingly, sildenafil treatment improved survival and reduced target organ damage during experimental SR-aGvHD. Our results demonstrate extensive damage, structural changes, and dysfunction of the vasculature during aGvHD. Therapeutic intervention by endothelium-protecting agents is an attractive approach for SR-aGvHD complementing current anti-inflammatory treatment options.

Introduction

Allogeneic hematopoietic stem cell transplantation (allo-HSCT) is the only curative treatment option for many patients suffering from hematological malignancies. A major complication of allo-HSCT is acute graft-*versus*-host disease (aGvHD), an inflammatory condition primarily affecting the skin, liver, and intestines. aGvHD occurs in more than two thirds of patients undergoing allo-HSCT.[1]

Correspondence:

OLAF PENACK
olaf.penack@charite.de

Received: March 27, 2020.

Accepted: July 13, 2020.

Pre-published: July 16, 2020.

https://doi.org/10.3324/haematol.2020.253716

Steroid treatment is successful in most of these patients (75%-80%). However, the 20%-25% of patients who fail initial treatment with steroids (steroid-refractory aGvHD [SR-aGvHD]) have very high mortality.[2,3] No standard treatment for SR-aGvHD is currently available, and its pathobiology is poorly understood, thereby hindering the development of novel therapeutic approaches.

The endothelium is the first contact for immunological effector cells in the blood and a key regulator in various inflammatory processes. In early complications after allo-HSCT such as transplantation-associated-microangiopathy,[4] veno-occlusive disease,[5] capillary leak syndrome[6] and diffuse alveolar hemorrhage[7] the endothelium was shown to be relevant. Recent studies also suggest a critical role of the endothelium in aGvHD. Angiogenesis appears to be a very early event during aGvHD, occurring before immune cell infiltration in target organs.[8] During later phases of aGvHD, endothelial apoptosis has been described in cutaneous aGvHD.[9,10] Clinical studies demonstrated that soluble markers of endothelial damage such as von Willebrand factor,[11] thrombomodulin,[12-14] micro particles released by endothelial cells (EC)[15] as well as the CD40/CD40 ligand axis,[16] can be used as biomarkers during aGvHD. Furthermore, factors of endothelial damage were correlated with the mortality rate of patients suffering from SR-aGvHD.[12,13,17] In addition to endothelial pathology in the microvasculature, arterial vessels were described to suffer from endothelial damage during aGvHD with consequences for their physiological properties.[18]

The characterization of endothelial function during aGvHD and SR-aGvHD is still incomplete and effective pharmacologic strategies aiming at the normalization of endothelial dysfunction to ameliorate aGvHD and SR-aGvHD are lacking.

Methods

Patient material and histology of human biopsies

Collection of human samples was approved by the institutional ethics committees of Charité Berlin and Medical University Hannover and was in accordance with the Declaration of Helsinki. From the Charité cohort, we included intestinal biopsies with aGvHD *versus* no aGvHD after allo-HSCT performed between 2007 and 2015. We identified 12 duodenal and 11 colon biopsies from patients with aGvHD grade III-IV. As a control, we used 19 duodenal and ten colon biopsies from allo-HSCT recipients without histological evidence of aGvHD.[19] From the Hannover cohort colon biopsies from 11 patients with aGvHD were included. From each patient, biopsies were taken at two time points: at diagnosis of aGvHD and later at diagnosis of SR-aGvHD. Detailed clinical data from both cohorts are given in the *Online Supplementary Tables S1, S2, S4* and *S6*.

Mice and acute graft-*versus*-host disease experiments

aGVHD models were used as described previously.[8,20,21] Control groups (no aGvHD) were transplanted with the same bone marrow (BM) cell numbers and T-cell numbers from syngeneic donors. In order to mimic SR-aGvHD, we used the chemotherapy based murine models 129→B6 major histocompatibility complex (MHC)-matched and B6→B6D2F1 (haploidentical) and the radiation based murine model BALB/c→B6 MHC-mismatch with conditioning and cell dosages analogue to the models described above. Recipient mice were treated intraperitoneal with 0.5 mg/kg/day dexamethasone beginning at day+4 after HSCT (Merck, Darmstadt, Germany).[22,23] We used dexamethasone because of its longer lasting effects compared to methyl-prednisolone or prednisolone enabling once daily dosing in the murine models. The rationale for starting at day+4 is that during this time leukocytes start to infiltrate target organs during aGvHD.[8,21,24] Clinical scores, weight loss and survival in the B6-BDF SR-aGVHD model are given in the *Online Supplementary Figure S1*.

Histology of murine tissues

Tissue samples were cryoembedded and scored as previously described.[19]

Evans blue assay

For assessment of endothelial leakage, Evans blue assay was performed as described in detail elsewhere.[25]

Immunolabeling against VE-cadherin for light sheet fluorescence microscopy

25 μg/mouse anti-VE-cadherin antibody (Thermo Scientific, eBioBV13-eFluor660) was intravenously (i.v.) injected in mice from B6→BDF aGvHD model. Mice were sacrificed and perfused with phosphate buffered saline (PBS) followed by 4% paraformaldehyde in PBS. Sample preparation and imaging of whole organs were performed by light sheet fluorescence microscopy as previously described.[26] Analysis of vasculature and its segmentation was performed using Imaris 8.1 software (Bitplane, Concord, MA, USA). Branch level was determined by branching point and diameter changes of the vasculature.[27]

Hepatic endothelial cell isolation

Single cell suspensions were generated via digestion with 2 mg/mL collagenase D and 5 μL deoxyribonuclease. Hepatic EC cell fraction was enriched by gradient centrifugation using 30% histodenz (Sigma Aldrich). For gene expression analysis, the obtained single cell suspension was further enriched for EC ($CD11b^-$, $CD45^{dim/-}$, $CD31^+$) by flow cytometry using a Bio-Rad S3 cell Sorter. EC purity was determined via flow cytometry analysis of $ICAM1^+$ and $CD31^+$ cells.

Statistics

Survival data were analyzed using the Kaplan–Meier method and compared with the Mantel–Cox log-rank test. For statistical analysis of all other data, Student's *t*-test was used, unless indicated otherwise. Values are presented as mean ± standard error of the mean (SEM). Values of $P \leq 0.05$ were considered statistically significant. All statistical analyses were performed using GraphPad Prism software (GraphPad Software Inc., La Jolla, CA, USA).

Additional experimental procedures are described in the *Online Supplementary Appendix*.

Results

Endothelial apoptosis during severe intestinal acute graft-*versus*-host disease in human biopsies

We stained colon and duodenum biopsies from allo-HSCT recipients with the apoptotic cell marker caspase 3 (Casp3). We found that Casp3 positive ($Casp^+$) EC were rare events in biopsies of allo-HSCT recipients without

aGvHD. In contrast, Casp3+ EC were frequent in intestinal biopsies of patients diagnosed for grade III-IV aGvHD. Figure 1 shows exemplary pictures of colon sections in human allo-HSCT recipients without aGvHD (Figure 1A) *versus* grade III-IV intestinal aGvHD (Figure 1B). Quantification revealed a significant increase in percentage of Casp3+ vessels in duodenal (Figure 1C) and colonic mucosa (Figure 1D) of grade III-IV aGvHD. Patient characteristics and clinical data are given in the *Online Supplementary Table S1* (for Figure 1C) and the *Online Supplementary Table S2* (for Figure 1D). Our data demonstrate endothelial apoptosis during severe intestinal aGvHD in human allo-HSCT recipients.

Micro-structural endothelial changes during experimental acute graft-*versus*-host disease in transmission electron microscopy

In order to further investigate micro-structural changes of the endothelium we used experimental aGvHD models. We first performed transmission electron microscopy (TEM) of liver (Figure 2A to F) and colon (*Online Supplementary Figure S2A* to *F*) at day+15 after allo-HSCT. We found that the hepatic sinusoidal endothelium in allo-HSCT recipients without aGvHD is not affected. The endothelial monolayer as well as the EC-cell contacts were intact (Figure 2A and B), and we observed a normal endothelial monolayer in hepatic sinusoids (Figure 2B). In contrast, the hepatic sinusoidal endothelium during aGvHD was severely damaged with close immune cell-EC interactions (Figure 2C). Furthermore, we observed a discontinuous endothelial monolayer at the EC-immune cell contact zone during hepatic aGvHD (Figure 2D). In addition, we found blistering of the endothelial monolayer (Figure 2E) as well as platelet adhesion on the sinusoidal endothelial monolayer (Figure 2E) and in the blistered endothelium (Figure 2F) during hepatic aGvHD. In colonic mucosa, vessels were again normal in allo-HSCT recipients without aGvHD (*Online Supplementary Figure S2A* to *F*). The endothelial monolayer was well-structured, smooth and surrounded by pericytes (*Online Supplementary Figure S2A*) with intact tight junctions (*Online Supplementary Figure S2B*). In contrast, during intestinal aGvHD the endothelial monolayer was ruffled (*Online Supplementary Figure S2C*) with perivascular fibrinogen deposits (*Online Supplementary Figure S2A, C, D* and *F*). Endothelial cytoplasm was enriched with vesicles

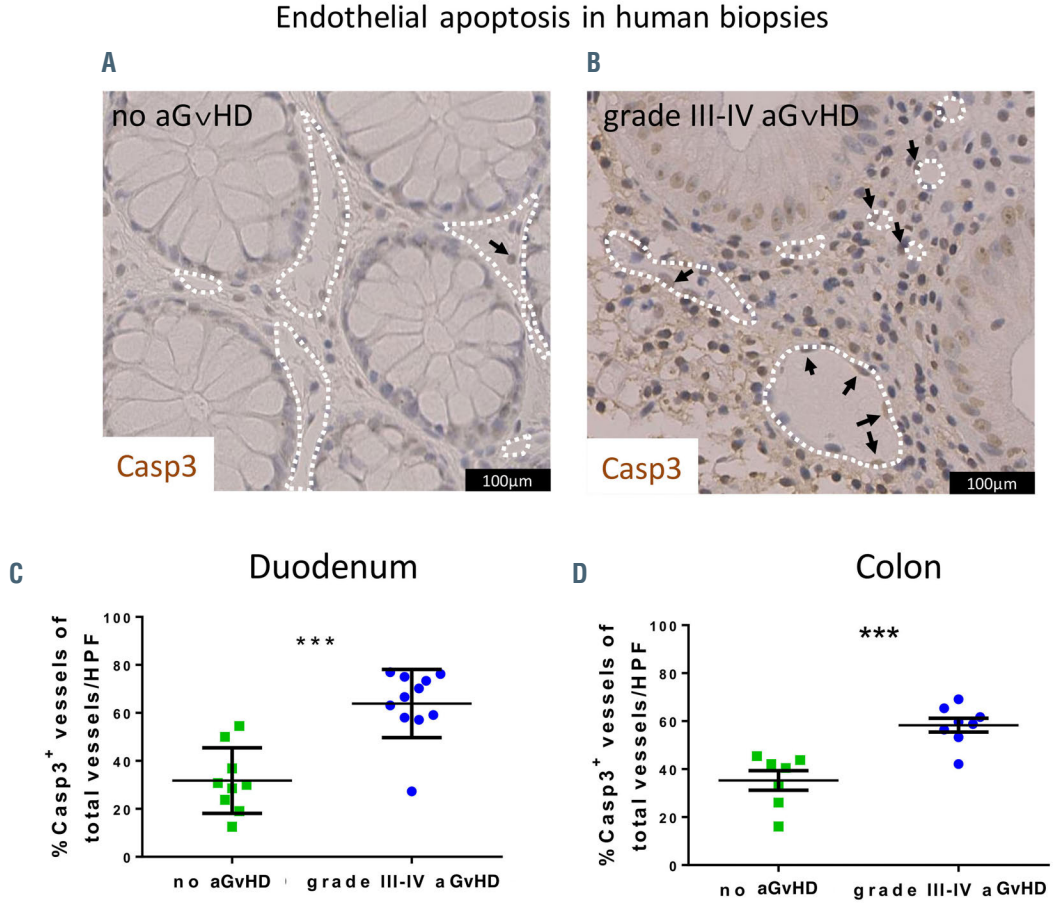

Figure 1. Endothelial damage in human intestinal biopsies. (A) Exemplary picture of a colon biopsy of a patient after allogeneic hematopoietic stem cell transplantation (allo-HSCT) without histologic evidence of acute graft-*versus*-host disease (aGvHD) and low level of endothelial apoptosis. The white dotted lines indicate vessel lumen and the arrow indicates one apoptotic caspase 3 positive (Casp3+) endothelial cell. (B) Exemplary picture of a colon biopsy of a patient with grade III-IV intestinal aGvHD and increased endothelial apoptosis. The white dotted lines indicate vessel lumen and the arrows indicate apoptotic Casp3+ endothelial cells. (C) Quantification of Casp3+ events in duodenal endothelium of allo-HSCT recipients given in percent of vessels in high-power fields (HPF). (D) Quantification of Casp3+ events in colonic endothelium of allo-HSCT recipients given in percent of vessels in HPF. Percentage of Casp3+ vessels was tested for significance by Student's *t*-test (***P<0.001; n=7-11 patients per group). Error bars indicate mean ± standard error of the mean.

and the endothelial monolayer was disrupted (*Online Supplementary Figure S2D* and *E*). During intestinal aGvHD, clotting was present in the colonic microvasculature as well as convolution of the endothelial monolayer (*Online Supplementary Figure S2E*). In conclusion, TEM revealed an extensive endothelial damage in target organs during aGvHD.

Pericyte coverage, tight junctions and endothelial leakiness during acute graft-*versus*-host disease

As a method to quantify endothelial damage in experimental aGvHD, we analyzed pericyte-coverage of $CD31^+$ vessels in the colon and liver by fluorescence microscopy. Representative pictures are shown in Figure 3A and G. We found reduced pericyte-coverage of vessels in hepatic sinusoids (Figure 3B) and in colonic mucosa (Figure 3H) during aGvHD, indicating a damaged endothelial monolayer. In order to address the question whether the endothelial barrier function is altered during aGvHD, we assessed the endothelial expression of the tight junction protein ZO-1 and the intercellular junction protein VE-cadherin in vessels of aGvHD target organs a shown in the representative pictures in Figure 3C and I. Immunostaining revealed reduced endothelial ZO-1 abundance during aGvHD, which correlates with reduced numbers of intact tight junction (Figure 3D and J). Moreover, colonic microvascular and hepatic sinusoidal endothelium VE-cadherin abundance was reduced (Figure 3E and K).

In order to investigate, if the reduced expression of tight junction and intercellular connection proteins of the endothelium during aGvHD have functional consequences *in vivo*, we injected Evans blue solution intravenously and analyzed the penetration into the organs. In allo-HSCT recipients with aGvHD endothelial leakage was significantly increased in liver (Figure 3F) and colon (Figure 3L) as compared to HSCT recipients without aGvHD.

Next, we were interested if the detected endothelial changes occurred exclusively in the target organs during

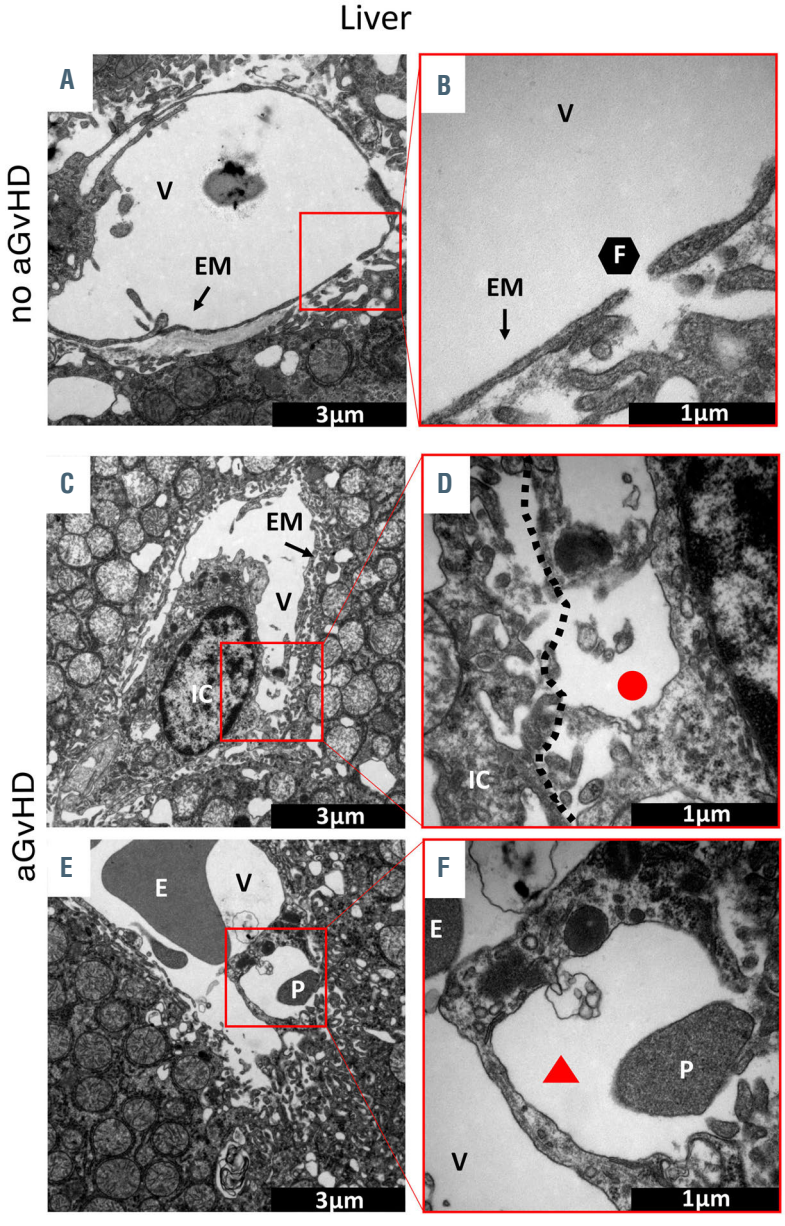

Figure 2. Visualization of acute graft-*versus*-host disease-associated ultrastructural changes in the liver by transmission electron microscopy. Representative pictures of sections from liver taken at day+15 after experimental hematopoietic stem cell transplantation (HSCT) in the chemotherapy based B6→BDF model. (A and B) Liver sinusoidal endothelial monolayer after syngeneic-HSCT (syn-HSCT) without acute graft-*versus*-host disease (aGvHD). (A) Normal, fenestrated sinusoidal blood vessel completely covered with endothelial monolayer. (B) Higher magnification of a 100 nm large fenestration of the endothelium in the liver. (C to-F) Sinusoidal liver endothelial monolayer after allo-HSCT during aGvHD. (C) Liver sinusoidal vessel with destroyed and unregularly shaped endothelial monolayer in contact with an immune cell. (D) Higher magnification of contact zone between immune cell and endothelial cell. (E) Blistering of the endothelial monolayer with a platelet in the region of injury. (F) Higher magnification of endothelial blistering. The perivascular space is marked by a red triangle. V: vessel lumen; EM: endothelial monolayer; F: fenestrated endothelium; IC: immune cell; E: erythrocyte; P: platelet; red circle: loss of endothelium; red triangle: endothelial blistering. Control groups (no aGvHD) were transplanted with the same bone marrow cell numbers and T-cell numbers from syngeneic donors.

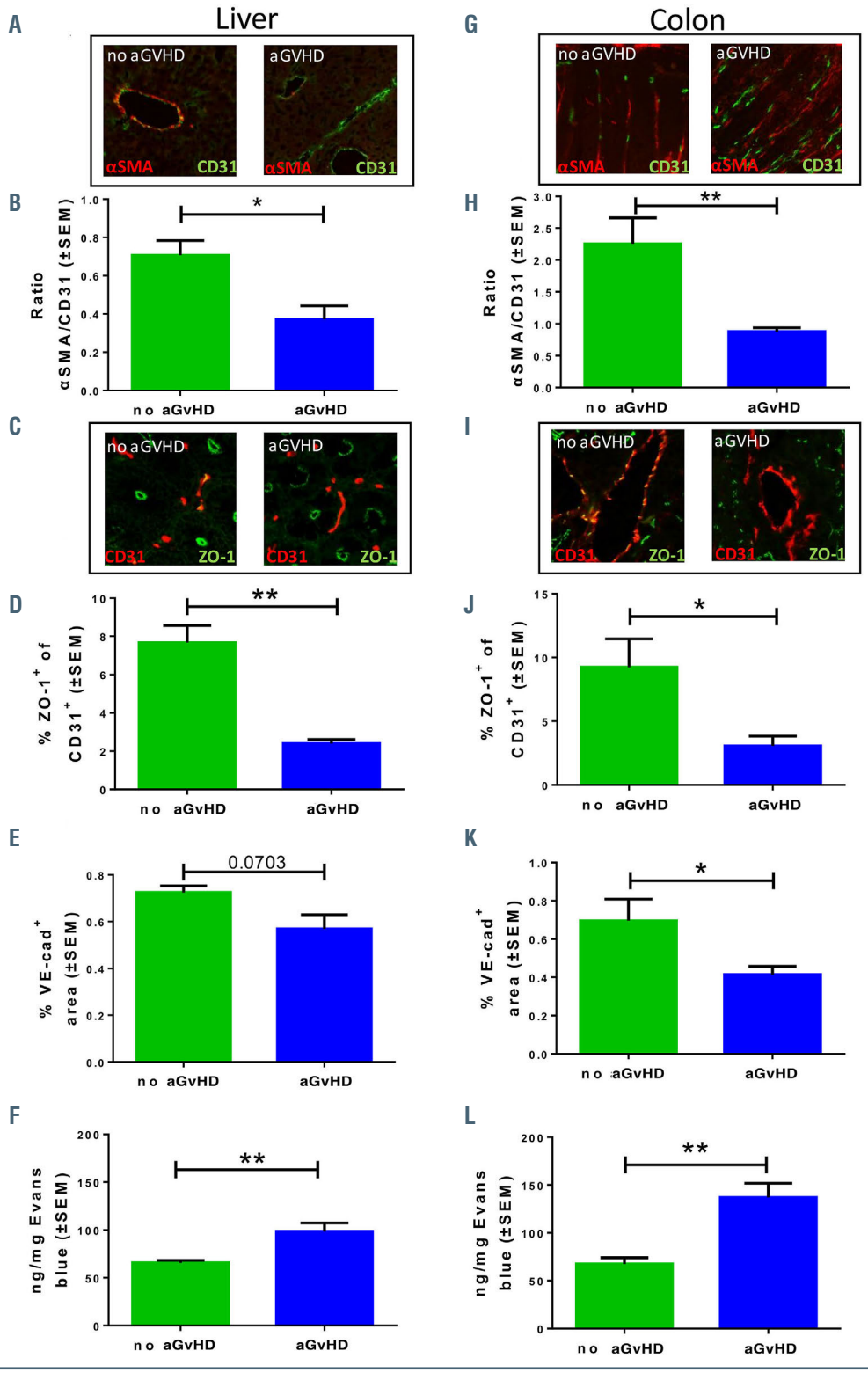

Figure 3. Pericyte coverage, tight junctions and endothelial leakiness during acute graft-*versus*-host disease. Organs were harvested at day+15 after experimental hematopoietic stem cell transplantation (HSCT) in the chemotherapy based LP/J→B6 model. Control groups (no acute graft-*versus*-host disease [aGvHD]) were transplanted with the same bone marrow cell numbers and T-cell numbers from syngeneic donors. (A, B, and G to H) Quantification of pericyte coverage of vessels. (A and G) Representative pictures of staining for pericyte marker α smooth muscle actin (αSMA) in red and endothelial cell marker CD31 in green. Right organs of animals without aGvHD and left organs of animals suffering from aGvHD. (B and H) Ratio of αSMA positive area and CD31 positive area in (B) liver sinusoidal endothelium and (H) in colonic mucosal vessels in aGvHD *versus* no aGvHD. (C, D, I and J) Quantification of endothelial tight junction protein expression ZO-1. (C and I) Representative pictures of staining ZO-1 in green and CD31 in red. Right organs of animals without aGvHD and left organs of animals suffering from aGvHD. (D and J) Percentage of ZO-1$^+$ CD31$^+$ area in (D) liver sinusoidal endothelium and (J) colonic mucosal vessels in aGvHD *versus* no aGvHD. (E and K) Quantification of endothelial adherence junction protein expression VE-cadherin. Percentage of VE-cadherin positive area in (E) liver sinusoidal endothelium and (K) colonic mucosal vessels in aGvHD *versus* no aGvHD. (F and L) Measurement of Evans blue extravasation in ng Evans blue per mg at day+15 after experimental allo-HSCT in the chemotherapy based B6→BDF model. (F) Liver and (L) colon of aGvHD *versus* no aGvHD. Significance was tested with Student's t-test (*P<0.05; **P<0.01; n=5 animals per group). All experiments were reproduced in a biological independent experiment and shown are representative results of one experiment. Error bars indicate mean ± standard error of the mean.

aGvHD or if this is a systemic effect. We therefore analyzed endothelial leakage in the kidney and skeletal muscle, which are typically not affected in human aGvHD. We have previously confirmed these organs to be unaffected by aGvHD in our models.[8,21] The Evans blue assay revealed no significant changes of endothelial leakage in these non-target organs during aGvHD (*Online Supplementary Figure 3A* and *B*) suggesting that increased endothelial leakiness predominantly occurs in aGvHD target organs.

Taken together, we found disturbed endothelial tight junctions and intercellular connections leading to increased vascular leakiness in target organs of aGvHD.

Structural changes of vasculature in target organs during aGvHD

In order to get a better overview of the three-dimensional (3D) changes of the vasculature, we compared aGvHD and non-GvHD colonic vessel structure and organization with light sheet fluorescence microscopy after *in vivo* perfusion with an anti-VE-cadherin antibody. Figure 4A and C show normal VE-cadherin staining and vessel branching in a 3D model in colon at d+15 after HSCT without aGvHD. During aGvHD, we found considerably different staining patterns for VE-cadherin (Figure 4B) and increased vessel branching in colon (Figure 4D). Using this 3D model to quantify vessel branch levels of vasculature, we found significantly increased total vessel branching in colonic vasculature during aGVHD as compared to HSCT recipients without aGvHD (Figure 4E). Accordingly, analysis of branching levels from vessel segments (Figure 4F) and vessel diameter (Figure 4G) revealed a significant increase during intestinal aGvHD. We conclude that aGvHD is associated with structural changes in colonic vasculature.

Dysfunction of the macrovasculature during acute graft-*versus*-host disease

As aGvHD is associated with severe signs of microvascular dysfunction, we became interested if aGvHD also influences the physiological functions of macrovasculature as suggested previously.[18] We examined vessel contraction and relaxation in mouse mesenteric arteries during aGvHD *versus* no aGVHD after HSCT by myographic measurements. We found that maximum contraction of mesenteric arteries in response to high doses of noradrenaline (NA) and phenylephrine (Phe) was not significantly changed (*Online Supplementary Figure S4A* and *B*). However, partial contraction at lower doses of NA and Phe was moderately increased during aGvHD *versus* no aGvHD *(Online Supplementary Figure S4C* and *D*). In addition, fractional relaxation after maximum contraction in response to ACh was slower in arteries from allo-HSCT recipients with aGvHD (*Online Supplementary Figure S4E*). Taken together we found increased contraction and reduced relaxation potential of mesenteric arteries during aGvHD indicating systemic hypertension.

Gene expression changes of endothelial cells during acute graft-*versus*-host disease

In order to better understand the molecular pathways involved in endothelial dysfunction during aGvHD we performed gene array expression analysis of flow cytometry sorted hepatic EC from HSCT recipients with aGvHD *versus* without aGvHD at day+15. We found significant endothelial gene expression changes in complement activation, apoptosis, oxidative damage, IL-1 signaling and cell cycle during aGvHD (*Online Supplementary Figures S5, S6 and S7; Online Supplementary Table S3*). Furthermore, barrier function and cytoskeleton pathways were differentially regulated, including expression changes of *Rho GTPases* (*Online Supplementary Table 3*). We performed interaction analysis of selected endothelium-specific genes (*Online Supplementary Figure 7*) and found differential expression of *Cdh1* and *Cdh13* (coding for cadherins), *Thbd* (coding for thrombomodulin), *Vegfc* (coding for vascular endothelial growth factor c) and *Anpgt1/2* (coding for angiopoietin 1 and 2). In summary, we detected endothelial gene expression changes in different clinically relevant pathways during aGvHD providing possible targets for future therapeutic interventions.

Inflammatory activity and endothelial damage during steroid-refractory acute graft-*versus*-host disease

Since recent clinical data has provided evidence on the importance of endothelial pathology specifically in SR-aGVHD,[12,17,28-31] we decided to characterize both inflammatory infiltrates and endothelial damage in this setting. Based on previous data,[22] we first performed dose-finding studies with steroids in different aGvHD models to establish a protocol with progressive aGvHD despite high dose steroid treatment. Treatment with dexamethasone starting at day+4 after allo-HSCT, showed progressive aGvHD in our models (*Online Supplementary Figure S1*; Figure 5).

We analyzed vascular pericyte coverage as well as infiltration by $CD4^+$ donor T cells in dexamethasone-treated SR-aGvHD *versus* untreated aGvHD at day+15 after allo-HSCT. We found reduced inflammatory T-cell infiltrates in SR-aGvHD *versus* untreated aGvHD (Figure 5A to D). The predominant remaining cell population in colon during SR-aGvHD were $CD4^+$ and $CD8^+$ T cells (Figure 5 C and D) as well as $CD11b^+$ and $F4/80^+$ myeloid cells (*Online Supplementary Figure S8A* and *B*). Endothelial damage as quantified by pericyte coverage reduction in colon vessels was equally severe in SR-aGvHD and untreated aGvHD (Figure 5E). In order to connect the experimental findings to the clinical context of SR-aGvHD, we quantified leukocyte infiltration in intestinal biopsies of patients at diagnosis of aGvHD and at later time points of SR-aGvHD in two independent cohorts. Figure panels 5F to J demonstrate significant lower infiltration of $CD45^+$ leukocytes in colon biopsies as well as duodenum biopsies (Figure 5I). The leukocyte reduction was mainly due to significantly lower infiltration by $CD3^+$ T cells in colon biopsies (Figure 5K, L, M and O) as well as duodenum biopsies (Figure 5N) during SR-aGvHD *versus* aGvHD at time of diagnosis. Figure 5K gives a typical example of colonic aGvHD at onset with high levels of inflammatory infiltrates by $CD3^+$ T cells and Figure 5L a representative colonic section after steroid treatment and diagnosis for SR-aGvHD, demonstrating reduced inflammatory infiltrates. In addition, we performed caspase 3 staining and demonstrated a high level of endothelial apoptosis during aGvHD both at diagnosis as well as during SR-aGVHD (Figure 5P). A typical example of high inflammatory activity at aGvHD diagnosis time point and low level of inflammatory activity at diagnosis of SR-GvHD in combination with

considerable tissue damage in hematoxylin and eosin (H&E) staining is given in the *Online Supplementary Figure S8, panels C* and *D*. Patient characteristics and clinical information is given in the *Online Supplementary Tables S4* to *S6*. Our data indicates that inflammatory activity in intestinal tissues is reduced after steroid treatment, while the endothelial damage is not influenced by steroid treatment during SR-aGvHD.

Endothelial protection by PDE5 inhibition in acute graft-*versus*-host disease (aGvHD) and steroid-refractory aGvHD

Based on our results demonstrating extensive endothelial damage and reduced inflammatory T-cell infiltration during SR-aGvHD, we hypothesized that pharmacologic protection of the endothelium would have stronger protective effects on SR-aGvHD *versus* treatment of aGvHD

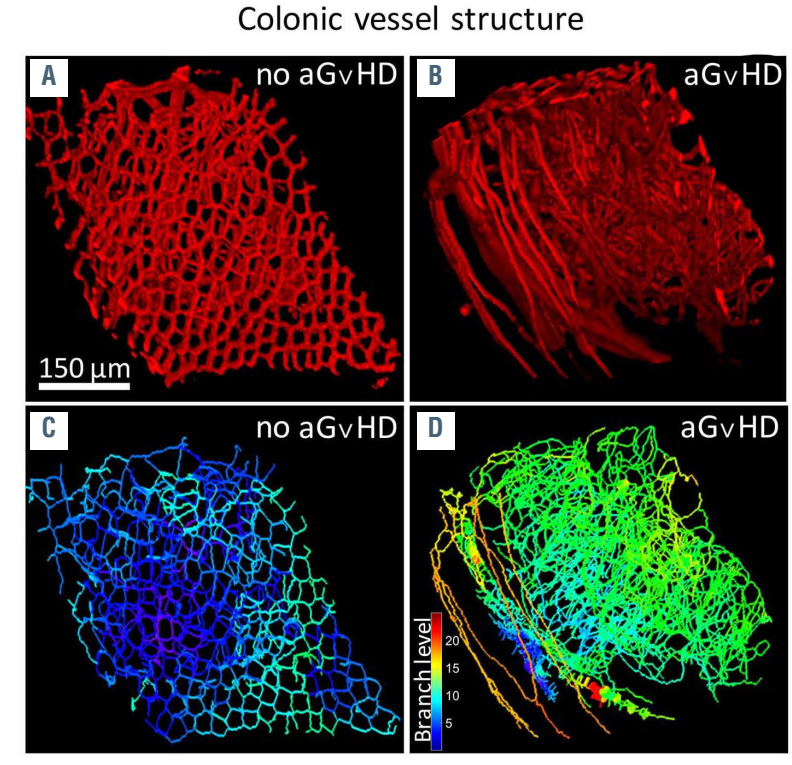

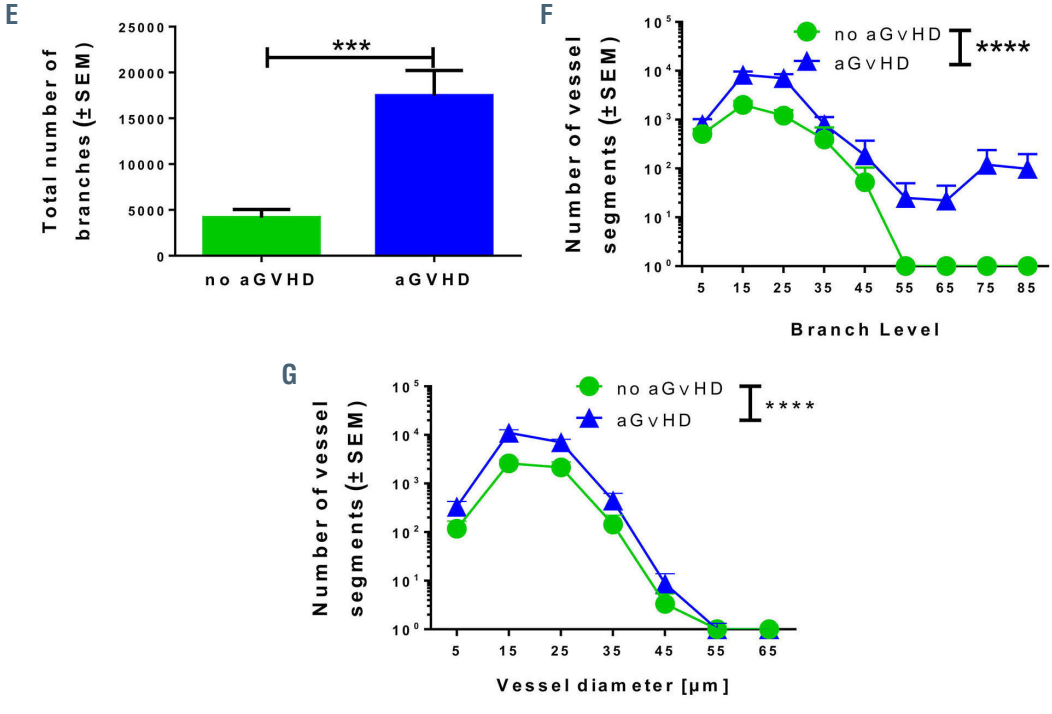

Figure 4. Structural changes of vasculature in target organs during acute graft-*versus*-host disease by scanning light sheet fluorescence microscopy. We analyzed organs at day+15 after experimental hematopoietic stem cell transplantation (HSCT) in the chemotherapy based B6→BDF model. Control groups (no aGvHD) were transplanted with the same bone marrow (BM) cell numbers and T-cell numbers from syngeneic donors. (A and B) VE-cadherin signal of vasculature in colon of (A) allogeneic-HSCT (allo-HSCT) recipients without aGvHD and (B) allo-HSCT recipients with aGvHD. (C-D) Computed three-dimensional (3D) model of colonic vasculature with number of branches (blue= low branch levels; red= high branch levels) of (C) allo-HSCT recipients without aGvHD and (D) allo-HSCT recipients with aGvHD. (E to G) Analysis of colonic vasculature parameters. Assessment of (E) total number of branches (F) distribution of vessels branching level and (G) vessel diameter distribution in allo-HSCT recipients with aGvHD *versus* without aGvHD. Significance of total number of branches was tested by Student's *t*-test (***P<0.001; n=3 animals per group) and significance of vessel branching level was tested by two-way ANOVA with Tukey's multiple comparison test (***P<0.001; n=3 animals per group). Error bars indicate mean ± standard error of the mean.

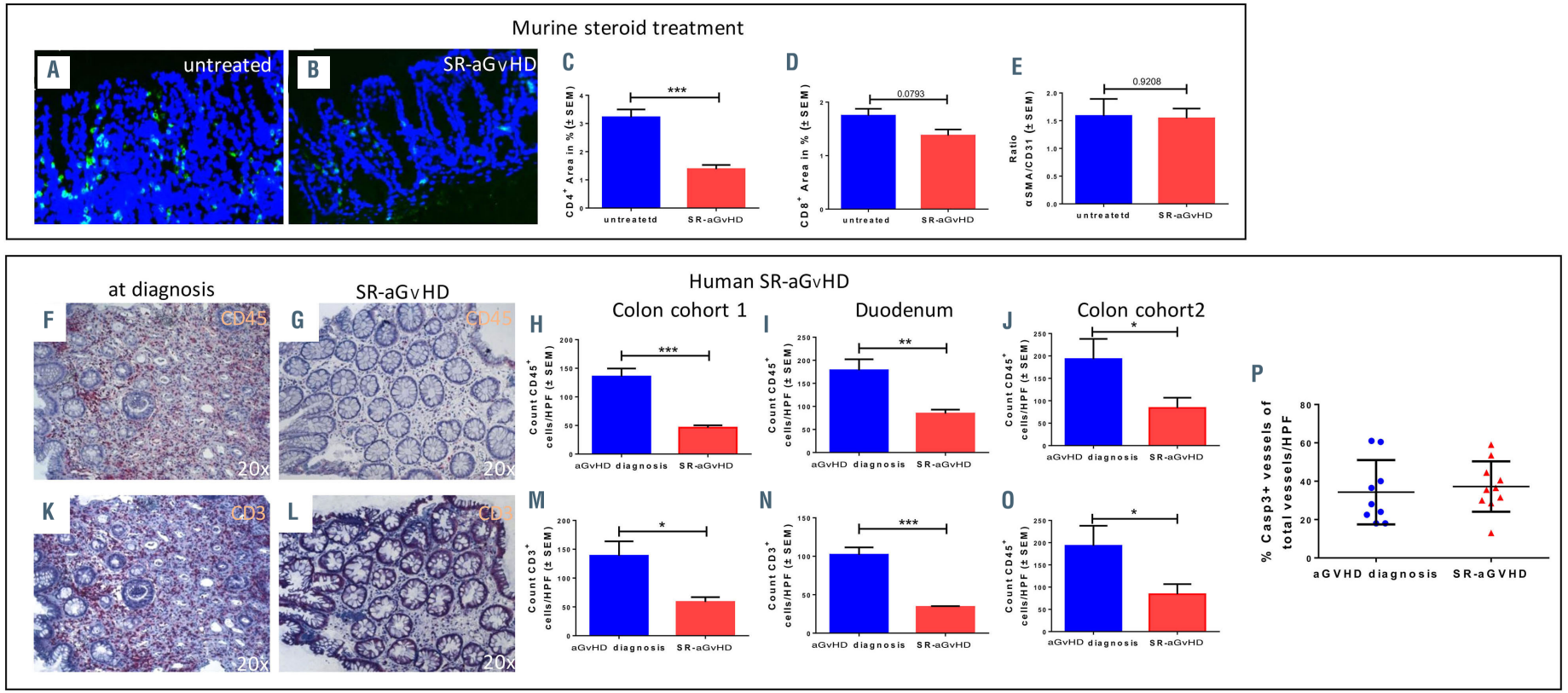

Figure 5. Inflammatory infiltration and endothelial damage in human steroid-refractory acute graft-*versus*-host disease (SR-aGvHD) and in an experimental model of SR-aGvHD. (A to E) Immune cell infiltration in colon samples at day+15 after experimental allogeneic hematopoietic stem cell transplantation (allo-HSCT) in the chemotherapy based B6→BDF model. Exemplary pictures of $CD4^+$ infiltrates (green) in colon mucosa of (A) control phosphate buffered saline (PBS) treated (untreated) aGvHD and (B) Dexamethasone treated aGvHD (SR-aGvHD, 0.5mg/kg/day Dexamethasone starting at day+4). (C) Quantification of $CD4^+$ area in colonic mucosa of untreated aGvHD *versus* SR-aGvHD. (D) Quantification of $CD8^+$ area in colonic mucosa of untreated aGvHD *versus* SR-aGvHD. (E) Ratio of pericyte marker α smooth muscle actin (αSMA) positive area and endothelial cell marker CD31 positive area in in colonic mucosa of untreated aGvHD *versus* SR-aGvHD. Significance was tested by Student's *t*-test (***P<0.001; n=5 animals per group). Error bars indicate mean ± standard error of the mean. (F to P) Human intestinal biopsies at aGvHD diagnosis and during the course of SR-aGvHD. (F to J) Intestinal biopsies at aGvHD diagnosis and SR-aGvHD stained against pan leukocyte marker CD45 (F) Colon biopsy stained against CD45 at aGvHD diagnosis with massive infiltrates. (G) Colon biopsy stained against CD45 during SR-aGvHD with low infiltrates. (H to J) Quantification of CD45 infiltrates at aGvHD diagnosis *versus* SR-aGvHD in (H) colon and (K) duodenum biopsies of cohort 1 and (J) in colon biopsies of cohort 2. (K-O) Intestinal biopsies at aGvHD diagnosis and SR-aGvHD stained against T-cell receptor marker CD3 (K) Colon biopsy stained against CD3 at aGvHD diagnosis with massive infiltrates. (L) Colon biopsy stained against CD3 during SR-aGvHD with low infiltrates. (M to O) Quantification of CD3 infiltrates at aGvHD diagnosis *versus* SR-aGvHD in (M) colon and (N) duodenum biopsies of cohort 1 and (O) in colon biopsies of cohort 2. (P) Quantification of capspase 3 positive (Casp3+) events in colonic endothelium of allo-HSCT recipients of cohort 2 at aGvHD diagnosis and during SR-aGvHD given in percent of vessels per high power field (HPF). Significance was tested by Student's *t*-test (*P<0.05; **P<0.01; ***P<0.001; n= 4-6 patients per group). Error bars indicate mean ± standard error of the mean.

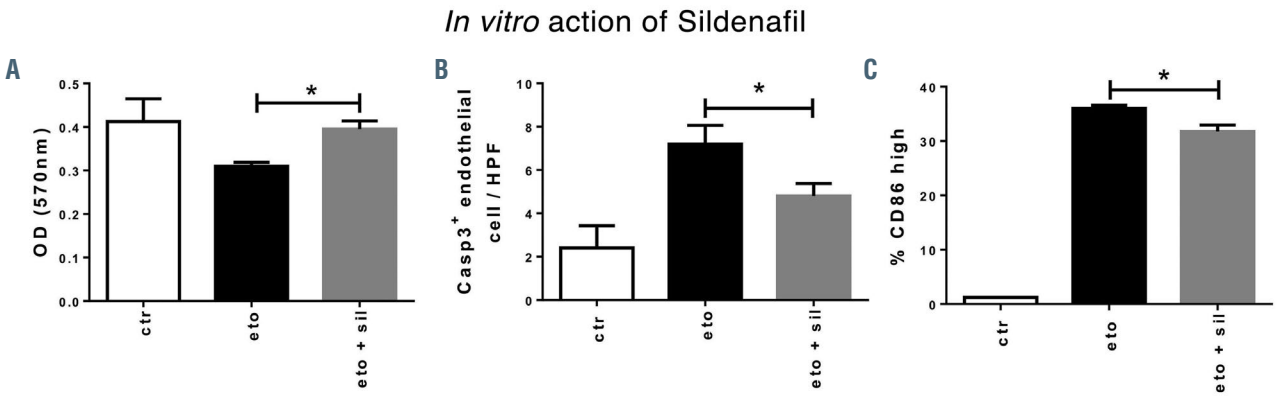

Figure 6. Reduction of endothelial apoptosis and endothelial activation by sildenafil *in vitro*. Mouse cardiac endothelial cells (MCEC) were incubated with either phosphate buffered saline (PBS)/ 0,1% dimethylsulfoxide (DMSO) (control [ctr]), 100 nm etoposide (eto), an inducer of cell death, or with 100 nm etoposide and 34 nm sildenafil (eto+sil) for 24 hours before analysis. (A) MTT assay showed higher optical density of eto+sil group *versus* eto-only group. (B) Staining for apoptotic cell marker caspase 3 (Casp3) showed reduced Casp3$^+$ cells per high-power field (HPF) in eto+sil group compared to eto-only group. (C) Flow cytometry analysis of CD86, a costimulatory and endothelial activation marker, showed reduced percentage of endothelial CD86^{high} cells in eto+sil group compared to eto-only group. Significance was tested by Student's *t*-test (*P<0.05; n=2-3 experiments with at least triplicates per condition). Error bars indicate mean ± standard error of the mean.

at its initiation stage. As a first example for such an approach, we used the PDE5 inhibitor sildenafil, which has been demonstrated to normalize endothelial dysfunction *in vivo* in different settings.[32-39] First, we tested sildenafil *in vitro* for EC protection from cytotoxic damage, mediated by etoposide. Sildenafil protected EC from etoposide-induced reduction of endothelial metabolic activity and proliferation (Figure 6A). Sildenafil significantly reduced etoposide-induced endothelial apoptosis, as quantified by Casp3$^+$ staining (Figure 6B). For co-stimulatory capacity, we checked CD86^{high} expression of EC by flow cytometry. Sildenafil treatment resulted in a significant reduction of etoposide-induced CD86 expression on EC (Figure 6C). Our data demonstrate a protective effect of sildenafil on etoposide-induced endothelial dysfunction *in vitro*.

We tested the effect of sildenafil in our experimental models of aGvHD (Figure 7A to F) and SR-aGvHD (Figure 7G to L). In the aGvHD model without steroid treatment, we found that sildenafil treatment had no significant effect on survival (Figure 7A). However, sildenafil-treated allo-HSCT recipients with aGvHD had significantly lower clinical scores at different time points (Figure 7B) as well as lower histopathological aGvHD scores in the liver (Figure 7C) and colon (Figure 7D) as compared to untreated allo-HSCT recipients with aGvHD. In addition, we found a non-significant trend towards reduced costimulatory capacity and antigen presentation potential of hepatic EC under sildenafil treatment (Figure 7E and F). The vascular density (*Online Supplementary Figure S9A*) as well as the density of lymphatic vessels was not significantly affected by sildenafil treatment (*Online Supplementary Figure S9B*).

During SR-aGvHD, sildenafil treatment significantly improved survival (Figure 7G). Due to high mortality, clinical scoring was only significant in the early phase (Figure 7H). Histopathological aGvHD scores in the iver (Figure 7I) and colon (Figure 7J) were significantly reduced in sildenafil-treated allo-HSCT recipients with SR-aGvHD. Additionally, we found a trend towards reduced co-stimulatory capacity as well as significantly reduced antigen presentation potential of hepatic EC in sildenafil-treated SR-aGvHD, demonstrated by lower MHC class I and II expression (Figure 7K). We confirmed these findings in another murine aGvHD model (129→B6, MHC-matched, *Online Supplementary Figure S10*). We found non-significant trends towards increased vascular density (*Online Supplementary Figure S9C*) and lymphatic vascular density in sildenafil-treated SR-GvHD *versus* controls (*Online Supplementary Figure S9D*). Next, we analyzed the effect of sildenafil on the endothelium during SR-aGvHD with electron microscopy analyses of liver and colon tissues (Figure 7M to P). We found endothelial damage in the liver and colon in untreated and sildenafil-treated SR-aGvHD. However, the sildenafil treated SR-aGvHD group showed reduced endothelial ruptures in liver (Figure 7N) and less prominent fibrinogen deposits in colonic biopsies (Figure 7P).

In order to analyze for effects of sildenafil on T-cell proliferation, we performed *in vivo* proliferation assays with carboxyfluorescein succinimidyl ester (CFSE) labeled allogeneic T cells. In irradiated mice, sildenafil had no significant effects on *in vivo* proliferation of allogeneic T cells (*Online Supplementary Figure S11A* to *C*). We next analyzed and quantified the impact on sildenafil on immune cell subsets in peripheral blood during SR-aGvHD and found no significant differences (*Online Supplementary Figure S11D* to *M*). Our data suggest that the observed positive effect of sildenafil on SR-aGvHD is predominantly mediated by its effect on EC as opposed to effects on immune cells.

Discussion

The standardized and well-described aGvHD mice models provide the unique opportunity to experimentally address the role of endothelial dysfunction after HSCT. We found that severe endothelial damage, structural changes of the vasculature and endothelial dysfunction occur during aGvHD. Due to lack of suitable animal models, less detailed data is available for other important endothelium-related complications of allo-HSCT, such as veno-occlusive disease and transplantation-associated microangiopathy. In line with the experimental results, we found that endothelial damage is present in the colon and duodenum of patients with severe aGvHD. This find-

ing is consistent with a previously published study, demonstrating increased endothelial injury in human skin biopsies during aGvHD.[10] Additionally, a series of clinical studies have collected supporting evidence on increased endothelial dysfunction during aGvHD, such as high numbers of circulating EC[40-43] and elevated serum levels of the endothelial stress markers ST2, von Willebrand factor, angiopoietin 2 and thrombomodulin.[31,44-46]

We have previously shown that aGvHD is associated with increased angiogenesis in target organs.[8,47] In the current study, we used light sheet fluorescence microscopy to demonstrate that target organ aGvHD is associated with vascular structural changes in terms of higher branching levels and larger diameter of the vasculature. Taking into account the available evidence from our previous studies as well as the experiments from this manuscript, it becomes clear that vascular destruction as well as pathological angiogenesis occur in parallel in the early phase during aGvHD in target organs. These processes finally result in restructuring of the vasculature as visualized and quantified in Figure 4. Interestingly, increased branching levels of vasculature were first reported during pathological angiogenesis in malignant tumors.[48] This finding led to the concept of 'vascular normalization' to improve antitumor therapies.[49] However, the significance of pathological vascular organization with increased branching level for the pathophysiology of aGvHD and possible therapeutic implications remains to be determined.

We found that the expression of tight junction- and adherence junction proteins were reduced during aGVHD, leading to increased vascular permeability in aGvHD target organs after allo-HSCT. The role of tight junction- and adherence junction proteins for vascular barrier maintenance[50-52] as well as leukocyte transmigration[53,54] has been described previously. Additionally, the promotion of the adherence junction protein VE-cadherin in tumor vasculature increased T-cell infiltration into the tumor.[55] These findings may open a new window for

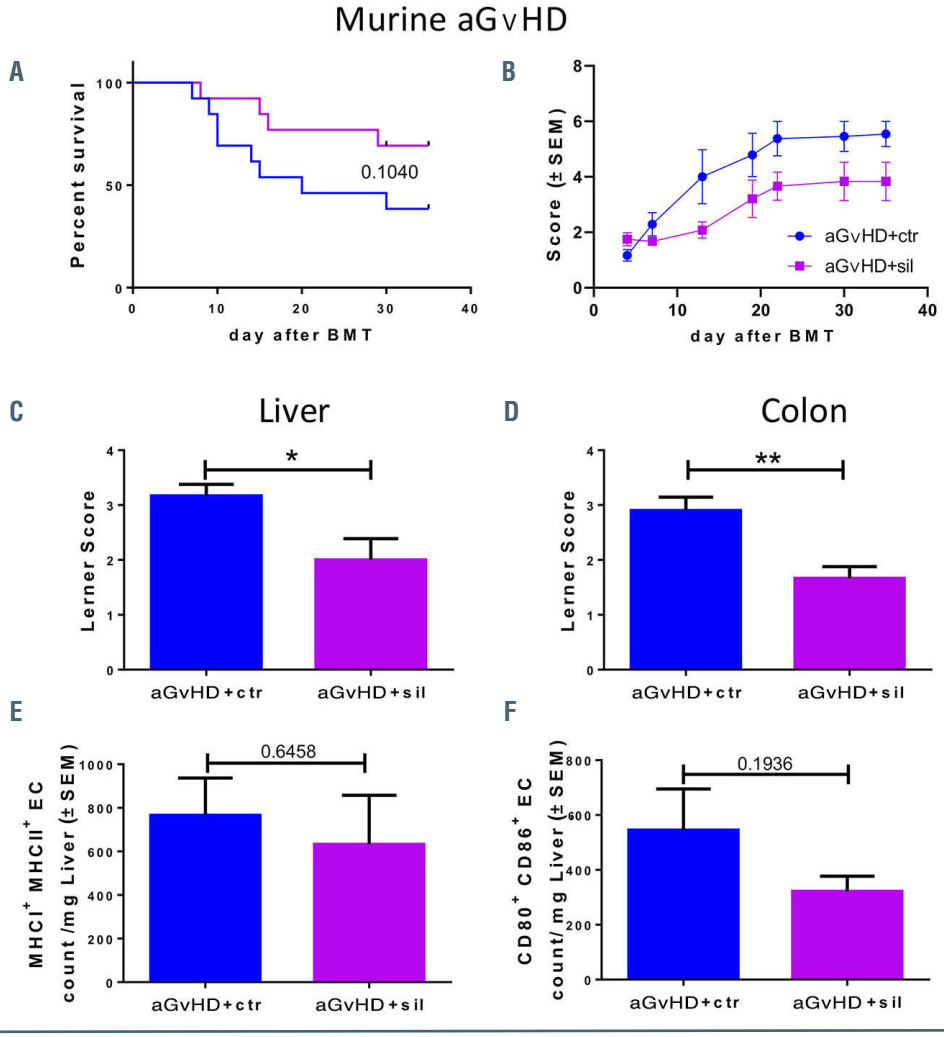

Figure 7. *In vivo* treatment of acute graft-*versus*-host disease (aGvHD) and steroid-refractory-aGvHD with sildenafil. (A to G) Treatment of aGvHD with 10 mg/kg/d sildenafil after experimental allogeneic hematopoietic stem cell transplantation (allo-HSCT) at day+15 after experimental allo-HSCT in the radiation based B6→BALB/c model. (A) Survival analysis and (B) clinical aGvHD manifestations of sildenafil (sil) treated allo-HSCT recipients with aGvHD *versus* control substance phosphate buffered saline/dimethylsulfoxide (PBS/DMSO, control [ctr]) treated allo-HSCT recipients with aGvHD. Histopathological assessment of aGvHD manifestations in (C) liver and (D) colon in sildenafil *versus* control substance treated allo-HSCT recipients at day+15. Flow cytometry quantification of (E) major histocompatibility complex I (MHCI) and MHCII expression and (F) CD80 and CD86 expression of isolated liver sinusoidal endothelial cells of sildenafil *versus* control substance treated allo-HSCT recipients at day+15. (G to L) Treatment with 10 mg/kg/d sildenafil in a murine model of SR-aGvHD at day+15 after experimental allo-HSCT in the radiation based B6→BALB/c model. (continued on next page.)

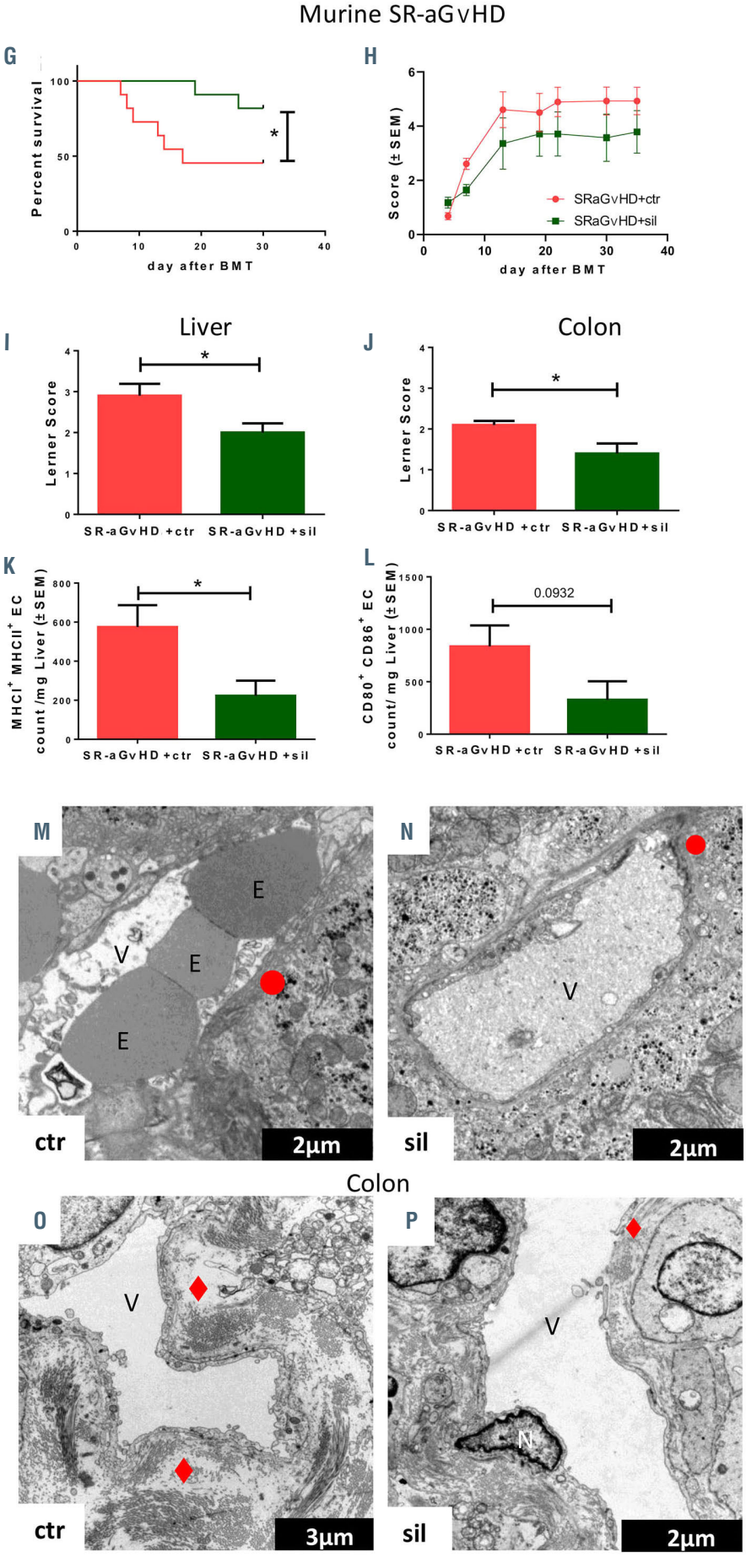

Figure 7. (G) Survival analysis and (H) clinical aGvHD manifestations of sildenafil (SR-aGvHD+sil) *versus* control substance treated (SR-aGvHD+ctr) SR-aGvHD. Histopathological assessment of aGvHD severity in (I) liver and (J) colon in SR-aGvHD+sil and SR-aGvHD+ctr at day+15 after allo-HSCT. Flow cytometry quantification of (K) MHCI and MHCII expression and (L) CD80 and CD86 expression of isolated liver sinusoidal endothelial cells of SR-aGvHD+sil and SR-aGvHD+ctr at day+15 after allo-HSCT. Significance was tested by Kaplan-Meier method and compared with the Mantel-Cox log-rank test (*P<0.05; n=8-10 animals per group) and Student's t-test (*P<0.05; **P<0.01; n=6 animals per group). Error bars indicate mean ± standard error of the mean. Survival data was pooled from two experiments. All experiments were reproduced in a biological independent experiment and shown are representative results of one experiment. (M to P) Visualization of SR-aGvHD and sildenafil treated SR-aGvHD associated ultrastructural changes in the liver and the colon by transmission electron microscopy. Shown are typical pictures of sections from liver and colon taken at day+15 after experimental allo-HSCT in the chemotherapy based 129→B6 model. (M and N) Sinusoidal liver endothelial monolayer during SR-aGvHD and sildeanfil (sil) treated SR-aGvHD. (M) Liver sinusoidal vessel of untreated SR-aGvHD with destroyed and unregularly shaped endothelial monolayer, marked by a red circle. (N) Liver sinusoidal vessel of Sildenafil treated SR-aGvHD with small ruptures of the endothelial monolayer, marked by a red circle. (O and P) Colonic mucosa endothelium during SR-aGvHD and sildeanfil treated SR-aGvHD. (O) The vessel of untreated SR-aGvHD is surrounded by massive perivascular fibrinogen deposits marked by a red rhombus. (P) Occasionally little perivascular fibrinogen deposits, marked by a red rhombus, could be detected in sildenafil treated SR-aGvHD. V: vessel lumen; E: erythrocyte; N: nucleus; red rhombus: perivascular fibrinogen deposits; red circle: loss of endothelium; red trapezoid: endothelial convolution).

aGvHD therapies aiming at reducing vascular permeability and stabilization of vascular tight-junctions as well as adherence-junctions. Vestweber and colleagues have generated mice with stabilized endothelial junctions; these mice had strongly reduced neutrophil and lymphocyte recruitment into inflamed tissues.[56] Examples for a therapeutic approach derive from the field of sepsis where reduction of vascular permeability with the αVβ3 antagonist cilengitide[57] or with an antibody binding to angiopoietin 2 and TIE2[58] which led to substantial biological benefits.

Recent clinical studies suggest a role of endothelial pathology particularly in SR-aGvHD[13,14,17,28,29,31] and a high medical need for development of respective therapies. We now demonstrate in two independent clinical cohorts as well as in experimental models that inflammatory infiltration in target organs is considerably reduced compared to aGvHD at diagnosis. Consequently, we found that dexamethasone treatment did not significantly reduce the severity of endothelial damage during SR-aGvHD. Pavan Reddy's group recently published the results of extensive experiments in murine models of SR-GvHD. In line with our findings, their results point towards the existence of T-cell independent mechanisms in the pathophysiology of SR-GvHD.[23] This may explain the historically disappointing clinical results of immunosuppressive treatments for SR-aGvHD. The low inflammatory status in connection with considerable endothelial pathology provides a rationale for therapies protecting the endothelium during SR-aGvHD. Based on previous encouraging data on normalization of endothelial dysfunction,[32-39] we used the PDE5 inhibitor sildenafil as a first attempt to treat SR-aGvHD by an 'endothelium-protective' approach. Sildenafil treatment ameliorated aGvHD and the effect was more pronounced in case of SR-aGvHD compared with previously untreated aGvHD. The latter observation may be explained by the high level of tissue inflammation in non-glucocorticoid treated aGvHD mice superimposing the beneficial effects of sildenafil on EC. However, we cannot exclude the possibility of a synergistic effect of sildenafil with steroids in our models.

The direct mechanisms of sildenafil treatment on the course of SR-aGvHD remain unclear. However, improvement of vascular barrier function and reduction of EC apoptosis probably contribute to the beneficial effects of sildenafil. During aGvHD we found increased vascular permeability in target organs and alterations of Rho GTPases, who are critical regulators of endothelial barrier function.[59] Sildenafil-mediated stabilization of endothelial barrier function[60,61] as well as impact of sildenafil on regulation of Rho GTPases[62] have been described previously. We found that apoptosis and expression of relevant genes, such as nitric oxide synthase (*Nos3*) and *BCL-2*, was increased in target organ EC during aGvHD. Sildenafil has been shown to have cyto-protective effects by regulation of nitric oxide synthase 3 signaling and BCL-2 expression.[63] In addition, sildenafil may have positive effects by stabilizing vessel surrounding pericytes and thereby vascular integrity: PDE5 targets cGMP, which has been demonstrated to inhibit the proliferation of smooth muscle cells by causing a delay in G_1/S transition in the cell cycle.[64] Interestingly, we detected differentially regulated cell cycle genes in EC during aGvHD. Of note, we found that sildenafil treatment led to reduction of aGvHD-associated expression of co-stimulatory molecules on target organ EC. However, our finding that sildenafil had no significant effects on *in vivo* proliferation of allogeneic donor T cells in irradiated hosts argue against the biologic significance of the observed impact of sildenafil on EC co-stimulatory molecule expression during aGvHD.

In conclusion, our results demonstrate extensive damage, structural changes, and dysfunction of the vasculature during aGvHD, and our findings suggest a novel concept of therapeutic intervention by endothelium-protecting agents as an attractive treatment approach for SR-aGvHD. A likely future perspective is to test endothelium-targeting approaches complementing treatment options with proven efficacy in SR-aGvHD, such as JAK-2 inhibition.[65]

Disclosures

No conflicts of interest to disclose.

Contributions

SC, AB, EC, MD-R, JM, LB, CPS and OP designed the study; SC, ZM, MB, YS, SM, KR, JM, MK, AM, JS, MP and GB performed experiments and analyzed results; SC and OP wrote the manuscript. All authors read, edited and approved the manuscript.

Acknowledgments

This work was supported by the José Carreras Leukämie-Stiftung (11R2016, 03R\2019), Deutsche Krebshilfe (70113519), Deutsche Forschungsgemeinschaft (PE 1450/7-1), Monika-Kutzner-Stiftung, and Wilhelm-Sander-Stiftung (2014.150.1).

Funding

MB was funded by the European Training and Research in Peritoneal Dialysis Program, funded by the European Union within the Marie Curie Scheme (287813). AB received funding from the German Research Foundation (DFG), collaborative research center TRR221 (B11, Z02) and ZM was funded by the DFG collaborative research center TRR225 (B08).

References

1. Garnett C, Apperley JF, Pavlu J. Treatment and management of graft-versus-host disease: improving response and survival. Ther Adv Hematol. 2013;4(6):366-378.
2. Deeg HJ. How I treat refractory acute GVHD. Blood. 2007;109(10):4119-4126.
3. Westin JR, Saliba RM, De Lima M, et al. Steroid-refractory acute GVHD: predictors and outcomes. Adv Hematol. 2011;2011:601953.
4. Gloude NJ, Khandelwal P, Luebbering N, et al. Circulating dsDNA, endothelial injury, and complement activation in thrombotic microangiopathy and GVHD. Blood. 2017;130(10):1259-1266.
5. Fan CQ, Crawford JM. Sinusoidal obstruction syndrome (hepatic veno-occlusive disease). J Clin Exp Hepatol. 2014;4(4):332-346.
6. Xie Z, Ghosh CC, Patel R, et al. Vascular endothelial hyperpermeability induces the clinical symptoms of Clarkson disease (the systemic capillary leak syndrome). Blood. 2012;119(18):4321-4332.
7. Ueda N, Chihara D, Kohno A, et al. Predictive value of circulating angiopoietin-2 for endothelial damage-related complications in allogeneic hematopoietic stem cell transplantation. Biol Blood Marrow Transplant. 2014;20(9):1335-1340.
8. Riesner K, Shi Y, Jacobi A, et al. Initiation of acute graft-versus-host disease by angiogenesis. Blood. 2017;129(14):2021-2032.
9. Murata H, Janin A, Leboeuf C, et al. Donor-derived cells and human graft-versus-host disease of the skin. Blood. 2007;109(6):2663-2665.

10. Dumler JS, Beschorner WE, Farmer ER, Di Gennaro KA, Saral R, Santos GW. Endothelial-cell injury in cutaneous acute graft-versus-host disease. Am J Pathol. 1989;135(6):1097-1103.
11. Mir E, Palomo M, Rovira M, et al. Endothelial damage is aggravated in acute GvHD and could predict its development. Bone Marrow Transplant. 2017;52(9):1317-1325.
12. Rachakonda SP, Penack O, Dietrich S, et al. Single-nucleotide polymorphisms within the thrombomodulin gene (THBD) predict mortality in patients with graft-versus-host disease. J Clin Oncol. 2014;32(30): 3421-3427.
13. Dietrich S, Falk CS, Benner A, et al. Endothelial vulnerability and endothelial damage are associated with risk of graft-versus-host disease and response to steroid treatment. Biol Blood Marrow Transplant. 2013;19(1):22-27.
14. Andrulis M, Dietrich S, Longerich T, et al. Loss of endothelial thrombomodulin predicts response to steroid therapy and survival in acute intestinal graft-versus-host disease. Haematologica. 2012;97(11):1674-1677.
15. Pihusch V, Rank A, Steber R, et al. Endothelial cell-derived microparticles in allogeneic hematopoietic stem cell recipients. Transplantation. 2006;81(10):1405-1409.
16. Rachakonda SP, Dai H, Penack O, et al. Single nucleotide polymorphisms in CD40L predict endothelial complications and mortality after allogeneic stem-cell transplantation. J Clin Oncol. 2018;36(8): 789-800.
17. Luft T, Benner A, Jodele S, et al. EASIX in patients with acute graft-versus-host disease: a retrospective cohort analysis. Lancet Haematol. 2017;4(9):e414-e423.
18. Schmid PM, Bouazzaoui A, Doser K, et al. Endothelial dysfunction and altered mechanical and structural properties of resistance arteries in a murine model of graft-versus-host disease. Biol Blood Marrow Transplant. 2014;20(10):1493-1500.
19. Lerner KG, Kao GF, Storb R, Buckner CD, Clift RA, Thomas ED. Histopathology of graft-vs.-host reaction (GvHR) in human recipients of marrow from HL-A-matched sibling donors. Transplant Proc. 1974;6(4):367-371.
20. Mertlitz S, Shi Y, Kalupa M, et al. Lymphangiogenesis is a feature of acute GVHD, and VEGFR-3 inhibition protects against experimental GVHD. Blood. 2017;129(13):1865-1875.
21. Riesner K, Kalupa M, Shi Y, Elezkurtaj S, Penack O. A preclinical acute GVHD mouse model based on chemotherapy conditioning and MHC-matched transplantation. Bone Marrow Transplant. 2016;51(3):410-417.
22. Bouazzaoui A, Spacenko E, Mueller G, et al. Steroid treatment alters adhesion molecule and chemokine expression in experimental acute graft-vs.-host disease of the intestinal tract. Exp Hematol. 2011;39(2): 238-249 e231.
23. Toubai T, Rossi C, Tawara I, et al. Murine models of steroid refractory graft-versus-host disease. Sci Rep. 2018;8(1):12475.
24. Beilhack A, Schulz S, Baker J, et al. In vivo analyses of early events in acute graft-versus-host disease reveal sequential infiltration of T-cell subsets. Blood. 2005;106(3): 1113-1122.
25. Radu M, Chernoff J. An in vivo assay to test blood vessel permeability. J Vis Exp. 2013(73):e50062.
26. Brede C, Friedrich M, Jordan-Garrote AL, et al. Mapping immune processes in intact tissues at cellular resolution. J Clin Invest. 2012;122(12):4439-4446.
27. Wertheimer T, Velardi E, Tsai J, et al. Production of BMP4 by endothelial cells is crucial for endogenous thymic regeneration. Sci Immunol. 2018;3(19):eaal2736.
28. Dietrich S, Okun JG, Schmidt K, et al. High pre-transplant serum nitrate levels predict risk of acute steroid-refractory graft-versus-host disease in the absence of statin therapy. Haematologica. 2014;99(3):541-547.
29. Luft T, Dietrich S, Falk C, et al. Steroid-refractory GVHD: T-cell attack within a vulnerable endothelial system. Blood. 2011;118(6):1685-1692.
30. Rotz SJ, Dandoy CE, Davies SM. ST2 and Endothelial injury as a link between GVHD and microangiopathy. N Engl J Med. 2017;376(12):1189-1190.
31. Vander Lugt MT, Braun TM, Hanash S, et al. ST2 as a marker for risk of therapy-resistant graft-versus-host disease and death. N Engl J Med. 2013;369(6):529-539.
32. Balarini CM, Leal MA, Gomes IB, et al. Sildenafil restores endothelial function in the apolipoprotein E knockout mouse. J Transl Med. 2013;11:3.
33. Bivalacqua TJ, Sussan TE, Gebska MA, et al. Sildenafil inhibits superoxide formation and prevents endothelial dysfunction in a mouse model of secondhand smoke induced erectile dysfunction. J Urol. 2009;181(2):899-906.
34. Aksu V, Yuksel V, Chousein S, et al. The effects of sildenafil and n-acetylcysteine on ischemia and reperfusion injury in gastrocnemius muscle and femoral artery endothelium. Vascular. 2015;23(1):21-30.
35. Valatsou A, Briasoulis A, Vogiatzi G, et al. Beneficial effects of sildenafil on tissue perfusion and inflammation in a murine model of limb ischemia and atherosclerosis. Curr Vasc Pharmacol. 2017;15(3):282-287.
36. Fahning BM, Dias AT, Oliveira JP, et al. Sildenafil improves vascular endothelial structure and function in renovascular hypertension. Curr Pharm Biotechnol. 2015;16(9):823-831.
37. McLaughlin K, Lytvyn Y, Luca MC, Liuni A, Gori T, Parker JD. Repeated daily dosing with sildenafil provides sustained protection from endothelial dysfunction caused by ischemia and reperfusion: a human in vivo study. Am J Physiol Heart Circ Physiol. 2014;307(6):H888-894.
38. Yin J, Kukucka M, Hoffmann J, et al. Sildenafil preserves lung endothelial function and prevents pulmonary vascular remodeling in a rat model of diastolic heart failure. Circ Heart Fail. 2011;4(2):198-206.
39. Yaguas K, Bautista R, Quiroz Y, et al. Chronic sildenafil treatment corrects endothelial dysfunction and improves hypertension. Am J Nephrol. 2010;31(4): 283-291.
40. Almici C, Skert C, Bruno B, et al. Circulating endothelial cell count: a reliable marker of endothelial damage in patients undergoing hematopoietic stem cell transplantation. Bone Marrow Transplant. 2017;52(12):1637-1642.
41. Woywodt A, Scheer J, Hambach L, et al. Circulating endothelial cells as a marker of endothelial damage in allogeneic hematopoietic stem cell transplantation. Blood. 2004;103(9):3603-3605.
42. Medinger M, Heim D, Gerull S, et al. Increase of endothelial progenitor cells in acute graft-versus-host disease after allogeneic haematopoietic stem cell transplantation for acute myeloid leukaemia. Leuk Res. 2016;47:22-25.
43. Yan Z, Zeng L, Jia L, Xu S, Ding S. Increased numbers of circulating ECs are associated with systemic GVHD. Int J Lab Hematol. 2011;33(5):507-515.
44. Tatekawa S, Kohno A, Ozeki K, et al. A novel diagnostic and prognostic biomarker panel for endothelial cell damage-related complications in allogeneic transplantation. Biol Blood Marrow Transplant. 2016;22(9):1573-1581.
45. Lindas R, Tvedt TH, Hatfield KJ, Reikvam H, Bruserud O. Preconditioning serum levels of endothelial cell-derived molecules and the risk of posttransplant complications in patients treated with allogeneic stem cell transplantation. J Transplant. 2014;2014:404096.
46. Biedermann BC, Tsakiris DA, Gregor M, Pober JS, Gratwohl A. Combining altered levels of effector transcripts in circulating T cells with a marker of endothelial injury is specific for active graft-versus-host disease. Bone Marrow Transplant. 2003;32(11): 1077-1084.
47. Penack O, Henke E, Suh D, et al. Inhibition of neovascularization to simultaneously ameliorate graft-vs-host disease and decrease tumor growth. J Natl Cancer Inst. 2010;102(12):894-908.
48. Less JR, Skalak TC, Sevick EM, Jain RK. Microvascular architecture in a mammary carcinoma: branching patterns and vessel dimensions. Cancer Res. 1991;51(1):265-273.
49. Huang Y, Goel S, Duda DG, Fukumura D, Jain RK. Vascular normalization as an emerging strategy to enhance cancer immunotherapy. Cancer Res. 2013;73(10): 2943-2948.
50. Tornavaca O, Chia M, Dufton N, et al. ZO-1 controls endothelial adherens junctions, cell-cell tension, angiogenesis, and barrier formation. J Cell Biol. 2015;208(6):821-838.
51. Fanning AS, Little BP, Rahner C, Utepbergenov D, Walther Z, Anderson JM. The unique-5 and -6 motifs of ZO-1 regulate tight junction strand localization and scaffolding properties. Mol Biol Cell. 2007;18(3):721-731.
52. Umeda K, Ikenouchi J, Katahira-Tayama S, et al. ZO-1 and ZO-2 independently determine where claudins are polymerized in tight-junction strand formation. Cell. 2006;126(4):741-754.
53. Reyat JS, Chimen M, Noy PJ, Szyroka J, Rainger GE, Tomlinson MG. ADAM10-interacting tetraspanins Tspan5 and Tspan17 regulate VE-cadherin expression and promote T lymphocyte transmigration. J Immunol. 2017;199(2):666-676.
54. Vockel M, Vestweber D. How T cells trigger the dissociation of the endothelial receptor phosphatase VE-PTP from VE-cadherin. Blood. 2013;122(14):2512-2522.
55. Zhao Y, Ting KK, Li J, et al. Targeting vascular endothelial-cadherin in tumor-associated blood vessels promotes T-cell-mediated immunotherapy. Cancer Res. 2017;77 (16):4434-4447.
56. Schulte D, Kuppers V, Dartsch N, et al. Stabilizing the VE-cadherin-catenin complex blocks leukocyte extravasation and vascular permeability. EMBO J. 2011;30 (20):4157-4170.
57. McHale TM, Garciarena CD, Fagan RP, et

al. Inhibition of vascular endothelial cell leak following Escherichia coli attachment in an experimental model of sepsis. Crit Care Med. 2018;46(8):e805-e810.
58. Han S, Lee SJ, Kim KE, et al. Amelioration of sepsis by TIE2 activation-induced vascular protection. Sci Transl Med. 2016;8(335):335ra355.
59. Wojciak-Stothard B, Tsang LY, Haworth SG. Rac and Rho play opposing roles in the regulation of hypoxia/reoxygenation-induced permeability changes in pulmonary artery endothelial cells. Am J Physiol Lung Cell Mol Physiol. 2005;288(4):L749-760.
60. Dias AT, Cintra AS, Frossard JC, et al. Inhibition of phosphodiesterase 5 restores endothelial function in renovascular hypertension. J Transl Med. 2014;12:250.
61. Chen W, Oberwinkler H, Werner F, et al. Atrial natriuretic peptide-mediated inhibition of microcirculatory endothelial Ca2+ and permeability response to histamine involves cGMP-dependent protein kinase I and TRPC6 channels. Arterioscler Thromb Vasc Biol. 2013;33(9):2121-2129.
62. Guilluy C, Sauzeau V, Rolli-Derkinderen M, et al. Inhibition of RhoA/Rho kinase pathway is involved in the beneficial effect of sildenafil on pulmonary hypertension. Br J Pharmacol. 2005;146(7):1010-1018.
63. Das A, Xi L, Kukreja RC. Phosphodiesterase-5 inhibitor sildenafil preconditions adult cardiac myocytes against necrosis and apoptosis. Essential role of nitric oxide signaling. J Biol Chem. 2005;280(13):12944-12955.
64. Fukumoto S, Koyama H, Hosoi M, et al. Distinct role of cAMP and cGMP in the cell cycle control of vascular smooth muscle cells: cGMP delays cell cycle transition through suppression of cyclin D1 and cyclin-dependent kinase 4 activation. Circ Res. 1999;85(11):985-991.
65. Zeiser R, von Bubnoff N, Butler J, et al. Ruxolitinib for glucocorticoid-refractory acute graft-versus-host disease. N Engl J Med. 2020;382(19):1800-1810.

ARTICLE

An international, multicenter study of intravenous bevacizumab for bleeding in hereditary hemorrhagic telangiectasia: the InHIBIT-Bleed study

Hanny Al-Samkari,[1,2] Raj S. Kasthuri,[3] Joseph G. Parambil,[4] Hasan A. Albitar,[5] Yahya A. Almodallal,[6] Carolina Vázquez,[7] Marcelo M. Serra,[7] Sophie Dupuis-Girod,[8] Craig B. Wilsen,[9] Justin P. McWilliams,[9] Evan H. Fountain,[10] James R. Gossage,[10] Clifford R. Weiss,[11] Muhammad A. Latif,[11] Assaf Issachar,[12] Meir Mei-Zahav,[12] Mary E. Meek,[13] Miles Conrad,[14] Josanna Rodriguez-Lopez,[1,15] David J. Kuter[1,2] and Vivek N. Iyer[16]

[1]Harvard Medical School, Boston, MA, USA; [2]Division of Hematology, Massachusetts General Hospital, Boston, MA, USA; [3]Division of Hematology/Oncology, University of North Carolina at Chapel Hill, Chapel Hill, NC, USA; [4]Respiratory Institute, Cleveland Clinic, Cleveland, OH, USA; [5]Department of Internal Medicine, Mayo Clinic, Rochester, MN, USA; [6]Department of Pediatrics, Mayo Clinic, Rochester, MN, USA; [7]HHT Center Argentina, Department of Internal Medicine, Hospital Italiano de Buenos Aires, Buenos Aires, Argentina; [8]Centre de Référence pour la Maladie de Rendu-Osler, Hospices Civils de Lyon, Lyon, France; [9]Division of Interventional Radiology, Department of Radiology, David Geffen School of Medicine at UCLA, Los Angeles, CA, USA; [10]Division of Pulmonary, Critical Care, and Sleep Medicine, Augusta University, Augusta, GA, USA; [11]Russel H. Morgan Department of Radiology and Radiological Science, Division of Interventional Radiology, Johns Hopkins University School of Medicine, Baltimore, MD, USA; [12]Schneider Children's Medical Center of Israel, Tel Aviv University, Tel Aviv, Israel; [13]Department of Radiology, University of Arkansas for Medical Sciences, Little Rock, AR, USA; [14]Department of Radiology, University of California San Francisco Medical Center, San Francisco, CA, USA; [15]Division of Pulmonary and Critical Care Medicine, Massachusetts General Hospital, Boston, MA, USA and [16]Division of Pulmonary and Critical Care Medicine, Mayo Clinic, Rochester, MN, USA

Ferrata Storti Foundation

Haematologica 2021
Volume 106(8):2161-2169

ABSTRACT

Hereditary hemorrhagic telangiectasia (HHT, Osler-Weber-Rendu disease) is a rare multisystem vascular disorder that causes chronic gastrointestinal bleeding, epistaxis, and severe anemia. Bevacizumab, an anti-vascular endothelial growth factor antibody, may be effective to treat bleeding in HHT. This international, multicenter, retrospective study evaluated the use of systemic bevacizumab to treat HHT-associated bleeding and anemia at 12 HHT treatment centers. Hemoglobin, Epistaxis Severity Score (ESS), red cell units transfused, and intravenous iron infusions before and after treatment were evaluated using paired means testing and mixed-effects linear models. Bevacizumab was given to 238 HHT patients for a median of 12 (range, 1-96) months. Compared with pretreatment, bevacizumab increased mean hemoglobin by 3.2 g/dL (95% confidence interval: 2.9-3.5 g/dL); i.e., from a mean hemoglobin of 8.6 (8.5-8.8) g/dL to 11.8 (11.5-12.1) g/dL; $P<0.0001$) and decreased the ESS by 3.4 (3.2-3.7) points (mean ESS 6.8 [6.6-7.1] *versus* 3.4 [3.2-3.7]; $P<0.0001$) during the first year of treatment. Compared with 6 months before treatment, the number of red blood cell units transfused decreased by 82% (median of 6.0 [interquartile range, 0.0-13.0] units *versus* 0 [0.0-1.0] units; $P<0.0001$) and iron infusions decreased by 70% (median of 6.0 [1.0-18.0] infusions *versus* 1.0 [0.0-4.0] infusions, $P<0.0001$) during the first 6 months of bevacizumab treatment. Outcomes were similar regardless of the underlying pathogenic mutation. Following initial induction infusions, continuous/scheduled bevacizumab maintenance achieved higher hemoglobin and lower ESS than intermittent/as-needed maintenance but with more drug exposure. Bevacizumab was well tolerated: hypertension, fatigue, and proteinuria were the most common adverse events. Venous thromboembolism occurred in 2% of patients. In conclusion, systemic bevacizumab was safe and effective for managing chronic bleeding and anemia in HHT.

Correspondence:

HANNY AL-SAMKARI
hal-samkari@mgh.harvard.edu

Received: June 4 2020.

Accepted: June 30, 2020.

Pre-published: July 16, 2020.

https://doi.org/10.3324/haematol.2020.261859

Introduction

Hereditary hemorrhagic telangiectasia (HHT, Osler-Weber-Rendu disease) is an autosomal dominant multisystem disease of disordered angiogenesis.[1] It occurs due to mutations in genes encoding proteins that mediate signaling via the transforming growth factor-β superfamily.[2] The vast majority of patients with HHT have mutations in endoglin (*ENG*) or activin receptor-like kinase 1 (*ACVRL1/ALK1*), resulting in angiogenic dysregulation, formation of telangiectasias on mucocutaneous surfaces, local hyperfibrinolysis within telangiectasias, and development of arteriovenous malformations in visceral organs.[3-5] Fragile mucocutaneous telangiectasias in the nasal mucosa (>95% of patients) and throughout the gastrointestinal tract (75% of patients) lead to severe, recurrent epistaxis and chronic gastrointestinal bleeding, with consequent severe iron deficiency anemia that is often transfusion-dependent.[6-8] Severe recurrent epistaxis, which may last for hours per day, also results in psychosocial morbidity, social isolation, and challenges with employment, travel, and routine daily activities.[9] Visceral arteriovenous malformations may involve the liver, lung, and central nervous system and can result in severe complications including high-output cardiac failure, liver failure, pulmonary hemorrhage, stroke and intracerebral hemorrhage.[10] Thus, chronic bleeding and visceral arteriovenous malformations in HHT are associated with considerable morbidity and mortality.[10,11]

With a prevalence of one case in 5,000 people, HHT is classified as a rare bleeding disorder by the Centers for Disease Control and Prevention, but is actually the second most common hereditary bleeding disorder in the USA and worldwide (following only von Willebrand disease in prevalence). Despite this, there are no United States Food and Drug Administration or European Medicines Agency-approved treatments for HHT-associated bleeding. The current standard of care for bleeding in HHT includes supportive red blood cell (RBC) transfusion and intravenous iron infusion to treat anemia and local nasal and endoscopic hemostatic procedures to reduce bleeding symptoms. Systemic non-specific hemostatic therapies, such as antifibrinolytic agents, are of limited benefit.[12] Most importantly, none of these modalities addresses the underlying pro-angiogenic pathophysiology, and the natural history of HHT in many patients is of unremitting telangiectasia formation and progressively worsening bleeding over the lifespan.[9,13-15]

Although several angiogenic proteins are dysregulated in HHT,[5,16] the raised level of vascular endothelial growth factor (VEGF)[17] is of particular clinical interest due to the availability of targeted anti-VEGF agents. Bevacizumab (Avastin®), a recombinant, humanized monoclonal IgG1 antibody that binds to and neutralizes circulating VEGF, is one such agent and is widely used to treat malignancies and age-related macular degeneration.[18,19] After promising case reports were published describing successful use of systemic bevacizumab to manage bleeding and anemia in HHT,[20-22] several HHT Centers of Excellence worldwide began using this agent off-label to treat HHT patients, given the profound unmet clinical need. Currently, data describing effectiveness and safety of systemic bevacizumab to treat chronic bleeding and anemia in HHT is limited to case reports and small, retrospective, single-center case series.[23-28] The International HHT Intravenous Bevacizumab Investigative Team study of Bleeding (InHIBIT-Bleed) was therefore designed as an international collaboration of 12 HHT centers seeking to better define the safety and effectiveness of systemic bevacizumab in the treatment of moderate-to-severe HHT-associated bleeding.

Methods

Patients and data collection

This study was approved by the Institutional Review Board of Partners Healthcare (approval 2016P002753/PHS). Nine centers in the USA and one center each in Argentina, Israel, and France participated in the study. All patients aged >18 years treated with systemic (intravenous) bevacizumab for HHT-associated bleeding (epistaxis, gastrointestinal bleeding, or both) from January 1, 2011 until May 1, 2019 were identified at each participating institution. General criteria used by centers to offer systemic bevacizumab for HHT-associated bleeding are detailed in *Online Supplementary Table S1*. Additional data collection information is given in the *Online Supplementary Methods*.

Effectiveness measures

Hemoglobin

Anemia was defined as a baseline hemoglobin (Hb) <11 g/dL regardless of gender. Baseline hemoglobin was calculated as the average of all measured hemoglobin values in the 6 months prior to bevacizumab initiation (at least 2 values required) and compared with mean on-treatment hemoglobin (mean of values collected at 3, 6, 9, and 12 months depending on treatment duration).

Epistaxis Severity Score

Background information regarding the Epistaxis Severity Score (ESS) is provided in the *Online Supplementary Methods*. The baseline ESS at initiation of bevacizumab was compared with the mean on-treatment ESS (mean of values collected at 3, 6, 9, and 12 months depending on treatment duration).

Red blood cell transfusion and iron infusion

The number of red blood cell (RBC) units transfused in the first 6 months on treatment was compared with the number of units transfused in the 6 months prior to treatment. Additionally, events in the second 6 months on treatment were compared with those in the first 6 months on treatment to evaluate ongoing response. The same analysis was performed for the number of intravenous iron infusions administered.

To be included in effectiveness analyses, patients needed to receive ≥3 months of treatment (Hb and ESS) or ≥6 months of treatment (RBC transfusion and iron infusion).

Subgroup analyses

Subgroup analyses for each effectiveness outcome were performed by genotype (*ENG vs. ACVRL1* mutation) as well as by maintenance dosing method (continuous *vs.* intermittent bevacizumab maintenance following an initial series of induction infusions).

Receipt of concurrent bleeding and anemia-directed therapies

Rates of freedom from hemostatic procedures and medical treatments (antifibrinolytic or erythropoiesis-stimulating agents) in the year following bevacizumab initiation were calculated, and effectiveness outcomes in patients who received these con-

current HHT-directed therapies were compared to those in patients who did not receive concurrent HHT-directed therapies.

Safety analysis

Treatment-emergent adverse events (TEAE) were defined according to Common Terminology Criteria for Adverse Events v. 5.0 (National Cancer Institute) and recorded. To evaluate any impact of longer-term treatment on TEAE incidence, the number of TEAE per patient in those treated for 2 years or longer was compared with the number of TEAE per patient in those treated for less than 2 years.

Statistical analysis

Baseline hemoglobin concentration and ESS were compared with on-treatment mean values using the paired *t*-test. Pretreatment RBC transfusion and iron infusion requirements were compared with on-treatment values using the Wilcoxon signed-rank test. To estimate the change in each outcome measure over time on treatment utilizing a method robust in the setting of missing data, a mixed effects linear model with a random intercept was also used for each outcome measure. Additional details regarding statistics, including analysis of subgroups, are detailed in the *Online Supplementary Methods*.

Results

Patients' characteristics

Two hundred fifty-seven HHT patients were treated with systemic bevacizumab for epistaxis, gastrointestinal bleeding, or both for the purpose of alleviating bleeding and consequent iron-deficiency anemia at the 12 participating centers during the study period. After 19 patients had been excluded because of inadequate chart data (missing baseline data or incomplete bevacizumab dosing information), 238 patients were included in the data analysis. Table 1 lists the patients' baseline characteristics. Patients were treated for a median of 12 (range, 1-96) months, receiving a median of 11 (range, 1-74) infusions of intravenous bevacizumab. This totaled 343.9 patient-years of systemic bevacizumab treatment of HHT-associated bleeding in the cohort.

Bevacizumab induction and maintenance dosing

Specific dosing protocols were institution-dependent. Two hundred twenty-one patients (93%) began treatment by receiving four to six induction infusions of bevacizumab 5 mg/kg administered every 2 weeks; 46 (19%)

Table 1. Baseline characteristics of 238 patients with hereditary hemorrhagic telangiectasia treated with bevacizumab for chronic bleeding and iron deficiency anemia.

Characteristic	Value
Age (years), mean (range)	63 (29-91)
% Female	62
% Definite HHT by Curaçao criteria[a]	97
Genetic mutation (HHT subtype)[a]	*ENG* (HHT-1): 52 (22%) *ACVRL1* (HHT-2): 92 (39%) *SMAD4* (HHT-JPS): 4 (2%) Other pathogenic HHT mutation: 6 (3%) Mutation not identified: 4 (2%) Genetic testing not done: 80 (34%)
Baseline GI AVM and prior treatments	Known upper GI AVM: 148 (62%) Known lower GI AVM: 47 (20%) Received local endoscopic hemostatic treatments: 119 (50%)
Baseline comorbidities relevant to bevacizumab treatment	Hypertension: 67 (29%) Chronic kidney disease: 14 (6%) Diabetes mellitus: 20 (9%) High-output heart failure: 32 (14%) Prior venous thromboembolism: 27 (11%)
Primary bleeding source	Epistaxis: 99 (42%) GI bleeding: 46 (19%) Both epistaxis and GI bleeding: 93 (39%)
Mean baseline hemoglobin (95% CI)	Treated for anemia (baseline Hb <11) (N=197): 8.6 g/dL (8.4, 8.8) All patients (N=232): 9.1 g/dL (8.9, 9.4)
Mean baseline epistaxis severity score (95% CI)	Treated for epistaxis (N=175): 6.75 (6.52, 6.99) All patients (N=213): 5.92 (5.60, 6.24)
Prior local hemostatic treatments for epistaxis	Any treatment: 182 (77%) Laser cautery: 118 (50%) Electrical or chemical cautery: 112 (47%) Nasal septodermoplasty: 38 (16%) Nasal sclerotherapy: 58 (24%) Nasal embolization: 21 (9%) Bevacizumab nasal spray: 26 (10%) Septal bevacizumab injection: 23 (9%) Nasal closure (Young's procedure): 9 (4%)
Prior nasal septum perforation (%)	32 (13%)

[a]The Curaçao criteria are used to establish the diagnosis of hereditary hemorrhagic telengiectasia (HHT); the presence of three or four out of four criteria denotes "definite HHT", while the presence of two out of four criteria signifies "possible HHT". Genetic testing is not required for a diagnosis of HHT but is done to identify HHT subtype. 95% CI: 95% confidence interval; GI, gastrointestinal. AVM, arteriovenous malformation. JPS, juvenile polyposis syndrome.

also received an additional four induction infusions administered every 4 weeks. Induction courses typically lasted 2-4 months but never extended beyond 6 months. A total of 181 patients received maintenance treatment, which was defined as additional bevacizumab doses administered to prevent or treat recurrent bleeding after completion of the initial induction infusion course. These maintenance doses were administered using one of two different protocols. The majority of patients (n=136) received continuous maintenance, defined as bevacizumab administered on a regular schedule every 4-12 weeks. The remainder (n=45) received intermittent maintenance, defined as retreatment only following recurrence or worsening of bleeding symptoms or anemia, with one to four doses administered every 2 weeks once the need for maintenance was triggered. Ninety-two percent of patients were given maintenance doses of 5 mg/kg per infusion (regardless of maintenance schedule) but doses of 1, 2.5, 3, and 7.5 mg/kg were also used occasionally. Compared with the relatively universal induction dose intensity of 10.0 mg/kg/month, mean maintenance dose intensity was 4.0 mg/kg/month in patients receiving continuous maintenance and 3.0 mg/kg/month in patients receiving intermittent maintenance.

Effect of bevacizumab on hemoglobin concentration

Of the 197 anemic (Hb <11 g/dL) patients treated, 185 patients had been treated for ≥3 months and were included in the hemoglobin analysis. Mean hemoglobin increased by 3.2 g/dL (95% confidence interval [95% CI]: 2.9-3.4, P<0.0001) from baseline following bevacizumab treatment (Table 2). In the evaluation of on-treatment mean hemoglobin, freedom from anemia (Hb ≥11 g/dL) was observed in 67% (n=123/185) of patients. In the evaluation of hemoglobin values at each time point, freedom from anemia was observed in 64% of patients at 3 months, 73% at 6 months, 76% at 9 months, and 71% at 12 months (Figure 1A). The change in hemoglobin concentration from baseline to on-treatment ranged from a 1.0 g/dL reduction to a 7.9 g/dL increase. A mixed linear model estimated the improvement in mean hemoglobin at between 3.0 g/dL (95% CI: 2.7-3.3 g/dL; P<0.0001) and 3.4 g/dL (95% CI: 3.1-3.7 g/dL; P<0.0001) at each time point, stable over the course of treatment (*Online Supplementary Table S2, Online Supplementary Figure S1A*).

Effect of bevacizumab on Epistaxis Severity Score

Of the 175 patients treated for epistaxis with complete ESS data available, 146 patients had been treated for ≥3 months and were included in the ESS analysis. Mean ESS decreased by 3.37 points (95% CI: -3.69 to -3.05; P<0.0001) from baseline following bevacizumab treatment (Table 2). Change in ESS from baseline to on-treatment ranged from a 1.92-point increase to a 10-point reduction. A clinically meaningful reduction in epistaxis (ESS decrease of ≥0.71 post-treatment) was seen in 92% (n=132/146) of patients. The ESS reduction was evident by 3 months (Figure 1B). A mixed linear model estimated the decrease in mean ESS to be between -2.96 (95% CI: -3.26 to -2.66; P<0.0001) and -3.73 (95% CI: -4.05 to -3.43; P<0.0001) at each time point, stable over the course of treatment (*Online Supplementary Table S2, Online Supplementary Figure S1B*).

Effect of bevacizumab on red blood cell transfusion

All patients

A total of 191 patients who had been treated for ≥6 months had complete RBC transfusion data available and were included in the RBC transfusion analysis. In analysis of all included patients (those who required RBC transfusion in the 6 months pretreatment and those who did not), the median number of RBC units transfused

Table 2. Impact of bevacizumab on hemoglobin, Epistaxis Severity Score, red blood cell transfusions, and iron infusions over the first year of treatment.

Outcome	Hemoglobin and Epistaxis Severity Score						
	Baseline	3 months	6 months	9 months	12 months	Mean on treatment	Baseline *vs.* mean on treatment, mean difference (95% CI)
Hemoglobin (g/dL), mean (95% CI), baseline anemia (Hb<11 g/dL) (n=185)	8.6 (8.5, 8.8)	11.6 (11.3, 11.9)	12.1 (11.8, 12.4)	12.0 (11.7, 12.4)	12.1 (11.7, 12.4)	11.8 (11.5, 12.1)	+3.2 (2.9, 3.4) P<0.0001*
Epistaxis Severity Score, mean (95% CI), treated for epistaxis (n=146)	6.81 (6.56, 7.06)	3.84 (3.49, 4.18)	3.02 (2.73, 3.31)	3.07 (2.70, 3.45)	3.22 (2.81, 3.62)	3.44 (3.17, 3.71)	-3.37 (-3.69, -3.05) P<0.0001*

Outcome	RBC transfusion and iron infusion			
	6 months pretreatment	First 6 months on treatment	Second 6 months on treatment	Pretreatment vs. on treatment, median difference (95% CI)
RBC transfusions, units, median (interquartile range) (N=191)	6.0 (0.0-13.0)	0.0 (0.0-2.0)	0.0 (0.0-0.0)	6 months pretreatment *vs.* 1st 6 months on treatment: -4.0 (-6.0, -3.0), P<0.0001† 1st 6 months on treatment *vs.* 2nd 6 months on treatment: 0.0 (0.0, 0.0), P=0.0005†
Iron infusions, median (interquartile range) (N=183)	6.0 (1.0-18.0)	1.0 (0.0-4.0)	0.0 (0.0-2.0)	6 months pretreatment *vs.* 1st 6 months on treatment: -4.0 (-6.0, -1.0), P<0.0001† 1st 6 months on treatment *vs.* 2nd 6 months on treatment: 0.0 (0.0, 0.0), P<0.0001†

*By a paired *t*-test. Normality for hemoglobin and Epistaxis Severity Score data confirmed with the D'Agostino and Pearson test. †By the Wilcoxon signed-rank test. 95% CI: 95% confidence interval; ESS: Epistaxis Severity Score; RBC: red blood cell.

decreased from 6.0 (interquartile range [IQR], 0.0-13.0) in the 6 months pretreatment to 0.0 (IQR, 0.0-1.0) in the first 6 months after treatment (P<0.0001) (Table 2). This improvement was maintained into the second 6 months of bevacizumab treatment (median of 0.0 units, IQR 0.0-0.0; P=0.0005). The findings of a mixed linear model were similar (*Online Supplementary Table S2*, *Online Supplementary Figure S1C*).

Patients requiring prior red blood cell transfusion

In an analysis of only those patients who required RBC transfusion in the 6 months prior to treatment (n=137), the median number of RBC units transfused decreased from 9.0 (IQR, 5.0-16.0) in the 6 months before treatment to 0.0 (IQR, 0.0-2.0) in the first 6 months after treatment (P<0.0001); 80/137 patients (58%), were RBC transfusion-free. There was maintained and continued reduction into the second 6 months of bevacizumab treatment (median of 0.0 units, IQR 0.0-0.0; P=0.0005), with 97/121 (80%) being RBC transfusion-free (Figure 1C). The decline in RBC transfusion requirements was observed regardless of baseline disease severity (Figure 2A).

Effect of bevacizumab on iron infusion

All patients

A total of 183 patients who had been treated for ≥6 months had complete iron infusion data available and were included in the iron infusion analysis. In the analysis of all included patients (those who required iron infusion in the 6 months prior to treatment and those who did not), the median number of iron infusions decreased from 6.0 (IQR, 1.0-18.0) in the 6 months before treatment to 1.0 (IQR, 0.0-4.0) in the first 6 months after treatment (P<0.0001) (Table 2). This improvement continued into the second 6 months of bevacizumab treatment (median of 0.0 infusions, IQR 0.0-2.0; P<0.0001). The findings of a mixed linear model were similar (*Online Supplementary Table S2*, *Online Supplementary Figure S1D*).

Patients requiring prior iron infusion

In the analysis of only those patients who received iron infusion in the 6 months prior to treatment (n=155), median number of iron infusions decreased from 8.0 (IQR, 3.0-20.0) in the 6 months before treatment to 2.0 (IQR, 0.0-5.0) in the first 6 months after treatment (P<0.0001); 48/155 (31%)

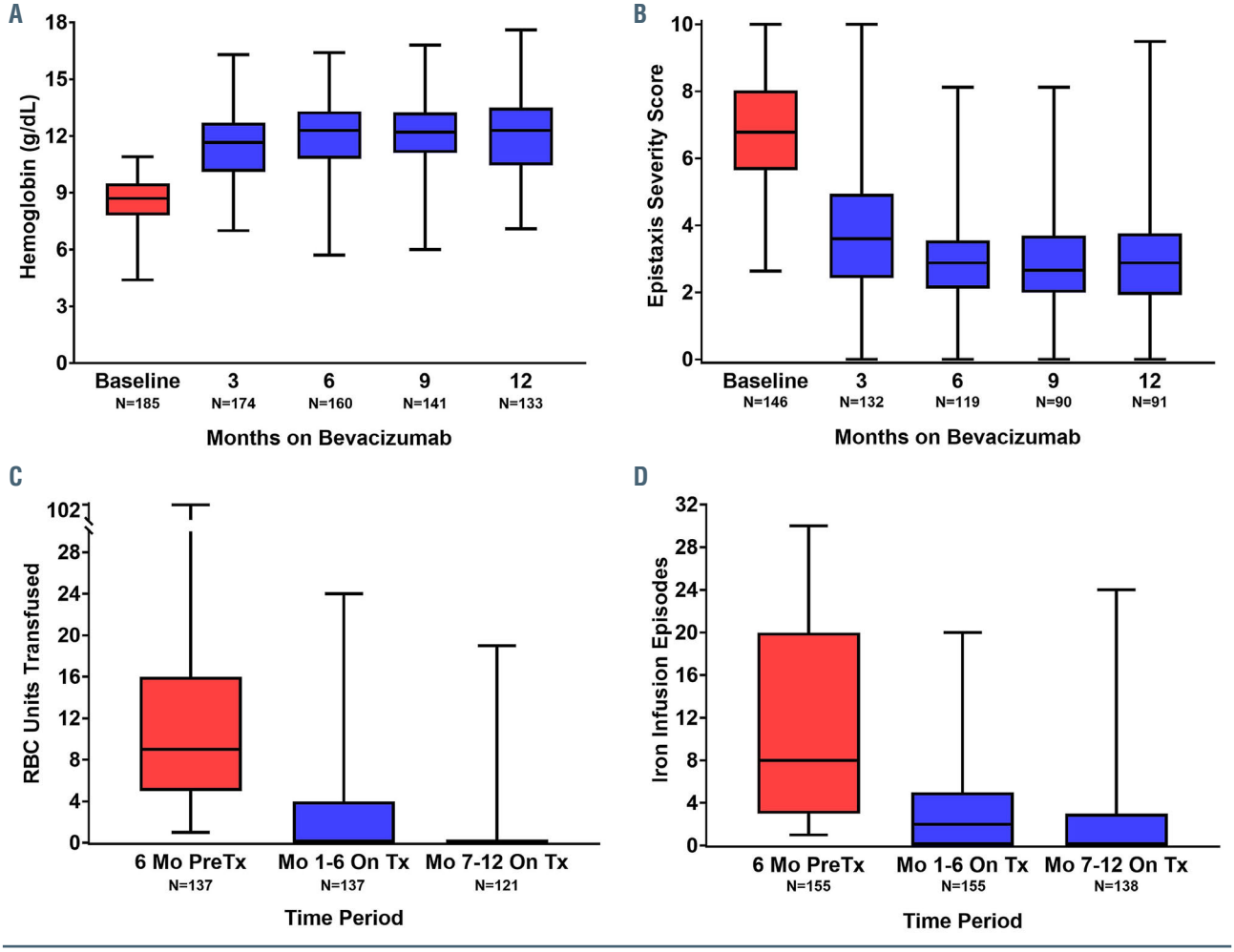

Figure 1. Box-and-whisker plots showing the effect of intravenous bevacizumab on hematologic parameters and epistaxis severity. A box represents the median and interquartile range and tails represent minimum and maximum values. Numbers at each time-point reflect the number of hereditary hemorrhagic telangiectasia (HHT) patients in a given analysis treated for at least that duration with complete data. (A) Effect on hemoglobin in HHT patients with baseline anemia (n=185). (B) Effect on Epistaxis Severity Score in patients treated for epistaxis (n=146). (C) Effect on red blood cell (RBC) transfusions in patients receiving transfusion in the 6 months prior to bevacizumab initiation (n=137). (D) Effect on iron infusion events in patients receiving intravenous iron in the 6 months prior to bevacizumab initiation (n=155). RBC: red blood cell; Mo: months; Tx: treatment.

patients were iron infusion-free. There was a maintained and continued reduction into the second 6 months of bevacizumab treatment (median of 0.0 units, IQR 0.0-3.0), with 84/138 (61%) patients being iron infusion-free (Figure 1D). The decline in iron infusion requirements was observed regardless of baseline disease severity (Figure 2B).

Subgroup analysis by genotype

There were no significant differences between baseline hematologic parameters or effect of bevacizumab treatment on these parameters between patients with *ENG* and *ACVRL1* mutations (*Online Supplementary Table S3*).

Subgroup analysis by maintenance dosing strategy

As compared with patients receiving continuous scheduled bevacizumab maintenance, those receiving intermittent (as-needed) bevacizumab maintenance had a lower mean hemoglobin (10.8 g/dL *vs.* 12.3 g/dL; P=0.0002) and higher ESS (4.96 *vs.* 2.88; P<0.0001) during the second 6 months of bevacizumab treatment (*Online Supplementary Table S4*). There were no significant differences in iron infusions or RBC transfusions between the two groups.

Use of concurrent therapies to treat hereditary hemorrhagic telengiectasia-associated bleeding

Fifty-three patients (22%) received one (39 patients) or more (14 patients) local hemostatic procedures to treat epistaxis (41 patients, 17%), gastrointestinal bleeding (12 patients, 5%), or both (1 patient) in the first year after initiating bevacizumab. Thirty-three patients (14%) received antifibrinolytic therapy and one patient received an erythropoiesis-stimulating agent during the first year after initiating bevacizumab. In total, 73 patients (31%) did receive and 165 patients (69%) did not receive any of these therapies.

Patients receiving concurrent therapies were similar at baseline to those not receiving them, except for a slightly higher mean ESS (*Online Supplementary Table S5*). On bevacizumab treatment, patients receiving concurrent treatments for HHT-associated bleeding had slightly lower on-treatment mean hemoglobin and slightly higher on-treatment mean ESS, median number of RBC transfusions, and median number of iron infusions than those not receiving concurrent treatments (*Online Supplementary Table S5*).

Safety analysis

The safety analysis included 232 patients with complete and continuous chart data available over the duration of bevacizumab treatment, totaling 340.1 patient-years at risk of bevacizumab administration. TEAE possibly or likely related to bevacizumab treatment are summarized in Table 3. The only TEAE reported in >1% of patients were hypertension (18%), fatigue (10%), proteinuria (9%), myalgia and/or arthralgia (6%), headache (4%), and venous thromboembolism (VTE, 2%). Overall, 88 patients (38%) experienced at least one TEAE possibly or likely related to beva-

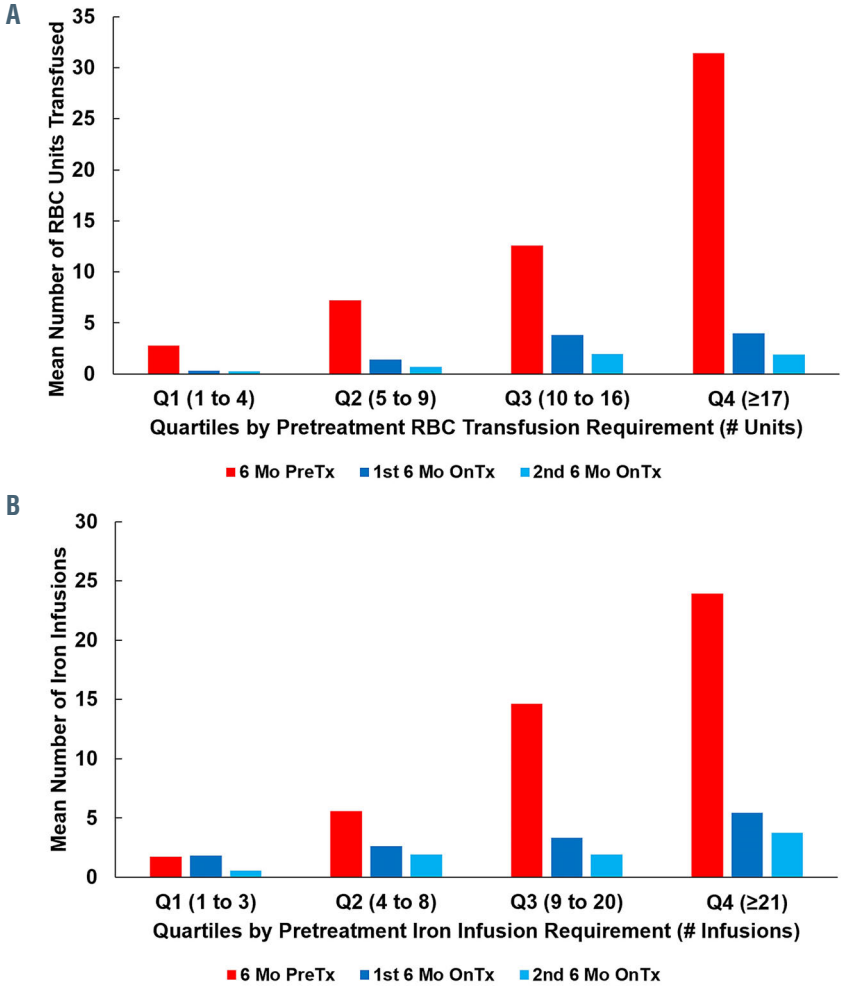

Figure 2. Red blood cell transfusions and iron infusions pretreatment and on-bevacizumab treatment by hematologic support requirements in the 6 months prior to bevacizumab initiation. (A) All patients requiring red blood cell (RBC) transfusion before treatment (n=137) were divided into quartiles (Q1-Q4) according to their pretreatment RBC transfusion requirements. Reductions in RBC transfusions were observed following bevacizumab treatment regardless of the pretreatment disease severity. (B) All patients requiring iron infusion pretreatment (n=155) were divided into quartiles according to their pretreatment iron infusion requirements. Reductions in iron infusions were observed following bevacizumab treatment regardless of the pretreatment disease severity. Mo: months; PreTx, pretreatment; OnTx, on treatment.

cizumab. There were no fatal TEAE. The TEAE rate was slightly higher in patients receiving intermittent maintenance (51%) than in those receiving continuous maintenance (32%). There was no significant difference in number of reported TEAE in patients with long-term exposure to bevacizumab (≥2 years) and those with shorter-term exposure (<2 years) with a mean of 0.57 versus 0.53 TEAE per patient, respectively (P=0.80, Mann-Whitney U test).

The rate of VTE in HHT patients receiving bevacizumab was 1.5 events per 100 patient-years at risk. *Online Supplementary Table S6* shows the venous thromboembolic events occurring in the cohort of patients.

Bevacizumab discontinuation

Twelve patients (5%) discontinued bevacizumab treatment because of adverse events. *Online Supplementary Table S7* describes the adverse events prompting treatment discontinuation. Eleven patients (5%) discontinued bevacizumab because of inadequate treatment effect. Discontinuation due to excessive financial cost for patients occurred in two cases (1%).

Discussion

We present a large, international, multicenter study of systemic bevacizumab treatment of HHT-associated bleeding, observing striking improvements in bleeding and anemia with bevacizumab treatment (Figure 1, *Online Supplementary Figure S1*). Historically, reports on bevacizumab treatment for HHT-related bleeding have been limited to single case reports and small cohorts from individual treatment centers. Before the present study, the largest study of systemic bevacizumab for bleeding and anemia in HHT, evaluating critical hematologic outcomes such as hemoglobin, blood transfusion and iron infusion, was a 13-patient case series.[23]

Table 3. Treatment-emergent adverse events (TEAE) identified by treating clinicians as likely or possibly due to bevacizumab. TEAE were evaluable in 232 patients.

TEAE	Number of patients (%)
Hypertension (new-onset or worse from baseline)	41 (18%)[a]
Fatigue	23 (10%)
Proteinuria	21 (9%)[b]
Myalgia and/or arthralgia	14 (6%)
Headache	9 (4%)
Venous thromboembolism	5 (2%)
Transaminase/alkaline phosphatase elevation	3 (1%)
Rash	3 (1%)
Abdominal pain/gastrointestinal upset	3 (1%)
Lightheadedness	2 (1%)
Dyspnea	2 (1%)
Hoarseness	2 (1%)
Bone marrow suppression	2 (1%)
Other[c]	7 (3%)

[a]26 patients with new-onset hypertension and 15 patients with hypertension worsened from baseline; [b]Occurred in one patient with baseline chronic kidney disease and three patients with baseline diabetes mellitus. [c]Includes one report each of lower extremity edema, worsened epistaxis, diarrhea, lower extremity venous ulceration, poor wound healing, non-cardioembolic stroke, and *Staphylococcus aureus* skin infection.

We found that bevacizumab was effective at reducing HHT-associated bleeding regardless of the patients' genotype, with an improvement in mean hemoglobin of 3.2 g/dL and resolution of anemia in two-thirds of patients. The severity of epistaxis also declined sharply, with a drop in mean ESS of 3.37 points, nearly five times the minimal clinically-important difference of 0.71 for this well-validated clinical bleeding score.[29] Concurrent with the improvements in hemoglobin, RBC transfusions and iron infusions dropped precipitously: 80% and 61% of patients previously requiring RBC transfusions and iron infusions, respectively, were liberated entirely from these hematologic support modalities after 6 months of treatment. Improvement was observed irrespective of baseline bleeding or anemia severity and included the most severely afflicted patients (Figure 2). Similar improvement was observed regardless of the underlying pathogenic mutation (*Online Supplementary Table S3*). Most patients did not receive any additional concurrent treatments to manage HHT-associated bleeding once on bevacizumab, and outcomes of the patients who did were actually slightly worse than those who did not (*Online Supplementary Table S5*). This is likely reflective of less improvement with bevacizumab in these patients prompting the need for additional therapies. The fact that patients not receiving any other bleeding-directed treatments had such significant improvement in hematologic parameters with bevacizumab initiation increases our confidence in the relationship between bevacizumab treatment and the dramatic improvement observed in these parameters.

The effectiveness observed with systemic bevacizumab treatment in this study is considerably better than that found for other systemic agents evaluated for HHT-associated bleeding.[30] Small randomized studies of tranexamic acid *versus* placebo suggest mild to moderate improvements in epistaxis severity but no improvement in hemoglobin with the active treatment.[12,31] A small randomized study of oral estrogen compared with placebo found no significant improvement in epistaxis.[32] Topical nasal pharmacotherapy has been similarly disappointing, with randomized studies of topical timolol, estrogen, and tranexamic acid all showing no difference in the comparison with placebo.[33,34] Bevacizumab via topical nasal spray has also been evaluated, with no improvement noted in epistaxis severity in the comparison with placebo.[33,35] Therefore, given the lack of other effective options and the continued lack of any Food and Drug Administration-approved treatment, our findings suggest it may be appropriate to consider systemic bevacizumab in patients with moderate-to-severe HHT-associated bleeding (*Online Supplementary Table S1*) without contraindications. This may be particularly true for patients with significant gastrointestinal bleeding, who constituted over half the cohort in the present study, for whom there are no studies of other pharmacological interventions. Oral anti-angiogenics such as pomalidomide[36] and pazopanib[37,38] are additionally under investigation for treatment of HHT-associated bleeding. Should these agents demonstrate efficacy, head-to-head studies comparing them with bevacizumab will be needed.

While initial bevacizumab induction treatment schedules were quite similar between different centers, maintenance strategies varied considerably, with some centers employing continuous scheduled maintenance and others opting for an intermittent, as-needed approach to minimize overall bevacizumab exposure. Both approaches were effective, but intermittent maintenance (which employed 75% of the

overall bevacizumab dose intensity used in continuous maintenance) resulted in significantly lower mean hemoglobin and higher mean ESS than continuous maintenance (*Online Supplementary Table S4*). This is not unexpected given that recurrence of bleeding and/or anemia are the triggers for re-treatment with an intermittent maintenance approach. It is unclear whether the financial savings of administering less drug in the intermittent maintenance approach offsets the potential disadvantages. Additionally, although patients in this study were treated for up to 8 years without any complications specifically attributed to extended-duration treatment, the impact of indefinite bevacizumab exposure in HHT (either positive or negative) is not known. How maintenance strategy and overall dose intensity could affect this impact is therefore also unknown.

Bevacizumab was well-tolerated overall, with hypertension, proteinuria, fatigue, and myalgia/arthralgia being the most common TEAE, consistent with prior reports in HHT patients.[23-27,39-42] Only 5% of patients discontinued treatment because of adverse events. An understanding of the adverse event profile of single-agent systemic bevacizumab in HHT patients is critical, given that the vast majority of prior bevacizumab studies added bevacizumab (typically at 2-3 times the common 5 mg/kg dose used in this study) to multiagent cytotoxic chemotherapy regimens and administered this combination to patients with metastatic cancer. Therefore, the adverse event rates described in the prescribing information, such as the relatively high rates of serious events including VTE or intestinal perforation, are not reflective of single-agent bevacizumab use in HHT patients. This point is highlighted by the VTE rate in this study of 2%, with a median duration of bevacizumab exposure considerably longer than that of most cancer studies finding VTE rates in the 5-10% range. Furthermore, two out of five of the VTE observed were provoked events immediately following major joint replacement surgery (*Online Supplementary Table S6*). We observed no central nervous system bleeding, hemoptysis, pulmonary hemorrhage, or intestinal perforation. Additionally, while anticoagulation in HHT patients can be very challenging and dramatically exacerbate bleeding, patients with VTE in this study receiving anticoagulation did well with concurrent bevacizumab treatment without significantly increased bleeding (*Online Supplementary Table S6*).

Our study has several limitations consistent with its retrospective nature. These include center variability in the management of HHT and variability in the use and availability of adjunctive measures to control bleeding. The lack of randomization allows for the presence of confounding factors that could have resulted in clinical improvement independent of bevacizumab use. However, the fact that significant improvements in all outcome measures occurred following initiation of bevacizumab treatment increases our confidence that bevacizumab was the cause of the clinical improvements. Additionally, we analyzed known confounders such as concurrent use of antifibrinolytics and receipt of local hemostatic procedures and found no significant difference in outcomes between the two groups. To minimize the impact of patient heterogeneity in this disease, we employed a pre/post-treatment analytical design with paired analyses such that each patient served as his or her own internal control in our effectiveness analyses. Adverse event reporting was limited by the retrospective design, but we expect it is unlikely that any serious adverse events would not have been appropriately documented. Finally, our study evaluated number of iron infusion events, not exact milligrams of elemental iron infused. Although less precise, we believe that the observed reduction in iron infusions to be valid for two reasons: the median number of iron infusions went from six before treatment to zero after treatment (and the amount of elemental iron in 0 iron infusions is none) and more importantly, the reduction in iron infusions paralleled the dramatic reduction in RBC transfusions.

In conclusion, we observed that systemic bevacizumab was effective in the management of severe HHT-related epistaxis and gastrointestinal bleeding in a cohort of 238 HHT patients. While data from large, randomized prospective studies are needed to confirm these findings, in this large observational study, bevacizumab was associated with significant improvements in hemoglobin and ESS, along with significant reductions in the need for RBC transfusion and intravenous iron infusion. Improvement was similar regardless of the underlying pathogenic mutation. Following an initial sequence of induction treatments, continuous scheduled maintenance therapy and intermittent as-needed maintenance therapy were both reasonable to maintain treatment effect. Hypertension, fatigue, proteinuria, and myalgia/arthralgia were the most common TEAE; VTE and treatment discontinuation for adverse events were rare, occurring in 2% and 5% of patients, respectively.

Disclosures

HA-S has provided consultancy services for Agios, Argenx, Rigel, Sobi, and Dova, and received research funding from Agios, Dova and Amgen. CRW has acted as a consultant for Medtronic and BTG/BSCI; and has received grant support from Medtronic, BTG/BSCI and Siemens Healthcare. MC: has provided consultancy services for Medtronic. DJK has received research funding from Protalex, Bristol-Myers Squibb, Rigel, Bioverativ, Agios, Syntimmune, Principia and Alnylam); and has acted as a consultant for ONO, Pfizer, 3SBios, Eisai, GlaxoSmithKline, Genzyme, Shire, Amgen, Shionogi, Rigel, Syntimmune, MedImmune, Novartis, Alexion, Bioverativ, Argenx, Zafgen, Fujifilm, Principia, Kyowa Kirin, Takeda and the Platelet Disorders Support Group. RSK, JGP, HAA, YAA, CV, MMS, SD-G, CBW, JPM, EHF, JRG, VNI, MAL, AI, MM-Z, MEM and JR-L have no conflicts of interest to disclose.

Contributions

HA-S wrote the first draft of the manuscript and contributed to the study design, data collection, data analysis, creation of tables and figures, critical revision of the manuscript, and its final approval; VNI contributed to the study design, data collection, critical revision of the manuscript, and its final approval; JGP, HAA, YAA, CV, MMS, SD-G, CBW, JPM, EHF, JRG, CBW, MAL, AI, MM-Z, MEM, MC, JR-L, DJK and RSK contributed to data collection, critical revision of the manuscript, and its final approval.

Acknowledgments

HA-S is the recipient of the National Hemophilia Foundation-Shire Clinical Fellowship Award, the Harvard KL2/Catalyst Medical Research Investigator Training Award, and the American Society of Hematology Scholar Award.

References

1. Fuchizaki U, Miyamori H, Kitagawa S, Kaneko S, Kobayashi K. Hereditary haemorrhagic telangiectasia (Rendu-Osler-Weber disease). Lancet. 2003;362(9394):1490-1494.
2. Kritharis A, Al-Samkari H, Kuter DJ. Hereditary hemorrhagic telangiectasia: diagnosis and management from the hematologist's perspective. Haematologica. 2018;103 (9):1433-1443.
3. Kwaan HC, Silverman S. Fibrinolytic activity in lesions of hereditary hemorrhagic telangiectasia. Arch Dermatol. 1973;107(4): 571-573.
4. Watanabe M, Hanawa S, Morishima T. Fibrinolytic activity in cutaneous lesions of hereditary hemorrhagic telangiectasia. Nihon Hifuka Gakkai Zasshi.1985;95(1):11.
5. Shovlin CL. Hereditary haemorrhagic telangiectasia: pathophysiology, diagnosis and treatment. Blood Rev. 2010;24(6):203-219.
6. Letteboer TG, Mager HJ, Snijder RJ, et al. Genotype-phenotype relationship for localization and age distribution of telangiectases in hereditary hemorrhagic telangiectasia. Am J Med Genet A. 2008;146A(21):2733-2739.
7. Abdalla SA, Geisthoff UW, Bonneau D, et al. Visceral manifestations in hereditary haemorrhagic telangiectasia type 2. J Med Genet. 2003;40(7):494-502.
8. Kasthuri RS, Montifar M, Nelson J, et al. Prevalence and predictors of anemia in hereditary hemorrhagic telangiectasia. Am J Hematol. 2017 Jun 22. [Epub ahead of print]
9. OS AA, Friedman CM, White RI Jr. The natural history of epistaxis in hereditary hemorrhagic telangiectasia. Laryngoscope. 1991; 101(9):977-980.
10. Donaldson JW, McKeever TM, Hall IP, Hubbard RB, Fogarty AW. Complications and mortality in hereditary hemorrhagic telangiectasia: a population-based study. Neurology. 2015;84(18):1886-1893.
11. Kjeldsen AD, Vase P, Green A. [Hereditary hemorrhagic telangiectasia. A population-based study on prevalence and mortality among Danish HHT patients]. Ugeskr Laeger. 2000;162(25):3597-3601.
12. Gaillard S, Dupuis-Girod S, Boutitie F, et al. Tranexamic acid for epistaxis in hereditary hemorrhagic telangiectasia patients: a European cross-over controlled trial in a rare disease. J Thromb Haemost. 2014;12(9): 1494-1502.
13. Ingrosso M, Sabba C, Pisani A, et al. Evidence of small-bowel involvement in hereditary hemorrhagic telangiectasia: a capsule-endoscopic study. Endoscopy. 2004;36(12):1074-1079.
14. Iyer VN, Brinjikji W, Apala D, et al. Impact of age on outcomes in hospitalized patients with hereditary hemorrhagic telangiectasia. Adv Hematol. 2018;2018:4798425.
15. Brinjikji W, Wood CP, Lanzino G, et al. High rates of bleeding complications among hospitalized patients with hereditary hemorrhagic telangiectasia in the United States. Ann Am Thorac Soc. 2016;13(9):1505-1511.
16. Letarte M, McDonald ML, Li C, et al. Reduced endothelial secretion and plasma levels of transforming growth factor-beta1 in patients with hereditary hemorrhagic telangiectasia type 1. Cardiovasc Res. 2005;68(1):155-164.
17. Cirulli A, Liso A, D'Ovidio F, et al. Vascular endothelial growth factor serum levels are elevated in patients with hereditary hemorrhagic telangiectasia. Acta Haematol. 2003;110(1):29-32.
18. Hurwitz H, Fehrenbacher L, Novotny W, et al. Bevacizumab plus irinotecan, fluorouracil, and leucovorin for metastatic colorectal cancer. N Engl J Med. 2004;350(23):2335-2342.
19. Michels S, Rosenfeld PJ, Puliafito CA, Marcus EN, Venkatraman AS. Systemic bevacizumab (Avastin) therapy for neovascular age-related macular degeneration twelve-week results of an uncontrolled open-label clinical study. Ophthalmology. 2005;112(6):1035-1047.
20. Bose P, Holter JL, Selby GB. Bevacizumab in hereditary hemorrhagic telangiectasia. N Engl J Med. 2009;360(20):2143-2144.
21. Oosting S, Nagengast W, de Vries E. More on bevacizumab in hereditary hemorrhagic telangiectasia. N Engl J Med. 2009;361 (9):931; author reply 931-932.
22. Brinkerhoff BT, Poetker DM, Choong NW. Long-term therapy with bevacizumab in hereditary hemorrhagic telangiectasia. N Engl J Med. 2011;364(7):688-689.
23. Al-Samkari H, Kritharis A, Rodriguez-Lopez JM, Kuter DJ. Systemic bevacizumab for the treatment of chronic bleeding in hereditary haemorrhagic telangiectasia. J Intern Med. 2019;285(2):223-231.
24. Al-Samkari H. Systemic bevacizumab for hereditary hemorrhagic telangiectasia: considerations from observational studies. Otolaryngol Head Neck Surg. 2019;160(2): 368.
25. Iyer VN, Apala DR, Pannu BS, et al. Intravenous bevacizumab for refractory hereditary hemorrhagic telangiectasia-related epistaxis and gastrointestinal bleeding. Mayo Clin Proc. 2018;93(2):155-166.
26. Guilhem A, Fargeton AE, Simon AC, et al. Intra-venous bevacizumab in hereditary hemorrhagic telangiectasia (HHT): a retrospective study of 46 patients. PLoS One. 2017;12(11):e0188943.
27. Epperla N, Kapke JT, Karafin M, Friedman KD, Foy P. Effect of systemic bevacizumab in severe hereditary hemorrhagic telangiectasia associated with bleeding. Am J Hematol. 2016;91(6):E313-314.
28. Epperla N, Kleman A, Karafin M, Foy P. Retreatment versus extended treatment strategy of systemic bevacizumab in hereditary hemorrhagic telangiectasia: which is better? Ann Hematol. 2018;97(9):1727-1729.
29. Yin LX, Reh DD, Hoag JB, et al. The minimal important difference of the epistaxis severity score in hereditary hemorrhagic telangiectasia. Laryngoscope. 2016;126(5): 1029-1032.
30. Hsu YP, Hsu CW, Bai CH, Cheng SW, Chen C. Medical treatment for epistaxis in hereditary hemorrhagic telangiectasia: a meta-analysis. Otolaryngol Head Neck Surg. 2018;160(1):22-35.
31. Geisthoff UW, Seyfert UT, Kubler M, Bieg B, Plinkert PK, Konig J. Treatment of epistaxis in hereditary hemorrhagic telangiectasia with tranexamic acid - a double-blind placebo-controlled cross-over phase IIIB study. Thromb Res. 2014;134(3):565-571.
32. Vase P. Estrogen treatment of hereditary hemorrhagic telangiectasia. A double-blind controlled clinical trial. Acta Med Scand. 1981;209(5):393-396.
33. Whitehead KJ, Sautter NB, McWilliams JP, et al. Effect of topical intranasal therapy on epistaxis frequency in patients with hereditary hemorrhagic telangiectasia: a randomized clinical trial. JAMA. 2016;316(9):943-951.
34. Dupuis-Girod S, Pitiot V, Bergerot C, et al. Efficacy of TIMOLOL nasal spray as a treatment for epistaxis in hereditary hemorrhagic telangiectasia. A double-blind, randomized, placebo-controlled trial. Sci Rep. 2019;9(1):11986.
35. Dupuis-Girod S, Ambrun A, Decullier E, et al. Effect of bevacizumab nasal spray on epistaxis duration in hereditary hemorrhagic telangectasia: a randomized clinical trial. JAMA. 2016;316(9):934-942.
36. Samour M, Saygin C, Abdallah R, Kundu S, McCrae KR. Pomalidomide in hereditary hemorrhagic telangiectasia: interim results of a phase I study. Blood. 2016;128(22):210.
37. Faughnan ME, Gossage JR, Chakinala MM, et al. Pazopanib may reduce bleeding in hereditary hemorrhagic telangiectasia. Angiogenesis. 2019;22(1):145-155.
38. Parambil JG, Woodard TD, Koc ON. Pazopanib effective for bevacizumab-unresponsive epistaxis in hereditary hemorrhagic telangiectasia. Laryngoscope. 2018;128 (10):2234-2236.
39. Buscarini E, Botella LM, Geisthoff U, et al. Safety of thalidomide and bevacizumab in patients with hereditary hemorrhagic telangiectasia. Orphanet J Rare Dis. 2019;14(1):28.
40. Dupuis-Girod S, Ginon I, Saurin JC, et al. Bevacizumab in patients with hereditary hemorrhagic telangiectasia and severe hepatic vascular malformations and high cardiac output. JAMA. 2012;307(9):948-955.
41. Al-Samkari H, Albitar HA, Olitsky SE, Clancy MS, Iyer VN. An international survey to evaluate systemic bevacizumab for chronic bleeding in hereditary haemorrhagic telangiectasia. Haemophilia. 2020;26(6): 1038-1045.
42. Al-Samkari H, Albitar HA, Olitsky SE, Clancy MS, Iyer VN. Systemic bevacizumab for high-output cardiac failure in hereditary hemorrhagic telangiectasia: an international survey of HHT centers. Orphanet J Rare Dis. 2019;14(1):256.

Ferrata Storti Foundation

Haematologica 2021
Volume 106(8):2170-2179

Antibody-mediated procoagulant platelets in SARS-CoV-2-vaccination associated immune thrombotic thrombocytopenia

Karina Althaus,[1,2*] Peter Möller,[3*] Günalp Uzun,[2] Anurag Singh,[1] Annika Beck,[3] Martin Bettag,[4] Hans Bösmüller,[5] Martina Guthoff,[6] Franziska Dorn,[7] Gabor C. Petzold,[8] Hans Henkes,[9] Nils Heyne,[6] Hassan Jumaa,[10] Kornelia Kreiser,[3] Caroline Limpach,[11] Beate Luz,[12] Matthias Maschke,[13] Janis A. Müller,[14] Jan Münch,[14] Simon Nagel,[15] Bernd Pötzsch,[16] Jens Müller,[16] Christoph Schlegel,[17] Andreas Viardot,[18] Hansjörg Bäzner,[19] Marc Wolf,[19] Lisann Pelzl,[1] Verena Warm,[5] Winfried A. Willinek,[20] Jochen Steiner,[21] Nicole Schneiderhan-Marra,[22] Dominik Vollherbst,[15] Ulrich J. Sachs,[23] Falko Fend[5#] and Tamam Bakchoul[1,2#]

[1]Institute for Clinical and Experimental Transfusion Medicine, Medical Faculty of Tübingen, Tübingen University Hospital, Tübingen; [2]Center for Clinical Transfusion Medicine, Tübingen University Hospital, Tübingen; [3]Institute for Pathology, Ulm University Hospital, Ulm; [4]Department of Neurosurgery, Krankenhaus der Barmherzigen Brüder Trier, Trier; [5]Institute for Pathology and Neuropathology, Tübingen University Hospital, Tübingen; [6]Department of Internal Medicine IV, Section of Nephrology and Hypertension, Tübingen University Hospital, Tübingen; [7]Department of Neuroradiology, Bonn University Hospital, Bonn; [8]Section of Vascular Neurology, University Hospital Bonn; [9]Department of Neuroradiology, Klinikum Stuttgart, Stuttgart; [10]Institute for Immunology, Ulm University Hospital, Ulm; [11]Department of Neurology, Krankenhaus der Barmherzigen Brüder Trier, Trier; [12]Institute of Transfusion Medicine, Klinikum Stuttgart, Stuttgart; [13]Department of Neurology, Krankenhaus der Barmherzigen Brüder Trier, Trier; [14]Institute of Molecular Virology, Ulm University Medical Center, Ulm; [15]Department of Neuroradiology, Heidelberg University Hospital, Heidelberg; [16]Institute for Experimental Hematology and Transfusion Medicine, Bonn; [17]Ulm University Hospital, Ulm; [18]Internal Medicine III, Ulm University Hospital, Ulm; [19]Department of Neurology, Klinikum Stuttgart, Stuttgart; [20]Department of Radiology, Krankenhaus der Barmherzigen Brüder Trier, Trier; [21]Anesthesiology and Intensive Care Medicine, Tübingen University Hospital, Tübingen; [22]Natural and Medical Sciences Institute, University of Tübingen, Reutlingen and [23]Department of Thrombosis and Hemostasis and Institute of Immunology and Transfusion Medicine, Giessen, Germany

*KA and PM contributed equally as co-first authors.

#FF and TB contributed equally as co-senior authors.

Correspondence:

TAMAM BAKCHOUL
tamam.bakchoul@med.uni-tuebingen.de

FALKO FEND
falko.fend@med.uni-tuebingen.de

Received: April 16, 2021.

Accepted: May 11, 2021.

Pre-published: May 20, 2021.

https://doi.org/10.3324/haematol.2021.279000

ABSTRACT

The COVID-19 pandemic has resulted in significant morbidity and mortality worldwide. In order to prevent severe infection, mass COVID-19 vaccination campaigns with several vaccine types are currently underway. We report pathological and immunological findings in eight patients who developed vaccine-induced immune thrombotic thrombocytopenia (VITT) after administration of SARS-CoV-2 vaccine ChAdOx1 nCoV-19. We analyzed patient material using enzyme immune assays, flow cytometry and heparin-induced platelet aggregation assay and performed autopsies on two fatal cases. Eight patients (five females, three males) with a median age of 41.5 years (range, 24-53) were referred to us with suspected thrombotic complications 6 to 20 days after ChAdOx1 nCoV-19 vaccination. All patients had thrombocytopenia at admission. Patients had a median platelet count of 46.5x10^9/L (range, 8-92). Three had a fatal outcome and five were successfully treated. Autopsies showed arterial and venous thromboses in various organs and the occlusion of glomerular capillaries by hyaline thrombi. Sera from VITT patients contain high-titer antibodies against platelet factor 4 (PF4) (optical density [OD] 2.59±0.64). PF4 antibodies in VITT patients induced significant increase in procoagulant markers (P-selectin and phosphatidylserine externalization) compared to healthy volunteers and healthy vaccinated volunteers. The generation of procoagulant platelets was PF4 and heparin dependent. We demonstrate the contribution of antibody-mediated platelet activation in the pathogenesis of VITT.

Introduction

COVID-19 infection has resulted in considerable morbidity and mortality in the last 15 months.[1] Within an exceptionally short time, several SARS-CoV-2 vaccines have been licensed and used worldwide.[2] Safety signals have been, however, noted. Center for Disease Control and Prevention (CDC) in the US reported in the beginning of March 26 cases of venous thromboembolism, 20 cases of thrombosis and 41 ischemic strokes in individuals vaccinated with mRNA vaccines in the US. More than 200 cases with thrombosis among 34 million persons vaccinated with ChAdOx1 nCoV-19 have been reported to the European database of suspected adverse reactions, EudraVigilance. After the investigation of reported cases, European Medical Association (EMA) found a link between ChAdOx1 nCoV-19 and unusual thrombotic events and concomitant thrombocytopenia. Although the World Health Organization (WHO) and EMA concluded that the benefit of vaccination with ChAdOx1 nCoV-19 outweighs the risks associated with thrombosis and thrombocytopenia, several countries instituted restrictions on the use of ChAdOx1 nCoV-19. The unusual clinical constellation of cerebral venous sinus thrombosis (CVST) and thrombocytopenia is called vaccine-induced immune thrombotic thrombocytopenia (VITT). We studied eight cases with thrombocytopenia and primarily with suspected CVST but also other thromboembolic complications to better understand the pathophysiology of VITT. In this study, we identified antibody-mediated procoagulant platelets as a novel mechanism associated with VITT.

Methods

Study cohort and evaluation of the clinical data

Eight patients were referred to different university hospitals with neurological or hematological symptoms after vaccination with ChAdOx1 nCoV-19 (AstraZeneca, London, UK) between February 1st and April 6th 2021. Six patients admitted to university hospitals and two patients, who were initially admitted to local hospitals, were later transferred to university hospitals. Medical records were used to collect treatments and outcome. Diagnosis of thromboembolic complications was made when indicated by clinical or laboratory findings and/or based on computed tomography, ultrasound imaging or in case of death by autopsy.

Blood samples were collected to exclude heparin-induced thrombocytopenia (HIT). Blood samples from non-vaccinated healthy blood donors (n=24, 17 females, mean age 36.1±13.7 years) and from healthy vaccinated before and after the first vaccination with ChAdOx1 nCoV-19 (n=41, 29 females, mean age 37.3±10.9 years) served as healthy controls.

In addition, sera from 29 COVID-19 patients who had serial HIT immunoglobulin G (IgG)-enzyme immune assay (EIA) measurements during hospitalization were also included in the study (seven females, mean age 65.3±14.1 years). Clinical data from the ICU COVID-19 patients and a VITT-patient (case #7) were reported in previous studies.[3,4]

Bead-based multiplex assay for detection of COVID-19 antibodies

COVID-19 antibodies were measured with a multiplex assay (NMI, Reutlingen, Germany) with the FLEXMAP 3D® system (Luminex Corporation, Austin, USA).[5]

Testing for anti-PF4/heparin antibodies

A commercially available EIA was used in accordance with the manufacturer's instructions (Hyphen Biomed, Neuville-sur-Oise, France). The ability of sera to activate platelets was tested using the functional assay heparin-induced platelet aggregation assay (HIPA) as previously described.[6] For more details, see the *Online Supplementary Appendix*.

Serological characterization of PF4 antibody

Antibody binding to PF4 and the receptor binding domain of Spike protein (Spike-RBD and S2 domain) was analyzed using an in-house EIA.

Assessment of antibody-mediated procoagulant platelets

Patients' sera were incubated with washed platelets ($7.5x10^6$) for 1.5 h* under different conditions at room temperature. Platelets were then stained with Annexin V-FITC and CD62-APC (Immunotools, Friesoythe Germany) and directly analyzed by flow cytometry (FC). For more details see the *Online Supplementary Appendix*.

Ethics statement

The study was conducted in accordance with the Declaration of Helsinki. The study protocol was approved by the Institutional Review Board of the University of Tuebingen (236/2021BO2, 224/2021BO2) and analysis of sera from ChAdOx1 nCoV-19 vaccinated individuals were performed at the University of Ulm (99/21).

Statistical analyses

The statistical analysis was performed using GraphPad Prism, Version 7.0 (GraphPad, La Jolla, USA). Since potential daily variations in FC measurements might result in bias in data analysis, test results were normalized to two healthy donors tested in parallel at the same time point. Data in the text are presented as median (range), mean ± standard deviation (SD) or numbers (n in %).

Data sharing statement

Data may be requested for academic collaboration from the corresponding author.

Results

Clinical and laboratory features of vaccine-induced immune thrombotic thrombocytopenia

Eight patients (five females, three males) with a median age of 41.5 years (range, 24-53) were referred with suspected thrombotic complications after ChAdOx1 nCoV-19 vaccination. Demographic data are summarized in Table 1. The patients were admitted to hospital 6 to 20 days after ChAdOx1 nCoV-19 vaccination. All patients had thrombocytopenia at admission with a median platelet count of $46.5x10^9$/L (range, 8-92). D-dimer was available in five patients, which was 9 µg/mL or higher. Thrombosis was detected in six patients at admission and two developed thrombosis during hospitalization (Figure 1). Thrombotic events included cerebral venous sinus thrombosis (five patients), pulmonary embolism (four patients), deep vein thrombosis (one patient), and thrombosis in other organs (three patients). Three of eight patients had more than one thrombotic event. Three patients presented initially with bleeding signs with easy

bruising and petechiae, which might be an early sign of VITT. One patient underwent a successful thrombus removal by endovascular rheolysis. Three of eight patients died (on day 6 [case #1], day 10 [case #2] and day 7 [case #3] of hospitalization). All surviving patients received anticoagulation. Four patients received intravenous immunoglobulin (IVIG) combined with non-heparin anticoagulation.

Pathological findings

Autopsy was performed in two of three deceased patients. Autopsy of case #2 showed complete thrombotic obstruction of the straight, sagittal and transversal cerebral sinuses, subarachnoidal hemorrhage, cerebral edema and bilateral pulmonary embolism in mid-sized arteries and obstruction of glomerular arterioles and capillaries by hyaline microthrombi containing fibrin and platelets (Figure 2A and B). Autopsy of case #3 showed massive cerebral hemorrhage and cerebral edema, bilateral pulmonary thromboembolism and obstruction of glomeruli by hyaline microthrombi (Figure 2C to G). Histology of the bone marrow was normal in both cases without any hint of increased thrombopoesis.

Table 1. Demographic and clinical data of cases with vaccine induced immune thrombotic thrombocytopenia.

Case #	Age	Sex	First symptoms after vaccination (days)	Thrombosis/ Bleeding	Thrombotic risk factors	PLT, (150-450x10^9/L)	D-Dimer, (<0.5 μg/mL)	Fibrinogen, (170-410 mg/dL)	INR	aPTT, (>40s)
1	47	f	7	CVST	none	10	>35	128	1.30	23
2	48	f	6	CVST, PE	n.a.	40	n.a.	n.a.	1.16	22.9
3	24	m	10	bleeding, multiple thrombosis	heterozygous FVL mutation	22	n.a.	109	1.20	42
4	53	m	9	DVT, PE	none	8	>35	126	1.01	25
5	47	f	7	CVST	none	56	9	263	1.25	35
6	32	m	20	PE	none	71	n.a.	n.a.	n.a.	n.a.
7	36	f	17	CVST	none	92	13	n.a.	1.19	22
8	29	f	7	CVST	contra-ception	53	32	274	1.00	23

CVST: indicates cerebral venous sinus thrombosis; DVT: deep vein thrombosis; FVL: Factor V Leiden; n.a.: not available; PE, pulmonary embolism; PLT: platelet.

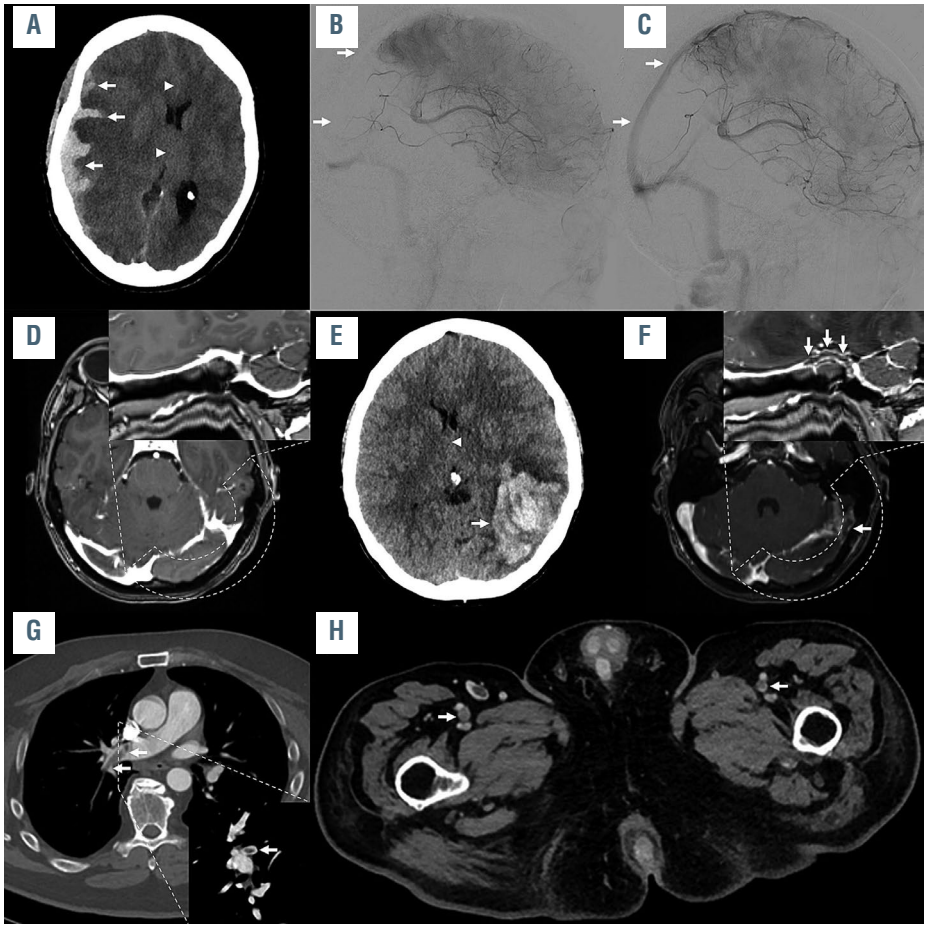

Figure 1. Imaging example of three illustrative cases. Imaging examples of case #1 (A to C), case #8 (D to F) and case #4 (G and H). In case #1, non-enhanced computed tomography imaging (A) showed a parenchymal and subdural hemorrhage (arrows in A), causing a midline shift (arrowheads in A). Digital subtraction angiography was performed (B) showing thrombosis of the right sigmoid and transverse sinus, superior sagittal sinus (arrows in B), and straight sinus. Angiography after mechanical recanalization (C) shows the recanalized cerebral sinuses (superior sagittal sinus marked with arrows). In case #8, cerebral imaging 7 days after vaccination was unremarkable (curved reconstruction of the left transverse and sigmoid sinus shown in the right upper corner of D and F). She worsened, which led to a repeated cerebral imaging, showing a large intraparenchymal hemorrhage in the left temporal lobe (arrow in E), causing midline shift (arrowhead in E), caused by a thrombosis of the transverse and sigmoid sinus (arrows in F), as well as of the adjacent tentorial veins. In case #4, a thrombus in the right pulmonary artery was observed (arrows in E; coronal reconstruction shown in the right lower corner of G). Further imaging also revealed thrombi in the femoral veins on both sides (arrows in H).

Immunoglobulin G binding profile of sera from vaccine-induced immune thrombotic thrombocytopenia

High-titer PF4/heparin antibodies were detected in all sera (eight of eight, 100%) using the IgG PF4/heparin EIA. Interestingly, binding of all sera was inhibited in the presence of high concentration of heparin (mean optical density [OD] of IgG antibodies against PF4/heparin complexes: 2.591±0.642 *versus* 0.176±0.073, respectively, $P<0.0001$, Figure 3A). No correlation was found between the PF4/heparin antibodies and the detected COVID-19 antibodies in VITT patients and in vaccinated controls (*Online Supplementary Figure S1A to D [I-IV]*). Among non-vaccinated controls only one subject (4%) had a PF4/heparin antibodies in EIA (*data not shown*).

We next investigated the PF4-seroconversion after vaccination with ChAdOx1 nCoV-19, as well as during severe SARS-CoV-2 infection (Figure 3B). We found that four of 41 (9.8%) vaccinated healthy individuals and four of 25 (16%) patients with severe COVID-19 seroconverted with IgG antibodies against PF4/heparin complexes within 14 days (Figure 3B). Next, we tested IgG binding to platelets by FC. An increase in IgG binding to test platelets was observed (fold increase [FI] in mean fluorescence [MF] intensity compared to healthy controls [FI of MFI]: 4.39±1.15 *vs.* 1±1.10, $P=0.026$, Figure 4, *Online Supplementary Figure S2A*). IgG binding to platelets was inhibited by heparin at high concentrations (FI of MFI IgG binding: 1.51±0.66, $P=0.016$), but not at low concentrations (FI of MFI of IgG binding: 3.60±2.01, $P=0.688$). Only one serum showed increased binding to platelets in the presence of PF4 and the vaccine ChAdOx1 nCoV-19 (case #4, Figure 4). Spike-RBD did not induce a significant change in IgG binding in VITT patients (Figure 5A). Similar results were observed when S2 protein was added (Figure 5B). IgG binding was also observed when sera from ChAdOx1 nCoV-19 vaccinated volunteers with IgG PF4 antibodies were tested (*Online Supplementary Figure 2B*). However, severe COVID-19 patients with IgG PF4 antibodies showed no increase in IgG binding (*Online Supplementary Figure S2C*).

The impact of Spike-RBD on the binding of anti-PF4 antibodies

Compared to healthy controls, sera from VITT patients showed strong binding to PF4 in the in-house EIA (OD IgG antibodies against PF4: 1.03±0.04 *vs.* 0.110±0.002, respec-

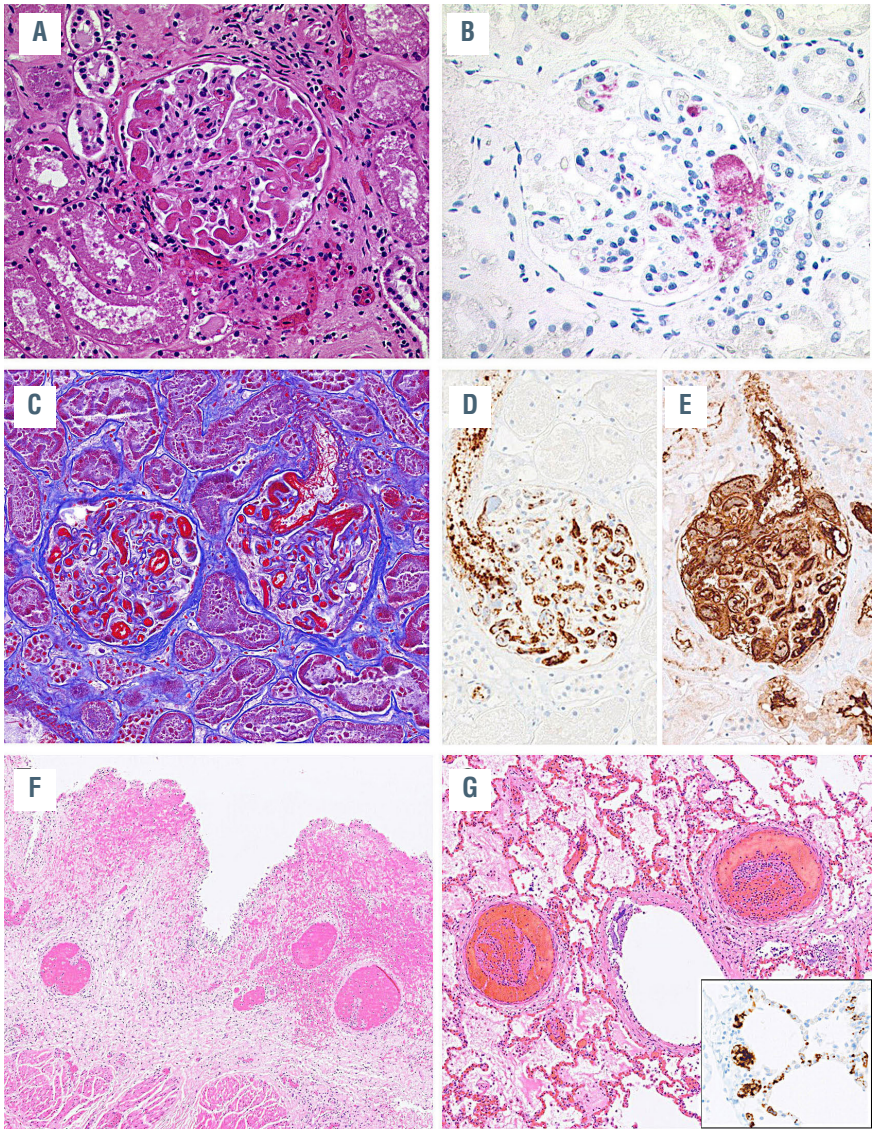

Figure 2. Histopathological findings in case #2 and case #3. (A) Case #2: occlusion of glomerular capillary loops by hyaline thrombi. Hematoxylin-Eosin (H&E) staining, original magnification 200x. (B) Deposition of platelets in glomerular vessels documented by CD42b staining, immunoperoxidase staining, magnification 200x. (C) Case #3: occlusion of glomerular capillary loops by hyaline thrombi with fibrin deposits highlighted in red, Masson's trichrome stain, magnification 200x. (D) Immunostaining for CD61 and (E) fibrin demonstrate the massive intravascular deposits of fibrin and platelets, immunoperoxidase staining, magnification 200x. (F) Thrombotic occlusions of submucosal vessels in the urinary bladder with hemorrhage. H&E staining, magnification 40x. (F) Thrombotic occlusion of medium-sized pulmonary vessels. H&E stining, magnification 40x. (G) Insert shows platelet deposits in pulmonary capillaries stained for CD61, immunoperoxidase staining, magnification 400x.

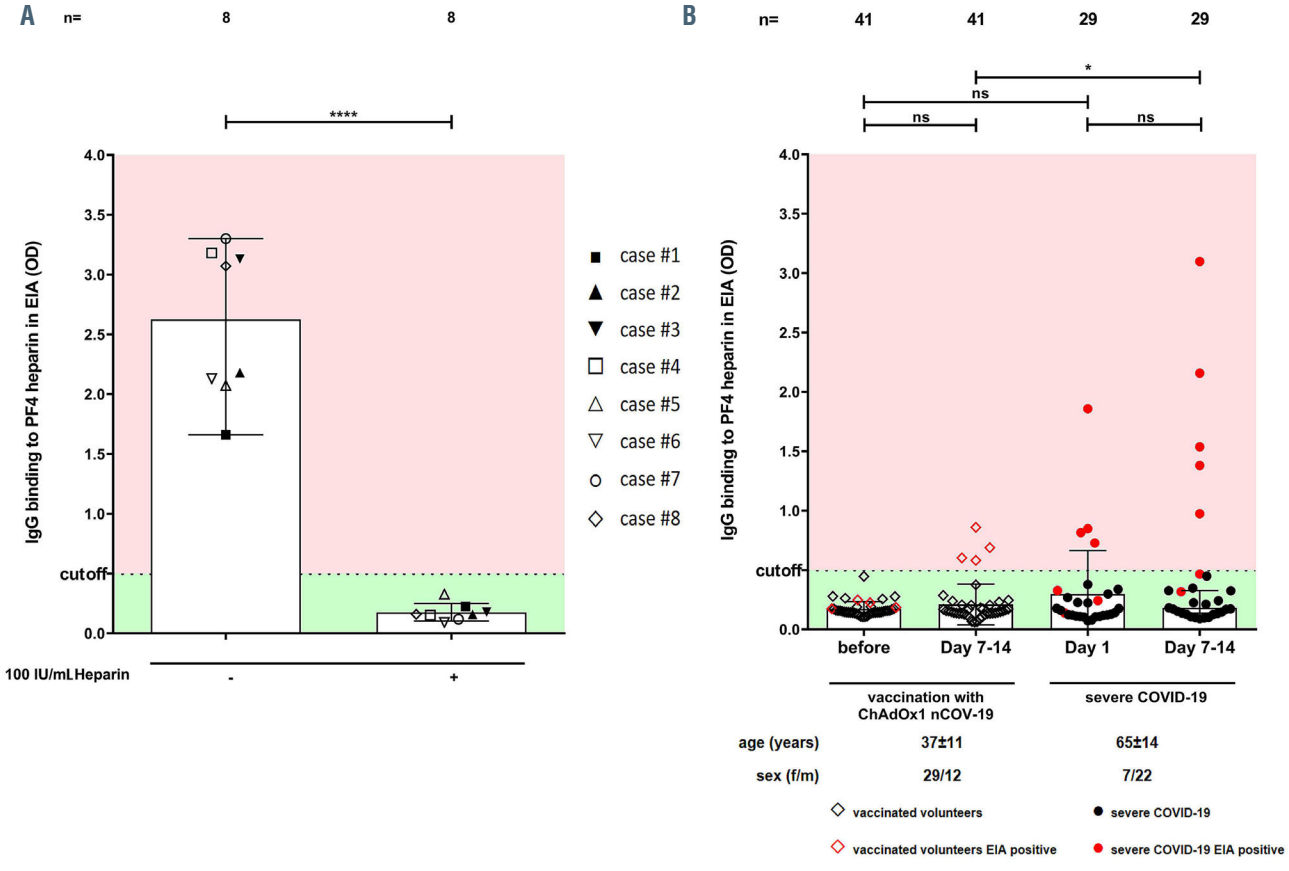

Figure 3. Binding profile of sera from vaccine-induced immune thrombotic thrombocytopenia. (A) Results of the PF4/heparin immunoglobulin G (IgG)-enzyme immune assay (EIA) in patients with vaccine-induced immune thrombotic thrombocytopenia (VITT) with and without 100 IU/mL heparin. All VITT patients showed an enhanced binding which was significantly inhibited at high dose of heparin (100 IU/mL). (B) PF4-seroconversion after vaccination and severe SARS-CoV2 infection was followed up. IgG PF4/heparin antibody binding results in healthy volunteers before and after vaccination and COVID-19 patients in intensive care units showed four vaccinated volunteers displaying a positive EIA result after 7-14 days post-vaccination (red empty diamonds). OD: optical density.

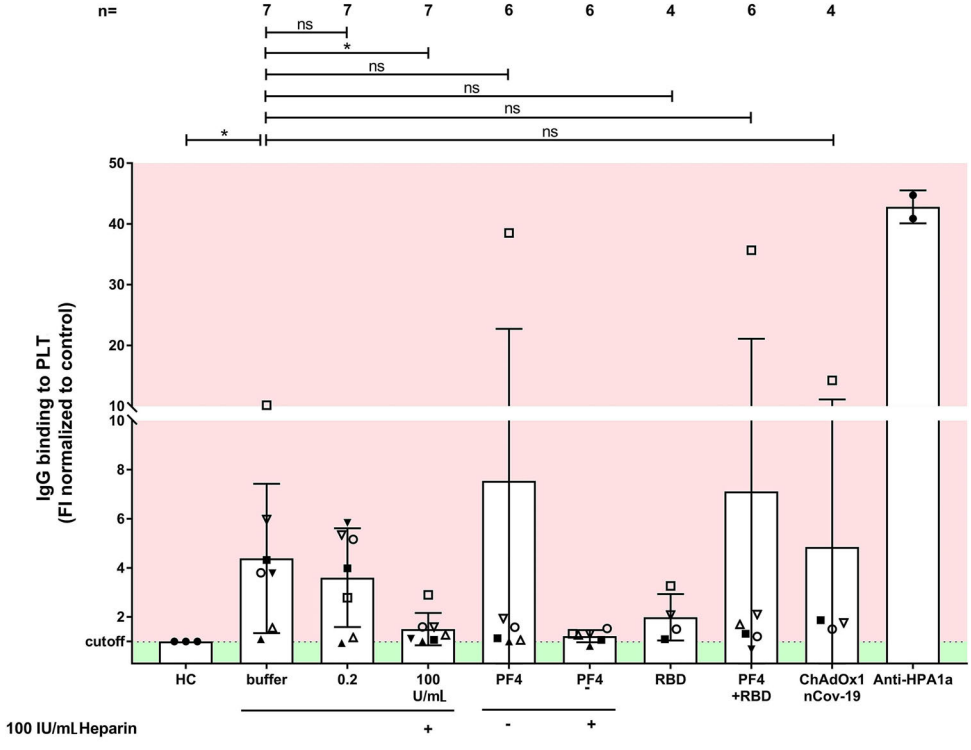

Figure 4. Immunoglobulin G binding to platelets by flow cytometry in sera of vaccine-induced immune thrombotic thrombocytopenia patients. Immunoglobulin G (IgG) binding to healthy washed platelets (PLT) after incubation with sera from vaccine-induced immune thrombotic thrombocytopenia (VITT) patients was measured (assessed by flow cytometry and expressed as fold increase (FI) normalized to controls). VITT patients showed significantly higher binding at the baseline in comparison to healthy controls, which was inhibited by high dose heparin. ns: not significant; **P*<0.05, ***P*<0.01, ****P*<0.001 and *****P*<0.0001.

tively, $P<0.0001$, Figure 5A). On the other hand, sera from VITT patients showed slight but not significant binding to Spike-RBD (*Online Supplementary Figure S2D*). Most importantly, in the presence of PF4 the IgG binding was reduced when the concentration of RBD is increased above 6.5 μg/mL (Figure 5A). However, sera from VITT patients did not show significant binding to S2 protein with and without PF4 (Figure 5B; *Online Supplementary Figure S2E*).

Platelet activation in the heparin-induced platelet aggregation assay assay

In order to investigate the ability of patients' sera to activate platelets, the HIPA assay was used with several modifications. Sera were incubated with washed platelets in the presence of i) buffer, ii) 0.2 IU/mL LMWH, iii) 100 IU/mL UFH, iv) an Fcγ receptor IIa (FcγRIIA)-blocking monoclonal antibody (mAb IV.3), v) 30mg/mL IVIG, vi) 25 μg/mL PF4, vii) 50 μg/mL Spike-RBD, viii) PF4/Spike-RBD complexes, ix) PF4+RBD or x) ChAdOx1 nCoV-19. Conditions with PF4 and RBD were also repeated in the presence of high concentration of heparin (100 IU/mL unfractionated heparin [UFH]). We observed platelet activation in the presence of buffer in eight of eight VITT patients (median time to platelet aggregation 5 minutes [min], no range 5-10 min [min*], Figure 6A), but not in sera from vaccinated individuals

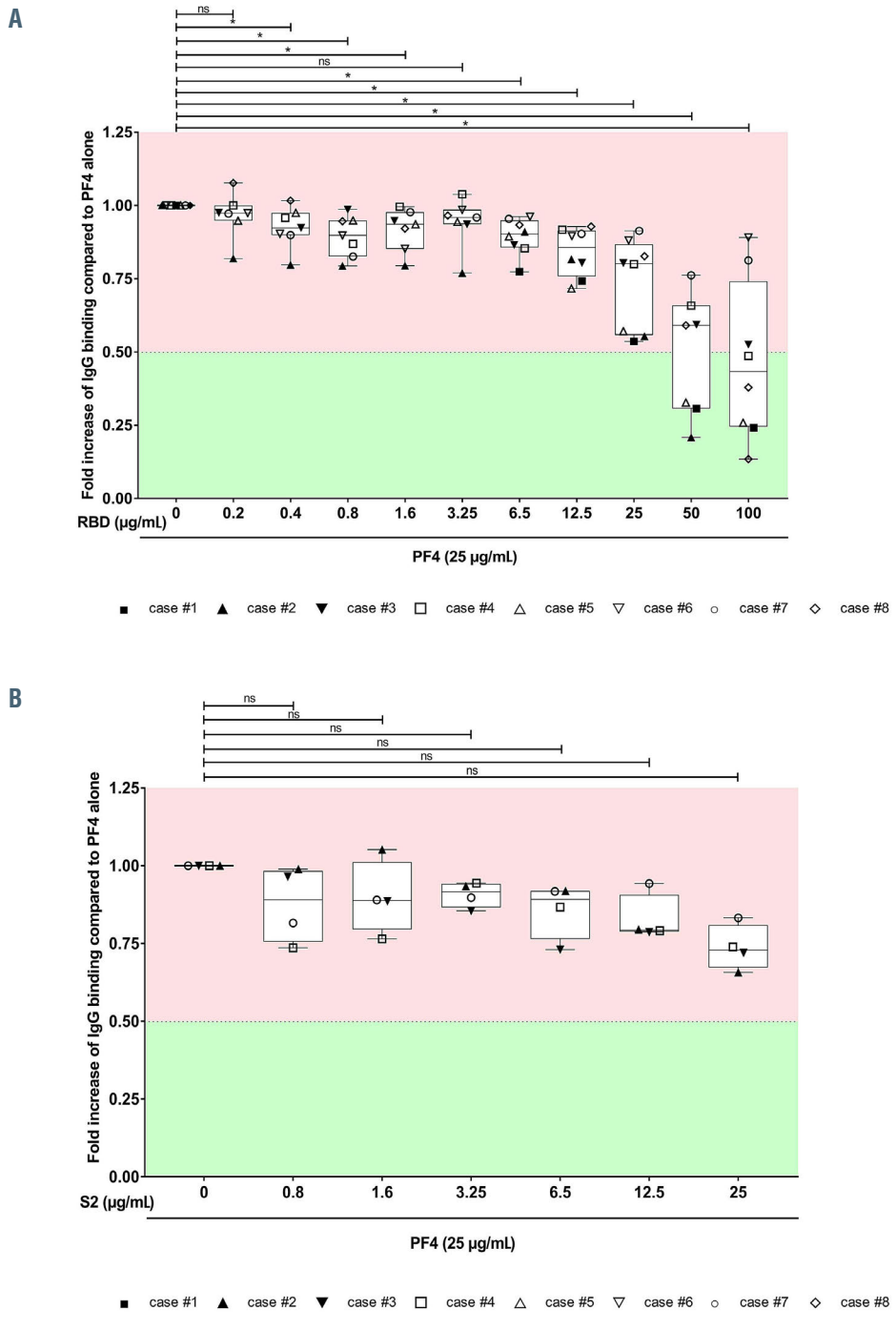

Figure 5. Immunoglobulin G binding to SARS-CoV-2 Spike-RBD and S2 in the presence and absence of PF4. (A) Immunoglobulin G (IgG) binding to SARS-CoV-2 Spike-RBD was assessed by IgG-enzyme immune assay (EIA) and expressed as fold increase to PF4 alone. (B) IgG binding to SARS-CoV-2 S2/PF4 complexes was assessed by EIA and expressed as fold increase to PF4 alone. ns: not significant; *$P<0.05$, **$P<0.01$, ***$P<0.001$ and ****$P<0.0001$.

with anti-PF4 antibodies, who did not develop any clinical sign of thromboembolic complications, without side effects (*Online Supplementary Figure S3A*). Moreover, only one of the sera from patients with severe COVID-19 who were tested positive in PF4/heparin EIA showed platelet activation in the HIPA assay. (*Online Supplementary Figure S3B*). Interestingly, the reaction was weaker in the presence of low molecular weight heparin (median time to aggregate: 5 min, 5-10 min [range] *vs.* 30 min, 5->45min [range], Figure 6A). All reactions were inhibited by a high dose of heparin (P=0.008, Figure 6A). In presence of PF4, sera from VITT patients showed

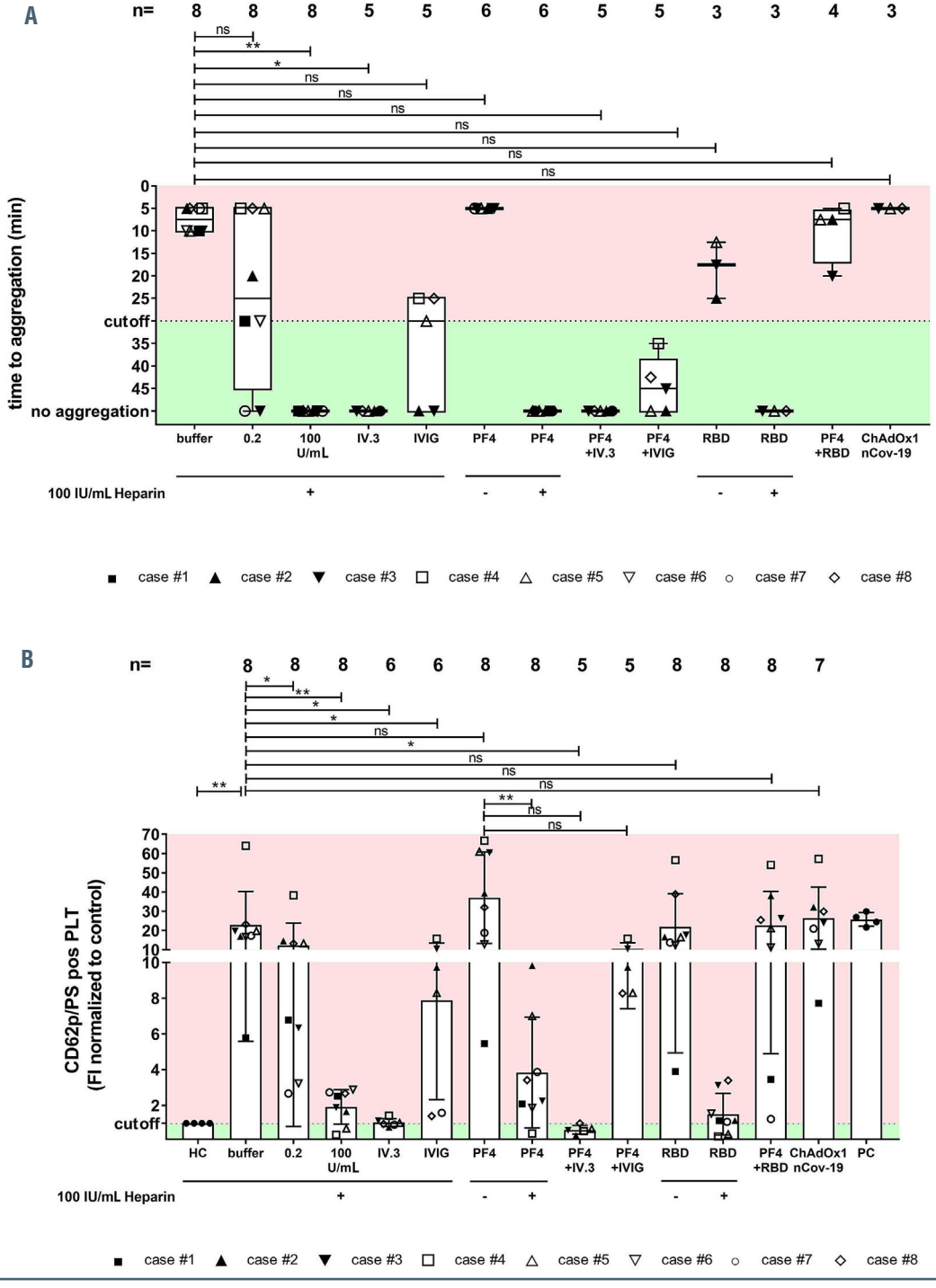

Figure 6. Antibody-mediated platelet activation and generation of procoagulant platelets. Results of the platelet activation assay (HIPA) with modifications in the vaccine-induced immune thrombotic thrombocytopenia (VITT) patients. Each dot represents the median of four different donors. (A) All VITT patients presented platelet (PLT) activation with buffer alone, which was significantly increased by PF4 but inhibited with high dose of heparin. Procoagulant platelets (CD62P/phosphatidylserine [PS] positive) in different settings were analyzed via Annexin V-FITC and CD62p-APC antibody staining. (B) Where indicated, platelets were treated with PF4, 0.2 U/mL and 100 IU/mL heparin, RBD and ChAdOx1 nCoV-19A. Data are presented as mean ± standard deviation of the measured fold increase compared to control. ns: not significant; *P<0.05, **P<0.01, ***P<0.001 and ****P<0.0001. The number of sera tested is reported in each graph. Dotted lines represent the cutoffs determined testing sera from healthy donors. FI: fold increase.

strong platelet activation (median time to platelet aggregation 5 min, 5-5 min [range], Figure 6A). Most importantly, platelet activation was completely inhibited by the mAb IV.3 that blocks the FcγRIIa and by high doses of IgG (>45 min, no aggregation, Figure 6A). No significant change was found when PF4/RBD complexes were added. Antibody-mediated platelet activation was inhibited when low molecular weight heparin (LMWH) was added at low concentrations by testing three sera. When sera from VITT patients were diluted, specific binding was observed to PF4 while no reaction in the buffer was found (Figure 7A).

Sera of vaccine-induced immune thrombotic thrombocytopenia patients induce PF4-dependent procoagulant phenotype

In order to explore the mechanism of coagulation dysregulation in VITT, sera were incubated with washed platelets from healthy donors in the presence of buffer, heparin, mAb IV.3, IVIG, PF4, PF4+IVIG, PF4+RBD, the Spike-RBD protein or the vaccine ChAdOx1 nCoV-19. FC analyses revealed that sera from VITT patients induce remarkable changes in the distribution of CD62p/PS positivity (FI CD62p/PS positive platelets [PLT]: 22.94±6.14 *vs.* 0.90±0.63, respectively, *P*=0.009, Figure 6B, *Online*

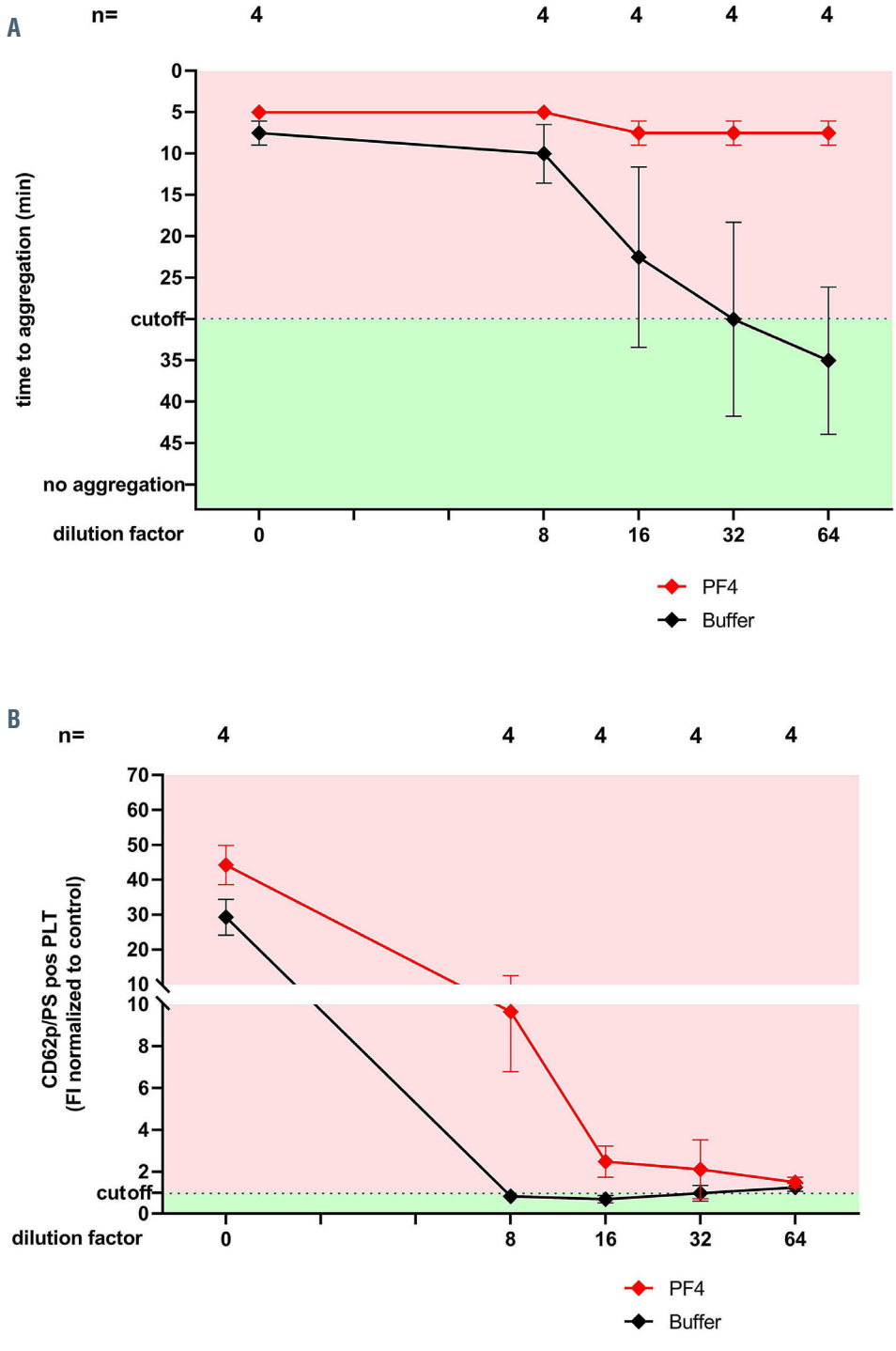

Figure 7. Antibody-mediated platelet activation and generation of procoagulant platelets with diluted sera. (A) Results of heparin-induced platelet aggregation assay (HIPA) at different titrations of sera from vaccine-induced immune thrombotic thrombocytopenia (VITT) patients. Note that diluted sera (from 1:64) activated platelets only in the presence e of PF4. (B) Effect of sera from VITT patients at different titrations on the development of procoagulant platelets. Note that diluted sera (from 1:8) activated platelets only in the presence e of PF4. Data are presented as mean ± standard deviation of the measured fold increase (FI) compared to control. ns: not significant; **P*<0.05; ***P*<0.01, ****P*<0.001 and *****P*<0.0001. The number of sera tested is reported in each graph. Dotted lines represent the cutoffs determined testing sera from healthy donors.

Supplementary Figure S4). In contrast, the platelet population was almost non-affected after incubation with sera from vaccinated controls (*Online Supplementary Figure S5A*). Interestingly, the generation of procoagulant platelets was reduced by 0.2 IU/mL LMWH (FI CD62p/PS positive PLT: 13.32±11.50, P=0.016, Figure 6B) and completely inhibited by high concentration of UFH in VITT patients (FI CD62p/PS positive PLT: 1.92±0.96, P=0.008, Figure 6B, *Online Supplementary Figure S4*). These reactions were also inhibited by the FcγRIIA blocking with mAb IV.3 as well as by high concentrations of IgG (FI CD62p/PS positive PLT: 1.04±0.22, *P*=0.031 and FI CD62p/PS positive PLT: 7.88±5.56, *P*= 0.031, respectively, Figure 6B). No significant increase of procoagulant platelets was also observed in presence of PF4 (FI CD62p/PS positive PLT: 37.07±23.73, *P*=0.078) and in the presence of Spike-RBD alone (FI CD62p/PS positive PLT: 22.02±17.09, *P*=0.195). While an increased generation of procoagulant platelets was observed after the incubation of sera from severe COVID-19 patients, no significant change was observed when sera from vaccinated individuals with anti-PF4 antibodies were tested (*Online Supplementary Figure S5A* and *B*).

In order to identify the target antigen of the platelet activating antibodies, the HIPA and FC analyses were repeated at different titrations of sera from VITT patients. Interestingly, diluted sera (from 1:64) were able to activate platelets and induce a procoagulant phenotype only in the presence of PF4 (Figure 7A and B, respectively).

Discussion

The increasing number of reports on rare thrombotic events after SARS-CoV-2 vaccination draw public attention and led to concerns regarding the safety of this vaccine due to the uncertainty of the origin of these undesired reactions.[7-9] In order to understand the pathophysiology of this phenomenon, the so-called VITT, we analyzed sera from eight patients. Our mostly young, generally fit cohort of patients, presented acutely with atypical thrombosis, primarily, but not exclusively involving the cerebral venous sinuses, an extremely rare manifestation of thrombosis in the general population. All cases developed symptoms within 6-20 days after the ChAdOx1 nCoV-19 vaccination showing a temporal relationship between vaccination and symptoms. The main findings in these cases were thrombocytopenia, high D-dimer, low fibrinogen, and high-titer IgG antibodies against PF4 that can induce procoagulant platelet phenotype.

After intensive laboratory investigations of the VITT cases, we were able to identify the serological profile of the pathological antibodies. In a small cohort of vaccinated volunteers, approximately 10% of the individuals developed IgG antibodies against PF4/polyanion complexes within 14 days after the first vaccination; none of them had been exposed to heparin in the past 100 days. We observed that IgG binding to PF4 in these sera as well as in VITT sera can be inhibited by heparin but also by increasing the concentration of Spike-RBD. These data may suggest that these antibodies are specific for conformational changes in PF4 that might be induced by negatively charged structures. Of note, no significant IgG binding to platelets was observed in the presence of the vaccine ChAdOx1 nCoV-19. Accordingly, it is very unlikely that the vector (pCDNA4) may be responsible for the high PF4-seroconversion rate in vaccinated individuals. Comparable data were reported by Greinacher *et al.*[7] and Schultz *et al.*[9] in two very recent reports that appeared while our manuscript was in preparation. In addition to their observations, we were also able to demonstrate that sera from VITT patients directly induce procoagulant platelets, suggesting a possible mechanism for thrombotic events seen in patients with VITT. This is further corroborated by the pathological studies in two of our patients. Despite the distinct immediate causes of death in these two fatal cases, namely fatal cerebral sinus thrombosis and intracerebral hemorrhage, the two autopsy reports showed striking similarities. In addition to arterial, arteriolar and venous thrombosis in various organs and pulmonary thromboembolism, both cases showed a striking occlusion of multiple glomeruli and afferent arterioles by hyaline thrombi composed of fibrin and platelets, but lacking erythrocytes. The kidney morphology bears resemblance to thrombotic microangiopathy, but we failed to identify erythrocyte fragmentation, a key feature of thrombotic microangiopathy.[10] Both patients, however, had normal kidney function (highest creatinine level 0.5 mg/dL in case #2 and 0.8 mg/dL in case#3) until briefly before death, indicating rapid pre-terminal development of glomerular microthrombosis. White thrombi have been associated with antibody-mediated platelet activation.[10,11]

Our data indicate that IgG antibodies against PF4 increase the generation of procoagulant platelets in VITT. However, we cannot exclude other co-factor(s) that could also induce thromboembolic complications *in vivo*. We report on VITT after ChAdOx1 nCoV-19, which is the only SARS-CoV-2 vaccine that includes a simian adenovirus. Disturbances of platelets have been described in association with the intravenous administration of adenovirus gene therapy vectors although it is unclear how that might relate to isolated thrombocytopenia as an adverse event of the vaccine.[8]

Finally, the observed clinical and laboratory features of the VITT are exceptional and rare. Therefore, the value of the COVID-19 vaccination to provide critical protection should be considered higher compared to the significant health risk of COVID-19. With the better recognition of this rare complication and the availability of efficient therapies, the risk-benefit ratio of ChAdOx1 nCoV-19 might be further reconsidered.

Conclusion

Although the incidence of VITT after ChAdOx1 nCoV-19 vaccination is very low, the mortality rate is high (37.5% in our case series). Since a global vaccination campaign is underway and large numbers of people will be vaccinated, an increase in the number of people with this side effect is to be expected, highlighting the importance of a better understanding of the pathophysiology of VITT. In this study, we present immunological and pathological findings in patients with VITT. Furthermore, we show the contribution of antibody-mediated platelet activation in the pathogenesis of VITT.

Disclosures

No conflicts of interest to disclose.

Contributions

KA, PM, UJS, FF, and TB designed the study; JS, MG, MP,

MB, AB, HB, FD, AV, HH, NH, KK, CL, BL, JM, MM, SN, CS, BP, UJS, MW and GCP were responsible for the treatment of patients and collected and analyzed the clinical data; TB, GU, KA and FF reviewed medical reports; KA, GU, JAM, AS and LP performed the experiments; WAW and DV analyzed the radiological images; HB, VW, FF, and PM analyzed the autopsy findings and performed tissue studies; HJ produced Spike protein; KA, LP, AS, GU, NS, FF and TB analyzed the data, interpreted the results and wrote the manuscript. All authors read and approved the manuscript.

Acknowledgments

We thank our technicians Karoline Weich, Simone Weit, Franziska Lyshy, Marco Mikus and Flavianna Rigoni for their excellent technical support. We also thank Harald Klüter and Martin Holderried for vaccines.

Funding

This work was supported by grants from the German Research Foundation and from the Herzstiftung to TB (BA5158/4 and TSG-Study), by special funds from the state of Baden-Württemberg for autopsy-based COVID-19 research and the DEFEAT PANDEMIcs network funded by the BMBF to PM and FF. JAM is supported by a grant from the German Research Foundation.

References

1. Grasselli G, Greco M, Zanella A, et al. Risk factors associated with mortality among patients with COVID-19 in intensive care units in Lombardy, Italy. JAMA Intern Med. 2020;180(10):1345-1355.
2. Castells MC, Phillips EJ. Maintaining safety with SARS-CoV-2 vaccines. N Engl J Med. 2021;384(7):643-649.
3. Althaus K, Marini I, Zlamal J, et al. Antibody-induced procoagulant platelets in severe COVID-19 infection. Blood. 2021; 137(8):1061-1071.
4. Wolf ME, Luz B, Niehaus L, Bhogal P, Bazner H, Henkes H. Thrombocytopenia and intracranial venous sinus thrombosis after "COVID-19 vaccine AstraZeneca" Exposure. J Clin Med. 2021;10(8):1599.
5. Becker M, Strengert M, Junker D, et al. Exploring beyond clinical routine SARS-CoV-2 serology using MultiCoV-Ab to evaluate endemic coronavirus cross-reactivity. Nat Commun. 2021;12(1):1152.
6. Greinacher A, Michels I, Kiefel V, Mueller-Eckhardt C. A rapid and sensitive test for diagnosing heparin-associated thrombocytopenia. Thromb Haemost. 1991;66(6):734-736.
7. Greinacher A, Thiele T, Warkentin TE, Weisser K, Kyrle PA, Eichinger S. Thrombotic thrombocytopenia after ChAdOx1 nCov-19 vaccination. N Engl J Med. 2021;384(22):2092-2101.
8. Othman M, Labelle A, Mazzetti I, Elbatarny HS, Lillicrap D. Adenovirus-induced thrombocytopenia: the role of von Willebrand factor and P-selectin in mediating accelerated platelet clearance. Blood. 2007;109(7):2832-2839.
9. Schultz NH, Sorvoll IH, Michelsen AE, et al. Thrombosis and Thrombocytopenia after ChAdOx1 nCoV-19 Vaccination. N Engl J Med. 2021;384(22):2124-2130.
10. Brocklebank V, Wood KM, Kavanagh D. Thrombotic Microangiopathy and the Kidney. Clin J Am Soc Nephrol. 2018;13(2): 300-317.
11. Pierangeli SS, Espinola RG, Liu X, Harris EN. Thrombogenic effects of antiphospholipid antibodies are mediated by intercellular cell adhesion molecule-1, vascular cell adhesion molecule-1, and P-selectin. Circ Res. 2001;88 (2):245-250.

Ferrata Storti Foundation

Membrane protein CAR promotes hematopoietic regeneration upon stress

Guojin Wu and Cheng Cheng Zhang

Department of Physiology, University of Texas Southwestern Medical Center, Dallas, TX, USA

Haematologica 2021
Volume 106(8):2180-2190

ABSTRACT

Adult hematopoietic stem cells (HSC) are quiescent most of the time, and how HSC switch from quiescence to proliferation following hematopoietic stress is unclear. Here we demonstrate that upon stress the coxsackievirus and adenovirus receptor CAR (also known as CXADR) is upregulated in HSC and critical for HSC entry into the cell cycle. Wild-type HSC were detected with more rapid repopulation ability than the *CAR* knockout counterparts. After fluorouracil treatment, *CAR* knockout HSC had lower levels of Notch1 expression and elevated protein level of Numb, a Notch antagonist. The Notch signaling inhibitor DAPT, dominant negative form of MAML (a transcriptional coactivator of Notch), or dominant negative mutant of LNX2 (an E3 ligase that acts on Numb and binds to CAR), all were capable of abrogating the function of CAR in HSC. We conclude that CAR activates Notch1 signaling by downregulating Numb protein expression to facilitate entry of quiescent HSC into the cell cycle during regeneration.

Correspondence:

CHENGCHENG ZHANG
Alec.Zhang@UTSouthwestern.edu

Received: November 28, 2019.

Accepted: June 22, 2020.

Pre-published: June 25, 2020.

https://doi.org/10.3324/haematol.2019.243998

Introduction

In adults stem cells with self-renewal and differentiation capabilities are required for tissue homeostasis and regeneration. Quiescence protects stem cells from exhaustion. Hematopoietic stem cells (HSC) are largely quiescent during normal hematopoiesis, [1] and adult hematopoiesis is sustained primarily by "short-term" HSC (ST-HSC).[1] During injury or inflammation, quiescent HSC enter the cell cycle to accelerate hematopoietic flux,[1-3] and cycling HSC return to quiescence after the injury is repaired or inflammation is resolved. Multiple signaling pathways are known to be important for regulation of cell fates and regeneration of HSC.[4-10] The molecular mechanisms that regulate HSC to transit from quiescence to proliferation during regeneration remain largely unknown.

The coxsackievirus and adenovirus receptor (CAR, also known as CXADR) was first reported to mediate viral attachment and infection[11] and later was demonstrated to be a tight junction protein.[12] CAR expression is required for normal atrioventricular conduction and cardiac function.[13] Its constitutive expression in various cancerous and normal tissues has also been reported.[14,15] CAR was also reported to be critical for survival of oral squamous cell carcinomas.[16] Interestingly, CAR expression increases during tissue regeneration,[17] suggesting that it plays an important role in repairing injury. Here we demonstrate that CAR expression is transiently increased in HSC during fluorouracil (5-FU)-induced hematopoietic injury and bone marrow (BM) transplantation and supports HSC regeneration. CAR does not alter HSC self-renewal but rather induces quiescent HSC to enter cell cycle. Mechanistic studies indicated that CAR activates Notch1 signaling in stressed HSC by degrading the Notch inhibitor Numb.

Methods

Mice

$CAR^{loxP/loxP}$ mice and UBC-Cre-ERT2 mice were purchased from Jackson Laboratory. Mice were maintained at the University of Texas Southwestern Medical Center animal facility. All animal experiments were performed with the approval of The University of Texas Southwestern Committee on Animal Care.

Competitive reconstitution analysis

CD45.2 donor bone marrow cells (3×10^5 unless otherwise indicated) were mixed with an equal number of freshly isolated CD45.1 competitor BM cells, and the mixture was injected intravenously via the retro-orbital route into 6- to 9-week-old CD45.1 mice that had been previously irradiated with a total dose of 10 Gy, essentially as we described.[18-20] BM cells ($1x10^6$) collected from primary recipients were used for the secondary transplantation. In order to measure reconstitution of transplanted mice, peripheral blood was collected at the indicated times after transplantation and the presence of $CD45.1^+$ and $CD45.2^+$ cells in lymphoid and myeloid compartments was measured.

5-fluorouracil treatment

5-FU was administered intraperitoneally to female wild-type (WT) or CAR conditional knockout (cKO) mice at a dose of 150, 250, or 300 mg/kg. In order to test Notch signaling, DAPT (Selleckchem, cat. #S2215) was injected at 10 mg/kg. Differences in survival of the two groups were analyzed using a log-rank test.

Retrovirus infection

LNX1 and *LNX2* were cloned from cDNA of mouse intestine. The dominant negative forms (DN-LNX1 and DN-LNX2) were sub cloned [21] and retroviral plasmids MSCV-DN-LNX1-IRES-GFP and MSCV-DN-LNX2-IRES-GFP were constructed using standard methods. The retroviral plasmids with PCL-ECO (2:1) were transfected using PolyJet (SignaGen) into 293 T cells. The resulting retroviral supernatant was collected 48-72 hours later and used for infection. At 6 days after 5-FU injection, the Lin^- cells from the BM of *CAR* cKO mice were isolated, and the Lin^- cells were resuspended in viral supernatants (1×10^5 cells/mL) with 4 μg/mL polybrene and centrifuged at 2,000 rpm for 2 hours before culturing for 24 hours in StemSpan (StemCell Technologies) in the presence of 10 ng/mL stem cell factor, 20 ng/mL thrombopoietin, and 10 ng/mL interleukin 3. Cells were then resuspended in viral supernatant for another round of infection. After 24 hours, green fluorescent protein positive (GFP^+) cells were isolated for repopulation assay.

Statistics

Statistical significance of differences was assessed using 2-tailed Student's *t*-test. Animal survival analysis was assessed with long-rank test. A *P*-value of 0.05 or less was considered significant. Values are reported as mean ± standard error of the mean.

Results

CAR expression is elevated in stressed hematopoietic stem cells

We compared *CAR* mRNA levels in HSC, hematopoietic progenitors, and differentiated hematopoietic cells before and after stress. As reported previously,[22] *CAR* is expressed in differentiated cells and not stem cells or hematopoietic progenitors with the exception of granulocyte-monocyte progenitor (GMP) cells (Figure 1A). Shortly after treatment of mice with 5-FU or after BM transplantation, *CAR* expression was greatly enhanced in phenotypical LT-HSC (identified as $Lin^-Sca1^+cKit^+CD135^-CD34^-$ or LSKFC) compared to untreated mice (Figure 1B). *CAR* expression returned to the original low level at the later time point (Figure 1B). However, ST-HSC, multipotent hematopoietic progenitors (MPP) and hematopoietic progenitors did not increase *CAR* expression after 5-FU treatment (*Online Supplementary Figure 1*). In order to prove CAR is expressed on plasma membrane of HSC, we stained BM cells from 5-FU treated mice with anti-mCAR. Real-time qantitative polymerase chain reaction (RT-qPCR) and *CAR* cKO BM cells both prove the specific binding of the anti-mCAR (*Online Supplementary Figure 2*; Figure 1B). The surface CAR expression was detected in LSK population after 5-FU treatment (Figure 1C). Competitive repopulation assay with sorted CAR negative and positive expressed LSKFC cells from 5-FU treated mice indicates that both subpopulations had similar repopulation abilities (Figure 1D and E; *Online Supplementary Figure 3*). These results imply that CAR plays a role in HSC during regeneration induced by stress.

CAR supports hematopoietic regeneration after injury

CAR deletion in mice is embryonically lethal.[23] In order to study the function of CAR, $CAR^{loxp/loxp}$ mice were crossbred with UBC-CreERT2 mice. In the resulting mice, global knockout (KO) of *CAR* can be induced with tamoxifen treatment; these mice are thereafter referred to as *CAR* conditional KO (cKO) mice. The hematopoietic system is damaged by treatment with the chemotherapy drug 5-FU.[24] *CAR* cKO mice were more sensitive to 5-FU treatment and died faster. After administration of 300 mg/kg 5-FU, 60% of *CAR* cKO mice died within 2 weeks, whereas all WT mice (which were UBC-CreERT2/$CAR^{wt/wt}$ mice with tamoxifen treatment) survived (Figure 2A). This indicates that CAR is important in the response to injury of the hematopoietic system. In order to compare kinetics of hematopoietic system recovery in WT and cKO mice, we treated mice with 250 mg/kg 5-FU, a dose that does not cause death of the WT mice. The complete blood count (CBC) data indicated CAR cKO mice had a slower recovery, although there was not a significant difference in hematopoietic cell counts between WT and *CAR* cKO mice before 5-FU treatment. On day 8 after 5-FU treatment, total white blood cell (WBC) and individual lineage cell numbers (including neutrophils, monocytes, eosinophils, basophils, and lymphocytes) had decreased relative to pretreatment levels. Numbers rebounded more rapidly in WT mice than in the *CAR* cKO mice. On day 14 post 5-FU treatment there were an average of $12.8x10^3$ ±1.5 WBC per μL in WT mice and only $6.2x10^3$±0.4 WBC per μl in cKO mice (Figure 2B). On day 17 post treatment, the *CAR* cKO mice and WT mice had equivalent WBC counts of about $12x10^3$ per μL. A significant difference in neutrophil numbers between WT and *CAR* cKO mice was detected on day 12 (Figure 2B). Red blood cell (RBC) numbers decreased more slowly than WBC counts and the lowest cell counts were detected on day 14 in both WT and *CAR* cKO mice. Although there were no significant differences detected before day 14, the WT mice had significant more RBC than cKO mice in peripheral blood between day 14 and 17 (Figure 2B). Specifically, $Mac1^+$ cells and $B220^+$ cells had significantly faster recovery in WT mice than in *CAR* cKO mice after 5-FU treatment (*Online Supplementary Figure 4*). These results indicate that *CAR* cKO mice produce hematopoietic blood cells more slowly after 5-FU treatment, which explains why mice lacking CAR die after a dose of 5-FU that is sub-lethal dose to WT mice.

CAR stimulates progenitor production during regeneration

The Lin$^-$Sca1$^+$cKit$^+$ (LSK) population of hematopoietic cells is primarily responsible for production of progenitors during regeneration.[25] We compared the production of hematopoietic progenitors by WT and *CAR* cKO mice after dosing with 150 mg/kg 5-FU and after BM transplantation (Figure 3A). The *CAR* cKO mice produced progenitors more slowly during recovery. Before 5-FU administration there were no differences in pre-B or myeloid colony forming units (CFU) in WT and *CAR* cKO mice. Four days after 5-FU injection, there were significantly more pre-B CFU and myeloid CFU but fewer granulocyte, erythrocyte, monocyte, megakaryocyte (GEMM) CFU in WT mice than in *CAR* cKO mice, suggesting a slower hematopoietic differentiation in *CAR* cKO mice upon 5-FU-induced injury. When the mice recovered from injury at 7 days after 5-FU injection, the CAR cKO mice had the same number of myeloid CFU and the difference in pre-B cell CFU between WT and *CAR* cKO mice was smaller than on day 4 (Figure 3A). We also injected WT or *CAR* cKO BM cells into lethally irradiated recipient mice and conducted CFU assays for the BM cells. WT donor cells produced more pre-B and myeloid CFU than *CAR* cKO donor cells on days 9 and 11 post transplantation (Figure 3B). The difference disappeared at 2 months after transplantation, suggesting *CAR* cKO only took effect during regeneration. These results indicate that CAR stimulates production of differentiated progenitors.

CAR stimulates entry of "long-term"-hematopoietic stem cells into cell cycle

Although CAR promotes progenitor production during regeneration, it did not affect frequency of progenitors or stem cells during homeostasis (*Online Supplementary Figure 5*). During regeneration, HSC enter the cell cycle and expand.[2] During expansion, HSC may self-renew or differentiate. In order to investigate whether CAR regulates the function of LT-HSC, ST-HSC, and MPP upon transplantation stress, we collected WT and cKO LT-HSC (LSKFC) and ST-HSC plus MPP (Lin$^-$Sca1$^+$cKit$^+$CD34$^+$) for competitive repopulation assays. From day 17 after trans-

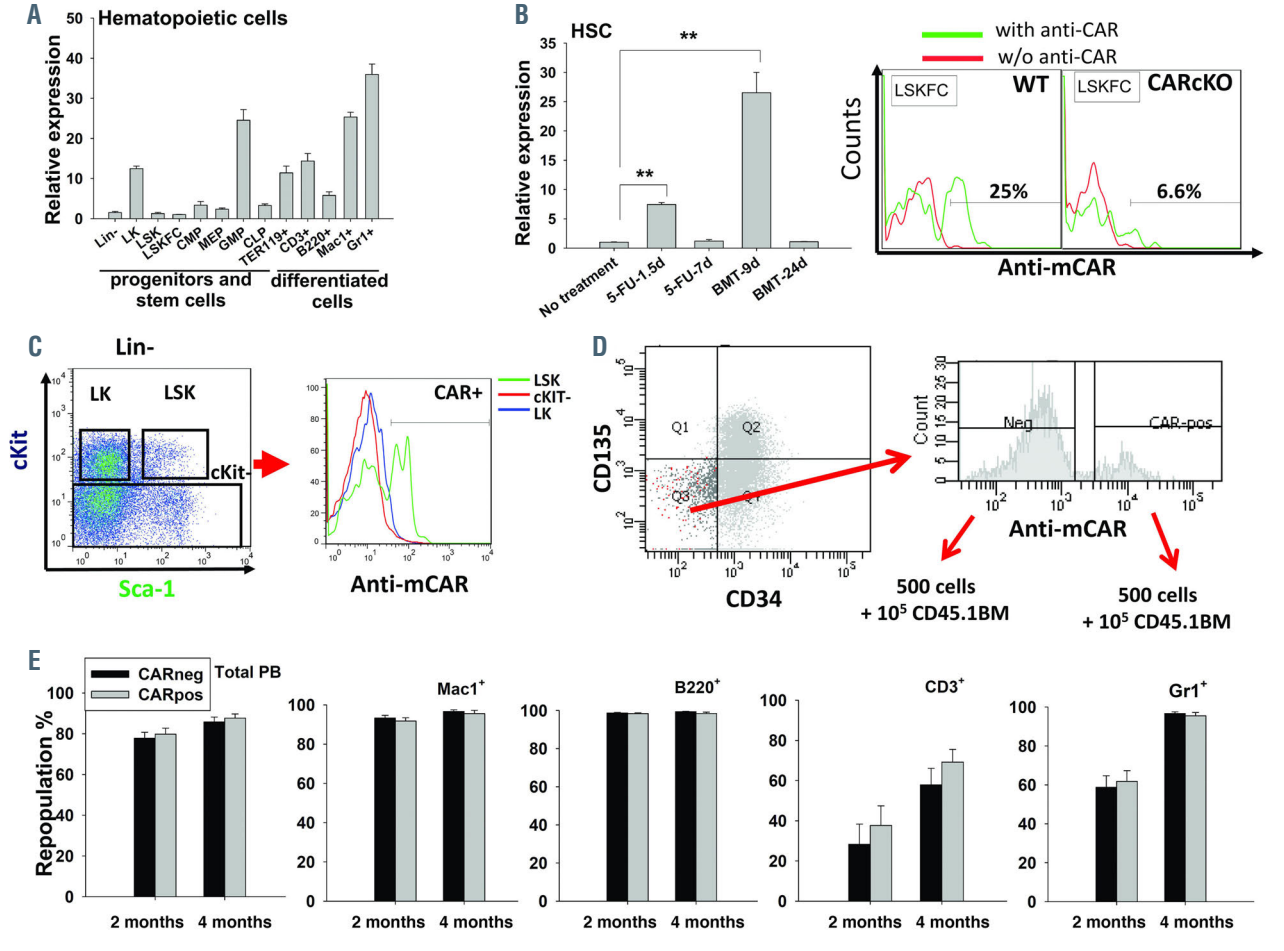

Figure 1. *CAR* is expressed in differentiated hematopoietic cells, and its expression increases in hematopoietic stem cells during regeneration. (A) *CAR* expression (determined by real-time qantitative polymerase chain reaction [RT-qPCR]) in hematopoietic cells, hematopoietic stem cells (HSC), and progenitors including Lin-, LK (Lin-cKit+Sca1-), LSK (Lin-cKit$^+$Sca1$^+$), LSKFC (Lin-Sca1$^+$cKit$^+$CD135$^-$CD34$^-$), CMP (LKCD34$^+$FcrR$^-$), MEP (LKCD34$^-$FcrR$^-$), granulocyte-monocyte progenitor (GMP) (LKCD34$^+$FcrR$^+$), and CLP (Lin-cKit^{low}Sca1^{low}CD135$^+$CD127$^+$). (B) Right panel, *CAR* expression (determined by RT-qPCR) in LT-HSC (selected as LSKFC) at day 1.5 and day 7 after 5-fluorouracil (5-FU) treatment (5-FU-1.5d and 5-FU-7d, respectively) and at 9 and 24 days post bone marrow (BM) transplantation (BMT-9d and BMT-24d, respectively); Left panel, BM cells from wild-type (WT) and CAR conditional knockout (cKO) for analysis CAR expression on LSKFC. (C) CAR surface expression on LK, LSK and Lin-cKit- population after 5-FU treatment. (D) Flow chart of repopulation experiment for LSKFC CAR- or CAR+. (E) Repopulation results of LSKFC CAR$^-$ or CAR$^+$ (n=7-9). One and half days after treated with 5-FU, BM cells from mice were isolated for flow cytometry analysis (panel B (left) and C) or for isolating LSKFC cells (D and E). The mRNA levels were calculated based on non-treated LSKFC, and experiments were repeated three times. $^{**}P<0.001$.

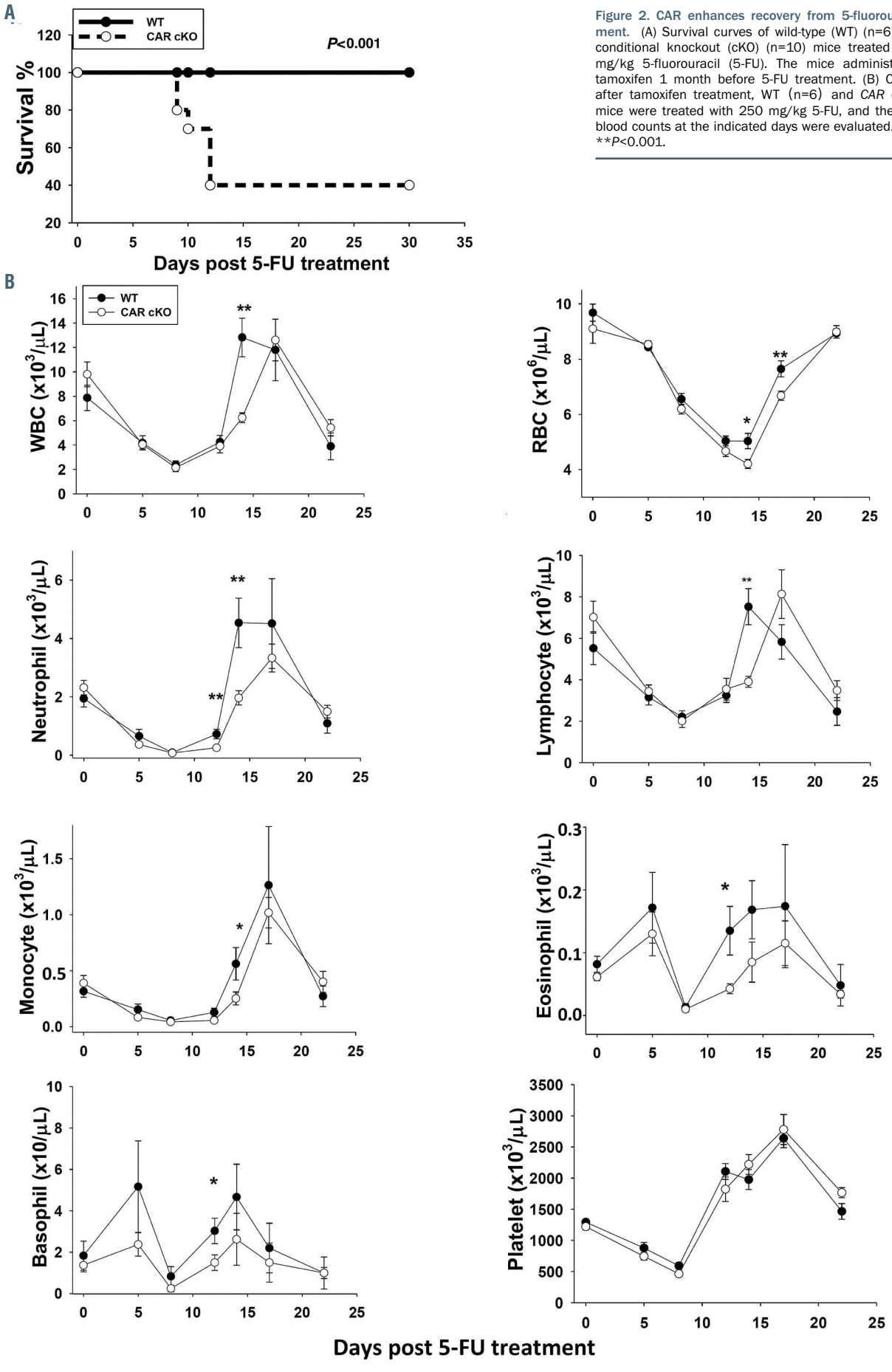

Figure 2. CAR enhances recovery from 5-fluorouacil treatment. (A) Survival curves of wild-type (WT) (n=6) and *CAR* conditional knockout (cKO) (n=10) mice treated with 300 mg/kg 5-fluorouracil (5-FU). The mice administered with tamoxifen 1 month before 5-FU treatment. (B) One month after tamoxifen treatment, WT (n=6) and *CAR* cKO (n=8) mice were treated with 250 mg/kg 5-FU, and the complete blood counts at the indicated days were evaluated. **P*<0.05, ***P*<0.001.

plantation, the repopulation percentage of WT LT-HSC donors gradually increased to above 35%, whereas the percentage decreased to below 2% for WT ST-HSC plus MPP (Figure 4A). This indicated that LT-HSC play the major role in regeneration and that ST-HSC and MPP are quickly exhausted.

When WT and *CAR* cKO donors were compared, WT LT-HSC repopulated about twice as efficiently as *CAR* cKO cells in the first 6 weeks (Figure 4A). There was only a small difference for ST-HSC plus MPP between WT and *CAR* cKO cells on days 21 and 23 in Mac1$^+$ population. In the B220$^+$ population there were significant differences in LT-HSC, but not in ST-HSC plus MPP, between WT and *CAR* cKO donors (Figure 4A). This suggests that CAR cKO impairs the function of LT-HSC but not of ST-HSC and MPP. At 170 days after transplantation, the repopulation percentages donor LSKFC of WT and *CAR* cKO LT-HSC groups did not differ significantly (Figure 4B), indicating that CAR deficiency does not alter LT-HSC activity during regeneration. These results indicate that CAR stimulates regeneration mainly by affecting LT-HSC.

In order to evaluate whether lack of CAR is detrimental after bone marrow transplantation, we conducted another repopulation assay (Figure 4C). Here WT or *CAR* cKO BM cells were mixed with an equal number of CD45.1 BM cells and were injected into lethally irradiated recipient mice. WT donor cells showed greater repopulation ability in both myeloid and lymphoid cells than *CAR* cKO donor cells in first 6 weeks after transplantation. After 6 weeks, the difference between WT and *CAR* cKO repopulation gradually diminished. At 16 weeks after BM transplantation, the repopulation percentage of the donor BM cells from *CAR* cKO mice was not significantly different from that in mice that received WT cells (Figure 4C). In the second transplantation, *CAR* cKO donor cells had no defects in long-term repopulation ability (Figure 4C). This serial transplantation analysis indicates that the self-renewal of LT-HSC was not affected by CAR. In addition, CAR did not affect homing ability of HSC (*Online Supplementary Figure 6*). The limiting dilution analysis indicates that *CAR* cKO did not change the frequency of HSC in BM (*Online Supplementary Table1*). This result suggests that CAR enhances the speed of hematopoietic repopulation after BM transplantation but does not change HSC activity over the long term. Together, these results demonstrate that CAR supports hematopoietic regeneration after stress. Furthermore, the donor BM cells from Scl-CreERT/CARloxp/loxp mice in which *CAR* was specifically cKO in hematopoietic cells also had defects in initial repopulation after BM transplantation (*Online Supplementary Figure 7*), indicating that CAR on the hematopoietic cells plays a major role in regeneration. In repopulation assay with *CAR* cKO recipient mice, *CAR* cKO in the donor hematopoietic cells still resulted in defects in repopulation (*Online Supplementary Figure 8*), suggesting that CAR in the BM microenvironment is not essential for the function of CAR in regeneration.

Next, we assessed phenotypical LT-HSC (LSKFC), stem cells, and multiple progenitors in WT and *CAR* cKO mice after 5-FU treatment. None of these populations altered once the mice recovered from 5-FU injury (Figure 4D). In order to test whether the functional LT-HSC were affected by CAR after injury, BM transplantation was conducted with the donor cells collected from mice 1 month after 5-

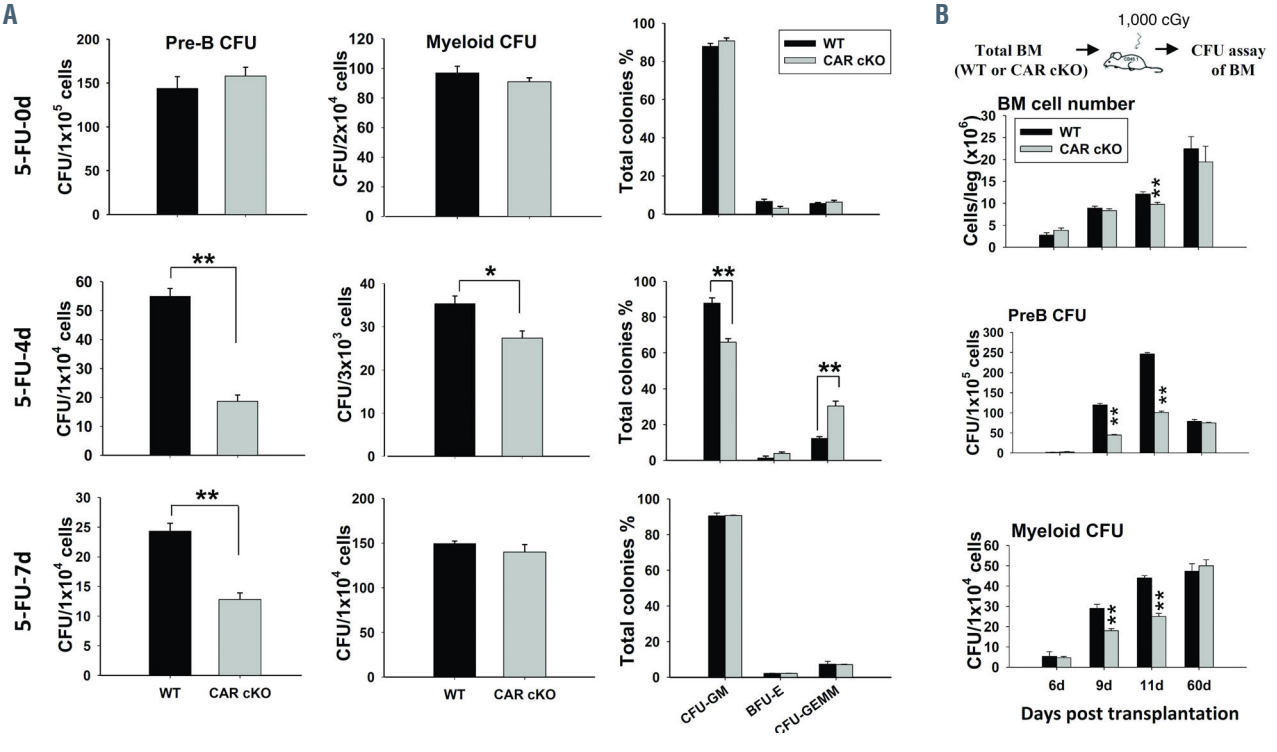

Figure 3. *CAR* stimulates progenitor production after 5-fluorouacil treatment and bone marrow transplantation. (A) One month after tamoxifen treatment, bone marrow (BM) cells from wild-type (WT) or *CAR* conditional knockout (cKO) mice were isolated before and at indicated days after 5-fluorouracil (5-FU) treatment (150 mg/kg) for colony forming units assays. (B) CFU assays of BM cells after transplantation of 1x10^6 total BM cells into lethally irradiated WT. *P<0.05; **P<0.001.

FU treatment. There was no difference in the long-term repopulation ability between WT and *CAR* cKO donors in this experiment (Figure 4E). Together, our results indicated that self-renewal of LT-HSC was not affected by CAR neither during homeostasis nor during regeneration.

In order to further understand how CAR affects LT-HSC, the population LSKFC cells were identified from mice on different days after 5-FU treatment and cell cycle states were analyzed (Figure 5). Before 5-FU injection, there was no difference between WT and *CAR* cKO cell cycle status. At 1.5 days after treatment, there was a significantly lower frequency of WT LSKFC in the G0 stage, and more WT LSKFC cells in apoptosis than prior to treatment because 5-FU kills cycling cells. After 3 days, more WT LSKFC than *CAR* cKO cells were in G1 stage and fewer were in G0 stage (Figure 5). These results suggest that CAR is needed for the transition into the cell cycle. On day 5 post 5-FU treatment, more than 90% of LSKFC cells were cycling and there were no differences between WT and *CAR* cKO populations. This implies that CAR is needed immediately after injury. Compared to *CAR* cKO mice, LSKFC of WT mice returned to homeostasis earlier, as more WT than *CAR* cKO LSKFC were at the G0 stage on day 6. In addition, CAR$^+$ LSKFC cells were positive for Ki67 staining and thus were cycling, whereas most CAR- LSKFC cells were Ki67 negative right after 5-FU treatment (*Online Supplementary Figure 9*). Thus, CAR appears to stimulate quiescent HSC to enter the cell cycle.

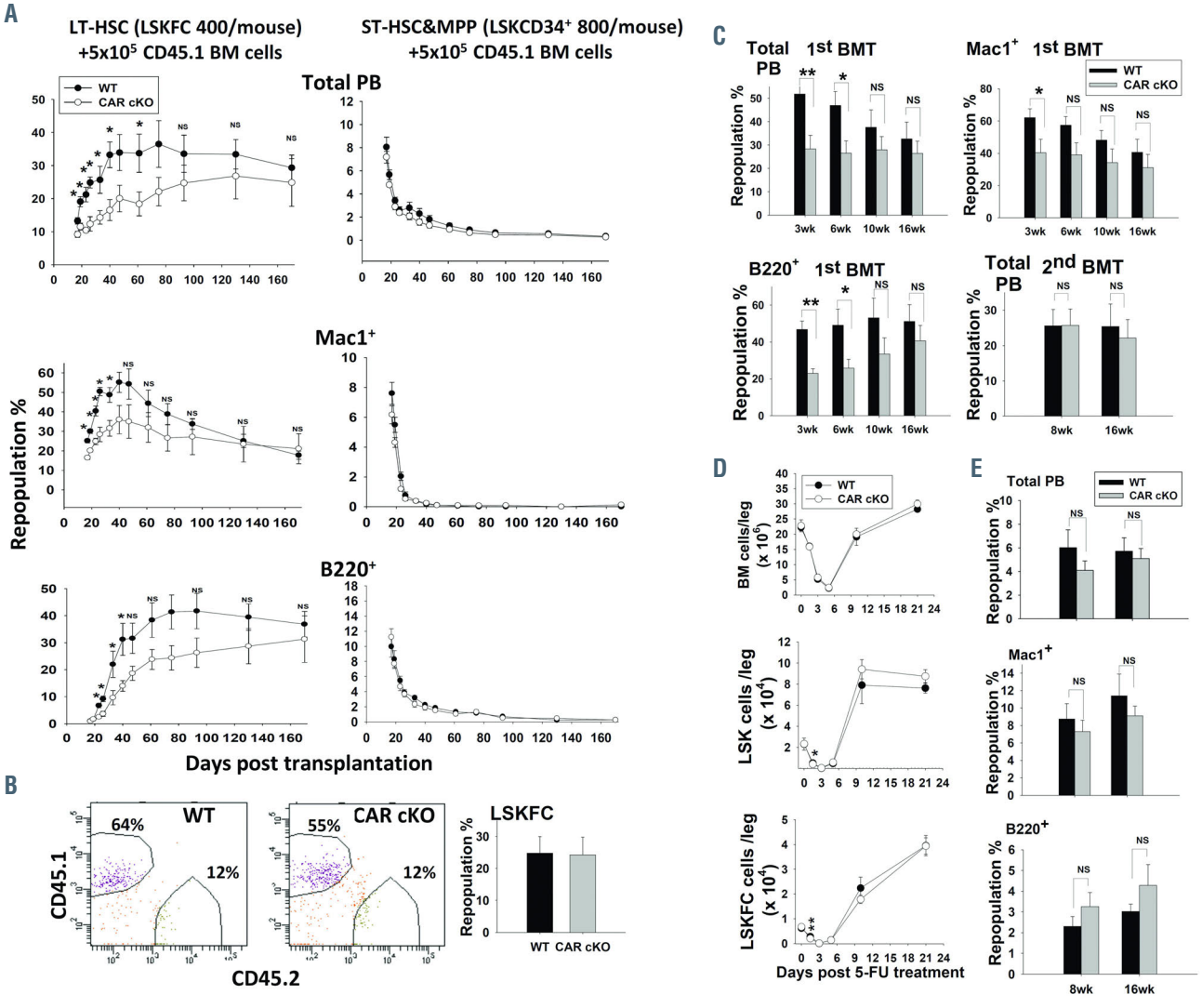

Figure 4. CAR stimulates regeneration by forcing hematopoietic stem cells into the cell cycle but does not affects self-renewal. (A) Competitive repopulation assays were performed with LT-HSC (LSKFC, LSKCD34-CD135$^-$) or "short-term" HSC (ST-HSC) plus multipotent hematopoietic progenitors (MPP) (LSKCD34$^+$) from wild-type (WT) or *CAR* conditional knockout (cKO) donors (1 month after tamoxifen treatment) and CD45.1 WT competitor bone marrow (BM). Percentages of donor peripheral leukocytes in total peripheral blood (PB), the Mac1$^+$ population, and the B220+ population after BM transplantation are plotted. (B) Percentages of donor LT-HSC (CD45.2) in total BM LT-HSC (CD45.1 plus CD45.2) 170 days after transplantation. (C) Competitive repopulation assays after initial BM transplantation were performed with a 1:1 ratio of donor (CD45.2) and CD45.1 WT competitor BM. Shown are the percentages of donor peripheral leukocytes (CD45.2) in total PB, the Mac1$^+$ population, and the B220+ population. Data are means ± standard error of the mean, n=7-9 mice. (D) Number of LSK and LSKFC cells in BM before and after treatment with 150 mg/kg 5-FU (n=3-9 mice per group). (E) Donor mice (1 month after tamoxifen treatment) were injected with 150 mg/kg 5-FU, and 1 month later, competitive repopulation assays were performed with a 1:1 ratio of donor and CD45.1 WT competitor BM. Shown are the percentages of donor peripheral leukocytes in total PB, the Mac1$^+$ population, and the B220$^+$ population. Data are means ± standard error of the mean, n=9-10 mice. **P*<0.05; ***P*<0.001. NS: no significant difference.

CAR stimulates Notch signaling

We sought to identify the underlying mechanism by which CAR mediates hematopoietic regeneration after stress. CAR binds to LNX, an E3 ligand of Numb,[21] suggesting the function of CAR may be related to Numb. After 5-FU treatment, Numb protein levels in HSC gradually decreased, and the population with no Numb staining increased from 5.7±0.3% on day 0 to 62.4±1.4% on day 5 (Figure 6A). On day 7, the Numb-negative population decreased to 6.8±1.5% (Figure 6A) as HSC had returned to homeostasis. Concordantly, the *Numb* mRNA levels decreased by more than 16 times on day 5 relative to pre-treatment levels and had returned to pre-treatment levels on day 7 (Figure 6A). HSC in WT mice entered the cell cycle earlier than did *CAR* cKO counterparts after 5-FU treatment (Figure 5). At 1.5 days after 5-FU treatment, there were fewer LSKFC cells that did not stain for Numb in *CAR* cKO mice than WT mice (Figure 6B), whereas there were no differences detected before or 5 days later after 5-FU treatment (*Online Supplementary Figure 10A*). The *Numb* mRNA levels in CAR cKO mice were similar to those in WT mice at 1.5 days after 5-FU treatment (*Online Supplementary Figure 10B*), suggesting that CAR mediates the degradation of Numb protein but does not affect Numb mRNA. In addition, there was fewer Numb protein in CAR^+ LSKFC cells than in CAR^- LSKFC cells (Figure 6C). Because Numb specifically inhibits Notch signaling,[26-28] these results suggest that Notch signaling is involved in CAR-mediated hematopoietic regeneration.

Notch signaling was previously reported to play an important role in hematopoietic regeneration.[6,29,30] In order to test how Notch signaling influences the function of CAR during regeneration, we treated mice with DAPT, an inhibitor of Notch signaling, with or without 300 mg/kg 5-FU. Whereas 5-FU treatment decreased survival of *CAR* cKO mice relative to WT counterparts, there was no difference in survival between 5-FU-treated WT and CAR cKO mice when Notch signaling was blocked by DAPT (Figure 6D). This implies that CAR stimulates regeneration via Notch signaling. At 1.5 days after 5-FU treatment, 4.2% of LSKFC cells were Notch1 positive in *CAR* cKO mice compared to 8.7% in WT mice, whereas 27.7% and 27% of LSKFC cells in *CAR* cKO and WT mice were positive for Notch2, respectively (Figure 6E). This indicate that Notch1, but not Notch2, is involved in the function of CAR. There were significantly lower levels of *hes1*, *hey1*, and *myc*, all Notch1 target genes, in *CAR* cKO mice compared to WT mice at 1.5 days after 5-FU treatment; there were no differences in levels of these mRNA prior to 5-FU treatment (Figure 6F). In addition, CAR cKO resulted in a defect in T-cell repopulation (*Online Supplementary Figure 11*), which further suggests a connection between CAR and Notch1, as Notch1 affects T-cell development.[31] Notch1 target genes indeed increased right after 5-FU treatment (*Online Supplementary Figure 12*). With 5-FU treatment, CAR+ HSC had more surface Notch1 protein than CAR- HSC (Figure 6G). Overexpression of CAR in LSKFC cells *in vitro* also increased Notch1 target gene expression (*Online Supplementary Figure 13*). In order to further confirm that CAR stimulates Notch signaling, we overexpressed the dominant negative MAML (dnMAML)[32-34] in 5-FU treated Lin- BM cells from UBC-Cre-ERT2/CARloxp/loxp mice

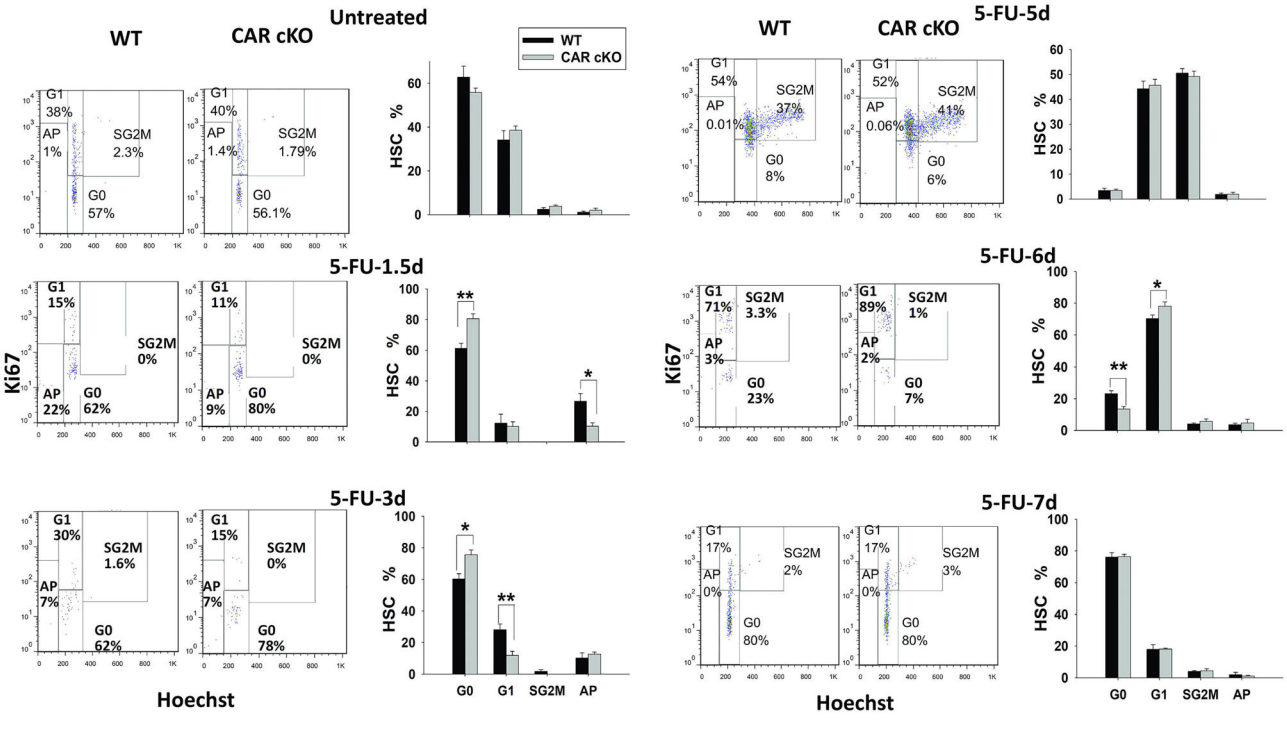

Figure 5. CAR stimulates hematopoietic stem cells proliferation after 5-fluorouracil treatment. Before and after 5-fluorouracil (5-FU) (150 mg/kg) treatment, cell cycle states of LSKFC cells were determined. The flow cytometry images are the representative results of bone marrow (BM) samples from wild-type (WT) or *CAR* conditional knockout (cKO) mice different times after 5-FU treatment, and the summaries of each time point after 5-FU treatment are on the right of flow cytometry images. The percentages of cell cycle states in total hematopoietic stem cells (HSC) (LSKFC) are indicated. Every groups include n=4-9 mice. G0: cell in G0 phase; G1; SG2M: cell in S, G2 and M phase; AP: cells in apoptosis. *P<0.05, **P<0.001.

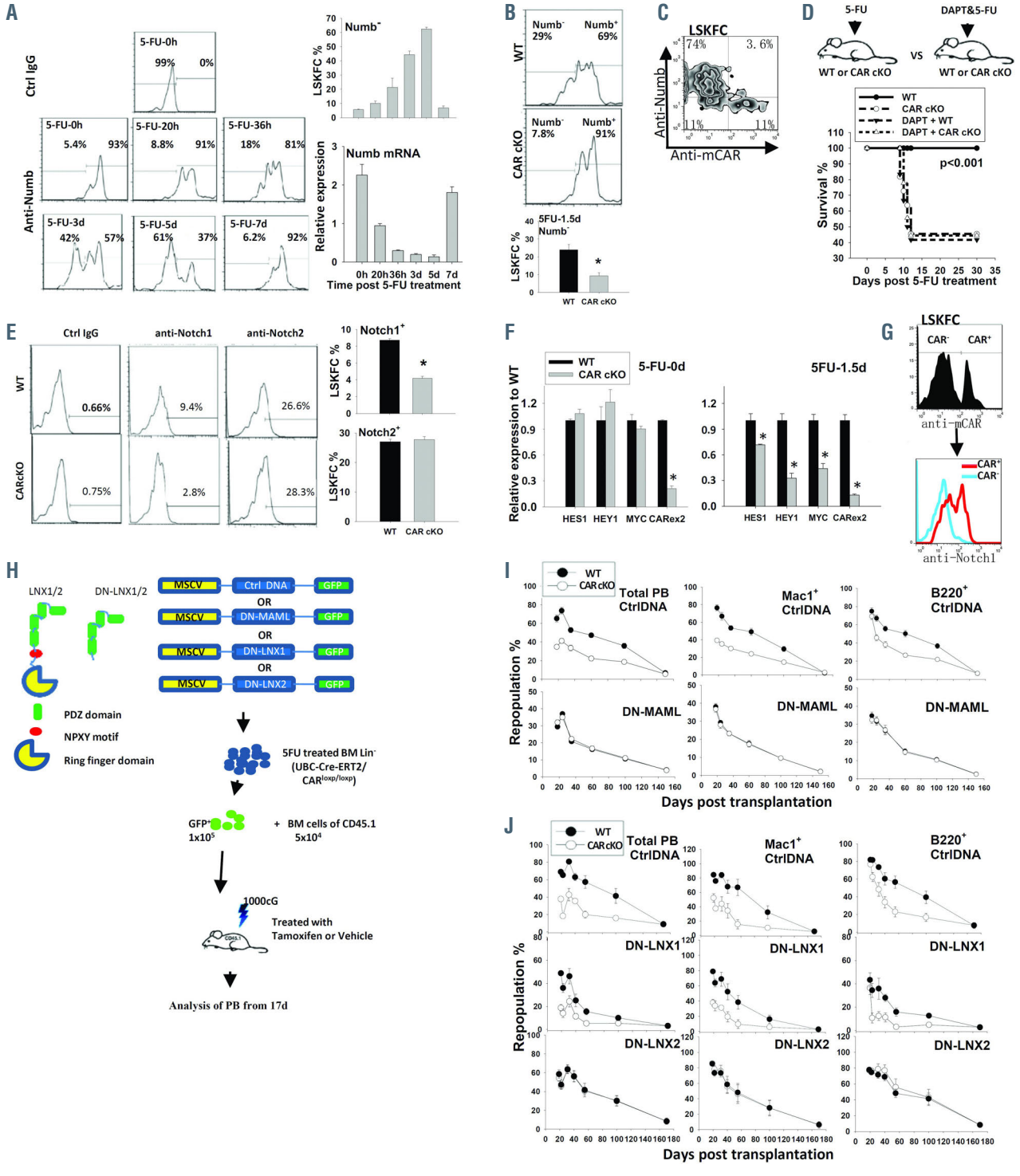

Figure 6. CAR enhances regeneration by stimulating Notch signaling. (A) Left panel: representative flow cytometry analyses of Numb negative and positive staining of LSKFC populations of 5-fluorouracil (5-FU) treated mice. Right top panel: Quantification of Numb negative staining in LSKFC. Right bottom panel: Quantification of *Numb* mRNA levels in LSKFC populations of 5-FU treated mice (the mRNA levels were calculated based on the 20-hour group, and experiments were repeated three times). (B) Top panel: representative flow cytometry analyses of Numb negative and positive staining in LSKFC populations at 36 hours after 5-FU treatment. Bottom panel: quantification of percentage of Numb negative LSKF cells in wild-type (WT) and *CAR* conditional knockout (cKO) cells, n=5 mice per group. (C) Numb and mouse CAR co-staining in LSKFC population of mice at 36 hours after 5-FU treatment. (D) Survival curves of WT and *CAR* cKO mice after injection with 300 mg/kg 5-FU and Notch signal inhibit DAPT, n=9-12 mice per group. (E) Right panel: representative flow cytometry analyses of membrane Notch1/2 staining in LSKFC populations at 36 hours after 5-FU treatment. Left top panel: quantification of percentage of Notch1-stained cells in LSKFC populations. Left bottom panel: quantification of percentage of Notoch2-stained cells in LSKFC populations, n=9 mice per group. (F) mRNA levels of *CAR* Notch target genes *hes1*, *hey1*, and *myc* in LSKFC populations before (right panel) and 36 hours after 5-FU treatment (left panel). (G) Notch1 and mCAR co-staining in LSKFC population of mice at 36 hours after 5-FU treatment. (H) Flow chart of experiment used to test whether Notch, LNX1 or LNX2 is involved in CAR function. DN-MAML, DN-LNX1 or DN-LNX2 was expressed in Lin- BM cells from *CAR* cKO mice without treatment of tamoxifen (UBC-Cre-ERT2/CAR$^{loxp/loxp}$), and these cells were used in repopulation assays. The recipient mice were treated with tamoxifen as *CAR* cKO group and treated with vehicle as WT group. (I and J) Percent repopulation of peripheral blood (PB) (left panels), the Mac1$^+$ population (middle panels), and the B220$^+$ population (right panels) by cells, n=8-10 mice per group. *P<0.05.

(*CAR* cKO mice before treatment with tamoxifen) to specifically inhibit Notch signaling (Figure 6H). In the competitive repopulation assay, the recipient CD45.1 mice were treated with tamoxifen to induce *CAR* cKO in the donor cells, with vehicle treatment as controls. With overexpressed dnMAML, the donor WT and *CAR* cKO BM cells showed the same repopulation abilities, whereas WT BM cells had a stronger repopulation ability than *CAR* cKO BM cells in the control condition (Figure 6I). In order to test whether enhanced Notch1 signaling rescues the phenotype of CAR deficiency, *CAR* cKO mice injected with 5-FU (300 mg/kg) were treated with valproic acid, a Notch1 activator.[35] These mice survived significantly longer than *CAR* cKO mice without valproic acid treatment (*Online Supplementary Figure 14*). In addition, valproic acid restored the repopulation ability of *CAR* cKO HSC (*Online Supplementary Figure 15*).

LNX contains a PDZ domain that may bind to the PDZ binding motif in the intracellular domain of CAR.[36, 37] There are two forms of LNX: LNX1 and LNX2.[36, 37] In order to test the roles of LNX1 and LNX2 in the function of CAR, the dominant negative (DN) forms of the LNX proteins (DN-LNX1 and DN-LNX2) with the ring finger domains and the NPXY motifs deleted [21] were over expressed in 5-FU treated Lin- BM cells from UBC-Cre-ERT2/CAR$^{loxp/loxp}$ mice (*CAR* cKO mice before treatment with tamoxifen), and a competitive repopulation assay was performed (Figure 6H). The cells expressing control DNA had significantly weaker repopulation ability in *CAR* cKO mice than in WT mice in both myeloid (Mac1^{+}) and lymphoid (B220^{+}) populations (Figure 6J). Repopulation of WT and *CAR* cKO mice was similar when donor cells expressed DN-LNX2, while donor cells expressing DN-LNX1 less effectively repopulated *CAR* cKO mice (Figure 6J). At 170 days after transplantation, repopulation percentages were similar in all groups (Figure 6J), indicating that lack of CAR had no effect on the total HSC pool. In order to further explore the relationship among CAR, LNX2 and Numb, we overexpressed CAR, LNX2 or DN-LNX2 in Lin- cells and evaluated the protein levels of Numb in LSK cells with flow cytometry. Overexpression of CAR or LNX2 decreased the Numb level in LSK cells, whereas DN-LNX2 elevated Numb expression (*Online Supplementary Figure 16*). These data suggest that LNX2, but not LNX1, is involved in the function of CAR (*Online Supplementary Figure 17*).

Discussion

Substantial efforts have been dedicated toward uncovering the mechanisms that regulate HSC niche maintenance.[7, 8] Recent studies demonstrated the essential roles of BM endothelial cells and osteolineage cells in regulating HSC regeneration following myelotoxicity[38-40] and identified two BM endothelial cell-derived paracrine factors, PTN and EGF, and osteolineage cell-derived Dkk1 as regulators of HSC regeneration *in vivo*.[38,41,42] Here we identified CAR as a membrane protein on HSC that is rapidly upregulated after stress, whose transient expression induces quiescent HSC to enter the cell cycle to counteract the hematopoietic injury. Without CAR, the process was delayed, and the mice in which CAR was conditionally deleted were more sensitive to injury than WT mice. Lack of *CAR* neither changed the pool nor altered the self-renewal of HSC. Mechanistically we showed that elevated CAR upon stress activates Notch1 signaling by down regulating expression of Notch antagonist Numb to facilitate entry of quiescent HSC into the cell cycle. To our knowledge, this is the first report demonstrating the role of CAR in HSC regeneration.

The Notch pathway plays an important part in many developmental processes and appears to regulate many adult stem cell fate decisions.[43, 44] While it was reported that Notch signaling is dispensable for HSC self-renewal and maintenance during hematopoiesis,[45, 46] Notch1 can promote the expansion of LT-HSC while preserving self-renewal ability.[47, 48] The expression of the canonical Notch ligands Jagged-1 and Jagged-2 by endothelial cells support hematopoietic regeneration.[10, 29] Varnum-Finney *et al.* showed that Notch2 enhances the rate of formation of short-term repopulating multi-potential progenitor cells as well as LT-HSC after 5-FU treatment.[6] Our results indicate that expression of CAR in quiescent LT-HSC increases Notch1 expression and induces HSC to enter the cell cycle immediately after injury and has no effect on HSC that have entered the cell cycle. Of note, this Notch1-mediated proliferation upon stress does not alter self-renewal of HSC.

Numb is a membrane-associated, evolutionarily conserved adaptor protein that regulates cell fate determination via its ability to antagonize Notch signaling.[49,50] Normal HSC differentiation and self-renewal occur in the absence of Numb during homeostasis.51 We observed that Numb expression decreased after injury and then returned to normal levels after the injury was repaired (Figure 6A), and CAR accelerated Numb protein degradation before *Numb* mRNA levels decreased (Figure 6B). A low level of Numb protein might be necessary for functional Notch signaling during regeneration. Low *Numb* mRNA levels during regeneration may be due to inhibition by Notch signaling.[52] LNX proteins are E3 ligases that act on Numb [53] and that may bind to the PDZ motif of CAR.[36, 37] Here we demonstrated that CAR expressed on HSC activates Notch signaling via LNX2, suggesting the PDZ motif of CAR plays a critical role in hematopoietic regeneration. CAR and CAR can form trans-interaction with a low affinity,[54] and this trans-interaction may stimulate CAR downstream signaling. However, in *CAR* cKO recipient mice, CAR expressed on donor hematopoietic cells still plays a critical role in regeneration in repopulation assay (*Online supplementary Figure 8*). Analysis of BM cells after 5-FU injection, HSC were more prone to increase CAR expression compared to other cells (Figure 1C). These results indicate that CAR expressed in the BM microenvironment is not important in HSC regeneration, and an unknown ligand may act on CAR and on HSC to regulate transition from quiescence to proliferation during hematopoietic stress. These possibilities warrant future investigations.

How HSC detect signals sent upon injury remains unknown. Low oxygen tension (hypoxia) is thought to be a characteristic of the quiescent HSC niche,[55] and oxygen levels may change markedly after radiation and chemotherapy.[56] CAR expression is repressed by hypoxia inducible factor-1a (Hif-1a).[57] We therefore propose that the oxygen increase resulting from hematopoietic injury may suppress Hif-1a expression, leading to induction of CAR expression. This transient elevation of CAR levels activates Notch1 signaling by down regulating expression of Notch antagonist Numb. Notch signaling could promote expansion of HSC by preventing hematopoietic cell differentiation upon

stress.[10,29,47,48] Our study suggests that the coupling of Notch with CAR enables a checked cell fate of HSC with increased cell cycling but not over-differentiation. Overall the mechanism facilitates the entry of quiescent HSC into the cell cycle with maintenance of stemness. Our continuous study in this subject may lead to development of novel strategies for promotion of stem cell regeneration.

Disclosures

No conflicts of interest to disclose.

Contributions

GW contributed to design, experimental performance, interpretation, and writing; CCZ contributed to design and writing.

Acknowledgments

We thank the NIH (1R01CA172268), the Leukemia & Lymphoma Society (1024-14), the March of Dimes Foundation (1-FY14-201), the Cancer Prevention and Research Institute of Texas (RP180435), and the Robert A. Welch Foundation (I-1834) for generous support.

References

1. Busch K, Klapproth K, Barile M, et al. Fundamental properties of unperturbed haematopoiesis from stem cells in vivo. Nature. 2015; 518(7540):542-546.
2. Wilson A, Laurenti E, Oser G, et al. Hematopoietic stem cells reversibly switch from dormancy to self-renewal during homeostasis and repair. Cell. 2008;135(6): 1118-1129.
3. Essers MA, Offner S, Blanco-Bose WE, et al. IFNα activates dormant haematopoietic stem cells in vivo. Nature. 2009;458(7240): 904-908.
4. Goessling W, North TE, Loewer S, et al. Genetic interaction of PGE2 and Wnt signaling regulates developmental specification of stem cells and regeneration. Cell. 2009;136(6):1136-1147.
5. Seita J, Weissman IL. Hematopoietic stem cell: self−renewal versus differentiation. Wiley Interdiscip Rev Syst Biol Med. 2010;2(6):640-653.
6. Varnum-Finney B, Halasz LM, Sun M, Gridley T, Radtke F, Bernstein ID. Notch2 governs the rate of generation of mouse long-and short-term repopulating stem cells. J Clin Invest. 2011;121(3):1207-1216.
7. Mendelson A, Frenette PS. Hematopoietic stem cell niche maintenance during homeostasis and regeneration. Nat Med. 2014;20(8):833-846.
8. Morrison SJ, Scadden DT. The bone marrow niche for haematopoietic stem cells. Nature. 2014;505(7483):327-334.
9. Zhang CC, Sadek HA. Hypoxia and metabolic properties of hematopoietic stem cells. Antioxid Redox Signal. 2014;20(12):1891-1901.
10. Guo P, Poulos MG, Palikuqi B, et al. Endothelial jagged-2 sustains hematopoietic stem and progenitor reconstitution after myelosuppression. J Clin Invest. 2017; 127(12):4242-4256.
11. Bergelson JM, Cunningham JA, Droguett G, et al. Isolation of a common receptor for Coxsackie B viruses and adenoviruses 2 and 5. Science. 1997;275(5304):1320-1323.
12. Cohen CJ, Shieh JT, Pickles RJ, Okegawa T, Hsieh J-T, Bergelson JM. The coxsackievirus and adenovirus receptor is a transmembrane component of the tight junction. Proc Natl Acad Sci U S A. 2001;98(26):15191-15196.
13. Lim B-K, Xiong D, Dorner A, et al. Coxsackievirus and adenovirus receptor (CAR) mediates atrioventricular-node function and connexin 45 localization in the murine heart. J Clin Invest. 2008;118(8): 2758-2770.
14. Anders M, Rösch T, Küster K, et al. Expression and function of the coxsackie and adenovirus receptor in Barrett's esophagus and associated neoplasia. Cancer Gene Ther. 2009;16(6):508-515.
15. Stecker K, Vieth M, Koschel A, Wiedenmann B, Röcken C, Anders M. Impact of the coxsackievirus and adenovirus receptor on the adenoma–carcinoma sequence of colon cancer. Br J Cancer. 2011;104(9):1426-1433.
16. Saito K, Sakaguchi M, Iioka H, et al. Coxsackie and adenovirus receptor is a critical regulator for the survival and growth of oral squamous carcinoma cells. Oncogene. 2014;33(10):1274-1286.
17. Nalbantoglu J, Pari G, Karpati G, Holland PC. Expression of the primary coxsackie and adenovirus receptor is downregulated during skeletal muscle maturation and limits the efficacy of adenovirus-mediated gene delivery to muscle cells. Hum Gene Ther. 1999;10(6):1009-1019.
18. Zheng J, Huynh H, Umikawa M, Silvany R, Zhang CC. Angiopoietin-like protein 3 supports the activity of hematopoietic stem cells in the bone marrow niche. Blood. 2011;117(2):470-479.
19. Zheng J, Umikawa M, Cui C, et al. Inhibitory receptors bind ANGPTLs and support blood stem cells and leukaemia development. Nature. 2012;485(7400):656-660.
20. Zheng J, Umikawa M, Zhang S, et al. Ex vivo expanded hematopoietic stem cells overcome the MHC barrier in allogeneic transplantation. Cell Stem Cell. 2011;9(2):119-130.
21. Kansaku A, Hirabayashi S, Mori H, et al. Ligand-of-Numb protein X is an endocytic scaffold for junctional adhesion molecule 4. Oncogene. 2006;25(37):5071-5084.
22. Rebel VI, Hartnett S, Denham J, Chan M, Finberg R, Sieff CA. Maturation and lineage−specific expression of the coxsackie and adenovirus receptor in hematopoietic cells. Stem Cells. 2000;18(3):176-182.
23. Dorner AA, Wegmann F, Butz S, et al. Coxsackievirus-adenovirus receptor (CAR) is essential for early embryonic cardiac development. J Cell Sci. 2005;118(15):3509-3521.
24. Grzegorzewski K, Ruscetti FW, Usui N, et al. Recombinant transforming growth factor beta 1 and beta 2 protect mice from acutely lethal doses of 5-fluorouracil and doxorubicin. J Exp Med. 1994;180(3):1047-1057.
25. Cheng C-W, Adams GB, Perin L, et al. Prolonged fasting reduces IGF-1/PKA to promote hematopoietic-stem-cell-based regeneration and reverse immunosuppression. Cell Stem Cell. 2014;14(6):810-823.
26. McGill MA, McGlade CJ. Mammalian numb proteins promote Notch1 receptor ubiquitination and degradation of the Notch1 intracellular domain. J Biol Chem. 2003;278(25): 23196-23203.
27. Bray SJ. Notch signalling: a simple pathway becomes complex. Nat Rev Mol Cell Biol. 2006;7(9):678-689.
28. Chapman G, Liu L, Sahlgren C, Dahlqvist C, Lendahl U. High levels of Notch signaling down-regulate Numb and Numblike. J Cell Biol. 2006;175(4):535-540.
29. Poulos MG, Guo P, Kofler NM, et al. Endothelial Jagged-1 is necessary for homeostatic and regenerative hematopoiesis. Cell Rep. 2013;4(5):1022-1034.
30. Mercher T, Cornejo MG, Sears C, et al. Notch signaling specifies megakaryocyte development from hematopoietic stem cells. Cell Stem Cell. 2008;3(3):314-326.
31. Radtke F, Wilson A, Stark G, et al. Deficient T cell fate specification in mice with an induced inactivation of Notch1. Immunity. 1999;10(5):547-558.
32. Moellering RE, Cornejo M, Davis TN, et al. Direct inhibition of the NOTCH transcription factor complex. Nature. 2009;462(7270): 182-188.
33. Weng AP, Nam Y, Wolfe MS, et al. Growth suppression of pre-T acute lymphoblastic leukemia cells by inhibition of notch signaling. Mol Cell Biol. 2003;23(2):655-664.
34. Maillard I, Weng AP, Carpenter AC, et al. Mastermind critically regulates Notch-mediated lymphoid cell fate decisions. Blood. 2004;104(6):1696-1702.
35. Platta CS, Greenblatt DY, Kunnimalaiyaan M, Chen HJJoSR. Valproic acid induces Notch1 signaling in small cell lung cancer cells. J Surg Res. 2008;148(1):31-37.
36. Mirza M, Raschperger E, Philipson L, Pettersson RF, Sollerbrant K. The cell surface protein coxsackie-and adenovirus receptor (CAR) directly associates with the Ligand-of-Numb Protein-X2 (LNX2). Exp Cell Res. 2005;309(1):110-120.
37. Sollerbrant K, Raschperger E, Mirza M, et al. The Coxsackievirus and adenovirus receptor (CAR) forms a complex with the PDZ domain-containing protein ligand-of-numb protein-X (LNX). J Biol Chem. 2003;278(9): 7439-7444.
38. Himburg HA, Doan PL, Quarmyne M, et al. Dickkopf-1 promotes hematopoietic regeneration via direct and niche-mediated mechanisms. Nat Med. 2017;23(1):91-99.
39. Doan PL, Russell JL, Himburg HA, et al. Tie2+ bone marrow endothelial cells regulate hematopoietic stem cell regeneration following radiation injury. Stem Cells. 2013;31(2):327-337.
40. Hooper AT, Butler JM, Nolan DJ, et al. Engraftment and reconstitution of hematopoiesis is dependent on VEGFR2-mediated regeneration of sinusoidal endothelial cells. Cell Stem Cell. 2009;4(3): 263-274.
41. Doan PL, Himburg HA, Helms K, et al. Epidermal growth factor regulates hematopoietic regeneration after radiation injury. Nat Med. 2013;19(3):295-304.
42. Himburg HA, Muramoto GG, Daher P, et al. Pleiotrophin regulates the expansion and regeneration of hematopoietic stem cells. Nat Med. 2010;16(4):475-482.
43. Pajcini K, Speck N, Pear W. Notch signaling in mammalian hematopoietic stem cells. Leukemia. 2011;25(10):1525-1532.
44. Bigas A, Espinosa L. Hematopoietic stem

cells: to be or Notch to be. Blood. 2012;119 (14):3226-3235.
45. Maillard I, Koch U, Dumortier A, et al. Canonical notch signaling is dispensable for the maintenance of adult hematopoietic stem cells. Cell Stem Cell. 2008;2(4):356-366.
46. Mancini SJ, Mantei N, Dumortier A, Suter U, MacDonald HR, Radtke F. Jagged1-dependent Notch signaling is dispensable for hematopoietic stem cell self-renewal and differentiation. Blood. 2005;105(6):2340-2342.
47. Varnum-Finney B, Xu L, Brashem-Stein C, et al. Pluripotent, cytokine-dependent, hematopoietic stem cells are immortalized by constitutive Notch1 signaling. Nat Med. 2000;6(11):1278-1281.
48. Stier S, Cheng T, Dombkowski D, Carlesso N, Scadden DT. Notch1 activation increases hematopoietic stem cell self-renewal in vivo and favors lymphoid over myeloid lineage outcome. Blood. 2002;99(7):2369-2378.
49. Spana EP, Doe CQ. Numb antagonizes Notch signaling to specify sibling neuron cell fates. Neuron. 1996;17(1):21-26.
50. Guo M, Jan LY, Jan YN. Control of daughter cell fates during asymmetric division: interaction of Numb and Notch. Neuron. 1996;17 (1):27-41.
51. Wilson A, Ardiet D-L, Saner C, et al. Normal hemopoiesis and lymphopoiesis in the combined absence of numb and numblike. J Immunol. 2007;178(11):6746-6751.
52. Wu Y-C, Lee K-S, Song Y, Gehrke S, Lu B. The bantam microRNA acts through Numb to exert cell growth control and feedback regulation of Notch in tumor-forming stem cells in the Drosophila brain. PLoS Genet. 2017;13(5):e1006785.
53. Nie J, McGill MA, Dermer M, Dho SE, Wolting CD, McGlade CJ. LNX functions as a RING type E3 ubiquitin ligase that targets the cell fate determinant Numb for ubiquitin–dependent degradation. EMBO J. 2002;21(1-2):93-102.
54. van Raaij MJ, Chouin E, van der Zandt H, Bergelson JM, Cusack S. Dimeric structure of the coxsackievirus and adenovirus receptor D1 domain at 1.7 Å resolution. Structure. 2000;8(11):1147-1155.
55. Simsek T, Kocabas F, Zheng J, et al. The distinct metabolic profile of hematopoietic stem cells reflects their location in a hypoxic niche. Cell Stem Cell. 2010;7(3):380-390.
56. Spencer JA, Ferraro F, Roussakis E, et al. Direct measurement of local oxygen concentration in the bone marrow of live animals. Nature. 2014;508(7495):269-273.
57. Küster K, Koschel A, Rohwer N, Fischer A, Wiedenmann B, Anders M. Downregulation of the coxsackie and adenovirus receptor in cancer cells by hypoxia depends on HIF-1α. Cancer Gene Ther. 2010;17(2):141-146.

ARTICLE

MYB bi-allelic targeting abrogates primitive clonogenic progenitors while the emergence of primitive blood cells is not affected

Zahir Shah,[1,2,3] Elena S. Philonenko,[1,2,4] Vasily Ramensky,[5,6] Chenyu Fan,[1,2,3] Cuihua Wang,[1,2] Hanif Ullah,[1,2,3] Baoyun Zhang,[1,2] Pavel Volchkov[5] and Igor M. Samokhvalov[1,2]

[1]Guangzhou Institutes of Biomedicine and Health, Chinese Academy of Science, Guangzhou, China; [2]Key Laboratory of Regenerative Biology, Chinese Academy of Science, Guangdong Provincial Key Laboratory of Stem Cells and Regenerative Medicine, Guangzhou, China; [3]University of Chinese Academy of Science, Beijing, China; [4]Vavilov Institute of General Genetics, Russian Academy of Science, Moscow, Russia; [5]Moscow Institute of Physics and Technology, Dolgoprudny, Moscow, Russia and [6]National Medical Research Center for Preventive Medicine, the Ministry of Healthcare of the Russian Federation, Moscow, Russia

Ferrata Storti Foundation

Haematologica 2021
Volume 106(8):2191-2202

ABSTRACT

MYB is a key regulator of definitive hematopoiesis and it is dispensable for the development of primitive hematopoietic cells in vertebrates. In order to delineate definitive *versus* primitive hematopoiesis during differentiation of human embryonic stem cells, we have introduced reporters into the *MYB* locus and inactivated the gene by bi-allelic targeting. In order to recapitulate the early developmental events more adequately, mutant and wild-type human embryonic stem cell lines were differentiated in defined culture conditions without the addition of hematopoietic cytokines. The differentiation of the reporter cell lines demonstrated that MYB is specifically expressed throughout emerging hematopoietic cell populations. Here we show that the disruption of the *MYB* gene leads to severe defects in the development and proliferation of primitive hematopoietic progenitors while the emergence of primitive blood cells is not affected. We also provide evidence that MYB is essential for neutrophil and T-cell development and the upregulation of innate immunity genes during hematopoietic differentiation. Our results suggest that the endothelial origin of primitive blood cells is direct and does not include the intermediate step of primitive hematopoietic progenitors.

Introduction

Mammalian hematopoietic development is a multistage process that occurs in two distinct sites of the vertebrate conceptus, the yolk sac and the embryo proper. The primitive hematopoietic program of the yolk sac is transient and restricted to a few blood cell lineages. The earliest clonogenic hematopoietic progenitors arise within the extraembryonic mesoderm of the mid-streak mouse conceptus and precede the appearance of first hemoglobinized erythroblasts by about 1.5 days of gestation.[1,2] The primitive hematopoietic progenitors are thought to give rise to all primitive erythroblasts and other primitive blood cells.[1,3,4] The progenitor-derived primitive erythroblasts gradually mature and ultimately enucleate within mouse embryo circulation.[5]

Myb, one of the key hematopoietic transcription factors, is essential for the maintenance of definitive hematopoietic progenitors with high proliferative potential.[6] In the developmental context, the *Myb* gene is expressed in the definitive erythroid precursors of mouse fetal liver but is not detected in primitive erythroid cells of the yolk sac.[7] The homozygous disruption of *Myb* is embryonic lethal by E15.5 due to progressive anemia caused by defects in the definitive erythropoiesis, whereas primitive hematopoiesis is not affected.[8] The role of MYB in human hematopoiesis has been studied using the hematopoietic differentiation of human pluripotent stem cells (hPSC) *in vitro* as a model of human hematopoietic develop-

Correspondence:

IGOR M. SAMOKHVALOV
igor@gibh.ac.cn

Received: February 4, 2020.

Accepted: July 28, 2020.

Pre-published: July 30, 2020.

https://doi.org/10.3324/haematol.2020.249193

ment. These studies have supported the established notion of MYB as the definitive hematopoietic factor that does not contribute to the development of the primitive wave.[9,10]

In an attempt to pinpoint the origin of the definitive hematopoiesis, we generated *MYB* reporter and *MYB*-null human embryonic stem cells (hESC) lines by gene targeting and subjected them to hematopoietic differentiation in defined conditions without exogenous hematopoietic cytokines. Unexpectedly, we have found that MYB is essential for the development and proliferation of primitive clonogenic progenitors. Our results suggest that the early primitive blood cells can develop independently of the primitive clonogenic progenitors that constitute a separate minor cell population of primitive hematopoiesis.

Methods

The hESC line used in this study was H1 (NIH code WA01). In order to initiate hematopoietic development, briefly formed embryoid bodies (EB) were allowed to attach to surfaces that were coated with extracellular matrix proteins. The cells were differentiated in a Stemline®II SFM (Sigma-Aldrich, St. Louis, MO, USA) – based medium supplemented with hVEGF165 (PeproTech, Rocky Hill, NJ). During the first 2 days post-attachment, hBMP4 (PeproTech) was added to initiate mesoderm formation. Additional information on materials and methods is provided in the *Online Supplementary Appendix*.

Results

Generation of reporter cell lines and bi-allelic inactivation of *MYB*

In order to create *MYB* reporter hESC lines, we have introduced alternative fluorescent gene reporters Venus and tdTomato into the second exon of *MYB* by TALEN-mediated homologous recombination (Figure 1A; *Online Supplementary Figure S1A* and *B*). The reporter insert containing a strong transcription stop signal has been placed downstream of the transcription elongation attenuation site and the second promoter both located in the first intron.[11,12] This position of the reporter genes maximized the probability of making reporter expression closely reflect transcription regulation of *MYB*.

Properly targeted clones were selected by Southern hybridization with two different biotin-labeled probes (*Online Supplementary Figure S1C* and *D*). For bi-allelic inactivation, we excised the *PGK-Puro*^{R} cassette by Cre recombinase and subjected resulting Puro^{S} clones to the second round of electroporation with the targeting construct and TALEN (*Online Supplementary Figure 1E* and *F*). Real-time reverse transcription polymerase chain reaction (RT-PCR) and western blotting showed that the *MYB* expression in differentiated bi-allelic knockout cells was effectively switched off (Figure 1B and C). Analysis of *MYB* exonal expression using RNA sequencing of differentiated mutant hESC confirmed that the gene transcription elongation is blocked by the inserted gene cassette (*Online Supplementary Figure S2A*). The analysis demonstrated that despite the presence of the PGK promoter in the second targeted allele the promoter leakage was negligible. Karyotyping of the targeted cells did not reveal any gross chromosomal aberrations (*Online Supplementary Figure S2B*).

MYB is specifically expressed in the early human blood cells

We subjected H1-isogenic hESC reporter lines (single knockout, SKO, cells) and *MYB*-null lines (double knockout, DKO, cells) to a modified planar hematopoietic differentiation in defined culture conditions.[13-15] These conditions improve the reproducibility of the data,[15] which is critical for reliable phenotypic analysis of the mutant hESC lines. Moreover, we did not add hematopoietic cytokines to the differentiation medium for closer recapitulation of the early hematopoietic development. The rationale for adopting such protocol was that high concentrations of hematopoietic cytokines are unlikely to occur in the early conceptus.[16]

The recapitulative quality of such hematopoietic cytokine-free *in vitro* differentiation was manifested by the spontaneous formation of vascular plexus-like structures and transitory blood island-like VE-Cadherin^{+} cell aggregates at which hematopoietic induction occurred in a process similar to the endothelial-to-hematopoietic transition (EHT) (Figure 1D). Single or clumped CD43^{+} cells emerged on the fringes of the "blood islands" after apparent downregulation of VE-Cadherin in the peripheral cells, and the loss of VE-Cadherin was followed by dissociation of the nascent blood cells from the aggregates (Figure 1D). The emerging CD43^{+} cells induced the expression of key hematopoietic transcription factors, such as GATA1, GATA2, GFI1, GFI1B, KLF1, LMO2, MYB, RUNX1, SPI1, TAL1, which attested the hematopoietic commitment of these cells in contrast to non-hematopoietic CD43-negative cells (Figure 1E). In accordance with the transcriptomics data, MYB-Venus^{+} cells emerge within these *in vitro* blood islands (Figure 1F). Our observations suggest that the segregation of the early blood cells from the hESC-derived hemogenic endothelium (HE) is similar to the initiation of hematopoiesis in the yolk sac.[2]

The SKO cells demonstrated vigorous hematopoietic development identical to that of the parent "wild-type" (WT) H1 hESC (*Online Supplementary Figure 3A*), indicating the absence of non-specific genetic lesions in these cells. Time course quantitation of MYB-Venus fluorescence in SKO cells and *MYB* mRNA in WT cells showed two peaks of expression, on day 6 and around day 14 (Figure 1G). The close correlation of MYB-Venus flow cytometry of SKO cells and the *MYB* qRT-PCR data of WT cells indicates that the knockin reporter system faithfully reflects *MYB* expression. Undifferentiated SKO hESC were Venus-negative while the MYB-Venus expression was induced upon the upregulation of the earliest hematopoietic markers and concomitant downregulation of pluripotency markers (Figure 2A). Starting on day 6 of hematopoietic differentiation, MYB-Venus was specifically expressed in overlapping blood cell populations (*Online Supplementary Figure S3A*). Within differentiated cultures on day 6 and day 10, the highest level of MYB-Venus expression was observed in the CD41a^{high}CD235a^{+} erythro-megakaryocyte precursors and the CD34^{low}CD45^{+} phenotypic progenitor population, respectively (*Online Supplementary Figure S3B* and *C*).

In agreement with the flow cytometry data, RNA sequencing demonstrated around 20 times higher levels of *MYB* mRNA in day 6 CD43^{+} cells compared to day 6 CD43^{-} non-blood cells (Figure 2B). The MYB^{+}/CD43^{+} cells also selectively expressed high levels of *GYPA* (CD235a) and *ITGA2B* (CD41a) mRNA. These markers were shown

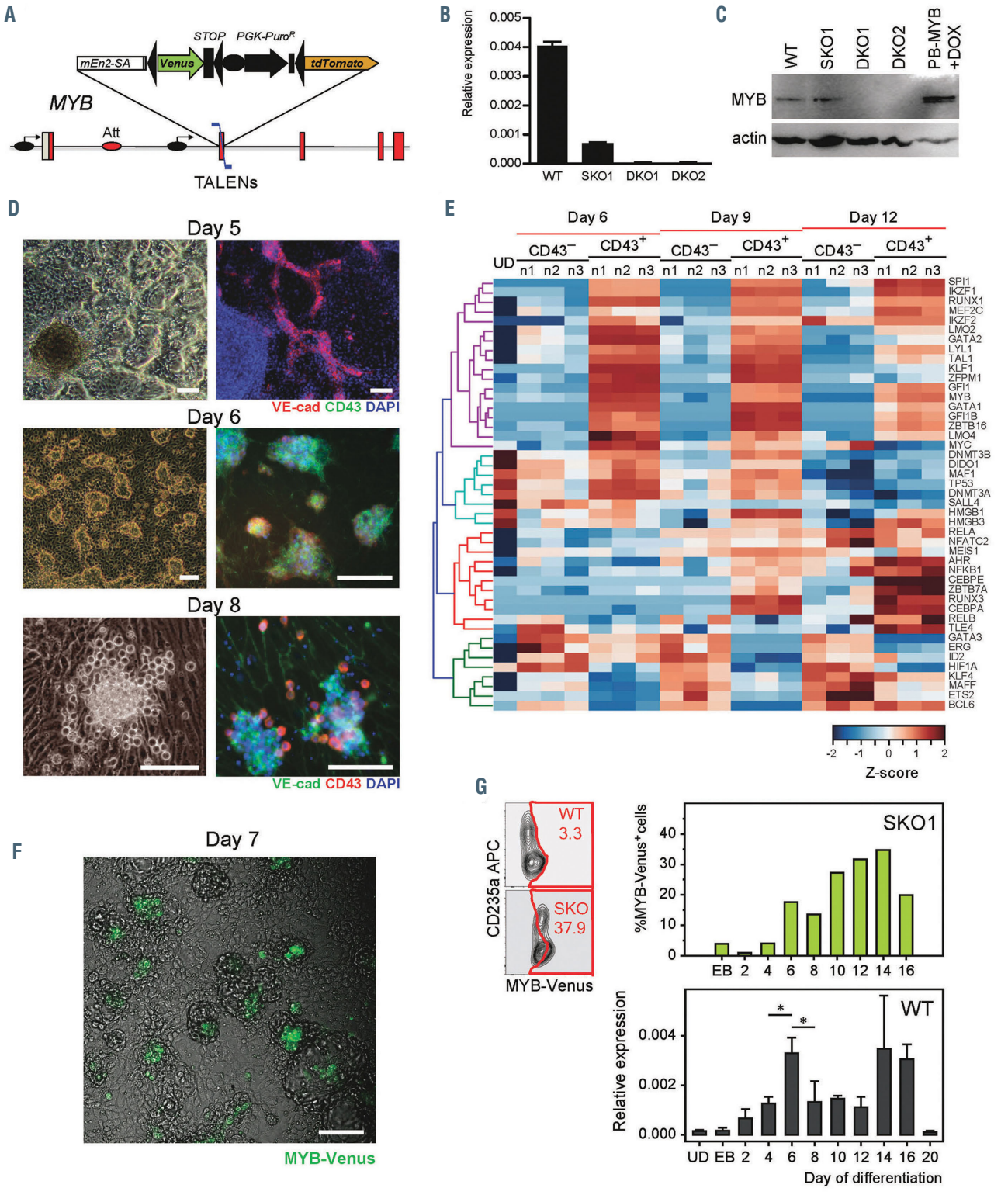

Figure 1. The outline of the experimental system for studying the role of MYB in early human hematopoietic development. (A) Scheme of the *MYB* gene targeting. Designations are as in *Online Supplementary Figure S1B*. (B) Quantitative real-time polymersase chain reaction (qRT-PCR) analysis of the *MYB* expression in day 6 differentiated wild-type (WT), SKO, and DKO cells. Here and elsewhere: SKO1, DKO1, and DKO2, independent single and double knockout H1-isogenic cell lines. (C) Western blot analysis of day 12 differentiated *MYB* knockout cells. PB-MYB+DOX, MYB-null cells transfected with a PiggyBack-TRE-CMV-MYB cDNA vector and activated by doxycycline (DOX). (D) *In vitro* blood islands in the cytokine-free hematopoietic differentiation of human embryonic stem cells (hESC). Upper panels show representative phase-contrast images of the early stages of H1 hESC differentiation, the lower panels – immunocytofluorescent staining of the cultures at the corresponding stages of differentiation. Scale bar – 100 μm. (E) Expression of selected transcription factors in $CD43^+$ *versus* $CD43^-$ cell population on day 6, 9, and 12 of hematopoietic differentiation of H1 hESC. Gene expression levels in the heatmap are normalized by Z-score transformation across the RNA-seq experiments, with three independent biological repeats for each cell population. (F) The emergence of MYB-$Venus^+$ DKO cells (DKO2) from the *in vitro* blood island structures on day 7 of differentiation. Scale bar – 100 μm. (G) Venus reporter expression faithfully reflects the dynamics of *MYB* mRNA levels during the time course of differentiation. The upper bar plot is the quantitation, exemplified by contour plots on the left, of the MYB-Venus expression dynamics in SKO cells (*Online Supplementary Figure S3A*). The lower bar plot demonstrates the quantitation of *MYB* mRNA by qRT-PCR in undifferentiated (UD) and differentiated WT H1 hESC on the EB stage (day 0) through day 20. The data are mean ± standard deviation, **P*<0.05, two-tailed Student's *t*-test.

to be specific for the hESC-derived primitive human hematopoiesis.[17,18] Correspondingly, cell populations expressing CD43, CD235a, and CD41a were strongly suppressed by SB-431542, the inhibitor of Activin/Nodal signaling and primitive human hematopoiesis[17] (Figure 2C). Principal component analysis (PCA) revealed a very close similarity of gene expression profiles in day 6 DKO/SKO MYB-Venus$^+$ cells and WT CD43$^+$ primitive blood cells whereas gene expression of day 6 DKO/SKO MYB-Venus$^-$ cells closely correlated with the profile of WT CD43$^-$ cells (Figure 2D). Taken together, these observations indicate that in contrast to mouse data[1,7] MYB is specifically expressed in the primitive human blood cells.

Defective development of myeloid and T cells derived from MYB-null human embryonic stem cells

The MYB-Venus fluorescence in differentiated DKO hESC was much stronger compared to SKO cells, while the hematopoietic specificity of the reporter expression was preserved (Figure 2E). The upregulation of MYB-Venus expression in the MYB-null cells was significantly higher than the expected two-fold rise in cells with the bi-allelic knockin of a reporter gene (Figure 2F) indicating negative transcriptional autoregulation of *MYB* transcription during the early human hematopoietic development.

Despite the specific expression of MYB in early human blood cells, its bi-allelic inactivation did not perturb the emergence of blood cells at the early stages of differentiation (Figures 2E and 3A). The vast majority of these MYB-independent early blood cell populations were CD235a$^+$/CD41a$^+$ cells of the primitive erythro-megakaryocytic lineage (Figure 3A). Minor qualitative alterations in the expression of hematopoietic markers were noticeable in the CD43$^+$CD45$^+$ DKO cell population starting from day 10 of differentiation. (Figure 3B). The phenotypical differences become increasingly prominent by day 12 (*Online Supplementary Figure 4A*). By day 20, DKO cells failed to develop into CD14^{low}CD66b$^+$CD86$^-$ neutrophil granulocytes, and the development of CD11b$^+$ immature myeloid cells was also negatively affected (Figure 3C). SKO cells demonstrated an intermediate myeloid phenotype, indicating a dose-dependent manner of MYB contribution to early human myeloid development and further validating the observed phenotype of MYB-null cells. The emergence of CD14$^+$CD86$^+$ monocytes and macrophages was apparently independent of MYB. The defect in the myeloid development of DKO cells was detected already on day 16 (*Online Supplementary Figure S4B*). Thus, MYB does not participate, or its deficiency is compensated, in the initial hematopoietic commitment, but the gene is critically important for granulocyte development and maturation.

The transcriptomes of MYB-Venus$^+$/CD43$^+$ early blood cell populations sustained significant changes between day 6 and day 12. In contrast, the gene expression profiles of non-blood MYB-Venus$^-$/CD43$^-$ remained almost the same (Figure 2D), except day 12 SKO MYB-Venus$^-$ populations containing blood cells that by day 12 further decreased the low MYB-Venus fluorescence of SKO cells and were sorted into the MYB-negative population. The day 6 – day 12 shift in gene expression of MYB-Venus$^+$/CD43$^+$ cells reflects a vigorous hematopoietic development in which MYB had limited influence because day 12 DKO/SKO MYB-Venus$^+$ cells continued to cluster with day 12 WT CD43$^+$ cells. The data support our phenotypic observations that the functional influence of MYB on the emergence of early blood cells is limited.

Nevertheless, the transcriptomes of DKO/SKO MYB-Venus$^+$ and WT CD43$^+$ cell populations were more divergent by day 12 compared to the close clustering of day 6 populations (Figure 2D). This divergence was sufficient for a reliable differential gene expression (DEG) analysis, and the GO term enrichment revealed a clear pattern of expression changes that occurred in MYB-null blood cells. Inactivation of MYB resulted in the downregulation of genes responsible for the innate immune and inflammatory response (Figure 4A; *Online Supplementary Figure S5A*). In DKO cells, mainly non-hematopoietic genes were upregulated, which suggests that MYB disruption switches hESC differentiation from hematopoietic to non-hematopoietic development. We also found that in addition to known MYB target genes such as GFI1, and BCL2, the MYB deficiency led to the suppression of two key regulators of myeloid differentiation, CEBPA and SPI1 (PU.1) (Figure 4B). Furthermore, the expression of CDK6, a key regulator of HSC activation,[19] was inhibited in DKO cells whereas several CDK inhibitors were upregulated including CDKN1A (CIP1/WAF1), a major mediator of p53-dependent tumor suppression.[20] The expression of myeloid cytokine receptor genes, CSF1R and CSF3R, as well as a number of genes encoding receptors for pro- and anti-inflammatory cytokines were negatively affected by MYB inactivation (*Online Supplementary Figure 5B*). The expression of CSF3R was most severely affected, which can explain the observed defects in the granulocyte development of MYB-null cells. In sum, the transcriptome profiling confirmed the involvement of MYB in the development of innate immune myeloid cells and indicated possible mechanisms of MYB regulation of the early human hematopoiesis.

We also confirmed the crucial role of MYB in the development of definitive hematopoiesis. Analysis of the T-cell potential is a standard procedure to monitor definitive hematopoietic development in differentiating cultures of hPSC.[17] We found that MYB inactivation led to complete failure of lymphoid cell development in the co-culture with OP9-DL4 stroma while WT cells efficiently produced CD5$^+$CD7$^+$ and CD4$^+$CD8$^+$ T cells (*Online Supplementary Figure S6*).

MYB inactivation results in the deficiency of primitive clonogenic progenitors

Next, we investigated whether MYB is required for the development of clonogenic hematopoietic progenitors. In our differentiation system, the earliest clonogenic progenitors arise on day 6, and their emergence coincides with the spontaneous formation of the *in vitro* blood islands (Figure 1D). All erythroid/erythro-myeloid progenitors corresponded to the primitive hematopoietic lineage producing primitive erythroblasts of characteristic morphology and primitive megakaryocytes distinguished by their relatively smaller size and less lobular nuclei (Figure 5A).[21] Moreover, gene expression profiling of pooled methylcellulose colonies showed the overwhelming predominance of embryonic hemoglobin expression (Figure 5B). We designated the hESC-derived primitive erythroid progenitors with higher proliferative potential as BFU-E^P (Burst Forming Unit – Erythroid, Primitive), and those with low proliferative potential as CFU-E^P (Colony Forming Unit –

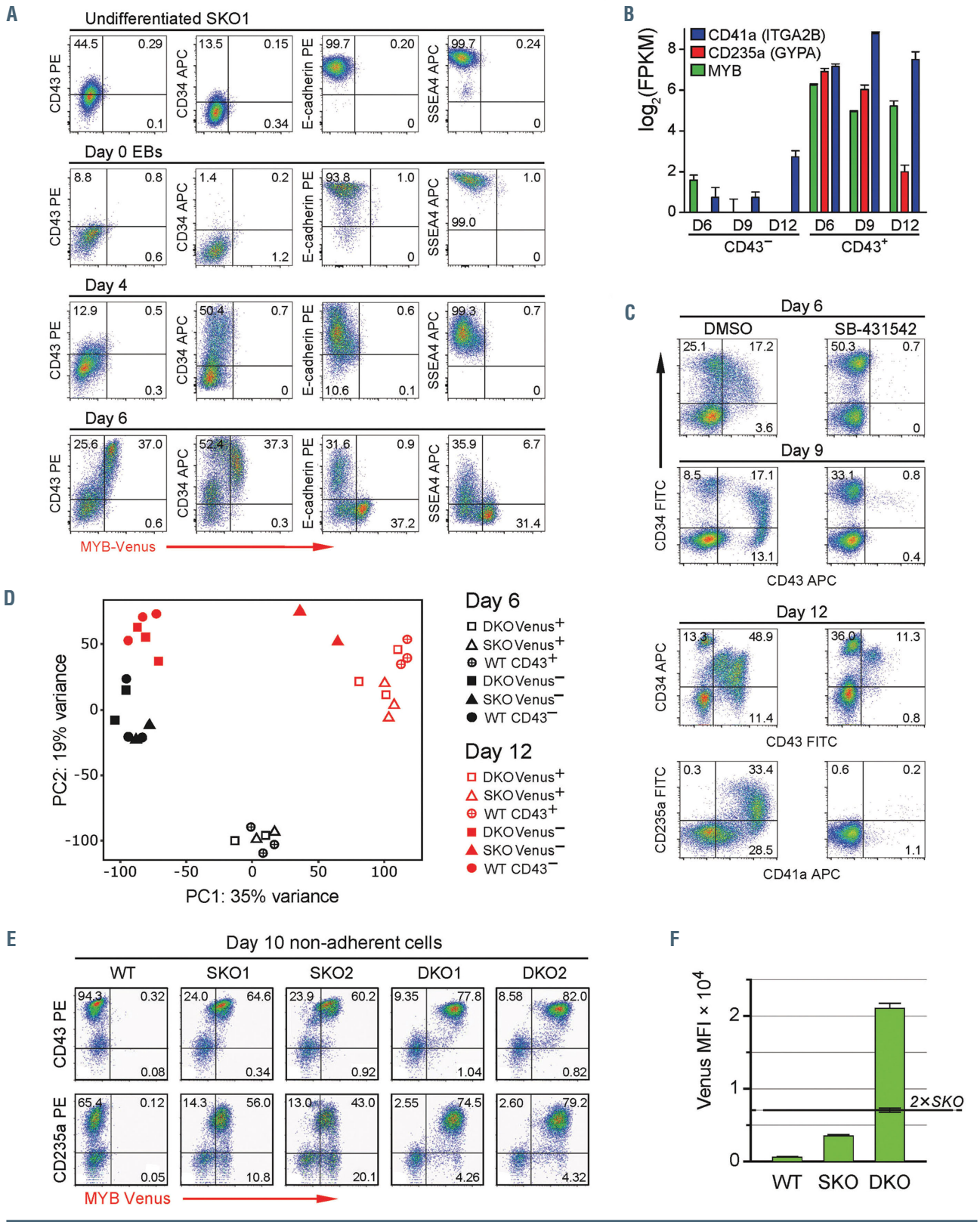

Figure 2. MYB is specifically expressed in the emerging hematopoietic cells. (A) Specific expression of MYB-Venus in the early blood cells during the initial phase of hematopoietic differentiation of SKO1 cells. Here and elsewhere, numbers in flow cytometry plots represent the percentages of cells within the respective quadrants. Representative flow cytometry data of four experiments are shown. (B) Human embryonic stem cells (hESC)-derived CD43$^+$ cells selectively co-express mRNA of *MYB* and the markers of primitive human blood cells, *ITGA2B* and *GYPA*. Differentiated wild-type (WT) H1 hESC were used for transcriptome analysis. (C) Inhibition of Activin/Nodal signaling by addition of 6 μM SB-431542 between day 2 and day 4 of differentiation strongly suppressed the development of CD43$^+$ and CD235a$^+$/CD41a$^+$ primitive blood cell populations. (D) Principal component analysis (PCA) of the sorted day 6 and day 12 WT, SKO1 and DKO1 cell populations, 31 samples, and entire gene set (19,796 genes). (E) Representative flow cytometry of day 10 live non-adherent blood cells generated by H1 and the isogenic mutant cell lines. (F) Quantitation of data represented in (E). MYB-Venus fluorescence (expressed as the mean fluorescence intensity [MFI]) in DKO cells is disproportionally stronger than the fluorescence in SKO cells. Data are mean ± standard deviation, n=4.

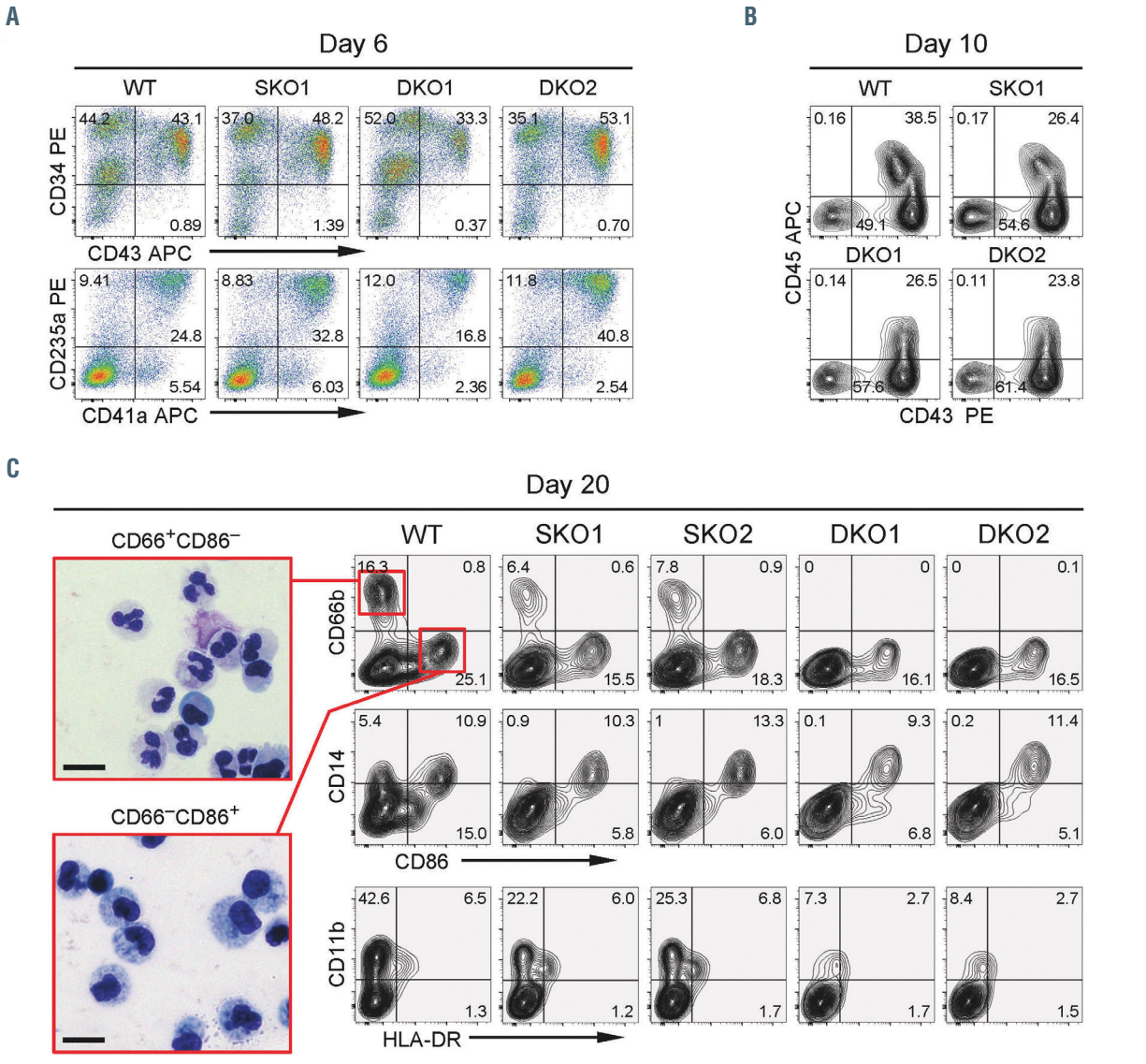

Figure 3. Blood cell populations are differently affected by the MYB deficiency depending on the stage of differentiation. (A) H1-isogenic *MYB* knockout cell lines develop normally on day 6 of differentiation. Total live differentiated cells were taken for the analysis, as in (B) and (C). Representative data of more than ten experiments are shown. (B) On day 10 the DKO cell lines demonstrate subtle differences in the CD43/CD45 cell staining. Representative data of three experiments are shown. (C) Day 20 phenotype of the *MYB* knockout cell lines. Representative data of six experiments are shown. Two cytospin panels on the left represent May-Grünwald staining of sorted CD66b$^+$CD86$^-$ neutrophils and CD66b$^-$CD86$^+$ cells of the monocyte-macrophage lineage. Scale bar, 10μm.

Erythroid, Primitive). The ability of the primitive progenitors to form large colonies of erythroid cells suggests that the assay medium is optimal for analyzing primitive progenitors generated in the cytokine-free differentiation.

First, we determined that the vast majority of hematopoietic progenitors were MYB-Venus$^+$ (Figure 5C). Of note, the analysis of the sorted cell populations demonstrated extremely high efficiency of hematopoietic progenitor generation in our differentiation system: up to 17% of all day 6 CD34$^+$MYB-Venus$^+$ blood cells generated CFU-C colonies in the assay medium. Then, we compared the generation of the progenitors by WT and mutant hESC lines on day 6 and day 10 of differentiation. Progenitors of higher proliferative potential, BFU-E^P and CFU-Mix^P, were practically absent in differentiated cultures of MYB-null hESC, and the myeloid progenitors were also affected (Figure 5D). Furthermore, we observed the effects of *MYB* haploinsufficiency on the generation of these progenitors from SKO cells. Only day 6 erythroid progenitors of low proliferation potential, CFU-E^P, could be detected at a comparable density in the MYB-null cultures. However, CFU-E^P in day 6 non-adherent DKO cell fractions were completely lost (Figure 5D). Moreover, instead of forming typical compact cell colonies, nearly all of day 6 MYB-null CFU-E^P generated aberrant loose colonies, and the morphology of cells from those colonies was abnormal (Figure 5E). Almost all CFU-myeloid colonies generated by the DKO cells were composed exclusively of macrophages and were notably smaller compared to the WT and SKO counterparts (Figure 5F). The survival of the CFU-M subset of CFU-myeloid progenitors confirms the previously published data on MYB-independence of hPSC-derived macrophages and macrophage progenitors.[10] Taken together, these observations demonstrate that primitive erythroid and primitive mixed progenitors are non-functional in differentiated cul-

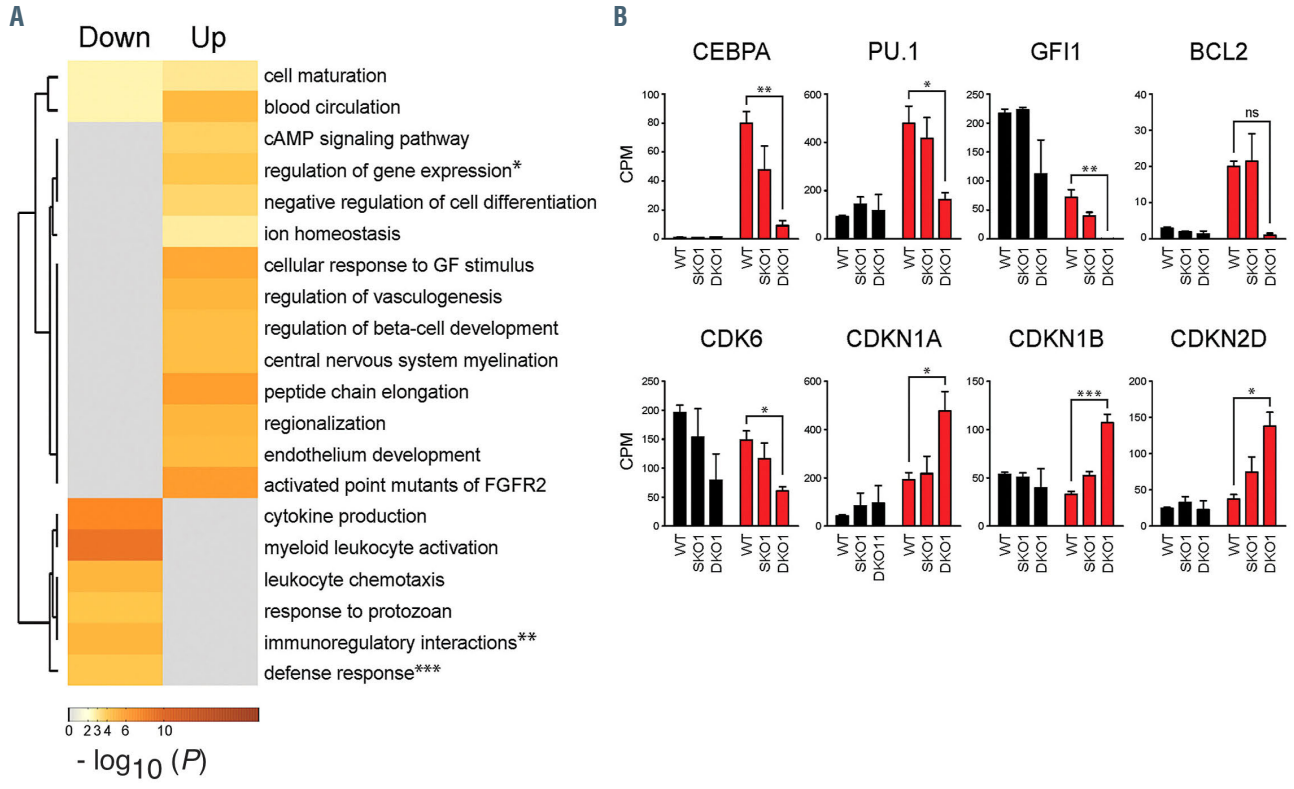

Figure 4. Innate immunity genes, hematopoietic transcription factors, and cell cycle regulatory genes negatively regulated in MYB-null cells. (A) Heat map of top 20 enriched terms across the two differential gene expression (DEG) lists (upregulated and downregulated, log_2FC >2, <−2) in MYB-null cells, colored by *P*-values. * – R-HSA-210747: "regulation of gene expression in early pancreatic precursor cells"; ** – R-HSA-198933: "immunoregulatory interactions between a lymphoid and a non-lymphoid cell"; *** – GO:0098542: "defense response to other organism". (B) Bar plots of mRNA expression of cell cycle regulatory genes and hematopoietic transcription factors in wild-type (WT) CD43$^+$, and MYB-Venus$^+$ SKO and DKO cells. Data are mean ± standard error of the mean (SEM), n=3 (biological repeats). *P*-values were calculated using one-way ANOVA with Tukey's test for multiple comparisons, where ***P<0.001; **P<0.01; *P<0.05.

tures of MYB-null hESC whereas non-macrophage myeloid progenitors are noticeably affected by the MYB inactivation. Such results are unexpected since previous studies denied any role of Myb/myb/MYB in primitive hematopoiesis.[7-9, 22] It was reported earlier that BFU-E and CFU-Mix progenitors failed to develop from Myb-null mESC, although whether such progenitors belonged to primitive or definitive hematopoiesis was unclear.[23]

In order to validate our discovery that MYB was required for the development of primitive human hematopoietic progenitors, we stimulated hESC-derived primitive hematopoiesis Activin A and studied the effects of such treatment on the hematopoietic differentiation of WT, DKO, and SKO cells. Primitive, but not definitive, human hematopoiesis is stimulated by Activin/Nodal signaling.[17,24] In our experiments, the Activin A treatment led to a reliable increase of MYB-Venus expression in both SKO and DKO blood cells (Figure 5G) and a significant expansion of all types of day 6 clonogenic progenitors derived from the WT hESC (Figure 5H). The latter observation further indicated that all these progenitors were primitive. As expected, MYB-null cells failed to boost the generation of BFU-E^P and CFU-Mix^P progenitors upon the Activin stimulation. The stimulation of CFU-E^P was not, however, precluded by the bi-allelic inactivation of MYB, although these MYB-null progenitors formed substandard colonies as described above. Activin-stimulated DKO myeloid progenitors formed only macrophage colonies confirming the resistance of the macrophage lineage to MYB inactivation.[10] These results confirm that MYB is required for the development and/or proliferation of primitive human hematopoietic progenitors.

VEGF is a major mitogen of early human hematopoiesis

Our results demonstrated that primitive blood cells emerged normally in the circumstances, at which primitive hematopoietic progenitors were severely compromised. Apparent progenitor-independence of the early blood cells poses a question of what factors drive the expansion of the early hematopoiesis.

VEGF is the only growth factor that was added to the culture medium after mesoderm induction and, therefore, it is an obvious candidate for a stimulatory molecule promoting the emergence and expansion of early blood cells. Indeed, the removal of VEGF from culture medium starting from day 3 of the differentiation timecourse led to a strong inhibition, but not a complete suppression, of the early hematopoiesis (Figure 6A), which indicates that this growth factor is responsible for mitogenic support of early human blood cells. In conjunction with the resistance of the early blood cells to MYB inactivation, these observations strongly suggest that MYB and VEGF regulate early human hematopoiesis independently. The VEGF removal also abolished the generation of clonogenic progenitors but did not prevent the robust generation of myeloid cells at the later stages (Figure 6B to D). The progenitor-independent myeloid cells do not originate from the MYB-

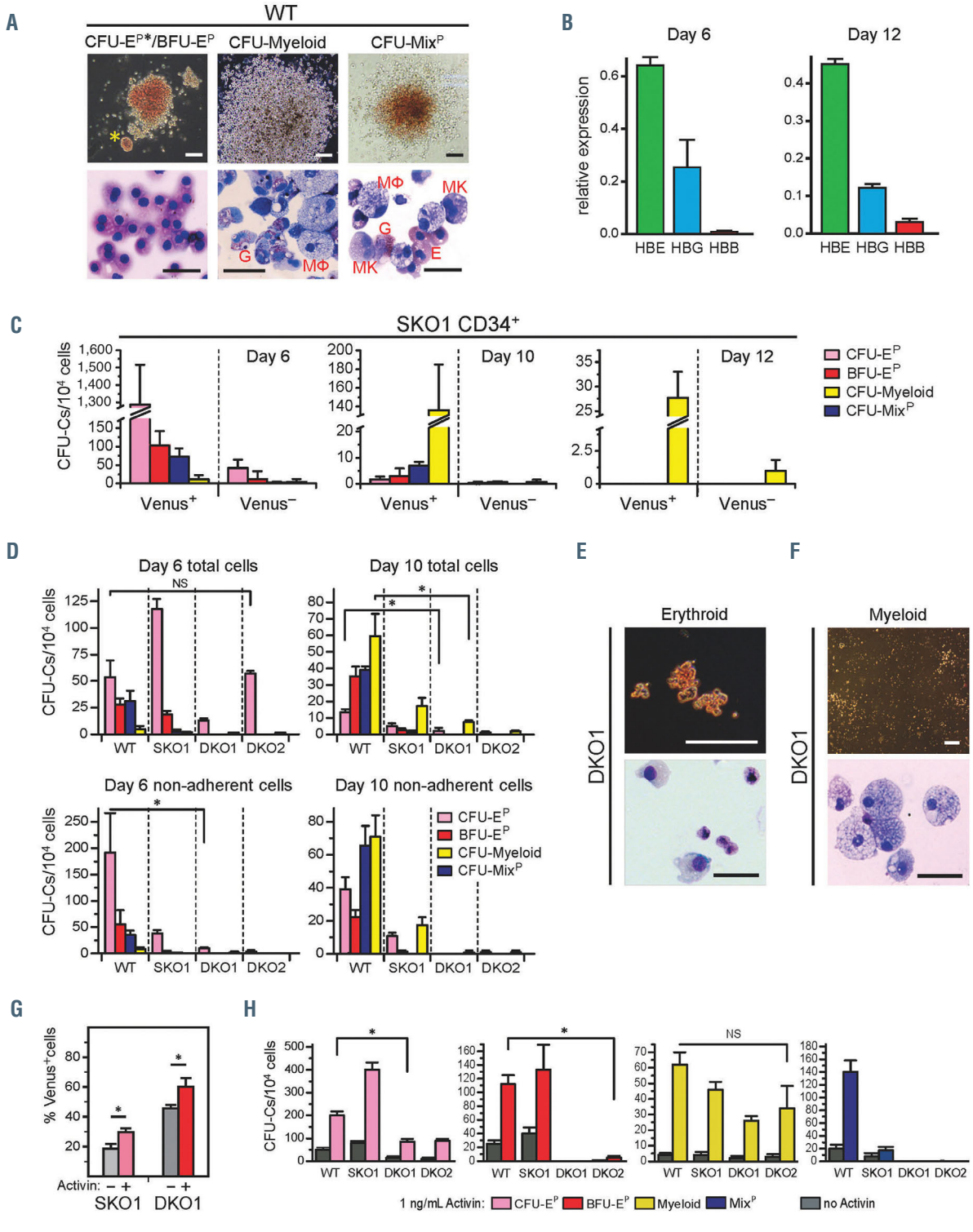

Figure 5. MYB inactivation leads to a severe deficiency of primitive clonogenic progenitors. (A) Morphology of individual CFU-C colonies derived from day 6 and day 10 hematopoietic progenitors (upper panels; scale bar, 100 μm), and May-Grünwald staining of cells from corresponding colonies (lower panels; scale bar, 20 μm). MΦ: macrophages; MK: megakaryocytes; E: erythroblasts; Gr: granulocytes. (B) Real-time polymerase chain reaction (RT-PCR) analysis of hemoglobin gene expression. Differentiated H1 embryonic stem cells (ESC) (1x10^4 cells) were grown in methylcellulose assay medium for 18 days, and all resulting CFU-C colonies (~100-150) were pooled for mRNA isolation. The data are mean ± standard deviation (SD). (C) Primitive human clonogenic progenitors express MYB. The frequency of the hematopoietic progenitors was measured in SKO1 CD34$^+$Venus$^+$ *versus* CD34$^+$Venus$^-$ cells. Data are mean ± SD, n=3. (D) The frequency of clonogenic hematopoietic progenitors in total or non-adherent cells of the three H1-isogenic *MYB* genotypes. Mean values ± SD are shown, n=3. *P<0.05; NS: non-significant; two-tailed Student's *t*-test. (E) Morphology of typical DKO erythroid colonies and cells. Upper panels, scale bar – 100 μm; lower panels, scale bar – 20 μm. (F) Morphology of typical DKO myeloid colonies and cells. Scale bar – 20 μm. (G) Activin stimulates MYB-Venus expression in the *MYB* knockout cell lines on day 6 of differentiation. Data are mean ± SD, n=4. *P<0.05; two-tailed Student's *t*-test. (H) Activin stimulation of day 6 primitive clonogenic progenitors of the three H1-isogenic *MYB* genotypes. Data are mean ± SD, n=3. *P<0.05; NS: non-significant; two-tailed Student's *t*-test.

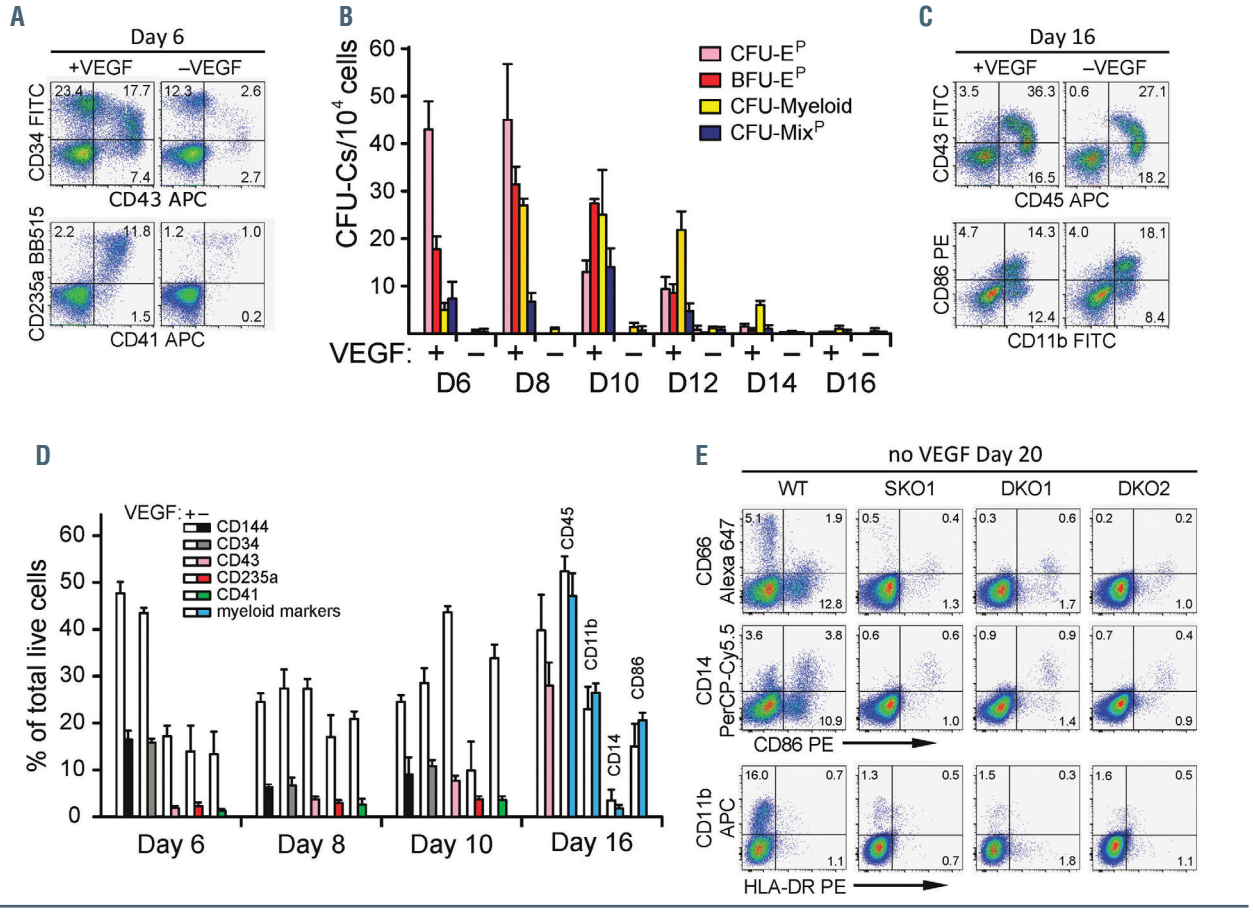

Figure 6. Vascular endothelial growth factor is a key cytokine for the early human hematopoiesis. (A) Human embryonic stem cells (hESC)-derived hematopoiesis on day 6 of differentiation is severely inhibited upon removal of vascular endothelial growth factor (VEGF) starting from day 3. Representative data of three experiments are shown. (B) Effect of the VEGF removal on the emergence of hematopoietic clonogenic progenitors during differentiation of H1 hESC (day 6 – day 16). Data are mean ± standard deviation (SD), n=4. (C) hESC-derived myeloid cells emerge normally on day 16 of differentiation in the absence of exogenous VEGF. Representative data of four experiments are shown. (D) Dynamics of hematopoietic marker expression during H1 hESC differentiation in the presence (open bars) or the absence of VEGF (colored bars). Data are presented as mean ± SD, n=3. (E) Day 20 phenotype of the *MYB* knockout cell lines differentiated in the absence of VEGF. Data are representative of three independent differentiation experiments.

independent early blood cells since these early cells are strongly suppressed by the VEGF removal (Figure 6A and D). Progenitor-independent monocyte/macrophages, granulocytes, and their immature precursors are likely to arise through the conversion of mesodermal or endothelial cells in a process similar to the aforementioned in vitro EHT. MYB inactivation severely affected the progenitor-independent myeloid cells with complete loss of granulocytes on day 20 of the VEGF-deprived differentiation (Figure 6E). Taken together, these results demonstrate that VEGF serves as a major mitogenic factor for the nascent human blood cells.

MYB is required for the development and proliferation of primitive progenitors

The progenitor defects upon MYB inactivation might be either due to the failure of progenitor proliferation in the methylcellulose assay or the interruption of progenitor development during the primary differentiation of hESC. In order to address this issue, we performed a series of rescue experiments in MYB-null cells using a Tet-On expression system PB-iDox that included a PiggyBac transposon vector[25] bearing *MYB* cDNA under the TRE-CMV promoter. One type of the doxycycline (DOX)-inducible vectors contained *mCherry* gene reporter attached to *MYB* cDNA via an *IRES* element (Figure 7A and B). In CFU-C colonies that were generated from DOX-activated DKO cells transfected by the PB-*MYB-mCherry* construct, the red reporter was downregulated at the colony fringes containing more mature cells (Figure 7C). The transgene's downregulation was even more profound than the silencing of MYB-Venus expression in the fringes (*Online Supplementary Figure S7A*). This observation suggests that the transgene's expression is controlled by post-transcriptional regulatory mechanisms, possibly via microRNA,[26] and the overexpression of MYB, a typical proto-oncogene, does not cause an uncontrolled proliferation of hematopoietic cells and progenitors. A time-course analysis of the PB-*MYB* transgene expression in DOX-treated DKO cells demonstrated stage-specific modulation of *MYB* mRNA levels further suggesting the post-transcriptional regulation by microRNA (*Online Supplementary Figure S7B*).

We have been able to rescue day 6 and day 12 clonogenic progenitors only when the transgenic *MYB* was induced by DOX both in the primary differentiation of hESC and the secondary methylcellulose cultures (Figure 7D; *Online Supplementary Figure S7C*). The most efficient was the recovery of BFU-E^P on day 6 (Figure 7D) and myeloid progenitors on day 12 (*Online Supplementary Figure S7C*) whereas the rescue of CFU-mix progenitors

was at a very low but detectable level at both stages. These results demonstrated that the gene is required not only for progenitor proliferation but also for their development from differentiated hESC. In addition, the progenitor recovery further evidenced that defects in the development of primitive hematopoietic progenitors were associated with the MYB inactivation rather than nonspecific genomic abnormalities.

We also studied whether the reactivation of MYB in the MYB-null cells could rescue maturating myeloid cells at day 20 of the primary differentiation. As shown in Figure 7E, the continuous expression of PB-*MYB* from day 4 to day 18 has led to a robust recovery of CD11b$^+$ and CD11c$^+$ monocyte-macrophage cells with strong upregulation of CD86 and HLA-DR. In contrast, only limited recovery of CD66b$^+$ granulocytes was observed on day

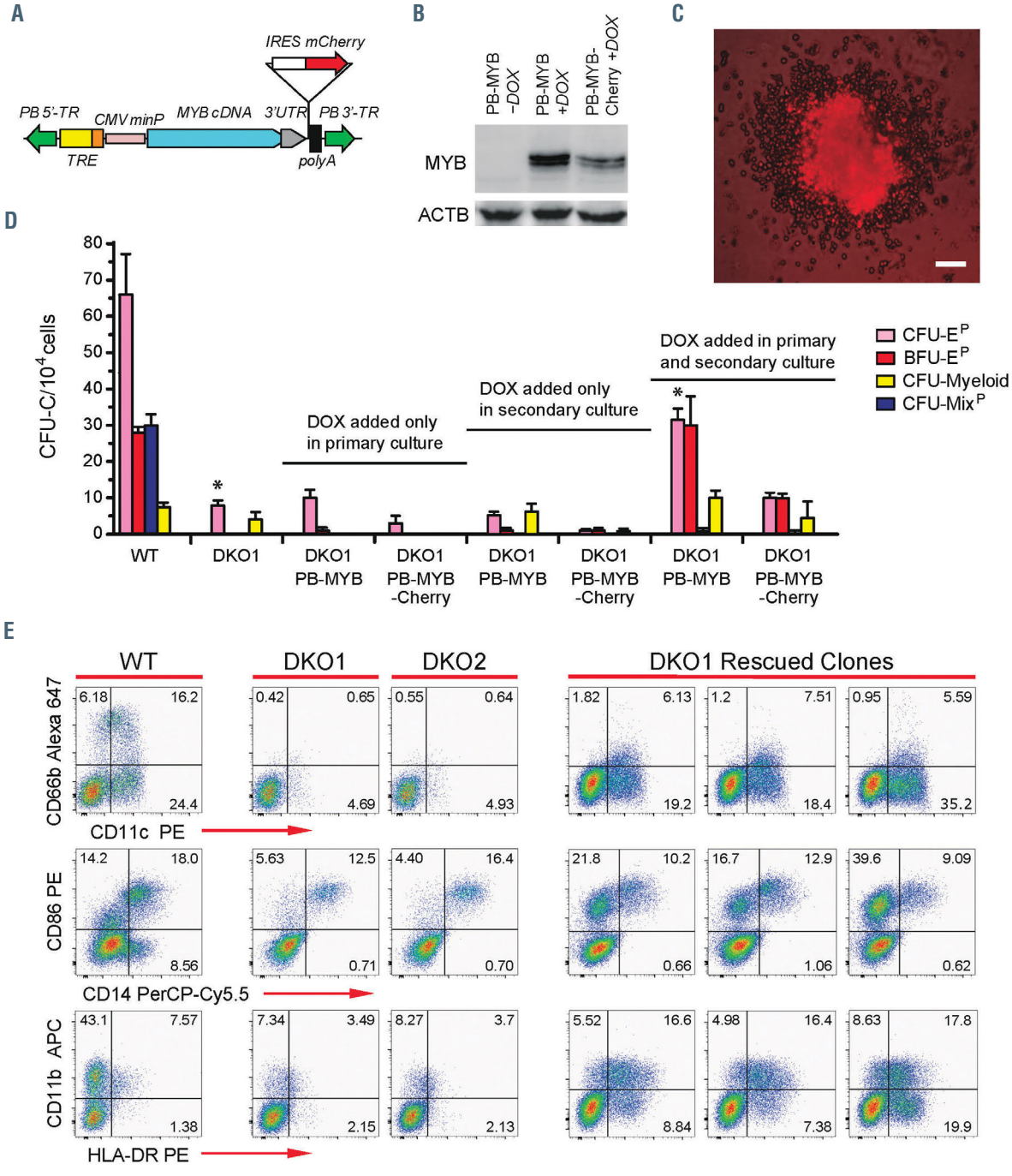

Figure 7. MYB is required for both emergence and proliferation of the primitive clonogenic progenitors. (A) Scheme of the PiggyBac-MYB transposon construct. (B) Western blotting of doxyclycline (DOX)-induced expression of transgenic MYB in day 12 DKO1-PB-MYB and DKO1-PB-MYB-Cherry cells. (C) A representative CFU-mix colony generated by DOX-stimulated day 6 DKO1-PB-MYB-Cherry cells. Scale bar, 100 μm. (D) Efficient rescue of day 6 clonogenic progenitors is achieved when DOX is added to both primary and secondary stages of hematopoietic differentiation of DKO1-PB-MYB cells. Data are mean ± standard deviation (SD), n=3. (E) MYB overexpression in the DKO1-PB-MYB clones during day 4 to day 18 period leads to the accumulation of immature myeloid cells on day 20. Representative data of three experiments are shown.

20, suggesting that the granulocyte differentiation and maturation were inhibited by MYB overexpression that resulted in the accumulation of immature $CD11c^{+}CD66b^{low}$ myeloid cells. The negative effect of Myb overexpression on granulocyte maturation has been observed in the mouse progenitor differentiation model.[27] Taken together with the limited recovery of CFU-mix progenitors, these data suggest that an excess of MYB dysregulates the hESC-derived hematopoietic development.

Discussion

In this study, we created a model in which the emergence of the early primitive blood cells was effectively uncoupled from the development of the primitive hematopoietic progenitors. The ability of differentiated hESC to generate large numbers of blood cells in the absence of cytokines provided an initial idea that early blood cells do not require the proliferation of clonogenic hematopoietic progenitors for their emergence. We have been unable to detect mRNA of *EPO, TPO, G-CSF, GM-CSF,* and *IL3* in differentiating cultures of hESC up to day 12; thereby the hESC-derived erythro-myeloid progenitors are unlikely to proliferate and produce day 6 primitive blood cells.

The conclusive evidence of progenitor independence of early human blood cells was obtained from our gene ablation studies of *MYB*. Primitive erythroid and CFU-Mix^{P} progenitors failed to develop in the absence of MYB and thus could not be a source of the MYB-independent cells of the erythro-megakaryocyte lineage. These data suggest that the primitive clonogenic progenitors and the first wave of primitive blood cells originate from HE independently (Figure 8). Our findings contradict the convention that all primitive blood cells are derived from primitive progenitors.[1,3,4] Despite their MYB-independence the early human blood cells specifically upregulated transcription from *MYB* promoters. One possible explanation of this observation is that the absence of the functional MYB protein is compensated by other transcription factors. Alternatively, the MYB expression is an insufficient prerequisite for turning HE and early blood cells into hematopoietic progenitors. In this view, additional developmental cues select cells for specification into functional progenitors.

We obtained ample evidence that MYB-dependent hematopoietic progenitors belonged to the primitive wave of hematopoiesis. These observations indicate the presence of MYB-dependent primitive erythro-myeloid progenitors (EMP) in the early human hematopoietic development. The issue of definitive *versus* primitive EMP in humans is disputed;[28] it is possible that both primitive and definitive cohorts of EMP participate in the establishment of human hematopoiesis. One report noticed abnormalities both in primitive and definitive hematopoiesis in a c-myb mutant of the medaka fish.[29] However, the *c-myb* mutation creates a dominant-negative allele that could inhibit the function of the related *a-myb* and *b-myb* genes.[30] Other mouse and zebrafish studies unequivocally denied Myb/myb a role in the primitive hematopoiesis.[8,22] Our data challenged the notion of MYB as a factor that does not have a function in the primitive hematopoiesis. The differences in the developmental role of MYB between small model animals and humans are likely to be associated with the requirement to facilitate the longer proliferation of primitive blood cells in order to sustain the growing needs of human conceptuses.

An important issue to consider is whether our findings are relevant to the onset of hematopoietic development in the human conceptus. Poor quality and scarcity of 3rd-week human conceptuses prevent reliable analysis of the early human hematopoietic cells.[31] Detailed mouse studies, however, suggest that around 300 EryP-CFC on E8.5[1] are unlikely to give rise to about 10^{5} erythroblasts in the E9.5 conceptus,[32] and there should be a progenitor-independent source of the primitive blood cells. Such large

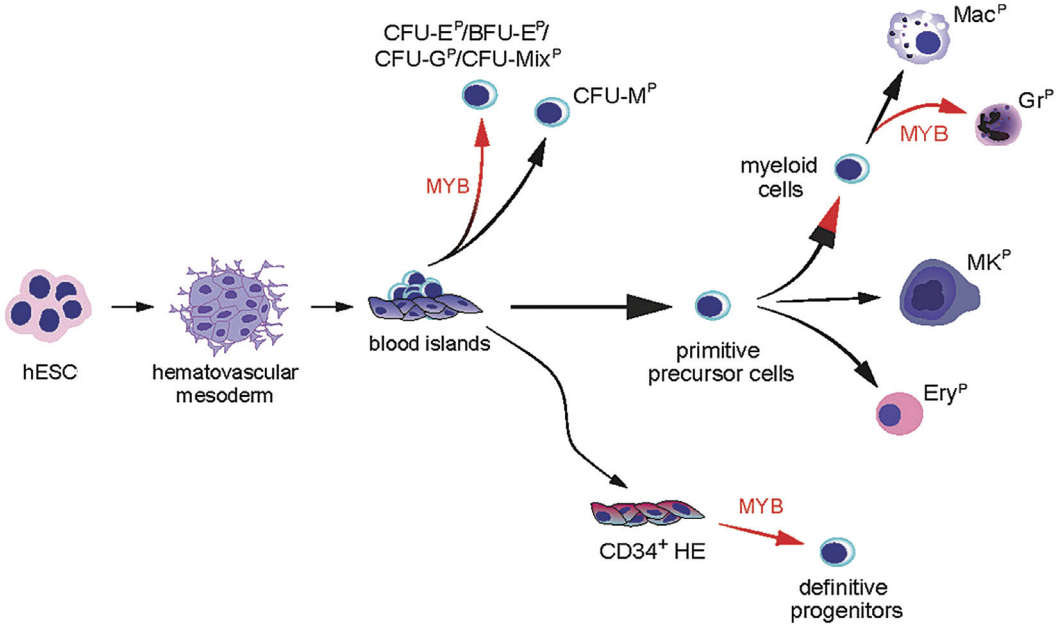

Figure 8. The role of MYB in the human embryonic stem cell-derived hematopoiesis. The *MYB* gene targeting and the cytokine-free differentiation system revealed progenitor-independent primitive hematopoiesis. Red arrows show MYB-dependent developmental events, black arrows – MYB-independent stages.

numbers of the primitive cells may be provided by the massive EHT in the yolk sac vasculature.

The detection of the progenitor-independent primitive blood cells was possible only in cytokine-free culture conditions because otherwise, it would be difficult to distinguish progenitor-derived from HE-derived blood cells. Our findings further emphasize the value of the *in vitro* differentiation of hESC as a practical tool for studying early hematopoiesis in humans.

Disclosures

No conflicts of interest to disclose.

Contributions

IMS designed and directed the study; ZSh co-designed the study, created the mutant cell lines, and performed most of the experiments; CF and HU performed a number of CFU-C assays, qRT-PCR, and VEGF-independent differentiation; BZ provided the experimental data on Activin/Nodal signaling inhibition; ESF conducted immunocytofluorescent staining; CW prepared cell samples for the RNA-seq analysis; VR, CW, PV performed bioinformatics analyses; IMS wrote the manuscript with input from ESF, ZSh, and PV.

Acknowledgments

The authors thank Dr. Kenjiro Adachi (MPI Münster) for providing the PiggyBac plasmids, Dr. Guangjin Pan (GIBH CAS) for providing H1 hESC line, and Andrew Sonin (MIPT) for assistance with bioinformatics analyses.

Funding

This work was supported by the National Key R&D Program of China 2017YFA0103101, Science and Technology Planning Project of Guangdong Province, China 2017B030314056, the National Basic Research Program of China 2015CB964900, the Guangdong Province Leading Talent Program 2014-2018 (to IMS).

References

1. Palis J, Robertson S, Kennedy M, Wall C, Keller G. Development of erythroid and myeloid progenitors in the yolk sac and embryo proper of the mouse. Development. 1999;126(22):5073-5084.
2. Ferkowicz MJ, Yoder MC. Blood island formation: longstanding observations and modern interpretations. Exp Hematology. 2005;33(9):1041-1047.
3. Wong PM, Chung SW, Reicheld SM, Chui DH. Hemoglobin switching during murine embryonic development: evidence for 2 populations of embryonic erythropoietic progenitor cells. Blood. 1986;67(3):716-721.
4. Porcher C, Chagraoui H, Kristiansen MS. SCL/TAL1: a multifaceted regulator from blood development to disease. Blood. 2017;129(15):2051-2060.
5. Kingsley PD, Malik J, Fantauzzo KA, Palis J. Yolk sac-derived primitive erythroblasts enucleate during mammalian embryogenesis. Blood. 2004;104(1):19-25.
6. Ramsay RG, Gonda TJ. MYB function in normal and cancer cells. Nat Rev Cancer. 2008;8(7):523-534.
7. Tober J, McGrath KE, Palis J. Primitive erythropoiesis and megakaryopoiesis in the yolk sac are independent of c-myb. Blood. 2008;111(5):2636-2639.
8. Mucenski ML, McLain K, Kier AB, et al. A functional c-myb gene is required for normal murine fetal hepatic hematopoiesis. Cell. 1991;65(4):677-689.
9. Vanhee S, De Mulder K, Van Caeneghem Y, et al. In vitro human embryonic stem cell hematopoiesis mimics MYB-independent yolk sac hematopoiesis. Haematologica ,2015;100(2):157-166.
10. Buchrieser J, James W, Moore MD. Human induced pluripotent stem cell-derived macrophages share ontogeny with MYB-independent tissue-resident macrophages. Stem Cell Rep. 2017;8(2):334-345.
11. Jacobs SM, Gorse KM, Westin EH. Identification of a second promoter in the human c-myb proto-oncogene. Oncogene. 1994;9(1):227-235.
12. Thompson MA, Flegg R, Westin EH, Ramsay RG. Microsatellite deletions in the c-myb transcriptional attenuator region associated with over-expression in colon tumor cell lines. Oncogene. 1997; 14(14):1715-1723.
13. Salvagiotto G, Burton S, Daigh CA, Rajesh D, Slukvin II, Seay NJ. A defined, feeder-free, serum-free system to generate in vitro hematopoietic progenitors and differentiated blood cells from hESCs and hiPSCs. PLoS One. 2011;6(3):e17829.
14. Niwa A, Heike T, Umeda K, et al. A novel serum-free monolayer culture for orderly hematopoietic differentiation of human pluripotent cells via mesodermal progenitors. PLoS One. 2011;6(7):e22261.
15. Uenishi G, Theisen D, Lee J-H, et al. Tenascin C promotes hematoendothelial development and T lymphoid commitment from human pluripotent stem cells in chemically defined conditions. Stem Cell Reports. 2014;3(6):1073-1084.
16. Malik J, Kim AR, Tyre KA, Cherukuri AR, Palis J. Erythropoietin critically regulates the terminal maturation of murine and human primitive erythroblasts. Haematologica. 2013;98(11):1778-1787.
17. Kennedy M, Awong G, Sturgeon CM, et al. T lymphocyte potential marks the emergence of definitive hematopoietic progenitors in human pluripotent stem cell differentiation cultures. Cell Rep. 2012; 2(6):1722-1735.
18. Sturgeon CM, Ditadi A, Awong G, Kennedy M, Keller G. Wnt signaling controls the specification of definitive and primitive hematopoiesis from human pluripotent stem cells. Nat Biotechnol. 2014;32(6):554-561.
19. Scheicher R, Hoelbl-Kovacic A, Bellutti F, et al. CDK6 as a key regulator of hematopoietic and leukemic stem cell activation. Blood. 2015;125(1):90-101.
20. Bunz F, Dutriaux C, Lengauer C, et al. Requirement for p53 and p21 to sustain G2 arrest after DNA damage. Science. 1998;282(5393):1497-1501.
21. Bluteau O, Langlois T, Rivera-Munoz P, et al. Developmental changes in human megakaryopoiesis. J Thromb Haemost. 2013;11(9):1730-1741.
22. Soza-Ried C, Hess I, Netuschil N, Schorpp M, Boehm T. Essential role of c-myb in definitive hematopoiesis is evolutionarily conserved. Proc Natl Acad Sci USA. 2010;107(40):17304-17308.
23. Clarke D, Vegiopoulos A, Crawford A, Mucenski M, Bonife, C, Frampton J. In vitro differentiation of c-myb–/– ES cells reveals that the colony forming capacity of unilineage macrophage precursors and myeloid progenitor commitment are c-Myb independent. Oncogene. 2000; 19(30):3343-3351.
24. Sturgeon CM, Ditadi A, Clarke RL, Keller G. Defining the path to hematopoietic stem cells. Nat Biotechnol. 2013;31(5):416-418.
25. Adachi K, Nikaido I, Ohta H, et al. Context-dependent wiring of Sox2 regulatory networks for self-renewal of embryonic and trophoblast stem cells. Mol Cell. 2013;52(3):380-392.
26. Wang X, Angelis N, Thein SL. MYB – a regulatory factor in hematopoiesis. Gene. 2018;665:6-17.
27. Bies J, Mukhopadhyaya R, Pierce J, Wolff L. Only late, non-mitotic stages of granulocyte differentiation in 32Dcl3 cells are blocked by ectopic expression of murine c-myb and its truncated forms. Cell Growth Differ. 1995;6(1):59-68.
28. Ivanovs A, Rybtsov S, Ng ES, Stanley EG, Elefanty AG, Medvinsky A. Human haematopoietic stem cell development: from the embryo to the dish. Development. 2017;144(13):2323-2337.
29. Moriyama A, Inohaya K, Maruyama K, Kudo A. Bef medaka mutant reveals the essential role of c-myb in both primitive and definitive hematopoiesis. Dev. Biol. 2010;345(2):133-143.
30. Lipsick JS. The c-MYB story – is it definitive? Proc Natl Acad Sci USA. 2010; 107(40):17067-17068.
31. Tavian M, Peault B. Embryonic development of the human hematopoietic system. Int J Dev Biol. 2005;49(2-3):243-250.
32. McGrath KE, Koniski AD, Malik J, Palis J. Circulation is established in a stepwise pattern in the mammalian embryo. Blood. 2003;101(5):1669-1676.

ARTICLE

BMP signaling is required for postnatal murine hematopoietic stem cell self-renewal

Sarah Warsi,* Ulrika Blank,* Maria Dahl, Tan Hooi Min Grahn, Ludwig Schmiderer, Silja Andradottir and Stefan Karlsson

Division of Molecular Medicine and Gene Therapy, Lund Stem Cell Center, Lund University, Lund, Sweden.

**SW and UB contributed equally as co-first authors.*

Ferrata Storti Foundation

Haematologica 2021
Volume 106(8):2203-2214

ABSTRACT

Life-long production of blood from hematopoietic stem cells (HSC) is a process of strict modulation. Intrinsic and extrinsic signals govern fate options like self-renewal – a cardinal feature of HSC. Bone morphogenetic proteins (BMP) have an established role in embryonic hematopoiesis, but less is known about its functions in adulthood. Previously, SMAD-mediated BMP signaling has been proven dispensable for HSC. However, the BMP type-II receptor (BMPR-II) is highly expressed in HSC, leaving the possibility that BMP function via alternative pathways. Here, we establish that BMP signaling is required for self-renewal of adult HSC. Through conditional knockout we show that *BMPR-II* deficient HSC have impaired self-renewal and regenerative capacity. *BMPR-II* deficient cells have reduced p38 activation, implying that non-SMAD pathways operate downstream of BMP in HSC. Indeed, a majority of primitive hematopoietic cells do not engage in SMAD-mediated responses downstream of BMP *in vivo*. Furthermore, deficiency of *BMPR-II* results in increased expression of *TJP1*, a known regulator of self-renewal in other stem cells, and knockdown of *TJP1* in primitive hematopoietic cells partly rescues the BMPR-II null phenotype. This suggests TJP1 may be a universal stem cell regulator. In conclusion, BMP signaling, in part mediated through TJP1, is required endogenously by adult HSC to maintain self-renewal capacity and proper resilience of the hematopoietic system during regeneration.

Introduction

Hematopoietic stem cells (HSC) have dual capacity to self-renew and give rise to differentiating progeny.[1,2] Self-renewal pertains to the ability of HSC to duplicate without losing developmental potential. Maintenance of the stem cell pool is dependent on self-renewal and loss thereof leads to erosion of regenerative capacity and hematopoietic failure. In order to ensure homeostasis, HSC are tightly regulated by internal factors and external signaling cues from the bone marrow (BM) niche.[3] Although many regulatory mechanisms have been identified, deeper understanding of the self-renewal machinery is required to fully utilize the therapeutic potential of HSC.

Bone morphogenetic proteins (BMP) belong to the TGF-β superfamily of secreted cytokines, which during embryogenesis regulate a wide variety of biological processes.[4-7] Mechanistically, BMP signal through cell surface receptors, which activate receptor-regulated SMAD transcription factors (R-SMAD) through phosphorylation.[8] Phosphorylated R-SMAD form complexes with SMAD4 resulting in nuclear accumulation of activated complexes, which together with cofactors regulate target gene transcription.[8] Two classes of receptors have been identified; type-I and type-II. BMP bind to and signal via the BMP type-II receptor (BMPR-II), in association with any type-I receptor (ALK2, ALK3, or ALK6).[8]

The importance of BMP signaling during development is well established and reflected in early embryonic lethality of mice with targeted deletions of components of the pathway.[9-12] Similarly, deletion of *SMAD1* and *SMAD5* results in embryonic lethality.[13-16] Beyond development, the TGF-β superfamily regulates tissue home-

Correspondence:

SARAH WARSI
sarah.warsi@med.lu.se

Received: August 28, 2019.

Accepted: July 10, 2020.

Pre-published: July 16, 2020.

https://doi.org/10.3324/haematol.2019.236125

ostasis and adult regeneration of a variety of organ systems. Several lines of evidence suggest that BMP play a role in adult HSC regulation, but conclusive evidence for direct BMP-requirement by HSC is still lacking. For instance, ALK3-mediated signaling is required by the HSC osteoblastic niche, with loss of *ALK3* leading to increased HSC numbers.[17] By contrast, decreased levels of BMP4 in the BM results in reduced HSC numbers, as shown in a hypomorphic BMP4 mutant mouse model.[18] Additionally, BMP4 maintains cord blood-derived human hematopoietic stem and progenitor cells (HSPC) during *ex vivo* culture, by acting as a survival factor.[19] Recently, Khurana *et al.* showed that BMP4 exposure *in vitro* maintains the expression of ITGA4 in murine HSC, thereby preventing culture-induced loss of homing capacity.[20] However, *SMAD1* and *SMAD5* are dispensable for adult HSC, leading to the conclusion that BMP signaling is not endogenously required by adult HSC.[21,22] Interestingly, *BMPR-II* is reportedly highly expressed in adult HSC, suggesting that BMP may signal via alternative circuitries in HSC.[23] Indeed, several pathways can be activated by BMP, including components of the MAPK pathway, such as p38 and JNK.[24,25] A role for p38 has been suggested in maintenance of ITGA4 expression in HSC *in vitro*, but a conclusive role for BMP in the regulation of HSC *in vivo* has never been shown.[20] Therefore, in order to investigate the complete role of BMP signaling in HSC *in vivo*, we conditionally deleted *BMPR-II* in hematopoietic cells using the Cre/loxP system. We report here that BMPR-II is essential for self-renewal of HSC with mutants displaying significantly reduced regenerative capacity upon BM transplantation. Steady state hematopoiesis is normal in mice deficient of BMPR-II and the differentiation capacity upon transplantation is likewise unaltered, indicating a specific role for BMPR-II in HSC self-renewal. In addition, we map the transcriptional activity of SMAD-mediated signaling in hematopoietic cells by using a *BRE-GFP* reporter mouse,[26] which suggests a failure to engage SMAD-dependent transcriptional response upon BMP exposure. Furthermore, our findings indicate that loss of BMPR-II results in up-regulation of tight junction protein 1 (*TJP1*) and that knockdown of *TJP1* partly rescues the *BMPR-II* knockout phenotype. *TJP1* is a protein previously implicated in self-renewal regulation of several types of stem cells, including both embryonic and adult stem cells. Together, our findings show that BMP signaling, via BMPR-II, is endogenously required by adult HSC to maintain self-renewal capacity *in vivo*.

Methods

Mice

Mice on C57Bl/6 background with loxP flanking one allele of exon 4-5 of the *BMPR-II* gene (MMRRC, University of North Carolina, Chapel Hill, NC, USA)[27] were bred to homozygosity and mated with *Vav-Cre*[28] transgenic mice to generate conditional *Vav-Cre;BMPR-II$^{fl/fl}$* mice. Detection of *Cre*, floxed (fl), wild-type (WT), and excised alleles was done by polymerase chain reaction (PCR) as previously described.[22,27] Mice were housed and bred in ventilated cages in the BMC animal facility. All experiments involving animals were approved by the regional Animal Ethical Committee in Lund.

Transplantation assays

For competitive transplantation assays, $0.2x10^6$ unfractionated BM cells from *BMPR-II$^{fl/fl}$;Vav-Cre*, *BMPR-II$^{fl/+}$;Vav-Cre*, and WT littermates (*BMPR-II$^{fl/fl}$* or *BMPR-II$^{fl/+}$*) (CD45.2) were transplanted with $0.2x10^6$ congenic CD45.1 BM cells by tail vein injection to lethally irradiated (900 cGy) congenic CD45.1/2 recipients (three recipients per donor). Donor, competitor, and recipient cells were monitored by peripheral blood (PB) samplings at several time points at 4-16 weeks. Sixteen weeks post-transplantation mice were killed, BM was analyzed and $2x10^6$ cells were transplanted to secondary recipients, monitored as above. After another 16 weeks secondary mice were killed and tertiary transplantations were performed using $20x10^6$ BM cells. Tertiary recipients were monitored as above for 16 weeks, after which final analyses of BM and PB were performed. For transplantations using purified HSC, ten LSK/CD48$^-$/CD150$^+$ cells from *BMPR-II$^{fl/fl}$;Vav-Cre* or WT littermates were transplanted together with $0.2x10^6$ whole BM support cells (CD45.1/2) to CD45.1 recipients. Reconstitution was monitored as above and BM was analyzed at 16 weeks. Homing assays were performed by transplantation of $15x10^6$ unfractionated BM cells to congenic CD45.1 recipients; BM analysis was done 20 hours post-transplantation. For competitive homing $10x10^6$ BM cells from donors were transplanted with an equal number of WT competitor cells.

Knockdown of *TJP1*

FFor knockdown of *TJP1*, lentiviral plasmid pGFP-C-shLenti containing short hairpin RNA (shRNA) targeting *TJP1* or scrambled shRNA (OriGene) was used to produce lentiviral particles at the Stem Cell Center Vector Core Facility (Lund University). C-kit-enriched BM cells (CD45.2; *BMPR-II$^{fl/fl}$;Vav-Cre* or WT) were placed into virus-loaded plates at a multiplicity of infection (MOI) of 30-50 and incubated over night (37°C, 5% CO2). Transduced cells were collected and transplanted into lethally irradiated CD45.1 recipient mice (two recipients/donor). An aliquot of cells was cultured for flow cytometry analysis of transduction efficiency after 48 hours. BM of transplanted animals was analyzed at 16 weeks. Additional information can be found in the *Online Supplementary Appendix*.

Results

BMPR-II is highly expressed in long-term hematopoietic stem cells

In order to map the extent of *BMPR-II* expression in distinct populations of primitive adult hematopoietic cells, we performed quantitative PCR (qPCR) analyses on sorted long-term HSC (LT-HSC) (LSK-CD34$^-$FLT3$^-$), short-term HSC (ST-HSC) (LSK-CD34$^+$FLT3$^-$), lymphoid-primed multipotent progenitors (LMPP) (LSK-CD34$^+$FLT3$^+$), as well as various progenitor populations.[29] Robust expression of *BMPR-II* was detected in all subsets, although LT-HSC exhibited the highest expression on average between tested populations (Figure 1A). Similarly, we examined expression of type-I receptors *ALK2*, *ALK3*, and *ALK6* in HSC populations (Figure 1B). In LT- and ST-HSC, both *ALK2* and *ALK3* were expressed, but expression of both receptors was more abundant in LT-HSC. In LMPP, *ALK2* was the dominating receptor. *ALK6* was undetectable in all hematopoietic subsets tested.

Normal steady state hematopoiesis despite reduced progenitor activity upon deletion of *BMPR-II*

Given the robust expression of *BMPR-II* in LT-HSC, we hypothesized that its deletion would blunt most signaling events initiated by BMP in HSC, allowing us to probe the

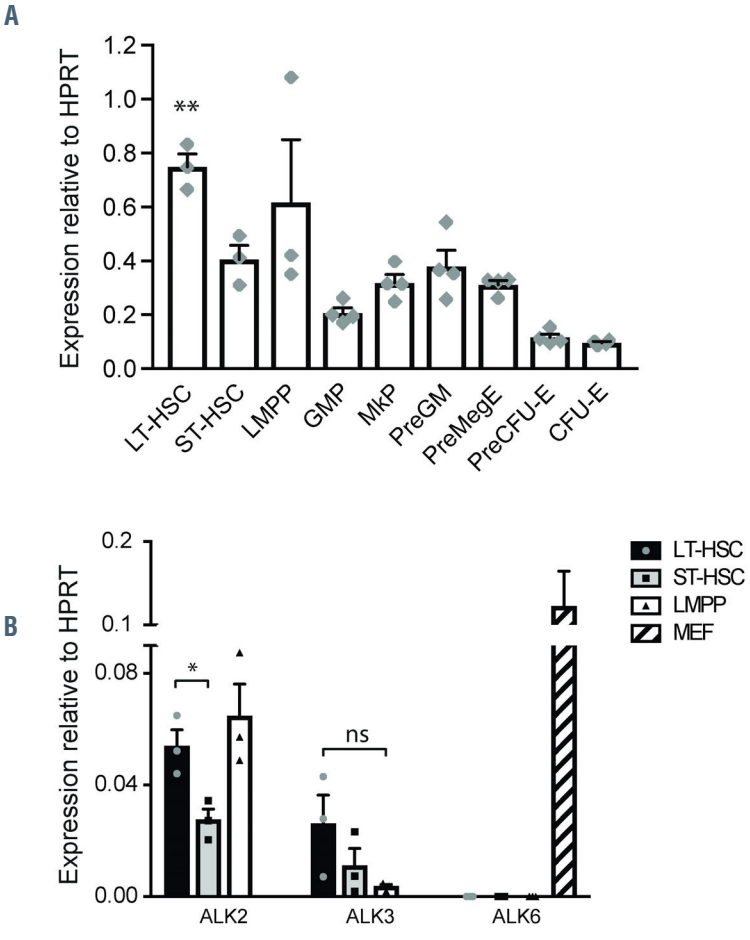

Figure 1. Expression of bone morphogenetic protein receptors in primitive hematopoietic subsets. (A) Expression of bone morphogenetic protein (BMP) receptor *BMPR-II* relative to *HPRT* in indicated subsets of bone marrow (BM) hematopoietic cell populations (n=3-4). LT-HSC: long term-hematopoietic stem cells; ST-HSC: short term-HSC; LMPP: lymphoid-primed multipotent progenitor; GMP: granulocyte-macrophage progenitor; MkP: megakaryocyte progenitor; PreGM: pre-granulocyte-macrophage progenitor; PreMegE: pre-megakaryocyte-erythroid progenitor; PreCFU-E: pre-colony-forming unit-erythroid progenitor; CFU-E: colony-forming unit-erythroid progenitor. (B) Expression of type-I receptors, *ALK2*, *ALK3*, and *ALK6* in indicated hematopoietic cell populations (n=3). $^{**}P<0.01$ in comparison to all other populations except for LMPP (A); $^{*}P<0.05$; ns:not significant; ALK6 data was not statistically tested (B). MEF: mouse embryonic fibroblasts.

full role of BMP in adult hematopoiesis. We conditionally deleted *BMPR-II* in hematopoietic cells, employing the Cre/loxP system with the *Vav-Cre* driver strain.[27,28] Efficient deletion of exon 4-5 of the *BMPR-II* gene in hematopoietic cells was confirmed by PCR analysis of individual colonies from BM, reaching 98.85% efficiency (n=160 alleles; *Online Supplementary Figure S1A*). Recombination at the *BMPR-II* locus resulted in efficient reduction of *BMPR-II* mRNA in purified LT-HSCs (*Online Supplementary Figure S1B* and *C*). *Vav-Cre* mediated deletion in mice homozygous for floxed *BMPR-II* alleles (*BMPR-II*$^{fl/fl}$;*Vav-Cre*, hereafter referred to as *BMPR-II*$^{-/-}$) did not result in embryonic lethality although the *Vav* promoter is active from embryonic day (E) 10.5,[30] indicating that BMPR-II signaling is not endogenously required in HSC for normal development after E10.5. All PB parameters were normal in adult *BMPR-II*$^{-/-}$ and *BMPR-II*$^{+/-}$ mice at steady state compared to WT littermates (Figure 2A and B). Similarly, B/T/myeloid lineage distribution and number of cells in the BM of mutant mice were unaltered compared to WT littermates (Figure 2C and *data not shown*). Megakaryocytic lineage distribution and progenitor populations were also unaltered (*Online Supplementary Figure S2A* and *B*). In order to further analyze HSPC lacking BMPR-II, we performed flow cytometry analyses on BM from *BMPR-II*$^{-/-}$, *BMPR-II*$^{+/-}$, and WT littermate mice. Interestingly, *BMPR-II*$^{-/-}$ mice had significantly fewer LSK cells in the BM as compared to WT mice (Figure 2D to E). Further analyses by SLAM markers did not reveal significant differences in more primitive subsets of LSK cells, such as LT-HSC (Figure 2D to E). Similarly, when assessing HSC phenotypic aging by CD41 expression[31] we saw no significant differences between WT and *BMPR-II*$^{-/-}$ LT-HSC (*Online Supplementary Figure S2C*). However, in agreement with the reduced number of LSK cells, the colony forming capacity of BM cells from *BMPR-II*$^{-/-}$ mice was significantly reduced compared to that of WT littermates (Figure 2F; *Online Supplementary Figure 2D*), suggesting that primitive hematopoiesis might be altered in *BMPR-II*$^{-/-}$ mice.

BMPR-II deficient hematopoietic stem cells exhibit reduced regenerative potential upon transplantation

In order to test the regenerative capacity of BMPR-II deficient HSC, we transplanted unfractionated BM cells from *BMPR-II*$^{-/-}$, *BMPR-II*$^{+/-}$, and WT mice at a 1:1 ratio with congenic WT competitor cells to lethally irradiated recipients (Figure 3A). *BMPR-II*$^{-/-}$ BM cells exhibited significantly reduced reconstitution capacity in PB short term at 4 weeks (data not shown) and a similar, though non-significant, reduction in PB long term at 16 weeks post-transplantation (Figure 3A to C). Deficiency of BMPR-II did not affect lineage distribution, though a slight decrease in donor contribution to myeloid cells could be observed (Figure 3D). In order to further investigate the ability of *BMPR-II*$^{-/-}$ cells to contribute to primitive hematopoietic cells, we quantified the number of donor-derived LSK-SLAM cells in BM. Interestingly, *BMPR-II*$^{-/-}$ cells exhibited a significantly reduced contribution to the entire LSK compartment including all LSK-

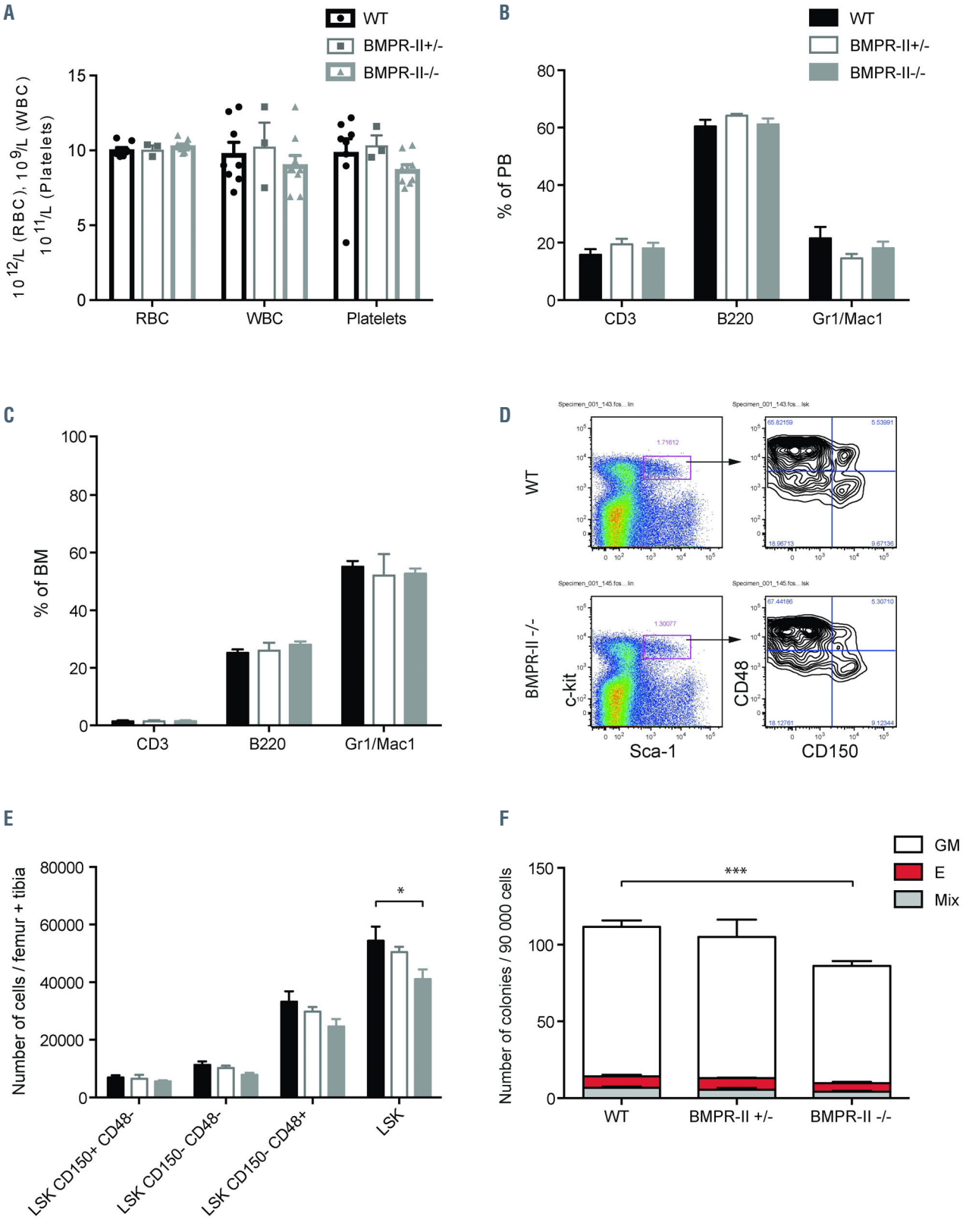

Figure 2. Normal steady state hematopoiesis in BMPR-II deficient mice. (A) Peripheral blood (PB) cell counts of adult mice (n=3-9). Y-axis indicates number of cells per L (liter) PB. RBC: red blood cell; WBC: white blood cell. (B) Lineage distribution in PB of adult mice at steady state by flow cytometry analysis. CD3: T cells; B220: B cells; Gr1/Mac1: myeloid cells (n=3-10). (C) Lineage distribution in BM of adult mice at steady state by flow cytometry analysis (n=3-10). (D) Representative fluorescence activated cell sorting (FACS) plot of an LSK-SLAM stain of BM cells from adult mice. (E) Quantification of LSK-SLAM populations in BM of adult mice at steady state. Number of LSK cells: 54,341±4,939 for wild-type (WT) (n=8) *vs.* 41,052±3,398 for BMPR-II$^{-/-}$ (n=10). (F) BM colony forming assay *in vitro*. Total number of colonies: 111.5±5.07 for WT (n=8) *vs.* 86.2±3.37 for BMPR-II$^{-/-}$ (n=10). **P*<0.05; *** *P*<0.001.

SLAM populations, including the LT-HSC (LSK-CD150^{+}CD48^{-}) (Figure 3E and F).

Deletion of *BMPR-II* results in compromised self-renewal capacity and altered long-term hematopoietic stem cell-quality

In order to assay the self-renewal ability of BMPR-II deficient HSC, secondary and tertiary BM transplantations were performed. We transplanted a fixed number of cells from primary recipients to lethally irradiated secondary recipients. Similarly, BM from secondary recipients was transplanted to lethally irradiated tertiary recipients. The overall donor contribution of *BMPR-II*$^{-/-}$ HSC dropped dramatically upon secondary transplantation, as compared to WT cells, which exhibited stable reconstitution across consecutive transplantations (Figure 3G). Upon tertiary transplantation, *BMPR-II*$^{-/-}$ cells dropped further, indicating a severely compromised ability to self-renew under stressed conditions (Figure 3G). *BMPR-II*$^{+/-}$ BM cells displayed sustained donor contribution in secondary recipients, but appeared to drop upon tertiary transplantation, although not significantly so (Figure 3G). Furthermore, quantification of LT-HSC revealed decreasing numbers of *BMPR-II*$^{-/-}$ derived cells across consecutive transplantations and in tertiary recipients the contribution to LT-HSC was essentially nonexistent (Figure 3H). These data show that BMPR-II-mediated signaling is essential for self-renewal of LT-HSC *in vivo*.

In agreement with the *in vivo* transplantation data stated above is the *in vitro* serial replating assay which shows a significant decrease in *BMPR-II*$^{-/-}$ colony number after three platings (*Online Supplementary Figure S2E*).

In order to verify that the observed defect in regenerative capacity was caused by a qualitative defect of HSC, we transplanted ten sorted *BMPR-II*$^{-/-}$ or WT LT-HSC in conjunction with congenic WT support BM cells (Figure 3I). In agreement with previous transplantations, overall donor contribution of *BMPR-II*$^{-/-}$ LT-HSC was significantly reduced at 16 weeks post-transplantation in PB (Figure 3J) and the lineage distribution was unaffected (Figure 3K). Furthermore, the LSK compartment in BM was significantly reduced, as was the CD150^{-}CD48^{-} and CD150^{-}CD48^{+} subset of LSK cells (Figure 3L). The LT-HSC showed a similar reduction, though it did not reach significance (P=0.09) (Figure 3L).

Loss of *BMPR-II* causes transcriptional cell cycle perturbation but has little or no effect on cell cycle and apoptosis in long-term hematopoietic stem cells

In order to investigate the biological properties of *BMPR-II*$^{-/-}$ primitive hematopoietic cells, we analyzed apoptosis and cell cycle parameters of BM cells from *BMPR-II*$^{-/-}$ and WT mice by flow cytometry. The fraction of apoptotic (AnnexinV+) cells within LSK/LSK-SLAM populations did not differ between *BMPR-II*$^{-/-}$ and WT BM (Figure 4A and B). Cell cycle distribution, analyzed using Ki67 and DAPI, was mostly unaltered in all hematopoietic populations tested between *BMPR-II*$^{-/-}$ and controls (Figure 4C). We observed a slight decrease in quiescent G0-phase LT-HSC and a slight increase in LT-HSC in G1-phase, though these differences did not reach significance (Figure 4D). Similar results were seen in other primitive hematopoietic populations, with a significant decrease of cells in G0 in the CD150^{-}CD48^{-} and CD150^{-}CD48^{+} subsets of LSK cells (*Online Supplementary Figure S3A to C*). In contrast to the lack of significant cell cycle perturbation in LT-HSC was the observed enrichment in gene sets pertaining to cell cycling (*Online Supplementary Figure S4A*). When the hematopoietic system was put under stress following *in vivo* treatment with 5-fluorouracil, the blood, BM, and spleen were mostly unaffected. Even though white blood cells and splenic LT-HSC were reduced, this was not significant (*Online Supplementary Figure S5A to D*). Furthermore, the proliferative capacity of *BMPR-II*$^{-/-}$ c-kit^{+} BM cells *in vitro* was normal when assayed under serum-free conditions in the presence of SCF, IL-3, and IL-6 (Figure 4E).

Homing is unaffected by deletion of *BMPR-II*

As BMP signaling has been linked to HSC homing via maintenance of ITGA4 expression during *ex vivo* culture, we investigated if loss of BMPR-II resulted in a homing defect.[20] We transplanted unfractionated *BMPR-II*$^{-/-}$ and WT BM cells, with or without competitor cells, to lethally irradiated recipients. Following 20 hours, BM was analyzed by flow cytometry. The donor contribution to Lin-Sca1^{+}CD150^{+} cells as well as to the overall Lin- population was not significantly altered between *BMPR-II*$^{-/-}$ and WT cells (Figure 4F; *Online Supplementary Figure S6A*). Donor contribution following competitive transplantation was also not significantly altered (*Online Supplementary Figure S6B to C*). Likewise, the expression of ITGA4 (CD49d) was unaltered between *BMPR-II*$^{-/-}$ and control LT-HSC, indicating that BMP signaling does not regulate ITGA4 expression *in vivo* (*Online Supplementary Figure S6D*).

Reduced phosphorylation of SMAD1 upon *BMPR-II* deletion

In order to investigate the SMAD signaling status of *BMPR-II*$^{-/-}$ hematopoietic cells, we performed western blots of purified c-kit^{+} cells incubated with/without BMP4 *in vitro*. As expected, *BMPR-II*$^{-/-}$ cells exhibited significantly reduced phosphorylated SMAD1/5, both in the presence and absence of BMP4 stimulation (Figure 5A). WT cells exhibited robust levels of phosphorylated SMAD1/5, but the level was not further increased upon BMP4 exposure, suggesting already saturated levels. These data confirm that deletion of *BMPR-II* translates into a functional reduction of SMAD signaling.

Limited SMAD-dependent transcriptional activity in hematopoietic populations

Although SMAD1/5-mediated BMP signaling is dispensable for HSC function, transcriptional activity of SMAD downstream of BMP has not been characterized in detail in hematopoietic cells. Using a BRE-GFP reporter mouse, a well-established model for gauging *in vivo* transcriptional activity of SMAD1/5/8,[26,32-34] cells responding transcriptionally to BMP through SMAD were measured by green fluorescent protein (GFP), allowing *in vivo* analysis. BRE-GFP BM cells displayed limited activation of the SMAD pathway, with the highest proportion of GFP+ cells reaching only 2.79 % on average (LSK CD150-CD48- population) (Figure 5B). In order to investigate whether hematopoietic cells could respond to BMP signaling via the SMAD pathway, BRE-GFP cells were stimulated *in vitro* for 16 hours with/without BMP4. No significant difference in GFP^{+} cells was found in any BM population (Figure 5C).

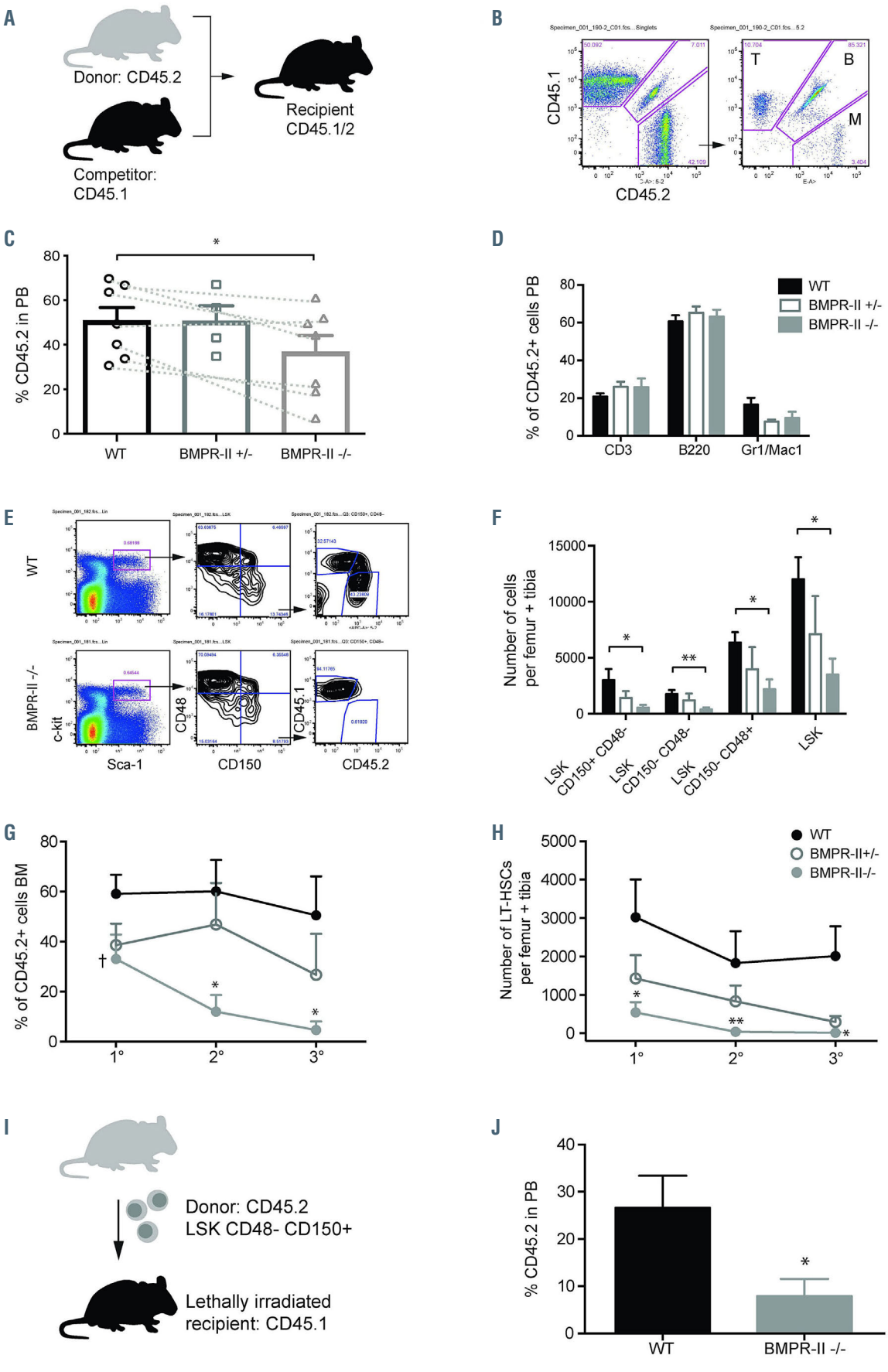

Figure 3. Continued on following page.

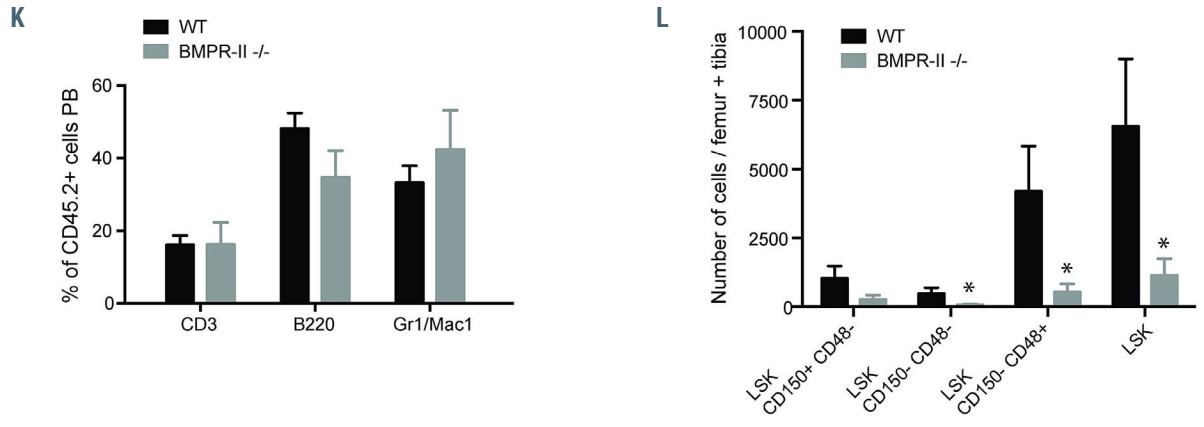

Figure 3. Reduced self-renewal capacity of hematopoietic stem cells upon loss of BMPR-II. (A) Competitive transplantation. (B) Representative fluorescence activated cell sorting (FACS) plots of peripheral blood (PB) showing CD45.1 competitor *vs.* CD45.2 donor contribution, and lineage distribution within the CD45.2 subset of cells. T: T cells; B: B cells; M: myeloid cells. (C) CD45.2 donor contribution in PB of primary recipients at 16 weeks post transplant. Mean engraftment 50.6%±6.2 for wild-type (WT) *vs.* 36.5%±7.6 for BMPR-II$^{-/-}$. Heterozygotes (BMPR-II$^{+/-}$) did not differ from WT in PB engraftment (50.4%±7.1). Due to statistically detectable variability between experiments, paired *t*-test was used to compare WT and *BMPR-II*$^{-/-}$ (n=4-7). (D) Lineage distribution within CD45.2 donor subset of PB in primary recipients at 16 weeks post transplant (n=4-7). (E) Representative FACS plots of LSK-SLAM CD45.1/2 stain of BM of primary recipients at 16 weeks post transplant. (F) Quantification of CD45.2^{+} LSK-SLAM populations in BM of primary recipients at 16 weeks post transplantation (n=4-7). (G) CD45.2 donor contribution in BM at 16 weeks post transplant in primary, secondary, and tertiary recipients (n=4-7). (H) Quantification of CD45.2^{+} Long-term hematopoietic stem cells (LT-HSC) in BM at 16 weeks post transplantation in primary, secondary, and tertiary recipients (n=4-7). (I) Transplantation of sorted LT-HSC to lethally irradiated recipients. (J) CD45.2 donor contribution in PB of recipients at 16 weeks post sorted LT-HSC transplant (n=6). (K) Lineage distribution within CD45.2 donor subset of PB in recipients at 16 weeks post sorted LT-HSC transplant (n=6). (L) Quantification of CD45.2+ LSK-SLAM populations in BM of recipients at 16 weeks post sorted LT-HSC transplantation (n=6). **P*<0.05; ***P*<0.01; †*P*=0.078.

Loss of *BMPR-II* results in a reduction of p38

As p38 has been implicated downstream of BMP in hematopoietic cells, we evaluated the level of phosphorylated p38 in c-kit^{+} progenitor cells by western blot. Phospho-p38 was reduced in un-stimulated *BMPR-II*$^{-/-}$ cells, though it did not reach significance, and its level did not change following stimulation with BMP4 (Figure 5D). We could not detect a robust increase of phospho-p38 in BMP4-stimulated WT cells. Instead, phospho-p38 was reduced following BMP4 stimulation in WT c-kit^{+} cells (Figure 5D). Additionally, the reduction of phospho-p38 in *BMPR-II*$^{-/-}$ cells may be a reflection of significantly reduced total p38 (Figure 5E). We found no significant differences in protein levels of other known signaling mediators such as phospho-Limk, phospho-Cofilin, or RhoA/B (*Online Supplementary Figure S7A* and *B*). In order to further investigate whether the reduction in LSK cell numbers in *BMPR-II* null mice is related to known downstream BMP signaling mediators such as the MAPK pathway, gene expression was evaluated in sorted LSK cells. No significant differences were found among the investigated genes (*Online Supplementary Figure S7C*). Finally, we assessed expression levels of BMP type-I and other type-II receptors in sorted WT and *BMPR-II*$^{-/-}$ primitive hematopoietic cells (LSK CD48-) to determine whether *BMPR-II* deletion leads to up- or down-regulation of other BMP receptors. We found no significant differences, despite a trend of increased Alk3 in the absence of BMPR-II (*Online Supplementary Figure S7D to E*).

Deficiency of *BMPR-II* results in up-regulation of TJP1 in long-term hematopoietic stem cells

In order to further explore underlying mechanisms behind the *BMPR-II*$^{-/-}$ phenotype, we performed microarray analysis on highly purified LT-HSC (LSK-CD150^{+}CD48^{-}CD9^{hi})[35] from adult mice. The analysis generated a number of differentially expressed genes (*Online Supplementary Figures S8* and *S4B*) and enriched gene sets (*Online Supplementary Figure S4A*). Selected genes, based on relevant known connections to stem cell function, hematopoiesis or BMP, were further validated. qPCR analyses confirmed a significant 2.4-fold up-regulation of *TJP1* in *BMPR-II*$^{-/-}$ LT-HSC (Figure 5F).

In order to further investigate whether the reduction in LSK cell numbers in *BMPR-II* null mice is related to factors known to associate with TJP1 such as SRC and STAT3, gene expression was evaluated in sorted LSK cells. No significant differences were found among the investigated genes (*Online Supplementary Figure S7C*). We also found no significant differences in expression of Alpk or microRNA 15a/23b/27a, which were other hits in the array (*Online Supplementary Figure S7F* and *G*).

TJP1 knockdown partly rescues the *BMPR-II* knockout phenotype

In order to evaluate the contribution of *TJP1* up-regulation to the observed *BMPR-II*$^{-/-}$ phenotype, *TJP1* knockdown was performed using shRNA lentiviral vectors in ckit-enriched BM cells from *BMPR-II*$^{-/-}$ and WT mice. Transduced cells were transplanted to WT recipients. Using shRNA-C knockdown of *TJP1* was achieved to at least 0.51-fold level (compared to un-transduced cells) (*Online Supplementary Figure 9A*). Average transduction efficiency at transplantation was 36 % and 33 % for scrambled-shRNA transduced WT and *BMPR-II*$^{-/-}$ groups respectively; 21 % and 26 % for *TJP1*-shRNA transduced WT and *BMPR-II*$^{-/-}$ groups (*Online Supplementary Figure S9B*).

In transplanted mouse BM the donor LSK compartment showed a partial rescue, as *TJP1*-shRNA transduced *BMPR-II*$^{-/-}$ cells no longer showed reduced engraftment in comparison to Scrambled-shRNA transduced WT cells (Figure 6A). A trend of increased engraftment was seen among HSC, although this did not reach significance (Figure 6B). In hierarchically lower populations no similar effect on engraftment was seen (Figure 6C and D), nor in PB (*data not shown*).

Discussion

A large body of work from a variety of model systems has established a critical role for BMP signaling during early development.[5-7] Studies performed *in vitro* indicate that BMP signaling continues to function in the regulation of HSC beyond development.[19,20,36] However, *SMAD1* and *SMAD5* are dispensable for adult HSC function in mice, leading to the conclusion that BMP play a limited role, if any, in adult HSC regulation *in vivo*.[21,22] The SMAD circuitry is undoubtedly the best characterized pathway downstream of BMP, but the lack of HSC phenotype in mice deficient of *SMAD1* and *SMAD5* does not automatically rule out a role for BMP signaling in adult HSC, as non-SMAD pathways can also be activated by BMP.[24,25] The fact that *BMPR-II* is highly expressed in LT-HSC has left a gap in knowledge between the BMP circuitry and its function in adult HSC *in vivo*.[23]

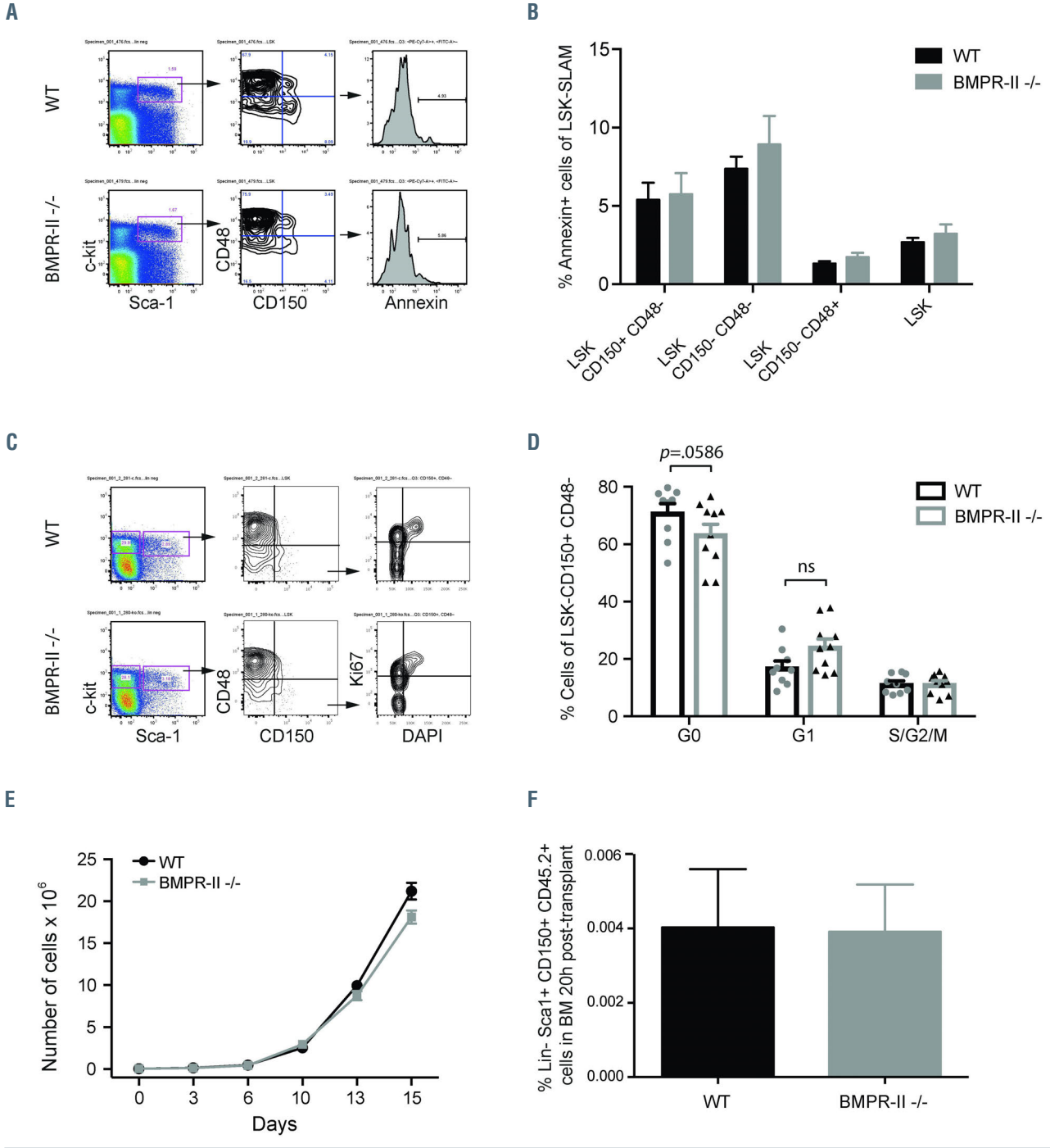

Figure 4. BMPR-II deficient mice exhibit normal apoptosis and cell cycle parameters of primitive hematopoietic cells. (A) Representative fluorescence activated cell sorting (FACS) plots of LSK-SLAM/Annexin V stain of bone marrow (BM). (B) Percentage of Annexin V$^+$ cells within indicated LSK-SLAM subsets of BM of adult mice at steady state (n=5). (C) Representative FACS plots of LSK-SLAM/Ki67/DAPI stain of BM. (D) Cell cycle distribution in percent within long-term hematopoietic stem cells (LT-HSC) (n=9-10). (E) *In vitro* growth of c-kit$^+$ cells (n=3). (F) Homing assay. Percentage of Lin/Sca1$^+$/CD150$^+$/CD45.2$^+$ cells in BM of transplanted recipients (n=5).

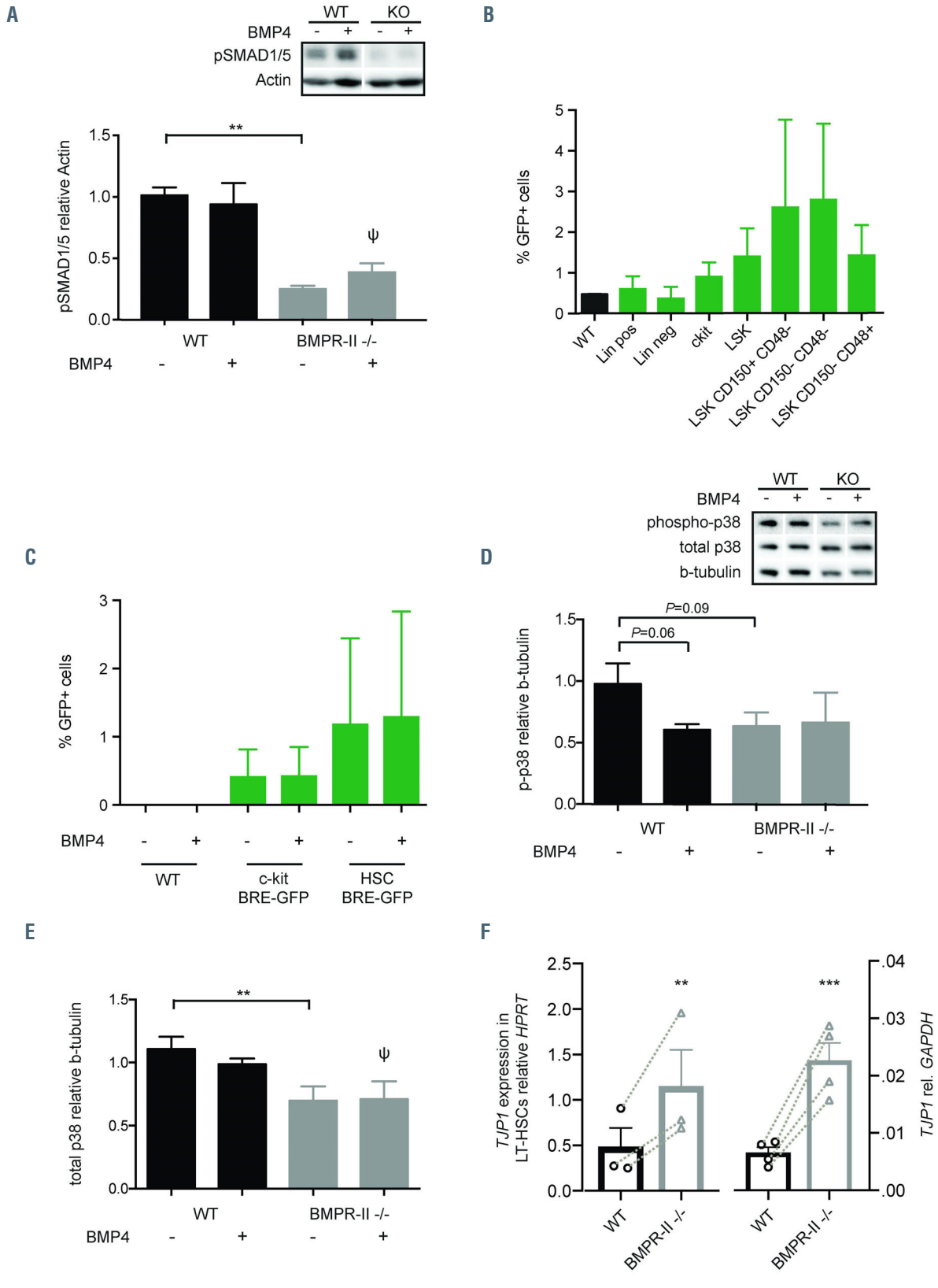

Figure 5. BMPR-II deficient cells have reduced p38 levels and up-regulation of TJP1. (A) Western blot analysis of SMAD1/5 phosphorylation in WT and BMPR-II deficient c-kit$^+$ cells, with and without BMP4 stimulation *in vitro* (n=3). ψP<0.05 compared to wild-type (WT) stimulated with BMP4 and P<0.01 compared to WT (without BMP4). (B) Western blot analysis of phospho-p38 in WT and BMPR-II$^{-/-}$ cells cultured over night with or without BMP4 (n=3).(C) Green fluorescent protein-positive (GFP$^+$) cells in BM from BRE-GFP reporter mice by flow cytometry analysis (n=3). (D) Western blot analysis of total p38 in WT and BMPR-II$^{-/-}$ cells cultured over night with or without BMP4 (n=3). ψP<0.05 compared to WT stimulated with BMP4 and P<0.01 compared to WT (without BMP4). (E) GFP$^+$ cells following over night *in vitro* culture with or without BMP4 (n=3). (F) Two separate quantitative polymerase chain reaction analyses of *TJP1* expression in WT and BMPR-II deficient LT-HSC (n=3-4). Due to statistically detectable variability between experiments and consistent ratio based changes in expression levels, ratio paired *t*-test was used to compare groups. TJP1 protein levels could not be investigated as all tested commercially available antibodies yielded no results (*data not shown*). **P<0.01; ***P<0.001.

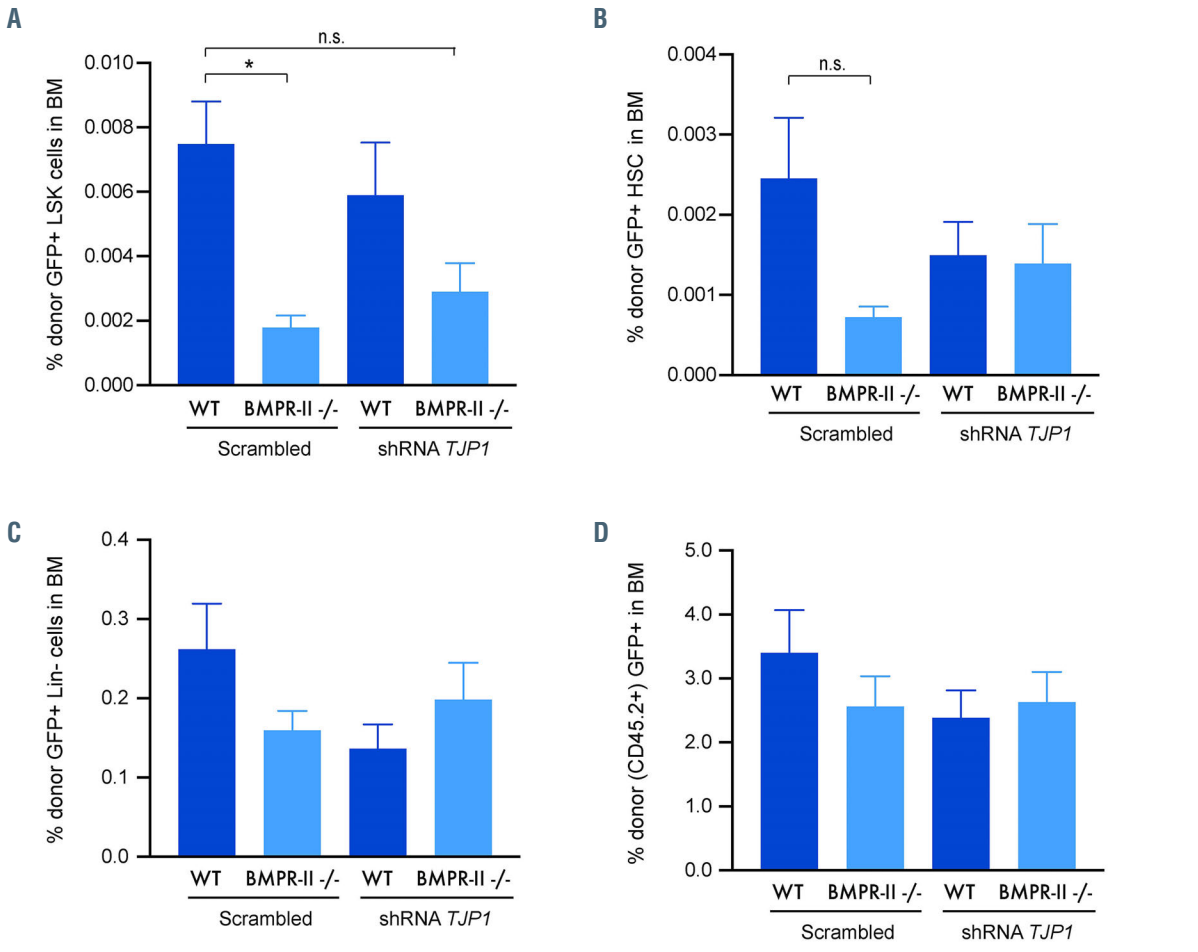

Figure 6. *TJP1* knockdown in BMPR-II deficient cells increases primitive cell engraftment. Engraftment of green fluorescent protein-positive (GFP$^+$) cells percent in bone marrow following transplantation of transduced cells in (A) CD45.2$^+$ (donor) GFP$^+$ LSK population, (B) CD45.2$^+$ GFP$^+$ HSC (LSKCD48-CD150$^+$) population, (C) CD45.2$^+$ GFP$^+$ Lin- population, and (D) CD45.2$^+$ GFP$^+$ population, analyzed at 16 weeks post transplant (n=8-9). In data set (A) and (B) outliers (one and two respectively) were detected using Grubb's test (α=0.01) and removed; this did not alter outcomes of statistical analyses. *P<0.05.

Here we aimed to elucidate the endogenous role of BMP signaling in adult murine HSC, by conditional deletion of *BMPR-II* specifically in hematopoietic cells. Unlike deletion of *SMAD1* and *SMAD5*, we report here that BMPR-II is essential for self-renewal of adult HSC. It is likely that this non-SMAD signal in HSC is mediated by BMPR-II associated with the BMP type-I receptor ALK2 or possibly ALK3, based on our transcriptional profiling of receptor expression in WT LT-HSC and that we find no significant change in expression levels of other BMP receptors in primitive hematopoietic cells from *BMPR-II*$^{-/-}$ mice. Additionally, there is limited knowledge about BMPR-II being able to activate downstream signaling pathways independently of type-I receptors. Despite the absence of significant differences in our measurements of above mentioned transcript levels, a trend of increased Alk3 seemed to be observed following *BMPR-II* deletion. This will require further studies to fully decipher the relation between BMP receptors and their cross-regulation, and to understand their relative function in the context of HSC regulation. Though it is possible that cross-talk and feedback regulation occurs within the BMP signaling pathway, *BMPR-II* deletion does not seem to have a regulatory effect at transcript level on other BMP family receptors in HSC.

In this study we show that BMPR-II deficient HSC fail to efficiently generate additional HSC upon transplantation, thus causing a significant reduction in hematopoietic regeneration following serial BM transplantation. Loss of BMPR-II did not affect homing capacity of HSC to the BM, suggesting that the reduced regenerative capacity observed upon transplantation derives from compromised self-renewal ability of LT-HSC. During steady state hematopoiesis, *BMPR-II*$^{-/-}$ mice display essentially normal hematopoietic parameters, lending further evidence to a specific role for BMPR-II in self-renewal of LT-HSC. Furthermore, as cell cycle distribution among LT-HSC is more or less unaffected by loss of BMPR-II and the hematopoietic system recovers almost normally following stress, our data suggest that a possible effect on cell cycle progression plays only a small part in HSC regulation by BMP. Instead, LT-HSC deficient of BMPR-II fail to maintain stemness during conditions when self-renewal divisions are required. This is in agreement with previous data, which shows that BMP stimulation does not affect proliferation of HSC *in vitro*.[23]

By investigating the transcriptional activity of the SMAD pathway, our data reveals that a majority of hematopoietic cells fail to respond transcriptionally to BMP and thus do not employ SMAD-dependent transcriptional response, despite phosphorylation of SMAD. We hypothesize that other regulatory mechanisms limit

the ability of the SMAD pathway to engage transcriptionally in response to BMP stimulation and that BMP preferentially signal through non-SMAD circuitries in hematopoietic cells. The BRE-reporter study is in agreement with the lack of hematopoietic phenotype seen upon deletion of *SMAD1/SMAD5*.

The p38 signaling pathway is an alternative signaling circuitry implicated downstream BMP receptors. Khurana *et al.* showed that p38 is phosphorylated in both human and mouse HSPC cultured in the presence of BMP4 *in vitro*.[20] In agreement with this, we observed a reduction in phosphorylation of p38 in hematopoietic progenitor cells lacking BMPR-II. However, we could not detect a robust induction of phosphorylation in response to BMP4 in WT progenitor cells. This may be due to the length of BMP stimulation, as Khurana *et al.* measured p38 signaling following 5 days of continuous BMP4 exposure. We assayed p38 after 30 minutes of BMP4 stimulation, a time point to measure direct activation. Reduced phosphorylation of p38 is therefore in agreement with a more long-term loss of *BMPR-II*, and may thus be due to secondary effects.

Interestingly, we observed a significant increase in expression of *TJP1* in purified *BMPR-II*$^{-/-}$ LT-HSC. TJP1 has previously been linked to regulation of self-renewal in embryonic stem cells where loss of TJP1 results in increased self-renewal.[37] Expression of *TJP1* is shared between HSC, ES cells, and neural stem cells, indicative of a universal role for TJP1 in self-renewal of stem cells.[38] Additionally, *TJP1* is downregulated in a multipotent hematopoietic cell line upon differentiation.[39] Taken together, these data substantiate the link between TJP1 and HSC self-renewal. Contrary to what is seen in hematopoietic cells *in vitro*,[39] our data suggests that loss of BMPR-II leads to disruption of HSC self-renewal via excessive expression of *TJP1*, which is in line with previous findings in ES cells.[37] It is possible that fine-tuned HSC regulation *in vivo* requires very specific levels of TJP1. Our findings further show that knockdown of *TJP1* partly rescues the *BMPR-II* null phenotype. Following transplantation of *BMPR-II*$^{-/-}$ cells with *TJP1* knockdown, we observed an increase in cell contribution to the donor LSK compartment. A similar trend was seen in the HSC compartment, but not in more differentiated populations. Our data suggests that the up-regulation of *TJP1* is, at least in part, one of the key mechanisms behind the observed *BMPR-II*$^{-/-}$ hematopoietic phenotype. Complete reversal of the phenotype may not have been achieved due to incomplete knockdown or that in addition to *TJP1* there could be other mechanisms playing a part in generating the phenotype.

In order to increase the therapeutic applicability of HSC, more detailed information is required regarding mechanisms controlling fate options such as self-renewal. In human hematopoiesis BMP have been shown to have an important role in adhesion to stroma, differentiation potential and *ex vivo* maintenance.[19,20,36] Here, we identify BMPR-II and TJP1 as important players regulating murine LT-HSC self-renewal *in vivo*. In light of our findings, further work should focus on investigating the role for BMPR-II and in particular TJP1 in human HSC self-renewal.

Disclosure

No conflicts of interest to disclose.

Contributions

SW, UB, and SK designed experiments; SW, UB, MD, THMG, LS, and SA performed experiments; SW and UB analysed data. SW, UB, and SK wrote the paper; SK supervised the study.

Acknowledgements

The authors would like to thank Leif Oxburgh from the Maine Medical Center for support in initial BRE-LacZ analyses, Elaine Dzierzak from the University of Edinburgh for providing BRE-GFP reporter mice, Shamit Soneji and Stefan Lang at the Stem Cell Center Bioinformatics Core Facility at Lund University for input on the microarray and advice on statistical analyses, and Göran Karlsson at Lund University for continuous feedback on the project and manuscript.

Funding

This work was supported by funds from the European Commission (Stemexpand); Hemato-Linné and Stemtherapy program project grants from the Swedish Research Council; a project grant to SK from the Swedish Research Council; the Swedish Cancer Society; the Swedish Childhood Cancer Fund; a Clinical Research Award from Lund University Hospital; and a grant to SK from The Tobias Foundation awarded by the Royal Academy of Sciences.

References

1. Ogawa M. Differentiation and proliferation of hematopoietic stem cells. Blood. 1993;81(11):2844-2853.
2. Orkin SH, Zon LI. Hematopoiesis: an evolving paradigm for stem cell biology. Cell. 2008;132(4):631-644.
3. Zon LI. Intrinsic and extrinsic control of haematopoietic stem-cell self-renewal. Nature. 2008;453(7193):306-313.
4. Massague J. TGFbeta signalling in context. Nature Rev M Cell Biol. 2012;13(10):616-630.
5. Sadlon TJ, Lewis ID, D'Andrea RJ. BMP4: its role in development of the hematopoietic system and potential as a hematopoietic growth factor. Stem Cells. 2004;22(4):457-474.
6. Snyder A, Fraser ST, Baron MH. Bone morphogenetic proteins in vertebrate hematopoietic development. J Cell Biochem. 2004;93(2):224-232.
7. Larsson J, Karlsson S. The role of Smad signaling in hematopoiesis. Oncogene. 2005;24(37):5676-5692.
8. Massague J. TGF-beta signal transduction. Annu Rev Biochem. 1998;67:753-791.
9. Mishina Y, Suzuki A, Ueno N, Behringer RR. Bmpr encodes a type I bone morphogenetic protein receptor that is essential for gastrulation during mouse embryogenesis. Genes Dev. 1995;9(24):3027-3037.
10. Winnier G, Blessing M, Labosky PA, Hogan BL. Bone morphogenetic protein-4 is required for mesoderm formation and patterning in the mouse. Genes Dev. 1995;9(17):2105-2116.
11. Beppu H, Kawabata M, Hamamoto T, et al. BMP type II receptor is required for gastrulation and early development of mouse embryos. Dev Biol. 2000;221(1):249-258.
12. Zhang H, Bradley A. Mice deficient for BMP2 are nonviable and have defects in amnion/chorion and cardiac development. Development. 1996;122(10):2977-2986.
13. Lechleider RJ, Ryan JL, Garrett L, et al. Targeted mutagenesis of Smad1 reveals an essential role in chorioallantoic fusion. Dev Biol. 2001;240(1):157-167.
14. Tremblay KD, Dunn NR, Robertson EJ. Mouse embryos lacking Smad1 signals display defects in extra-embryonic tissues and germ cell formation. Development. 2001;128(18):3609-3621.
15. Chang H, Huylebroeck D, Verschueren K, Guo Q, Matzuk MM, Zwijsen A. Smad5 knockout mice die at mid-gestation due to multiple embryonic and extraembryonic defects. Development. 1999;126(8):1631-1642.
16. Yang X, Castilla LH, Xu X, et al. Angiogenesis defects and mesenchymal apoptosis in mice lacking SMAD5. Development. 1999;126(8):1571-1580.

17. Zhang J, Niu C, Ye L, et al. Identification of the haematopoietic stem cell niche and control of the niche size. Nature. 2003;425(6960):836-841.
18. Goldman DC, Bailey AS, Pfaffle DL, Al Masri A, Christian JL, Fleming WH. BMP4 regulates the hematopoietic stem cell niche. Blood. 2009;114(20):4393-4401.
19. Bhatia M, Bonnet D, Wu D, et al. Bone morphogenetic proteins regulate the developmental program of human hematopoietic stem cells. J Exp Med. 1999;189(7):1139-1148.
20. Khurana S, Buckley S, Schouteden S, et al. A novel role of BMP4 in adult hematopoietic stem and progenitor cell homing via Smad independent regulation of integrin-alpha4 expression. Blood. 2013;121(5):781-790.
21. Singbrant S, Karlsson G, Ehinger M, et al. Canonical BMP signaling is dispensable for hematopoietic stem cell function in both adult and fetal liver hematopoiesis, but essential to preserve colon architecture. Blood. 2010;115(23):4689-4698.
22. Singbrant S, Moody JL, Blank U, et al. Smad5 is dispensable for adult murine hematopoiesis. Blood. 2006;108(12):3707-3712.
23. Utsugisawa T, Moody JL, Aspling M, Nilsson E, Carlsson L, Karlsson S. A road map toward defining the role of Smad signaling in hematopoietic stem cells. Stem Cells. 2006;24(4):1128-1136.
24. Blank U, Brown A, Adams DC, Karolak MJ, Oxburgh L. BMP7 promotes proliferation of nephron progenitor cells via a JNK-dependent mechanism. Development. 2009;136(21):3557-3566.
25. Derynck R, Zhang YE. Smad-dependent and Smad-independent pathways in TGF-beta family signalling. Nature. 2003;425(6958):577-584.
26. Monteiro RM, de Sousa Lopes SM, Bialecka M, de Boer S, Zwijsen A, Mummery CL. Real time monitoring of BMP Smads transcriptional activity during mouse development. Genesis. 2008;46(7):335-346.
27. Beppu H, Lei H, Bloch KD, Li E. Generation of a floxed allele of the mouse BMP type II receptor gene. Genesis. 2005;41(3):133-137.
28. Stadtfeld M, Graf T. Assessing the role of hematopoietic plasticity for endothelial and hepatocyte development by non-invasive lineage tracing. Development. 2005;132(1):203-213.
29. Pronk CJ, Rossi DJ, Mansson R, et al. Elucidation of the phenotypic, functional, and molecular topography of a myeloerythroid progenitor cell hierarchy. Cell Stem Cell. 2007;1(4):428-442.
30. Chen MJ, Yokomizo T, Zeigler BM, Dzierzak E, Speck NA. Runx1 is required for the endothelial to haematopoietic cell transition but not thereafter. Nature. 2009;457(7231):887-891.
31. Gekas C, Graf T. CD41 expression marks myeloid-biased adult hematopoietic stem cells and increases with age. Blood. 2013;121(22):4463-4472.
32. Blank U, Seto ML, Adams DC, Wojchowski DM, Karolak MJ, Oxburgh L. An in vivo reporter of BMP signaling in organogenesis reveals targets in the developing kidney. BMC Dev Biol. 2008;8:86.
33. Crisan M, Kartalaei PS, Vink CS, et al. BMP signalling differentially regulates distinct haematopoietic stem cell types. Nat Commun. 2015;6:8040.
34. Crisan M, Solaimani Kartalaei P, Neagu A, et al. BMP and hedgehog regulate distinct AGM hematopoietic stem cells ex vivo. Stem Cell Reports. 2016;6(3):383-395.
35. Karlsson G, Rorby E, Pina C, et al. The tetraspanin CD9 affords high-purity capture of all murine hematopoietic stem cells. Cell Rep. 2013;4(4):642-648.
36. Jeanpierre S, Nicolini FE, Kaniewski B, et al. BMP4 regulation of human megakaryocytic differentiation is involved in thrombopoietin signaling. Blood. 2008;112(8):3154-3163.
37. Xu J, Lim SB, Ng MY, et al. ZO-1 regulates Erk, Smad1/5/8, Smad2, and RhoA activities to modulate self-renewal and differentiation of mouse embryonic stem cells. Stem Cells. 2012;30(9):1885-1900.
38. Ramalho-Santos M, Yoon S, Matsuzaki Y, Mulligan RC, Melton DA. "Stemness": transcriptional profiling of embryonic and adult stem cells. Science. 2002;298(5593):597-600.
39. Bruno L, Hoffmann R, McBlane F, et al. Molecular signatures of self-renewal, differentiation, and lineage choice in multipotential hemopoietic progenitor cells in vitro. Mol Cell Biol. 2004;24(2):741-756.

ARTICLE

Co-occurrence of cohesin complex and Ras signaling mutations during progression from myelodysplastic syndromes to secondary acute myeloid leukemia

Marta Martín-Izquierdo,[1*] María Abáigar,[1*] Jesús M. Hernández-Sánchez,[1] David Tamborero,[2,3] Félix López-Cadenas,[4] Fernando Ramos,[5] Eva Lumbreras,[1] Andrés Madinaveitia-Ochoa,[6] Marta Megido,[7] Jorge Labrador,[8] Javier Sánchez-Real,[5] Carmen Olivier,[9] Julio Dávila,[10] Carlos Aguilar,[11] Juan N. Rodríguez,[12] Guillermo Martín-Nuñez,[13] Sandra Santos-Mínguez,[1] Cristina Miguel-García,[1] Rocío Benito,[1] María Díez-Campelo[4*] and Jesús M. Hernández-Rivas[1,4#]

[1]Institute of Biomedical Research of Salamanca (IBSAL), Cytogenetics-Molecular Genetics in Oncohematology, Cancer Research Center-University of Salamanca (IBMCC, USAL-CSIC), Salamanca, Spain; [2]Research Program on Biomedical Informatics, Hospital del Mar Medical Research Institute (IMIM), Universitat Pompeu Fabra, Barcelona, Spain; [3]Department of Oncology-Pathology, Science for Life Laboratory, Karolinska Institutet, Stockholm, Sweden; [4]University of Salamanca, IBSAL, Hematology, Hospital Clínico Universitario, Salamanca, Spain; [5]Hematology, Hospital Universitario de León, Institute of Biomedicine (IBIOMED)-University of León, León, Spain; [6]Hematology, Hospital Universitario Miguel Servet, Zaragoza, Spain; [7]Hematology, Hospital del Bierzo, Ponferrada, León, Spain; [8]Hematology, Hospital Universitario de Burgos, Burgos, Spain; [9]Hematology, Hospital General de Segovia, Segovia, Spain; [10]Hematology, Hospital Nuestra Señora de Sónsoles, Ávila, Spain; [11]Hematology, Hospital Santa Bárbara, Soria, Spain; [12]Hematology, Hospital Juan Ramón Jiménez, Huelva, Spain and [13]Hematology, Hospital Virgen del Puerto, Plasencia, Spain

*MA and MMI contributed equally as co-first authors.
#MDC and JMHR contributed equally as co-senior authors.

Ferrata Storti Foundation

Haematologica 2021
Volume 106(8):2215-2223

ABSTRACT

Myelodysplastic syndromes (MDS) are hematological disorders at high risk of progression to secondary acute myeloid leukemia (sAML). However, the mutational dynamics and clonal evolution underlying disease progression are poorly understood at present. In order to elucidate the mutational dynamics of pathways and genes occurring during the evolution to sAML, next-generation sequencing was performed on 84 serially paired samples of MDS patients who developed sAML (discovery cohort) and 14 paired samples from MDS patients who did not progress to sAML during follow-up (control cohort). Results were validated in an independent series of 388 MDS patients (validation cohort). We used an integrative analysis to identify how mutations, alone or in combination, contribute to leukemic transformation. The study showed that MDS progression to sAML is characterized by greater genomic instability and the presence of several types of mutational dynamics, highlighting increasing (*STAG2*) and newly-acquired (*NRAS* and *FLT3*) mutations. Moreover, we observed co-operation between genes involved in the cohesin and Ras pathways in 15-20% of MDS patients who evolved to sAML, as well as a high proportion of newly acquired or increasing mutations in the chromatin-modifier genes in MDS patients receiving a disease-modifying therapy before their progression to sAML.

Introduction

Myelodysplastic syndromes (MDS) are a heterogeneous group of clonal hematopoietic disorders characterized by peripheral blood (PB) cytopenia with dysplastic bone marrow (BM) morphology and an increased risk of progression to secondary acute myeloid leukemia (sAML).[1-3] Approximately one third of patients diag-

Correspondence:
JESÚS M HERNÁNDEZ-RIVAS
jmhr@usal.es

Received: February 3, 2020.
Accepted: July 14, 2020.
Pre-published: July 16, 2020.

https://doi.org/10.3324/haematol.2020.248807

nosed with MDS eventually transform into sAML.[4] Disease progression is associated with a dismal prognosis, partly because most of these patients are resistant to currently available treatments, and the long-term survival rate of treated patients is less than 10% after a couple of years.[5-7]

In recent years, new high-throughput genomic technologies, such as next-generation sequencing (NGS), have enabled a large number of studies to elucidate some of the mechanisms involved in MDS pathogenesis such as epigenetic regulation, transcription, signaling pathways, splicing, cohesin complex, apoptosis and angiogenesis. However, MDS exhibit great genetic and clinical heterogeneity, so the nature of their pathogenesis is still not fully understood.[8-10]

The mutational dynamics and clonal evolution underlying disease progression have just begun to become clear. Previous studies have identified multiple genes recurrently mutated in MDS and sAML and these have provided insight into the great intratumoral heterogeneity typical of progression from MDS to sAML.[8-13] These studies have shown that the evolution of the disease is a complex process involving new additional alterations co-existing with the MDS founder clone.[14] Moreover, recent studies have described the association of mutations in genes such as *TET2, RUNX1, ASXL1,* and *STAG2* with high-risk MDS, as well as the presence of mutations in genes activating signaling pathways, such as *FLT3, PTPN11, NPM1*, and *NRAS*, which are newly acquired in sAML and associated with faster progression.[15-17] However, this complexity and the lack of large cohorts of serial samples means that molecular mechanisms of disease progression are only partly understood. Thus, longitudinal sequencing genomic studies are still required to determine which mutations or combinations of them are important in leukemic transformation.

In this study, we performed whole-exome sequencing (WES) and/or targeted deep sequencing (TDS) on serial samples from MDS patients who evolved to sAML (discovery cohort) before and after progression, as well as TDS on additional MDS patients who did not progress to sAML during follow-up (control cohort). The results were validated in an independent series of MDS patients (validation cohort). Interestingly, we undertook an integrative analysis to determine the mutational dynamics of the pathways and genes and to identify how mutations, alone or in combination, contribute to leukemic transformation. The study showed involvement of co-occurrence of alterations in the cohesin and Ras pathways in the MDS transformation to sAML, as well as a high proportion of newly acquired or increased clonal selection of mutations in the chromatin-modifier genes in MDS patients who received a disease-modifying therapy before their progression to sAML.

Methods

Study design

In order to study the mutational changes occurring during the evolution to sAML from a previous myelodysplastic phase, 486 samples from 437 patients were included in the study. The patient series was divided into three cohorts (*Online Supplementary Figure S1*): i) discovery cohort: a cohort of MDS → sAML progressing patients that included 42 patients diagnosed with MDS who progressed to sAML; according to the study design, 84 BM serial patient-matched samples were collected and sequenced on two occasions with the first sampling, at initial presentation of the disease (diagnosis, MDS stage), and the second sampling, after progression to sAML (disease evolution, leukemic phase); all samples were analyzed by a TDS strategy; furthermore, 16 of those progressing patients (32 samples) were initially studied by WES; information about the treatment received before progression was available for all 42 patients: azacytidine (n=16), lenalidomide (n=4) and no treatment or supportive care (n=22); ii) control cohort: a cohort of MDS non-progressing patients consisted of 14 BM paired samples from seven MDS patients who did not progress to sAML after a minimum of 3-year follow-up for low-risk MDS (LR-MDS) and 1 year for high-risk MDS (HR-MDS) (median follow-up of 52 months; range, 20-89 months); according to the study design, the second sampling in this control cohort corresponded to a time when the disease was stable and TDS was performed on all these samples; iii) validation cohort: a cohort of 388 BM or PB samples from patients suffering MDS at diagnosis and for which only one time-point (sample) was studied by TDS;. notably, 63 of these patients eventually evolved to sAML, while 325 had not progressed to sAML after a median follow-up of 19.6 months. The main patient clinical characteristics are summarized in the *Online Supplementary Table S1*.

This research was performed in accordance with the Declaration of Helsinki guidelines, and was approved by the Local Ethics Committee ("Comité Ético de Investigación Clínica, Hospital Universitario de Salamanca"). All patients provided written informed consent.

Sequencing analysis

Whole-exome sequencing

WES was performed on matched diagnosis-progression samples from 16 patients of the discovery cohort. The mean coverage of WES was 77.6x (range, 36-124) and at least 73% of the captured regions had a coverage of 30x or more for all 32 samples (*Online Supplementary Table S2*). See the *Online Supplementary Appendix* for full details.

Targeted-deep sequencing

All genomic DNA samples underwent TDS using an in-house custom capture-enrichment panel of 117 genes previously related to the pathogenesis of myeloid malignancies (*Online Supplementary Table S3*). The mean coverage of TDS was 665x (range, 251-1,198) where 99.5% of target regions were captured at a level greater than 100x. See the *Online Supplementary Appendix* for full details.

Analysis of mutational dynamics

The main aim of this study was to analyze the mutational changes occurring between the first sampling (MDS stage) and the second sampling (stable disease/sAML stage) in the discovery and control cohorts. To this end, variant allele frequency (VAF) at these two stages were compared using two approaches: i) VAF ratio between second and first sampling, where thresholds of >1.2 and <0.8 were used to classify mutations as increasing or decreasing, respectively, while ratios between these thresholds were considered to be stable; and ii) Fisher´s exact test where values of $P<0.05$ were taken to indicate statistically significant changes during progression.

Results

Molecular landscape of the progression from myelodysplastic syndromes to secondary acute myeloid leukemia

In order to characterize the main cohort of the study, the discovery cohort, 16 patients (patients #27 - #45) were analyzed by WES at the time of diagnosis and at leukemic

transformation, as previously explained. After a stringent analysis[18] as described in the *Online Supplementary Appendix*, 61 variants were identified as likely somatic mutations: 40 were called driver and 21 were called passenger using the novel bioinformatics tool "Cancer Genome Interpreter"[19] (*Online Supplementary Table S4*). A total of 47 variants in genes known to drive myeloid malignancies were further validated with a true positive rate of >89% using TDS and VAF correlation between two platforms was high (Pearson´s r=0.90) (*Online Supplementary Figure S2*). However, the application of TDS revealed that several driver mutations were not detected by WES as they were poorly covered and displayed a low VAF. Then, we decided to more comprehensively study disease progression by applying the TDS panel in a larger cohort of serially collected samples.

We performed TDS on these 16 patients of the initial discovery cohort and in additional 26 patients. A total of 159 mutations were identified at diagnosis of the 42 patients (*Online Supplementary Table S5*). The most recurrently mutated genes were *TET2* (14 of 42, 33%), *SF3B1* (13 of 42, 31%), *SRSF2* (ten of 42, 24%), *DNMT3A* (10 of 42, 24%), *STAG2* (8 of 42, 19%), *TP53* (8 of 42, 19%) and *ASXL1* (6 of 42, 14%). At the time of the second sampling, the sAML

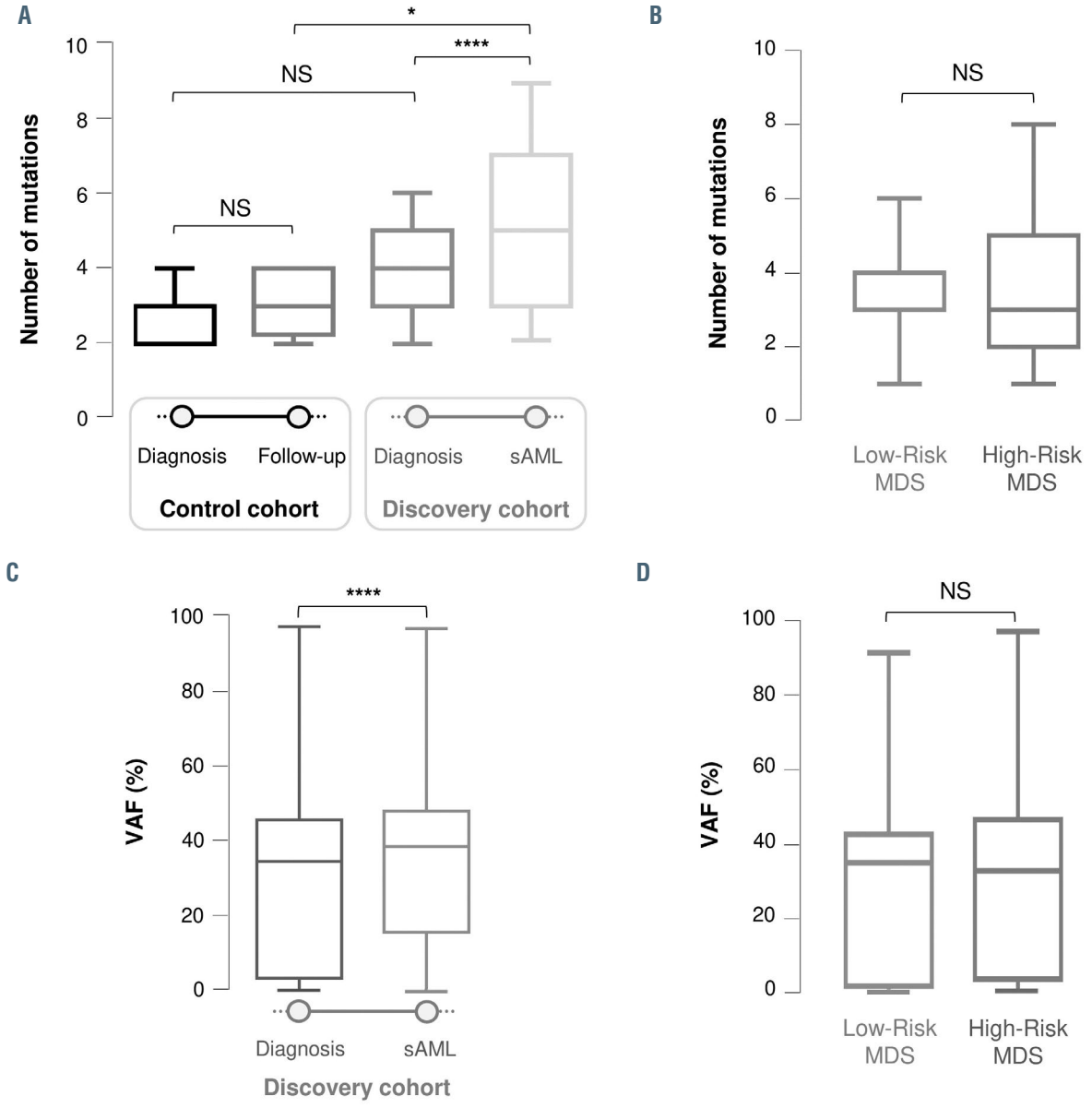

Figure 1. Boxplots showing the differences in the number of mutations (A-B) and variant allele frequency (C-D) between the two times analyzed during the evolution of the disease and between the different French-American-British/World Health Organization (FAB/WHO) subtypes at the time of diagnosis. (A) Differences in the number of mutations between diagnosis and follow-up/secondary acute myeloid leukemia (sAML) stages within and between the control and discovery cohorts. These graphs show a statistically significant increase in the number of mutations during disease evolution in patients who progressed to sAML (P<0.0001). (B) No significant differences in the number of mutations between the FAB/WHO subtypes at time of diagnosis (number of mutations low-risk myelodysplastic syndromes [LR-MDS] *vs.* high-risk MDS [HR-MDS], P=0.588). (C) Differences in variant allele frequency (VAF) of detected mutations between diagnosis and sAML stage in the discovery cohort. The VAF was higher at the time of sAML progression (P<0.0001). (D) No significant difference in VAF between the FAB/WHO subtypes at time of diagnosis (VAF: LR-MDS *vs.* HR MDS, P=0.528). NS: not significant; *P<0.05; ****P<0.0001.

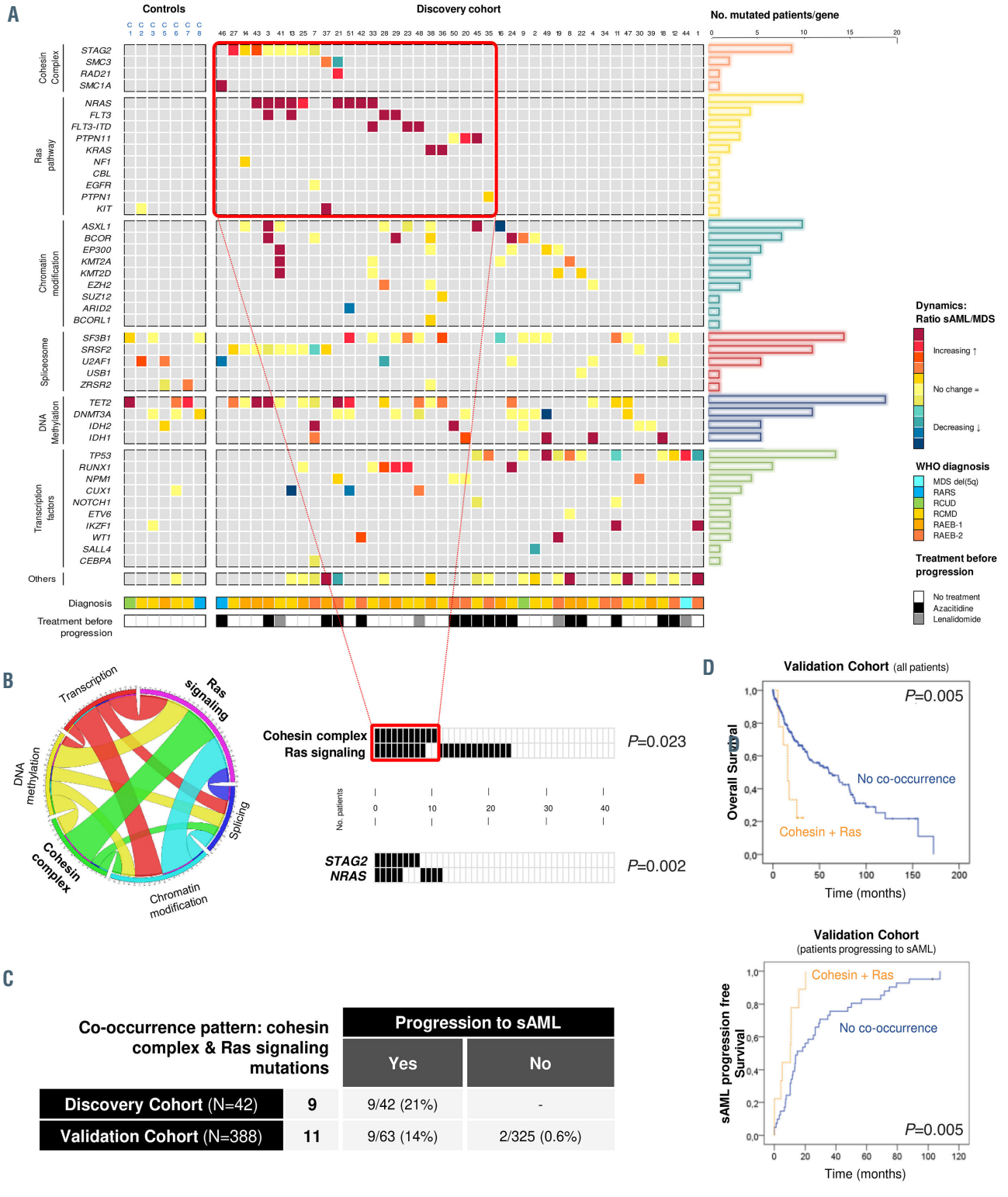

C

Co-occurrence pattern: cohesin complex & Ras signaling mutations		Progression to sAML	
		Yes	No
Discovery Cohort (N=42)	9	9/42 (21%)	-
Validation Cohort (N=388)	11	9/63 (14%)	2/325 (0.6%)

Figure 2. Dynamics of gene mutations in the myelodysplastic syndromes to secondary acute myeloid leukemia progression axis. (A) Comprehensive landscape of mutational dynamics in the discovery and control cohorts. Genes are grouped by cellular functions and are represented in rows; each column represents a patient. Dynamics are represented by a color gradient: red/orange for newly acquired/increasing mutations, yellow for stable mutations, and blue/green colors for decreasing mutations. (B) Co-occurrence of cohesin complex and Ras signaling mutations in the discovery cohort. Circos plot of statistically significant associations between mutations detected in the discovery cohort, grouped by functional pathways. Graphs represent patients with mutations in the cohesin complex and Ras signaling, and the most frequently mutated genes in these pathways, *STAG2* and *NRAS*, showing a statistically significant association (P=0.023 and P=0.002, respectively). (C) Incidence of this co-occurrence pattern in the discovery and validation cohorts. The table contains the number of patients with the combination of cohesin and Ras signaling mutations in the discovery and validation cohorts and an indication of whether they evolved to secondary acute myeloid leukemia (sAML). (D) Prognostic impact of the co-occurring mutations in the cohesin complex and Ras pathway. Kaplan-Meier curves for overall survival and sAML progression-free survival in patients bearing co-occurring cohesin and Ras pathway mutations in the entire validation cohort. VAF: variant allele frequency; LR: low-risk; HR: high-risk; NS: not significant; *P<0.05.

stage, 210 mutations were detected, 159 of which were already known to be present in the MDS stage, at clonal or subclonal levels (128 were retained and 31 evolved during disease progression), while 51 were detected only at the second sampling. The most recurrently mutated genes at the sAML stage were similar to those noted at the MDS stage: *TET2* (17 of 42, 40%), *SF3B1* (13 of 42, 31%), *TP53* (12 of 42, 29%), *SRSF2* (ten of 42, 24%), *DNMT3A* (ten of 42, 24%), *ASXL1* (nine of 42, 21%) and *STAG2* (eight of 42, 19%). However, the *NRAS* gene (9 of 42, 21%) also stood out at this stage. It should be noted that 32 of 54 genes (59%) were mutated only in fewer than three (<7%) patients, highlighting the great heterogeneity in the mechanisms of disease evolution.

Regardless of World Health Organization diagnosis subtypes, patients progressing to secondary acute myeloid leukemia present a higher number of mutations than those that do not progress

In order to analyze the changes in clonal size and distribution during evolution to sAML, we compared the number of mutations identified at diagnosis and at the second sampling in the discovery and control cohorts. The control cohort presented a median of three mutations at both sampling times (p10-p90: 2-4 in both), indicating no significant differences (P=0.449). By contrast, the discovery cohort had a median of four (p10-p90: 1-6) and five (p10-p90: 2-9) mutations at the first and second samplings, respectively, representing a highly significant increase in the number of mutations during disease progression (P<0.0001). Remarkably, the control and discovery cohorts had a similar number of mutations at the time of diagnosis (P=0.097), although a slight trend was observed, while patients who progressed showed a significantly higher number of mutations at the time of sAML than the control patients at the second sampling (P=0.027) (Figure 1A). Considering the discovery cohort patients by World Health Organization diagnosis subtype (LR-MDS and HR-MDS) did not reveal any significant differences in the number of mutations in patients progressing to sAML (P=0.588) (Figure 1B).

In order to further study what characterizes disease evolution, we compared the VAF of mutations at both times. Patients who evolved to sAML presented a significantly higher VAF median at second sampling (29.11% *vs.* 36.76%, P<0.0001) (Figure 1C). However, no differences were identified in the median VAF between each subtype at the time of diagnosis (P=0.528). (Figure 1D).

Therefore, taking all these results together, MDS patients, irrespective of their diagnostic subtype, displayed a greater genomic instability during disease progression than patients who did not evolve to sAML.

Mutational dynamics during the progression to secondary acute myeloid leukemia: clonal evolution

In order to study the mutational dynamics and identify which mutations could be involved in clonal evolution and play an important role during disease progression, the VAF of mutations detected at both times (follow-up/sAML *vs.* diagnosis) were compared in all patients of the discovery and control cohorts.

Four types of clonal dynamics were identified: type 1, in which mutations were initially present in the MDS stage, but whose VAF increased significantly in the sAML stage; type 2, mutations whose VAF significantly decreased; type 3, mutations that were newly acquired at the sAML stage; type 4, mutations that persisted with a similar allelic burden at both stages.

Stable mutations (Figure 2A, type 4, depicted in yellow) were detected in genes involved in the spliceosome and DNA methylation pathways, such as the splicing factor *SRSF2* (diagnosis *vs.* sAML median VAF, P=0.4922) and the DNA methylation gene *DNMT3A* (diagnosis *vs.* sAML median VAF, P=0.7695) (*Online Supplementary Figure S3*).

Only a minority of the mutations detected at diagnosis showed a decrease in their allelic burden (Figure 2A, type

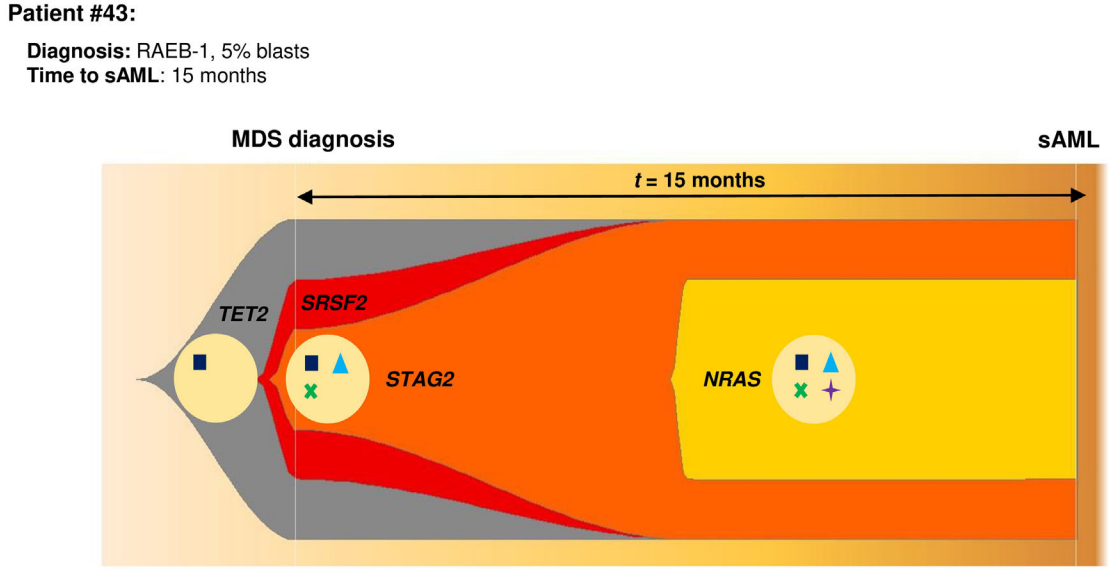

Figure 3. Model of clonal evolution during myelodysplastic syndrome progression to secondary acute myeloid leukemia using patient #43 as an example and applying the Fishplot R package.[29] In this patient diagnosed as RAEB-1, an myelodysplastic syndrome (MDS) founder clone was present at the time of diagnosis with typical myeloid mutations such as *TET2* and *SRSF2*. This clone also harbored a mutation in *STAG2*, thus it triggered the acquisition of a subsequent mutation in a Ras pathway gene, namely *NRAS*. This clone expanded, driving the evolution of the disease.

2, in green-blue), and these were randomly distributed throughout all the genes without showing a pattern.

The most interesting dynamic patterns were those of newly acquired mutations (Figure 2A, type 3, represented in red) or increased in clonal size (Figure 2A, type 1, in orange) at the time of sAML progression. These mutational patterns were mainly found in the cohesin complex and Ras signaling, where they were clustered in the *STAG2* and *NRAS, KRAS* and *FLT3* genes. These profiles were also detected in transcription factors and epigenetic modifiers, but in these cases they were randomly distributed among the genes. In fact, the *STAG2* VAF median was significantly higher at sAML stage (diagnosis *vs.* sAML median VAF, P=0.023) and this gene was mutated in eight patients of the discovery cohort, in five of which the VAF had increased by the time they had become sAML (*Online Supplementary Figure S3*). The increase was statistically significant in three of these five patients, while it was not significant in the other two, although a trend was observed (P<0.08), probably because the VAF at diagnosis was already very high. Moreover, most of the mutations (nine of 12) in the cohesin complex genes were of the frameshift or stop gained (loss of function) type and the cohesin-mutated patients showed a higher number of mutations than wild-type patients (median number of mutations: seven *vs.* four, P=0.0179). On the other hand, *NRAS* and *FLT3* mutations were newly acquired (diagnosis *vs.* sAML median VAF, P=0.0029 and P=0.0078, respectively) during the evolution and so were detected at the sAML stage (*Online Supplementary Figure S3*).

Co-occurrence of cohesin complex and Ras signaling mutations in patients after progressing to secondary acute myeloid leukemia

Within this heterogeneous landscape of mutational dynamics, we focused our study on increasing (type 1) and newly acquired (type 3) mutations because their dynamic patterns suggested that they were positively selected during disease evolution. Moreover, in order to better characterize the mechanisms driving sAML progression, we studied which pathways and combination of them were affected by these types of mutations.

In the discovery cohort, a high proportion of Ras signaling-mutated patients at the sAML stage, already harbored cohesin complex mutations. In fact, 26% (11 of 42) of the discovery cohort patients carried mutations in the cohesin complex at diagnosis. On the other hand, 52% (22 of 42) of the patients had at least one Ras pathway mutation at the sAML stage, mainly acquired during the evolution of the disease. Of interest, nine of these cohesin-mutated patients (nine of 11, 82%) carried a co-occurring Ras signaling mutation at the sAML stage. Considering only the most recurrently mutated gene, *STAG2* (n=eight of 11), seven patients (seven of eight, 88%) carried another mutation in the Ras pathway, this being a *NRAS* mutation in five patients. Therefore, there was a statistically significant co-occurrence of these two pathways (P=0.023) and of the most recurrently mutated genes of these pathways, *STAG2* and *NRAS* (P=0.002) (Figure 2B).

In order to confirm these observations and their impact on MDS progression to sAML, the combination of the cohesin complex and Ras pathway mutations was sought in the validation cohort, an independent cohort of 388 patients in which the disease was studied on only one occasion, at diagnosis. In fact, these co-occurring mutations were detected in eleven additional patients: nine of which finally transformed into sAML (nine of 63), while two patients did not evolve during the median follow-up of 19.6 months (two of 325) (Figure 2C). Although all samples of this cohort were studied at diagnosis, these nine patients carried cohesin and Ras co-occurring mutations at an advanced stage of the disease, indeed these were detected in sAML sampling or in patients who transformed in a median time of 11 months from sampling.

The discovery cohort included only patients who evolved to sAML, and therefore displayed a very poor outcome. This made it difficult to measure the impact of this co-occurrence in these patients. For that reason and also to further study the clinical consequences of this co-occurrence on outcome, the effects on overall survival and progression-free survival in the validation cohort (median follow-up of 19.6 months) were analyzed. In our validation cohort, where 16.2% of patients evolved to sAML and 44.76% died (*Online Supplementary Table S1*), those patients harboring both the cohesin complex and Ras signaling mutations had significantly shorter overall survival (16 *vs.* 60 months, P=0.005) and significantly earlier progression to sAML (10 *vs.* 15 months, P=0.005) (Figure 2D). Moreover, in order to study the contribution of the cohesin and Ras mutations alone to these effects, comparison of median overall survival of the double-mutant and cohesin and Ras single mutant patients was performed and patients harboring double mutations showed shorter overall survival than patients with Ras or cohesin single mutations (16 *vs.* 25 *vs.* 37 months, respectively, P=0.018, *Online Supplementary Figure S4*).

Higher proportion of newly acquired or increasing mutations in chromatin modifiers in treated myelodysplastic syndrome patients

As previously mentioned, 48% of the patients in the discovery cohort of this study were treated with 5-azacytidine (AZA) (n=16) or lenalidomide (n=4), and progressed to sAML after therapy, whereas the other 52% received no treatment (only supportive care). Thus, we investigated whether the mechanisms of progression could be slightly different between patients who were treated with disease-modifying agents (AZA and lenalidomide) before transformation into sAML and non-treated patients.

In order to achieve this aim, the proportions of the different mutational dynamics were compared between treated and untreated patients. Thereby, the mutational dynamics featured a significantly higher proportion of newly acquired or increasing mutations in chromatin modifiers at the time of sAML in treated patients (eight of 15 mutations), while in untreated patients the majority of mutations were stable (53% [eight of 15] *vs.* 19% [four of 21], P=0.031). By contrast, and with respect to the treatment, no differences were detected in the dynamics of the cohesin complex (50% [three of six] of newly acquired or increasing mutations in treated patients *vs.* 50% [three of six] in untreated, P=1.00) or Ras pathway mutations (91% [ten of 11] in treated *vs.* 76% [13 of 17] in untreated patients, P=0.3299) (*Online Supplementary Figure S5*). Thus, our study suggests that mutations in chromatin-modifier genes could be related to the evolution of patients who receive disease-modifying treatment before progression to sAML.

Discussion

Our study characterizes the landscape of mutations during progression toward sAML and how mutations, alone or in combination, contribute to leukemic transformation, based on the analysis of a large number of serial samples from patients who progressed to sAML. Moreover, the comparison of a control and a validation cohort supports the identification of mechanisms mostly related to evolution to sAML.

Previous studies have documented the clonal evolution and greater clonal heterogeneity during cancer development and, specifically, as MDS evolves to advanced stages and transforms into sAML,[8,9,14-16,20] and according to this fact, the study demonstrates that MDS patients, irrespective of their diagnostic subtype, gain more mutations and a higher VAF during disease progression. Therefore, these results are evidence that progression toward sAML is associated with pronounced genomic instability and a heavy mutational burden.

The mechanisms of disease evolution showed a great heterogeneity.[14-17] However, this study identified four distinct types of mutational dynamics and their roles during sAML progression. It is of particular note that this study shows a higher incidence of mutations in the cohesin complex and Ras signaling genes than in previously published MDS series,[8,9,21,22] probably because this cohort consisted only of patients who progressed to sAML. Moreover, increasing mutations (type 1) were mainly found in genes of this pathway, such as *STAG2*, most of which were loss of function mutations. Previous studies of cohesin mutations had already shown that these mutations could be related to sAML progression,[15,21,22] but the dynamics observed in this study confirm that mutations of cohesin complex genes could be an early event in sAML progression, and the loss of function of these genes could play an important role in the leukemic transformation. Similarly, the dynamics of Ras signaling genes observed here, mainly newly acquired mutations (type 3), highlight the importance of this pathway in sAML progression. Earlier studies have described how alterations in Ras pathway genes, such as *NRAS* and *FLT3*, could drive the progression to sAML[23-25] but these results confirm that they are late events that may drive leukemic transformation. Furthermore, this study reveals a significant co-occurrence of mutations in these two pathways and, also, in the main genes of these pathways (*STAG2* and *NRAS*), excluding the *FLT3*-ITD mutations which could have a different behavior than other mutations in Ras pathway and they could be involved in an independent mechanism of sAML progression.[26,27] Although Walter *et al.*[28] described that *NRAS* and cohesin mutations tend to be mutually exclusive, this work included a low number of patients and, conversely, this co-occurrence was briefly described in another study with a higher number of patients.[21] Thus, this study, due to detecting in a cohort of sAML-progressing patients, demonstrates that this progressive combination of the cohesin complex, mainly *STAG2*, and Ras signaling mutations, mostly *NRAS*, could play an important role in the progression of MDS to sAML. In addition, the results from the validation cohort confirmed the impact of this co-occurrence on sAML progression not only in the discovery cohort, but also in the validation cohort. Therefore, these findings support a hypothesis of genetic "predisposition", that early mutations shape the future trajectories of clonal evolution from MDS to sAML. Therefore, a new model of genetic evolution could be suggested consisting of cohesin mutations as an early event in the evolution of the disease that trigger to acquire new mutations, mainly Ras signaling mutations. Consequently, this clone expands, driving the disease evolution (Figure 3, model of clonal evolution using Fishplot R package).[29] Recent studies have described that cohesins are involved in DNA damage repair, chromatin accessibility and transcription factor activity[30-32] and our results show than cohesin-mutated patients displayed a higher number of mutations, thereby cohesins could cause an instability where new mutations are generated, mainly Ras mutations, leading the disease progression. These are not absolute rules and, unfortunately, this novel model does not fully explain the progression to sAML, but it could explain the evolution in 15-20% of all sAML transformations. Moreover, cohesin mutations potentiate the subsequent acquisition of Ras mutations, so these mutations could be used to identify patients whose disease is progressing before symptoms associated with progression to sAML are manifested.

On the other hand, the mutations that were stable during the evolution (type 4) were found in splicing and DNA methylation genes. This is in line with the finding of some recent reports showing that variants affect these pathways in this steady-state pattern.[16] Moreover, mutations in DNA methylation and RNA splicing pathways are well known to have a heavier mutational burden than those in other genes, suggesting an early event in MDS development.[8,9] Considering these findings together, these results showed that mutations in these pathways, which have high VAF and are stable during the disease evolution, could be directly involved in MDS pathogenesis (driver role) but not in sAML progression (passenger role). The mutations whose VAF decreased during progression (type 2) were distributed randomly throughout all the genes without showing a particular pattern. This could be the result of clone sweeping, a previously described event,[15] that is specific to each patient rather than to a specific pattern of each gene or pathway.

Furthermore, a mechanism that could be linked to the evolution of patients who receive disease-modifying treatment before progression to sAML was detected. Several studies have described the mutational dynamics in treated MDS patients and have demonstrated that therapy alters clonal distribution, but the predictive impact of the dynamics is still unclear.[33-37] A significantly higher proportion of newly acquired or increasing mutations in chromatin modifiers at the time of sAML was identified in treated patients. Thus, these results suggest that mutations in chromatin-modifier genes could be related to the evolution of treated patients. However, more studies with larger numbers of patients are required to validate this result.

In summary, MDS progression to sAML is characterized by greater genomic instability, irrespective of the MDS subtypes at diagnosis, and there are four types of mutational dynamics during the disease evolution, increasing and newly acquired mutations (type 1 and type 3, respectively) being of particular importance. Moreover, a co-occurrence of cohesin complex and Ras signaling mutations could play an important role in the 15-20% of MDS patients who evolved to sAML. With regard to treatment, we found that mutations in chro-

matin-modifier genes could be related to the evolution of MDS patients who received disease-modifying treatment before progression to sAML.

Disclosures

No conflicts of interest to disclose.

Contributions

MMI designed the experiments, performed targeted-deep sequencing experiments, analyzed the data and wrote the paper; MA designed the experiments, performed whole-exome sequencing experiments, contributed to interpret the results and wrote the paper; JMHS performed NGS data analysis and contributed to the experiment design; DT analyzed the whole-exome sequencing data; FLC, FR, EL, AMO, MM, JL, JSR, CO, JD, CA, JNR and GMN provided patient samples and clinical information and SSM and CMG contributed to perform the NGS experiments; RB contributed to data analysis, interpretation of the results and critically reviewed the manuscript and MDC and JMHR conceived the study, designed the experiments and wrote the manuscript. All authors discussed the results and revised the manuscript.

Acknowledgments

The authors would like to thank to Sara González, Irene Rodríguez, Teresa Prieto, Mª Ángeles Ramos, Filomena Corral, Mª Almudena Martín, Ana Díaz, Ana Simón, María del Pozo, Isabel M Isidro, Vanesa Gutiérrez, Sandra Pujante and Mª Ángeles Hernández from the Cancer Research Center of Salamanca, Spain, for their technical support. We also thank to Teresa González and Alba Redondo-Guijo for providing patients samples and clinical information and we are deeply grateful to Miguel Quijada Álamo for his helpful suggestions and personal support.

Funding

This work was supported by grants from the Spanish Fondo de Investigaciones Sanitarias FIS PI18/01500, PI17/01741, Instituto de Salud Carlos III (ISCIII), Fondo de Investigación Sanitaria (Instituto de Salud Carlos III – Contratos Río Hortega (CM17/0017), European Regional Development Fund (ERDF), Una manera de hacer Europa, European Union Seventh Framework Programme [FP7/2007-2013] under Grant Agreement nº306242-NGS-PTL, SYNtherapy: Synthetic Lethality for Personalized Therapy-based Stratification in Acute Leukemia (ERAPERMED2018-275); ISCIII (AC18/00093), Proyectos de Investigación del SACYL, Gerencia Regional de Salud de Castilla y León: GRS1850/A18, GRS1653/A17, and Centro de Investigación Biomédica en Red de Cáncer (CIBERONC CB16/12/00233). MMI is supported by a predoctoral grant from the Junta de Castilla y León, and by the Fondo Social Europeo (JCYL-EDU/556/2019 PhD scholarship) and JMHS is supported by a research grant from Fundación Española de Hematología y Hemoterapia.

References

1. Cazzola M, Della Porta MG, Malcovati L. The genetic basis of myelodysplasia and its clinical relevance. Blood. 2013;122(25):4021-4034.
2. Lindsley RC, Ebert BL. Molecular pathophysiology of myelodysplastic syndromes. Annu Rev Pathol. 2013;8:21-47.
3. Tefferi A, Vardiman JW. Classification and diagnosis of myeloproliferative neoplasms: the 2008 World Health Organization criteria and point-of-care diagnostic algorithms. Leukemia. 2008;22(1):14-22.
4. Greenberg PL, Tuechler H, Schanz J, et al. Revised international prognostic scoring system for myelodysplastic syndromes. Blood. 2012;120(12):2454-2465.
5. Shukron O, Vainstein V, Kundgen A, Germing U, Agur Z. Analyzing transformation of myelodysplastic syndrome to secondary acute myeloid leukemia using a large patient database. Am J Hematol. 2012 87(9):853-860.
6. Montalban-Bravo G, Garcia-Manero G. Myelodysplastic syndromes: 2018 update on diagnosis, risk-stratification and management. Am J Hematol. 2018;93(1):129-147.
7. Steensma DP, Bennett JM. The myelodysplastic syndromes: diagnosis and treatment. Mayo Clin Proc. 2006;81(1):104-130.
8. Papaemmanuil E, Gerstung M, Malcovati L, et al. Clinical and biological implications of driver mutations in myelodysplastic syndromes. Blood. 2013;122(22):3616-3627.
9. Haferlach T, Nagata Y, Grossmann V, et al. Landscape of genetic lesions in 944 patients with myelodysplastic syndromes. Leukemia. 2014;28(2):241-247.
10. Abaigar M, Robledo C, Benito R, et al. Chromothripsis is a recurrent genomic abnormality in high-risk myelodysplastic syndromes. PLoS One. 2016; 11(10): e0164370.
11. Lindsley RC, Mar BG, Mazzola E, et al. Acute myeloid leukemia ontogeny is defined by distinct somatic mutations. Blood. 2015; 125(9):1367-1376.
12. da Silva-Coelho P, Kroeze LI, Yoshida K, et al. Clonal evolution in myelodysplastic syndromes. Nat Commun. 2017;8:15099.
13. Sperling AS, Gibson CJ, Ebert BL. The genetics of myelodysplastic syndrome: from clonal haematopoiesis to secondary leukaemia. Nat Rev Cancer. 2017;17(1):5-19.
14. Walter MJ, Shen D, Ding L, et al. Clonal architecture of secondary acute myeloid leukemia. N Engl J Med. 2012;366(12):1090-1098.
15. Makishima H, Yoshizato T, Yoshida K, et al. Dynamics of clonal evolution in myelodysplastic syndromes. Nat Genet. 2017; 49(2):204-212.
16. Kim T, Tyndel MS, Kim HJ, et al. The clonal origins of leukemic progression of myelodysplasia. Leukemia. 2017;31(9):1928-1935.
17. Stosch JM, Heumuller A, Niemoller C, et al. Gene mutations and clonal architecture in myelodysplastic syndromes and changes upon progression to acute myeloid leukaemia and under treatment. Br J Haematol. 2018;182(6):830-842.
18. Ibanez M, Carbonell-Caballero J, Such E, et al. The modular network structure of the mutational landscape of acute myeloid leukemia. PLoS One. 2018;13(10):e0202926.
19. Tamborero D, Rubio-Perez C, Deu-Pons J, et al. Cancer Genome Interpreter annotates the biological and clinical relevance of tumor alterations. Genome Med. 2018;10(1):25.
20. Reiter JG, Baretti M, Gerold JM, et al. An analysis of genetic heterogeneity in untreated cancers. Nat Rev Cancer. 2019;19(11):639-650.
21. Thota S, Viny AD, Makishima H, et al. Genetic alterations of the cohesin complex genes in myeloid malignancies. Blood. 2014;124(11):1790-1798.
22. Viny AD, Levine RL. Cohesin mutations in myeloid malignancies made simple. Curr Opin Hematol. 2018;25(2):61-66.
23. Pellagatti A, Roy S, Di Genua C, et al. Targeted resequencing analysis of 31 genes commonly mutated in myeloid disorders in serial samples from myelodysplastic syndrome patients showing disease progression. Leukemia. 2016;30(1):247-250.
24. Takahashi K, Jabbour E, Wang X, et al. Dynamic acquisition of FLT3 or RAS alterations drive a subset of patients with lower risk MDS to secondary AML. Leukemia. 2013;27(10):2081-2083.
25. Meggendorfer M, de Albuquerque A, Nadarajah N, et al. Karyotype evolution and acquisition of FLT3 or RAS pathway alterations drive progression of myelodysplastic syndrome to acute myeloid leukemia. Haematologica. 2015;100(12):e487-490.
26. Badar T, Patel KP, Thompson PA, et al. Detectable FLT3-ITD or RAS mutation at the time of transformation from MDS to AML predicts for very poor outcomes. Leuk Res. 2015;39(12):1367-1374.
27. Xu F, Han R, Zhang J, et al. The Role of FLT3-ITD Mutation on de novo MDS in Chinese population. Clin Lymphoma Myeloma Leuk. 2019;19(2):e107-e115.
28. Walter MJ, Shen D, Shao J, et al. Clonal diversity of recurrently mutated genes in myelodysplastic syndromes. Leukemia. 2013;27(6):1275-1282.
29. Miller CA, McMichael J, Dang HX, et al. Visualizing tumor evolution with the fishplot package for R. BMC Genomics. 2016; 17(1):880.
30. Mazumdar C, Shen Y, Xavy S, et al. Leukemia-associated cohesin mutants dominantly enforce stem cell programs and impair human hematopoietic Progenitor differentiation. Cell Stem Cell. 2015; 17(6):675-688.
31. Mondal G, Stevers M, Goode B, Ashworth A, Solomon DA. A requirement for STAG2 in

replication fork progression creates a targetable synthetic lethality in cohesin-mutant cancers. Nat Commun. 2019;10(1):1686.
32. Meisenberg C, Pinder SI, Hopkins SR, et al. repression of transcription at DNA breaks requires cohesin throughout interphase and prevents genome instability. Mol Cell. 2019; 73(2):212-223.e7.
33. Kuendgen A, Muller-Thomas C, Lauseker M, et al. Efficacy of azacitidine is independent of molecular and clinical characteristics - an analysis of 128 patients with myelodysplastic syndromes or acute myeloid leukemia and a review of the literature. Oncotarget. 2018; 9(45):27882-27894.
34. Polgarova K, Vargova K, Kulvait V, et al. Somatic mutation dynamics in MDS patients treated with azacitidine indicate clonal selection in patients-responders. Oncotarget. 2017;8(67):111966-111978.
35. Tobiasson M, McLornan DP, Karimi M, et al. Mutations in histone modulators are associated with prolonged survival during azacitidine therapy. Oncotarget. 2016;7(16):22103-22115.
36. Cabezon M, Bargay J, Xicoy B, et al. Impact of mutational studies on the diagnosis and the outcome of high-risk myelodysplastic syndromes and secondary acute myeloid leukemia patients treated with 5-azacytidine. Oncotarget. 2018;9(27):19342-19355.
37. Dohner H, Dolnik A, Tang L, et al. Cytogenetics and gene mutations influence survival in older patients with acute myeloid leukemia treated with azacitidine or conventional care. Leukemia. 2018; 32(12):2546-2557.

Ferrata Storti Foundation

Haematologica 2021
Volume 106(8):2224-2232

Identification of the atypically modified autoantigen Ars2 as the target of B-cell receptors from activated B-cell-type diffuse large B-cell lymphoma

Lorenz Thurner,[1] Sylvia Hartmann,[2] Moritz Bewarder,[1] Natalie Fadle,[1] Evi Regitz,[1] Claudia Schormann,[1] Natalia Quiroga,[1] Maria Kemele,[1] Wolfram Klapper,[3] Andreas Rosenwald,[4] Lorenz Trümper,[5] Rainer Maria Bohle,[6] Anna Nimmesgern,[7] Christina Körbel,[8] Matthias W. Laschke,[8] Michael D. Menger,[8] Stefan Barth,[9] Boris Kubuschok,[10] Anja Mottok,[11] Dominic Kaddu-Mulindwa,[1] Martin-Leo Hansmann,[2] Viola Pöschel,[1] Gerhard Held,[12] Niels Murawski,[1] Stephan Stilgenbauer,[1] Frank Neumann,[1] Klaus-Dieter Preuss[1] and Michael Pfreundschuh[1†]

[1]Saarland University Medical School, José Carreras Center for Immuno- and Gene Therapy and Internal Medicine I, Homburg/Saar, Germany; [2]Dr. Senckenberg Institute of Pathology, Goethe University Hospital of Frankfurt am Main, Frankfurt am Main, Germany; [3]Institute of Pathology, University of Kiel, Kiel, Germany; [4]Institute of Pathology, University of Würzburg and CCC Mainfranken, Würzburg, Germany; [5]Department of Hematology and Medical Oncology, University Hospital Göttingen, Göttingen, Germany; [6]Saarland University Medical School, Institute of Pathology, Homburg/Saar, Germany; [7]Institute of Medical Microbiology and Hygiene, University of Saarland, Homburg, Germany; [8]Institute for Clinical & Experimental Surgery, University of Saarland, Homburg/Saar, Germany; [9]Institute for Infectious disease & Molecular Medicine, University of Cape Town, Cape Town, South Africa; [10]Department of Internal Medicine II, Augsburg University Medical Center, Augsburg, Germany; [11]Institute of Human Genetics, Ulm University and Ulm University Medical Center, Ulm, Germany and [12]Department of Hematology/Oncology, Westpfalzklinikum, Kaiserslautern, Germany

[†]*Deceased.*

ABSTRACT

It has been suggested that stimulation of B-cell receptors (BCR) by specific antigens plays a pathogenic role in diffuse large B-cell lymphoma (DLBCL). Here, it was the aim to screen for specific reactivities of DLBCL-BCR in the spectrum of autoantigens and antigens of infectious origin. Arsenite resistance protein 2 (Ars2) was identified as the BCR target of three of five activated B-cell type DLBCL cell lines and two of 11 primary DLBCL cases. Compared to controls, Ars2 was hypophosphorylated exclusively in cases and cell lines with Ars2-specific BCR. In a validation cohort, hypophosphorylated Ars2 was found in eight of 31 activated B-cell type DLBCL, but in only one of 20 germinal center B-cell like type DLBCL. Incubation with Ars2 induced BCR-pathway activation and increased proliferation, while an Ars2/ETA' toxin conjugate induced killing of cell lines with Ars2-reactive BCR. Ars2 appears to play a role in a subgroup of activated B-cell-type DLBCL. Moreover, transformed DLBCL lines with Ars2-reactive BCR still showed growth advantage after incubation with Ars2. These results provide knowledge about the pathogenic role of a specific antigen stimulating the BCR pathway in DLCBL.

Correspondence:

LORENZ THURNER
lorenz.thurner@uks.eu

Received: October 28, 2019.

Accepted: July 9, 2020.

Pre-published: July 16, 2020.

https://doi.org/10.3324/haematol.2019.241653

Introduction

Diffuse large B-cell lymphoma (DLBCL) is the most common aggressive B-cell non-Hodgkin lymphoma. According to the World Health Organization (WHO) classification, DLBCL can be classified based on gene expression profiling (GEP) into an activated B-cell (ABC)-like type, a germinal center B-cell (GCB)-like type and primary mediastinal B-cell lymphoma.[1,2] In contrast to relatively well-studied genetic or epigenetic pathway alterations, little is known about specific and complementary external

stimuli of different subgroups of DLBCL.[3,4] In particular, DLBCL of the ABC-type or the recently specified MCD-type or Cluster 5 harbor recurrent mutations in *MYD88* and *CD79B* genes with dependency on constitutive BCR signaling.[5-8] For primary central nervous system lymphoma, which represents a specific extranodal subtype of DLCBL with molecular similarities to MCD type or C5 with frequent mutations in MYD88 and CD79,[9,10] SAMD14/neurabin-I were recently identified as antigens of BCR, and were hyper-N-glycosylated specifically in patients with SAMD14/neurabin-I-reactive BCR.[11] In systemic DLBCL, a *cis* and *trans* stimulation of the BCR by a so far uncharacterized autoantigen was reported for the HBL1 line. Moreover, an anti-idiotype reactivity of complementarity determining region 3 of the BCR of the TMD8 line against an epitope within its own FR2 ($V^{37}R^{38}$) was described, and for U2932 and OCI-LY10 lines BCR reactivity against apoptotic cell debris was reported.[8] This prompted us to screen for and characterize possible target antigens of BCR of systemic DLBCL using expression cloning of primary cryopreserved specimens and DLBCL lines and subsequent protein array screening.[12-14]

Methods

The study was approved by the local ethics committee (Ärztekammer des Saarlandes 12/13). For expression cloning of DLBCL-BCR, patients' snap-frozen specimens were obtained from the Dr. Senckenberg Institute of Pathology (Frankfurt am Main, Germany). Sera of a second cohort of patients with DLBCL were obtained from the DSHNHL RICOVER-60 trial.

DLBCL cryospecimens, of a third cohort of patients, of which the cell-of-origin had been determined by GEP, were obtained from the Institutes of Pathology of Würzburg and Kiel Universities.

B-cell receptor screening for autoantigens

BCR from nine DLBCL cell lines were prepared by digestion with papain. Moreover, expression cloning of recombinant BCR derived from primary DLBCL cryospecimens was performed, as described in the *Online Supplementary Material*. These DLBCL line-derived BCR and the pooled recombinantly expressed BCR (each at a concentration of 10 μg/mL) were screened on protein macroarrays containing clones of UniPEx 1 and 2 cDNA expression libraries (Bioscience, Dublin, Ireland), as previously described.[13,14] To search for further antigens, all recombinant DLBCL-derived antigen-binding fragments (Fab) without reactivity against arsenite resistance protein 2 (Ars2) were screened against variously post-translationally modified UniPEx 1 and 2 protein macroarrays, including sumoylation, ubiquitination, citrullination, and acetylation. Protein macroarrays were sumoylated as described elsewhere[15] and ubiquitination was performed with synchronized HeLa cell extracts.[16] The screening for antigens of infectious origin is described in the *Online Supplementary Material*.

Expression of target antigens and immunotoxins

The expression clone of Ars2 and subsequently the epitope-containing region consisting of amino acids 342-375 of Ars2 were recombinantly expressed with a C-terminal FLAG tag by a pSFI vector in HEK293 cells. Additionally, C-terminally FLAG-tagged full-length Ars2 was transfected by electroporation into U2932 and TMD8 via a pRTS vector.[17] C-terminally FLAG-tagged FamH83 and JmjD4 were recombinantly expressed in HEK293 cells. Site-directed mutagenesis of Ars2 and secondary modification of antigens is described in the *Online Supplementary Material*.

Immunotoxins with monomethyl auristatin E (MMAE) are effective *in vivo* and established in the clinics, but the synthesis of toxin conjugates with MMAE requires enzyme-cleavable dipeptide linkers and is therefore challenging for academic laboratories.[18,19] Hence, a truncated form of *Pseudomonas aeuroginosa* exotoxin A (ETA') was used, as the ETA' conjugate can be recombinantly expressed directly. Recombinantly expressed immunotoxins, consisting of Ars2 amino acids 342-375 conjugated to ETA' were either obtained from the Fraunhofer Institute of Experimental Medicine and Immunotherapy (Aachen, Germany) or recombinantly expressed in our laboratory in *E. coli* BL21 and purified by the His-Tag, as described by Nachreiner *et al.*[20]

Enzyme-linked immunosorbent assay (ELISA) for B-cell receptor and serum reactivity against target antigens and competition ELISA with apoptotic debris

Ars2, ubiquitinated FamH83, and sumoylated JmjD4 were confirmed as BCR antigens by ELISA, as previously described.[13] ELISA and competition assays with apoptotic debris are described in detail in the *Online Supplementary Material*.

Western blot and isoelectric focusing

Lysates of DLBCL lines or of whole blood from patients were loaded and separated by 10% sodium dodecylsulfate polyacrylamide gel electrophoresis and transferred to a polyvinylidene fluoride membrane using a transblot semidry transfer cell (Bio Rad). After blocking overnight at 4°C in phosphate-buffered saline/10% nonfat dry milk, a recombinant Ars2-reactive His-tagged Fab was incubated at a concentration of 2 μg/mL for 1 h at room temperature, followed by incubation for 1 h at room temperature with murine anti-his antibody at a ratio of 1:2,000 (Qiagen), with horseradish peroxidase-labeled anti-mouse IgG antibody (Bio Rad). Chemiluminescence reagent (New England BioLabs) was used for immunoblot detection. Isoelectric focusing was performed as previously described. Proliferation, BCR pathway activation assays, cytotoxicity and apoptosis assays are described in the *Online Supplementary Material*.

Results

Recombinant BCR in the form of Fab were successfully synthesized from 11 DLBCL cases. Moreover, Fab of "natural" BCR were obtained by papain digestion from nine DLBCL cell lines. From three of these cell lines, recombinant Fab were generated (*Online Supplementary Table S1*).

Screening of protein macroarrays and a library of infective agents

The screening of DLBCL Fab identified an expression clone of Ars2 transcript variant 2 (RZPDp828K0526 from Unipex 2, UnigeneID: Hs.111801) spanning from amino acids 253 to 416 as the candidate antigenic target. The screening of the Fab of DLBCL cases and cell lines on post-translationally modified protein macroarrays revealed sumoylated JmJD4 (RZPDp9027E0216D from Unipex 1; UnigeneID: Hs.555974) and ubiquitinylated FamH83 (RZPDp828G0328 from Unipex 2; UnigeneID: Hs.676336) as candidate antigens. The screening against bacterial lysates of 11 bacterial strains did not reveal any specific reactivity. Screening of an Infectious Disease Epitope Microarray (PEPperCHIP® Heidelberg, Germany) consisting of 3,760 database-derived B-cell epitopes associated with 196 pathogens, including various bacterial, fungal, parasitic,

and viral pathogens, revealed no significant binding of the pooled DLBCL-BCR.

Confirmation of Ars2, sumoylated JmjD4, and ubiquitinated FamH3 as targets of diffuse large B-cell lymphoma B-cell receptors and determination of the B-cell receptor-binding epitope

ELISA with recombinant Ars2 (UnigeneID: Hs.111801) expressed with a C-terminal FLAG-tag in HEK293 confirmed Ars2 as the BCR target antigen from three of five (60%) ABC-derived cell lines (OCI-Ly3, OCI-Ly10, and U2932; but not HBL1 and TMD8) and none of four GCB-DLBCL cell lines (Figure 1A). Recombinant BCR from two of 11 DLBCL cases (with unknown cell of origin), but none of nine mantle cell lymphomas and none of 11 primary central nervous system lymphomas were reactive with Ars2 (Figure 1B). Of the two Ars2-reactive DLBCL, one was a non-GCB type and one was unclassified according to immunohistochemistry using the Hans classifier.[21] ELISA with fragments of different lengths of Ars2 as the coat identified a region spanning amino acids 350 to 416 as the BCR-binding epitope (Figure 1C), and all

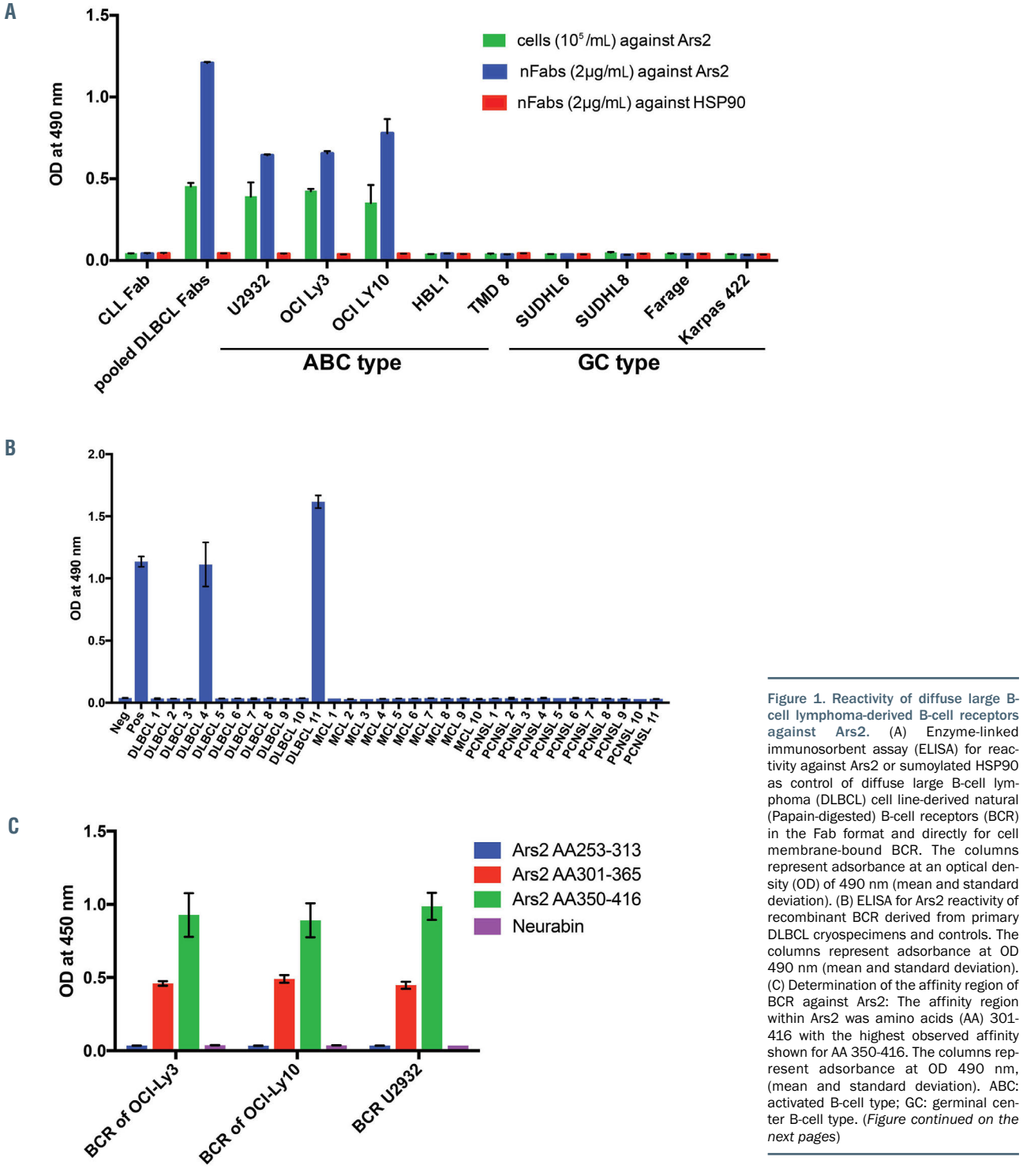

Figure 1. Reactivity of diffuse large B-cell lymphoma-derived B-cell receptors against Ars2. (A) Enzyme-linked immunosorbent assay (ELISA) for reactivity against Ars2 or sumoylated HSP90 as control of diffuse large B-cell lymphoma (DLBCL) cell line-derived natural (Papain-digested) B-cell receptors (BCR) in the Fab format and directly for cell membrane-bound BCR. The columns represent adsorbance at an optical density (OD) of 490 nm (mean and standard deviation). (B) ELISA for Ars2 reactivity of recombinant BCR derived from primary DLBCL cryospecimens and controls. The columns represent adsorbance at OD 490 nm (mean and standard deviation). (C) Determination of the affinity region of BCR against Ars2: The affinity region within Ars2 was amino acids (AA) 301-416 with the highest observed affinity shown for AA 350-416. The columns represent adsorbance at OD 490 nm, (mean and standard deviation). ABC: activated B-cell type; GC: germinal center B-cell type. (*Figure continued on the next pages*)

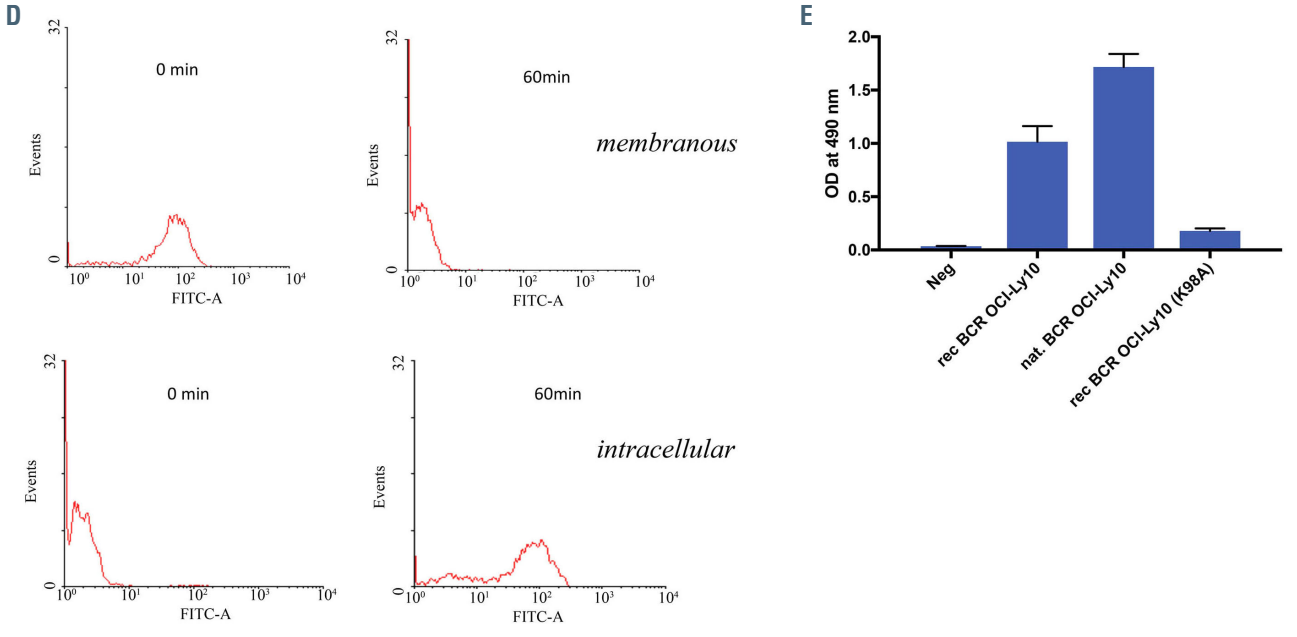

Figure 1. Continued from previous page. (D) Binding of Ars2 and internalization into U2932 cells. At time 0 (left) Ars2 (a fragment of 253 to 416 amino acids) bound to the cell surface of U2932 cells (above) and was not detected intracellularly (below). After 60 min incubation at 37°C (right) and washing, Ars2 was no longer detected on the cell surface (above), but was found intracellularly (below). Non-specific binding was determined by incubation with antibodies alone. (E) ELISA for reactivity against Ars2 of the BCR of OCI-Ly10 wt and K98A. Recombinant and papain-digested (natural) Fab of OCI-Ly10 bound to Ars2. K98A mutagenesis of recombinant OCI-Ly10 BCR resulted in the loss of reactivity of the recombinant BCR against Ars2. K98A had previously been described for OCI-Ly10 as being responsible for loss of BCR autoreactivity against apoptotic debris. The columns represent adsorbance at OD 490 nm (mean and standard deviation).

Ars2-specific BCR derived from cell lines and cryospecimens bound to this epitope. ELISA with recombinant sumoylated JmjD4 or ubiquitinylated FamH83 expressed with a C-terminal FLAG-tag in HEK293 confirmed each as target antigens of one DLBCL-derived recombinant Fab and ubiquitinated FamH83 in addition as a target of a recombinant mantle-cell lymphoma–derived Fab (*Online Supplementary Figures S1* and *S2*). Fab did not bind to non-modified JmjD4 and FamH83. Binding of Ars2 to membrane BCR was demonstrated by flow cytometry of DLBCL cell lines with Ars2-reactive BCR, but not for the TMD8 line without Ars2-reactive BCR. Internalization of C-terminally FLAG-tagged Ars2 into U2932 cells was observed after 60 min (Figure 1D). For OCI-Ly10, mutagenesis of K98A of the BCR heavy chain gene had been reported to result in loss of autoreactivity.[8] OCI-Ly10 K98A resulted in loss of affinity against Ars2 (Figure 1E).

Characterization of Ars2 in diffuse large B-cell lymphoma with Ars2-specific B-cell receptors

No obvious differences in molecular weight of Ars2 from DLBCL cases with Ars2-reactive and Ars2-non-reactive BCR and controls were observed in western blots; similarly, Sanger sequencing revealed identical DNA sequences, excluding mutations in the coding sequence as an explanation for the immunogenicity of Ars2. However, isoelectric focusing of cell lines (Figure 2A) and DLBCL cases (Figure 2B) with an Ars2-reactive BCR revealed a less negatively charged Ars2 isoform. Dephosphorylation with alkaline phosphatase treatment led to a stronger reduction of the negative charges of Ars2 from DBLCL cases and cell lines without Ars2-specific BCR than in cases with Ars2-reactive BCR and resulted in the disappearance of the differences in electric charge between both isoforms of Ars2 (Figure 2C), demonstrating that the different isoelectric focusing pattern of Ars2 was due to hypophosphorylation in cases with Ars2-specific BCR. The hypophosphorylated Ars2 isoform was detected in all of the three DLBCL cell lines with Ars2-reactive BCR (i.e., OCI-Ly3, OCI-Ly10, and U2932), but in none of six DLBCL lines without Ars2-reactive BCR. This association in the nine analyzed DLBCL cell lines between BCR reactivity against Ars2 and the presence of the hypophosphorylated isoform of Ars2 was statistically significant (Fisher exact *t*-test: two-tailed P=0.0119). Regarding the 11 DLBCL cases with recombinantly expressed Fab (*Online Supplementary Table S1*) derived from cryospecimens, only the two cases with Ars2-reactive Fab (#3 and #11) showed hypophosphorylation of Ars2. In this cohort of 11 cases of cryospecimens and recombinantly expressed Fab, the association between Ars2 reactivity and presence of hypophosphorylated Ars2 isoform was also statistically significant (Fisher exact *t*-test: two-tailed P=0.0182). Looking at the association between BCR reactivity of DLBCL cells and the presence of hypophosphorylated Ars2 isoform overall, considering data from both cell lines and cases with cryospecimen-derived recombinant Fab, the association was statistically highly significant (Fisher exact *t*-test: two-tailed P<0.0001).

Hypophosphorylated Ars2 was detected in the biopsies of eight of 31 (26%) ABC-type DLBCL cases characterized by GEP, but in only one of 20 (5%) GCB-type DLBCL and in the peripheral blood from one in 100 healthy controls.

The hypophosphorylated sites were identified as serine 328 and serine 341 by site-directed point mutagenesis of various predicted sites in Ars2 transfected with a C-termi-

nal FLAG tag in OCI-Ly10, OCI-Ly3 and, as a control, HBL1 (Figure 2D and *Online Supplementary Figure S4*).

Frequency, titers, and IgG subclasses of Ars2 serum antibodies

Ars2 antibodies were detected by ELISA in the sera of four of 98 patients with DLBCL, with titers ranging from 1:800 to 1:1600, and in one of 400 healthy controls. All four patients with Ars2 antibodies in their sera (#22, #27, #41, #73) were carriers of hypophosphorylated Ars2 in the cells of their peripheral blood (Figure 2B), but this isoform was not detected in the peripheral blood of any of the 94 other patients, resulting in a statistically significant relationship between serum Ars2-autoantibodies and the presence of the hypophosphorylated Ars2 in peripheral blood (Fisher exact *t*-test: two-tailed $P<0.0001$).

Effects of Ars2 on diffuse large B-cell lymphoma lines

Western blot analysis of BCR pathway activation after addition of recombinant Ars2 revealed a strong activation in the U2932 cell line with Ars2-reactive BCR, demonstrated by a strong upregulation of pTyr525/526 SYK, pTyr96 BLNK, pTyr759 PLCγ2, and pTyr223 BTK. Moreover, this BCR stimulation by Ars2 led to increases in MYC expression. However, regarding MYC two cases with Ars2-reactive BCR (#4 and #10) did not have MYC-overexpression, as determined by immunohistochemical analysis (*data not shown*). No BCR pathway activation was induced by the control antigen MAZ in the U2932 line or by addition of Ars2 to the HBL1 line (Figure 3A). Addition of recombinant Ars2 induced proliferation of U2932 and OCI-Ly3 cells, but not of DLBCL cell lines without Ars2-reactive BCR, such as TMD8, analyzed by the tetrazolium/formazan EZ4U assay (Figure 3B). This Ars2-induced growth stimulus could be reverted by addition of Ars2-neutralizing recombinant Fab derived from patient #4 (Figure 3C). Furthermore, flow cytometry analysis of U2932 cells showed a strong increase of cytoplasmic calcium levels after incubation with the Ars2 epitope, but not the control antigen (Figure 3D).

Cytotoxicity of the Ars2/ETA' conjugate

Addition of Ars2-ETA' resulted in inhibition of growth analyzed in proliferation assays. This inhibition could be reverted by preincubation of Ars2/ETA' toxin with the Ars2-reactive recombinant Fab derived from case #4 (Figure 4A). The Ars2-ETA' conjugate exerted a specific and dose-dependent toxicity against the Ars2-reactive

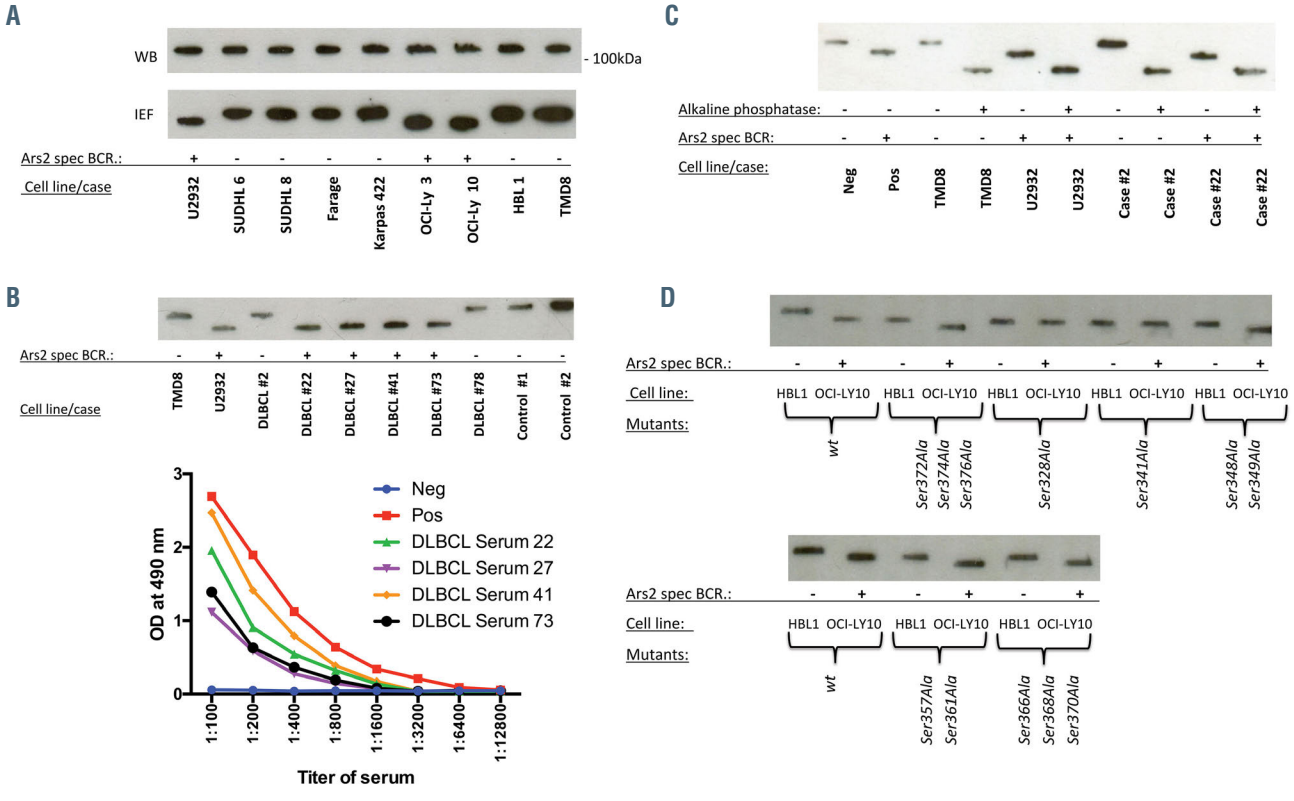

Figure 2. Ars2 is exclusively hypophosphorylated in patients with Ars2-reactivity of lymphoma B-cell receptors. (A) Western blot and isoelectric focusing (IEF) of Ars2 derived from diffuse large B-cell lymphoma (DLBCL) cell lines. Western blot of Ars2 in nine DLBCL cell lines revealed no difference in Ars2 between cell lines with and without Ars2-reactive B-cell receptors (BCR) (above). However, IEF of Ars2 in the DLBCL lines showed a less negative charge of Ars2 in OCI-Ly3, OCI-Ly10 and U2932. These three cell lines had exclusively Ars2-reactive BCR. (B) IEF of Ars2 of whole blood derived from DLBCL patients with Ars2-autoantibodies (#22, #27, #41, #73). The less negatively charged Ars2 isoform was also detected In the peripheral blood of these four patients. Ars2 autoantibody titers ranged between 1:800 and 1:1600 in these four patients. (C) Alkaline phosphatase treatment led to disappearance of differences in IEF of Ars2. A stronger reduction of negative charges of Ars2 by dephosphorylation was observed in cases/cell lines without Ars2-reactive BCR. (D) Identification of the hypophosphorylated sites by site-directed mutagenesis and transfection of C-terminally FLAG-tagged Ars2 into U2932 and HBL1. In contrast to wild-type Ars2, mutations in Ser372Ala, Ser374Ala, Ser376Ala, Ser348Ala, Ser349 Ala, Ser357Ala, Ser361Ala, Ser365Ala, Ser368Ala and Ser370Ala resulted in hypophosphorylated Ars2 isoforms in both HBL1 and U2932; however the Ars2 isoform of U2932 was still less negatively charged compared to that of HBL1. Only the mutants Ser328Ala and Ser341Ala resulted in the disappearance of this difference in electric charge, identifying both Ser328 and Ser341 as the sites of hypophosphorylation. Murine anti-FLAG-antibody was used as the primary antibody.

BCR-expressing cell lines, but had no observable effect on DLBCL lines lacking Ars2-reactive BCR (Figure 4B). No toxic effect was observed with the control toxin LRPAP1-ETA' against OCI-Ly3. Trypan blue staining after addition of 5 μg/mL Ars2-ETA' showed that 35%, 2% and 0% of OCI-Ly3 cells were alive after 24 h, 48 h and 72 h, respectively, contrasting with findings for the wild-type HBL1 cell line without BCR reactivity against Ars2 (97% viable cells at 24 h; 96% at 48 h; and 97% at 72 h) (Figure 4B). In accordance with this, an increase of apoptotic cells was detected after incubation with Ars2-ETA' in U2932 cells expressing Ars2-reactive BCR (Figure 4C), as demonstrated in the annexin V/propidium iodide assay.

Discussion

Beside the two relatively rare target antigens, ubiquitinated FamH83 and sumoylated JmJD4, in the present study, hypophosphorylated Ars2 was identified as a more frequent antigen of BCR from DLBCL lines and recombinant BCR from primary DLBCL cryospecimens. Ars2 is also known as serrate RNA effector molecule (SRRT). Its gene is located on chromosome 7q21 and the protein is a zinc finger protein consisting of 875 amino acids with a molecular weight of around 100 kDa. Ars2 was described as being involved in miRNA silencing by interacting with the nuclear cap binding complex,[22] and as being involved in the innate immune response against RNA viruses by

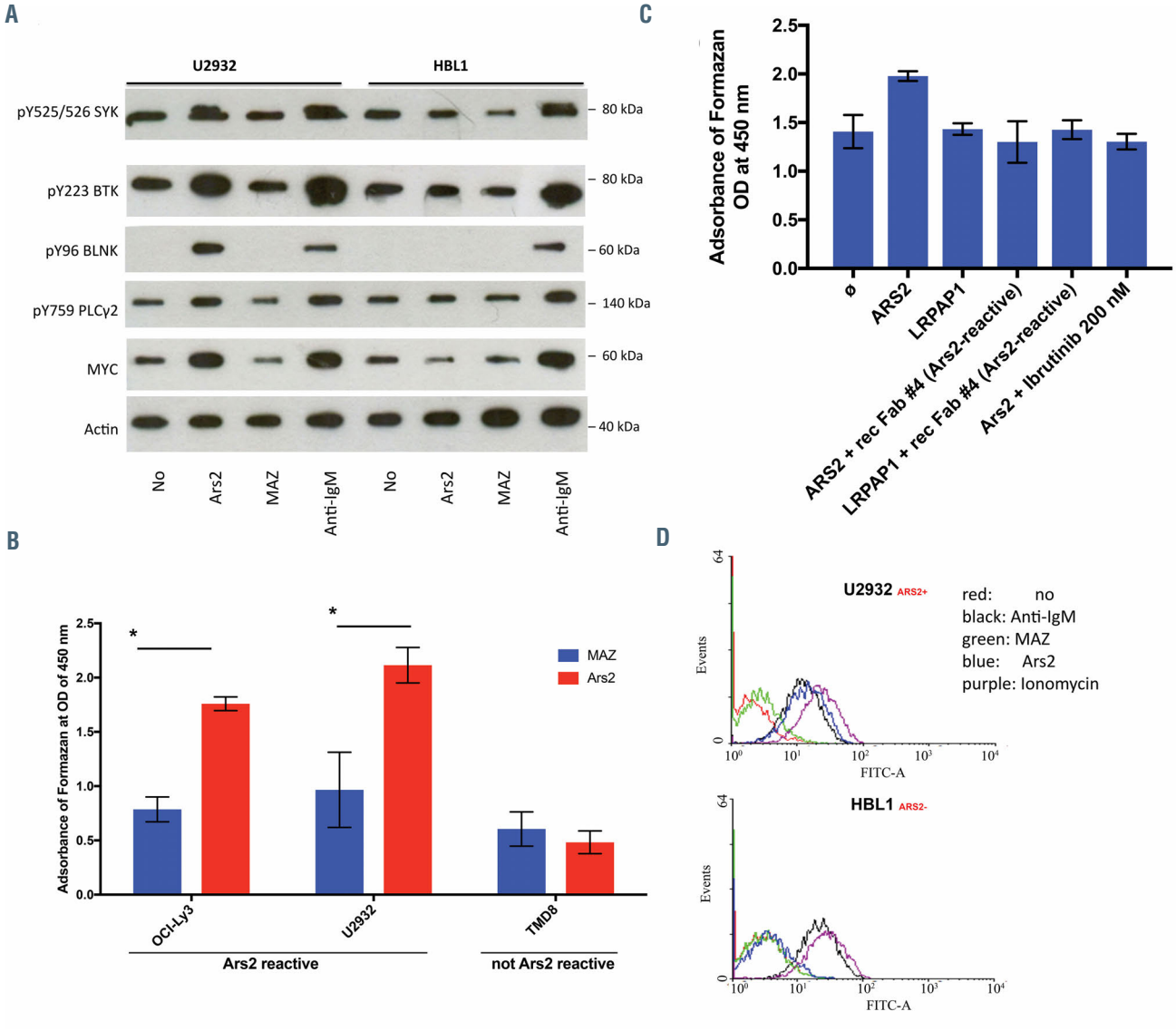

Figure 3. B-cell receptor pathway activation and induction of proliferation by Ars2. (A) B-cell receptor (BCR) pathway analysis by western blot in U2932 and HBL1 after addition of cognate/control antigens Ars2 or MAZ showed strong activation due to the addition of ARS2 to U2932 cells with upregulation of pTyr525/526 SYK, pTyr96 BLNK, pTyr759 PLCγ2 and pTyr223 BTK and higher expression of MYC. In contrast, no effect of ARS2 on the BCR pathway was observed in HBL1 cells. (B) Induction of proliferation by Ars2. Addition of Ars2 to OCI-Ly3 and U2932 lines resulted in a statistically significant (P<0.01: Student t-test) increase of proliferation, as determined by the EZ4U assay (columns represent formazan at an optical density [OD] of 450 nm), while addition of Ars2 had no effect on the TMD8 cell line. Columns and bars represent mean and standard deviation of three experiments. (C) Inhibition of Ars2-induced proliferation by neutralizing Ars2-reactive Fab. Addition of Ars2 together with Ars2-reactive (patient derived, case #4) recombinant Fab prevented induction of growth in U2932 cells. (D) Elevation of cytoplasmatic calcium levels by addition of Ars2. Flow cytometry analysis of cytoplasmic calcium levels using Fluo-4 dye showed an increase after addition of the cognate antigen ARS2 (blue) comparable to the effect of adding anti-IgM (black) to U2932 cells, but not after the addition of a control antigen MAZ (green). Addition of Ars2 to control the diffuse large B-cell lymphoma line HBL1 did not result in elevated calcium levels.

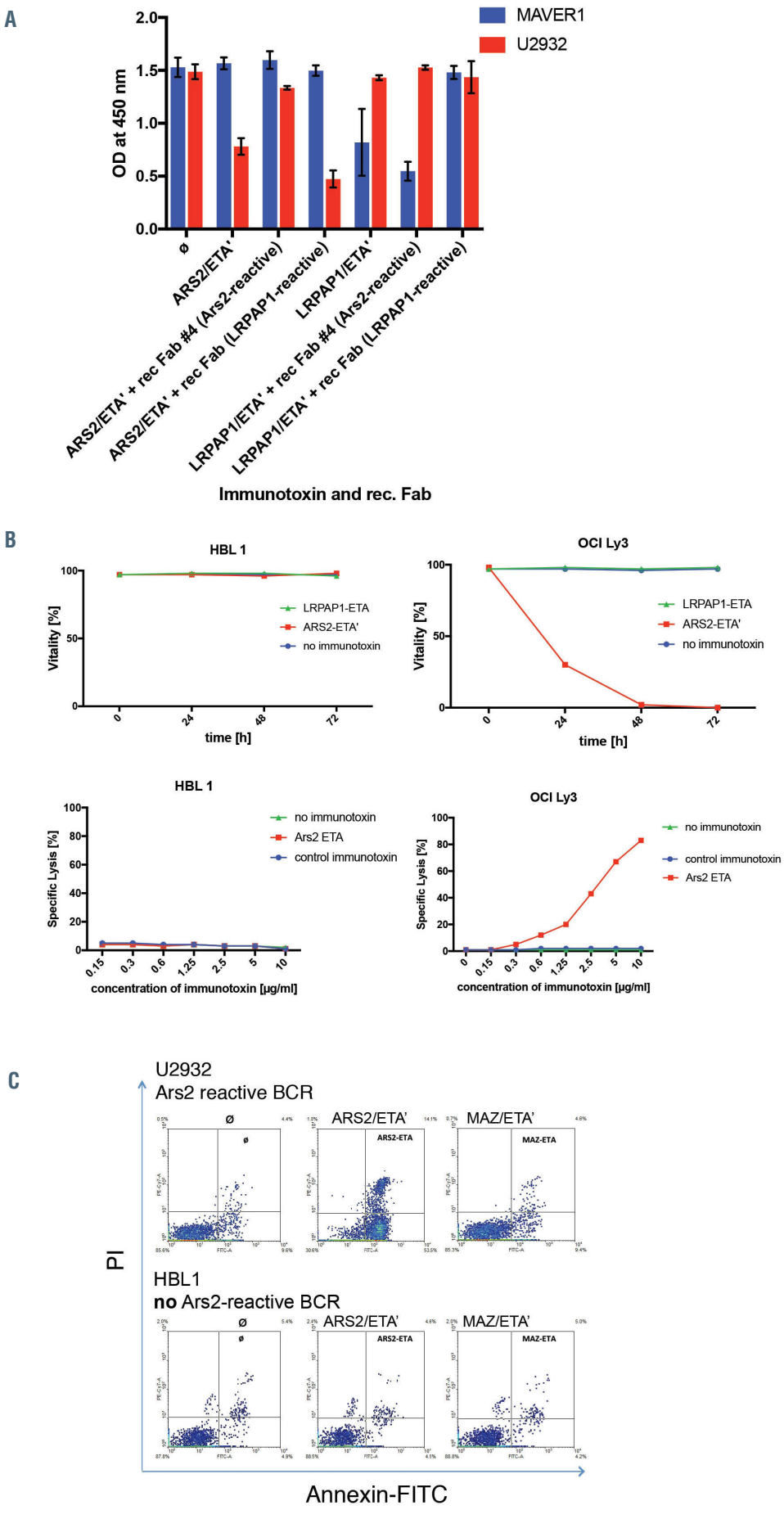

Figure 4. Targeting Ars2-reactive diffuse large B-cell lymphoma with Ars2-containing immunotoxins. (A) Growth inhibition by B-cell receptor (BCR)-antigen/immunotoxins. Growth of U2932 cells was inhibited by addition of Ars2/ETA', an immunotoxin of the epitope of the cognate antigen Ars2 fused to a truncated form of *Pseudomonas aeruginosa* exotoxin A. This growth inhibition could be prevented by co-incubation with neutralizing Ars2-reactive Fab but not by LRPAP1-reactive Fab. Columns (formazan formation detected at an optical density of 450 nm) represent cell proliferation (mean and standard deviation). (B) BCR-specific lysis of DLBCL cell lines by Ars2/ETA' immunotoxin. Above: cytotoxic effect after 24 h, 48 h and 72 h of incubation with 5 µg/mL of recombinant Ars2/ETA' or LRPAP1/ETA' immunotoxins. Cell viability of HBL-1 (left) and OCI-LY3 (right) cell lines determined by trypan blue staining. Below: Dose-dependent cytotoxic effect of Ars2/ETA' determined in a lactate dehydrogenase (LDH) release assay. Curves indicate percent specific lysis of the HBL1 line (left) or OCI Ly3 line (right) with and without Ars2-reactive BCR, after incubation with doses from 0 µg/mL to 10 µg/mL Ars2/ETA', LRPAP1/ETA' or phosphate-buffered saline. (C) Induction of apoptosis by addition of Ars2/ETA' immunotoxins. Flow cytometric characterization of apoptotic U2932 or HBL1 cells 24 h after addition of Ars2/ETA' or MAZ/ETA' by annexin-V/propidium iodide staining. U2932 cells have Ars2-reactive BCR resulting in a strong increase of early and late apoptotic cells after addition of Ars2/ETA'.

miRNA processing.[23] Ars2 expression was shown to be linked to proliferative states[24] and different roles were described in malignant disesases.[25,26]

All three target antigens of DLBCL-BCR identified in this study share the characteristic of being atypically post-translationally modified, which represents the most likely reason for their immunogenicity. For ubiquitinated FamH83 and sumoylated JmJD4, the lymphoma BCR were specific for the secondary modified isoforms. In contrast, Ars2-reactive BCR of DLBCL bound both the hypophosphorylated and the normally phosphorylated isoforms of Ars2. However, the hypophosphorylated isoform of Ars2 was only observed in cell lines or cryospecimens of DLBCL with BCR reactivity for Ars2 (P<0.0001). Similarly, regarding peripheral blood, the hypophosphorylated isoform of Ars2 was only observed in lysates of peripheral blood cells of patients seropositive for Ars2 autoantibodies (P<0.0001). These statistically significant associations between Ars2-reactivity and the presence of hypophosphorylated Ars2 indicate that this post-translational modification is involved in the immunogenicity.

Bringing this into the context of other B-cell neoplasias, in plasma cell dyscrasia SLP2-reactive paraprotein was also not specific for the differentially phosphorylated SLP2 isoform.[27] As for $CD4^+$ T-helper cells specific for hyperphosphorylated SLP2 in plasma cell dyscrasia,[28] one might speculate about a possible role of hypothetical $CD4^+$ T-helper cells specific for hypophosphorylated Ars2 epitopes, which might stimulate Ars2-reactive B cells, which by themselves do not differentiate between normally phosphorylated and hypophosphorylated Ars2. Generally, atypical post-translational modifications represent an accepted mechanism for the breakdown of self-tolerance, with numerous examples in clinical immunology, such as modified wheat gliadin in celiac disease,[29] N-terminally acetylated myelin basic protein in multiple sclerosis,[30] citrullinated fibrin/vimentin in rheumatoid arthritis,[31,32] phosphorylated SR proteins during stress-induced apoptosis in systemic lupus erythematosus,[33,34] immunogenic pSer81 progranulin isoform and progranulin autoantibodies,[35,36] phosphorylated enolase in pancreatic carcinoma,[37-39] and the involvement of atypically modified BCR target antigens in lymphomagenesis including hyperphosphorylated SLP2, ATG13, and sumoylated HSP90 in plasma cell dyscrasia and hyper-N-glycosylated SAMD14/neurabin-I in primary central nervous system lymphoma.[11,15,27,40,41]

Of interest, Ars2 hypophosphorylation and reactivity of DLBCL BCR against Ars2 was nearly exclusively detected in DLBCL of the ABC type. All the cell lines with anti-Ars2 reactivity were of this cell of origin, and in a validation cohort of DLBCL with cell of origin characterized by GEP, hypophosphorylated Ars2 was detected in eight of 31 cases (26%) of the ABC type of DLBCL, but in only one of 20 cases (5%) of GCB-type DLBCL. In a combined analysis of GEP-typed cryospecimens and analyzed cell lines, the hypophosphorylated Ars2 isoform was statistically significantly associated with ABC type (P=0.0188).

Considering possible functional effects of Ars2, we observed that its addition stimulated growth of DLBCL lines with Ars2-specific BCR (Figure 3), indicating that these lines still depend to some extent on BCR stimulation by their cognate antigen Ars2. Regarding the mutational background of these cell lines with Ars2-reactive BCR and expression of hypophosphorylated Ars2, OCI-Ly10 has mutated MYD88 (L265P)[42] and a truncating mutation of CD79A,[7,43] U2932 has a mutated NFκB-pathway by TAK1 mutation,[44] but wild-type CARD11, and wild-type MYD88,[7,45] and OCI-Ly3 has a mutated CARD11 and mutated MYD88 (L265P).[7,42] This demonstrates that, despite pathway-activating mutations, the proliferation of these cell lines might still benefit from an upstream BCR pathway stimulation by a cognate antigen.

From a therapeutic point of view, two hypothetical approaches arise from these data. Firstly, BCR antigens might be used as baits to target lymphoma cells in a specific way (i.e., targeting of a cell-bound antibody by an antigen), similarly to anti-idiotype antibodies or peptibodies,[46] with the advantage of not having to be selected and synthesized individually for each patient, since all Ars2-reactive DLBCL BCR bind the same epitope. Physiologically it is the major task of a surface immunoglobulin to bind its cognate antigen and then internalize it, enabling processing and antigen presentation via MHC class II molecules. Targeting Ars2-reactive BCR of DLBCL cell lines resulted in a specific and efficacious killing. Beside this, the Ars2 epitope could be used for bispecific constructs for T- or NK-cell engaging (e.g., CD3/Ars2 or CD16/Ars2),[47] or as an additional ectodomain for chimeric antigen receptor T cells.[48] Secondly, regarding the high relative risk of carriers of atypically hypophosphorylated Ars2, investigating ways of modulating this post-translational modification might be worthwhile in the future.

Disclosures

No conflicts of interest to disclose. MP died during the preparation of the manuscript. Saarland University has applied for a relevant patent.

Contributions

LTh, SH, KDP, BK and MP designed the study. SH and MLH performed microdissection of DLBCL cases and interpreted data. WK, AW YJK, RMB, BK, FvB, LTr, MZ, NM, DKM VP and GH were of great help in the acquisition of DLBCL samples and clinical data. NF performed the protein array, phosphorylation and proteomic experiments. ER did site-directed point mutagenesis of Ars2. MK and ER performed sequencing studies. LTh, MK, ER and TB performed seminested IgV gene PCR and BCR expression cloning. LTh, MB, MK, ER and NF performed expression of Ars2-immunotoxins. LTh and MP were responsible for data analysis, interpretation of results and writing the manuscript. This article is dedicated to the memory of MP, who died during its preparation.

Acknowledgments

We are grateful to the entire team of the José-Carreras-Center for Immuno- and Gene Therapy, the DSHNHL and GLA, the Department of Internal Medicine I of Saarland University Medical School for continuous logistic and intellectual support. We also thank Hans Drexler from DSMZ for constant support.

Funding

This work was supported by a grant from Wilhelm-Sander-Stiftung.

References

1. Rosenwald A, Staudt LM. Gene expression profiling of diffuse large B-cell lymphoma. Leuk Lymphoma. 2003;44(Suppl 3):S41-47.
2. Alizadeh AA, Eisen MB, Davis RE, et al. Distinct types of diffuse large B-cell lymphoma identified by gene expression profiling. Nature. 2000;403(6769):503-511.
3. Reddy A, Zhang J, Davis NS, et al. Genetic and functional drivers of diffuse large B cell lymphoma. Cell. 2017;5;171(2):481-494.
4. Lenz G, Wright G, Dave SS, et al. Stromal gene signatures in large-B-cell lymphomas. N Engl J Med. 2008;27;359(22):2313-2323.
5. Schmitz R, Wright GW, Huang DW, et al. Genetics and pathogenesis of diffuse large B-cell lymphoma. N Engl J Med. 2018;12;378(15):1396-1407.
6. Chapuy B, Stewart C, Dunford AJ, et al. Molecular subtypes of diffuse large B cell lymphoma are associated with distinct pathogenic mechanisms and outcomes. Nat Med. 2018;24(5):679-690.
7. Davis RE, Ngo VN, Lenz G, et al. Chronic active B-cell-receptor signalling in diffuse large B-cell lymphoma. Nature 2010;463 (7277):88-92.
8. Young RM, Wu T, Schmitz R, et al. Survival of human lymphoma cells requires B-cell receptor engagement by self-antigens. Proc Natl Acad Sci U S A. 2015;112(44):13447-13454.
9. Montesinos-Rongen M, Godlewska E, Brunn A, Wiestler OD, Siebert R, Deckert M. Activating L265P mutations of the MYD88 gene are common in primary central nervous system lymphoma. Acta Neuropathol. 2011;122(6):791-792.
10. Montesinos-Rongen M, Schafer E, Siebert R, Deckert M. Genes regulating the B cell receptor pathway are recurrently mutated in primary central nervous system lymphoma. Acta Neuropathol. 2012;124(6): 905-906.
11. Thurner L, Preuss K-D, Bewarder M, et al. Hyper N-glycosylated SAMD14 and neurabin-I as driver CNS autoantigens of PCNSL. Blood. 2018;132(26):2744-2753.
12. Cepok S, Zhou D, Srivastava R, et al. Identification of Epstein-Barr virus proteins as putative targets of the immune response in multiple sclerosis. J Clin Invest. 2005;115(5):1352-1360.
13. Preuss KD, Pfreundschuh M, Ahlgrimm M, et al. A frequent target of paraproteins in the sera of patients with multiple myeloma and MGUS. Int J Cancer. 2009;125(3):656-661.
14. Thurner L, Müller A, Cérutti M, et al. Wegener's granuloma harbors B lymphocytes with specificities against a proinflammatory transmembrane protein and a tetraspanin. J Autoimmun. 2011;36(1):87-90.
15. Preuss KD, Pfreundschuh M, Fadle N, Regitz E, Kubuschok B. Sumoylated HSP90 is a dominantly inherited plasma cell dyscrasias risk factor. J Clin Invest. 2015;125(1):316-323.
16. Merbl Y, Kirschner MW. Large-scale detection of ubiquitination substrates using cell extracts and protein microarrays. Proc Natl Acad Sci U S A. 2009;106(8):2543-2548.
17. Bornkamm GW, Berens C, Kuklik-Roos C, et al. Stringent doxycycline-dependent control of gene activities using an episomal one-vector system. Nucleic Acids Res. 2005;33(16):1-11.
18. Doronina SO, Toki BE, Torgov MY, et al. Development of potent monoclonal antibody auristatin conjugates for cancer therapy. Nat Biotech. 2003;21(7):778-784.
19. Oflazoglu E, Kissler KM, Sievers EL, Grewal IS, Gerber HP. Combination of the anti-CD30-auristatin-E antibody-drug conjugate (SGN-35) with chemotherapy improves antitumour activity in Hodgkin lymphoma. Br J Haematol. 2008;142(1):69-73.
20. Nachreiner T, Kampmeier F, Thepen T, Fischer R, Barth S, Stocker M. Depletion of autoreactive B-lymphocytes by a recombinant myelin oligodendrocyte glycoprotein-based immunotoxin. J Neuroimmunol. 2008;195(1-2):28-35.
21. Hans CP, Weisenburger DD, Greiner TC, et al. Confirmation of the molecular classification of diffuse large B-cell lymphoma by immunohistochemistry using a tissue microarray. Blood. 2004;103(1):275-282.
22. Gruber JJ, Olejniczak SH, Yong J, LaRocca G, Dreyfuss G, Thompson CB. Ars2 promotes proper replication-dependent histone mRNA 3' end formation. Mol Cell. 2012;45(1):87-98.
23. Sabin LR, Zhou R, Gruber JJ, et al. Ars2 regulates both miRNA- and siRNA- dependent silencing and suppresses RNA virus infection in Drosophila. Cell. 2009;138(2):340-351.
24. Gruber JJ, Zatechka DS, Sabin LR, et al. Ars2 links the nuclear cap-binding complex to RNA interference and cell proliferation. Cell. 2009;138(2):328-339.
25. He Q, Huang Y, Cai L, Zhang S, Zhang C. Expression and prognostic value of Ars2 in hepatocellular carcinoma. Int J Clin Oncol. 2014;19(5):880-888.
26. Cui L, Gao C, Zhang RD, et al. Low expressions of ARS2 and CASP8AP2 predict relapse and poor prognosis in pediatric acute lymphoblastic leukemia patients treated on China CCLG-ALL 2008 protocol. Leuk Res. 2015;39(2):115-123.
27. Grass S, Preuss KD, Pfreundschuh M. Autosomal-dominant inheritance of hyperphosphorylated paratarg-7. Lancet Oncol. 2010;11(1):12.
28. Neumann F, Pfreundschuh M, Preuss KD, et al. CD4(+) T cells in chronic autoantigenic stimulation in MGUS, multiple myeloma and Waldenstrom's macroglobulinemia. Int J Cancer. 2015;137(5):1076-1084.
29. Arentz-Hansen H, Korner R, Molberg O, et al. The intestinal T cell response to alpha-gliadin in adult celiac disease is focused on a single deamidated glutamine targeted by tissue transglutaminase. J Exp Med. 2000; 191(4):603-612.
30. Zamvil SS, Mitchell DJ, Moore AC, Kitamura K, Steinman L, Rothbard JB. T-cell epitope of the autoantigen myelin basic protein that induces encephalomyelitis. Nature. 1986;324(6094):258-260.
31. Schellekens GA, de Jong BA, van den Hoogen FH, van de Putte LB, van Venrooij WJ. Citrulline is an essential constituent of antigenic determinants recognized by rheumatoid arthritis-specific autoantibodies. J Clin Invest. 1998;101(1):273-281.
32. van Venrooij WJ, Pruijn GJ. Citrullination: a small change for a protein with great consequences for rheumatoid arthritis. Arthritis Res. 2000;2(4):249-251.
33. Neugebauer KM, Merrill JT, Wener MH, Lahita RG, Roth MB. SR proteins are autoantigens in patients with systemic lupus erythematosus. Importance of phosphoepitopes. Arthritis Rheum. 2000;43(8): 1768-1778.
34. Utz PJ, Hottelet M, Schur PH, Anderson P. Proteins phosphorylated during stress-induced apoptosis are common targets for autoantibody production in patients with systemic lupus erythematosus. J Exp Med. 1997;185(5):843-854.
35. Thurner L, Preuss KD, Fadle N, et al. Progranulin antibodies in autoimmune diseases. J Autoimmun. 2013;42:29-38.
36. Thurner L, Fadle N, Regitz E, et al. The molecular basis for development of proinflammatory autoantibodies to progranulin. J Autoimmun. 2015;61:17-28.
37. Cappello P, Tomaino B, Chiarle R, et al. An integrated humoral and cellular response is elicited in pancreatic cancer by α-enolase, a novel pancreatic ductal adenocarcinoma-associated antigen. Int J Cancer 2009;125 (3):639–648.
38. Tomaino B, Cappello P, Capello M, et al. Circulating autoantibodies to phosphorylated α-enolase are a hallmark of pancreatic cancer. J Proteome Res. 2011;10(1):105-112.
39. Zhou W, Capello M, Fredolini C, et al. Mass spectrometry analysis of the post-translational modifications of alpha-enolase from pancreatic ductal adenocarcinoma cells. J Proteome Res. 2010;9(6):2929-2936.
40. Grass S, Preuss KD, Wikowicz A, et al. Hyperphosphorylated paratarg-7: a new molecularly defined risk factor for monoclonal gammopathy of undetermined significance of the IgM type and Waldenstrom macroglobulinemia. Blood. 2011;117(10): 2918-2923.
41. Preuss KD, Pfreundschuh M, Fadle N, et al. Hyperphosphorylation of autoantigenic targets of paraproteins is due to inactivation of PP2A. Blood. 2011;118(12):3340-3346.
42. Ngo VN, Young RM, Schmitz R, et al. Oncogenically active MYD88 mutations in human lymphoma. Nature. 2011;470 (7332):115-121.
43. Gordon MS, Kanegai CM, Doerr JR, Wall R. Somatic hypermutation of the B cell receptor genes B29 (Igβ, CD79b) and mb1 (Igα, CD79a). Proc Natl Acad Sci U S A. 2003;100(7):4126-4131.
44. Compagno M, Lim WK, Grunn A, et al. Mutations of multiple genes cause deregulation of NF-kappaB in diffuse large B-cell lymphoma. Nature. 2009;459(7247):717-721.
45. Mondello P, Brea EJ, De Stanchina E, et al. Panobinostat acts synergistically with ibrutinib in diffuse large B cell lymphoma cells with MyD88 L265 mutations. JCI Insight. 2017;2(6):e90196.
46. Torchia J, Weiskopf K, Levy R. Targeting lymphoma with precision using semisynthetic anti-idiotype peptibodies. Proc Natl Acad Sci U S A. 2016;113(19):5376-5381.
47. Bewarder M, Preuss KD, Fadle N, Regitz E, Thurner L, Pfreundschuh M. CD3/Bars: a novel bispecific format for the treatment of B-cell lymphomas. Blood. 2016;128(22): 3516.
48. Kochenderfer JN, Dudley ME, Kassim SH, et al. Chemotherapy-refractory diffuse large B-cell lymphoma and indolent B-cell malignancies can be effectively treated with autologous T cells expressing an anti-CD19 chimeric antigen receptor. J Clin Oncol. 2015;33(6):540-549.

ARTICLE

Genetic variation near *CXCL12* is associated with susceptibility to HIV-related non-Hodgkin lymphoma

Christian W. Thorball,[1,2] Tiphaine Oudot-Mellakh,[3] Nava Ehsan,[4,5] Christian Hammer,[6,7] Federico A. Santoni,[8] Jonathan Niay,[3] Dominique Costagliola,[9] Cécile Goujard,[10,11] Laurence Meyer,[12] Sophia S. Wang,[13] Shehnaz K. Hussain,[14] Ioannis Theodorou,[3] Matthias Cavassini,[15] Andri Rauch,[16] Manuel Battegay,[17] Matthias Hoffmann,[18] Patrick Schmid,[19] Enos Bernasconi,[20] Huldrych F. Günthard,[21,22] Pejman Mohammadi,[4,5] Paul J. McLaren,[23,24] Charles S. Rabkin,[25] Caroline Besson[25-27] and Jacques Fellay[1,2,28]

[1]School of Life Sciences, École Polytechnique Fédérale de Lausanne, Lausanne, Switzerland; [2]Swiss Institute of Bioinformatics, Lausanne, Switzerland; [3]Centre de Génétique Moléculaire et Chromosomique, GH La Pitié Salpêtrière, Paris, France; [4]The Scripps Research Translational Institute, La Jolla, CA, USA; [5]Department of Integrative Structural and Computational Biology, The Scripps Research Institute, La Jolla, CA, USA; [6]Department of Cancer Immunology, Genentech, South San Francisco, CA, USA; [7]Department of Human Genetics, Genentech, South San Francisco, CA, USA; [8]Service of Endocrinology, Diabetology and Metabolism, Lausanne University Hospital, Lausanne, Switzerland; [9]Sorbonne Universités, INSERM, UPMC Université Paris 06, Institut Pierre Louis d'Épidémiologie et de Santé Publique (IPLESP UMRS 1136), Paris, France; [10]INSERM, CESP, U1018, Paris-Sud University, Le Kremlin-Bicêtre, France; [11]Department of Internal Medicine, Bicêtre Hospital, AP-HP, Le Kremlin-Bicêtre, France; [12]INSERM U1018, Centre de Recherche en Épidémiologie et Santé des Population, Paris-Sud University, Paris-Saclay University, Le Kremlin-Bicêtre, France; [13]Division of Health Analytics, City of Hope Beckman Research Institute and City of Hope Comprehensive Cancer Center, Duarte, CA, USA; [14]Department of Medicine, Cedars-Sinai Medical Center, Los Angeles, CA, USA; [15]Service of Infectious Diseases, Lausanne University Hospital and University of Lausanne, Lausanne, Switzerland; [16]Department of Infectious Diseases, Bern University Hospital, University of Bern, Switzerland; [17]Department of Infectious Diseases and Hospital Epidemiology, University Hospital Basel, University of Basel, Basel, Switzerland; [18]Division of Infectious Diseases and Hospital Epidemiology, Kantonsspital Olten, Olten, Switzerland; [19]Division of Infectious Diseases, Cantonal Hospital of St. Gallen, St. Gallen, Switzerland; [20]Division of Infectious Diseases, Regional Hospital of Lugano, Lugano, Switzerland; [21]Department of Infectious Diseases and Hospital Epidemiology, University Hospital Zurich, Zurich, Switzerland; [22]Institute of Medical Virology, University of Zurich, Zurich, Switzerland; [23]JC Wilt Infectious Diseases Research Center, National Microbiology Laboratory, Public Health Agency of Canada, Winnipeg, Manitoba, Canada; [24]Department of Medical Microbiology and Infectious Diseases, University of Manitoba, Winnipeg, Manitoba, Canada; [25]Infections and Immunoepidemiology Branch, Division of Cancer Epidemiology and Genetics, National Cancer Institute, Rockville, MD, USA; [26]CESP, UVSQ, INSERM, Université Paris-Saclay, Villejuif, France; [27]Department of Hematology and Oncology, Hospital of Versailles, Le Chesnay, France and [28]Precision Medicine Unit, Lausanne University Hospital (CHUV) and University of Lausanne, Lausanne, Switzerland.

Ferrata Storti Foundation

Haematologica 2021
Volume 106(8):2233-2241

ABSTRACT

Human immunodeficiency virus (HIV) infection is associated with an increased risk of non-Hodgkin lymphoma (NHL). Even in the era of suppressive antiretroviral treatment, HIV-infected individuals remain at higher risk of developing NHL compared to the general population. In order to identify potential genetic risk loci, we performed case-control genome-wide association studies and a meta-analysis across three cohorts of HIV-infected patients of European ancestry, including a total of 278 cases and 1,924 matched controls. We observed a significant association with NHL susceptibility in the C-X-C motif chemokine ligand 12 (*CXCL12*) region on chromosome 10. A fine mapping analysis identified rs7919208 as the most likely causal variant (P=4.77e-11), with the G>A polymorphism creating a new transcription factor binding site for BATF and JUND. These results suggest a modulatory role of *CXCL12* regulation in the increased susceptibility to NHL observed in the HIV-infected population.

Correspondence:

JACQUES FELLAY
jacques.fellay@epfl.ch

Received: January 9, 2020.

Accepted: July 14, 2020.

Pre-published: July 16, 2020.

https://doi.org/10.3324/haematol.2020.247023

Introduction

Human immunodeficiency virus (HIV) infection is associated with a markedly increased risk of several types of cancer compared to the general population.[1–3] This elevated cancer risk can be attributed partly to viral-induced immunodeficiency, frequent co-infections with oncogenic viruses (*e.g.*, Epstein-Barr virus [EBV], hepatitis B and hepatitis C viruses, human herpesvirus 8 [HHV-8] and papillomavirus), and increased prevalence of traditional risk factors such as smoking.[4,5] However, all of these risk factors may not entirely explain the excess cancer burden seen in the HIV-infected (HIV+) population.[5,6]

A previous study performed in the Swiss HIV Cohort Study (SHCS) identified two AIDS-defining cancers, Kaposi sarcoma and non-Hodgkin lymphoma (NHL) as the main types of cancer found among HIV+ patients (NHL representing 34% of all identified cancers).[4] The relative risk of developing NHL in HIV+ patients was highly elevated compared to the general population (period-standardized incidence ratio [SIR] = 76.4).[4] High HIV plasma viral load, absence of antiretroviral therapy (ART) as well as low CD4+ T-cell counts are known predictive factors for NHL.[7,8] The introduction of ART into clinical practice has led to improved overall survival and restoration of immunity by decreasing viral load and increasing CD4+ T-cell counts, and has led to a decreased risk of developing NHL. However, the risk remains substantially elevated compared to the general population (suboptimal immune response [SIR] 9.1[range, 8.3–10.1])[9] and NHL still represents 20% of all cancers in people living with HIV in the ART era.[10] NHL associated with HIV are predominantly aggressive B-cell lymphomas. Although they are heterogeneous, they share several pathogenic mechanisms involving chronic antigen stimulation, impaired immune response, cytokine deregulation and reactivation of the oncogenic viruses EBV and HHV-8.[11]

The emergence of genome-wide approaches in human genomics has led to the discovery of many associations between common genetic polymorphisms and susceptibility to several diseases including HIV infection and multiple types of cancer.[12,13] Recent genome-wide association studies (GWAS) of NHL have identified multiple susceptibility loci in the European population.[14–22] These variants are located in the genes *LPXN*[21], *BTNL2*[23], *EXOC2*, *NCOA1*[14], *PVT1*[14,22], *CXCR5*, *ETS1*, *LPP*, and *BCL2*[22] for various subtypes of NHL, as well as *BCL6* in the Chinese population.[24] Strong associations with variation in human leukocyte antigen (HLA) genes have also been reported.[15,18,22] However, in the setting of HIV infection, no genome-wide analysis has been reported concerning the occurrence of NHL and the specific mechanisms driving their development remain largely unknown.

Here we report the results of the first genome-wide analysis of NHL susceptibility in individuals chronically infected with HIV. We combined three HIV cohort studies from France, Switzerland and the USA and searched for associations between >6 million single nucleotide polymorphisms (SNP) and a diagnosis of NHL. We identified a novel genetic locus near *CXCL12* to be associated with the development of NHL among HIV+ individuals.

Methods

Ethics statement

The SHCS, the Primo ANRS and ANRS CO16 Lymphovir cohorts (ANRS) and the Multicenter AIDS Cohort Study (MACS) cohorts have been approved by the competent Ethics Committees /Institutional Review Boards of all participating institutions. A written informed consent, including consent for human genetic testing, was obtained from all study participants.

Study participants and contributing centers

Genotyping and phenotypic data were obtained from a total of 2,202 HIV+ individuals enrolled in the SHCS, ANRS and MACS cohorts (278 cases and 1,924 controls) (Table 1). For details on inclusion criteria and cohorts, refer to the *Online Supplementary Appendix*.

Quality control and imputation of genotyping data

The genotyping data from each cohort was filtered and imputed in a similar way, with each genotyping array processed separately to minimize potential batch effects. All variants were first flipped to the correct strand orientation with BCFTOOLS (v1.8) using the human genome build GRCh37 as reference. Variants were removed if they had a larger than 20% minor allele frequency (MAF) deviation from the 1,000 genomes phase 3 EUR reference panel or if they showed a larger than 10% MAF deviation between genotyping chips in the same cohort.

The quality control (QC) filtered genotypes were phased with EAGLE2[25] and missing genotypes were imputed using PBWT[26] with the Sanger Imputation Service,[27] taking the 1,000 genomes project phase 3 panel as reference. Only high-quality variants with an imputation score (INFO >0.8) were retained for further analyses.

Genome-wide association testing and meta-analysis

In order to search for associations between human genomic variation and the development of HIV-related NHL, we first performed separate GWAS within each cohort (SHCS, ANRS and MACS) prior to combining the results in a meta-analysis.

For each cohort separately, the imputed variants were filtered out using PLINK (v2.00a2LM)[28] based on missingness (>0.1), MAF (<0.02) and deviation from Hardy-Weinberg Equilibrium (P_{HWE}<1e-6). Determination of population structure and calculation of principal components was done using EIGENSTRAT (v6.1.4)[29] and the HapMap3 reference panel.[30] All individuals not clustering with the European HapMap3 samples were excluded from further analyses. The samples were screened using KING (v2.1.3)[31] to ensure no duplicate or cryptic related samples were included. Single-marker case-control association analyses were performed using linear mixed models, with genetic relationship matrices calculated between pairs of individuals according to the leave-one-chromosome-out principle, as implemented in GCTA mlma-loco (v1.91.4beta).[32,33] Sex was included as a covariate, except in the MACS cohort, which only includes men.

The results of the three GWAS were combined across cohorts using a weighted Z-score-based meta-analysis in PLINK (v1.90b5.4), after exclusion of the variants that were not present in all three cohorts.

Other methods

The details of the cohorts and other methods used, *i.e.*, fine mapping, prediction of causal variants, long-range chromatin interactions, transcriptomic effects, comparisons to GWAS in

the general population and information on data sharing can be found in the *Online Supplementary Appendix*.

Results

Study participants and association testing

In order to identify human genetic determinants of HIV-associated NHL, we performed case-control GWAS in three groups of HIV+ patients of European ancestry (SHCS, ANRS and MACS). The characteristics of the study participants are presented in Table 1. In total, genotyping data were obtained for 278 cases (NHL+/HIV+) and 1,924 matched controls (NHL-/HIV+). With this sample size, we had 80% power to detect a common genetic variant (10% minor allele frequency) with a relative risk of 2.5, assuming an additive genetic model and using Bonferroni correction for multiple testing ($P_{threshold}$=5e-8).[34]

After genome-wide imputation and quality control, 6.2 million common variants were tested for association with the development of NHL using linear mixed models including sex as a covariate. Results were combined across cohorts using a weighted Z-score-based meta-analysis (Figure 1A). The genomic inflation factor (lambda) was in all cases very close to 1 [1.00–1.01], indicating an absence of systematic inflation of the association results (Figure 1B; *Online Supplementary Figure S2*).

Association results

We observed significant associations with the development of HIV-related NHL at a single locus on chromosome 10, downstream of *CXCL12* (Figure 1C). A total of seven SNP in this locus had *P*-values lower than the genome-wide significance threshold (*P*<5e-8), with rs7919208 displaying the strongest association (Table 2). This association was only detected in the SHCS and ANRS cohorts and not among MACS study participants (*Online Supplementary Table S1*).

Fine mapping of the *CXCL12* locus

In order to identify the causal variant(s) among associated SNP and determine their potential functional effects, we used a multi-level fine mapping approach, combining the statistical fine mapping tool PAINTOR to obtain a 99% credible set and the deep learning framework DeepSEA to predict any effects on chromatin marks and transcription factor binding these variants may have.

Using PAINTOR, we identified a single variant, rs7919208, having a high posterior probability (=100%) of being causal among the 99% credible set based on the integration of the association results, linkage disequilibrium (LD) structure and enrichment of genomic features in this locus (Figure 2).

Consistent with the PAINTOR result, DeepSEA also identified rs7919208 as the sole variant, among the 99% credible set, predicted to have a functional impact by significantly increasing the probability of binding by the B-cell transcription factors BATF (log$_2$ fold-change=3.27) and JUND (log$_2$ fold-change=2.91) (*Online Supplementary Table S2*). Further analysis of the genomic sequence surrounding rs7919208 and the JASPAR transcription factor binding site (TFBS) motifs for BATF and JUND revealed that rs7919208 G->A polymorphism creates the TFBS motif required for the binding of these transcription factors (Figure 3A).

Long-range chromatin interactions

In order to assess the potential functional links between the TFBS created in the presence of the minor allele of rs7919208 and the nearby genes, we performed an analysis of promoter capture Hi-C data and topologically associating domains (TAD). We used the well-characterized GM12878 lymphoblastoid cell line produced by EBV transformation of B lymphocytes collected from a female European donor as a model.

First, in order to examine the interaction potential of the rs7919208 region with nearby promoters, we analyzed available promoter capture Hi-C data obtained from the GM12878 cell line. This analysis revealed a significant interaction between the rs7919208 region and the *CXCL12* promoter, suggesting a possible modulating impact of rs7919208 on the transcription of that gene (Figure 3B). Second, in order to further validate this observed genomic interaction, we analyzed available TAD calls from GM12878 cells,[35] using the 3D Genome Browser for visualization[36] (Figure 3C). We observed that rs7919208 is located within a large TAD together with *CXCL12*, signifying the interaction potential of the new TFBS at rs7919208 and *CXCL12*.

Transcriptomic effects of rs7919208

We did not observe any association between rs7919208 and mRNA expression levels of *CXCL12* in peripheral

Table 1. Summary of included samples and studies.

Cohort	Cases	Controls	Lambda	Genotyping chips	Years of NHL diagnosis	Control inclusion criteria
SHCS	145	1,090	1.00	Illumina HumanOmniExpress-24, Human1M, Human610, HumanHap550, HumanCore-12	2000 - 2017	HIV < 2005, no cancer diagnosis as of 2017 & matched with age
Age (median)	61	58				
Sex (male, %)	91%	80%				
ANRS	61	562	1.00	Illumina Human Omni5 Exome 4v 1-2, Illumina 300	2008 - 2015	No cancer diagnosis
Age (median)	50	34				
Sex (male, %)	89%	87%				
MACS	72	272	1.01	Illumina 1MV1, Human1M-Duo, HumanHap550	1985 - 2013	Matched to cases in terms of age, treatment & time of infection
Age (median)	69	68				
Sex (male, %)	100%	100%				

Cohort and patient characteristics for the Swiss HIV Cohort Study (SHCS), the Primo ANRS and ANRS CO16 Lymphovir cohorts (ANRS) and the Multicenter AIDS Cohort Study (MACS) cohorts. Lambda indicates the genomic inflation factor from the individual cohort genome-wide association studies (GWAS). NHL: non-Hodgkin lymphoma; HIV: human immunodeficiency virus.

blood or peripheral blood mononuclear cells (PBMC) from multiple publicly available datasets, including GTEx,[37] GEUVADIS[38] and the Milieu Intérieur Consortium[39] (*Online Supplementary Figure S3*). Of note, *CXCL12* expression levels were very low in all datasets (*Online Supplementary Figure S4A)*.

Using allele-specific expression analysis in the GTEx dataset, we observed a significant effect in individuals heterozygous of rs7919208, with increased allelic imbalance of *CXCL12* in fibroblasts (false discovery rate adjusted *P*=0.0006, one-sided rank sum test), which was not observed in other tissues (*Online Supplementary Figure 4B*).

HIV infection causes many profound transcriptomic changes.[40] Thus, in order to examine the effect of rs7919208 on *CXCL12* in the context of HIV infection, we extracted RNA from PBMC of 452 individuals in the SHCS with available genotyping data and sequenced them using the Bulk RNA Barcoding and sequencing (BRB-seq) approach.[41] However, the expression levels of *CXCL12* were below the limit of detection for most individuals, preventing an expression quantitative trait loci (eQTL) analysis.

Multiple isoforms of *CXCL12* exist, with variable degrees of expression and potency described in the context of HIV infection.[42] We observed a single significant correlation between rs7919208 and *CXCL12* transcript usage, which was restricted to visceral adipose tissue. The presence of the rs7919208 minor allele was associated with higher relative expression of the longer and rarer transcript isoform ENST00000374429.6 (*Online Supplementary Figure S5*).

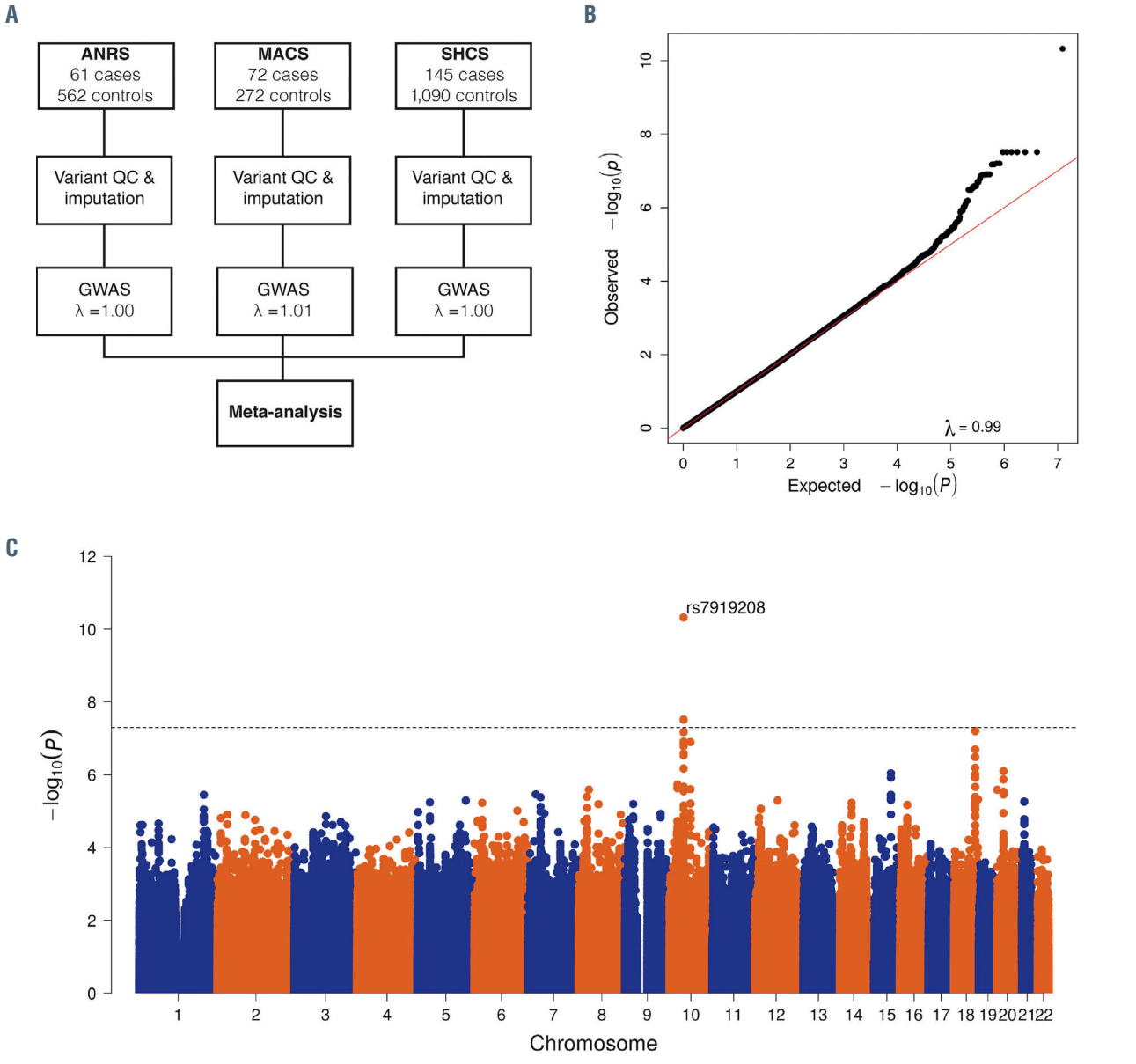

Figure 1. Genome-wide association analysis. (A) Schematic of analysis pipeline. (B) Quantile-quantile plot of the observed -log$_{10}$(*P*-value) (black dots, y-axis) *vs.* expected -log$_{10}$(*P*-values) under the null hypothesis (red line) to check for any genomic inflation of the observed *P*-values. No genomic inflation is observed, with the genomic inflation factor λ=0.99. (C) Manhattan plot of all obtained *P*-values for each variant included in the meta-analysis. The genome-wide threshold (*P*=5e-8) for significance is marked by a dotted line. Only variants at the *CXCL12* locus were found to be significant.

No replication of susceptibility loci found in the general population

In order to assess whether the genetic contribution to the risk of developing NHL is similar or distinct in the HIV+ population compared to the general population, we extracted the *P*-values of all variants found to be genome-wide significant in previous GWAS performed in the general population[14,21–24,43] and compared them to our results. We did not replicate any of the previously published genome-wide associated variants, even at nominal significance level ($P<0.05$), despite sufficient statistical power for many of the variants, thus indicating that the genetic susceptibility of NHL is distinct between the HIV+ and the general population (*Online Supplemental Table S3*). In order to further examine this possibility, we tested whether the NHL/HIV+ associated variant rs7919208 is associated

Table 2. Significant association with human immunodeficiency virus-related non-Hodgkin lymphoma.

Chr	Pos	SNP	Ref	Alt	*P*	OR
10	44673557	rs7919208	A	G	4.77e-11	1.23
10	44677967	rs149399290	T	C	3.09e-08	1.20
10	44678218	rs17155463	T	A	3.09e-08	1.20
10	44678262	rs17155474	C	T	3.09e-08	1.20
10	44678454	rs17155478	T	C	3.09e-08	1.20
10	44678898	rs12249837	G	A	3.09e-08	1.20
10	44680902	rs10608969	T	TAAAGA	3.09e-08	1.20

Variants significantly associated with human immunodeficiency virus (HIV)-related non-Hodgkin lymphoma in a weighted Z-score-based meta-analysis of all individuals included in the Swiss HIV Cohort Study (SHCS), the Primo ANRS and ANRS CO16 Lymphovir cohorts (ANRS) and the Multicenter AIDS Cohort Study (MACS) cohorts. Odds ratios (OR) were transformed from betas using the formula OR=exp(beta). Chr: chromosome; pos: position; SNP: single nucleotide polymorphisms; Ref: reference allele, Alt: alternative allele.

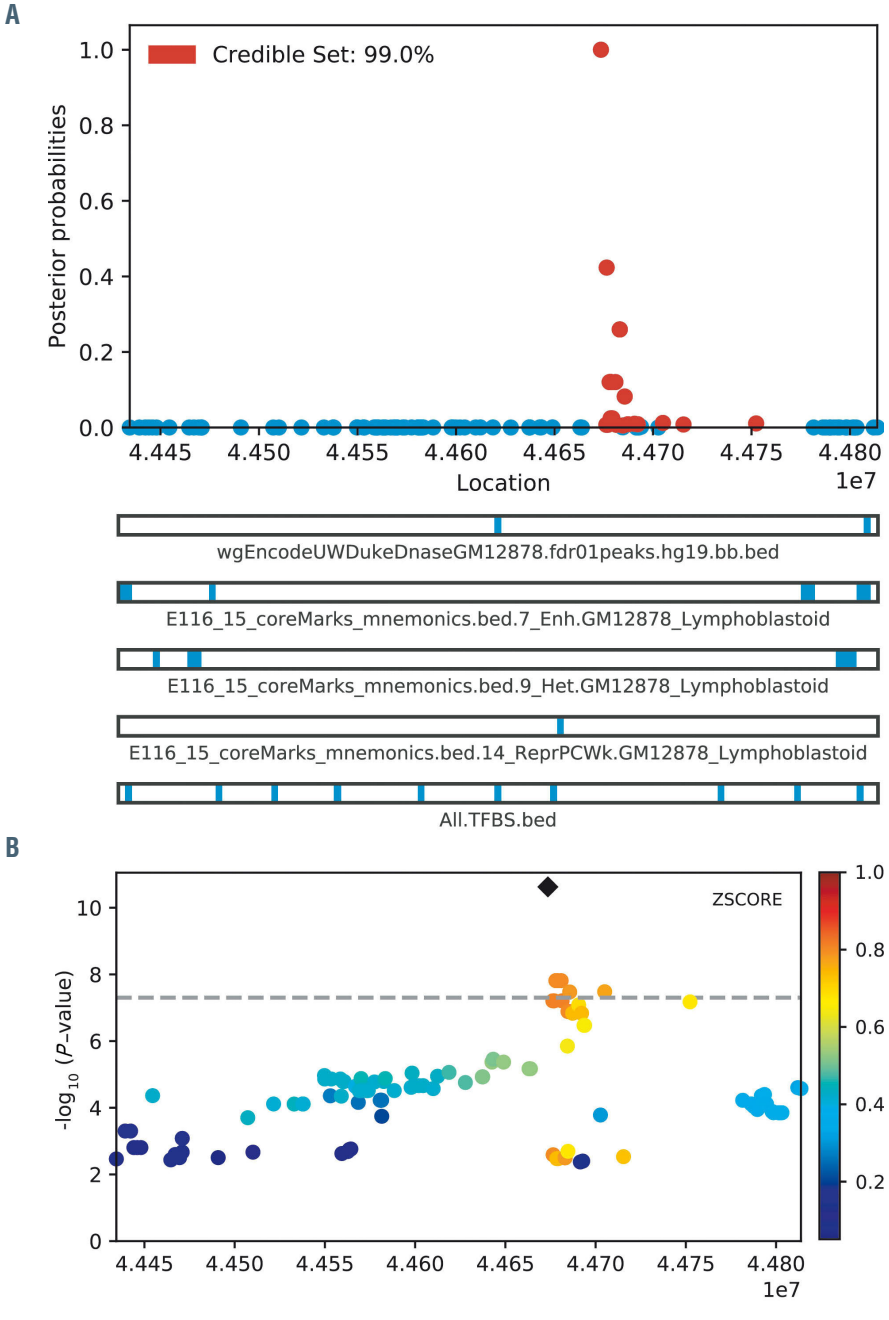

Figure 2. Fine mapping of genome-wide significant hits with PAINTOR. (A) The 99% credible set and posterior probabilities of being the causal variant. The genomic positions are listed on the x-axis. Bottom tracks represent DNAase and chromatin marks obtained from GM12878 cells as well as transcription factor binding site (TFBS) from the Roadmap Epigenomics Project and ENCODE in the region. (B) Locus plot of the associated variants, highlighting the LD relationship, based on the Swiss HIV Cohort Study cohort. The top variant rs7919208 is marked by a black diamond.

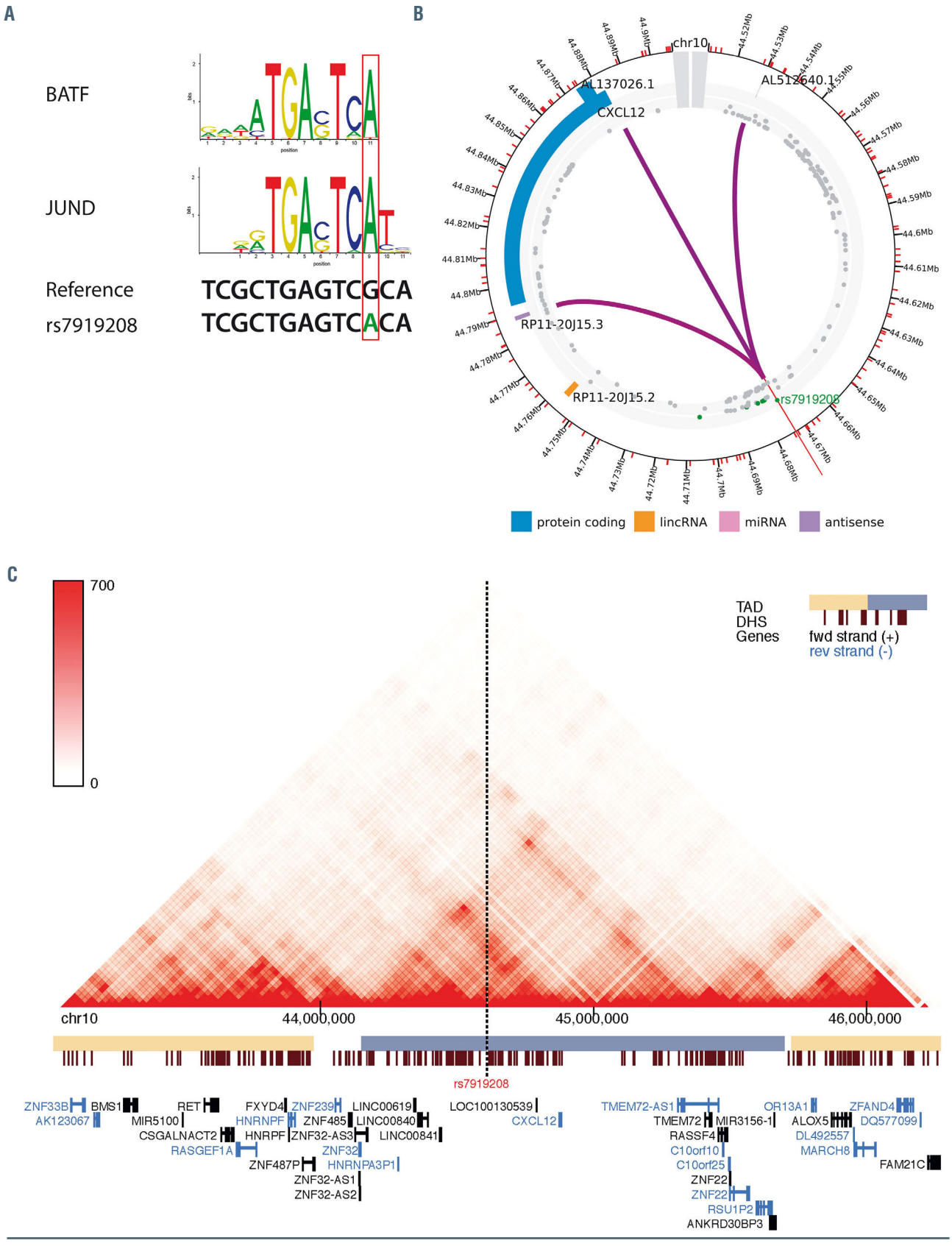

Figure 3. Novel transcription factor binding site and long-range interactions. (A) Canonical motifs of BATF and JUND with the underlying genomic reference sequence and the nucleotide change caused by rs7919208. (B) Promoter capture Hi-C analysis in the GM12878 cell line of the region with the predicted causal variant and *CXCL12*. Variants and their level of association in the meta-analysis are marked in the inner grey circle. Genome-wide significant variants are colored green. Purple lines indicate significant interactions between promoter and other genomic regions. (C) Topologically associating domains (TAD) in the GM12878 cell line in the region of *CXCL12*. The yellow and blue boxes indicate the called TAD from the Hi-C contact map above. The plot is centered on rs7919208. DHS: DNase I hypersensitive sites.

with an increased risk of NHL in the general population. We performed a series of case/control GWAS of four NHL subtypes (CLL, DLBCL, FL and MZL) as well as a combined GWAS with all NHL subtypes (*Online Supplementary Table S4*; *Online Supplementary Figure S6*) and assessed the association evidence at rs7919208. We found no association between rs7919208 and any of the subtypes in the general population, even at nominal significance.

Discussion

In this genome-wide analysis, including a total of 278 NHL HIV+ cases and 1,924 HIV+ controls from three independent cohorts, we identified a novel NHL susceptibility locus on chromosome 10 near the *CXCL12* gene. The strong signal observed in the meta-analysis was driven by the associations detected in the SHCS and ANRS cohorts and there was no evidence of association in the MACS cohort. Notably, most NHL cases in the MACS cohort date back to the pre-ART era, while only NHL cases diagnosed after the year 2000 were included in the SHCS and ANRS analyses. Conceivably, NHL occurring in the early years of the HIV pandemic may have been primarily driven by severe immunosuppression, which could have obscured any influence of human genetic variation among the cases in the MACS sample. Precise phenotype definition is crucial in designing large-scale genetic studies since any environmental noise tends to decrease the likelihood of identifying potential genetic influences.

NHL is a relatively rare cancer even among HIV infected individuals, making it difficult to collect the large numbers of cases that would typically be included in contemporary genome-wide genetic studies. Indeed, a recent study from the Data Collection on Adverse events of Anti-HIV Drugs (D:A:D) group showed an NHL incidence rate of 1.17/1,000 person-years of follow-up over the past 15 years (392 new cases in >40,000 HIV+ individuals).[8] Still, we were able to obtain clinical and genetic data from a total of 278 patients with confirmed NHL diagnosis. By matching them with a larger number of controls from the same cohorts, we had enough power to identify associated variants of relatively large effects in the *CXCL12* region.

Several groups have already suggested a potential role for *CXCL12* variation in HIV-related NHL. A prospective study correlated increased *CXCL12* expression with subsequent NHL development in HIV+ children but not in uninfected children.[44] The number of A alleles at the CXCL12-3' variant (rs1801157) has also previously been associated with an increased risk of developing HIV-related NHL during an 11.7 year follow-up period.[45] Thus, our data further support the role of CXCL12 as a critical modulator of the individual risk of developing NHL in the HIV+ population.

The role of CXCL12 and its receptor chemokine receptor 4 (CXCR4) in cancer in the general population is well established, with the levels of *CXCL12* and *CXCR4* found to be increased in multiple types of cancer and to be associated with tumor progression.[46,47] Furthermore, *in vivo* inhibition of either CXCR4 or CXCL12 signaling is capable of disrupting early lymphoma development in severe combined immunodeficient (SCID) mice transfused with EBV+ PBMC.[48] These results and others have already led to the development and testing of several small molecules targeting either CXCL12 or CXCR4 to inhibit tumor progression.[46]

We could not identify any significant relationship between rs7919208 and the expression levels of *CXCL12* in PBMC or EBV transformed lymphocytes. This could be due to the low expression levels of *CXCL12* in most tissues, apart from stromal cells. Still, our analysis of allele-specific expression showed a significant allelic imbalance for heterozygous carriers of rs7919208 for *CXCL12*. This signal was only observed in fibroblasts, the GTEx tissue most closely resembling stromal cells. Furthermore, we identified a significant association between rs7919208 and CXCL12 transcript isoform usage in the visceral adipose tissue, which is known to also contain a minority of stromal cells.[49] Combined these results underscore the potential importance of these cells in the development of HIV-related NHL and the ability of rs7919208 to modify transcription.

The new BATF and JUND binding site created by rs7919208 could act as an induced or dynamic eQTL, specifically triggered by HIV infection. Such eQTL can be found in regions deprived of regulatory annotations, since these have been mostly examined in static cell types.[50] Supporting this hypothesis, HIV has been shown to induce overexpression of BATF.[51] This would explain why rs7919208 is only a risk factor for HIV+ individuals and not in the general population.

Previous analyses in the general population have discovered both shared and distinct associations for NHL subtypes.[14,21–24,43] However, similar analyses were not possible in our sample since NHL subtype information was not available for many of our cases. Furthermore, information on serostatus for relevant co-infections with EBV or other oncogenic viruses was not available and could therefore not be assessed. In particular, EBV has been largely associated with the development of NHL and other lymphomas and is considered a driver of a subset of NHL in the general population.[52] Variants in the HLA region have consistently been associated with all NHL subtypes in HIV uninfected populations regardless of EBV serostatus, although different HLA associations have been observed for each NHL subtype. We did not find any evidence of HLA associations in our analyses of HIV-related NHL. This might be due to a lack of power, due to our limited sample size in comparison to the NHL GWAS performed in the general population. However, this lack of replication of HLA variants and all other risk variants previously identified in the general population strongly suggests that distinct genes or pathways influence susceptibility to NHL in the HIV+ population compared to the general population.[53] This distinction may be due to the unique pathogenic mechanisms involved in HIV-associated NHL, such as cytokine deregulation, chronic antigen stimulation and impaired immune response, among others.[11]

In summary, we have identified variants significantly associated with the development of NHL in the HIV+ population. Fine mapping of the associated locus and subsequent analyses of TAD, promoter capture Hi-C data as well as deep-learning models of mutational effects on transcription factor binding, points to a causative model involving the gain of a BATF and JUND transcription binding site downstream of *CXCL12* capable of physically interacting with the *CXCL12* promoter. These results suggest an important modulating role of CXCL12 in the development of HIV-related NHL.

Disclosure

CH is a full-time employee of F. Hoffmann–La Roche/Genentech; all other authors declare no conflicts of interest.

Contributions

CWT, JF, PJM, CSR, CB, CH and TOM contributed to the conception and design of the study; CWT, JF, PJM, FAS, DC, LM, CG, IT, SKH, MC, AR, MB, MH, PS, EB, HFG, CSR and CB contributed to the acquisition of data; CWT, TOM, CH, FAS, CB, CSR, NE, PM, and JF contributed to the analysis and interpretation of data; CWT, JF, CSR, CB and SW contributed to drafting the article and revising it critically for important intellectual content; all authors critically reviewed and approved the final manuscript.

Acknowledgments

The data are gathered by the Five Swiss University Hospitals, two Cantonal Hospitals, 15 affiliated hospitals and 36 private physicians (listed in http://www.shcs.ch/180-health-care-providers). The datasets have been accessed through the National Institutes of Health (NIH) database for Genotypes and Phenotypes (dbGaP) under accession # phs000801. A full list of acknowledgements can be found in the supplementary note (Berndt SI et al., Nature Genet., 2013, PMID: 23770605).

Funding

This study has been financed within the framework of the Swiss HIV Cohort Study, supported by the Swiss National Science Foundation (grant #177499), by SHCS project #789 and by the SHCS research foundation. This work further benefited from the ANRS funding of both the Primo and Lymphovir cohorts. Foundation Monahan and Fulbright funded the stay of CB at the National Cancer Institute (NCI). The Genome-Wide Association Study (GWAS) of Non-Hodgkin Lymphoma (NHL) project was supported by the intramural program of the Division of Cancer Epidemiology and Genetics (DCEG), National Cancer Institute (NCI), NIH.

References

1. Patel P, Hanson DL, Sullivan PS, et al. Incidence of types of cancer among HIV-infected persons compared with the general population in the United States, 1992–2003. Ann Intern Med 2008;148(10):728-736.
2. Vogel M, Friedrich O, Lüchters G, et al. Cancer risk in HIV-infected individuals on HAART is largely attributed to oncogenic infections and state of immunocompetence. Eur J Med Res. 2011;16(3):101.
3. Robbins HA, Pfeiffer RM, Shiels MS, Li J, Hall HI, Engels EA. Excess cancers among HIV-infected people in the United States. J Natl Cancer Inst. 2015;107(4):dju503.
4. Clifford GM, Polesel J, Rickenbach M, et al. Cancer risk in the Swiss HIV Cohort Study: associations with immunodeficiency, smoking, and highly active antiretroviral therapy. J Natl Cancer Inst. 2005;97(6):425-432.
5. Engels EA. Non-AIDS-defining malignancies in HIV-infected persons: etiologic puzzles, epidemiologic perils, prevention opportunities. AIDS. 2009;23(8):875-885.
6. Borges ÁH, Dubrow R, Silverberg MJ. Factors contributing to risk for cancer among HIV-infected individuals, and evidence that earlier combination antiretroviral therapy will alter this risk: Curr Opin HIV AIDS. 2014;9(1):34-40.
7. Guiguet M, Boué F, Cadranel J, Lang J-M, Rosenthal E, Costagliola D. Effect of immunodeficiency, HIV viral load, and antiretroviral therapy on the risk of individual malignancies (FHDH-ANRS CO4): a prospective cohort study. Lancet Oncol. 2009;10(12):1152-1159.
8. Shepherd L, Ryom L, Law M, et al. Differences in virological and immunological risk factors for non-Hodgkin and Hodgkin lymphoma. J Natl Cancer Inst. 2018;110(6):598-607.
9. Hleyhel M, Belot A, Bouvier AM, et al. Risk of AIDS-defining cancers among HIV-1–infected patients in France between 1992 and 2009: results from the FHDH-ANRS CO4 Cohort. Clin Infect Dis. 2013;57(11):1638-1647.
10. Robbins HA, Pfeiffer RM, Shiels MS, Li J, Hall HI, Engels EA. Excess cancers among HIV-infected people in the United States. J Natl Cancer Inst. 2015;107(4):dju503.
11. Swerdlow SH. WHO classification of tumours of haematopoietic and lymphoid tissues. International Agency for Research on Cancer; 2017.
12. McLaren PJ, Carrington M. The impact of host genetic variation on infection with HIV-1. Nat Immunol. 2015;16(6):577-583.
13. Sud A, Kinnersley B, Houlston RS. Genome-wide association studies of cancer: current insights and future perspectives. Nat Rev Cancer. 2017;17(11):692-704.
14. Cerhan JR, Berndt SI, Vijai J, et al. Genome-wide association study identifies multiple susceptibility loci for diffuse large B cell lymphoma. Nat Genet. 2014;46(11):1233-1238.
15. Conde L, Halperin E, Akers NK, et al. Genome-wide association study of follicular lymphoma identifies a risk locus at 6p21.32. Nat Genet. 2010;42(8):661-664.
16. Frampton M, da Silva Filho MI, Broderick P, et al. Variation at 3p24.1 and 6q23.3 influences the risk of Hodgkin's lymphoma. Nat Commun. 2013;4:2549.
17. Kumar V, Matsuo K, Takahashi A, et al. Common variants on 14q32 and 13q12 are associated with DLBCL susceptibility. J Hum Genet. 2011;56(6):436-439.
18. Moutsianas L, Enciso-Mora V, Ma YP, et al. Multiple Hodgkin lymphoma–associated loci within the HLA region at chromosome 6p21.3. Blood. 2011;118(3):670-674.
19. Skibola CF, Bracci PM, Halperin E, et al. Genetic variants at 6p21.33 are associated with susceptibility to follicular lymphoma. Nat Genet. 2009;41(8):873-875.
20. Urayama KY, Jarrett RF, Hjalgrim H, et al. Genome-wide association study of classical Hodgkin lymphoma and Epstein–Barr virus status–defined subgroups. J Natl Cancer Inst. 2012;104(3):240-253.
21. Vijai J, Kirchhoff T, Schrader KA, et al. Susceptibility loci associated with specific and shared subtypes of lymphoid malignancies. PLoS Genet. 2013;9(1):e1003220.
22. Skibola CF, Berndt SI, Vijai J, et al. Genome-wide association study identifies five susceptibility loci for follicular lymphoma outside the HLA region. Am J Hum Genet. 2014;95(4):462-471.
23. Vijai J, Wang Z, Berndt SI, et al. A genome-wide association study of marginal zone lymphoma shows association to the HLA region. Nat Commun. 2015;6:5751.
24. Tan DEK, Foo JN, Bei J-X, et al. Genome-wide association study of B cell non-Hodgkin lymphoma identifies 3q27 as a susceptibility locus in the Chinese population. Nat Genet. 2013;45(7):804-807.
25. Loh P-R, Danecek P, Palamara PF, et al. Reference-based phasing using the Haplotype Reference Consortium panel. Nat Genet. 2016;48(11):1443-1448.
26. Durbin R. Efficient haplotype matching and storage using the positional Burrows–Wheeler transform (PBWT). Bioinformatics. 2014;30(9):1266-1272.
27. McCarthy S, Das S, Kretzschmar W, et al. A reference panel of 64,976 haplotypes for genotype imputation. Nat Genet. 2016;48(10):1279-1283.
28. Chang CC, Chow CC, Tellier LC, Vattikuti S, Purcell SM, Lee JJ. Second-generation PLINK: rising to the challenge of larger and richer datasets. Gigascience. 2015;4(1):1-16.
29. Price AL, Patterson NJ, Plenge RM, Weinblatt ME, Shadick NA, Reich D. Principal components analysis corrects for stratification in genome-wide association studies. Nat Genet. 2006;38(8):904-909.
30. The International HapMap 3 Consortium. Integrating common and rare genetic variation in diverse human populations. Nature. 2010;467(7311):52-58.
31. Manichaikul A, Mychaleckyj JC, Rich SS, Daly K, Sale M, Chen W-M. Robust relationship inference in genome-wide association studies. Bioinformatics. 2010;26(22):2867-2873.
32. Yang J, Lee SH, Goddard ME, Visscher PM. GCTA: a tool for genome-wide complex trait analysis. Am J Hum Genet. 2011;88(1):76-82.
33. Yang J, Zaitlen NA, Goddard ME, Visscher PM, Price AL. Advantages and pitfalls in the application of mixed-model association methods. Nat Genet. 2014;46(2):100-106.
34. Johnson JL, Abecasis GR. GAS Power Calculator: web-based power calculator for genetic association studies. bioRxiv. 2017;164343.
35. Rao SSP, Huntley MH, Durand NC, et al. A 3D Map of the human genome at kilobase resolution reveals principles of chromatin looping. Cell. 2014;159(7):1665-1680.
36. Wang Y, Song F, Zhang B, et al. The 3D Genome Browser: a web-based browser for visualizing 3D genome organization and long-range chromatin interactions. Genome Biol. 2018;19(1):151.
37. GTEx Consortium. Genetic effects on gene expression across human tissues. Nature. 2017;550(7675):204-213.

38. Lappalainen T, Sammeth M, Friedländer MR, et al. Transcriptome and genome sequencing uncovers functional variation in humans. Nature. 2013;501(7468):506-511.
39. Piasecka B, Duffy D, Urrutia A, et al. Distinctive roles of age, sex, and genetics in shaping transcriptional variation of human immune responses to microbial challenges. PNAS. 2018;115(3):e488-E497.
40. Mohammadi P, Desfarges S, Bartha I, et al. 24 hours in the life of HIV-1 in a T cell line. PLOS Pathogens. 2013;9(1):e1003161.
41. Alpern D, Gardeux V, Russeil J, et al. BRB-seq: ultra-affordable high-throughput transcriptomics enabled by bulk RNA barcoding and sequencing. Genome Biol. 2019;20(1):71.
42. Janssens R, Struyf S, Proost P. The unique structural and functional features of CXCL12. Cell Mol Immunol. 2018;15(4):299-311.
43. Lim U, Kocarnik JM, Bush WS, et al. Pleiotropy of cancer susceptibility variants on the risk of non-Hodgkin lymphoma: The PAGE Consortium. PLoS One. 2014;9(3):e89791.
44. Sei S, O'Neill DP, Stewart SK, et al. Increased level of stromal cell-derived factor-1 mRNA in peripheral blood mononuclear cells from children with AIDS-related lymphoma. Cancer Res. 2001;61(13):5028-5037.
45. Rabkin CS, Yang Q, Goedert JJ, Nguyen G, Mitsuya H, Sei S. Chemokine and chemokine receptor gene variants and risk of non-Hodgkin's lymphoma in human immunodeficiency virus-1–infected individuals. Blood. 1999;93(6):1838-1842.
46. Meng W, Xue S, Chen Y. The role of CXCL12 in tumor microenvironment. Gene. 2018;641:105-110.
47. Peled A, Klein S, Beider K, Burger JA, Abraham M. Role of CXCL12 and CXCR4 in the pathogenesis of hematological malignancies. Cytokine. 2018;109:11-16.
48. Piovan E, Tosello V, Indraccolo S, et al. Chemokine receptor expression in EBV-associated lymphoproliferation in hu/SCID mice: implications for CXCL12/CXCR4 axis in lymphoma generation. Blood. 2005;105(3):931-939.
49. Vijay J, Gauthier M-F, Biswell RL, et al. Single-cell analysis of human adipose tissue identifies depot- and disease-specific cell types. Nat Metab. 2020;2(1):97-109.
50. Strober BJ, Elorbany R, Rhodes K, et al. Dynamic genetic regulation of gene expression during cellular differentiation. Science. 2019;364(6447):1287-1290.
51. Quigley M, Pereyra F, Nilsson B, et al. Transcriptional analysis of HIV-specific CD8+ T cells shows that PD-1 inhibits T cell function by upregulating BATF. Nat Med. 2010;16(10):1147-1151.
52. Gasser O, Bihl FK, Wolbers M, Loggi E, Steffen I, Hirsch HH. HIV patients developing primary CNS lymphoma lack EBV-specific CD4þ T cell function irrespective of absolute CD4þ T cell counts. PLoS Med. 2007;4(3):6.
53. Swerdlow SH, Campo E, Harris NL, et al. WHO classification of tumours of haematopoietic and lymphoid tissues.

The *EBF1-PDGFRB* T681I mutation is highly resistant to imatinib and dasatinib *in vitro* and detectable in clinical samples prior to treatment

EBF1-PDGFRB accounts for 3% of cases of childhood Philadelphia chromosome-like acute lymphoblastic leukemia (Ph-like ALL),[1] represents the most common fusion gene in the Ph-like ABL-class subtype,[2] and is notoriously associated with high rates of induction failure.[1-3] *EBF1-PDGFRB* fusions exhibited exquisite sensitivity to ABL tyrosine kinase inhibitors (TKI) in preclinical models,[3] and durable remissions have been reported in patients harboring *EBF1-PDGFRB* when treated with either imatinib or dasatinib.[4] Collectively, these observations provide a compelling rationale for investigating the incorporation of ABL TKI in combination with conventional chemotherapy for Ph-like ABL-class ALL patients in clinical trials. However, the emergence of kinase domain (KD) mutations as the primary mechanism of acquired resistance to TKI has been well described and occurs in many adults with relapsed/refractory Philadelphia chromosome-driven leukemias.[5] The mechanisms of TKI resistance in Ph-like ABL-class ALL have not been extensively studied, although we hypothesize that similar resistance mechanisms may occur between the two subsets. Hence, we sought to characterize the spectrum of TKI-resistant KD mutations in *EBF1-PDGFRB* Ph-like ALL as a mechanism of acquired resistance by using a validated *in vitro* saturation mutagenesis screen, as previously described.[6]

Among 245 imatinib-resistant and 416 dasatinib-resistant colonies isolated from our *in vitro* screens, 233 (95%) and 363 (87%) colonies, respectively, harbored a single KD mutation. The predominant recurrent single KD mutation was the gatekeeper T681I point mutation for both imatinib (n=233/245, 95%) and dasatinib (n=338/416, 81%). The next most common recurrent KD mutation was N666S (n=18/416, 4%), which conferred resistance to dasatinib only. The T681I mutation in *EBF1-PDGFRB* is analogous to the gatekeeper mutation T315I in *BCR-ABL1*, while the N666S mutation is analogous to the N676S mutation in *FLT3*-ITD.[7] The full spectrum of KD mutations in *EBF1-PDGFRB* identified from the *in vitro* saturation mutagenesis screens with imatinib and dasatinib is reported in *Online Supplementary Table S1*.

We then focused on the two most common KD mutations to assess their proliferative properties and characterize their biochemical resistance to the relevant TKI. Introduction of *EBF1-PDGFRB* T681I and N666S mutant isoforms into Ba/F3 cells rendered them independent of interleukin-3, illustrating that the transforming capacity of the *EBF1-PDGFRB* fusion gene is preserved in the presence of these mutations. In viability assays, the T681I mutation was highly resistant to imatinib and dasatinib, while the N666S mutation showed intermediate resistance to dasatinib. The half maximal inhibitory concentra-

Table 1. Clinical characteristics and outcomes of the 23 *EBF1-PDGFRB* patients with or without a subclonal T681I mutation at diagnosis, as determined by droplet digital polymerase chain reaction.

ID#	Age at diagnosis (years)	WBC at diagnosis x10^9/L	BM blasts (%)	CR	EOI MRD (%)	Relapse	Months to relapse	HSCT	Status
1	3	18.4	95	Yes	>1	No		Yes	Alive (11.1 years)
2	12	114.3	98	IF	>1	BM	12	Yes	Died of disease (1.2 years)
3	14	419.8	92	IF	>1	No		Yes	Died in remission (1.2 years)
4	7	79.9	85	IF	>1	No		Yes	Died in remission (1.5 years)
5	17	396	69	Yes	0.1-0.99	CNS	27	No	Alive (7.4 years)
6*	17	13.4	96	Yes	>1	BM	28	Yes	Alive (6.8 years)
7	12	32.5	89	Yes	>1	BM	32	Yes	Alive (6.8 years)
8	19	54.8	97	IF	>1	No		Yes	Alive (6.2 years)
9	14	41.7	90	Unknown	>1	No		Yes	Alive (6.0 years)
10	11	28.2	85	IF	>1	No		Yes	Alive (5.2 years)
11	6	80.7	91	IF	>1	No		Yes	Alive (5.6 years)
12	14	3.3	90	Unknown	Unknown	No		No	Induction death (19 days)
13	9	39	74	IF	>1	No		Yes	Alive (5.0 years)
14	6	212	98	Yes	Unknown	BM/CNS	31	No	Died of disease (5.0 years)
15	12	17	68	Yes	Unknown	No		No	Alive (7.6 years)
16*	12	5	Unknown	Yes	Unknown	BM	39	No	Alive (7.4 years)
17	4	49	95	Yes	>0.1	No		No	Alive (7.5 years)
18	19	8	99	Yes	>10	CNS	40	No	Alive (6.8 years)
19	18	3	Unknown	Yes	>10	No		Yes	Alive (5.2 years)
20*	14	26	94	Yes	>10	BM	18	No	Died of disease (1.8 years)
21	8	34	99	Yes	>10	BM	50	No	Alive (3.8 years)
22	16	68	95	Unknown	>0.01	No		No	Died in remission (4 months)
23	16	102	72	IF	>10	No		No	Died of disease (3 months)

ID#: identification number; WBC: white blood cell; BM: bone marrow; CR: complete remission defined as M1 marrow or <5% blasts on microscopic assessment; EOI MRD: end of induction minimal residual disease; HSCT: hematopoietic stem cell transplantation; IF: induction failure; CNS: central nervous system, *patients with subclonal T681I mutation.

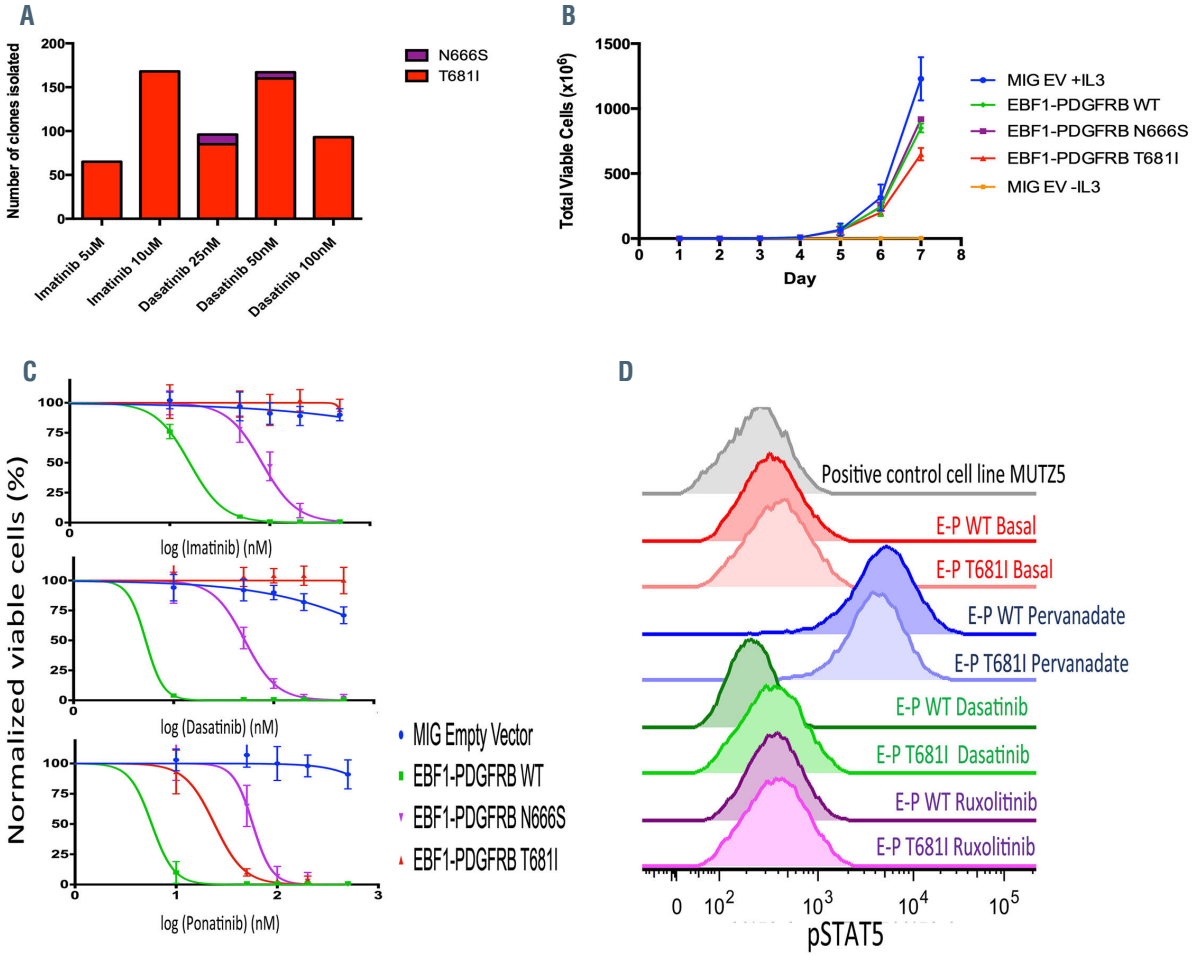

Figure 1. *In vitro* mutational screen of *EBF1-PDGFRB* reveals kinase domain mutations causing varying degrees of resistance to imatinib and dasatinib. (A) The proportion of T681I and N666S kinase domain mutations identified in *EBF1-PDGFRB in vitro* screens to different concentrations of imatinib and dasatinib. (B) Proliferation assays demonstrating the cytokine-independent proliferation of wild-type and mutant *EBF1-PDGFRB* Ba/F3 cells. (C) Drug-sensitivity profiles of Ba/F3 cells harboring wild-type and mutant *EBF1-PDGFRB* in response to imatinib, dasatinib and ponatinib. (D) Phosphorylation of STAT5 is elevated at basal in Ba/F3 cells harboring *EBF1-PDGFRB* and can be inhibited in wild-type but not mutant *EBF1-PDGFRB* in response to dasatinib. E-P: *EBF1-PDGFRB*; EV: empty vector; IL3: interleukin-3: WT: wild-type; pSTAT5: phosphorylated STAT5.

tion (IC_{50}) values for wild-type *EBF1-PDGFRB* were 15.74 nM, 5.26 nM and 5.73 nM for imatinib, dasatinib and ponatinib, respectively. The IC_{50} values for the *EBF1-PDGFRB* T681I mutant isoform were 602.5 nM and 23.93 nM for imatinib and ponatinib, respectively, while the IC_{50} was not reached with the highest concentration of dasatinib used. Moreover, phosphorylation of STAT5 was not abrogated by dasatinib in Ba/F3 constructs harboring the T681I *EBF1-PDGFRB* compared to wild-type *EBF1-PDGFRB* (Figure 1).

To understand the molecular mechanism of TKI resistance from KD mutations, we modeled the wild-type and mutant structures of PDGFRB in relationship with the relevant TKI. Co-crystal structure analysis of the T681I mutation demonstrated that substitution from a threonine to the bulkier hydrophobic isoleucine at the gatekeeper position leads to steric incompatibility between the ligand and the pocket, thus preventing dasatinib from binding both the active and inactive kinase conformations. As for the N666S substitution, the PDGFRB N666S model demonstrated that the mutation likely disrupts a network of stabilizing hydrogen bonds, which might have long-range effects on the conformation of the ATP binding pocket (*Online Supplementary Figure S1*).

We then hypothesized that KD mutations might be present at very low levels at diagnosis in patients with *EBF1-PDGFRB* when assessed by more sensitive technologies and emerge as the dominant clone at relapse under the selective pressure of therapy, as suggested by a few adult studies.[8,9] We designed a droplet digital polymerase chain reaction (ddPCR) assay to identify the T681I mutation in patients' diagnostic samples prior to any exposure to a TKI. Among the 23 diagnostic *EBF1-PDGFRB* patients' samples we analyzed, the gatekeeper T681I mutation was identified in 13% (n=3/23) by our ddPCR assay (Figure 2). This cohort comprised 13 patients enrolled on the Children's Oncology Group ALL trials (AALL0232: n=1, AALL1131: n=12) and ten patients on United Kingdom ALL trials (UK ALL 97/99: n=3, UK ALL 2003: n=7) (Table 1). The median age of the entire cohort was 12 years (range, 8-16), and the median white blood cell count at diagnosis was 39.0 (17-80.7) x 10^9 cells/L. The median duration of follow-up was 60 (14-81) months. None of the patients was treated with TKI. Baseline characteristics, leukemia response and clinical outcomes among the three *EBF1-PDGFRB* patients with subclonal T681I mutation detected by ddPCR at diagnosis were not significantly different from those of the 20

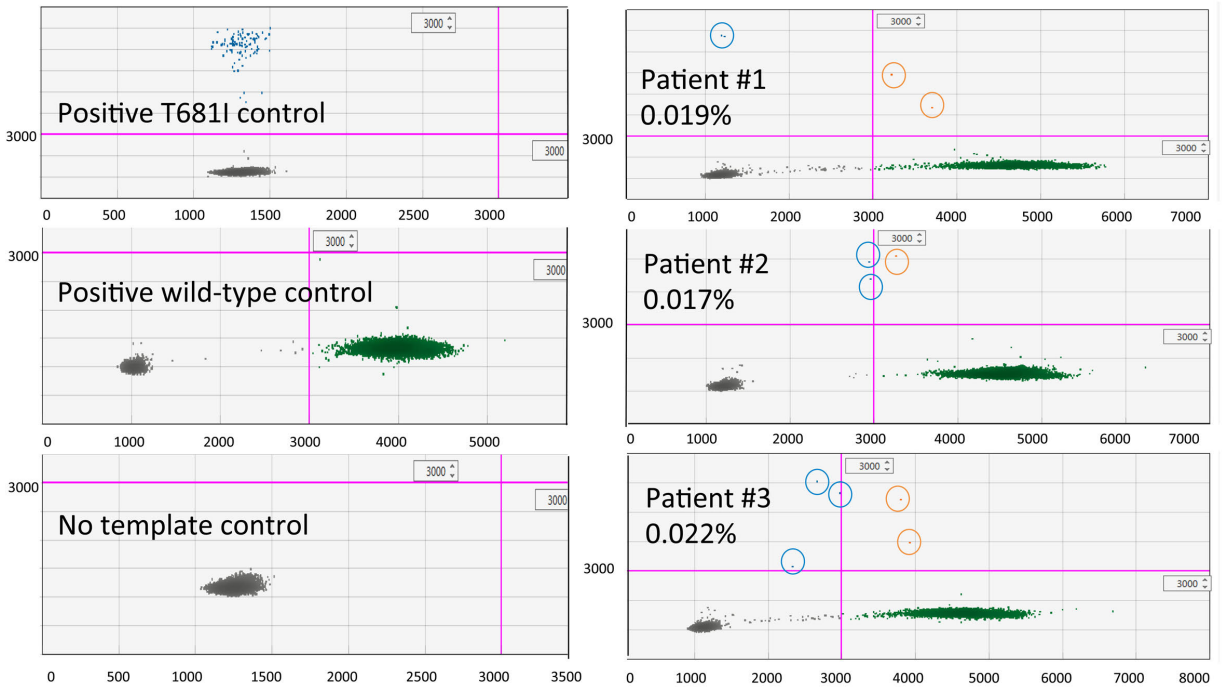

Figure 2. Droplet digital polymerase chain reaction can detect subclonal T681I mutation in clinical samples at diagnosis. Droplet digital polymerase chain reaction (ddPCR) experiments including positive T681I, wild-type and no template controls in the left panel. In the right panel, three *EBF1-PDGFRB* patients were found to have subclonal T681I mutationd at diagnosis by ddPCR. Patient #1 had four droplets containing the mutant T681I out of 20,879 total generated droplets (0.019%); Patient #2 had three positive droplets out of 17,987 generated (0.017%) and patient #3 had five positive droplets out of 22,799 generated (0.022%).

patients without a subclonal T681I mutation, although there was a trend towards a higher likelihood of relapse in the T681I-positive group *versus* the T681I-negative group (100% *vs.* 35%; *P*=0.0678) (*Online Supplementary Table S2*).

To the best of our knowledge, our study is the first to report that KD mutations represent a potential mechanism of acquired resistance in children with *EBF1-PDGFRB* Ph-like ALL. The gatekeeper T6811 mutation was the predominant KD mutation in our *in vitro* screens which was resistant to both imatinib and dasatinib, but could be rescued by ponatinib as predicted. The paucity of KD mutations in *EBF1-PDGFRB* recovered in the dasatinib mutational screen was similar to that in other BCR-ABL1 mutational screens, since dasatinib is active against most imatinib-resistant KD mutations.[10] However, to our surprise, the gatekeeper mutation was the only KD mutation in *EBF1-PDGFRB* retrieved in the imatinib mutational screen, while over 90 imatinib-resistant KD mutations have been reported with *BCR-ABL1*.[11] This finding could be explained by the higher dose that was used in our screen compared to previous reports, but it is also known that imatinib is much more potent in *PDGFR* family fusions than in the *BCR-ABL1* fusion. The IC_{50} of imatinib for *EBF1-PDGFRB* in our hands was 15.74 nM, while Cools *et al.* reported that the IC_{50} of imatinib for cells expressing *FIP1L1-PDGFRA* was 3.2 nM, whereas the IC_{50} for *BCR-ABL1* was 582 nM.[12] Thus, mutations that impart a modest degree of imatinib resistance may not have been detected by our screens.

The analogous N666S mutation has not been previously reported in *BCR-ABL1 in vitro* screens with either imatinib or dasatinib. However, the residue N666 in *EBF1-PDGFRB* is adjacent to its analogous residue V299 in *BCR-ABL1*, which represents the third most common contact residue where KD mutations to dasatinib arise, after T315 and F317 amino acid residues.[10] Smith *et al.* identified the N676S mutation in *FLT3*-ITD in their *in vitro* mutagenesis screen with the FLT3 inhibitor PLX3997, but only N676K/T mutations rather than N676S were isolated from adult acute myeloid leukemia patients with acquired clinical resistance to PLX3997.[7] Moreover, *FLT3* N676K mutations have been identified in core-binding factor leukemia at diagnosis and may represent a cooperating mutation in leukemogenesis. The *FLT3* N676K mutant alone can induce cytokine-independent growth in Ba/F3 cells and confer resistance to FLT3 inhibitors.[13]

In contrast to the report by Zhang *et al.*,[14] our *EBF1-PDGFRB in vitro* saturation mutagenesis screen did not identify the C843G KD mutation that was seen in *AGGF1-PDGFRB* Ph-like ALL. In their experiments, the reported IC_{50} of *AGGF1-PDGFRB* C843G and *EBF1-PDGFRB* C843G to dasatinib was 0.78 nM and 0.121 nM, respectively. Thus, we may not recover this mutant in our screens even at 25 nM of dasatinib, the lowest dasatinib concentration used in our screen, which is more than 200-fold above the measured IC_{50} of *EBF1-PDGFRB* C843G.

The detection of drug-resistant KD mutations at diagnosis has been reported in 21% to 40% of cases of TKI-naïve chronic myelogenous leukemia with advanced disease and in Ph^+ ALL samples.[8,15] The frequency of T315I mutation at diagnosis ranges from 12.5% to 17%,[15] which is in keeping with the frequency of the analogous gatekeeper T681I mutation in our cohort of *EBF1-PDGFRB* patients. Nevertheless, the clinical and prognostic significance of pre-existing KD mutation detected by sensitive technologies prior to TKI remains unclear. Willis *et al.* showed that mutation detection at

low levels by allele-specific oligonucleotide polymerase chain reaction does not invariably predict relapse, or have a negative impact on cytogenetic response or event-free survival.[15] Patients with subclonal T681I mutations detected by ddPCR at diagnosis had a trend towards increased risk of relapse compared to the T681I-negative subgroup; however, these analyses were hindered by small numbers of patients and should be validated in larger cohorts of uniformly treated patients. Furthermore, confirmation of the T681I mutation in relapsed samples would be essential in future studies to validate that relapse was driven by the clonal expansion of drug-resistant mutations under the selective pressure of TKI therapy. However, none of our 23 patients was treated with TKI and relapse samples after TKI treatment were not available for testing.

In conclusion, KD point mutations represent a potential mechanism of acquired resistance in *EBF1-PDGFRB* Ph-like ALL. The T681I gatekeeper KD mutation was the most common KD mutation in *EBF1-PDGFRB* Ph-like ALL that was resistant to both imatinib and dasatinib, and could be identified in clinical samples at diagnosis by ddPCR. Validation of our *in vitro* saturation mutagenesis screens would be important in future clinical trials of Ph-like ALL and concerted efforts should focus on exploring novel therapies targeting the T681I KD mutation.

Thai Hoa Tran,[1,2] Jonathan V. Nguyen,[2] Adrian Stecula,[3] Jon Akutagawa,[2] Anthony V. Moorman,[4] Benjamin S. Braun,[2] Andrej Sali,[3] Charles G. Mullighan,[5] Neil P. Shah,[6] Yunfeng Dai,[7] Meenakshi Devidas,[8] Kathryn G. Roberts,[5] Catherine C. Smith[6] and Mignon L. Loh[2]

[1]Division of Pediatric Hematology-Oncology, Charles-Bruneau Cancer Center, CHU Sainte-Justine, University of Montreal, Montreal, Quebec, Canada; [2]Department of Pediatrics, Benioff Children's Hospital and the Helen Diller Family Comprehensive Cancer Center, University of California San Francisco, San Francisco, CA, USA; [3]Department of Bioengineering and Therapeutic Sciences, Department of Pharmaceutical Chemistry, California Institute for Quantitative Biosciences, University of California San Francisco, San Francisco, CA, USA; [4]Wolfson Childhood Cancer Research Centre, Northern Institute for Cancer Research, Newcastle University, Newcastle upon Tyne, UK; [5]Department of Pathology, St. Jude Children's Research Hospital, Memphis, TN, USA; [6]Division of Hematology-Oncology and the Helen Diller Family Comprehensive Cancer Center, University of California San Francisco, San Francisco, CA, USA; [7]Department of Biostatistics, College of Medicine and Public Health & Health Professions, University of Florida, Gainesville, FL, USA and [8]Department of Global Pediatric Medicine, St. Jude Children's Research Hospital, Memphis, TN, USA

Correspondence: THAI HOA TRAN - thai.hoa.tran@umontreal.ca

doi:10.3324/haematol.2020.261354

Received: June 11, 2020.

Accepted: February 2, 2021.

Pre-published: February 25, 2021.

Disclosures: no conflicts of interest to disclose.

Contributions: THT and MLL designed the study; JN and THT performed the experiments and analyzed the data; AS performed comparative protein structure modeling of PDGFRB; JA, JN and THT performed the drug screens; AVM, YD and MD provided the clinical data; THT and MLL wrote the manuscript. All authors reviewed the manuscript.

Acknowledgments: we thank the Children's Oncology Group ALL Biology Committee and the UK Childhood Leukemia Cell Bank for providing the patients' precious samples.

Funding: this work was supported by National Institutes of Health grants U10 CA98543 and U10 CA180886 (COG Chair's grants), U10 CA98413 and U10 CA180899 (COG Statistics and Data Center grants), U24 CA114766 and U24-CA196173 (COG Specimen Banking), and by the American Lebanese Syrian Associated Charities. MLL is the Benioff Chair of Children's Health and the Deborah and Arthur Ablin Endowed Chair for Pediatric Molecular Oncology at Benioff Children's Hospital. THT and MLL were supported by the Innovation Grant of Alex's Lemonade Stand Foundation as well as the Frank A. Campini Foundation.

References

1. Reshmi SC, Harvey RC, Roberts KG, et al. Targetable kinase gene fusions in high-risk B-ALL: a study from the Children's Oncology Group. Blood. 2017;129(25):3352-3361.
2. den Boer ML, Cario G, Moorman AV, et al. Outcome of ABL-class acute lymphoblastic leukemia in children in the pre-tyrosine kinase inhibitor era; an international retrospective study of the Ponte di Legno group. Lancet Haematol. 2021;8(1):e55-e66.
3. Roberts KG, Li Y, Payne-Turner D, et al. Targetable kinase-activating lesions in Ph-like acute lymphoblastic leukemia. N Engl J Med. 2014;371(11):1005-1015.
4. Tanasi I, Ba I, Sirvent N, et al. Efficacy of tyrosine kinase inhibitors in Ph-like acute lymphoblastic leukemia harboring ABL-class rearrangements. Blood. 2019;134(16):1351-1355.
5. Soverini S, Branford S, Nicolini FE, et al. Implications of BCR-ABL1 kinase domain-mediated resistance in chronic myeloid leukemia. Leuk Res. 2014;38(1):10-20.
6. Smith CC, Wang Q, Chin CS, et al. Validation of ITD mutations in FLT3 as a therapeutic target in human acute myeloid leukaemia. Nature. 2012;485(7397):260-263.
7. Smith CC, Zhang C, Lin KC, et al. Characterizing and overriding the structural mechanism of the quizartinib-resistant FLT3 "gatekeeper" F691L mutation with PLX3397. Cancer Discov. 2015;5(6):668-679.
8. Pfeifer H, Wassmann B, Pavlova A, et al. Kinase domain mutations of BCR-ABL frequently precede imatinib-based therapy and give rise to relapse in patients with de novo Philadelphia-positive acute lymphoblastic leukemia (Ph+ ALL). Blood. 2007;110(2):727-734.
9. Hofmann WK, Komor M, Wassmann B, et al. Presence of the BCR-ABL mutation Glu255Lys prior to STI571 (imatinib) treatment in patients with Ph+ acute lymphoblastic leukemia. Blood. 2003;102(2):659-661.
10. Burgess MR, Skaggs BJ, Shah NP, Lee FY, Sawyers CL. Comparative analysis of two clinically active BCR-ABL kinase inhibitors reveals the role of conformation-specific binding in resistance. Proc Natl Acad Sci U S A. 2005;102(9):3395-3400.
11. Azam M, Latek RR, Daley GQ. Mechanisms of autoinhibition and STI-571/imatinib resistance revealed by mutagenesis of BCR-ABL. Cell. 2003;112(6):831-843.
12. Cools J, DeAngelo DJ, Gotlib J, et al. A tyrosine kinase created by fusion of the PDGFRA and FIP1L1 genes as a therapeutic target of imatinib in idiopathic hypereosinophilic syndrome. N Engl J Med. 2003;348(13):1201-1214.
13. Opatz S, Polzer H, Herold T, et al. Exome sequencing identifies recurring FLT3 N676K mutations in core-binding factor leukemia. Blood. 2013;122(10):1761-179.
14. Zhang Y, Gao Y, Zhang H, et al. PDGFRB mutation and tyrosine kinase inhibitor resistance in Ph-like acute lymphoblastic leukemia. Blood. 2018;131(20):2256-2261.
15. Willis SG, Lange T, Demehri S, et al. High-sensitivity detection of BCR-ABL kinase domain mutations in imatinib-naive patients: correlation with clonal cytogenetic evolution but not response to therapy. Blood. 2005;106(6):2128-2137.

The TRPV2 channel mediates Ca^{2+} influx and the Δ9-THC-dependent decrease in osmotic fragility in red blood cells

Water and ionic homeostasis of red blood cells (RBC) is regulated by various active and passive transport mechanisms in the RBC membrane, including channels like aquaporins,[1] the mechanically activated non-selective cation channel Piezo1[2] and the Ca^{2+}-activated potassium channel KCa3.1.[3] The human genome contains 27 genes that code for transient receptor potential (TRP) channels. The only TRP channel protein that has been detected in circulating mouse RBC is TRPC6,[4] which might be associated with basal Ca^{2+} leakage and stress-stimulated Ca^{2+} entry.[4] TRPC2 and TRPC3 are expressed by murine erythroid precursors and splenic erythroblasts, and in these cells, erythropoietin stimulates an increase in intracellular calcium concentration via TRPC2 and TRPC3.[5] In this study we identified the TRP vanilloid (TRPV) 2 channel protein in mouse and human RBC by specific antibodies and mass spectrometry. TRPV2-dependent currents and Ca^{2+} entry were activated by the TRPV2 agonists cannabidiol (CBD) and Δ9-tetrahydrocannabinol (Δ9-THC)[6] resulting in a left-shift of the hypotonicity-dependent hemolysis curve. This effect was reversed in the presence of the KCa3.1 inhibitor TRAM-34, whereas the knockout of *Trpv2* right-shifted the hemolysis curve to higher tonicities.

We separated mouse RBC from other blood cells by centrifugation and analyzed protein lysates by nanoflow liquid chromatography tandem mass spectrometry (nano-LC-MS/MS). The identified proteins included TRPV2 (*Online Supplementary Figure S1A*). To enrich the TRPV2 protein we generated an antibody which recognizes the TRPV2 protein in RBC from wild-type (WT) animals but not in RBC from *Trpv2* gene-deficient (KO) mice (Figure 1A). As an additional control, we used anti-TRPC6 antibody and identified TRPC6 in RBC (Figure 1B). Total eluates of anti-mTRPV2 affinity purifications from RBC membranes of WT mice were analyzed by nano-LC-MS/MS, which retrieved peptides covering 54% of the accessible TRPV2 primary sequence (*Online Supplementary Figure S1B*).

To obtain a more comprehensive protein profile, we lysed WT and *Trpv2*-KO RBC, extracted the proteins, and measured the resulting tryptic peptides by nano-LC-MS/MS. A total of 1,450 proteins were identified (*Online Supplementary Figure S1E*), with TRPV2 present in all WT samples. Eighty-seven of the identified proteins were detected exclusively or with more than a 2-fold increase in WT RBC, while 13 proteins were detected with more than a 2-fold increase in *Trpv2*-KO RBC (Figure 1C, *Online Supplementary Figure S1F*) by semiquantitative exponentially modified protein abundance index (emPAI) analysis. Next, we evaluated the frequency of the identified proteins by spectral counting and normalized the data to band 3 (Figure 1D). TRPV2 ranked at position 560, about 0.4% of band 3, 50% and 84% less than ferroportin and Piezo1, respectively. In addition to TRPV2 and Piezo1, other channels such as aquaporin1 and transmembrane channel like 8 (*Online Supplementary Figure S1D*) were identified. The KCa3.1 protein, on the other hand, seemed to be much less abundant, as we could identify only one KCa3.1 peptide in our experiments, which was below the threshold for unambiguous protein identification.

According to the proteomic profiling, Piezo1 and aquaporin1 proteins were present in equal amounts in murine RBC from *Trpv2*-KO and WT animals. In contrast, several proteins that affect ion and fluid homeostasis were significantly less abundant in *Trpv2*-KO RBC, including the STE20-like- and the WNK1-serine/threonine protein kinases SLK (in humans also dubbed SPAK) and WNK1 (Figure 1C). Both kinases regulate the Na^+-K^+-Cl^- symporter NKCC1 present in the erythrocyte membrane, resulting in the flux of NaCl and KCl into the cell with subsequent rehydration.[7] This mechanism would be attenuated in *Trpv2*-KO RBC with decreased WNK1, similar to renal cells that are also equipped with NKCC1 and WNK1 and in which WNK1 is inhibited under hypotonic conditions. Likewise, the significantly reduced amount of the casein kinase II (CKII)-α subunit (CSK21) in *Trpv2*-KO RBC (Figure 1C) could be part of mechanisms that compensate for the absence of TRPV2, as pharmacological inhibition of CKII-α causes shrinkage of RBC.[8]

Hematologic parameters from blood of *Trpv2*-KO and WT animals (Figure 1E), were not significantly different. However, when RBC were exposed to hypotonic solutions, keeping extracellular [Ca^{2+}] at 76 μM, hemolysis of *Trpv2*-KO RBC occurred at higher tonicity (Figure 1F). The relative tonicity at half maximal lysis (C_{50}) (Figure 1G) was 49.19±0.62 (WT, n=5) and 53.7±0.68 (*Trpv2*-KO, n=5; $P<0.0001$).

To isolate TRPV2 currents from murine RBC we applied the non-specific TRPV2 agonist 2-APB. Inward and outward currents with the outwardly rectifying current-voltage (IV) relationship typical of TRPV2 currents were recorded by whole cell patch-clamping (Figure 2A, B) or by a miniaturized patch system (Figure 2C, D). A fraction of these 2-APB-induced currents was blocked by ruthenium red. Similar, but much larger currents were recorded from COS-7 cells, which overexpress the murine *Trpv2* cDNA (*Online Supplementary Figure S2E*). Upon application of 2-APB, cytoplasmic [Ca^{2+}] increased in WT RBC (*Online Supplementary Figure S2A*). The Ca^{2+} increase was blocked in the presence of ruthenium red but could also be induced in *Trpv2*-KO RBC (*Online Supplementary Figure S2B-D*). 2-APB blocks TRPC6 and KCa3.1 present in RBC and acts on additional targets.[9] Thereby it may affect the RBC membrane potential and Ca^{2+}-signaling pathways independently of TRPV2 during monitoring cytoplasmic Ca^{2+}. As shown in COS-7 cells (*Online Supplementary Figures S2E-I* and *S3A*), which do not endogenously express TRPC6 or KCa3.1, the 2-APB-induced increase in cytosolic Ca^{2+} and plasma membrane currents required the presence of overexpressed mouse or human TRPV2. We therefore applied the more specific TRPV2 agonist Δ9-THC, which elicited Ca^{2+} influx in WT RBC; this influx was significantly reduced in *Trpv2*-KO RBC (Figure 2E, F) indicating that part of the Ca^{2+} increase was mediated by TRPV2. The antagonists of the G protein-coupled cannabinoid receptors type 1 (CB1) and type 2 (CB2), AM251 (AM) and JTE907 (JTE), had no effect on the Δ9-THC-elicited Ca^{2+}-response in WT RBC (Figure 2G, H), demonstrating that TRPV2 mediates a significant fraction of THC-elicited Ca^{2+} influx and that the action of THC on TRPV2 is direct, and not mediated by CB1 or CB2 receptors.

The primary sequences of human and mouse TRPV2 are 80.4% identical, but the antibody against mTRPV2 does not recognize the hTRPV2 protein. We therefore generated an antibody that recognizes the hTRPV2 protein by western blot (Figure 3A). Next, total eluates of anti-hTRPV2 affinity purifications from RBC membranes were analyzed by nano-LC-MS/MS that retrieved peptides covering 54.8% of the hTRPV2 primary sequence (*Online Supplementary Figure S1G*). In similar experiments but with an antibody for hTRPC6, TRPC6 was not detectable in human RBC by either western blot or nano-LC-MS/MS.

The cannabinoid TRPV2 agonists CBD and Δ9-THC

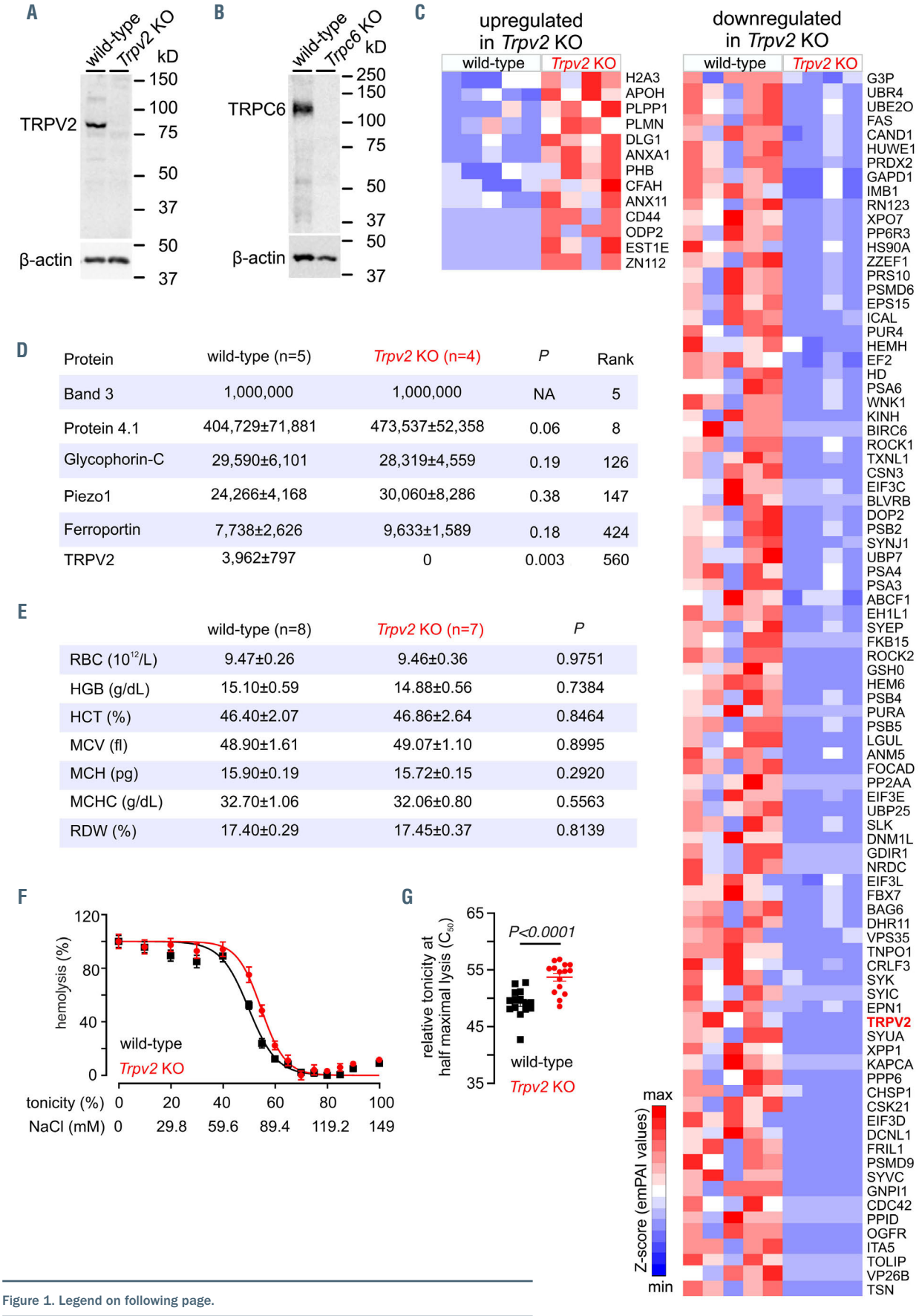

D

Protein	wild-type (n=5)	*Trpv2* KO (n=4)	*P*	Rank
Band 3	1,000,000	1,000,000	NA	5
Protein 4.1	404,729±71,881	473,537±52,358	0.06	8
Glycophorin-C	29,590±6,101	28,319±4,559	0.19	126
Piezo1	24,266±4,168	30,060±8,286	0.38	147
Ferroportin	7,738±2,626	9,633±1,589	0.18	424
TRPV2	3,962±797	0	0.003	560

E

	wild-type (n=8)	*Trpv2* KO (n=7)	*P*
RBC (10^{12}/L)	9.47±0.26	9.46±0.36	0.9751
HGB (g/dL)	15.10±0.59	14.88±0.56	0.7384
HCT (%)	46.40±2.07	46.86±2.64	0.8464
MCV (fl)	48.90±1.61	49.07±1.10	0.8995
MCH (pg)	15.90±0.19	15.72±0.15	0.2920
MCHC (g/dL)	32.70±1.06	32.06±0.80	0.5563
RDW (%)	17.40±0.29	17.45±0.37	0.8139

Figure 1. Legend on following page.

Figure 1. TRPV2 protein in mouse red blood cells. (A, B) Western blot of wild-type, *Trpv2* knockout (KO) (A) and *Trpc6* KO (B) red blood cell (RBC) proteins, using antibodies against mouse TRPV2, TRPC6 and β-actin. (C) Semi-quantitative analysis of differentially expressed proteins identified by mass spectrometry in wild-type and *Trpv2* KO RBC lysates. Up- and down-regulated proteins were identified based on at least 2-fold changes with a *P*-value <0.05, calculated by an unpaired two-tailed Student *t* test. The heatmap shows the Z-scores of the exponentially modified protein abundance index (emPAI) values of mass spectrometry measurements of five independent wild-type and four independent *Trpv2* KO samples. (D) Relative abundance of the TRPV2 protein compared to that of the 1,450 proteins identified in mouse erythrocyte membrane fractions. Rank represents the order of the identified protein obtained by spectral counting with the *P*-value calculated by an unpaired Student *t* test. NA, not applicable. (E) Hematologic parameters of the blood from wild-type and *Trpv2* KO. RBC: red blood cell; HGB: hemoglobin; HCT: hematocrit; MCV: mean corpuscular volume; MCH: mean corpuscular hemoglobin; MCHC: mean corpuscular hemoglobin concentration; RDW: red cell distribution width with *P*-value calculated by an unpaired two-tailed Student *t* test. (F) Hemolysis (%) of RBC collected from wild-type (black) and *Trpv2* KO mice (red) in buffer A (149 mM NaCl, 2 mM $CaCl_2$, 4 mM KCl, 2 mM HEPES, pH7.4), diluted 26-fold in buffer B (0-149 mM NaCl, 2 mM HEPES, pH 7.4) as indicated; extracellular [Ca^{2+}] was kept at ~76 μM. (G) Tonicity at which 50% lysis occurred (C_{50}), calculated by sigmoidal fitting from experiments in (F). Single values and mean ± standard error of mean from five independent experiments performed in triplicate are shown with the *P*-value calculated by an unpaired two-tailed Student *t* test.

elicited Ca^{2+} influx in human RBC (Figure 3B-D). Inward and outward currents with the outward rectifying IV relation were obtained by patch clamp recordings from human RBC after application of Δ9-THC (Figure 3E-G). Although the currents obtained from human RBC have a small amplitude, their IV match the TRPV2 current signature obtained from COS-7 overexpressing human TRPV2 cDNA upon application of Δ9-THC or CBD (*Online Supplementary Figure S3B, C*).

Assessment by confocal microscopy revealed that 95.3±2.4% of the human RBC had a biconcave disc-shaped form. Adding CBD or Δ9-THC shifted the morphology of these biconcave discocytes to concave RBC, the stomatocytes, which in the presence of CBD and Δ9-THC make up 92.7±1.3% (CBD) and 66.3±17.1% (THC) of the total RBC, the remaining cells being discocytes and more spherical-shaped spherocytes (Figure 3H, I). The TRPV2 agonist-induced shape change of the RBC was maintained in the presence of the CB1 and CB2 antagonists (*Online Supplementary Figure S3D, E*), indicating that the major fraction of the cannabinoids' effect on RBC morphology is mediated by TRPV2. After addition of Δ9-THC, human RBC showed reduced osmotic fragility, as demonstrated by the left-shifted hemolysis curve in response to the hypotonicity challenge, independently of whether cannabinoid receptor antagonists were absent or present (Figure 3J, K). Similarly, but to a lesser extent, Δ9-THC shifts the C_{50} value after treating WT murine RBC to lower tonicities (C_{50}, in the absence, 49.05±1.53, and in the presence of Δ9-THC, 46.08±1.55). This effect was reversed by pretreatment with the KCa3.1 antagonist TRAM-34, in the presence of 76 μM (*Online Supplementary Figure S3F, G*)

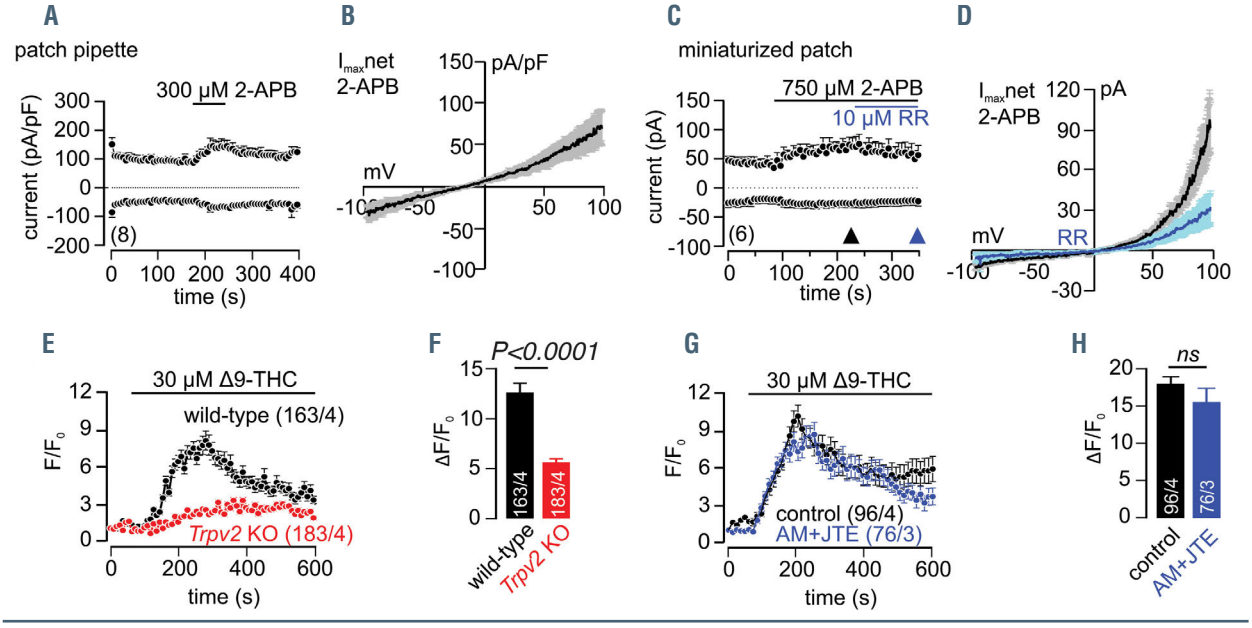

Figure 2. TRPV2 function in mouse red blood cells. (A-D) In- and outward currents at -80 and +80 mV shown as mean ± standard error of mean (SEM), recorded from mouse red blood cells (RBC) using a patch pipette (A) or a miniaturized patch clamp system (port-a-patch) (C) plotted *versus* time (number of cells in brackets). TRPV2 currents were activated by the application of 2-APB (black line) in the absence and presence of 10 μM ruthenium red (RR, blue line) with the corresponding current-voltage relationships (IV) at the peak net currents (I_{max} net), shown as mean ± SEM in (B) and (D). Patch pipette resistances were 10 - 15 MΩ when filled with standard internal solution (in mM): 120 Cs-glutamate, 8 NaCl, 1 $MgCl_2$, 10 HEPES, 10 1,2-bis(2-aminophenoxy)ethane-N,N,N',N'-tetraacetic acid tetracesium salt (Cs-BAPTA), 3.1 $CaCl_2$ (100 nM free Ca^{2+}, calculated with WebMaxC), pH7.2 with CsOH. Standard external solution contained (in mM): 140 NaCl, 2 $MgCl_2$, 1 $CaCl_2$, 10 HEPES, 10 glucose, pH 7.2 with NaOH. For experiments with the miniaturized patch system, the intracellular solution contained (in mM): 60 Cs-methansulfonate, 8 NaCl, 1 $MgCl_2$, 3.1 $CaCl_2$, 60 CsF, 10 HEPES, 10 BAPTA (100 nM free Ca^{2+}, calculated with WebMaxC), 10 glucose, pH 7.2 with CsOH and the extracellular solution contained (in mM): 140 NaCl, 2 $MgCl_2$, 1.35 $CaCl_2$, 10 HEPES, 10 glucose, pH 7.2 with NaOH. (E, G) Mean Fluo-4 fluorescence (F/F_0) traces showing changes in the cytosolic [Ca^{2+}] of RBC isolated from wild-type (black) and *Trpv2* KO mice (red) in the absence (E) and presence (G, blue) of the CB1/CB2-receptor antagonists AM251 and JTE907 (100 nM each), challenged by the application of 30 μM Δ9-tetrahydrocannabinol (Δ9-THC, line). Ca^{2+}-imaging measurements were performed in the presence of a Tyrode solution (in mM): 135 NaCl, 5.4 KCl, 1 $MgCl_2$, 10 HEPES, 10 glucose, and 1.8 $CaCl_2$, pH 7.35; RBC were loaded with 5 μM Fluo-4 and the fluorescence was excited at 488 nm every 3 seconds with the emitted fluorescence detected at >515 nm. (F, H) Summary of peak amplitudes from (E) and (G) shown as mean ± SEM with *P*-values calculated by the unpaired two-tailed Student *t* test (ns, not significant). Numbers of measured cells (x) within (y) independent experiments are indicated in brackets and bars.

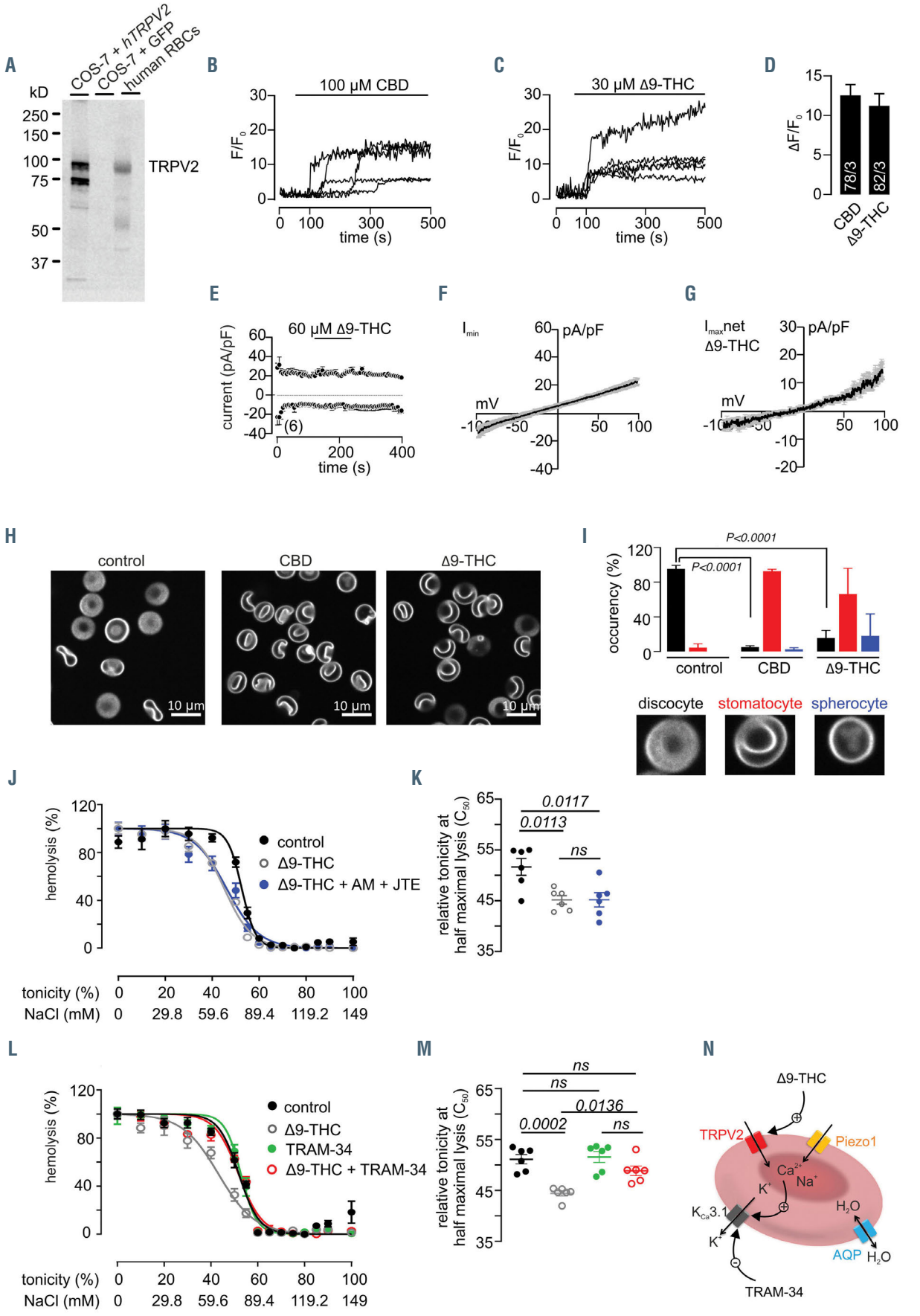

Figure 3. Legend on following page.

Figure 3. TRPV2 protein and function in human red blood cells. (A) Western blot of protein lysates of COS-7 cells transfected with human *TRPV2* cDNA, the cDNA of green fluorescent protein (GFP) as a control, and human red blood cells (RBC) using anti-human TRPV2. (B, C) Representative traces of cytosolic Ca^{2+} changes, detected as Fluo-4 fluorescence (F/F_0), in human RBC challenged by the application of 100 μM cannabidiol (CBD) (B) or 30 μM Δ9-tetrahydrocannabinol (Δ9-THC) (C). (D) Summary of the peak amplitudes in (B) and (C) as mean ± standard error of mean (SEM) (78 and 82 cells measured in 3 independent experiments each). (E) In- and outward currents at -80 and +80 mV in the absence and presence of Δ9-THC (black line) recorded from human RBC and plotted versus time. The corresponding current-voltage relationships (IV) of the basic current (I_{min}) and the peak net current in Δ9-THC (I_{max} net) are depicted in (F) and (G). Data are shown as mean ± SEM (number of cells indicated in brackets). (H) Confocal microscopic images of human RBC not treated (control, left) or treated with 100 μM cannabidiol (CBD, middle) or 30 μM Δ9-THC (right). (I) Bar graphs showing the percentage of discocytes (black), stomatocytes (red) and spherocytes (blue) as mean ± SEM, from three independent healthy donors, treated as in (H), with *P*-values calculated by one-way analysis of variance (ANOVA), followed by the Bonferroni multiple comparison. The classification was done with 3-D stacks of confocal images. (J) Hemolysis (%) of human RBC treated with the vehicle (control, black), 30 μM Δ9-THC (gray open circle) or 30 μM Δ9-THC in the presence of 100 nM CB1- and CB2-receptor antagonists AM251 and JTE907 (Δ9-THC + AM + JTE, blue) plotted *versus* the extracellular NaCl concentration (mM) and respective tonicity (%), with extracellular [Ca^{2+}] kept at 76 μM as described in Figure 1F. (K) Tonicity at which 50% lysis occurred (C_{50}), calculated by sigmoidal fitting of the individual experiments in (J). (L) Hemolysis (%) of human RBC in buffer A (149 mM NaCl, 2 mM $CaCl_2$, 4 mM KCl, 2 mM HEPES, pH 7.4), treated with vehicle (control, black), 30 μM Δ9-THC (gray open circle), 2 μM TRAM-34 (green) or 30 μM Δ9-THC plus TRAM-34 (red) for 30 min, after 26-fold dilution in buffer B (0-149 mM NaCl, 2 mM $CaCl_2$, 4 mM KCl, 2 mM HEPES, pH 7.4); extracellular [Ca^{2+}] was kept at 2 mM. (M) Tonicity at which 50% lysis occurred (C_{50}), calculated by sigmoidal fitting of the individual experiments in (L). Data in (K) and (M) are shown as means ± SEM from two independent experiments performed in triplicate with the *P*-value calculated by one-way ANOVA, followed by the Bonferroni multiple comparison. (N) Working model for how TRPV2, activated by Δ9-THC, modulates the TRAM-34 sensitive KCa3.1 activity in a human RBC. Note that TRPC6 was not detectable in human RBC.

or 2 mM extracellular Ca^{2+} (Figure 3L, M). The data indicate that TRPV2, like Piezo1 and, maybe TRPC6, enables an influx of cations including Ca^{2+}. The increase of intracellular Ca^{2+} by TRPV2 activates KCa3.1 which allows K^+ efflux, resulting in the shift of the hemolysis curve. This shift does not occur in the presence of the KCa3.1 antagonist TRAM-34 (Figure 3L-N).

Stabilization of the RBC membrane against hypotonic hemolysis by Δ9-THC and CBD has been described[10] and it has been shown that in the presence of Δ9-THC at concentrations of >15 μM almost all RBC assume a stomatocyte-like concave shape.[11] Some of those results were attributed to interactions between the hydrophobic, naturally occurring cannabinoids and the membrane lipids of the RBC. However, membrane partitioning experiments, electron spin resonance spectrometry and experiments with artificial liposomes of different compositions which were tested for the release of trapped markers in the presence of Δ9-THC, suggested additional mechanisms.[12-14]

The data described in our study point to TRPV2 being a specific molecular target for Δ9-THC and CBD in RBC. Activation of the TRPV2 channel by the compounds present in the *Cannabis sativa* plant makes RBC more resistant to lysis in response to hypotonic solutions. Whether our data explain why hemp products have been used in folk medicine to treat malaria since ancient times[15] needs to be shown by further studies.

Anouar Belkacemi,[1] Claudia Fecher-Trost,[1] René Tinschert,[1] Daniel Flormann,[2] Mahsa Malihpour,[1] Christian Wagner,[2,3] Markus R. Meyer,[1] Andreas Beck[1] and Veit Flockerzi[1]

[1]Experimentelle und Klinische Pharmakologie und Toxikologie und Präklinisches Zentrum für Molekulare Signalverarbeitung (PZMS), Universität des Saarlandes, Homburg, Germany; [2]Experimentalphysik, Universität des Saarlandes, Saarbrücken, Germany and [3]University of Luxembourg, Physics and Materials Science Research Unit, Esch-sur-Alzette, Luxembourg

Correspondence: VEIT FLOCKERZI - veit.flockerzi@uks.eu

doi:10.3324/haematol.2020.274951

Received: October 26, 2020.

Accepted: February 8, 2021.

Pre-published: February 18, 2021.

Disclosures: no conflicts of interest to disclose.

Contributions: ABelkacemi, CFT, RT, DF, MM, and ABeck performed experiments, ABelkacemi, CFT, DF, ABeck and VF analyzed data. MRM provided reagents. ABelkacemi, ABeck and VF conceived and supervised the study. CFT, ABeck, CW and MRM edited the manuscript. ABelkacemi and VF wrote the manuscript.

Acknowledgments: we thank Dr. Petra Weissgerber and the Transgene Unit of the SPF animal facility (project P2 of SFB 894) of the Medical Faculty, Homburg, for taking care of the mice; Christine Wesely, Martin Simon-Thomas, Oliver Glaser and Armin Weber for excellent technical assistance; Prof. Dr. Michael J. Caterina, the Johns Hopkins University (Baltimore) and the University of California San Francisco (UCSF), for providing the Trpv2 KO mouse strain.

Funding: the study was funded by the Deutsche Forschungsgemeinschaft (DFG) Collaborative Research Center 894 Project A3 (to ABelkacemi, VF) and A14 (to ABeck, VF) and FE 629/2-1 (to CFT).

References

1. Agre P, Preston GM, Smith BL, et al. Aquaporin CHIP: the archetypal molecular water channel. Am J Physiol. 1993;265(4 Pt 2):F463-476.
2. Cahalan SM, Lukacs V, Ranade SS, Chien S, Bandell M, Patapoutian A. Piezo1 links mechanical forces to red blood cell volume. Elife. 2015;4:e07370.
3. Maher AD, Kuchel PW. The Gardos channel: a review of the Ca^{2+}-activated K^+ channel in human erythrocytes. Int J Biochem Cell Biol. 2003;35(8):1182-1197.
4. Foller M, Kasinathan RS, Koka S, et al. TRPC6 contributes to the Ca^{2+} leak of human erythrocytes. Cell Physiol Biochem. 2008;21(1-3):183-192.
5. Hirschler-Laszkiewicz I, Zhang W, Keefer K, et al. Trpc2 depletion protects red blood cells from oxidative stress-induced hemolysis. Exp Hematol. 2012;40(1):71-83.
6. Pumroy RA, Samanta A, Liu Y, et al. Molecular mechanism of TRPV2 channel modulation by cannabidiol. Elife. 2019;8:e48792.
7. Zheng S, Krump NA, McKenna MM, et al. Regulation of erythrocyte $Na^+/K^+/2Cl^-$ cotransport by an oxygen-switched kinase cascade. J Biol Chem. 2019;294(7):2519-2528.
8. Kostova EB, Beuger BM, Klei TR, et al. Identification of signalling cascades involved in red blood cell shrinkage and vesiculation. Biosci Rep. 2015;35(2):e00187.
9. Hermosura MC, Monteilh-Zoller MK, Scharenberg AM, Penner R, Fleig A. Dissociation of the store-operated calcium current I(CRAC) and the Mg-nucleotide-regulated metal ion current MagNuM. J Physiol. 2002;539(Pt 2):445-458.
10. Chari-Bitron A. Stabilization of rat erythrocyte membrane by 1 - tetrahydrocannabinol. Life Sci II. 1971;10(22):1273-1279.
11. Chari-Bitron A, Shahar A. Changes in rat erythrocyte membrane induced by delta 1-tetrahydrocannabinol, scanning electron microscope study. Experientia. 1979;35(3):365-366.
12. Alhanaty E, Livne A. Osmotic fragility of liposomes as affected by antihelmolytic compounds. Biochim Biophys Acta. 1974;339(1):146-155.
13. Laurent B, Roy PE. Alteration of membrane integrity by delta1-tetrahydrocannabinol. Int J Clin Pharmacol Biopharm. 1975;12(1-2):261-266.
14. Leuschner JT, Wing DR, Harvey DJ, et al. The partitioning of delta 1-tetrahydrocannabinol into erythrocyte membranes in vivo and its effect on membrane fluidity. Experientia. 1984;40(8):866-868.
15. Touw M. The religious and medicinal uses of Cannabis in China, India and Tibet. J Psychoactive Drugs. 1981;13(1):23-34.

Rationale for the combination of venetoclax and ibrutinib in T-prolymphocytic leukemia

T-prolymphocytic leukemia (T-PLL) is an aggressive mature T-cell neoplasm that responds poorly to conventional chemotherapy and has a dismal outcome.[1] Patients with active T-PLL present with an exponential rise of post-thymic T cells with prolymphocytic morphology, hepatosplenomegaly, skin rash, lymphadenopathy, and effusions.[1] T-PLL cells commonly demonstrate rearrangements involving T-cell leukemia/lymphoma 1 (TCL1) family genes *TCL1A, MTCP1* (mature T-cell proliferation), or *TCL1B* as molecular hallmarks.[2] The anti-CD52 antibody alemtuzumab has improved initial responses up to 90%; however, nearly all cases eventually relapse, and allogeneic stem cell transplantation remains the only curative treatment option for a small subset of patients.[3]

Recently, we and others have demonstrated *in vitro* activity and clinical efficacy of the Bcl-2 inhibitor venetoclax as a single agent in relapsed/refractory T-PLL (r/r-T-PLL).[4,5] Since clinical responses were transient, we set out to identify effective combination partners for venetoclax. We probed putative mechanisms and demonstrated clinical feasibility and activity of a putative combination by treating two patients with active, r/r-T-PLL.

We employed combinatorial drug screening to identify synergistic combination partners to enhance the efficacy of venetoclax in T-PLL patients. Twenty-four candidate compounds were selected based on their clinical approval status, literature data, and mechanisms of drug action. Venetoclax was used in pairwise combinations (Figure 1A) in primary T-PLL samples with a mean post-thawing viability of 93% and mean purity of 94% (Table 1). Drug screening was performed as previously described.[4] Here ibrutinib demonstrated the strongest synergism with

Table 1. Characteristics of patients included in the high throughput combinatorial drugs screen. Overview of clinical and molecular characteristics as well as sample quality information for patients included in the combinatorial drug screen.

Patient ID	Sex	Age	Cytogenetics	FISH	TCL1A-expression	Consensus Dx	Tumor cell content (%)	Post thawing viability (%)
1	M	73	Complex karyotype	44,XY,-18,-22,der(6),t(6;22)(p?;q?),idic(6p?), idic(8)(q11),del(11)(q14),der(12),t(12;22)(q?;q?), der(13), t(13;14)(q?;q?),dup(15)(q22),der(15), t(15;18)(q?;q?)[cp5]; TCL1A rearrangement	Negative	**TCL1 positive T-PLL:** WBC >5x10^9/L, TCL1 rearrangement, complex karyotype, TCR rearrangement	93	89
2	F	58	Complex karyotype	NA	Negative	**TCL1 negative T-PLL:** WBC >5x10^9/L, complex karyotype, TCR-rearrangement	98	95
3	M	41	Complex karyotype	NA	Positive	**TCL1 positive T-PLL:** WBC >5x10^9/L, TCL1 expression, complex karyotype, TCR rearrangement	>90	95
4	M	76	NA	TCL1A rearrangement	Negative	**TCL1 positive T-PLL:** WBC > 5x10^9/L, TCL1 rearrangement, TCR rearrangement, splenomegaly, effusion	93	96
5	F	81	Complex karyotype	TP53_del MYB_del	Negative	**TCL1 negative T-PLL:** WBC > 5x10^9/L, complex karyotype, TCR-rearrangement	98	NA
6	F	67	Normal	TCL1A rearrangement ATM_del MYC_amp	Positive	**TCL1 positive T-PLL:** WBC >5x10^9/L, TCL1 rearrangement, TCR rearrangement, trisomy 8, ATM abnormality	99	89
7	M	64	NA	TLC1A rearrangement	Positive	**TCL1 positive T-PLL:** WBC > 5x10^9/L, TCL1 rearrangement, TCR rearrangement, effusion	90	NA

M: male; F: female; FISH: fluorescence *in situ* hybridization; WBC: white blood cell count; TCR: T-cell receptor; NA: not available.

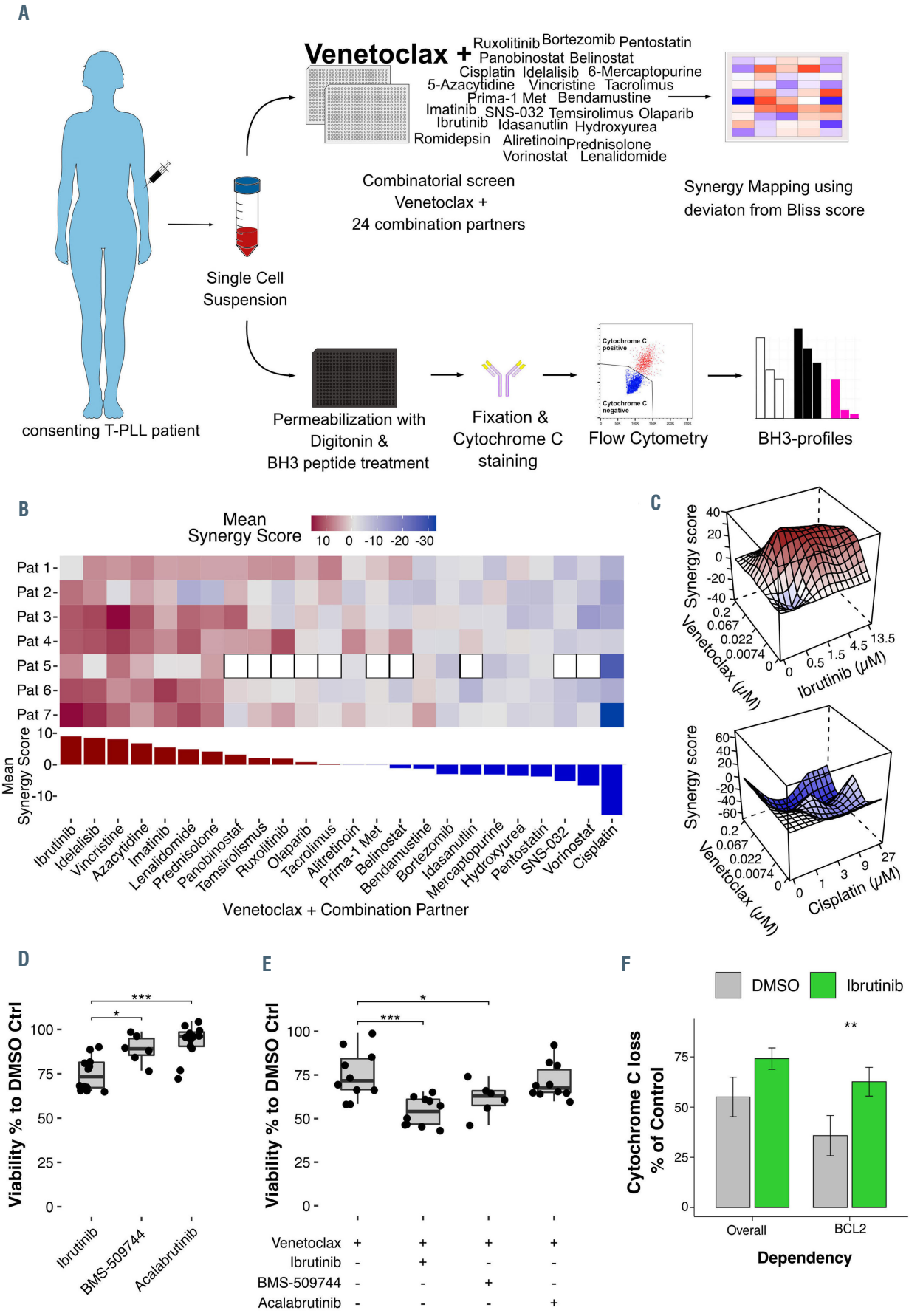

Figure 1. Legend on following page.

Figure 1. Ibrutinib synergizes with venetoclax in T-prolymphocytic leukemia via inhibition of ITK and enhances Bcl2-dependent apoptotic priming. (A) Single cell suspensions of blood or bone marrow samples were subjected to combinatorial drug screens with venetoclax and 24 potential combination partners. Deviation from the Bliss Independence score was evaluated for each combination. For BH3-profiling single cells were stained for cytochrome and analyzed by flow cytometry. (B) Heatmap demonstrating deviation from the Bliss independence score for each combination and individual patients (n=7). Synergy is denoted in red while antagonism is shown in blue. Clear boxes represent missing data for Patient 5 whose material was only screened for a subset of drugs due to sample availability. The bar plot in the lower half shows the synergy score as a mean over all patients. Drug synergy was calculated using the Synergy finder R package by integrating data of three independent runs (*Online Supplementary Figure S1B*). (C) A representative three-dimensional drug synergy plot (data from Patent 7) for ibrutinib and cisplatin with venetoclax. (D) Annexin V assay showing viability compared to that with a DMSO control for ibrutinib (n=12 different T-PLL patient samples), ITK-inhibitor BMS-509744 (n=6), and BTK-inhibitor acalabrutinib (n=12, Wilcoxon-Mann-Whitney test, ***P<0.001, *P<0.05, all compounds tested at 10 μM with drug exposure for 24 h under NKtert co-culture). (E) Annexin V assay demonstrating viability of T-PLL samples under NKtert co-culture treated with venetoclax alone (n=10), or in combination with ibrutinib (n=10), BMS-509744 (n=6), and acalabrutinb (n=10) compared to DMSO-Ctrl. (t-test,*P≤0.05, ***P<0.001, ibrutinib, acalabrutinib and BMS-509744 were used at a dose of 10 μM with drug exposure for 24 h, venetoclax was used at a dose of 100 nM with drug exposure for 4 h both as a single agent and in combination. After annexin V/Hoechst staining, cells were fixed with paraformaldehyde and analyzed using a BD Fortessa with a 96-well HTS plate-reader. NKTert cells were excluded using forward and side scatter parameters. Primary antibodies were directed against cytochrome c (Alexa Fluor 488-labeled, 6H2.B4/612308, Biolegend), CD19 (PE/Cy7-labeled, H13B19/302216, BioLegend), anti–CD5 (PE-labeled, UCHT2/300608, Biolegend). The analysis was performed on the CD5+CD19– cell fraction. (F) BH3-profiling in primary T-PLL samples treated with ibrutinib: cytochrome C release compared to control for overall mitochondrial priming and specific BCL2-dependence is shown for samples treated with either DMSO or ibrutinib 10 μM for 24 h (t-test,**P≤0.01). T-PLL: T-prolymphocytic leukemia; DMSO: dimethylsulfoxide; Ctrl. Control.

venetoclax, whereas cisplatin appeared the most antagonistic (Figure 1B and C, *Online Supplementary Figure S1B*). The activity of ibrutinib as a single agent was very modest (*Online Supplementary Figure S1A* and *B*), consistent with previous reports.[6] In addition, independent annexin V/Hoechst assays of primary T-PLL cells on NK-Tert stromal support demonstrated modest single-agent activity of ibrutinib (Figure 1D, *Online Supplementary Figure S2A*). Moreover, selective inhibition of Bruton tyrosine kinase (BTK) by acalabrutinib had no effect on viability (Figure 1D). In contrast, ibrutinib has substantial inhibitory activity on the intracellular mediator of T-cell receptor signaling IL-2-inducible T-cell kinase (ITK; half maximal inhibitory concentration [IC_{50}]: 2.2 nM), which has been reported to play a functional role in T-PLL.[5,7] In line with previous observations, single-agent treatment with BMS-509744, a specific ITK inhibitor, had no effect on viability in primary T-PLL samples (Figure 1D).[8]

To elucidate the mechanism of the combinatorial effect, we treated primary T-PLL samples with venetoclax alone and in combination with ibrutinib, BMS509744 or acalabrutinib. In contrast to BTK-specific inhibition, only drugs that inhibit ITK (ibrutinib, and BMS509744) enhanced Bcl2-inhibitor-induced cell death (Figure 1E). We performed dynamic BH3-profiling of primary T-PLL samples treated *ex vivo* with ibrutinib to elucidate changes in apoptotic priming. The assay measured cytochrome C release upon stimulation with BH3-mimetics as a readout for a cellular tendency towards apoptosis.[9] The data demonstrated enhanced overall mitochondrial priming for apoptosis and a shift to increased functional dependence on Bcl-2 for survival upon ibrutinib treatment (Figure 1F, *Online Supplementary Figure S2B*).

Based on our *in vitro* drug synergy findings, we initiated combined treatment with venetoclax and ibrutinib in two r/r-T-PLL patients after alemtuzumab-based therapy. Both patients presented with active disease after multiple treatment lines with no further standard treatment options available. We employed tandem mass spectrometry coupled to liquid chromatography (LC-MS/MS) to measure venetoclax and ibrutinib serum levels and *in vivo* BH3 profiling to evaluate overall and Bcl2-dependent apoptotic priming during treatment. The expression of phospho-ITK, ITK and BH3 family members was evaluated by immunoblotting of patients' cells obtained during treatment (Figure 2, *Online Supplementary Figure S3*).

Patient A (male, aged 78 years) was admitted with r/r-T-PLL after three previous treatment lines (alemtuzumab monotherapy, alemtuzumab + FCM [fluradabine, cyclophosphamide and mitoxantrone], rechallenged with alemtuzumab monotherapy). He presented with dyspnea, a white blood cell (WBC) count of 519x10^9/L, elevated lactate dehydrogenase (LDH; 5,230 U/L), fever, absolute lymphocytosis (472x10^9/L) and neutrophilia (42x10^9/L) (Figure 2A, *Online Supplementary Figure S3A*), and splenomegaly (diameter: 26 cm). Fluorescence *in situ* hybridization analyses of interphase nuclei revealed multiple cytogenetic aberrations (TCL1 and TCRA/D translocations, heterozygous deletions of several 6q and 13q loci, trisomies 8 and 12, duplication of the MLL locus as well as MYC amplifications), suggesting the presence of a complex aberrant karyotype. Venetoclax treatment was commenced with a daily ramp-up from 20 mg to 800 mg, which was well-tolerated. However, the clinical response was limited with the WBC count still above 300x10^9/L and LDH above 3,000 U/L after 2 weeks. When co-treatment with ibrutinib at a dose of 420 mg was initiated on day 16, both the WBC count and LDH decreased steadily (Figure 2A). The patient's overall clinical condition improved, and the spleen size decreased to 22 cm after 20 days of co-treatment. Serum levels of venetoclax and ibrutinib were continuously monitored. Interruption of ibrutinib on day 24 was associated with a rise of WBC count that declined after ibrutinib was reintroduced. The course of patient A was complicated by influenza A infection and subsequent bacterial pneumonia requiring multiple admissions to hospital, and mechanical respiratory support resulting in discontinuation of anti-T-PLL therapy. After resolution of the pneumonia, T-PLL therapy was reinitiated, however treatment adherence dropped, when the patient returned to his local treatment team who eventually switched to best supportive care.

Patient B (female, aged 75 years) had r/r-T-PLL that relapsed after initial therapy with CHOP (cyclophosphamide, doxorubicin, vincristine and prednisone) and was refractory to alemtuzumab. She presented with dyspnea, pleural effusion, a WBC count of 300x10^9/L, elevated LDH (581 U/L), and absolute neutrophilia (27x10^9/L) during alemtuzumab treatment (Figure 2B, *Online Supplementary Figure S3B*). The cytogenetic report demonstrated a complex karyotype including inv(14) and isochromosome 8q. Ibrutinib was started at a dose of 420 mg once daily before venetoclax daily at a dose increased from 20 mg to 400 mg. The combination of ibrutinib and venetoclax led to a rapid reduction of WBC count and LDH as well as an improvement of clinical status (Figure 2B). On day 26, the patient experienced a minimal subarachnoidal hemorrhage (grade 2). Ibrutinib was withheld but venetoclax continued. As serum levels of ibrutinib dropped to undetectable levels, a concomitant

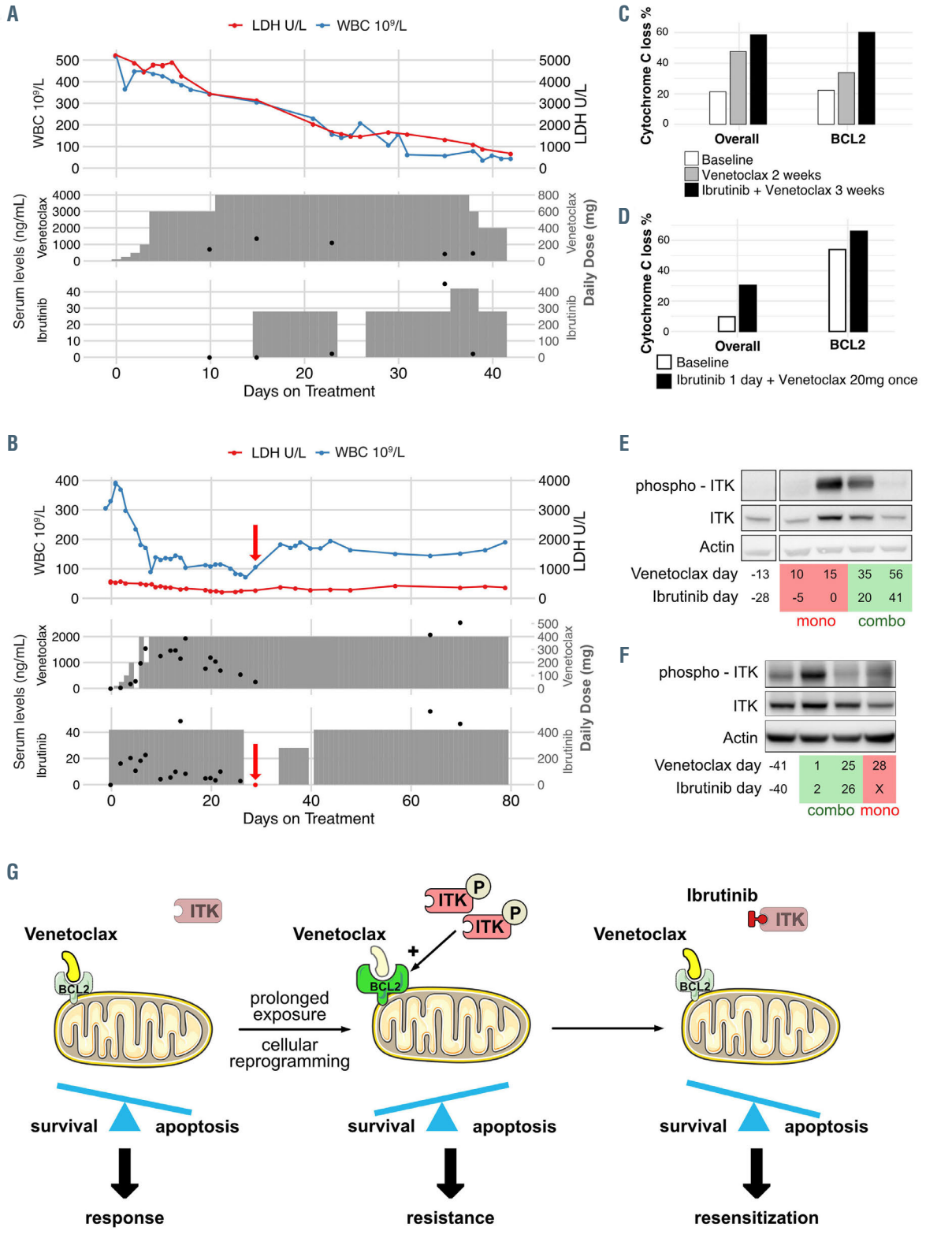

Figure 2. The combination of ibrutinib and venetoclax is clinically active in T-prolymphocytic leukemia. (A, B) Clinical follow-up of two patients treated with the combination of ibrutinib and venetoclax, patient A (A) and patient B (B). The WBC count and LDH concentration are plotted as blue and red lines, respectively. The lower part of each panel represents drug serum levels as black dots and drugs given as gray rectangles. Drug levels were determined by mass spectrometry. The red arrow denotes the time point at which the serum ibrutinib concentration dropped below the level of detection with a concomitant rise of WBC. (C, D) *In vivo* BH3 profiling of primary patients' samples during co-treatment: patient A (C) and patient B (D). (E, F) Western blot analysis of primary cells showing changes in protein levels of ITK and phospho-ITK during co-treatment of patient A (E) and patient B (F). Primary antibodies were directed against phospho-ITK (Tyr512, Life Technologies, #PA564523), ITK (Cell Signaling Technology, #2380S) and β-actin (Santa Cruz Biotechnology, #SC-47778) (G) Proposed mechanism. Monotherapy with venetoclax may lead to drug resistance via upregulation and activation of ITK and reduced apoptotic priming. ITK inhibition might increase Bcl-2-dependent apoptotic priming and restore the activity of venetoclax. WBC: white blood cell; LDH: lactate dehydrogenase.

increase of the WBC count was observed (Figure 2B). The hemorrhage resolved with supportive care, and ibrutinib was restarted, with stabilization of the WBC count. Three weeks later the patient died due to secondary bacterial pneumonia.

Despite high tumor burden neither patient showed signs of tumor lysis syndrome. In both patients, interruption of ibrutinib was associated with an increase of WBC count that declined (patient A) or stabilized (patient B) when ibrutinib was re-introduced. The clinical course of both patients was complicated by severe bacterial pneumonia which eventually led to treatment termination. The combination of venetoclax and ibrutinib had a tolerable safety profile but was associated with increased frequencies of neutropenia and respiratory infections in studies including patients with other hematologic diseases such as mantle cell lymphoma or chronic lymphocytic leukemia.[10,11] Both patients we treated had received alemtuzumab treatment as a re-induction attempt and experienced increased neutrophil counts (*Online Supplementary Figure S3A* and *B*). Thus, it is plausible that prior anti-CD52 could increase infectious complications of the combination.

In vivo dynamic BH3-profiling with samples from the two patients while on treatment showed a modest increase in overall apoptotic priming by ibrutinib, driven by an enhanced dependence on Bcl-2. This effect was further enhanced by venetoclax (Figure 2C and D), which is consistent with our *in vitro* data on T-PLL samples (Figure 1F). Immunoblotting analysis demonstrated that venetoclax treatment alone led to the induction of both phosphorylated and total ITK, an effect that was abrogated by the addition of ibrutinib as demonstrated in samples of patient A while on treatment (Figure 2E). In patient B, treatment with venetoclax was started 1 day after ibrutinib. ITK activity (phospho-ITK) decreased during treatment and regained activity upon interruption of ibrutinib treatment (Figure 2F). Intracellular T-cell receptor signaling via increased phospho-ITK expression is known to be associated with inferior prognosis in T-cell lymphomas, and ITK inhibition has been shown to prime apoptosis of malignant T cells by downregulating anti-apoptotic proteins, including Bcl-2, MCL-1, and Bcl-XL.[12] At the protein level, in patient A expression of Mcl-1 and Bcl-2 was induced during venetoclax monotherapy, but was reduced upon combinatorial treatment. In contrast, patient B showed a predominant induction of pro-apoptotic BH3 family members in response to combined ibrutinib and venetoclax treatment (*Online Supplementary Figure S3C* and *D*). However, previous research has shown that immunoblotting does not accurately reflect the clinical efficacy of BH3 mimetics.[9] Our previous report and data presented here suggest that exposure to venetoclax monotherapy leads to ITK activation and increased Bcl-2 and Mcl-1 expression, and Bcl-2 dependence with a suboptimal clinical response.[4] Co-treatment with venetoclax plus ibrutinib may reduce ITK activity, increase Bcl-2 dependence, and restore susceptibility to venetoclax (Figure 2G). Similarly, Mcl-1 inhibition has been shown to act synergistically with venetoclax in T-PLL cells.[13]

Our high-throughput screen identified ibrutinib as a synergistic combination partner for venetoclax in T-PLL. In this study, we favored synergy over potency, since we hypothesized that synergism would be associated with a more favorable clinical safety profile. Indeed, the combination of venetoclax and ibrutinib has been considered safe in other indications.[10,11] We acknowledge strong single-agent potency of other compounds such as the histone deacetylase inhibitor, panobinostat; however the added effect of its combination to venetoclax was negligible (*Online Supplementary Figure S1B*).

Recently, anecdotal cases of venetoclax combinatorial treatments of T-PLL patients have been published: In line with our findings Oberbeck *et al*. reported disease stabilization after short-term treatment of one patient with venetoclax plus ibrutinib, but progression after cessation of treatment.[14] Alfayez *et al*. treated one patient with venetoclax plus pentostatin who achieved complete remission for 10 months.[15] This combination, however, did not demonstrate synergism in our screen (Figure 1B), but future studies could determine a putative benefit for T-PLL patients.

Our *in vitro* studies demonstrated that the combination of venetoclax and ibrutinib increased T-PLL cell priming for apoptosis and Bcl-2 dependence. The combination produced clinical responses in two heavily pretreated patients with r/r-T-PLL and enhanced Bcl2-dependence *in-vivo* while reducing ITK activity. These results prompted the initiation of the first international multicenter clinical study in T-PLL, the phase II VIT-trial (NCT03873493) testing the combination of venetoclax and ibrutinib in r/r-T-PLL in a larger cohort of patients.

Christoph Kornauth,[1] Charles Herbaux,[2] Bernd Boidol,[3] Chantal Guillemette,[4] Patrick Caron,[4] Marius E. Mayerhöfer,[5] Stéphanie Poulain,[6] Olivier Tournilhac,[7] Tea Pemovska,[1] Stephen J.F. Chong,[2] Emiel van der Kouwe,[1] Lukas Kazianka,[1] Georg Hopfinger,[8] Daniel Heintel,[9] Roland Jäger,[10] Markus Raderer,[11] Ulrich Jäger,[1] Ingrid Simonitsch-Klupp,[12] Wolfgang R. Sperr,[1] Stefan Kubicek,[3] Matthew S. Davids[2#] and Philipp B. Staber[1#]

[#]MSD and PBS contributed equally as co-senior authors.

[1]Department of Medicine I, Division of Hematology and Hemostaseology, Medical University of Vienna, Vienna, Austria; [2]Department of Medical Oncology, Dana-Faber Cancer Institute, Harvard Medical School, Boston, MA, USA; [3]Center for Molecular Medicine (CeMM), Austrian Academy of Sciences, Vienna, Austria; [4]Centre Hospitalier Universitaire de Québec – Université Laval and Faculty of Pharmacy, Université Laval, Québec, Canada; [5]Department of Biomedical Imaging and Image-Guided Therapy, Medical University of Vienna, Vienna, Austria; [6]UMR CANTHER, INSERM 1277-CNRS 9020 UMRS 12, University of Lille, Hematology Laboratory, Biology and Pathology Center, CHU de Lille, Lille, France; [7]Service d'Hematologie Clinique et de Therapie Cellulaire, CHU, Universite Clermont Auvergne, EA7453 CHELTER, CIC1405, Clermont Ferrand, France; [8]3rd Medical Department, Centre for Oncology and Haematology, Kaiser Franz Josef-Spital, Vienna Austria; [9]1st Austria Medical Department, Center for Oncology and Hematology, Wilhelminenhospital Vienna, Vienna, Austria; [10]Department of Laboratory Medicine, Medical University of Vienna, Vienna, Austria; [11]Department of Medicine I, Division of Oncology, Medical University of Vienna, Vienna, Austria and [12]Clinical Department of Pathology, Medical University of Vienna, Vienna, Austria

Correspondence: PHILIPP B. STABER
philipp.staber@meduniwien.ac.at

doi:10.3324/haematol.2020.271304

Received: September 8, 2020.

Accepted: February 11, 2021.

Pre-published: February 25, 2021.

Disclosures: UJ and PBS have received honoraria and advisory board fees from Abbvie and Janssen. MSD has provided consultancy or scientific advisory board services for AbbVie, Adaptive Biotechnologies, Ascentage, AstraZeneca, Beigene, Celgene,

Genentech, Janssen, MEI Pharma, Pharmacyclics, Research to Practice, Syros Pharmaceuticals, TG Therapeutics, Verastem, and Zentalis, and has received institutional research funding from Ascentage, AstraZeneca, Genentech, MEI Pharma, Pharmacyclics, Surface Oncology, TG Therapeutics, and Verastem. The other authors have no conflicts of interest to disclose.

Contributions: CK, CH, BB, CG, PC, SJFC, LK and EK performed research; SP, OT, RJ, MEM and ISK provided material and performed expanded diagnostics on patients' samples; GH, WRS, DH, MR, UJ and PBS managed and treated patients; CK, CH, TP, SK, MSD and PBS analyzed the data; CK, TP, PBS wrote the manuscript; MSD and PBS supervised the study.

Acknowledgments: our screening compound libraries are from the NIH clinical collection, gifts from F. Bracher, T. Nielsen, S. Nijman, J. Bradner, The Broad Institute, and Haplogen GmbH.

Funding: we acknowledge funding from the Austrian Science Fund (FWF) TRANSCAN-2 grant ERANET-PLL I 4156B, FWF TRANSCAN-2 grant EuroTCLym I 4154B, FWF grant P27132-B20 (to PBS), Vienna Science and Technology Fund (WWTF) grant LS16-034 (to UJ)and the Anniversary Fund of the Oesterreichische Nationalbank (OeNB) grant P15936 (to PBS). We further acknowledge funding from the Canadian Institutes of Health Research (CIHR; FRN-152986 and FRN-408093 (to CG), and the Canada Research Chair Program. CG holds a Canada Research Chair in pharmacogenomics (Tier 1).

References

1. Staber PB, Herling M, Bellido M, et al. Consensus criteria for diagnosis, staging, and treatment response assessment of T-cell prolymphocytic leukemia. Blood. 2019;134(14):1132-1143.
2. Stengel A, Kern W, Zenger M, et al. Genetic characterization of T-PLL reveals two major biologic subgroups and JAK3 mutations as prognostic marker. Genes Chromosomes Cancer. 2016;55(1):82-94.
3. Wiktor-Jedrzejczak W, Drozd-Sokolowska J, Eikema DJ, et al. EBMT prospective observational study on allogeneic hematopoietic stem cell transplantation in T-prolymphocytic leukemia (T-PLL). Bone Marrow Transplant. 2019;54(9):1391-1398.
4. Boidol B, Kornauth C, Kouwe E van der, et al. First-in-human response of BCL-2 inhibitor venetoclax in T-cell prolymphocytic leukemia. Blood. 2017;130(23):2499-2503.
5. Andersson EI, Pützer S, Yadav B, et al. Discovery of novel drug sensitivities in T-PLL by high-throughput ex vivo drug testing and mutation profiling. Leukemia. 2018;32(3):774-787.
6. Dietrich S, Oleś M, Lu J, et al. Drug-perturbation-based stratification of blood cancer. J Clin Invest. 2018;128(1):427-445.
7. Dubovsky JA, Beckwith KA, Natarajan G, et al. Ibrutinib is an irreversible molecular inhibitor of ITK driving a Th1-selective pressure in T lymphocytes. Blood. 2013;122(15):2539-2549.
8. Dondorf S, Schrader A, Herling M. Interleukin-2-inducible T-cell kinase (ITK) targeting by BMS-509744 does not affect cell viability in T-cell prolymphocytic leukemia (T-PLL). J Biol Chem. 2015; 290(16):10568-10569.
9. Koch R, Christie AL, Crombie JL, et al. Biomarker-driven strategy for MCL1 inhibition in T-cell lymphomas. Blood. 2019;133(6):566-575.
10. Tam CS, Anderson MA, Pott C, et al. Ibrutinib plus venetoclax for the treatment of mantle-cell lymphoma. N Engl J Med. 2018; 378(13):1211-1223.
11. Jain N, Keating M, Thompson P, et al. Ibrutinib and venetoclax for first-line treatment of CLL. N Engl J Med. 2019;380(22):2095-2103.
12. Liu Y, Wang X, Deng L, et al. ITK inhibition induced in vitro and in vivo anti-tumor activity through downregulating TCR signaling pathway in malignant T cell lymphoma. Cancer Cell Int. 2019; 19(1):32.
13. Smith VM, Lomas O, Constantine D, et al. Dual dependence on BCL2 and MCL1 in T-cell prolymphocytic leukemia. Blood Adv. 2020; 4(3):525-529.
14. Oberbeck S, Schrader A, Warner K, et al. Noncanonical effector functions of the T-memory–like T-PLL cell are shaped by cooperative TCL1A and TCR signaling. Blood. 2020;136(24):2786-2802.
15. Alfayez M, Thakral B, Jain P, et al. First report of clinical response to venetoclax combination with pentostatin in T-cell-prolymphocytic leukemia (T-PLL). Leuk Lymphoma. 2020;61(2):445-449.

Stem cell yield and transplantation in transplant-eligible newly diagnosed multiple myeloma patients receiving daratumumab plus bortezomib/thalidomide/dexamethasone in the phase III CASSIOPEIA study

High-dose therapy (HDT) followed by autologous stem cell transplantation (ASCT) is the standard of care for transplant-eligible patients with newly diagnosed multiple myeloma (NDMM).[1,2] An adequate stem cell yield is essential for timely hematopoietic reconstitution after ASCT.[3] Daratumumab is a human immunoglobulin (Ig) Gκ monoclonal antibody targeting CD38 with a direct on-tumor[4-6] and immunomodulatory mechanism of action.[7-9] Multiple studies have demonstrated the clinical benefits of adding daratumumab to standard-of-care regimens or as monotherapy across lines of therapy in multiple myeloma.[10]

The phase III CASSIOPEIA study investigated daratumumab plus the standard-of-care regimen bortezomib/thalidomide/dexamethasone (D-VTd) *versus* bortezomib/thalidomide/dexamethasone (VTd) in ASCT-eligible patients with NDMM.[11] In part 1 of the study, patients received induction, ASCT, and consolidation therapy, which was followed by part 2 of the study where patients with a partial response or better after consolidation were re-randomized to receive maintenance therapy or observation. Here we report stem cell yield/harvest and transplantation results in part 1 of CASSIOPEIA.

The study design and eligibility criteria of CASSIOPEIA have been previously reported (*clinicaltrials gov. Identifier: NCT02541383*) (Figure 1).[11] Briefly, eligible patients were 18 to 65 years of age, had NDMM, had an Eastern Cooperative Oncology Group performance status of 0 to 2, and were candidates for HDT and ASCT. Major exclusion criteria included the following: hemoglobin concentration <7.5 g/dL; absolute neutrophil count $<1.0\times10^9$/L; platelet count $\leq50\times10^9$/L (or $<70\times10^9$/L if <50% of bone marrow nucleated cells were plasma cells); aspartate aminotransferase and alanine aminotransferase levels >2.5 times the upper limit of normal (ULN); total bilirubin level >1.5 times ULN; calculated creatinine clearance <40 mL/min; corrected serum calcium concentration >14 mg/dL (3.5 mmol/L); primary amyloidosis, monoclonal gammopathy of undetermined significance, smoldering multiple myeloma, solitary plasmacytoma, or Waldenström macroglobulinemia; previous systemic therapy or stem cell transplantation for any plasma cell dyscrasia; and grade ≥2 peripheral neuropathy or grade ≥2 neuropathic pain. All patients provided written informed consent; the trial was approved by Institutional Review Board/ethics committees at each site and was conducted in accordance with the Declaration of Helsinki, Good Clinical Practices, and applicable regulatory requirements.

Following induction, patients underwent stem cell

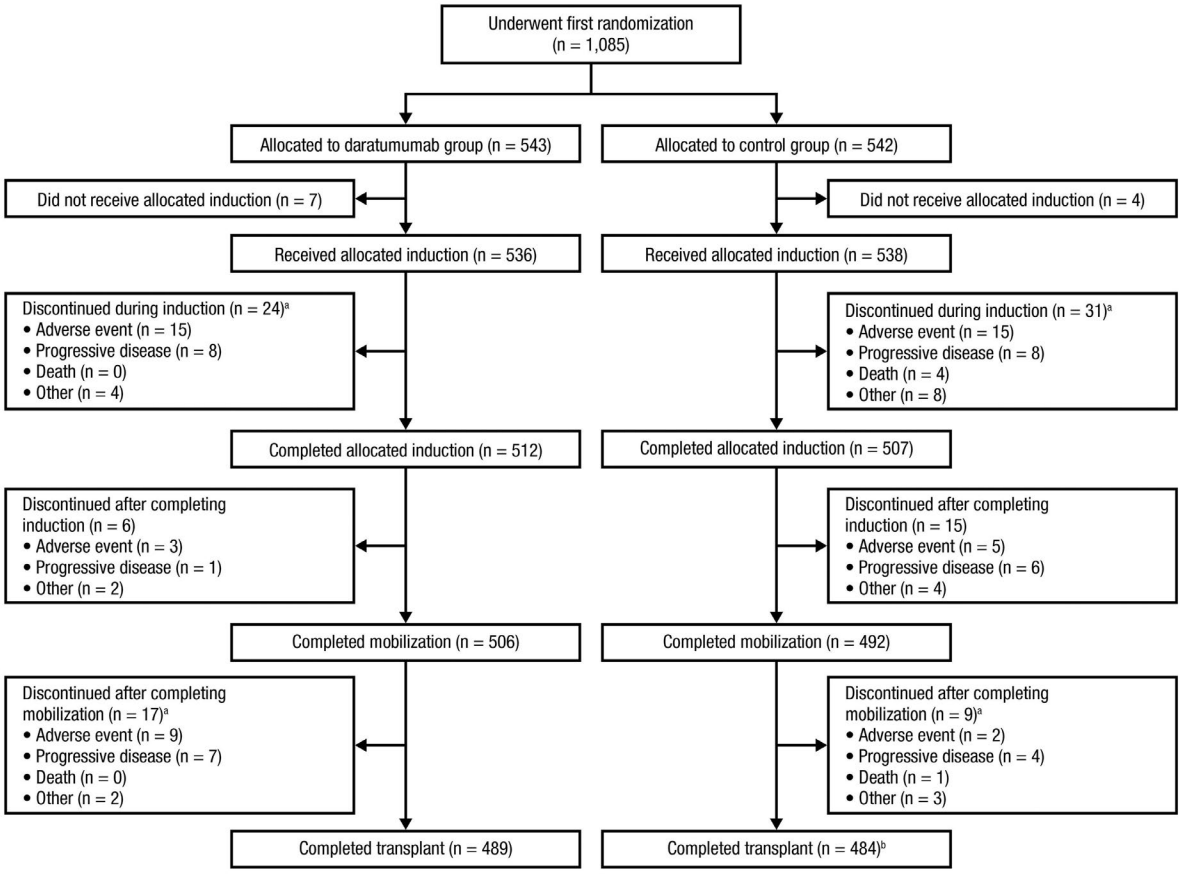

Figure 1. CONSORT diagram for the CASSIOPEIA study. The study flow diagram is shown for the CASSIOPEIA study from first randomization through completion of autologous stem cell transplant. The daratumumab group received daratumumab/bortezomib/thalidomide/dexamethasone; the control group received bortezomib/thalidomide/dexamethasone. Other: includes patient withdrawal, investigator decision, and others. [a]Reasons for discontinuation are not mutually exclusive. [b]One patient had successful CD34$^+$ stem cell collection without any previous mobilization treatment.

Table 1. Stem cell mobilization, harvesting, and transplantation.

	D-VTd	VTd	*P*
Patients with stem cell mobilization	**N=506**	**N=492**	
PBSC mobilizing agents, n (%)[a]			
Cyclophosphamide/G-CSF	506 (100)	492 (100)	
Plerixafor	110 (21.7)	39 (7.9)	<0.0001[b]
PBSC apheresis performed, n (%)	504 (99.6)[c]	490 (99.6)[d]	>0.999[b]
Patients with PBSC apheresis performed	**N=504**	**N=490**	
Number of days of apheresis, mean [SD] (range)	1.9 [0.92] (1–6)	1.4 [0.67] (1–4)	<0.0001[e]
Number of days of apheresis, n (%)			<0.0001[f]
1	184 (36.5)	327 (66.7)	
2	204 (40.5)	125 (25.5)	
3	91 (18.1)	32 (6.5)	
4	18 (3.6)	6 (1.2)	
5	4 (0.8)	0	
6	3 (0.6)	0	
Total number of $CD34^+$ stem cells collected (10^6/kg) among patients with PBSC apheresis performed			
Mean [SD] (range)	6.7 [2.63] (0.5–18.7)	10.0 [5.25] (2.2–36.9)	<0.0001[e]
≥2 × 10^6/kg, n (%)	501 (99.4)	490 (100)	0.2494[b]
≥4 × 10^6/kg, n (%)	444 (88.1)	470 (95.9)	<0.0001[b]
≥5 × 10^6/kg, n (%)	380 (75.4)	434 (88.6)	<0.0001[b]
Patients who underwent transplantation, n (%)	489 (97.0)	484 (98.8)	0.0758[b]
Number of $CD34^+$ stem cells transplanted (10^6/kg), Mean [SD] (range)	3.6 [1.59] (0.5–12.6)	5.0 [2.80] (1.2–23.3)	<0.0001[e]

Percentages were calculated with N in each group as the denominator. [a]Several PBSC mobilizing agents were possible. [b]*P*-value calculated from Fisher's exact test. [c]Bone marrow harvest was performed for one patient in the D-VTd arm and no patients in the VTd arm. No patients had only bone marrow collection. The D-VTd patient received a stem cell collection from bone marrow in addition to apheresis from peripheral blood. Here both numbers are summed as a total of $CD34^+$ stem cells collected from this patient. [d]Based on available information from the investigator, one patient in the VTd arm had successful $CD34^+$ stem cell collection without a record of mobilization treatment. However, unrecorded mobilization likely occurred, although details are undocumented. [e]*P*-value calculated from two-sample *t*-test. [f]*P*-value calculated from Cochran-Armitage trend test. D-Vtd: daratumumab/bortezomib/thalidomide/dexamethasone; Vtd: bortezomib/thalidomide/dexamethasone; PBSC: peripheral blood stem cell; G-CSF: granulocyte colony-stimulating factor; SD: standard deviation.

mobilization with cyclophosphamide (recommended dose, 3 g/m^2) and granulocyte colony-stimulating factor (G-CSF) (recommended dose, 10 μg/kg/day until the last day of the collection for a maximum of 10 days) after cycle 4. The recommended cyclophosphamide dose (3 g/m^2) was not mandatory and varied by region (e.g., more patients received 2 g/m^2 in the Netherlands and Belgium, while more received 3 g/m^2 in France). Plerixafor use was permitted per institutional practice in case of failure. Peripheral blood stem cells were harvested based on response to mobilization. Patients underwent conditioning with intravenous melphalan 200 mg/m^2 prior to ASCT. Per protocol, sufficient stem cells should be harvested to enable multiple transplants, in accordance with institutional standards. Cell counting after harvesting was conducted locally, per institutional practice. Consolidation therapy was initiated after hematopoietic reconstitution, but not earlier than 30 days after transplantation. Intergroupe Francophone du Myélome and Janssen statisticians were involved in all stages of the study and data analysis.

A total of 1,085 patients were randomized to D-VTd (n=543) or VTd (n=542) (Figure 1). Results for stem cell mobilization, harvesting, and transplantation are presented in Table 1. At the clinical cutoff of June 19, 2018, among those undergoing induction (D-VTd, n=536; VTd, n=538), 506 (94.4%) patients in the D-VTd group and 492 (91.4%) patients in the VTd group received cyclophosphamide/G-CSF; 504 (94.0%) and 490 (91.1%) patients, respectively, underwent stem cell harvesting. Plerixafor was administered in the course of stem cell mobilization to 110 patients (21.7% of the 506 patients who underwent mobilization) in the D-VTd group *versus* 39 patients (7.9% of the 492 patients who underwent mobilization) in the VTd group (*P*<0.0001). One patient who received VTd had no record of mobilization treatment but had successful collection of $CD34^+$ cells from peripheral blood in 2 consecutive days of apheresis; this patient received HDT with stem cell transplant with engraftment. One patient in the D-VTd group had stem cells collected from bone marrow in addition to apheresis from peripheral blood. Five patients (D-VTd, n=2; VTd, n=3) who received mobilizing agents did not undergo stem cell harvesting; of these, mobilization failure was noted in three patients (D-VTd, n=2; VTd, n=1). The two patients in the D-VTd group who failed mobilization underwent two mobilization procedures and failed both. The single patient in the VTd group who failed mobilization did not have a second procedure. The remaining two patients in the VTd group who received mobilizing agents did not undergo stem cell harvest and discontinued treatment due to death (n=1; serious adverse event of large intestine perforation with a history of sigmoid diverticulosis) or disease progression (n=1).

The mean number of days of apheresis were 1.9 for D-VTd *versus* 1.4 for VTd (*P*<0.0001; Table 1). Apheresis

Table 2. Stem cell transplantation outcomes.

Patients with transplantation	D-VTd N=489	VTd N=484	P
Patients with hematopoietic reconstitution, n (%)	488 (99.8)	482 (99.6)	0.6227[a]
Platelet recovery (achieving sustained platelets >20,000 cells/mm^3 without transfusion), n (%)	413 (84.5)	361 (74.6)	0.0001[a]
Number of days to achieve sustained platelets >20,000 cells/mm^3 without transfusion, mean [SD] (range)	14.9 [5.38] (2–56)	13.6 [4.64] (1–47)	0.0004[b]
Neutrophil recovery (achieving sustained absolute neutrophil counts >500 cells/mm^3), n (%)	475 (97.1)	474 (97.9)	0.5363[a]
Number of days to achieve sustained absolute neutrophil counts >500 cells/mm^3, mean [SD] (range)	14.4 [4.07] (6–54)	13.7 [4.20] (4–43)	0.0155[b]

D-Vtd: daratumumab/bortezomib/thalidomide/dexamethasone; Vtd: bortezomib/thalidomide/dexamethasone; SD: standard deviation. [a]*P*-value calculated from Fisher's exact test.[b]*P*-value calculated from two-sample *t*-test.

lasting 4-6 days occurred in 5.0% (25 of 504) and 1.2% (six of 490) of patients in the D-VTd and VTd groups who received apheresis. The mean number of CD34$^+$ stem cells collected was lower for patients receiving D-VTd versus VTd (6.7×10^6/kg *vs.* 10.0×10^6/kg, respectively; *P*<0.0001; Table 1). Nevertheless, among those who received apheresis, a similar percentage of D-VTd-treated patients and VTd-treated patients underwent ASCT (97.0% *vs.* 98.8%, respectively; *P*=0.0758; Table 1). Of the patients who completed mobilization without receiving transplant, the most common reasons for discontinuation were adverse events in the D-VTd group (D-VTd, n=8; VTd, n=2) and disease progression in the VTd group (D-VTd, n=7; VTd, n=4).

ASCT was undergone by 489 patients in the D−VTd-group and 484 patients in the VTd group. The mean number of CD34$^+$ stem cells transplanted was 3.6×10^6/kg in the D-VTd group compared with 5.0×10^6/kg in the VTd group (*P*<0.0001; Table 1). Hematopoietic reconstitution rates were high and similar in transplanted patients receiving D-VTd and VTd (99.8% *vs.* 99.6%, respectively; *P*=0.6227; Table 2). The mean (standard deviation) time to achieve sustained platelet counts >20,000 cells/mm^3 without transfusion was 14.9 days for D-VTd *versus* 13.6 days for VTd (*P*=0.0004), and the mean time to achieve sustained absolute neutrophil counts >500 cells/mm^3 was 14.4 days for D-VTd *versus* 13.7 days for VTd (*P*=0.0155; Table 2). Despite the greater mean number of days needed to achieve sustained platelet counts >20,000 cells/mm^3 without transfusion and absolute neutrophil counts >500 cells/mm^3 with D-VTd *versus* VTd, the percentage of patients who achieved platelet recovery was higher with D-VTd (84.5% *vs.* 74.6%; *P*=0.0001) and the percentages of patients who achieved neutrophil recovery were similar between the two treatment groups (97.1% *vs.* 97.9%; *P*=0.5363; Table 2).

Although there was lower stem cell yield and higher plerixafor use in the D-VTd group, the addition of daratumumab to VTd did not impair the feasibility and safety of performing transplant or the success of engraftment post transplant. Potential reasons why daratumumab results in lower stem cell yield in this study are unknown; however, daratumumab may possibly cause some degree of interference through an unknown mechanism, as CD34$^+$ committed stem cells express a low level of CD38.[12] Factors that have previously been demonstrated to impact yield, such as age, sex and weight, are not specifically associated with daratumumab or daratumumab-treated patients.[13,14] Close monitoring and early implementation of plerixafor could be considered for patients with risk factors for lower yield.[15]

Differences between treatment arms reached statistical significance for several parameters of stem cell mobilization, harvesting, and transplant. However, these differences were ultimately not clinically relevant, as post-transplant hematopoietic reconstitution was nearly identical (99.8% *vs.* 99.6%) in both treatment arms. Transplantation should be managed on an individual basis and with clinical judgment considering the overall situation of the patient.

In conclusion, the addition of daratumumab to VTd during induction therapy did not impair the feasibility and safety of transplantation with successful engraftment, even though stem cell yield was lower with D-VTd. Combined with the primary efficacy and safety data reported previously, D-VTd is considered a valid treatment option for patients with NDMM who are transplant-eligible.

Cyrille Hulin,[1] Fritz Offner,[2] Philippe Moreau,[3] Murielle Roussel,[4] Karim Belhadj,[5] Lotfi Benboubker,[6] Denis Caillot,[7] Thierry Facon,[8] Laurent Garderet,[9] Frédérique Kuhnowski,[10] Anne-Marie Stoppa,[11] Brigitte Kolb,[12] Mourad Tiab,[13] Kon-Siong Jie,[14] Matthijs Westerman,[15] Jérôme Lambert,[16] Lixia Pei,[17] Veronique Vanquickelberghe,[18] Carla de Boer,[19] Jessica Vermeulen,[19] Tobias Kampfenkel,[19] Pieter Sonneveld,[20] and Niels W.C.J. van de Donk[21] on behalf of the Intergroupe Francophone du Myélome (IFM) and Dutch-Belgian Cooperative Trial Group for Hematology Oncology (HOVON)

[1]*Department of Hematology, Hôpital Haut-Lévêque, University Hospital Bordeaux, Pessac, France;* [2]*Hematology, University Hospital Ghent, Ghent, Belgium;* [3]*Service d'Hématologie Clinique, University Hospital Hôtel-Dieu, Nantes, France;* [4]*Service d'Hématologie Clinique, /IUC Oncopole, Toulouse, France;* [5]*Hémopathies Lymphoïdes, Hôpital Henri Mondor, Creteil, France;* [6]*CHU de Tours, Hôpital de Bretonneau, Tours, France;* [7]*CHU Dijon, Hôpital Du Bocage, Dijon, France;* [8]*University of Lille, CHU Lille, Service des Maladies du Sang, Lille, France;* [9]*Sorbonne Université, INSERM, UMR_S 938, Centre de Recherche Saint-Antoine, Team Proliferation and Differentiation of Stem Cells, Assistance Publique-Hôpitaux de Paris, Hôpital Pitié Salpetrière, Département d'Hématologie, Paris, France;* [10]*Institut Curie Paris, Paris, France;* [11]*Institut Paoli-Calmettes, Marseille, France;* [12]*CHU de Reims, Hôpital Robert Debré, Reims, France;* [13]*CHD Vendée, La Roche-sur-Yon, France;* [14]*Zuyderland MC, Sittard, the Netherlands;* [15]*Northwest Clinics, Alkmaar, the Netherlands;* [16]*Biostatistical Department, Hôpital Saint Louis, Paris, France;* [17]*Janssen Research & Development, LLC, Raritan, NJ, USA;* [18]*Janssen Research & Development, Beerse, Belgium;* [19]*Janssen Research & Development, LLC, Leiden, the Netherlands;* [20]*Erasmus University Medical Center Cancer Institute, Rotterdam, the Netherlands and* [21]*Amsterdam UMC, Vrije Universiteit Amsterdam, Department of Hematology, Amsterdam, the Netherlands*

Correspondence:

CYRILLE HULIN - cyrille.hulin@chu-bordeaux.fr

doi:10.3324/haematol.2020.261842

Received: June 9, 2020.

Accepted: February 18, 2021.

Pre-published: March 4, 2021.

Disclosures: CH has received honoraria from Celgene, Janssen, Amgen, and Takeda; and travel, accommodations, and expenses from Celgene, Janssen, and Amgen. PM has received honoraria from and served as a consultant or in an advisory role for Celgene, Janssen, Amgen, and AbbVie. MR has received research funding from Amgen, Janssen, Takeda, and Celgene; travel, accommodation, and expenses from Amgen, Janssen, Celgene, Takeda, and Sanofi; and lecture fees from Amgen, Janssen, Celgene, and Takeda. KB has received personal fees from Celgene, Amgen, Takeda, and Janssen. TF has severed as a consultant or in an advisory role, participated in a speakers' bureau, and received travel, accommodations, or expenses from Janssen. LG has served as a consultant or in an advisory role for Amgen, Celgene, Takeda, Novartis, and Janssen. A-MS has received honoraria from Janssen, Celgene, Amgen, Novartis, and Takeda. LP, VV, CB, JV and TK are employees of Janssen Research & Development. PS has received research funding and/or honoraria from Amgen, Celgene, Janssen, Karyopharm, and Bristol Myers Squibb. NWCJD has served as a consultant or in an advisory role for Janssen, Celgene, Bristol Myers Squibb, Amgen, Novartis, Bayer, Servier, and Takeda; and has received research funding from Janssen, Celgene, Bristol Myers Squibb, Amgen, and Novartis. FO, LB, DC, BK, MT, K-SJ, MW and JL have nothing to disclose.

Contributions: CH, FO, PM, MR, KB, LB, DC, TF, LG, FK, A-MS, BK, MT, K-SJ, MW, PS, and NWCJvdD enrolled patients and collected data; NWCJvdD, JL, LP, VV, CdB, JV, and TK analyzed the data. All authors interpreted the data, contributed to the drafting and critical review of the manuscript, and approved the final version for submission. Janssen Research & Development, LLC, the Intergroupe Francophone du Myélome (IFM), and the Dutch-Belgian Cooperative Trial Group for Hematology Oncology (HOVON) collaborated to design the study.

Acknowledgments: the Intergroupe Francophone du Myélome (IFM) and Dutch-Belgian Cooperative Trial Group for Hematology Oncology (HOVON) sponsored this trial. This analysis was funded by Janssen Global Services, LLC. The authors, IFM, HOVON, and Janssen gratefully acknowledge the valued scientific contribution from Dr. Brigitte Kolb. Dr. Kolb passed away on the 5th of October, 2020, and will be dearly missed by the research teams that she contributed to or led. The authors would also like to thank the patients who participated in this study and their families, study investigators, staff members at each study site, and staff members involved in data collection and analyses. Medical writing and editorial support were provided by Kimberly Carmony, PhD, and Grace Wang, PharmD, of MedErgy, and were funded by Janssen Global Services, LLC.

References

1. Moreau P, San Miguel J, Sonneveld P, et al. Multiple myeloma: ESMO Clinical Practice Guidelines for diagnosis, treatment and follow-up. Ann Oncol. 2017;28(Suppl_4):iv52-iv61.
2. Mikhael J, Ismaila N, Cheung MC, et al. Treatment of multiple myeloma: ASCO and CCO joint clinical practice guideline. J Clin Oncol. 2019;37(14):1228-1263.
3. Corso A, Caberlon S, Pagnucco G, et al. Blood stem cell collections in multiple myeloma: definition of a scoring system. Bone Marrow Transplant. 2000;26(3):283-286.
4. Overdijk MB, Verploegen S, Bogels M, et al. Antibody-mediated phagocytosis contributes to the anti-tumor activity of the therapeutic antibody daratumumab in lymphoma and multiple myeloma. MAbs. 2015;7(2):311-321.
5. Overdijk MB, Jansen JH, Nederend M, et al. The therapeutic CD38 monoclonal antibody daratumumab induces programmed cell death via Fcgamma receptor-mediated cross-linking. J Immunol. 2016; 197(3):807-813.
6. de Weers M, Tai YT, van der Veer MS, et al. Daratumumab, a novel therapeutic human CD38 monoclonal antibody, induces killing of multiple myeloma and other hematological tumors. J Immunol. 2011;186(3):1840-1848.
7. Krejcik J, Casneuf T, Nijhof IS, et al. Daratumumab depletes CD38+ immune-regulatory cells, promotes T-cell expansion, and skews T-cell repertoire in multiple myeloma. Blood. 2016;128(3):384-394.
8. Adams HC III, Stevenaert F, Krejcik J, et al. High-parameter mass cytometry evaluation of relapsed/refractory multiple myeloma patients treated with daratumumab demonstrates immune modulation as a novel mechanism of action. Cytometry A. 2019;95(3):279-289.
9. Casneuf T, Adams HC III, van de Donk N, et al. Deep immune profiling of patients treated with lenalidomide and dexamethasone with or without daratumumab. Leukemia. 2021;35(2):573-584.
10. DARZALEX® (daratumumab) injection, for intravenous use [package insert]. Horsham, PA: Janssen Biotech, Inc. 2020. https://www.janssenlabels.com/package-insert/product-monograph/prescribing-information/DARZALEX-pi.pdf
11. Moreau P, Attal M, Hulin C, et al. Bortezomib, thalidomide, and dexamethasone with or without daratumumab before and after autologous stem-cell transplantation for newly diagnosed multiple myeloma (CASSIOPEIA): a randomised, open-label, phase 3 study. Lancet. 2019;394(10192):29-38.
12. Ma X, Wong SW, Zhou P, et al. Daratumumab binds to mobilized CD34+ cells of myeloma patients in vitro without cytotoxicity or impaired progenitor cell growth. Exp Hematol Oncol. 2018;7:27.
13. Ungerstedt JS, Watz E, Uttervall K, et al. Autologous hematopoietic stem cell transplantation in multiple myeloma and lymphoma: an analysis of factors influencing stem cell collection and hematological recovery. Med Oncol. 2012;29(3):2191-2199.
14. Ings SJ, Balsa C, Leverett D, Mackinnon S, Linch DC, Watts MJ. Peripheral blood stem cell yield in 400 normal donors mobilised with granulocyte colony-stimulating factor (G-CSF): impact of age, sex, donor weight and type of G-CSF used. Br J Haematol. 2006; 134(5):517-525.
15. Shah EE, Young RP, Wong SW, et al. Impact of plerixafor use at different peripheral blood CD34(+) thresholds on autologous stem cell collection in patients with multiple myeloma. Biol Blood Marrow Transplant. 2020;26(5):876-883.

The significance of gradient expression of chromosome region maintenance protein 1 in large cell lymphoma

Tumor cells depend on nuclear export of macromolecules to sustain their survival.[1] Chromosome region maintenance protein1 (CRM1), encoded by the *XPO1* gene, is the principle receptor mediating the nuclear efflux of proteins.[1] CRM1 (XPO1) is overexpressed in tumor cells to facilitate the increased demand for nuclear export of tumor suppressor proteins, leading to enhanced cell survival.[1-3] The intensity of CRM1 expression has an independent prognostic value in several solid tumors and in acute myeloid leukemia where high-expression was associated with an inferior survival.[2,4] Studies evaluating the presence and degree of CRM1 expression in diffuse large B-cell lymphoma (DLBCL) with respect to prognosis are limited. This topic is important given the recent approval of selinexor, a first-in-class small molecule inhibitor of CRM1, for the treatment of relapsed and/or refractory (R/R) DLBCL without the requirement to demonstrate tumor CRM1 expression.[5] Therefore, we assessed the gradient expression of CRM1 in DLBCL with respect to outcomes in patients treated with anti-CD20 antibody based chemoimmunotherapy.

The study was conducted in accordance with the Declaration of Helsinki following Institutional Review Board approval at Mayo Clinic, Rochester, MN. Patients with DLBCL, primary mediastinal (thymic) large B-cell lymphoma and high-grade B-cell lymphoma with *MYC* and *BCL2* and/or *BCL6* rearrangements from the Molecular Epidemiology Resource (MER) cohort at the Mayo Clinic and the University of Iowa were eligible. Paraffin embedded tumor tissue obtained prior to the initiation of treatment from patients who were subsequently treated with chemoimmunotherapy was assessed for CRM1 expression through immunohistochemistry (IHC) on a tissue microarray (TMA) by using a CRM1 monoclonal antibody. Standard slide preparation from paraffin blocks was performed and staining was done in the following order: i) CRM1 (Cell Signaling, catalog-no: 46249, dilution 1:100), ii) MACH 3™ Rabbit Probe HRP Polymer Kit (Biocare Medical, Walnut Creek, CA), iii) R-Polymer HRP: MACH 3™ Rabbit Probe HRP Polymer Kit (Biocare Medical, Walnut Creek, CA, USA), iv) Chromogen: DAB+ (DakoCytomation, Carpinteria, CA, USA), v) two 5-minute incubations with water rinse. Hemotoxylin was used as the counter stain. CRM1 expression by tumor cells was graded based on comparing tumor cell CRM1 staining to background, non-malig-

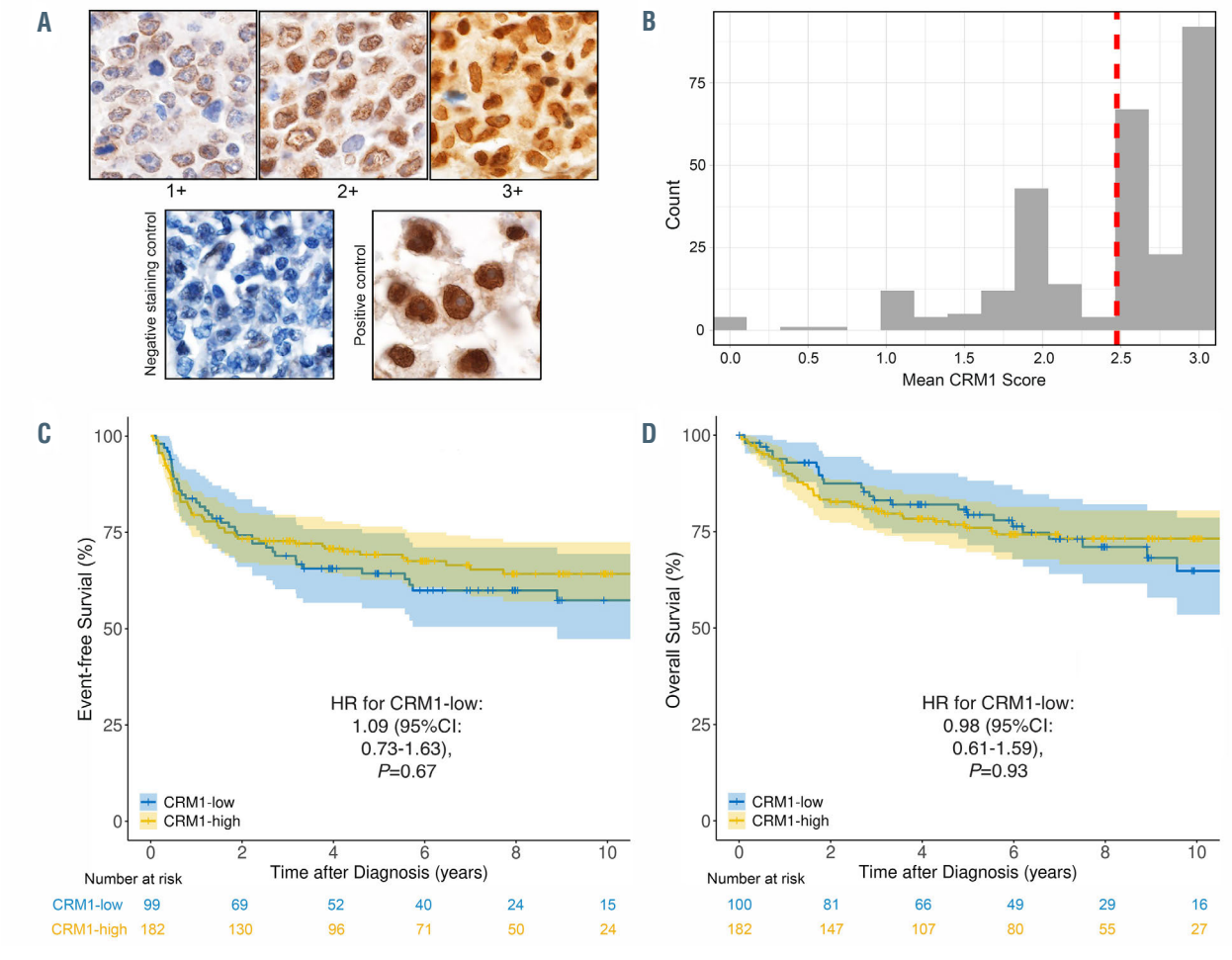

Figure 1. Distribution of the scores of histopathology grading of CRM1 expression on tumor tissue and the prognosis of patients with large-cell lymphoma based on CRM1 protein expression on primary tumor cells. (A) Spectrum of chromosome region maintenance protein1(CRM1) expression on tumor tissue assessed via immunohistochemistry; (B) histogram showing the distribution of the mean expression scores of CRM1, median score for the entire population was 2.5 (vertical red dashed line); ©event-free survival based on high and low CRM1 expression; (D) overall survival based on high and low CRM1 expression.

Table 1. Baseline characteristics of patients with large-cell lymphoma based on CRM1 protein expression on primary tumor cells.

Variable	CRM1-low (N=100)	CRM1-high (N=182)	*P*
Sex, n, (%)			0.827
Female	42 (42.0)	74 (40.7)	
Male	58 (58.0)	108 (59.3)	
Diagnosis Age			0.239
Median, years, (range)	59.0 (20.0 - 84.0)	61.5 (18.0 - 93.0)	
Subtype, n, (%)			0.7
DLBCL	98 (98.0)	177 (97.3)	
Mediastinal large B-cell	2 (2.0)	5 (2.7)	
Initial Treatment, n, (%)			0.845
MR-CHOP	6 (6.0)	16 (8.8)	
Other IC	4 (4.0)	3 (1.6)	
R-CHOP	66 (66.0)	122 (67.0)	
R-EPOCH	16 (16.0)	23 (12.6)	
R-HYPERCVAD	1 (1.0)	3 (1.6)	
R2-CHOP	6 (6.0)	12 (6.6)	
RAD-RCHOP	1 (1.0)	2 (1.1)	
RCHOP/Zevalin	0 (0.0)	1 (0.5)	
Stage Group n, (%)			0.751
I-II	42 (42.0)	80 (44.0)	
III-IV	58 (58.0)	102 (56.0)	
LDH Group n, (%)			0.454
Missing/unknown	15	17	
≤ Normal n, (%)	47 (55.3)	83 (50.3)	
> Normal n, (%)	38 (44.7)	82 (49.7)	
ECOG PS Group			0.707
< 2	81 (81.0)	144 (79.1)	
≥ 2	19 (19.0)	38 (20.9)	
Num. Extranodal Group n, (%)			0.658
≤ 1	85 (85.0)	151 (83.0)	
> 1	15 (15.0)	31 (17.0)	
IPI n, (%)			0.692
0	17 (17.0)	27 (14.8)	
1	29 (29.0)	43 (23.6)	
2	26 (26.0)	51 (28.0)	
3	19 (19.0)	41 (22.5)	
4	9 (9.0)	17 (9.3)	
5	0 (0.0)	3 (1.6)	
Cell of origin per Hans criteria			0.236
Missing/unknown	28	38	
GCB n, (%)	40 (55.6)	92 (63.9)	
non-GCB n, (%)	32 (44.4)	52 (36.1)	
Cell of origin per Nanostring			0.934
Missing/unknown	52	84	
ABC n, (%)	16 (33.3)	32 (32.7)	
GCB n, (%)	32 (66.7)	66 (67.3)	
MYC Double Hit (FISH) n, (%)			0.617
Missing/unknown	8 (8.0)	10 (5.5)	
Negative	89 (89.0)	164 (90.1)	
Positive	3 (3.0)	8 (4.4)	

ABC: activated B-cell; CRM1: chromosome region maintenance protein1; DLBLC: diffuse large B-cell lymphoma; IPI: international prognostic index; GCB: germinal center B-cell; FISH: fluorescent in-situ hybridization; LDH: lactate dehydrogenase; MR-CHOP: methotrexate, rituximab, cyclophosphamide, doxorubicin, vincristine, prednisone; RCHOP: rituximab, cyclophosphamide, doxorubicin, vincristine and prednisone; R-EPOCH: rituximab, etoposide, prednisone, vincristine, cyclophosphamide and doxorubicin; R-HYPERCVAD: rituximab, cyclophosphamide, vincristine, doxorubicin and dexamethasone; R2-CHOP: revlimid, rituximab, cyclophosphamide, doxorubicin, vincristine and prednisone; RAD-RCHOP: radiation with rituximab, cyclophosphamide, doxorubicin, vincristine and prednisone.

nant lymphocytes (negative control) and renal cell carcinoma (positive control; known to have a high CRM1 expression).[6] Two expert hematopathologists (RLK, AJW) independently scored CRM1 nuclear staining and assigned a score of 0-3; 0 (no nuclear staining; equal to non-malignant background cells), 1 (dim/weak nuclear staining but greater than background), 2 (moderate nuclear staining with nuclear detail still visible behind the stain) and 3 (strong nuclear staining obscuring most nuclear detail; staining intensity equivalent to renal cell carcinoma), Figure 1A. The average CRM1 score per case across all available cores on the TMA was calculated and the median CRM1 score for the entire cohort was 2.5. Low and high-CRM1 expression were defined as scores of 0-2.4 (CRM1-low) and 2.5-3.0 (CRM1-high), respectively. Scoring reliability between reviewers and between cores was assessed and an intra-class correlation coefficient of 0.75-0.90 was defined as "good scoring reliability". All time-to-event analyses were conducted from the time of diagnosis. Event-free survival (EFS) was defined as time from diagnosis to progression, retreatment, or death. The association of CRM1 expression and risk of failing to achieve EFS at 24 months after diagnosis (EFS24) was estimated using odds ratios (OR) and 95% Confidence Intervals (CI) from logistic regression models, while the association of CRM1 expression with continuous EFS and overall survival (OS) was estimated using Kaplan-Meier method and hazard ratios (HR) and 95% CI were calculated through Cox regression models.

Eighteen DLBCL TMA with optimal overlap with ongoing sequencing projects were used. After excluding non-chemoimmunotherapy treated patients, tumor tissue cores from 282 patients were analyzed (Table 1). The median age was 61 years (range, 18-93) and 166 (59%) were males. The median follow-up was 88.6 months (95% CI: 82.9-95.5). Quantitative expression of CRM1 was detected in 99% of cases (score of 1 or higher, n=278); therefore the intensity of CRM1 expression was assessed with respect to patient outcomes. One-hundred patients (35%) were categorized in to the CRM1-low intensity cohort; 182 (65%) patients were in the CRM1-high cohort, (Figure 1B). The intra-class correlation coefficient to measure scoring reliability of CRM1 expression was 0.79, meeting the criteria of good reliability between the hematopathologists.

There were no differences in International Prognostic Index (IPI), performance score, lactate dehydrogenase level, age, high-risk disease (double or triple-hit lymphoma), cell-of-origin, or treatment modality at diagnosis between the CRM1-high and the CRM1-low cohorts, (Table 1). The EFS24 was similar in the CRM1-high cohort (30%) compared to CRM1-low cohort (27%), OR 1.09, 95% CI: 0.73-1.63; *P*=0.67, (Figure 1C). The OS was not different between cohorts (Figure 1D). The EFS and OS results were similar when adjusted for age, sex, IPI, cell-of-origin, and MYC, BCL2 and BCL6 protein expression and rearrangement status (*data not shown*).

CRM1 is being exploited as a therapeutic target in cancer.[1] The recent United States Food and Drug Administration approval of selinexor for the treatment of R/R DLBCL was based on an overall response rate of 28% with single-agent selinexor suggesting the potential that the intensity level of CRM1 expression may have prognostic significance.[5] In a prior study in DLBCL, the qualitative expression level of CRM1 was an independent negative prognostic marker which associated with higher clinical stage and inferior OS.[7] However, that study was small (n=131), limited by short follow-up (median was not reported; range, 14-65 months), and heterogeneous treatments with nearly half of the patients receiving chemotherapy instead of the current standard of chemoimmunotherapy.[8] A second study assessed the expression of CRM1 by using a polyclonal-antibody in patients with DLBCL who were treated with chemoimmunotherapy and reported inferior OS associated with high-level of CRM1 expression in activated B-cell or double-expresser types.[9] The median follow-up of the patients was not mentioned in that study and the OS was lower than typical real-world patients with DLBCL treated with chemoimmunotherapy.[10] Importantly, the frequency of CRM1 expression in tumor cells in that study was low at only 40% of cases. This result differs from our study where 99% of cases were CRM1 positive but with variable intensity. The low expression level in that study is surprising given that CRM1/XPO1 is a protein critical for normal cellular function and is expected to be present in all cells to varying degrees.[11] Our study utilized a monoclonal-antibody in contrast to the polyclonal-antibodies used in the two prior studies. In general, monoclonal-antibodies are preferred for clinical use due to their improved specificity for a given epitope.[12] While technical differences in IHC protocols may contribute to different staining outcomes, we hypothesize that CRM1 polyclonal-antibodies may have lower sensitivity in detecting the particular epitope of CRM1 as compared to monoclonal-antibodies, accounting for the differences in positivity rates across DLBCL.

The expression of CRM1 in solid tumors has also been assessed in the past and shown a negative prognostic value with high CRM1 expression.[2] The heterogeneity of tumor biology, patient populations, and treatments may contribute to the disparate findings between solid cancers and ours here in DLBCL. The prevalence of *XPO1* mutation has been documented in DLBCL to be 2-4%, in which the majority were *XPO1*^{E571K} mutation.[13,14] In primary mediastinal B-cell lymphoma and Hodgkin lymphoma, the prevalence of *XPO1*^{E571K} is close to 25% in some studies.[15] Moreover, the *XPO1*^{E571K} mutation has been shown to promote lymphomagenesis and cellular proliferation, alter nuclear cytoplasmic compartmentation of CRM1, and better sensitize cells for CRM1 inhibitors *in vitro* and *in vivo*.[1] The relatively low prevalence of *XPO1* mutation in LCL, and lack of whole exome sequencing (WES) data on our current patient population prevented us from assessing the prognostic significance of *XPO1* mutations in LGL. However, future studies that include WES data on large LCL patient populations may be able to shed further light on this matter.

Strengths of our study include a large dataset, all patients received standard chemoimmunotherapy in a real-world setting, uniform assessment of CRM1 expression using a monoclonal-antibody, independent interpretation by two expert hematopathologists, and long follow-up. We report that CRM1/XPO1 protein is expressed in virtually all DLBCL but the difference in expression intensity did not predict outcomes in patients treated with regimens not containing the CRM1/*XPO1*-inhibitor, selinexor. Limitations of our study include that, although we have used easily reproducible methods to assess CRM1 expression in tumor cells with good scoring reliability between the two reviewers, the intensity grading algorithm used has not been tested among larger numbers of pathologists. However, based on differences in staining intensities (Figure 1) we demonstrated, there may be potential for this assay to be used in future prospective trials to learn if intensity predicts response to CRM1/*XPO1*-inhibitor treatment. This issue has not been described in any of the clinical trials which have

used selinexor to-date. The aggressive lymphoma field needs treatment selection factors now more than another marker of overall prognosis. We recommend that CRM1 staining and intensity grading be included in ongoing and future clinical trials to learn if CRM1 intensity predicts selinexor response.

Jithma P. Abeykoon,[1] Paul J. Hampel,[1*] Rebecca L. King,[2*] Adam J. Wood,[2*] Melissa C. Larson,[3*] Kevin E. Nowakowski,[1] Saurabh S. Zanwar,[1] Surendra Dasari,[3] Gordon J. Ruan,[1] Aishwarya Ravindran,[2] Linda E. Wellik,[1] Jonas Paludo,[1] Brian K. Link,[4] James R. Cerhan,[3] Stephen M. Ansell,[1] Grzegorz S. Nowakowski,[1] Carrie A Thompson,[1] Matthew J. Maurer,[3] Kerstin Wenzl,[1] Anne J. Novak,[1] Xiaosheng Wu,[1] Thomas M. Habermann[1] and Thomas E. Witzig[1]*

[1]Division of Hematology, Department of Internal Medicine, Mayo Clinic, Rochester, MN; [2]Division of Hematopathology, Department of Laboratory Medicine and Pathology, Mayo Clinic, Rochester, MN; [3]Department of Health Sciences Research, Mayo Clinic, Rochester, MN and [4]Division of Hematology, University of Iowa, Iowa City, IA, USA

**JPA, PJH, RLK, AJW and MCL contributed equally as co-first authors.*

Correspondence:

THOMAS E. WITZIG - witzig.thomas@mayo.edu

doi:10.3324/haematol.2020.278277

Received: December 30, 2020.

Accepted: February 23, 2021.

Pre-published: March 4, 2021.

Disclosures: TEW served on an advisory board meeting in 2018 and 2020 for Karyopharm Pharmaceuticals-personally compensated and serves on other advisory boards but none have any bearing on the subject of this manuscript; MM serves on the advisory board of MorphoSys, Kite Pharama, Pfizer, and receives research funding (to Mayo Clinic) from Celgene, NanoString Technologies, Genetech and Morphosys; SMA receives research funding (to Mayo Clinic) from Bristol Myers Squibb, Seattle Genetics, Takeda, Regeneron, ADC Therapeutics, Affimed, Trillium, and AI Therapeutics; BKL serves as a consultant for Genentech and MEI inc. The rest of the authors declare no competing financial interests.

Contributions: JPA, PJH, RLK, AJW, XW, TMH and TEW conceptually designed the study; JPA, PJH, RK, AJW, MCL, KEN, SSZ, SD, GJR, JP, BKL, JRC, SMA, GSN, CAT, KW, AJN, MJM, AR acquired analyzed and interpreted data; RLK, AJW were the expert pathologists; LEW performed IHC staining.

Funding: this work was funded by ASCO Conquer Cancer Young Investigator Award, supported by The Hearst Foundation. Any opinions, findings, and conclusions expressed in this material are those of the author(s) and do not necessarily reflect those of the American Society of Clinical Oncology®, Conquer Cancer®, or The Hearst Foundation. This research was also supported in part by the University of Iowa/Mayo Clinic Lymphoma SPORE (CA97274), the Mayo Clinic and the Predolin Foundation Biobank.

References

1. Taylor J, Sendino M, Gorelick AN, et al. Altered nuclear export signal recognition as a driver of oncogenesis. Cancer Discov. 2019; 9(10):1452-1467.
2. Yue L, Sun ZN, Yao YS, et al. CRM1, a novel independent prognostic factor overexpressed in invasive breast carcinoma of poor prognosis. Oncol Lett. 2018;15(5):7515-7522.
3. Abeykoon JP, Paludo J, Nowakowski KE, et al. The effect of CRM1 inhibition on human non-Hodgkin lymphoma cells. Blood Cancer J. 2019;9(3):24.
4. Kojima K, Kornblau SM, Ruvolo V, et al. Prognostic impact and targeting of CRM1 in acute myeloid leukemia. Blood. 2013;121(20):4166-4174.
5. Kalakonda N, Maerevoet M, Cavallo F, et al. Selinexor in patients with relapsed or refractory diffuse large B-cell lymphoma (SADAL): a single-arm, multinational, multicentre, open-label, phase 2 trial. Lancet Haematol. 2020;7(7):e511-e522.
6. Inoue H, Kauffman M, Shacham S, et al. CRM1 blockade by selective inhibitors of nuclear export attenuates kidney cancer growth. J Urol. 2013;189(6):2317-2326.
7. Luo B, Huang L, Gu Y, et al. Expression of exportin-1 in diffuse large B-cell lymphoma: immunohistochemistry and TCGA analyses. Int J Clin Exp Pathol. 2018;11(12):5547-5560.
8. Coiffier B, Lepage E, Brière J, et al. CHOP chemotherapy plus rituximab compared with CHOP alone in elderly patients with diffuse large B-cell lymphoma. N Engl J Med. 2002;346(4):235-242.
9. Deng M, Zhang M, Xu-Monette ZY, et al. XPO1 expression worsens the prognosis of unfavorable DLBCL that can be effectively targeted by selinexor in the absence of mutant p53. J Hematol Oncol. 2020;13(1):148.
10. Maurer MJ, Ghesquieres H, Jais JP, et al. Event-free survival at 24 months is a robust end point for disease-related outcome in diffuse large B-cell lymphoma treated with immunochemotherapy. J Clin Oncol. 2014;32(10):1066-1073.
11. Nguyen KT, Holloway MP, Altura RA. The CRM1 nuclear export protein in normal development and disease. Int J Biochem Mol Biol. 2012;3(2):137-151.
12. Lipman NS, Jackson LR, Trudel LJ, Weis-Garcia F. Monoclonal versus polyclonal antibodies: distinguishing characteristics, applications, and information resources. ILAR J. 2005;46(3):258-268.
13. Chapuy B, Stewart C, Dunford AJ, et al. Molecular subtypes of diffuse large B cell lymphoma are associated with distinct pathogenic mechanisms and outcomes. Nat Med. 2018;24(5):679-690.
14. Reddy A, Zhang J, Davis NS, et al. Genetic and functional drivers of diffuse large B cell lymphoma. Cell. 2017;171(2):481-494.e15.
15. Miloudi H, Bohers É, Guillonneau F, et al. XPO1(E571K) Mutation modifies exportin 1 localisation and interactome in B-cell lymphoma. Cancers (Basel). 2020;12(10):2829.

Ibrutinib interferes with innate immunity in chronic lymphocytic leukemia patients during COVID-19 infection

Severe acute respiratory syndrome coronavirus 2 (SARS-CoV-2) is a novel coronavirus that from December 2019 is spreading throughout the world causing a pandemic of Coronavirus Disease 2019 (COVID-19).[1] COVID-19 is characterized by severe activation of inflammatory response that is thought to be a major cause of disease severity and death. Immune response to COVID-19 infection is constituted by two steps: during the phase of incubation, an adaptive immune response is able to control virus proliferation preventing disease progression. In the later phase, an uncontrolled inflammatory response could determine major clinical complications. This response, known as cytokine storm, is induced by the activation of T cells, natural killer (NK) cells, monocytes/macrophage, neutrophils and any cells that run into the virus itself or degrade viral products. During the cytokine storm TNF-α, IFN-γ, IL-1β, IL-6, IL-12 and IL-17 are of crucial importance.[2] Given the aberrant response of immune cells to viral infection, acute respiratory distress syndrome appears to be the most acute and fatal event of this disease. It's evident that COVID-19 poses several challenges to the management of patients with hematologic malignancies since patients appear to be vulnerable to COVID-19.[3] Chronic lymphocytic leukemia (CLL) is the most common leukemia in Western countries that mainly affects older people. CLL is characterized by several clinical complications related to alterations in the immune system. Predisposition to infections in CLL patients includes both immunodeficiency related to the leukemia itself and the results of cumulative immunosuppression caused by treatments. Given these evidences CLL patients might represent a high-risk group for SARS-CoV-2 infection and the outcome of patients needed admission is poor with high mortality rate.[4] As supposed by different studies, BTK inhibitors (BTKi), in particular ibrutinib, may have a possible protective effect against lung injury in patients with COVID-19, tempering the hyper-inflammatory state.[5,6] Some different retrospective studies, in particular an observational study conducted in Europe identified treatment with ibrutinib or BTKi as a factor associated with better outcome during COVID-19, with a shorter hospitalization of CLL patients. On the contrary, a similar study conducted in US did not confirm this observation. Of importance, BTKi treatment was interrupted at the onset of COVID-19 in the majority of cases.[4,7] On this line, even though off-label administration of acalabrutinib in patients with severe COVID-19 had demonstrated reduction of the host inflammatory immune response and improved clinical outcomes, the CALAVI phase II trial for acalabrutinib in patients hospitalized with respiratory symptoms did not meet the primary efficacy endpoint of increasing the proportion of patients who remained alive and free of respiratory failure (*https://www.astrazeneca.com/media-centre/press-releases/2020/update-on-calavi-phase-ii-trials-for-calquence-in-patients-hospitalised-with respiratory-symptoms-of-covid-19.html*).[8] Ibrutinib exerts an immunomodulatory action, both on innate and adaptive immunity, sustaining a Th1 polarization and, at the same time, an anti-inflammatory polarization of macrophages.[9,10]

In the present study, we examined the modulation of ibrutinib treatment on the cytokine release by T cells and monocytes in CLL patients during infection with SARS-CoV-2.

Blood samples from patients that matched standard diagnostic criteria for CLL were obtained from the Hematology Unit of Modena Hospital, Italy with a protocol approved by the local Institutional Review Board and adhered to the tenets of the Declaration of Helsinki. Peripheral blood mononuclear cells (PBMC) were isolated and used fresh or cryopreserved until use. This study was performed on samples isolated from CLL patients who have not experienced SARS-CoV-2 infection. PBMC isolated from CLL patients were treated with ibrutinib or vehicle then stimulated with SARS-CoV-2 Peptide Pools Protein S, S1, S+, N and M (Miltenyi Biotech) and analyzed using cytokine secretion assay (CSA) for TNF-α and IFN-γ (Miltenyi Biotech). In order to identify the monocytic and T-cell population, PBMC were stained with CD14 and CD3 antibody respectively. For the *ex vivo* analysis, PBMC from CLL patients before and after 3 months of ibrutinib therapy were collected and stored in liquid nitrogen. PBMC were stimulated with SARS-CoV-2 Peptide Pools Protein and monocytes or T cells were identified by staining with CD14 or CD3. Secretion of TNF-α and IFN-γ was analyzed by CSA. Conditioned media were collected by centrifugation at 1,600 rpm for 10 minutes and stored at -20°C before being assayed. The levels of IL-6 were determined by human enzyme linked immunosorbent assay kit high sensitivity (Abcam). All data are presented as mean ± standard error of the mean. The *t*-test or Wilcoxon matched-pair signed rank test were used to determine statistical significance (GraphPad v6, GraphPad Software Inc).

CLL is typically characterized by perturbations of the immune system, involving both innate and adaptive immune responses. Firstly, we examined the impact of SARS-CoV-2 infection *in vitro* on the adaptive and innate immunity in CLL collected from treatment-naïve patients. As shown in Figure 1, following stimulation with SARS-CoV-2 peptides, we measured a strong and significant release of pro-inflammatory cytokines both by $CD3^+$ T cells and $CD14^+$ monocytes characterized by significant increase of TNF-α and IFN-γ secretion (*P<0.05; **P<0.01). Then, we analyzed if treatment with ibrutinib can modify the immunological response during infection. Ibrutinib targets T cells by irreversibly binding Tec family kinase, ITK, skewing toward Th1 phenotype and affecting Th2 immunity.[9] ITK is critically involved in T-cell-mediated immune response and depletion of its expression impairs influenza virus replication.[11] As shown in Figure 1A and B and in the *Online Supplementary Figure S1* ibrutinib did not determine a significant alteration in TNF-α secretion either in presence or absence of stimulation with SARS-CoV-2 peptides (P=not significant [ns]), in addition secretion of IFN-γ was not altered by ibrutinib and after stimulation we detected a slight increase (*P<0.05). Ibrutinib targets BTK in CLL-derived macrophages (nurse-like cells [NLC]) potentiating its immunosuppressive M2-skewed features.[10] BTK inhibition hampered the inflammatory response of NLC during *A. fumigatus* infection.[12] According to this evidence, we aimed to characterize the response of CLL monocytes to SARS-CoV-2 in the presence of ibrutinib. As reported in Figure 1C and D and in the *Online Supplementary Figure S1*, ibrutinib strongly impaired the release of TNF-α and IFN-γ by CLL monocytes induced by SARS-CoV-2 (*P<0.05). IL-6 is one of the key mediators of inflammation and cytokine storm in COVID-19 patients. Therefore, we measured the amount of secreted IL-6 in conditioned media collected after stimulation with sSARS-CoV-2 peptides either in the presence or absence

of ibrutinib treatment. As shown in Figure 1E, SARS-CoV-2 caused an increased release of IL-6 in the conditioned media (*P<0.05) that was significantly mitigated by BTK inhibition (*P<0.05).

Furthermore, we planned to analyze *ex vivo* matched samples isolated from CLL patients before treatment and after 3 months of treatment with ibrutinib comparing the response of $CD3^+$ and $CD14^+$ cells to SARS-CoV-2. Our data did not show any significant modification in pro-inflammatory cytokines release by CD3 during treatment with ibrutinib (Figure 2A and B; *Online Supplementary Figure S2*; P=ns). On the contrary, the secretion of TNF-α and IFN-γ by monocytes measured during the first 3 months of therapy was significantly reduced as compared to pre-treatment condition (Figure 2C and D; *Online Supplementary Figure S2*; *P<0.05).

Ibrutinib treatment continuation in CLL patients affected by COVID-19 is feeding an important clinical and sci-

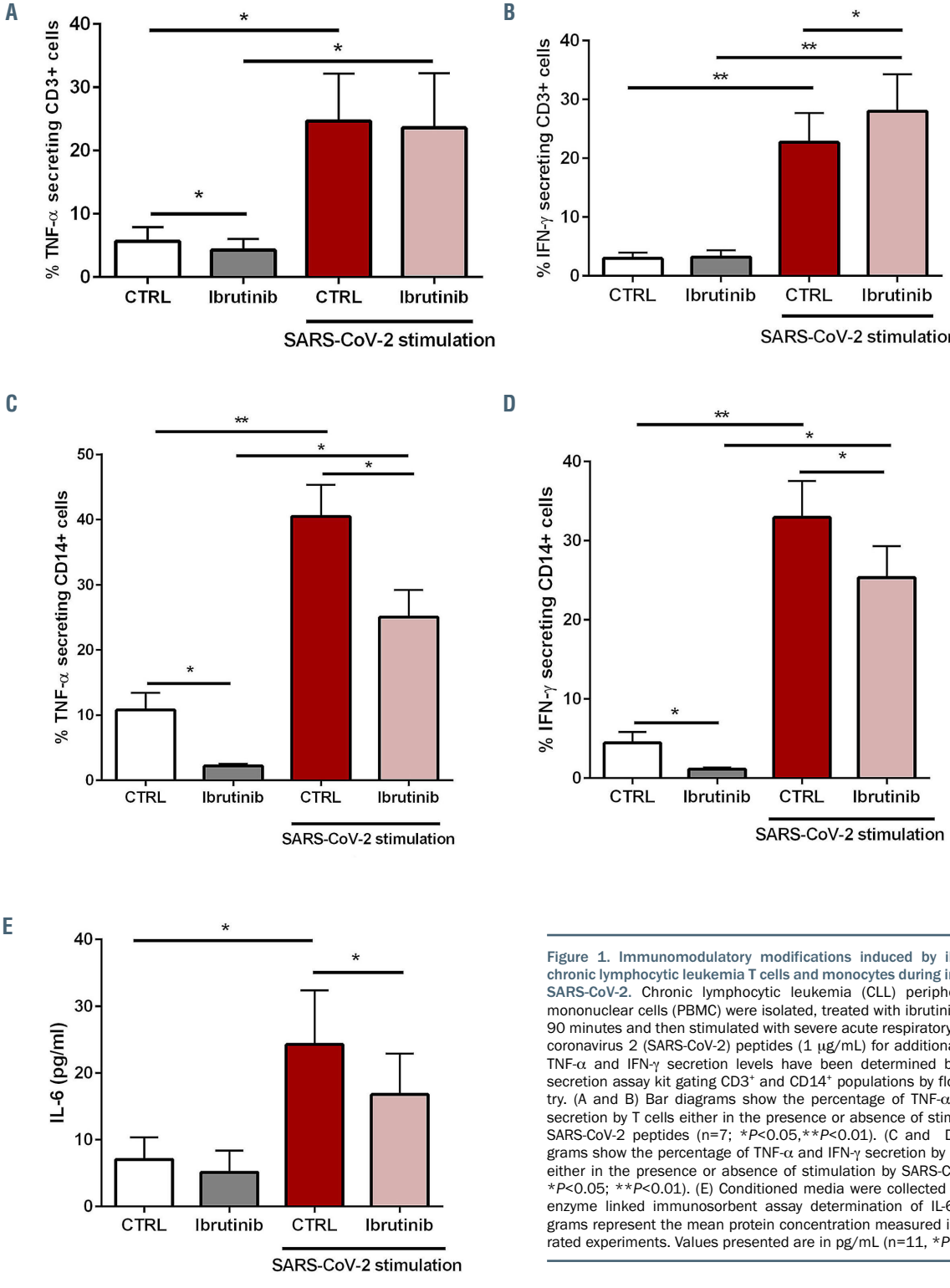

Figure 1. Immunomodulatory modifications induced by ibrutinib in chronic lymphocytic leukemia T cells and monocytes during infection by SARS-CoV-2. Chronic lymphocytic leukemia (CLL) peripheral blood mononuclear cells (PBMC) were isolated, treated with ibrutinib 1 μM for 90 minutes and then stimulated with severe acute respiratory syndrome coronavirus 2 (SARS-CoV-2) peptides (1 μg/mL) for additional 6 hours. TNF-α and IFN-γ secretion levels have been determined by cytokine secretion assay kit gating $CD3^+$ and $CD14^+$ populations by flow cytometry. (A and B) Bar diagrams show the percentage of TNF-α and IFN-γ secretion by T cells either in the presence or absence of stimulation by SARS-CoV-2 peptides (n=7; *P<0.05,**P<0.01). (C and D) Bar diagrams show the percentage of TNF-α and IFN-γ secretion by monocytes either in the presence or absence of stimulation by SARS-CoV-2 (n=7; *P<0.05; **P<0.01). (E) Conditioned media were collected for human enzyme linked immunosorbent assay determination of IL-6. Bar diagrams represent the mean protein concentration measured in 11 separated experiments. Values presented are in pg/mL (n=11, *P<0.05).

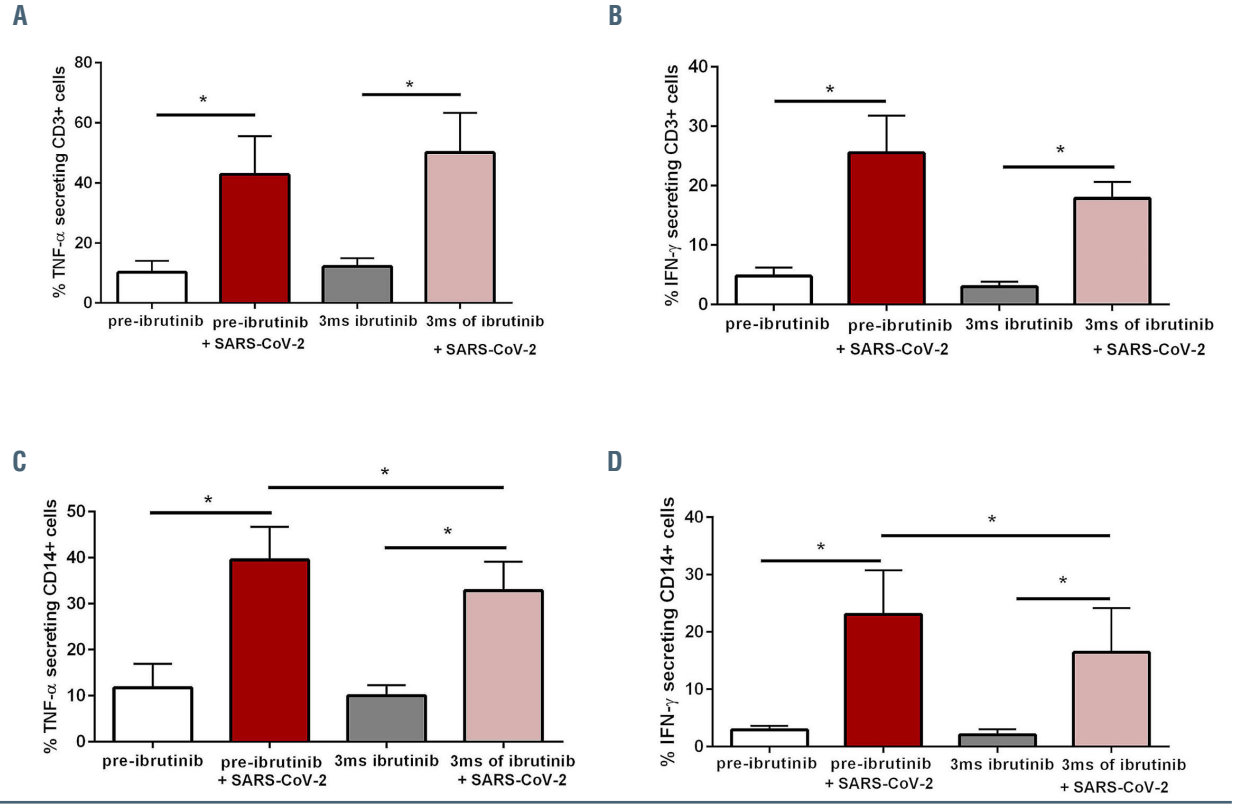

Figure 2. Immunological alterations in chronic lymphocytic leukemia patients under ibrutinib therapy during infection by SARS-CoV-2. Chronic lymphocytic leukemia (CLL) peripheral blood mononuclear cells (PBMC) were isolated from CLL patients before and after 3 months of treatment with ibrutinib and stimulated with severe acute respiratory syndrome coronavirus 2 (SARS-CoV-2) peptides (1 μg/ml) for 6 hours. TNF-α and IFN-γ secretion levels have been determined by cytokine secretion assay kit gating $CD3^+$ and $CD14^+$ populations by flow cytometry. (A and B) Bar diagrams show the percentage of TNF-α and IFN-γ secretion by T cells either in the presence or absence of stimulation by SARS-CoV-2 (n=7; **P*<0.05). (C and D) Bar diagrams show the percentage of TNF-α and IFN-γ secretion by monocytes either in the presence or absence of stimulation by SARS-CoV-2 (n=7; **P*<0.05).

entific debate about the opportunity to maintain or discontinue treatment in the presence of SARS-CoV-2 infection. In this scenario, some concerns are related to the evidence that an immunosuppressive activity of ibrutinib has been related to the occurrence of early-onset invasive fungal infections in treated-patients. For this reason, the choice of ibrutinib discontinuation may be related to a potentially increased risk of secondary infections and impaired humoral immunity.[13] Our results demonstrate how ibrutinib may have protective effects on COVID-19 in CLL patients by limiting the cytokine storm preventing lung injury. On one hand, ibrutinib may influence T-cell function, by skewing T cells from a Th2-dominant to a Th1 and $CD8^+$ cytotoxic population promoting Th1 immunity.[9] On the other hand, BTK is involved in the regulation of macrophage lineage commitment towards M1 polarization and ibrutinib is able to skew towards an immunosuppressive phenotype also in response to pro-inflammatory stimuli as fungal infection.[12] Inhibition of BTK, expressed by myeloid immune cells, affects the induction of inflammatory cytokines through the NFκB pathway and in mice intratracheal injection of BTK small interfering RNA confers potent protection against sepsis-induced acute lung injury with significant reduction of pulmonary edema, inflammatory cytokines and neutrophil infiltration in the lung tissues.[14] In the setting of influenza A infection, ibrutinib mitigates inflammation and improves resolution of infection.[15] Our results seem to strongly support a protective action of ibrutinib mitigating the feared cytokine storm sustaining the suggestion that there are no evident reasons to prematurely interrupt ibrutinib in these patients as recently suggested.[13] In the light of these observations, since ibrutinib seems to not worsen COVID-19 specific immune response, our study provides a biological rationale for continuation of BTKi in CLL patients who develop COVID-19. Noteworthy, a better overview on the potential use of BTKi against COVID-19 is under evaluation in clinical trials (clinicaltrials.gov Identifier: NCT04439006, NCT04375397) conducted in patients not affected by B-cell malignancies.

Stefania Fiorcari,[1] Claudio Giacinto Atene,[1*] Rossana Maffei,[2] Giulia Debbia,[1] Leonardo Potenza,[1,2] Mario Luppi[1,2] and Roberto Marasca[1,2]*

[1]Department of Medical and Surgical Sciences, Section of Hematology, University of Modena and Reggio Emilia, Modena and [2]Hematology Unit, Department of Oncology and Hematology, A.O.U of Modena, Policlinico, Modena, Italy

[*]SF and CGA contribute equally as co-first authors.

Correspondence:

STEFANIA FIORCARI - stefania.fiorcari@unimore.it

ROBERTO MARASCA - roberto.marasca@unimore.it

doi:10.3324/haematol.2020.277392

Received: December 3, 2020.

Accepted: February 26, 2021.

Pre-published: March 11, 2021.

Disclosures: no conflicts of interest to disclose.

Contributions: SF conceived the research, coordinated the research and interpreted the results; SF, CGA analyzed the results and SF wrote the manuscript; SF and CGA acquired and analyzed flow cytometric data; SF performed the statistical analyses; RMaf and RMar supervised the work-flow, revised the results and the manuscript critically; GD, LP, ML approved the final version of the paper.

Funding: this work was supported by Associazione Italiana per la Ricerca sul Cancro (IG21436 RM), Progetto Dipartimenti di Eccellenza 2018-2022. SF is supported by Fondazione Umberto Veronesi, Milan, Italy. The funding bodies had no role in study design, data collection and analysis, decision to publish or preparation of the manuscript.

References

1. Zhou P, Yang X-L, Wang X-G, et al. A pneumonia outbreak associated with a new coronavirus of probable bat origin. Nature. 2020; 579(7798):270-273.
2. Riva G, Nasillo V, Tagliafico E, Trenti T, Comoli P, Luppi M. COVID-19: more than a cytokine storm. Crit Care. 2020;24(1):549.
3. Passamonti F, Cattaneo C, Arcaini L, et al. Clinical characteristics and risk factors associated with COVID-19 severity in patients with haematological malignancies in Italy: a retrospective, multicentre, cohort study. Lancet Haematol. 2020;7(10):e737-e745.
4. Mato AR, Roeker LE, Lamanna N, et al. Outcomes of COVID-19 in patients with CLL: a multicenter international experience. Blood. 2020;136(10):1134-1143.
5. Treon SP, Castillo JJ, Skarbnik AP, et al. The BTK inhibitor ibrutinib may protect against pulmonary injury in COVID-19-infected patients. Blood. 2020;135(21):1912-1915.
6. Thibaud S, Tremblay D, Bhalla S, Zimmerman B, Sigel K, Gabrilove J. Protective role of Bruton tyrosine kinase inhibitors in patients with chronic lymphocytic leukaemia and COVID-19. Br J Haematol. 2020;190(2):e73-e76.
7. Scarfò L, Chatzikonstantinou T, Rigolin GM, et al. COVID-19 severity and mortality in patients with chronic lymphocytic leukemia: a joint study by ERIC, the European Research Initiative on CLL, and CLL Campus. Leukemia. 2020;34(9):2354-2363.
8. Roschewski M, Lionakis MS, Sharman JP, et al. Inhibition of Bruton tyrosine kinase in patients with severe COVID-19. Science Immunol. 2020;5(48):eabd0110.
9. Dubovsky JA, Beckwith KA, Natarajan G, et al. Ibrutinib is an irreversible molecular inhibitor of ITK driving a Th1-selective pressure in T lymphocytes. Blood. 2013;122(15):2539-2549.
10. Fiorcari S, Maffei R, Audrito V, et al. Ibrutinib modifies the function of monocyte/macrophage population in chronic lymphocytic leukemia. Oncotarget. 2016;7(40):65968–65981.
11. Fan K, Jia Y, Wang S, et al. Role of Itk signalling in the interaction between influenza A virus and T-cells. J Gen Virol. 2012;93(Pt 5):987-997.
12. Fiorcari S, Maffei R, Vallerini D, et al. BTK inhibition impairs the innate response against fungal infection in patients with chronic lymphocytic leukemia. Front Immunol. 2020;11:2158.
13. Chong EA, Roeker LE, Shadman M, Davids MS, Schuster SJ, Mato AR. BTK inhibitors in cancer patients with COVID-19: "The winner will be the one who controls that chaos" (Napoleon Bonaparte). Clin Cancer Res. 2020;26(14):3514-3516.
14. Zhou P, Ma B, Xu S, et al. Knockdown of Burton's tyrosine kinase confers potent protection against sepsis-induced acute lung injury. Cell Biochem Biophys. 2014;70(2):1265-1275.
15. Florence JM, Krupa A, Booshehri LM, Davis SA, Matthay MA, Kurdowska AK. Inhibiting Bruton's tyrosine kinase rescues mice from lethal influenza-induced acute lung injury. Am J Physiol Lung Cell Mol Physiol. 2018;315(1):L52-L58.

Derepression of retroelements in acute myeloid leukemia with 3q aberrations

Acute myeloid leukemia (AML) with chromosomal rearrangements inv(3)/t(3;3) (3q-AML) is a rare but highly fatal subtype of leukemia. It is characterized by an aberrant transcription of the proto-oncogene *EVI1* (ecotropic viral integration site 1, *MECOM*) as a result of the chromosomal 3q21q26 rearrangements that lead to the relocation of a master *GATA2* distal hematopoietic enhancer to the *EVI1* locus and deregulation of both genes.[1,2] To date, little is known about what triggers chromosomal rearrangements in 3q-AML that ultimately lead to the deregulation of *EVI1* via the repositioning of *G2DHE*. However, recent studies have shown evidence for the involvement of endogenous transposable elements of RNA family (retroelements [RE]) in the formation of complex chromosomal aberrations, including translocations, large-scale duplications and amplifications through retrotransposition across different cancer entities.[3] Furthermore, hypomethylation of RE has been linked to their pathogenic mobility in epithelial tumors.[4–6]

Here we present the results of functional genomics analysis of a cohort of 3q-AML patients. Based on our data, we hypothesized that breakpoint-associated RE (breakpoint-RE) could play an important regulatory and activating role in this AML subtype. Therefore, we performed an array of *in vitro* studies using CRISPR-Cas9 approach to dissect their role in 3q-AML.

Targeted chromosome 3q-capture sequencing of 3q-AML patient samples and cell lines with *EVI1* overexpression previously revealed a characteristic 3q21q26 pattern of patient-specific breakpoints, demarcating a leukemogenic *EVI1*-activating super-enhancer that is found uniquely in inv(3)/t(3;3) AML and contains *G2DHE*.[1] In order to identify a commonality between breakpoints relevant for super-enhancer formation, we reanalyzed 3q-capture sequencing data and found that in 38 of 41 samples, chromosomal breakpoints at 3q21.3 and 3q26.2 mapped to sequences of RE, including long interspersed elements (LINE), short interspersed elements (SINE) and long terminal repeats (LTR) (Figure 1A). Of note, RNA sequencing (RNA-Seq) of 3q-AML patients revealed a characteristic RNA readthrough spanning the large super-enhancer region at 3q21.3 (Figure 1B, top panel). A similar enhancer RNA (eRNA) signature was observed in non-3q-rearranged AML cases (Figure 1B, top panel; *Online Supplementary Figure S3*), indicating active *G2DHE* regulating *GATA2* in its native environment. In 3q-AML, however, the RNA readthrough frequently originated at 3q21.3 breakpoint sites, extending beyond the super-enhancer region. Additionally, allele-specific bisulfite amplicon sequencing performed on selected AML cases revealed focal demethylation of CpG sites around the chromosomal breakpoints exclusively on the rearranged allele, whereas the intact allele in 3q-AML and both alleles in non-rearranged leukemic cell lines did not show any hypomethylation pattern (Figure 1B, bottom panel). Focal hypomethylation around breakpoints on the rearranged allele could be the consequence of chromosomal rearrangements and super-enhancer-related epigenetic reprogramming, including the deposition of active chromatin marks and physical interaction between the *EVI1* promoter and *G2DHE*.[1]

Based on our RNA-Seq and bisulfite sequencing data, we investigated whether derepression of breakpoint-RE could possibly represent a priming event for an enhancer rearrangement by relaxation of the local chromatin compaction and may play a role in the ectopic activation of *EVI1* by the super-enhancer. In order to test this hypothesis, we performed a CRISPR-Cas9 gene editing experiment using a homology-directed repair (HDR) template to insert selected 3q21.3 breakpoint-RE sequences or *G2DHE* in the vicinity of the *EVI1* locus in the *EVI1*-positive myeloid leukemia reporter cell line K562 that does not harbor inv(3)/t(3;3) rearrangements (Figure 2A, top panel) (Ottema *et al.*, 2021, under review). The presence of a *T2A-eGFP* fusion sequence inserted downstream of *EVI1* allows for correlation of EVI1 expression with the synchronously expressed green fluorescent protein (GFP). The parental reporter cell line is tolerant of increased EVI1 levels given that its baseline expression is already increased in K562. The insertion sequences were derived from 3q21.3 breakpoints of two leukemia cases: AML 3071, a patient with inv(3) AML and MOLM-1, a near-triploid myeloid leukemia cell line harboring two chromosome 3 alleles with inv(3) (Figure 2A, bottom panel).7 The HDR templates were inserted in the corresponding 3q26.2 breakpoint loci as found in AML 3071 and MOLM-1, that is downstream of *EVI1* and within the last *EVI1* intron, respectively.

Single-cell clones validated by polymerase chain reaction (PCR) and Sanger sequencing (*Online Supplementary Figure S1A*) harboring the ectopic *G2DHE* showed a shift in GFP fluorescence indicating successful *EVI1* activation, whereas clones with 3q21.3 breakpoint-RE sequences showed no change in the GFP signal compared with untreated cells (Figure 2B). Furthermore, single-cell clones were analyzed by quantitative PCR (qPCR) and western blot, which showed results consistent with the flow cytometry analysis (Figure 2C and D, respectively), suggesting that the ectopic activation of *EVI1* occurs via *G2DHE*, whereas breakpoint-RE themselves are insufficient to induce *EVI1* transcriptional activation in the K562 reporter cell line.

In order to further dissect a potential regulatory role of breakpoint-RE in 3q-AML, a reciprocal experimental CRISPR-Cas9 approach was applied to delete the original breakpoint-RE in MOLM-1 and UCSD-AML1, the latter being a t(3;3) AML cell line. We expressed pairs of single guide RNA (sgRNA) in stably Cas9-expressing cells to induce a segmental deletion of a fragment containing either the inverted (MOLM-1) or translocated (UCSD-AML1) breakpoint-RE at 3q26.2 on the rearranged alleles located within the last *EVI1* intron in MOLM-1, and upstream of the *EVI1* promoter in UCSD-AML1 (Figure 3A). Targeting on the non-rearranged allele was expected to result only in generation of indels at the 3q21.3 and 3q26.2 site but not segmental RE deletions. In total, two MOLM-1 and six UCSD-AML1 clones harboring the desired deletion validated by PCR and Sanger sequencing (*Online Supplementary Figure S1B*) were derived successfully from single cells. Together with the nontargeting control (NTC) clones (targeted with sgRNA against mCherry and eGFP) and the wild-type (WT) cell line, we performed phenotypic analysis of obtained deletion clones. We observed no differences in proliferation between deletion and control samples (Figure 3B). Slightly reduced EVI1 expression on mRNA and protein level was observed exclusively in the MOLM-1 deletion clones (Figure 3C, left panel).

In order to identify potential genome-wide effects of CRISPR-Cas9-induced RE deletion, we performed genomic and epigenomic analyses of the MOLM-1 and UCSD-AML1 deletion and control clones using circularized chromatin conformation capture sequencing (4C-Seq) and chromatin immunoprecipitation followed by

sequencing (ChIP-Seq). Neither 4C-Seq nor ChIP-Seq revealed an impact of RE deletion on the interaction frequency of *G2DHE* with the *EVI1* promoter or on the deposition of active chromatin marks, such as H3K27ac and H3K4me3, in any of the two edited cell lines (results for MOLM-1 shown in the *Online Supplementary Figure S2A*), making it unlikely that the expression changes in EVI1 are caused by changes in the regulatory function of *G2DHE*.

Since the reduction of EVI1 expression was specific only to the MOLM-1, but not UCSD-AML1 deletion clones, we speculated that this effect might be due to other features present in the sequence deleted in MOLM-1, rather than the consequence of the breakpoint-RE-

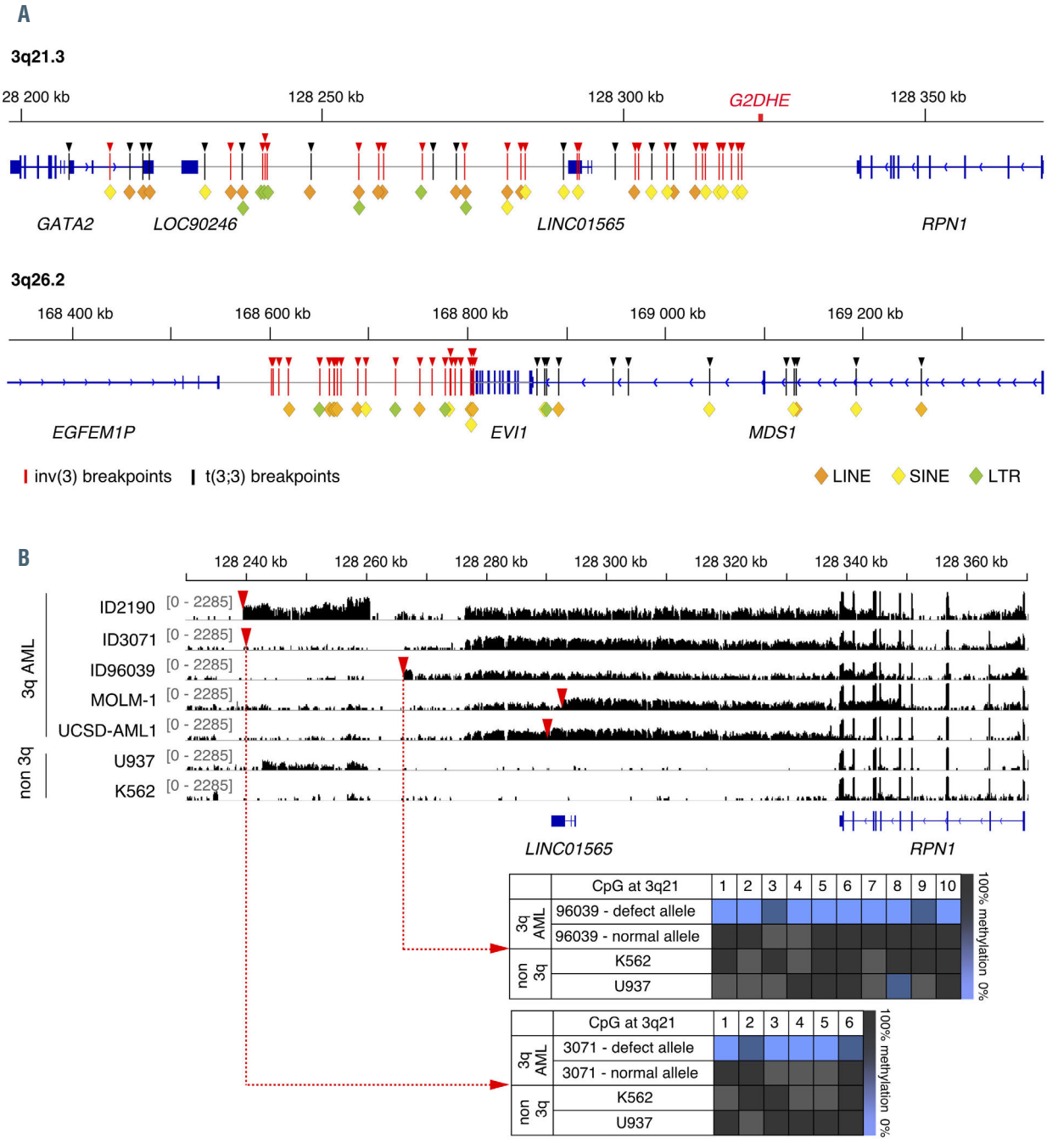

Figure 1. Chromosomal breakpoints in acute myeloid leukemia inv(3)/t(3;3) (3q-AML) are enriched in retroelements. (A) 3q-capture sequencing revealed a characteristic breakpoint pattern (red and black arrowheads) at 3q21.3 (upper tracks) and 3q26.2 (lower tracks). At 3q21.3, a breakpoint-free region downstream (left) of *RPN1* was identified as a commonly translocated segment containing *G2DHE*. At 3q26.2, breakpoints of inversion cases map exclusively downstream (left) or within the last *EVI1* intron, whereas translocation cases have breakpoints upstream of *EVI1*. Color-coded diamonds indicate the position of RE: long interspersed elements (LINE), short interspersed elements (SINE) or long terminal repeats (LTR), annotated by RepeatMasker. (B) RNA sequencing of 3q-AML samples revealed a characteristic RNA readthrough signature at 3q21.3. Bisulfite amplicon sequencing on representative 3q-AML samples showed focal hypomethylation of breakpoint regions (red arrowheads) on the rearranged allele but not on the normal allele and non-3q samples.

deletion. To this end, we reanalyzed the deleted sequences in the two cell lines. The original 3q21.3 fragment overlapping with *LINC01565* relocated to the 3q26.2 site and deleted in the MOLM-1 clones displays high degree of conservation (Figure 3A, left panel), which might indicate functional importance of this sequence. ENCODE transcription factor (TF) ChIP data generated in K562 cells revealed a plethora of TF binding to this region (*Online Supplementary Figure S2B*). Some of these TF have predicted binding sites within the *G2DHE* sequence, including IKZF1, MAX, TAL1 and MAZ (Kiehlmeier *et al.*, 2021, under review). Furthermore, EVI1 has been functionally linked to some of these TF, including MTA1/2, HDAC1/2 and GATAD2B. All these proteins belong to the nucleosome remodeling and deacetylase (NuRD) complex,[8] which was shown to specifically interact with the MDS-EVI1 (PRDM3) but not the EVI1 protein,[9] while both EVI1 protein isoforms were shown to interact with HDAC1.[10] Contrary to MOLM-1, no TF binding in the region deleted in the UCSD-AML clones was found (*Online Supplementary Figure S2B*).

Taken together, the observed reduction in EVI1 expression upon breakpoint-RE deletion in MOLM-1 is more likely the consequence of TF binding loss within the

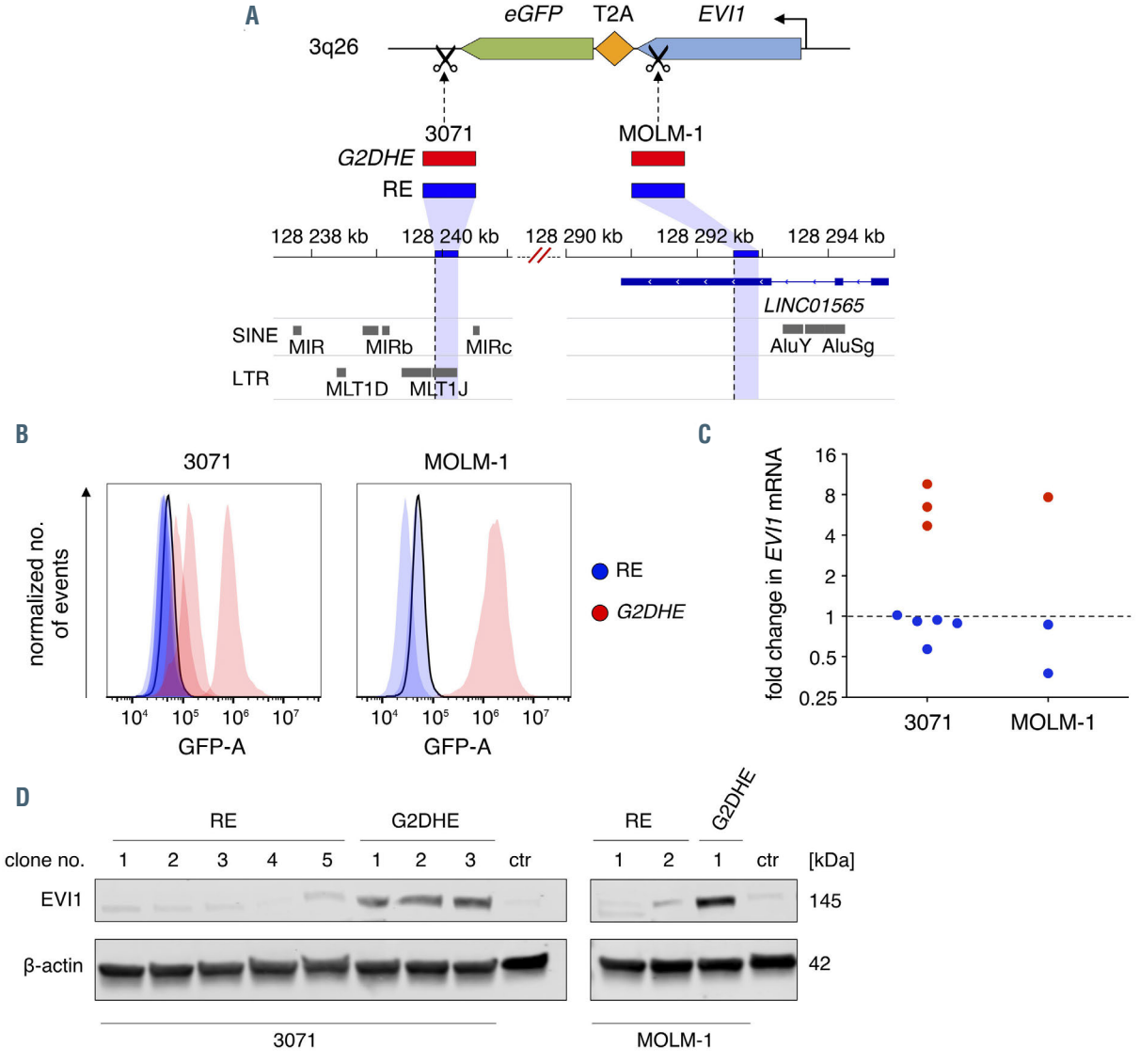

Figure 2. Ectopic activation of *EVI1* occurs via *G2DHE*, whereas breakpoint-associated retroelements do not display activating potential in the K562 cells. (A) Experimental strategy of CRISPR-Cas9-mediated genomic insertions. Donor templates containing either *G2DHE* (736 bp, red boxes) or 3q21.3 breakpoint-associated retroelements (breakpoint-RE) from selected 3q-AML cases (3071: 353 bp and MOLM-1: 280 bp, blue boxes) were inserted in the non-3q K562 reporter cell line (K562 *eGFP-T2A-EVI1*) using CRISPR-Cas9 downstream of *EVI1* and within the last *EVI1* intron. A genomic view shows the origin of 3q21.3 breakpoint sequences used in CRISPR experiments, dashed lines indicate 3q21.3 breakpoints in 3071 (left) and MOLM-1 (right). 3,071 homology-directed repair (HDR) template contains a part of MLT1J LTR element. *G2DHE* (red) and 3q21.3 breakpoint-RE samples (blue) are consistently colored throughout the figure. (B) Flow cytometry analysis on the K562 *eGFP-T2A-EVI1* single clones bearing the desired *G2DHE* or 3q21.3 breakpoint insertions. Peaks corresponding to the green fluorescent protein (GFP) signal from single clones targeted at the same region are presented together on one graph, with peaks for untreated cells shown as a black outline. (C) Quantitative polymerase chain reaction (qPCR) analysis of the *EVI1* mRNA levels in single clones shown in (B), relative to *HMBS* and normalized to the untreated *eGFP-T2A-EVI1* cells. (D) Representative western blot of the full-length EVI1 isoform from the clones and untreated cells (ctr) shown in (B) and (C). Data shown in (C) are means of three technical replicates from one independent experiment. SINE: short interspersed nuclear elements; LTR: long terminal repeats.

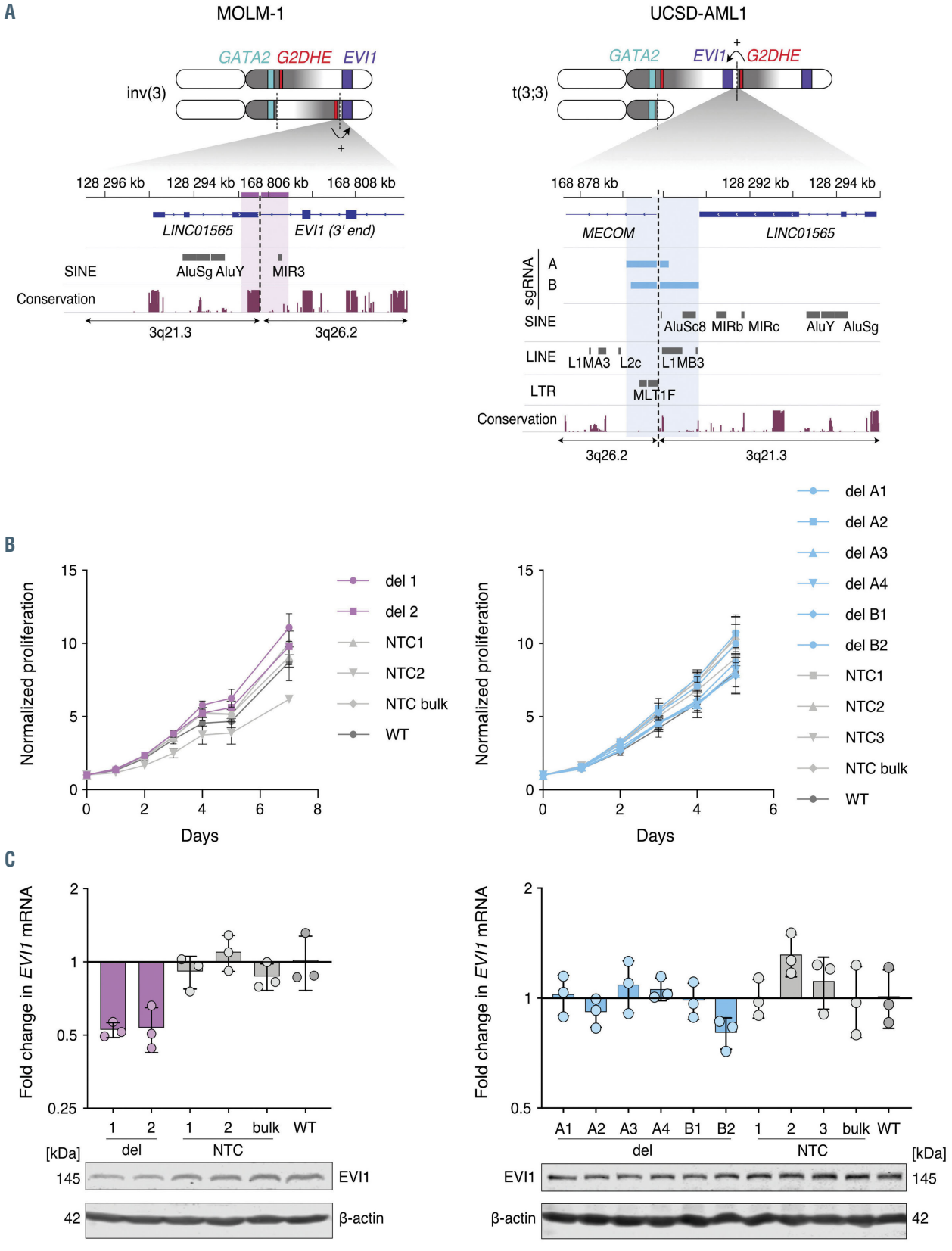

Figure 3. MOLM-1 single clones harboring the deletion of breakpoint-associated retroelements exhibit no phenotypic changes but show reduced *EVI1* expression. (A) Illustration of the CRISPR-Cas9 mediated segmental deletion surrounding the breakpoint on the rearranged allele of chromosome 3 in MOLM-1 (left) and UCSD-AML1 (right). The deleted regions (MOLM-1: purple, UCSD-AML1: blue) encompass a MIR3 SINE element in MOLM-1, and representatives of all three RE subclasses in UCSD-AML1. Normalized proliferation (B) of deletion (del), nontargeting control (NTC) clones, NTC bulk of cells and wild-type (WT) cell line. (C) Quantitative polymerase chain reaction analysis of *EVI1* mRNA levels (top panel) and representative western blot (bottom panel) of the full-length EVI1 isoform from samples shown in (B). Data shown in (B) and (C, top panel) are mean ± standard deviation from three independent experiments. Conservation across vertebrate genomes is taken from phastCons.[13] SINE: short interspersed nuclear elements; LINE: long interspersed nuclear elements; LTR: long terminal repeats.

G2DHE super-enhancer structure. However, we could not observe any specific pattern of TF binding sites commonly relocated to the *EVI1* locus in 3q-AML patient and cell line data. Meanwhile, we conclude that breakpoint-RE are not essential for the regulation and maintenance of *EVI1* expression in 3q-AML.

In summary, our data show that RE are highly enriched at inv(3)/t(3;3) breakpoint sites in AML and represent a source of genomic vulnerability without providing additional regulatory or activating signal for *EVI1* in this leukemia subtype, as evidenced by CRISPR-Cas9 editing experiments in 3q-rearranged cell lines. However, we cannot exclude the involvement of full-length source RE sequences in the formation of 3q rearrangements in earlier stages of malignant transformation. Since many retrotransposition-competent RE often become truncated or undergo internal reshuffling upon insertion in a new genomic location,[11,12] the presence of resulting chimeric breakpoint-RE sequences would bear no functional consequences, which stands in line with the lack of effects observed upon CRISPR-Cas9 editing of breakpoint-RE fusion sequences in our cell line models.

Additionally, the data from the K562 reporter cell line provide an orthogonal confirmation of the minimal *G2DHE* being sufficient for *EVI1* transcriptional activation.[1]

Jagoda Mika,[1] Sophie Ottema,[2] Sandra Kiehlmeier,[1] Sabrina Kruse,[1] Leonie Smeenk,[2] Judith Müller,[1] Sabrina Schweiggert,[1] Carl Herrmann,[3] Mathijs Sanders,[2] Ruud Delwel[2] and Stefan Gröschel[1,4,5]

[1]Molecular Leukemogenesis Group, German Cancer Research Center, Heidelberg, Germany; [2]Department of Hematology, Erasmus University Medical Center, Oncode Institute, Rotterdam, the Netherlands; [3]Health Data Science Unit, Medical Faculty Heidelberg and BioQuant, Heidelberg, Germany; [4]Internal Medicine V, Heidelberg University Hospital, Heidelberg, Germany and [5]Oncology Center Worms, Worms, Germany

Correspondence:

STEFAN GROESCHEL - stefan.groeschel@dkfz.de

doi:10.3324/haematol.2020.277400

Received: December 9, 2020.

Accepted: March 12, 2021.

Pre-published: March 25, 2021.

Disclosures: the authors declare no competing financial interests.

Contributions: JMi, SO, LS, SKi, JMü, SS and SG performed experiments; SO and RD provided RNA-seq data; JMi, SKr, MS and CH analyzed results; JMi made the figures; JMi and SG designed the experiments; JMi and SG wrote the manuscript with input from all authors.

Acknowledgments: the authors would like to thank Claudia Scholl and Stefan Fröhling (German Cancer Research Center, Heidelberg, Germany and National Center for Tumor Diseases, Heidelberg, Germany). We thank the DKFZ Genomics and Proteomics Core Facility for providing excellent sequencing services and Mathias Utz (German Cancer Research Center, Heidelberg, Germany) for technical assistance.

Funding: this research was supported with a Starting Grant (677209) of the European Research Council (SG), the program "ENHancers And Non-coding Cancer (Epi-)Mutations (ENHANCE)" funded within the DKFZ-NCT3.0 initiative on 'Integrative Projects in Basic Cancer Research' (CH, SG), a scholarship of the Helmholtz International Graduate School for Cancer Research (JMi, SKi), a grant of the NCT3.0 basic research (SG), a fellowship from the Daniel den Hoed, Erasmus MC Foundation (LS) and a grant of the Koningin Wilhelmina Fonds from the Dutch Cancer Society (RD, SO).

References

1. Gröschel S, Sanders MA, Hoogenboezem R, et al. A single oncogenic enhancer rearrangement causes concomitant EVI1 and GATA2 deregulation in leukemia. Cell. 2014;157(2):369-381.
2. Yamazaki H, Suzuki M, Otsuki A, et al. A remote GATA2 hematopoietic enhancer drives leukemogenesis in inv(3)(q21;q26) by activating EVI1 expression. Cancer Cell. 2014;25(4):415-427.
3. Rodriguez-Martin B, Alvarez EG, Baez-Ortega A, et al. Pan-cancer analysis of whole genomes identifies driver rearrangements promoted by LINE-1 retrotransposition. Nat Genet. 2020;52(3):306-319.
4. Tubio JMC, Li Y, Ju YS, et al. Extensive transduction of nonrepetitive DNA mediated by L1 retrotransposition in cancer genomes. Science. 2014;345(6196):1251343.
5. Lee E, Iskow R, Yang L, et al. Landscape of somatic retrotransposition in human cancers. Science. 2012;337(6097):967-971.
6. Cajuso T, Sulo P, Tanskanen T, et al. Retrotransposon insertions can initiate colorectal cancer and are associated with poor survival. Nat Commun. 2019;10(1):4022.
7. Matsuo Y, Adachi T, Tsubota T, Imanishi J, Minowada J. Establishment and characterization of a novel megakaryoblastic cell line, MOLM-1, from a patient with chronic myelogenous leukemia. Hum Cell. 1991;4(3):261-264.
8. Torrado M, Low JKK, Silva APG, et al. Refinement of the subunit interaction network within the nucleosome remodelling and deacetylase (NuRD) complex. FEBS J. 2017;284(24):4216-4232.
9. Ivanochko D, Halabelian L, Henderson E, et al. Direct interaction between the PRDM3 and PRDM16 tumor suppressors and the NuRD chromatin remodeling complex. Nucleic Acids Res. 2019; 47(3):1225-1238.
10. Vinatzer U, Taplick J, Seiser C, Fonatsch C, Wieser R. The leukaemia-associated transcription factors EVI-1 and MDS1/EVI1 repress transcription and interact with histone deacetylase. Br J Haematol. 2001;114(3):566-573.
11. Sassaman DM, Dombroski BA, Moran J V, et al. Many human L1 elements are capable of retrotransposition. Nat Genet. 1997; 16(1):37-43.
12. Brouha B, Badge RM, Farley AH, et al. Hot L1s account for the bulk of retrotransposition in the human population. Proc Natl Acad Sci U S A. 2003;100(9):5280-5285.
13. Siepel A, Bejerano G, Pedersen JS, et al. Evolutionarily conserved elements in vertebrate, insect, worm, and yeast genomes. Genome Res. 2005;15(8):1034-1050.

One third of alloantibodies in patients with sickle cell disease transfused with African blood are missed by the standard red blood cell test panel

Studies on red blood cell (RBC) antibodies in Africa routinely use standard test cells from donors of Caucasian descent. There are no systematic data on alloimmunization against antigens that are almost exclusively present in Africans. We studied the prevalence of antibodies in transfused Ghanaian patients with sickle cell disease (SCD) using standard test cells (representing predominantly antigens more common in Caucasians (Caucasian antigens) and cells expressing antigens more common among Africans (African antigens). Antibodies were present in 16% of 221 patients; 31% of these were directed against African antigens that were not detected with standard test cells. Our findings are not only relevant for an African setting, but also for Western blood banks that are developing strategies to recruit more African donors.

Transfusions in patients with SCD are associated with high rates of red blood cell (RBC) alloimmunization against multiple antigens. Alloantibody screening is performed with standard reagent test cells, mostly from donors of Caucasian descent that lack antigens that are more prevalent in Africans. Alloimmunisation involving antigens that are almost exclusively present in Africans has not been studied systematically in a setting where both patients and donors are Africans. We determined the prevalence of RBC antibodies against Caucasian and African antigens in multi-transfused patients with SCD in Ghana, where pre-transfusion antibody screening and indirect antiglobulin crossmatch are not routine.

Our cross-sectional study recruited patients between July and December 2018, from two tertiary hospitals. Patients were eligible for inclusion if they were at least 2 years of age and had received at least two transfusions at least 6 weeks before study enrolment (to allow time to develop antibodies). Patients were episodically transfused with non-leucoreduced whole blood from African donors. Donors were not screened for sickle cells. Participants' demographics and transfusion history were retrieved from hospital files. Patients or caretakers provided this information, if missing from hospital files, using a standard questionnaire.

Plasma and buffy coat samples, taken at enrolment, were frozen at –80°C and transported to Sanquin, Amsterdam, the Netherlands, for routine antibody testing against a standard three-cell reagent panel (Bio-Rad Laboratories AG, Cressier, Switzerland), not expressing antigens that are more common in Africans, using a low ionic strength solution (LISS) indirect anti-globulin gel column agglutination test. Using the same method, antibody identification was performed with commercial panels of reagent RBC of selected phenotypes and against eight selected cells with antigens that are very rare (<0.01% to 1%) in Caucasians but more frequent (0.5% to 32%) in Africans (*i.e.*, MNS6 [He], MNS25 [Dantu], RH10 [V], RH20 [VS], RH30 [Go^a], RH32, RH43 [Crawford] and KEL6 [Js^a]).[1] These antigens were selected based on the availability of RBC expressing rare antigens archived in the Immunohaematology Diagnostics laboratory at Sanquin. Antibody specificities were confirmed by re-testing with two RBC expressing and two RBC not expressing the target antigens. For patients with anti-D, *RHD* genotyping was done on genomic DNA by Multiplex Ligation-dependent Probe Amplification (MLPA) assay according to the manufacturers' protocol (MRC Holland, Amsterdam, the Netherlands) using a thermocycler (Veriti, Applied Biosystems, Nieuwerkerk aan de IJssel, the Netherlands).[2] When MLPA results were equivocal, DNA sequencing was performed to determine the *RHD* genotype. Sequence products were analyzed on a genetic analyzer (3730xl, Applied Biosystems).

Table 1. Specificities of the 36 red blood cell antibodies in the 35 alloimmunized multi-transfused Ghanaian patients with sickle cell disease.

Blood group system	Antibody specificity, (n)	
	Panel expressing antigens more common in Caucasians	African panel expressing antigens more common in Africans
Rh	E (10); D (7); G (2)	V/VS (2); VS (1); Go^a (1); RH32 (1)
Kell	K (1)	
MNS	s (1)	Dantu (3); He (2)
Unidentified	Pan-reactive (3); Non-specified* (1)	Non-specified* (1)

*The non-specified antibodies were probably against low frequency antigens. One patient had anti C+D.

The study was approved by the Committee on Human Research, Publication and Ethics, Kwame Nkrumah University of Science and Technology, and Korle Bu Teaching Hospital and Liverpool School of Tropical Medicine Institutional Review Boards. Patients or their caretakers gave written informed consent to participate in the study.

Statistical analyses were performed using the SPSS (IBM Corp., Armonk, NY, USA). Results for continuous variables were presented as medians (range) and categorical variables as frequencies (percentages).

We recruited 221 Ghanaian patients (123 women and 98 men; 89% hemoglobin [Hb] SS, 10% HbSC, one HbSD and one HbSβ^0-thalassemia). The median age at enrolment was 17 years (range, 2-66 years). Patients had received a median of three (range, 2-40) whole blood transfusions and the median period between last transfusion and study enrolment was 2.1 years (range, 6 weeks to 55.5 years).

Antibody screening, using standard test cells, was positive in 24 patients (10.9%) and revealed 25 antibody specificities (Table 1). Although D antigen matching was routine in Ghana, anti-D was present in seven patients. *RHD* genotyping of these patients revealed that three women and two men had only *RHD*-null alleles (three *RHD*01N.01/RHD*01N.01*, one *RHD*01N.01/RHD*01N.03* and one *RHD*08N.01/RHD*08N.01*). In the three D negative (D-) women, anti-D could have been induced by a D positive (D+) pregnancy. For the two D- men, errors in blood group typing or mistakenly transfusing patients with D+ blood are possible causes for the anti-D. The presence of RH variants expressing weak D among D- African donors might have contributed to these mismatched transfusions. Two patients possessed variant *RHD* genes (*RHD*03.04* and *RHD*04.01*) associated with D+ serology and carriers of these variants can make anti-D after D-antigen exposure.[3,4]

The nine patients with D, G and s antibodies and the three patients with pan-reactive antibodies, were not tested against the African antigens because African test cells lacking these antigens were not available. Of the

remaining 209 patients, eleven (5.3%) patients who did not have alloantibodies against the standard three-cell screen panel, had a total of eleven antibodies against African antigens; three anti-Dantu (for one, confirmation by a second Dantu+ test cell was not performed, due to lack of Dantu+ cells), two anti-He, two anti-V/VS, one anti-VS, one anti-RH32, one anti-Go^a and one antibody probably against a low frequency antigen but no plasma was available for further investigation (Table 1).

Overall, 31.4% of alloimmunized patients had antibodies against African antigens that were not detected during standard antibody screening. Other studies in patients with SCD have reported antibodies against African antigens[5-13] but these patients were transfused in the US and Europe and thus not exclusively with blood from African donors. Furthermore, these antibodies were encountered during complex antibody workup, crossmatch incompatibilities and hemolytic transfusion reactions rather than through systematic screening. The antibody frequency against African antigens in these studies ranged from 0.7% to 13.3%, with anti-V/VS, anti-Js^a and anti-Go^a representing 90% of specificities. So far, only one study in France systematically screened a heavily transfused patient cohort with SCD using selected African red cells. After receiving a mean of 144 RBC transfusions (11.5% from donors of African descent) 5.2% of 211 patients had antibodies against African-specific antigens (MNS6, RH10, RH20, RH23, RH30 and KEL6).[14] However, unlike our study, these patients received blood matched for major Rh and K antigens, which precludes insight in differences in immunogenicity of African and the classical 'major' blood group antigens. Surprisingly, in our study seven of 36 (19%) antibodies were against low frequency African antigens (*i.e.*, Go^a 2%, RH32 1%, He 1% and Dantu 0.5% in Africans).[1] This suggests that these antigens are immunogenic in Ghanaians and may be more immunogenic than antigens for which we test in the European setting. The results from these studies stress the importance of testing against African antigens when patients receive transfusions from African donors.

Antibodies in patients with SCD are notorious for their high evanescence rate, which may be up to 60-80%.[15] Because our study had a cross-sectional design, it is likely that antibody frequency was underestimated. In the French study, none of the eight previously detected African antibodies, were detectable at study enrollment, suggesting that African antibodies also have a high evanescence rate.[14] Furthermore, African antibodies have been implicated in severe hemolytic transfusion reactions upon receipt of transfusions with the cognate antigens.[12]

Our study was limited by the scarcity of test cells expressing African antigens, so antibodies against other African antigens, such as RH49 (STEM), GE6 (Ls^a) and CROM3 (Tc^b), might have been missed.[1] Furthermore, antibodies against antigens that are more frequently expressed on RBC of Ghanaian donors might have been missed, because we did not specifically test Ghanaian RBC.

Since we found African antibodies in African patients transfused with African blood, it is also quite likely that similar antibodies may be elicited in Caucasian patients receiving blood from African donors and through pregnancy. These antibodies cannot be detected during pre-transfusion antibody screening using standard test cells and without performing an indirect antiglobulin crossmatch with donor cells (and many countries only perform type and screen). Our findings are relevant for blood banks in Western countries since many are developing strategies to recruit more African donors. Unless they can supply antigen compatible blood, African antibodies may increasingly be missed as the pool of African donors expands.

This is the first study to systematically screen for RBC antibodies against African antigens in a large cohort of transfused patients with SCD who were exclusively transfused with blood from African donors. In order to increase the availability of test cells with African antigens, African donors should be typed, for relevant antigens and then retain them as repeat donors for the preparation of test cells. As long as antigens commonly expressed in Africans are not incorporated on the RBC testing panel, transfusions for patients with SCD should be cross-matched using an indirect antiglobulin test, even when they do not have RBC antibodies using the standard three-cell screen panel.

Lilian A. Boateng,[1,2] Henk Schonewille,[3] Peter C. Ligthart,[3] Ahmad Javadi,[3] Barbera Veldhuisen,[3] Alex Osei-Akoto,[4,5] Yvonne Dei-Adomakoh,[6,7] Imelda Bates[1] and C. Ellen van der Schoot[3]

[1]Center for Capacity Research, International Public Health, Liverpool School of Tropical Medicine, Liverpool, UK; [2]Medical Diagnostics, Kwame Nkrumah University of Science and Technology, Kumasi, Ghana; [3]Experimental Immunohaematology, Sanquin, Amsterdam, the Netherlands; [4]Child Health, School of Medicine and Dentistry, Kwame Nkrumah University of Science and Technology, Kumasi, Ghana; [5]Directorate of Child Health, Komfo Anokye Teaching Hospital, Kumasi, Ghana; [6]Hematology, University of Ghana Medical School, University of Ghana, Accra, Ghana and [7]Ghana Institute of Clinical Genetics, Korle Bu Teaching Hospital, Adult Sickle Cell Clinic, Accra, Ghana

Correspondence:

LILIAN A. BOATENG - lilian.boateng@lstmed.ac.uk

doi:10.3324/haematol.2021.278451

Received: January 28, 2021.

Accepted: March 11, 2021.

Pre-published: April 1, 2021.

Disclosures: the authors declare no competing financial interests.

Contributions: LB, HS, AO, YD, EVS and IB conceived the idea and designed the study; LB, PL, AJ and BV performed the laboratory test and interpreted the results; LB, HS, IB and EVS analyzed and interpreted the data; LB and HS drafted the manuscript.

Acknowledgments: the authors would like to thank the staff, patients and donors at the sickle cell clinics and blood banks in KATH and KBTH, Ghana, for their contributions in obtaining blood samples for the research project.

Funding: this work was supported by grant GHCA-2017-18 to LB, from the Commonwealth Scholarship Commission, UK and from Sanquin Blood Supply, The Netherlands.

References

1. Reid ME, Lomas-Francis C, Olsson ML. The blood group antigen factsbook. London, UK: Academic Press Limited; 2012.
2. Haer-Wigman L, Veldhuisen B, Jonkers R, et al. RHD and RHCE variant and zygosity genotyping via multiplex ligation–dependent probe amplification. Transfusion. 2013;53(7):1559-1574.
3. von Zabern I, Wagner FF, Moulds JM, Moulds JJ, Flegel WA. D category IV: a group of clinically relevant and phylogenetically diverse partial D. Transfusion. 2013;53(11pt2):2960-2973.
4. Wagner FF, Frohmajer A, Ladewig B, et al. Weak D alleles express distinct phenotypes. Blood. 2000;95(8):2699-2708.
5. Rosse WF, Gallagher D, Kinney TR, et al. Transfusion and alloimmunization in sickle cell disease. Blood. 1990;76(7):1431-1437.
6. Telen MJ, Afenyi-Annan A, Garrett ME, Combs MR, Orringer EP, Ashley-Koch AE. Alloimmunization in sickle cell disease: changing antibody specificities and association with chronic pain and decreased survival. Transfusion. 2015;55(6 Pt 2):1378-1387.

7. Castro O, Sandler SG, Houston-Yu P, Rana S. Predicting the effect of transfusing only phenotype-matched RBCs to patients with sickle cell disease: theoretical and practical implications. Transfusion. 2002;42(6):684-690.
8. Karafin MS, Field JJ, Gottschall JL, Denomme GA. Barriers to using molecularly typed minority red blood cell donors in support of chronically transfused adult patients with sickle cell disease. Transfusion. 2015;55(6):1399-1406.
9. Yee ME, Josephson CD, Winkler AM, et al. Red blood cell minor antigen mismatches during chronic transfusion therapy for sickle cell anemia. Transfusion. 2017;57(11):2738-2746.
10. Campbell-Lee SA, Gvozdjan K, Choi KM, et al. Red blood cell alloimmunization in sickle cell disease: assessment of transfusion protocols during two time periods. Transfusion. 2018;58(7):1588-1596.
11. Miller ST, Kim H-Y, Weiner DL, et al. Red blood cell alloimmunization in sickle cell disease: prevalence in 2010. Transfusion. 2013;53(4):704-709.
12. Coleman S, Westhoff CM, Friedman DF, Chou ST. Alloimmunization in patients with sickle cell disease and underrecognition of accompanying delayed hemolytic transfusion reactions. Transfusion. 2019;59(7):2282-2291.
13. Chou ST, Evans P, Vege S, et al. RH genotype matching for transfusion support in sickle cell disease. Blood. 2018;132(11):1198-1207.
14. Floch A, Gien D, Tournamille C, et al. High immunogenicity of red blood cell antigens restricted to the population of African descent in a cohort of sickle cell disease patients. Transfusion. 2018;58(6):1527-1535.
15. Harm SK, Yazer MH, Monis GF, Triulzi DJ, Aubuchon JP, Delaney M. A centralized recipient database enhances the serologic safety of RBC transfusions for patients with sickle cell disease. Am J Clin Pathol. 2014;141(2):256-261.

A phase II study of brentuximab vedotin in patients with relapsed or refractory Epstein-Barr virus-positive and CD30-positive lymphomas

Epstein-Barr virus (EBV) has etiological implications in the development of a wide range of lymphoproliferative lesions and malignant lymphomas of B-cell or T/NK-cell origin. Among peripheral T-cell lymphomas and diffuse large B-cell lymphomas, EBV-associated cases have a poorer prognosis compared to that of EBV-negative lymphomas.[1,2] Given that CD30, a member of the tumor necrosis factor receptor family, is frequently expressed in EBV-infected lymphoid cells, CD30 might represent an ideal target for the treatment of EBV-positive and CD30-positive lymphomas. Brentuximab vedotin is an antibody-drug conjugate comprising the chimeric IgG1 antibody cAC10 specific for human CD30 and the microtubule-disrupting agent monomethyl auristatin E via a protease-cleavable linker.

An open-label, multicenter, investigator-initiated phase II study was designed to evaluate the activity of brentuximab vedotin in patients with EBV-positive and CD30-positive non-Hodgkin lymphomas with various levels of CD30 in the relapsed or refractory setting (registered at Clinicaltrials.gov as NCT02388490). The optimal Simon two-stage design was used to test the null hypothesis of an objective response rate (ORR) of 20% against the alternative hypothesis of a 45% ORR. According to this design, ten patients were accrued in the first stage. Stage II was delayed until the completion of four or more cycles of study medication in the last subject in stage I. If more than three responders were observed, 15 additional patients would be accrued for a total of 25. This study design yields a type I error of 10% and a power of 90%. The study was approved by the institutional review board at each participating site and written informed consent was obtained in accordance with the Declaration of Helsinki.

A total of 25 patients with relapsed or refractory EBV-positive lymphomas also positive for CD30 (≥ 1% of tumor cells) were enrolled in this study between March 2016 and January 2018 at Seoul National University Hospital and Seoul National University Bundang Hospital. Positivity for EBV and CD30 expression was reviewed by experienced hematopathologists in each participating center and confirmed by a specialized hematopathologist (YKJ). All patients were administered 1.8 mg/kg brentuximab vedotin intravenously every 3 weeks for up to 16 cycles or until disease progression. Tumor measurements were assessed at screening, after completion of cycle 2, every 6 weeks until cycle 16, and at 4 to 8 weeks after the last dose of brentuximab vedotin. The patients' baseline characteristics and diagnostic data are presented in *Online Supplementary Table S1*. The median age of the 20 men and 5 women was 67 years (range, 38-87) and most patients had EBV-positive mature T/NK-cell neoplasms (88%). Most patients were diagnosed at advanced stage (III or IV) and about a quarter of the patients were heavily pretreated; one patient had undergone a prior autologous stem cell transplant. Patients received a median of nine cycles of brentuximab vedotin (range, 1-16), and nine patients completed the planned 16 cycles of brentuximab vedotin administration. The most common reasons for discontinuation were progressive disease (n=14, 56%) and adverse events (n=2, 8%).

The primary endpoint was the ORR based on the revised Cheson criteria or modified Severity Weighted Assessment Tool (SWAT) criteria in the case of cutaneous lymphomas.[3,4] The ORR in the intention-to-treat population of 25 patients was 48% (90% confidence interval [CI]: 31%-64%) (Table 1). The amount of tumor shrinkage of the target lesion from baseline for individual patients is shown in Figure 1. The correlation of CD30 expression level with the clinical response was assessed according to subgroup analysis. However, CD30 expression levels and ORR were not considerably different, although clinical responses were noted across all expression levels (Table 1).

Secondary objectives of the study were to evaluate the safety profile, progression-free survival, duration of response, and overall survival. The duration of response was assessed in 12 patients who had objective responses and the median duration was 10 months (95% CI: 4.2-21.0). The response continued even after the completion of the planned 16 cycles of brentuximab vedotin administration in three of these 12 patients (25%) at the time of data cut-off. The median duration of follow-up was 20 months (range, 1.7-30.4 months). For the intention-to-

Table 1. Clinical outcomes of brentuximab vedotin treatment according to lymphoma subtype and CD30 expression.

		Lymphoma subtype		CD30 expression		
	All (n=25)	Mature T/NK cell (n=22)	Mature B cell (n=3)	< 10% (n=13)	10-49% (n=5)	≥ 50% (n=7)
ORR	48%	46%	67%	46%	60%	43%
CR	20% (n=5)	18% (n=4)	33% (n=1)	15% (n=2)	60% (n=3)	0% (n = 0)
PR	28% (n=7)	27% (n=6)	33% (n=1)	31% (n=4)	0% (n=0)	43% (n = 3)
DoR (months)	10.1 (95% CI: 4.2-NE)	9.7 (95% CI: 7.1-12.4)	2.2 (95% CI: NE)	10.5 (95% CI: 3.7-17.2)	8.7 (95% CI: 3.9-13.6)	5.0 (95% CI: 0.6-9.3)
PFS (months)	6.1 (95% CI: 2.8-13.5)	6.1 (95% CI: 0-13.9)	3.0 (95% CI: 0.5-5.5)	5.5 (95% CI: 0-15.3)	9.7 (95% CI: 0-24.3)	6.1 (95% CI: 0-14.6)
OS (months)	15.6 (95% CI: 6.1-NE)	15.7 (95% CI: 4.2-27.1)	NE	11.1 (95% CI: 0.8-21.5)	NE	21.1 (95% CI: NE)

ORR: objective response rate; CR: complete remission; PR: partial remission; SD: stable disease; PD: progressive disease; DoR: duration of response; PFS: progression-free survival; OS: overall survival; NE: not estimable; 95% CI: 95% confidence interval.

treat population, the median progression-free survival and overall survival were 6·2 months (95% CI: 2.9-13.6) and 15.7 months (95% CI: 6.1-not reached), respectively (*Online Supplementary Figure S1A, B*). As of January 2, 2019, 13 patients had died of disease progression. Pretreatment serum samples were collected from the whole blood of all patients. The level of soluble CD30 (sCD30) was determined using an enzyme-linked immunosorbent assay. The median value of sCD30 was 99.03 ng/mL (range 2.67-2155.78 ng/mL), and the ORR in the groups with high sCD30 (≥ 99.03 ng/mL) and low sCD30 (<99.03 ng/mL) were not significantly different (46% *vs.* 50%; *P*=0.85). In addition, the sCD30 level was not significantly associated with either progression-free survival or overall survival (*Online Supplementary Figure S1C, D*).

Adverse events were graded according to the National Cancer Institute Common Terminology Criteria for Adverse Events (NCI CTCAE), version 4.03. Treatment-related adverse events are summarized in *Online Supplementary Table S2*. All patients except for one had adverse events of any grade, among which 45% were considered treatment-related by the investigators. Nine patients (36%) had 15 serious adverse events during the study. The most common treatment-related adverse events were peripheral neuropathy (48%), neutropenia (44%), thrombocytopenia (20%), and rash (16%). The most common treatment-related adverse events of grade 3/4 were neutropenia (20%), thrombocytopenia (12%), and anemia (8%). Overall, the grade 3/4 adverse events were manageable with the standard guidelines and patients recovered completely.

To explore the potential molecular biomarkers and resistance mechanisms, DNA obtained from formalin-fixed paraffin-embedded tumor tissues was deeply sequenced using a customized multigene panel test comprising 120 genes. The mutational profiles of 18 tumors in 14 patients are summarized in Figure 2. The samples of tumor tissue were taken pretreatment from ten patients and both before and after treatment with brentuximab vedotin from four patients. A majority of patients (n=8, 57%) carried *TET2* mutations and five patients (36%) carried *RHOA* mutations. In addition, *DMNT3A* and *IHD2* mutations were detected in four and three patients, respectively. Among the four patients with genomic profiles from paired pre- and post-treatment samples, a novel *TRAF3*^{D483E} mutation (variant allele frequency, 5.2%) was only identified in resistant tumors of patient SNU20. In addition, *CARD11*^{V1073M} (variant allele frequency, 3.18%) mutations were acquired at disease progression in patient SNU13.

In this phase II study, the clinical activity of brentuximab vedotin in relapsed or refractory EBV-positive and CD30-positive non-Hodgkin lymphomas was significant and durable with an ORR of 48% and a duration of response of 10.1 months, and thus met the primary endpoint. In addition, brentuximab vedotin was well tolerated with manageable toxicities in these heavily pretreated patients with advanced diseases.

Several studies with brentuximab vedotin alone or in combination with chemotherapy have shown its remarkable success in Hodgkin lymphoma and systemic anaplastic large cell lymphoma with high CD30 expression in both the frontline as well as refractory settings.[5-8] These previous studies provided the scientific rationale for considering that brentuximab vedotin might be active

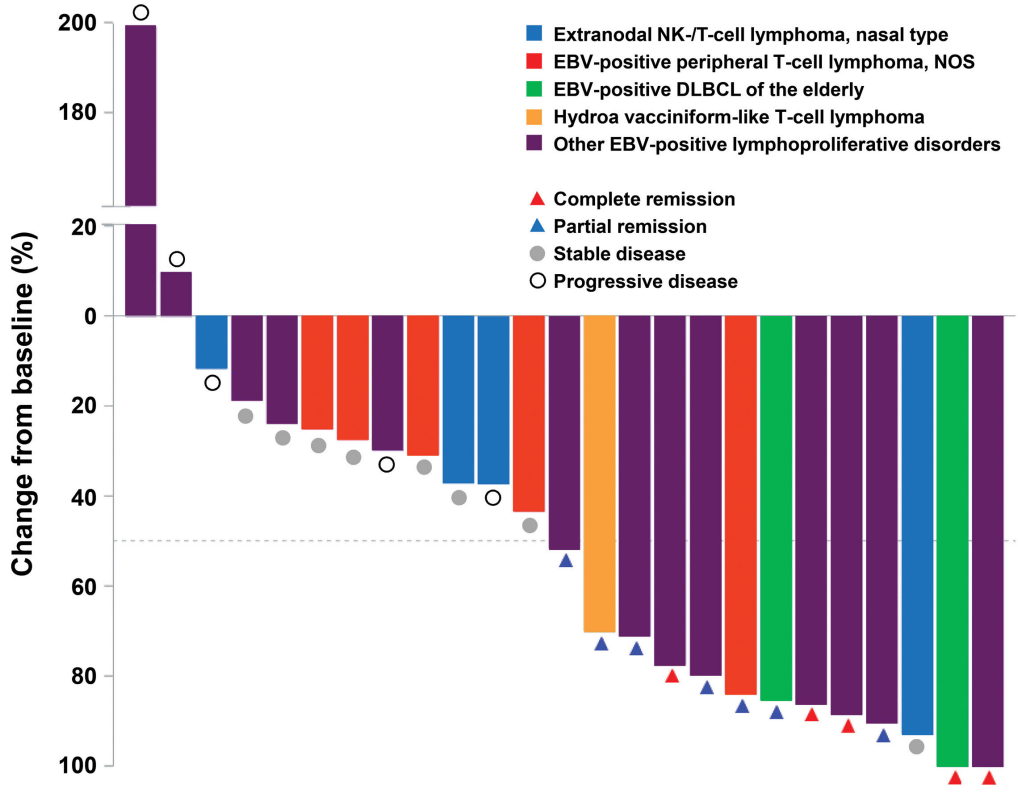

Figure 1. Response to brentuximab vedotin. Waterfall plot of maximum percent change in tumor size of target lesions from baseline. NK: natural killer; NOS: not otherwise specified; EBV: Epstein-Barr virus; DLBCL: diffuse large B-cell lymphoma.

against other lymphomas expressing CD30 at varying rates (0-100%). So far, brentuximab vedotin has shown promising results in relapsed or refractory diffuse large B-cell lymphoma, T-cell lymphomas, and mycosis fungoides/Sézary syndrome.[9-12] The ORR of our study was similar to that of a previous study in relapsed and refractory T-cell lymphomas.[10] However, considering the poor prognostic group of EBV-positive lymphomas in our study, the survival outcomes were encouraging and support the use of brentuximab vedotin for CD30-positive T- and B-cell lymphomas listed in National Comprehensive Cancer Network guidelines.

Although the nuclear factor kappa B (NF-κB) and mitogen-activated protein kinase pathways are known to be involved in CD30-mediated signaling,[13] pleiotropic effects were observed *in vitro* after stimulation with CD30L or the monoclonal antibody Ki-1.[14] This suggests that the CD30 signaling pathway might be differentially

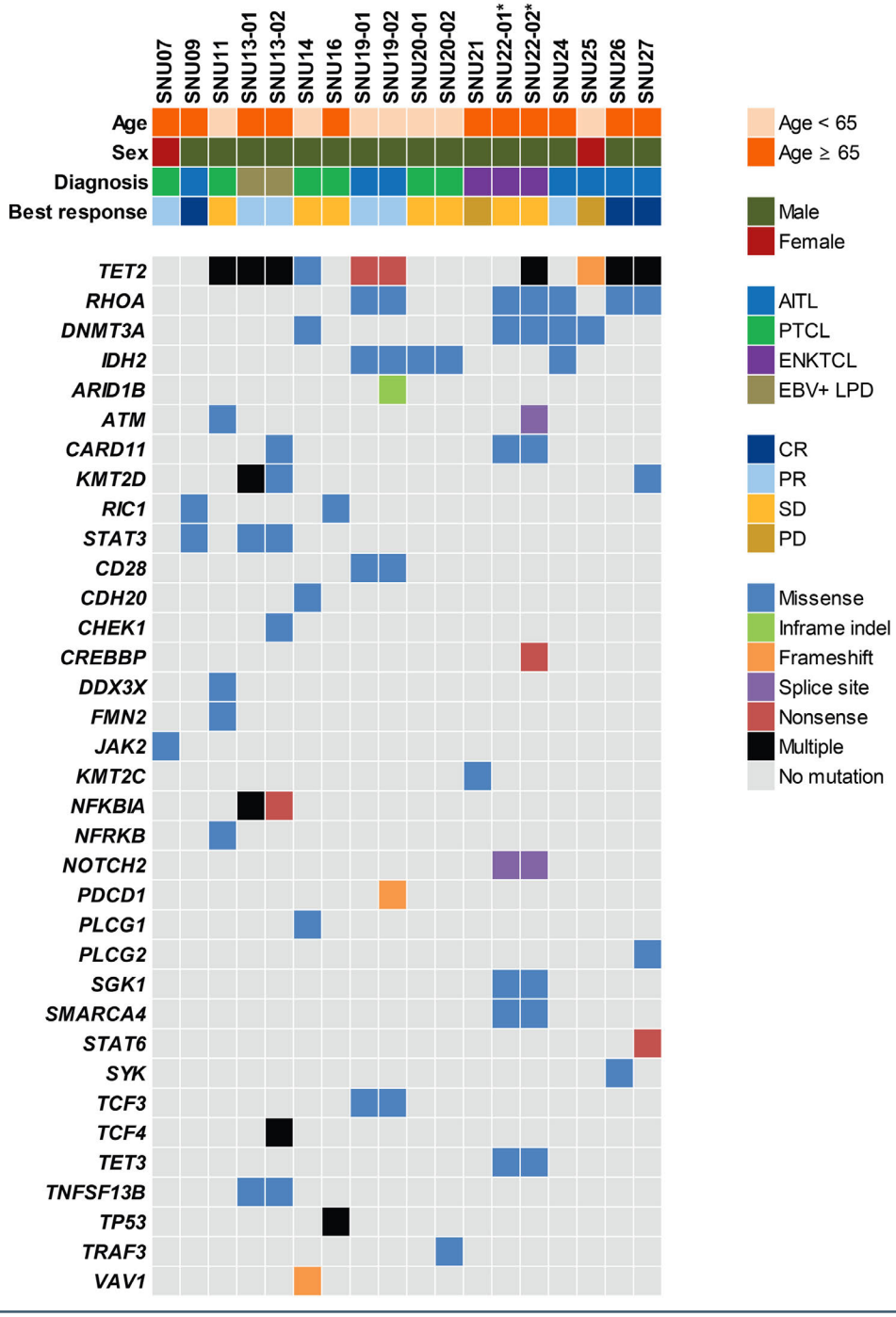

Figure 2. Mutational profiles of 14 patients in this trial. Samples for 14 patients, including four pairs of sequentially acquired samples, were subjected to targeted sequencing encompassing 120 lymphoma-associated genes. *Patient SNU22 was initially diagnosed as having extranodal NK/T-cell lymphoma according to the patient's referral record from another hospital. CR: complete remission; PR: partial remission; SD: stable disease; PD: progressive disease; AITL: angioimmunoblastic T-cell lymphoma; PTCL: peripheral T-cell lymphoma; ENKTCL: extranodal NK/T-cell lymphoma, nasal type; EBV+ LPD: Epstein-Barr virus-positive T-cell lymphoproliferative disorders.

regulated depending on the cell type or tumor microenvironment. This would partly explain why other lymphomas, albeit with high CD30 expression, are not as responsive as Hodgkin lymphoma and systemic anaplastic large cell lymphoma, as evident from recent studies, thereby showing no clear relation between CD30 expression and clinical response.[9-11] Conversely, even if CD30 expression was very low, tumor response was observed. Furthermore, tumor heterogeneity or unrevealed mechanisms of resistance may also contribute to the irrelevance of CD30 expression and efficacy of brentuximab vedotin. A recent study demonstrated that A20 negatively regulates the NF-κB pathway, and upregulation of NF-κB activity mediates resistance to brentuximab vedotin in Hodgkin lymphoma cell lines.[15] In this study, targeted sequencing of paired tumor tissues revealed *CARD11* and *TRAF3* mutations related to constitutive NF-κB activation, and the mutations were identified as possible resistance mechanisms to brentuximab vedotin.

In conclusion, brentuximab vedotin alone demonstrated significant and durable clinical activity with a manageable toxicity profile in relapsed or refractory EBV-positive and CD30-positive non-Hodgkin lymphomas. However, the results of this study, including correlative outcomes, should be interpreted cautiously because of the small number of patients, the single-arm design as well as the heterogeneous group of diseases. Thus, brentuximab vedotin warrants further investigational study, either as monotherapy or in combination, on a larger scale in this patient population.

Miso Kim,[1,2] Jeong-Ok Lee,[3] Jiwon Koh,[4] Tae Min Kim,[1,2] Ji Yun Lee,[3] Yoon Kyung Jeon,[2,4] Bhumsuk Keam,[1,2] Dong-Wan Kim,[1,2] Jong Seok Lee[3] and Dae Seog Heo[1,2]

[1]Department of Internal Medicine, Seoul National University Hospital, Seoul, Republic of Korea; [2]Seoul National University Cancer Research Institute, Seoul, Republic of Korea; [3]Department of Internal Medicine, Seoul National University Bundang Hospital, Seongnam, Republic of Korea and [4]Department of Pathology, Seoul National University Hospital, Seoul, Republic of Korea.

Correspondence: TAE MIN KIM - gabriel9@snu.ac.kr

doi:10.3324/haematol.2021.278301

Received: January 8, 2021.

Accepted: March 11, 2021.

Pre-published: April 1, 2021.

Disclosures: TMK received a research grant from AstraZeneca-KHIDI not related to this work. DWK received travel and accommodation support for advisory board meeting attendance from Amgen and Daiichi-Sankyo not related to this work. All other authors declare that they have no competing interests.

Contributions: TMK designed the study; MK and TMK wrote the manuscript; YKJ did the pathological review. All authors provided study materials or patients, contributed to the collection and assembly of data, data analysis, and interpretation, and reviewed and approved the final draft of the manuscript.

Acknowledgments: we thank the patients who participated in this trial and their families. We also thank Soyeon Kim, Ph.D., Sujung Huh, and Daye Paek for their contribution to the soluble CD30 experiments and Seonah Ha, Ph.D., who assisted in medical writing. Statistical analyses were supported by the Medical Research Collaborating Center (MRCC), Seoul National University, Seoul, Korea.

Funding: this study was funded by Takeda Pharmaceuticals Co, Ltd. and supported by a grant from the Korean Health Technology R&D Project "Strategic Center of Cell and Bio Therapy for Heart, Diabetes & Cancer" through the Korea Health Industry Development Institute (KHIDI), funded by the Ministry of Health & Welfare (MHW) (grant number: HI-17C-2085).

References

1. Dupuis J, Emile JF, Mounier N, et al. Prognostic significance of Epstein-Barr virus in nodal peripheral T-cell lymphoma, unspecified: a Groupe d'Etude des Lymphomes de l'Adulte (GELA) study. Blood. 2006;108(13):4163-4169.
2. Park S, Lee J, Ko YH, et al. The impact of Epstein-Barr virus status on clinical outcome in diffuse large B-cell lymphoma. Blood. 2007; 110(3):972-978.
3. Cheson BD, Pfistner B, Juweid ME, et al. Revised response criteria for malignant lymphoma. J Clin Oncol. 2007;25(5):579-586.
4. Olsen EA, Whittaker S, Kim YH, et al. Clinical end points and response criteria in mycosis fungoides and Sezary syndrome: a consensus statement of the International Society for Cutaneous Lymphomas, the United States Cutaneous Lymphoma Consortium, and the Cutaneous Lymphoma Task Force of the European Organisation for Research and Treatment of Cancer. J Clin Oncol. 2011;29(18):2598-2607.
5. Younes A, Gopal AK, Smith SE, et al. Results of a pivotal phase II study of brentuximab vedotin for patients with relapsed or refractory Hodgkin's lymphoma. J Clin Oncol. 2012;30(18):2183-2189.
6. Pro B, Advani R, Brice P, et al. Brentuximab vedotin (SGN-35) in patients with relapsed or refractory systemic anaplastic large-cell lymphoma: results of a phase II study. J Clin Oncol. 2012; 30(18): 2190-2196.
7. Connors JM, Jurczak W, Straus DJ, et al. Brentuximab vedotin with chemotherapy for stage III or IV Hodgkin's lymphoma. N Engl J Med. 2018;378(4):331-344.
8. Horwitz S, O'Connor OA, Pro B, et al. Brentuximab vedotin with chemotherapy for CD30-positive peripheral T-cell lymphoma (ECHELON-2): a global, double-blind, randomised, phase 3 trial. Lancet. 2019;393(10168):229-240.
9. Jacobsen ED, Sharman JP, Oki Y, et al. Brentuximab vedotin demonstrates objective responses in a phase 2 study of relapsed/refractory DLBCL with variable CD30 expression. Blood. 2015;125(9):1394-1402.
10. Horwitz SM, Advani RH, Bartlett NL, et al. Objective responses in relapsed T-cell lymphomas with single-agent brentuximab vedotin. Blood. 2014;123(20):3095-3100.
11. Duvic M, Tetzlaff MT, Gangar P, Clos AL, Sui D, Talpur R. Results of a phase II trial of brentuximab vedotin for CD30+ cutaneous T-cell lymphoma and lymphomatoid papulosis. J Clin Oncol. 2015; 33(32):3759-3765.
12. Kim YH, Tavallaee M, Sundram U, et al. Phase II investigator-initiated study of brentuximab vedotin in mycosis fungoides and Sézary syndrome with variable CD30 expression level: a multi-institution collaborative project. J Clin Oncol. 2015;33(32):3750-3758.
13. Nishikori M, Ohno H, Haga H, Uchiyama T. Stimulation of CD30 in anaplastic large cell lymphoma leads to production of nuclear factor-kappaB p52, which is associated with hyperphosphorylated Bcl-3. Cancer Sci. 2005;96(8):487-497.
14. Gruss HJ, Boiani N, Williams DE, Armitage RJ, Smith CA, Goodwin RG. Pleiotropic effects of the CD30 ligand on CD30-expressing cells and lymphoma cell lines. Blood. 1994;83(8):2045-2056.
15. Wei W, Lin Y, Song Z, et al. A20 and RBX1 regulate brentuximab vedotin sensitivity in Hodgkin lymphoma models. Clin Cancer Res. 2020;26(15):4093-4106.

Dynamic contrast-enhanced magnetic resonance imaging quantification of leukemia-induced changes in bone marrow vascular function

In this study we show that dynamic contrast enhanced (DCE) magnetic resonance imaging (MRI) can quantify the impact of human acute myeloid leukemia (AML) on bone marrow (BM) vasculature by optimizing an *in vivo* DCE-MRI method and assessing the method's diagnostic and prognostic potential.

AML, the most common acute leukemia in adults,[1] is a very heterogeneous disease with regard to both its genetic basis and outcome of treatment. The BM microenvironment is important because leukemia cells are able to change the functions of normal tissues, favoring proliferation of the cells and protecting them from external harm.[2-4] BM vascular remodeling induced by AML cells favors a more hypoxic microenvironment,[4] and is thought to protect leukemia stem cells from therapy, being a poor prognostic factor in AML.[5,6] Most preclinical studies use microscopy-based methods to assess environmental changes, namely vascular leakiness and perfusion,[7,8] leaving little space for direct translation of the optimized methodology. In the clinic, perfusion imaging is an important tool in the diagnosis and management of various diseases. The advantages of using MRI for perfusion imaging are its superiority in terms of soft tissue contrast, absence of ionizing radiation (compared to computerized tomography and nuclear imaging such as positron emission tomography and single photon emission computed tomography) and the possibility of imaging larger body areas or even the whole body. DCE-MRI is a method commonly used to measure perfusion.[9] DCE-MRI quantifies signal changes due to the passing of a contrast agent through the imaging area. By modeling the signal kinetics, it is possible to quantify vascular parameters such as perfusion, leakiness, and blood volume. Even though it has been around for over 20 years, DCE-MRI has not yet been fully implemented in many clinical pathways because of the lack of standardization in image acquisition and analysis methods, rendering it mostly a research-based tool.

We used DCE-MRI to quantify the impact of human AML on BM vasculature in an animal model. In-house MatLab scripts were used to quantify non-model-based parameters taken directly from the contrast agent kinetic curves (see below). The parameters quantified are illustrated in Figure 1A. Changes in the first part of the DCE curve reflect blood flow and blood volume, while changes in the second part of the DCE curve reflect changes in vascular permeability and extravascular space (Figure 1A).[9]

We have previously reported that leukemia induces BM vascular leakiness, using intravital imaging of the calvaria,[4] which was not observed in mice injected with cord blood (*Online Supplementary Figure S1A, B*), when compared to healthy, age-matched mice that were not injected (NI). To test the sensitivity of DCE-MRI in quantifying leukemia-induced BM vascular dysfunction, three different leukemia cell lines were used (U937, HL60, and ML1), and mice were scanned at different stages of the disease (*Online Supplementary Figure S1C*). When compared to healthy, age-matched NI controls, leukemia mice showed altered BM DCE kinetics (Figure 1B), with reduced contrast enhancement (CE; BM vascular density), reduced wash-in rate (WiR; blood flow), increased initial wash-out rate and wash-out rate (iWoR and WoR; vascular permeability and extravascular space) (Figure 1C). BM vascular dysfunction was not dependent on high leukemia burden, as even low levels of leukemia engraftment (<20% $mCD45^{-}hCD33^{+}$ cells present in the BM) significantly altered BM vascular function (Figure 1C, open circles). Leukemia is known to promote angiogenesis, but with disorganized and leaky vessels.[2,4,10] The reduced CE in our leukemia cohort is in agreement with this, as CE relates to the proportion of functional blood vessels per pixel. With deregulated BM vascular parameters correlating with aging in healthy mice (*Online Supplementary Figure S1D*), we compared younger (12-16 weeks) *versus* older (19-32 weeks) mice to understand whether age was affecting leukemia-induced BM vascular dysfunction. As shown in *Online Supplementary Figure S1D*, older, NI mice showed significantly reduced BM vascular density and increased BM vascular permeability, but we observed no effect of age in leukemia-injected mice (Figure 1C). This indicates that aging and leukemia seem to alter BM vascular permeability (WoR) and functional density (CE) to a similar extent. However, decreased BM blood flow/perfusion (WiR) seems to be a leukemia-specific effect, as it was the only parameter unaltered by aging (*Online Supplementary Figure S1E*). In fact, receiver operating characteristic (ROC) analysis highlighted WiR as the best parameter for distinguishing healthy from leukemic BM (Figure 1D; $AUC_{WiR} = 1.000$).

Differences in vascular density and function between different areas of the bone have been reported.[3] Using intravital two-photon imaging of the calvaria, we confirmed that at early stages of the disease the areas of leukemia engraftment (GFP^{+} cells) coincided with areas of reduced perfusion and irregular vessel structure, confirming a heterogeneous vascular dysfunction linked with leukemia burden (*Online Supplementary Figure S1F*). For this reason, we hypothesize that averaged DCE-MRI parameters could have some limitations in heterogeneous and low-engrafted mice. To obtain a detailed picture of DCE-MRI-measured vascular aberrations and evaluate their spatial distribution along the femur, we performed pixel-by-pixel (pbp, with each pixel corresponding to an area of ~200 μm) analysis for three DCE-MRI parameters: CE, WiR, and WoR. NI mice present a homogeneous distribution of functional vessels in the epiphysis and along the endosteum of the diaphysis (Figure 1E, CE); high vascular perfusion in the central marrow of the diaphysis (Figure 1E, WiR), and higher vascular permeability at the epiphysis and in proximity with the endosteum of the diaphysis. In the presence of AML, there is an aberrant, heterogeneous distribution of these parameters along the femur. In groups injected with HL60 and ML1, pbp analysis highlighted areas (pockets) with severe vascular dysfunction (Figure 1E, white rectangles), surrounded by less affected vasculature. Importantly, areas that showed lower functional vascular density (low CE) corresponded to areas in which both the vascular perfusion (WiR) and permeability (WoR) were mostly affected (Figure 1E, white rectangles). In the group injected with U937 cells, there were no obvious pockets of vascular dysfunction, with this being present throughout the femur. Thus, our pbp analysis approach was successful in resolving the spatial distribution of vascular parameters along the femur and unveiling the heterogeneity of vascular dysfunction in AML xenografts.

To further test the clinical potential of BM DCE-MRI, we scanned mice engrafted with samples from AML patients (i.e., with patient-derived xenografts, PDX). Different AML samples had different engraftment capacities (*Online Supplementary Figure S2A*) and DCE kinetics (Figure 2A), echoing the heterogeneous nature of this dis-

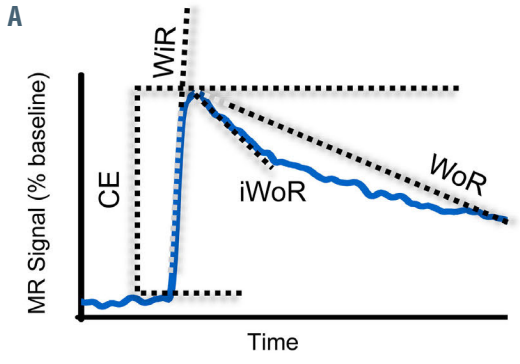

Parameters	Related to
CE: Contrast Enhancement	Functional vascular density
WiR: Wash-in Rate	Blood inflow/velocity; perfusion
WoR: Wash-out Rate	Tissue clearance capacity; permeability
iWoR: initial Wash-out Rate	Same as above, but shorter time frame

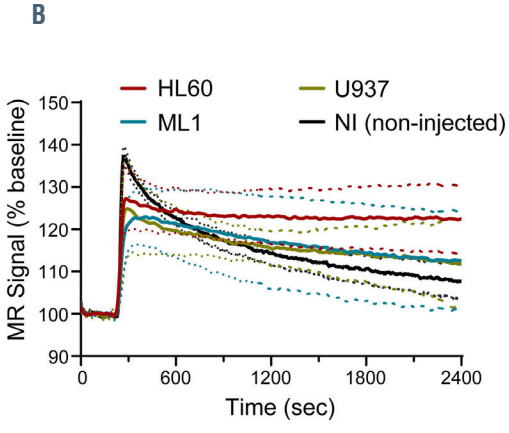

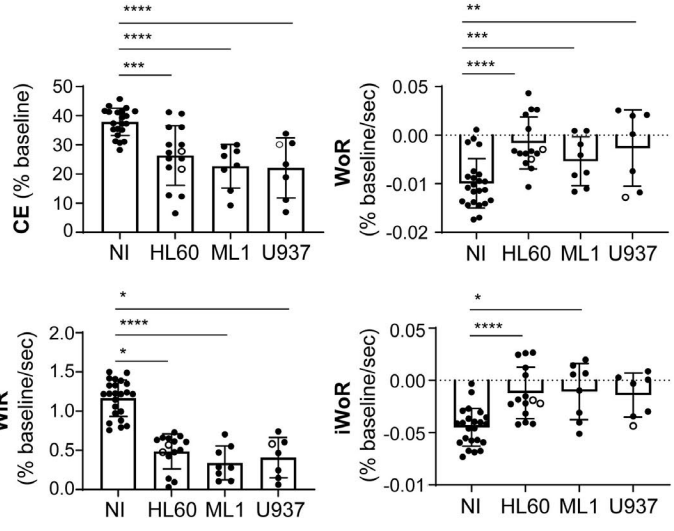

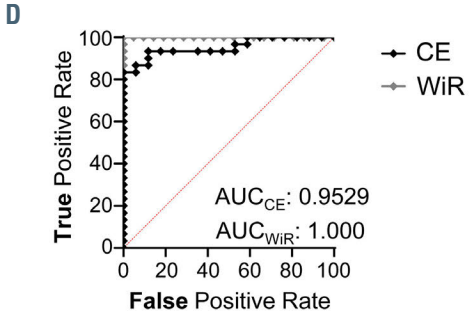

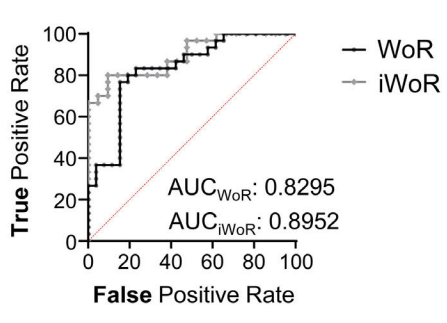

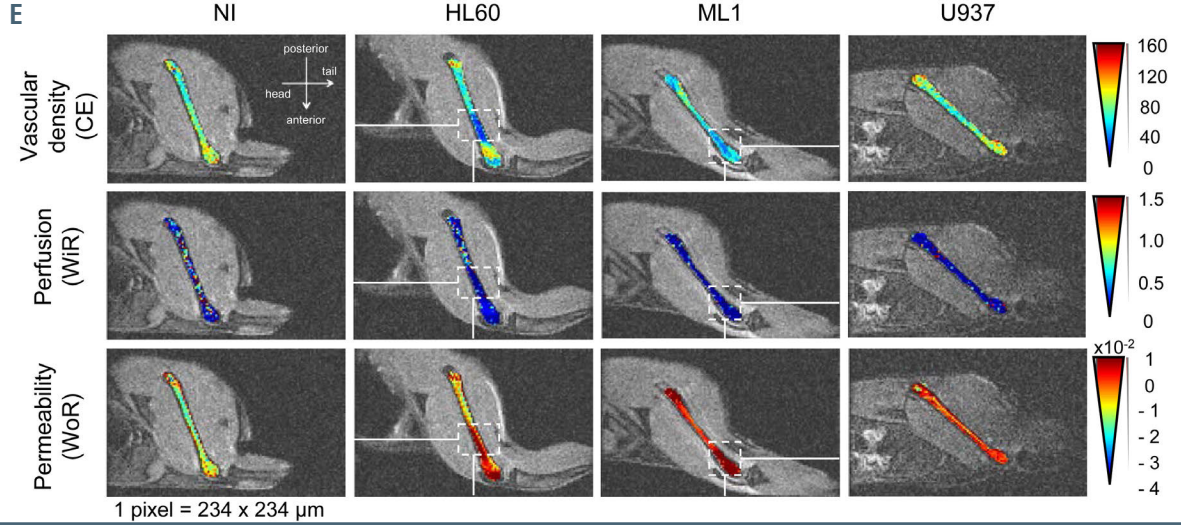

Figure 1. Legend on following page.

Figure 1. Bone marrow vascular changes in aging and leukemia cell line models, measured by dynamic contrast enhanced magnetic resonance imaging. (A) Schematic representation of a dynamic contrast enhanced magnetic resonance imaging (DCE-MRI) time intensity curve and the parameters measured. The table explains what each parameter relates to. (B) Bone marrow (BM) DCE-MRI time intensity curves of non-injected mice (black), mice injected with HL60 (red), ML1 (blue) or U937 (olive green). (C) Quantification of BM DCE-MRI parameters CE, WIR, WoR, and iWoR in non-injected mice (NI) and mice injected with either HL60, ML1 and U937. White circles represent mice with a leukemia burden <20%. Each dot represents one mouse. White columns represent the average of the group and error bars represent the standard deviation of the mean. (D) Receiver operating characteristic analysis of the diagnostic capabilities of the BM DCE-MRI parameters to distinguish malignant from non-malignant BM in the cell line model. (E) Pixel by pixel analysis of BM DCE-MRI parameters showing leukemia-induced changes to the BM tissue. For the HL60 and ML1 groups, white rectangles represent the same area in the BM. MR: magnetic resonance; NI: not injected: AUC: area under the curve; CE: contrast enhancement; WiR: wash-in rate; WoR: wash-out rate; iWoR: initial wash-out rate; *P<0.05; **P<0.01; ***P<0.001; ****P<0.0001.

ease. Mice injected with AML1 had the highest degree of vascular dysfunction (Figure 2A, B), which could also be seen in the pbp analysis (Figure 2C, AML1). Mice from the remaining AML PDX experiments showed no significant changes in CE or WoR, when compared to age-matched controls (old NI mice), similarly to the results from the experiments with AML cell lines (*Online Supplementary Figure S1E*). However, grafts from all the AML patients induced a significant deregulation of the four DCE-MRI parameters compared to those in young NI controls (Figure 2B). As hypothesized, averaged DCE-MRI vascular parameters were not sensitive enough to detect altered BM vasculature in the AML PDX model of low disease burden (<20% $hCD33^+$ cells present in the BM) (Figure 2B, open circles), a limitation that we were able to overcome with pbp analysis (detailed below). Our data highlight the heterogeneous nature of the primary disease compared to cell line models. However, regardless of the broad spectrum of vascular dysfunction, the reduction in BM vascular perfusion (WiR) was again the most significantly affected parameter (Figure 2B) in AML PDX, with ROC curve analysis showing that WiR is of clinical relevance in distinguishing normal from leukemic BM (*Online Supplementary Figure S2B*).

To determine whether DCE-MRI could be used to monitor the BM vascular response to chemotherapy, PDX cohorts were treated with a standard chemotherapy protocol and analyzed during the remission phase. Although cytarabine significantly reduced leukemia burden (*Online Supplementary Figure S2C*), it did not rescue the altered BM vascular phenotype. BM vascular response to cytarabine treatment was diverse, with some groups showing partial rescue (AML1, AML2), and other groups showing no effect at all (*Online Supplementary Figure S2D*).

Pbp analysis showed that vascular dysfunction in some AML samples was located in the whole or most of the diaphysis (AML1, AML3), while in others it was located in small pockets (AML2). Mice injected with sample AML1 exhibited severe BM vascular dysfunction throughout the whole diaphysis, with hardly any perfused pixels (Figure 2C). Cytarabine treatment partly rescued the lack of vascularity in the diaphysis but could not rescue either the vascular perfusion or permeability (Figure 2C, AML1). Even though AML3 did respond to cytarabine treatment (*Online Supplementary Figure S2C*), it showed great similarities with AML1 in terms of most of the vasculature in the diaphysis being compromised, with little to no perfused pixels corresponding to high vascular permeability areas (Figure 2C, AML3). AML4 and AML5 showed similar patterns of pixel distribution. Before therapy, both AML samples showed a modest effect on BM vasculature, and for both samples, cytarabine treatment seemed to worsen the phenotype for both perfusion and permeability (Figure 2C, AML4 and AML5).

Imaging the microenvironment can provide important insights and has diagnostic power.[11,12] In leukemia, clinical imaging is not part of the routine follow-up of patients, although clinical studies have shown the utility of DCE-MRI.[5,13] Our preclinical imaging data, focusing on femoral BM, sheds some lights on the nature of the vascular microenvironment involvement in AML at diagnosis and during remission, and our in-house image analysis pipeline maximizes the translational potential of the technique, without the need of complex modeling analysis. This strategy resolves the caveats encountered with standard model-based quantification of the parameters, whose clinical relevance depends strongly on the mathematical model chosen.[14] Our results pave the way for the implementation of a novel human BM tailored DCE-MRI model which would help to provide an absolute or correlative biomarker in clinical settings. Among the various parameters analyzed, the WiR has the best diagnostic potential as measured by ROC analysis. This could potentially be helpful in the scenario of long-term disease, patients' refusal to have a bone marrow puncture, or high-risk and/or older patients in whom frequent and thorough follow-up monitoring might be a value. Future clinical investigations will be needed to formally address the utility of this technique.

We were also able to show that vascular dysfunction occurs in healthy aging. Recent reports suggest that a damaged BM niche could have a role in the aging process of the hematopoietic system.[15] High vascular permeability being associated with increased HSC activation and egress from the niche,[8] our data are in line with these findings and point to a possible therapeutic benefit from restoring normal vascular functionality.

All animal experiments in this study were performed under the project license (PPL 70/8904) approved by the UK Home Office and in accordance with the Francis Crick Institute AWERB (Animal Welfare and Ethics Review Board) guidelines. NOD.Cg-*Prkdc*^{scid}*Il2rg*^{tm1Wjl} (NSG) strains were obtained from Jackson Laboratory (Bar Harbor, ME, USA) and were bred in-house.

Cell lines (HL60, ML1, U937) came originally from the American Type Culture Collection (distributor LGC standards, UK) and were grown by our cell service at the Institute. Before use, these lines were authenticated using short tandem repeat profiling. Once authenticated, $2x10^6$ cells per mouse were injected intravenously into NSG mice of different ages. BM engraftment was assessed by FACS analysis of BM aspirate 2-4 weeks after injection. For specific experiments, cell lines were transfected with GFP-Luciferase lentivirus vector, as previously described.[4]

The collection and use of all human samples were approved by the East London Research Ethical Committee (REC:06/Q0604/110) and performed in accordance with the Declaration of Helsinki. Umbilical cord blood samples were obtained from normal full-term deliveries after signed informed consent.

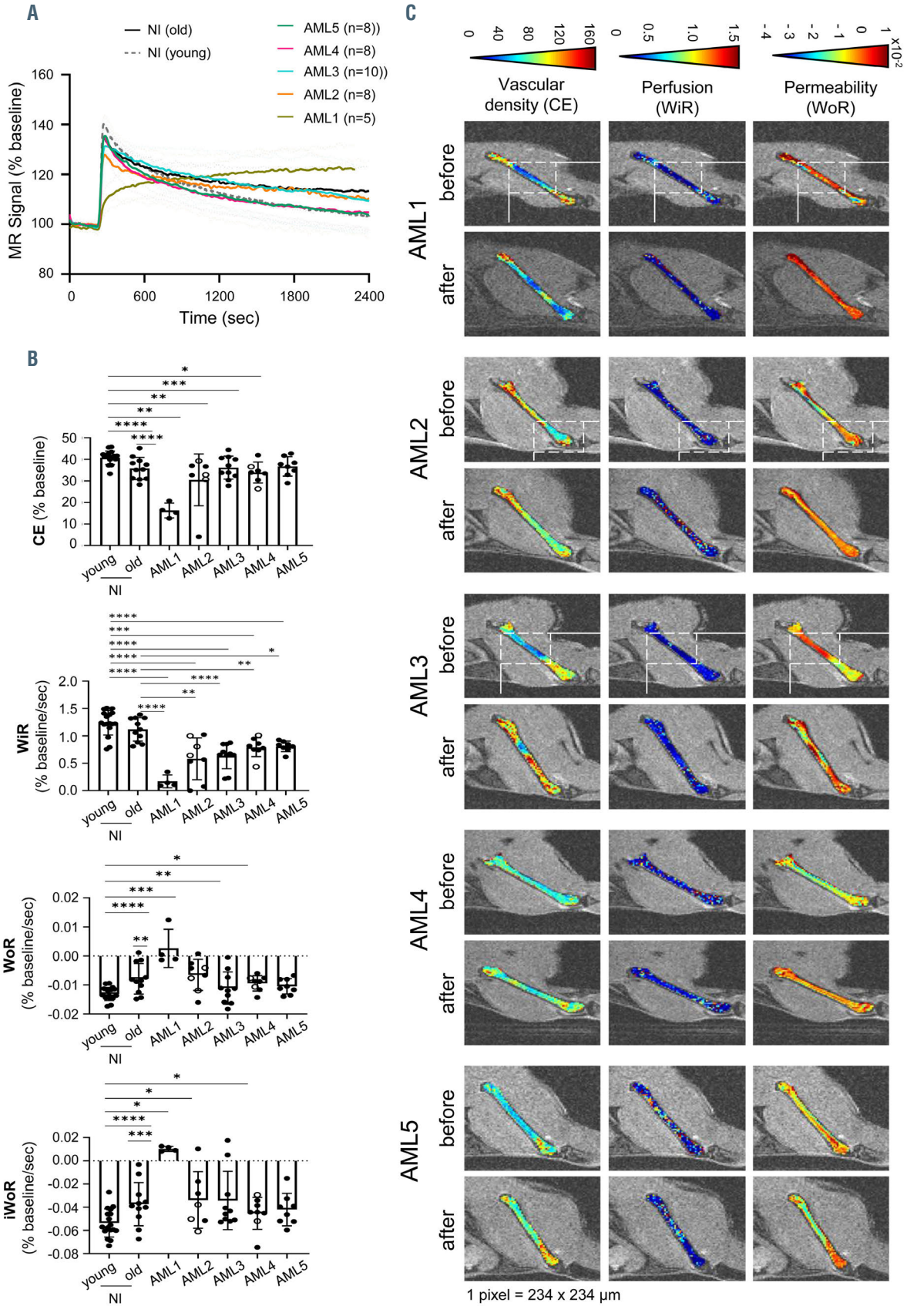

Figure 2. Legend on following page.

Figure 2. Dynamic contrast enhanced magnetic resonance imaging can help to distinguish normal from leukemic bone marrow in acute myeloid leukemia patient-derived xenograft models. (A) Bone marrow (BM) dynamic contrast enhanced magnetic resonance imaging (DCE-MRI) time intensity curves of non-injected young mice (NI, black), non-injected age-matched mice (NI, dashed black) and mice injected with samples from patients 1-5 with acute myeloid leukemia (AML1-AML5). (B) Quantification of the BM DCE-MRI parameters contrast enhancement, wash-in rate, wash-out rate and initial wash-out rate for the mice represented in (A). White circles represent mice with leukemia burden <20%. Each dot represents one mouse. White columns represent the average of the group and error bars represent the standard deviation of the mean. (C) Pixel by pixel analysis of BM DCE-MRI parameters from mice in *Online Supplementary Figure S1F*, showing leukemia-induced changes to the BM tissue. White rectangles represent the same area in the BM for that specific mouse. MR: magnetic resonance; NI: not injected; BM: bone marrow; AML: acute myeloid leukemia; DCE-MRI: dynamic contrast enhanced magnetic resonance imaging; CE: contrast enhancement; WiR: wash-in rate; WoR: wash-out rate; iWoR: initial wash-out rate; **P*<0.05; ***P*<0.01; ****P*<0.001; *****P*<0.0001.

AML samples were obtained after informed consent at St Bartholomew's Hospital (London, UK). T-cell depleted AML samples were injected intravenously into 8- to 12-weeks old unconditioned NSG mice ($2x10^6$ cells per mouse). Ten to 14 weeks after injection, mice were treated with a daily subcutaneous injection of cytarabine (10 mg/kg) for 7 consecutive days. Response to treatment response was assessed 2 weeks after the start of treatment, by flow cytometry analysis of BM aspirates.

At the end of each experiment, animals were euthanized and bone processed as already reported for FACS analysis.[4] The antibodies used were anti-mouse CD45-PerCPCy5 (1:200, eBioscience, #45045182); anti-human CD33-PE (1:100, BD Pharmingen, #555450); anti-human CD45- APC-eFluor 780 (1:100, eBioscience, #47045942). Flow cytometry analysis was performed using a Fortessa flow cytometer (BD Biosciences, Oxford, UK).

For magnetic resonance imaging, mice injected with leukemia cell lines were scanned 2-4 weeks after injection. Mice injected with AML patients' samples were scanned before and after treatment with cytarabine. MRI was performed on a 9.4 T horizontal bore system (Bruker GmbH) equipped with a B-GA12SH gradient coil system. RF transmission and reception were performed with a 40 mm ID quadrature birdcage coil (Bruker GmbH). A series of fast low-angle shot (FLASH) scans were used for femur localization and for slice positioning.

DCE scans were performed using a FLASH with the following parameters: repetition time = 17.639 ms; echo time = 1.859 ms; flip angle = 10°; repetition = 1100; field of view 30x30x0.5 mm^3; matrix 128x128, and resolution of 234 µm. Dotarem (0.4 mL/Kg, Guerbet, France) was injected 4 min after the start of the scan. The total duration of the scan was 41 min. All mice were placed in a head-first prone position for imaging. Anesthesia was induced and maintained using isoflurane (1-4%) in room air supplemented with oxygen (80%/20%). Temperature and respiration rate were monitored using an SA Instruments system (Bayshore, NY, USA).

To assess vascular perfusion in BM vessels by two-photon microscopy, we used a previously described protocol.[4] Images were obtained on a Zeiss 710 NLO laser scanning multiphoton microscope with a 20x 1.0 NA water immersion lens. The bone signal (second harmonic generation) was collected at 380-485 nm; GFP signals from AML cells was collected at 500-550 nm; the signal from Qtracker® 655 Vascular Label was collected at 640-690 nm by not descanned detectors. Each z stack of images (100-150 µM) was rendered in three dimensions using Imaris software (Bitplane).

We used Matlab 2019a for all DCE-MRI image analyes. One region-of-interest (ROI) was drawn for the BM and another for the muscle, per scan, per mouse. The signal in each ROI was then averaged and normalized to its baseline, so that it reflected percentage change from baseline. Signals from frames 3-90 were used as baseline. The muscle ROI was used as the internal control to rule out problems with the injection and/or systemic issues with blood circulation. Mice that showed abnormal DCE muscle kinetics were excluded from the analysis.

Parameters quantified from DCE time intensity curves were CE, WiR, WoR and iWoR. The CE was quantified as the percentage signal difference between baseline and maximum value from frames 95-300. The WiR was determined from the slope of the linear fit between the frame at which CE was reached and the frame at which the signal started to increase. The WoR was determined from the slope of the linear fit between the frame at which CE was reached and the end of the scan. The iWoR was determined from the slope of the linear fit between the frame at which CE was reached and the frame 5 mins later; Pbp analysis was done using the same scripts but applying them to every pixel inside of the bone marrow ROI.

Statistical differences in parameters between mice groups were calculated using two-tailed unpaired *t*-tests. Correlation analysis was done using two-tailed Pearson correlation analysis. ROC curves were calculated using the Wilson/Brown method.

Ana L. Gomes,[1] John Gribben,[2] Bernard Siow,[3#] Diana Passaro[1,4#] and Dominique Bonnet[1#]

[1]Haematopoietic Stem Cell Laboratory, The Francis Crick Institute; [2]Department of Haemato-Oncology, Barts Cancer Institute, Queen Mary University of London and [3]In Vivo Imaging, The Francis Crick Institute, London, UK

[#]BS, DP and DB contributed equally as co-senior authors.

Correspondence:

DOMINIQUE BONNET - dominique.bonnet@crick.ac.uk

DIANA PASSARO - diana.passaro@inserm.fr

BERNARD SIOW - bernard.siow@crick.ac.uk

doi:10.3324/haematol.2020.277269

Received: December 4, 2020.

Accepted: March 18, 2021.

Pre-published: March 25, 2021.

Disclosures: no conflicts of interest to disclose.

Contributions: ALG, DP and DB: wrote the manuscript; ALG, DP and DB designed the experiments; ALG and DP performed experiments and analyzed data; DB and DP secured funding; ALG and BS developed and optimized the MRI protocol; JG provided human AML samples.

Acknowledgments: the authors would like to thank the Biological Research Facility, Flow Cytometry and In Vivo Imaging core facilities at the Francis Crick Institute for their valuable help. The authors are grateful to Prof. John Gribben (St. Bartholomew's Hospital, London, UK) for providing human AML samples.

Funding: ALG was supported by an i2i translational grant scheme

from the Francis Crick Institute. DP was supported by a non-clinical junior research fellowship from the European Hematology Association. This work was supported by The Francis Crick Institute, which receives its core funding from Cancer Research UK (FC001045), The UK Medical Research Council (FC001045), and the Welcome Trust (FC001045).

Data sharing statement: scan data are available upon request. Please contact the corresponding author.

References

1. Sant M, Allemani C, Tereanu C, et al. Incidence of hematologic malignancies in Europe by morphologic subtype: results of the HAEMACARE project. Blood. 2010;116(19):3724-3734.
2. Hanoun M, Zhang D, Mizoguchi T, et al. Acute myelogenous leukemia-induced sympathetic neuropathy promotes malignancy in an altered hematopoietic stem cell niche. Cell Stem Cell. 2014; 15(3):365-375.
3. Duarte D, Hawkins ED, Lo Celso C. The interplay of leukemia cells and the bone marrow microenvironment. Blood. 2018;131(14):1507-1511.
4. Passaro D, Di Tullio A, Abarrategi A, et al. Increased vascular permeability in the bone marrow microenvironment contributes to disease progression and drug response in acute myeloid leukemia. Cancer Cell. 2017;32(3):324-341.
5. Padro T, Ruiz S, Bieker R, et al. Increased angiogenesis in the bone marrow of patients with acute myeloid leukemia. Blood. 2000;95(8):2637-2644.
6. Medyouf H. The microenvironment in human myeloid malignancies: emerging concepts and therapeutic implications. Blood. 2017; 129(12):1617-1626.
7. Bixel MG, Kusumbe AP, Ramasamy SK, et al. Flow dynamics and HSPC homing in bone marrow microvessels. Cell Rep. 2017;18(7): 1804-1816.
8. Itkin T, Gur-Cohen S, Spencer JA, et al. Distinct bone marrow blood vessels differentially regulate haematopoiesis. Nature. 2016; 532 (7599):323-328.
9. Cuenod CA, Balvay D. Perfusion and vascular permeability: basic concepts and measurement in DCE-CT and DCE-MRI. Diagn Interv Imaging. 2013;94(12):1187-1204.
10. Hussong JW, Rodgers GM, Shami PJ. Evidence of increased angiogenesis in patients with acute myeloid leukemia. Blood. 2000; 95(1):309-313.
11. Subashi E, Choudhury KR, Johnson GA. An analysis of the uncertainty and bias in DCE-MRI measurements using the spoiled gradient-recalled echo pulse sequence. Med Phys. 2014;41(3):032301.
12. Cao J, Pickup S, Clendenin C, et al. Dynamic contrast-enhanced MRI detects responses to stroma-directed therapy in mouse models of pancreatic ductal adenocarcinoma. Clin Cancer Res. 2019; 25(7): 2314-2322.
13. Hou HA, Shih TT, Liu CY, et al. Changes in magnetic resonance bone marrow angiogenesis on day 7 after induction chemotherapy can predict outcome of acute myeloid leukemia. Haematologica. 2010; 95(8):1420-1424.
14. Paudyal R, Lu Y, Hatzoglou V, et al. Dynamic contrast-enhanced MRI model selection for predicting tumor aggressiveness in papillary thyroid cancers. NMR Biomed. 2020;33(1):e4166.
15. Lazzari E, Butler JM. The instructive role of the bone marrow niche in aging and leukemia. Curr Stem Cell Rep. 2018;4(4):291-298.

Non-inhibitory antibodies inducing increased emicizumab clearance in a severe hemophilia A inhibitor patient

Hemophilia A is a bleeding disorder that results from coagulation factor VIII (FVIII) deficiency, which can be treated via substitution therapy using FVIII concentrates. However, the generation of neutralizing antibodies renders treatment ineffective in up to 30% of the severe patients.[1,2] Emicizumab is a humanized bispecific antibody that binds simultaneously to activated factor IX (FIXa) and factor X (FX), thereby mimicking the cofactor function of activated factor VIII (FVIIIa), even in the presence of FVIII inhibitors.[3,4] Once-weekly subcutaneous administration of emicizumab markedly decreased the bleeding rate in patients who had hemophilia A with or without FVIII inhibitors.[5-8] However, anti-drug antibodies with neutralizing potential can develop in a small number of patients and have been associated with decreased emicizumab plasma concentrations and loss of efficacy.[9,10] Although the development of neutralizing anti-emicizumab antibodies is rare and routinely biological monitoring is not recommended in patients treated with emicizumab, it is still important to detect the presence of such antibodies in case of bleeding events. In this study, we describe the development of non-inhibitory anti-emicizumab antibodies that selectively provoke increased emicizumab clearance in a severe hemophilia A patient with inhibitors.

A 2-year-old boy with severe hemophilia A developed an anti-FVIII inhibitor (1 BU/mL) at 19 exposure days. The patient failed to respond to immune tolerance induction and venous access became extremely complicated. Treatment with emicizumab was therefore initiated with four loading doses (3 mg/kg/week) followed by weekly treatment (1.5 mg/kg/week). Clinical outcomes were excellent with no bleeding episodes or bruising. Blood samples were taken as part of routine care, with excess being stored for research (The Hôpital Necker's hemophilia bio-library/Necker Biobank, registration number: DC-2009-955; procedure is in accordance with the Helsinki declaration and participants gave written informed consent). Analysis revealed emicizumab concentrations in the expected range (66 µg/mL 52 days after emicizumab initiation),[5] and a dramatic decrease in activated partial thromboplastin time (APTT) ratio (0.74, normal range <1.2) was measured (Figure 1).

A spontaneous hemarthrosis of the ankle occurred 6 months after emicizumab initiation, which was confirmed via clinical examination and ultrasound evaluation. Simultaneously, the APTT-ratio rose to 2.67, and circulating emicizumab concentrations were below 1 µg/mL (Figure 1). Hence, the development of anti-emicizumab antibodies was suspected, and the presence of emicizumab-specific immunoglobulin G (IgG) in the patient's serum was analyzed in immunosorbent assays, using normal serum and IgG-depleted patient serum as controls. Binding of IgG to immobilized emicizumab (5 µg/mL) was determined using isotype-specific peroxidase-labeled monoclonal antibodies. Whereas no specific IgG2 or IgG3 anti-emicizumab antibodies were detected, the patient's serum was indeed enriched in anti-emicizumab antibodies of the IgG1 subtype (Figure 2A and B). We could not test for IgG4 antibodies, since emicizumab is of this subtype.[3]

Treatment of the hemarthrosis included rFVIIa and oral

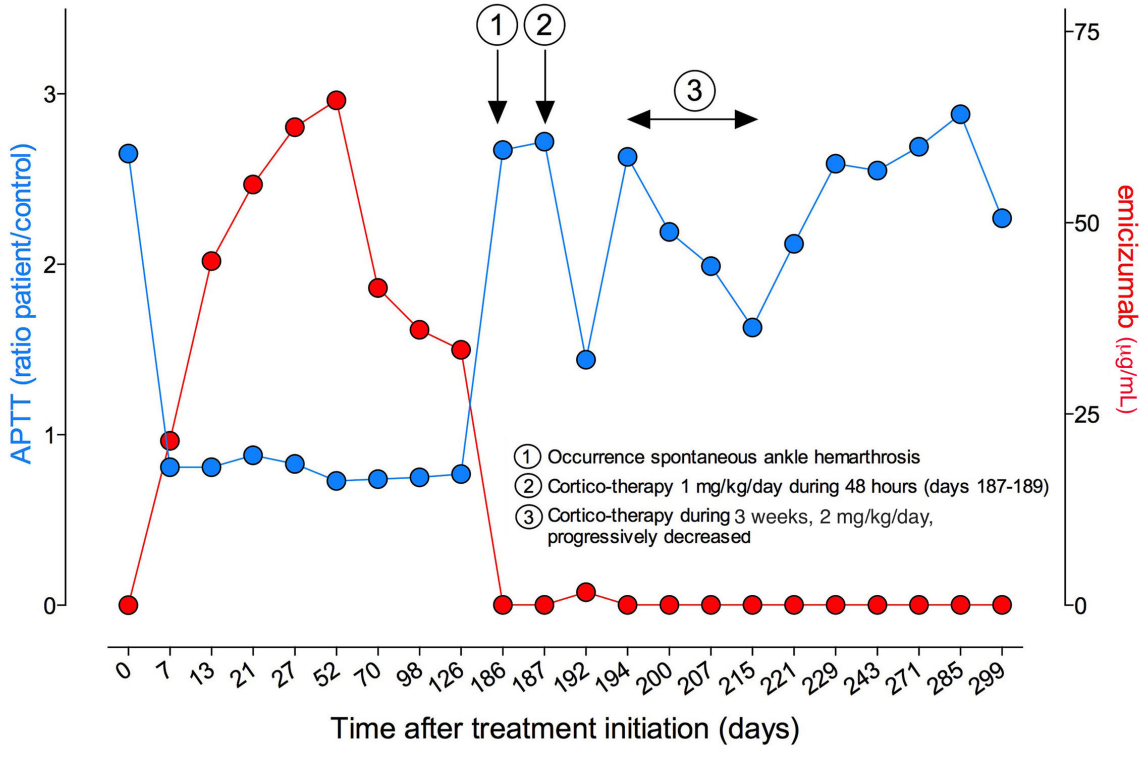

Figure 1. Evolution of APTT and emicizumab plasma concentration over time. At indicated time points, blood samples were taken from the patient. Plasma was then analyzed for APTT (left Y-axis, blue circles) and emicizumab concentration (right Y-axis; red circles). Arrow 1 indicates bleeding event; arrows 2-3 indicate periods of cortico-therapy (2: 1 mg/kg/day for 48 hours during day 187-189; 3: 2 mg/kg/day during 3 weeks during days 194-214, with progressive decrease in dosing). ATPP: activated partial thromboplastin time.

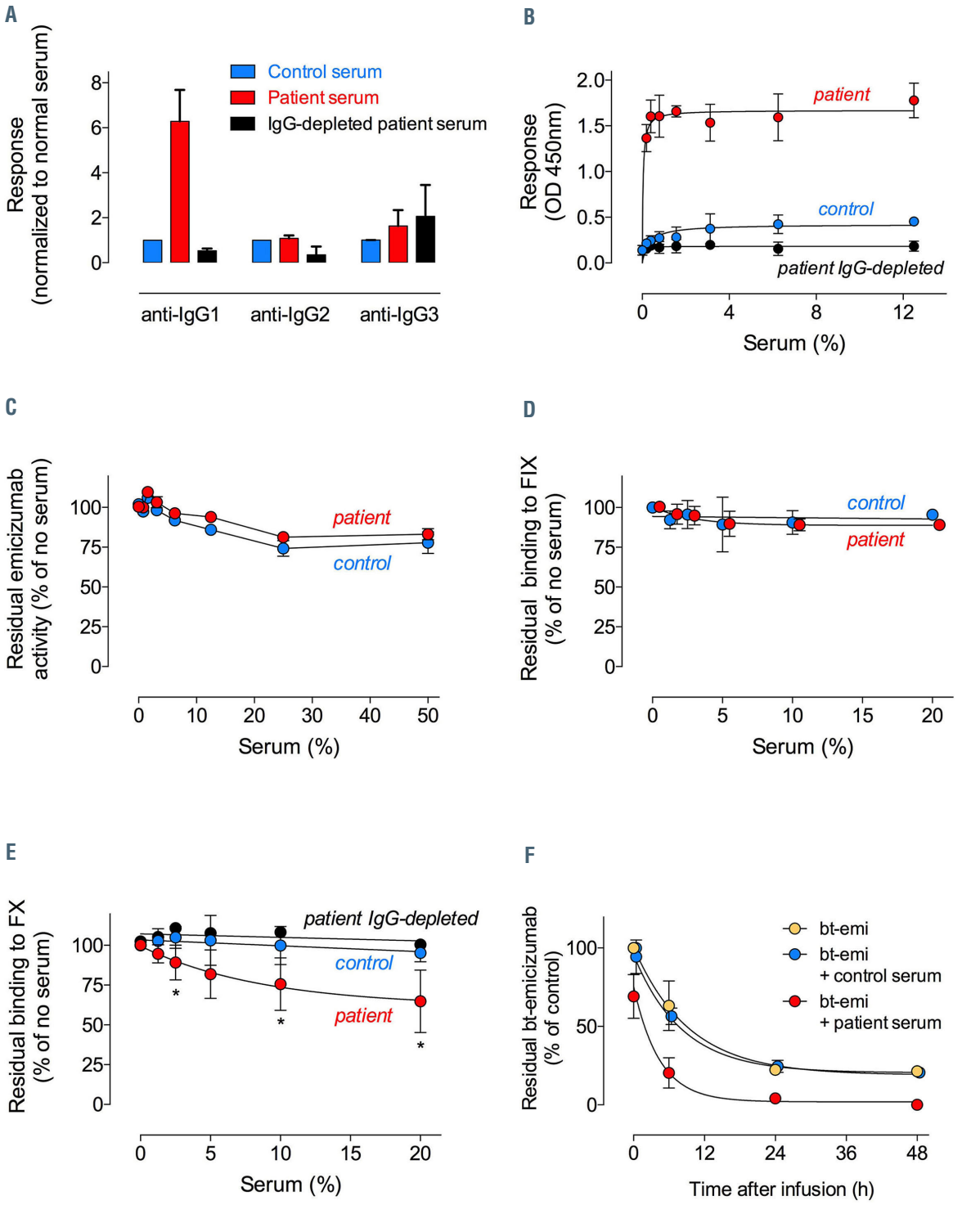

Figure 2. Characterization of anti-emicizumab antibodies. (A and B) Emicizumab was immobilized (5 μg/mL) and incubated with control serum (blue), patient serum (red) or immunoglobulin G (IgG)-depleted patient serum (black). Bound anti-emicizumab antibodies were probed using peroxidase-labeled IgG-subtype specific antibodies, and detected via 3,3',5,5'-tetramethyl benzidine (TMB) hydrolysis. For panel A, samples were diluted 256-fold, and response was normalized to that of normal plasma, which was arbitrarily set at 1. For panel B, the dose-response for binding of IgG1 antibodies to emicizumab is shown. (C) Emicizumab (25 μg/mL) was incubated in the absence or presence of various dilutions of control serum (blue circles) or patient serum (red circles). Presented is the percentage residual emicizumab activity relative to the absence of serum as measured in a chromogenic factor VIII (FVIII)-activity assay using human FIXa and factor X (FX). (D) Binding of bt-emicizumab (50 μg/mL) to immobilized factor IX (FIX) (5 μg/mL) was performed in the absence or presence of various dilutions of control serum (blue circles) or patient serum (red circles). Bound bt-emicizumab was probed with peroxidase-labeled streptavidin and detected via TMB hydrolysis. Shown is the percentage residual FIX binding relative to the absence of serum. (E) Binding of bt-emicizumab (10 μg/mL) to immobilized FX (5 μg/mL) was performed in the absence or presence of various dilutions of control serum (blue circles) or patient serum (red circles). Bound bt-emicizumab was probed with peroxidase-labeled streptavidin and detected via TMB hydrolysis. Shown is the percentage residual FX binding relative to the absence of serum. Statistical assessment was performed using multiple *t*-test analysis between control and patient serum. Stars indicate $P<0.05$ as analyzed in a multiple *t*-test comparing control serum and patient serum. (F) Immuno-deficient mice received bt-emicizumab (0.25 mg/kg) alone (orange circles) or in the presence of control serum (100 μL; blue circles) or patient serum (100 μL; red circles) via intravenous injection in the retro-orbital plexus. At indicated time points, samples were taken and plasma was analyzed for the presence of residual bt-emicizumab. Presented is the percentage of residual bt-emicizumab relative to bt-emicizumab alone at 3 minutes after injection, which was arbitrarily set at 100%. Lines were generated by fitting the data to an equation describing a single-exponential decay. Data represent the mean ± standard deviation of three experiments.

corticoids (1 mg/kg/day for 48 hours [h] to reduce periarticular inflammation). A minor increase in emicizumab concentrations (1.7 μg/mL) and reduction in APTT-ratio (1.44) was observed (Figure 1), suggesting a potential cortico-sensitivity of the anti-emicizumab antibody-producing plasmocytes. Although no bleeds were observed during a 3-week period, emicizumab levels remained undetectable following a short corticosteroid therapy (2 mg/kg/day, conform to the management of children's immunologic thrombocytopenic purpura). Corticosteroid-therapy was therefore halted. Since anti-emicizumab antibodies have been reported to be transient in some patients,[11] emicizumab therapy (1.5 mg/kg/week) was continued for 3 months. As no improvement was observed, emicizumab therapy was terminated.

In order to further characterize the anti-emicizumab antibodies, additional tests were performed. We next analyzed eventual inhibition of emicizumab activity using the chromogenic activity assay (Biophen FVIII:C activity assay [ref 221402]; Hyphen BioMed, Andresy, France). Surprisingly, no reduction in emicizumab activity was observed, irrespective of whether normal or patient serum was tested (Figure 2C). Similar data were obtained using a one-stage clotting assay, suggesting that the anti-emicizumab antibodies are essentially non-inhibitory.

This was further assessed by analyzing binding of biotinylated (bt)-emicizumab to immobilized purified recombinant FIX (Pfizer, Paris, France) or plasma-derived FX (Cryopep; Montpellier, France). Biotinylation was performed using the NHS-PEO4-biotin kit (ref: UPR2027B; Griener Bio-one; Frickenhausen, Germany) without loss of cofactor activity. No inhibition of emicizumab binding to FIX was observed with normal or patient serum (Figure 2D). However, a modest inhibition of emicizumab binding to FX was observed using patient serum (Figure 2E). Maximal inhibition was 35±20% (n=4, *P*=0.0124 compared to normal serum) using 5-fold diluted serum. The absence of a dominant inhibitory effect on the interactions between emicizumab and FIX/FX is compatible with the non-inhibitory nature of the patient's anti-emicizumab antibodies in the activity assays. Indeed, a modest decrease in emicizumab-FX complex formation would still allow for sufficient ternary complex to be formed (555 pM *vs.* 851 pM in the absence of inhibitor, when calculated according to Kitazawa *et al.*).[12] We previously showed that a threshold of about 300 pM ternary complex is needed to produce sufficient hemostatic activity *in vivo*.[13]

As low emicizumab levels in the patient can be explained by an increased clearance, we determined survival of bt-emicizumab in the absence or presence of serum in immuno-deficient mice. Bt-emicizumab was added to 0.9% NaCl, 100 μL control serum or 100 μL patient serum (both 5 μg per 100 μL), and incubated for 30 minutes (min) at ambient temperature. Mixtures were then injected via the retro-orbital plexus (at a dose of 0.25 mg/kg bt-emicizumab) to male NOD.CB17-Prkdcscid/NCrHsd-mice (age 9 weeks; ENVIGO, Gannat, France). Housing and experiments of NOD.CB17-Prkdcscid/NCrHsd-mice were performed in accordance with French regulations and the experimental guidelines of the European Community. Experimentation was approved by the local ethical committee of the Université Paris-Sud (Comité d'Éthique en Experimentation Animale no. 26, protocol APAFIS#4400-2016021716431023v5). Blood samples were taken at 15 min, 6 h, 24 h and 48 h after infusion. Plasma was used to determine residual bt-emicizumab levels in an enzyme-linked immonosorbent assay (ELISA) in which streptavidin-coated microtiter wells were incubated with plasma samples, and bound bt-emicizumab was probed using peroxidase-labeled anti-human IgG4-Fc antibodies. No difference in the disappearance from the circulation was found between bt-emicizumab alone or the bt-emicizumab/normal serum combination ($t_{1/2}$=8.5 h and 8.3 h, respectively; Figure 2F). In contrast, bt-emicizumab was eliminated significantly faster in the presence of patient serum ($t_{1/2}$=2.2 h; *P*=0.0013; Figure 2F), with no bt-emicizumab detectable at 48 h after infusion (compared to 21% for both other conditions). It, thus, seems that the main effect of the anti-emicizumab antibodies is to accelerate clearance of emicizumab.

Contrary to previously reported inhibitors of emicizumab, we here describe the presence of antibodies that leave emicizumab activity unaffected, but that provoke the rapid elimination of emicizumab in mice, providing an explanation for the low emicizumab levels in the patient. Although the occurrence of anti-emicizumab antibodies is rare, their presence may severely diminish its clinical efficacy, resulting in the re-appearance of spontaneous bleeds. Clinical monitoring will usually be sufficient for patients receiving emicizumab therapy. However, in case of bleeding in the absence of any compliance concerns, biological monitoring (APTT and emicizumab concentration) is therefore helpful to detect possible anti-drug antibodies.

Annie Harroche,[1,] Thibaud Sefiane,[2,*] Maximilien Desvages,[2,3] Delphine Borgel,[2,3] Dominique Lasne,[2,3] Caterina Casari,[2] Ivan Peyron,[2] Laurent Frenzel,[1] Stéphanie Chhun,[4] Peter J. Lenting[2] and Cécile Bally[1]*

[1]Centre de Traitement de l'Hémophilie, AP-HP, Hôpital Necker Enfants Malades, Paris; [2]Laboratory for Hemostasis, Inflammation & Thrombosis, Unité Mixed de Recherche 1176, Institut National de la Santé et de la Recherche Médicale, Université Paris-Saclay, Le Kremlin-Bicêtre; [3]Laboratoire d'Hématologie, AP-HP, Hôpital Necker Enfants Malades, Paris and [4]Laboratoire d'Immunologie Biologique, AP-HP, Hôpital Necker Enfants Malades, Paris, France

**AH and TS contributed equally as co-first authors.*

Correspondence: PETER J. LENTING - peter.lenting@inserm.fr

doi:10.3324/haematol.2021.278579

Received: February 15, 2021.

Accepted: May 3, 2021.

Pre-published: May 20, 2021.

Disclosures: AH received fees for consultancy and board expert membership from Roche, Takeda, LFB, CSL-Behring, Sobi and NovoNordisk; DL received consulting fees from Roche (with fees going to Association de Recherche en Hématologie à Necker-Enfants Malades; ARHNEM); PJL received speaker fees from Biotest, Chugai, CSL-Behring, LFB-Biomedicament, NovoNordisk, Roche, Sanofi, Takeda and research support from Sobi, Catalyst Biosciences. All other authors declare no conflicts of interest.

Contributions: AH, CB were in charge of the patients and provided the clinical samples; MD, DB and DL performed the coagulation tests; TS, CC, IP and PJL designed and performed the in vitro and in vivo experiments. All authors contributed to the interpretation of the data. AH, CB and PJL wrote the first draft of the manuscript, and all authors contributed to the editing of the final manuscript.

Acknowledgments: we thank Dr. Alyanakian MA who leads the biological Necker Biobank.

Data sharing statement: data are available upon reasonable request to the corresponding author.

References

1. Cormier M, Batty P, Tarrant J, Lillicrap D. Advances in knowledge of inhibitor formation in severe haemophilia A. Br J Haematol. 2020;189(1):39-53.
2. Scott DW, Pratt KP. Factor VIII: perspectives on immunogenicity and tolerogenic strategies. Front Immunol. 2019;10:3078.
3. Kitazawa T, Igawa T, Sampei Z, et al. A bispecific antibody to factors IXa and X restores factor VIII hemostatic activity in a hemophilia A model. Nat Med. 2012;18(10):1570-1574.
4. Sampei Z, Igawa T, Soeda T, et al. Identification and multidimensional optimization of an asymmetric bispecific IgG antibody mimicking the function of factor VIII cofactor activity. PLoS One. 2013; 8(2):e57479.
5. Oldenburg J, Mahlangu JN, Kim B, et al. Emicizumab prophylaxis in hemophilia A with inhibitors. N Engl J Med. 2017;377(9):809-818.
6. Mahlangu J, Oldenburg J, Paz-Priel I, et al. Emicizumab prophylaxis in patients who have hemophilia A without inhibitors. N Engl J Med. 2018;379(9):811-822.
7. Young G, Liesner R, Chang T, et al. A multicenter, open-label phase 3 study of emicizumab prophylaxis in children with hemophilia A with inhibitors. Blood. 2019;134(24):2127-2138.
8. Pipe SW, Shima M, Lehle M, et al. Efficacy, safety, and pharmacokinetics of emicizumab prophylaxis given every 4 weeks in people with haemophilia A (HAVEN 4): a multicentre, open-label, non-randomised phase 3 study. Lancet Haematol. 2019;6(6):e295-e305.
9. Harkins Druzgal C, Kizilocak H, Brown J, Sennett M, Young G. Neutralizing antidrug antibody to emicizumab in a patient with severe hemophilia A with inhibitors: new case with detailed laboratory evaluation. J Thromb Haemost. 2020;18(9):2205-2208.
10. Valsecchi C, Gobbi M, Beeg M, et al. Characterization of the neutralizing anti-emicizumab antibody in a patient with hemophilia A and inhibitor. J Thromb Haemost. 2021;19(3):711-718.
11. Paz-Priel I, Chang T, Asikanius E, et al. Immunogenicity of emicizumab in people with hemophilia A (PwHA): results from the HAVEN 1-4 studies. Blood. 2018;132(Suppl 1):S633.
12. Kitazawa T, Esaki K, Tachibana T, et al. Factor VIIIa-mimetic cofactor activity of a bispecific antibody to factors IX/IXa and X/Xa, emicizumab, depends on its ability to bridge the antigens. Thromb Haemost. 2017;117(7):1348-1357.
13. Ferriere S, Peyron I, Christophe OD, et al. A hemophilia A mouse model for the in vivo assessment of emicizumab function. Blood. 2020;136(6):740-748.

Post-mortem findings in vaccine-induced thrombotic thombocytopenia

Greinacher *et al*.[1] and Schultz *et al*.[2] were the first to independently report the main clinical and laboratory features of 11 and five respective patients from Germany, Austria and Norway who developed life-threatening thrombohemorrhagic complications 5 to 16 days after the administration of the first dose of the chimpanzee adenoviral vector vaccine ChAdOx1nCoV-19 against SARS-CoV-2 and COVID-19. Subsequently Scully *et al*.[3] reported similar findings in 23 patients treated with the same vaccine in the United Kingdom. More recently, See *et al*.[4] reported a case series of 12 patients from the USA with cerebral venous sinus thrombosis following the vaccination with Ad26.CoV2.S employing a human adenoviral vector. The main post-vaccination features common to the case series were the occurrence of venous thromboembolism mainly in unusual sites (cerebral and abdominal veins) and the concomitant presence of bleeding symptoms associated with severe thrombocytopenia, often accompanied by laboratory signs of consumption coagulopathy with low plasma fibrinogen and hugely increased levels of D-dimer. The majority of reported patients reacted positively for serum immunoglobulin G (IgG) antibodies to the platelet factor 4 PF4/heparin complex.[1-4] Another common feature was the high mortality rate. The mechanism of this very rare thrombohemorrhagic syndrome was postulated to be a vaccine-triggered autoimmune reaction, with the development of antibodies against a still ill-defined PF4/polyanion complex that causes platelet activation as in heparin-induced thrombocytopenia (HIT),[1-4] notwithstanding the fact that no cases were exposed to heparin before the onset of thrombosis and thrombocytopenia. We report herewith the detailed post-mortem macroscopic and microscopic findings in two similar cases that occurred in the Italian region of Sicily.

Case Reports. Patient 1 was a 50-year-old man (body weight 90 kg) with abdominal pain that developed 10 days after vaccination with ChAdOx1 nCoV-19. He had neither a history for thrombosis risk factors nor had he any intake of drugs increasing this risk. At the emergency room he presented with severe thrombocytopenia, low plasma fibrinogen and very high D-dimer (Table 1). The results of other blood tests were normal except for moderately elevated white blood cells and inflammatory serum markers. Computed tomography (CT) showed portal vein thrombosis with smaller thrombi in the splenic and upper mesenteric veins. During the next 4 days after admission platelets and fibrinogen remained low and D-dimer very high with no substantial changes. An initial dose of the low molecular weight heparin nadroparin was given subcutaneously at a dosage of 5,700 IU followed by a second dose after 8 hours. Clinical conditions deteriorated and a new CT scan showed massive intracerebral hemorrhage. Treated with multiple transfusions of platelet concentrates that failed to control bleeding the patient died 4 days after the onset of symptoms and 16 days after vaccination. A serum sample obtained before nadroparin showed the presence of anti PF4/polyanion complex IgG antibodies by enzyme-linked immunosorbent assay (ELISA) (Lifecodes PF4 IgG assay, Immucor, USA).

Patient 2, a 37-year old previously healthy woman (61 kg) with a negative history for significant disease and drug intake developed 10 days after the administration of the same vaccine first low back pain and then a strong headache. She became progressively drowsy and ultimately unconscious, and was, therefore, admitted to the emergency room of her local hospital. With laboratory tests similar of those of patient 1 (Table 1), a CT scan showed an occlusive thrombus in the superior sagittal venous sinus and a very large hemorrhage in the frontal cerebral lobe. Transported comatose by helicopter to a larger hub hospital she underwent craniotomy in order to control intracranial hypertension and remove the frontal lobe hemorrhage. She survived the operation but remained comatose and died 10 days after the first hospital admission and 23 days after vaccination. Anti-PF4/polyanion complex antibody reactivity was detected by ELISA and confirmed in a stored serum sample (Table 1).

Table 1. Clinical and laboratory characteristics.

	Case 1	Case 2
Age, years	50	37
Sex	Male	Female
Pre-existing conditions	None of significance	None of significance
Time from vaccination to admission, days	10	10
Presenting symptoms	Abdominal pain	Low back pain, headache
Thrombosis location	Portal, splenic and superior mesenteric veins	Superior sagittal sinus
Platelet count nadir, per mm^3	7,000	9,000
D-dimer peak, mg/dL	52	290
Fibrinogen nadir, g/L	0.66	0.34
Sars-CoV-2 molecular test	Negative	Negative
Anti-PF4/polyanion complex testing	Positive for IgG	Positive for IgG
Anticoagulation	Nadroparin	None
Outcome	Fatal	Fatal

The reference ranges for platelet count are 130.000-400.000 per mm3, for D-dimer less than 0.5 mg/dL for fibrinogen 1.7-4.0 g/L. Ig: immunoglobulin.

Autopsy findings. The anatomic dissection showed a multi-district catastrophic picture of venous thrombosis, but neither entrapment or nutcracker nor any compression which may produce blood stasis and facilitate venous thrombosis. In both cases the sites of venous thrombosis identified by imaging were confirmed, coupled with dramatic pictures of cerebral hemorrhages. While case 1 was confirmed to have had portal and mesenteric thrombosis with extension into the splenic vein, case 2 showed besides cerebral sinus thrombosis a massive thrombosis of the whole venous tree of the left upper limb extending from the hand to the axillary vein, with symmetric lesions in the veins of the right hand and the right axillary vein. In addition, the superficial veins of both feet appeared to be thrombosed. The histological evaluation revealed the presence of vascular thrombi associated with hemorrhagic phenomena localized in the meningeal space and focally involving the brain. The thrombotic phenomena also involved small- and medium-sized vessels. The immunohistochemical findings detailed in Figure 1 suggested endothelial activation associated with the dense recruitment of inflammatory myeloid cells, presumably sustaining procoagulant conditions and thrombus formation.

From a clinical and laboratory standpoint these two fatal cases of venous thrombosis located in unusual sites

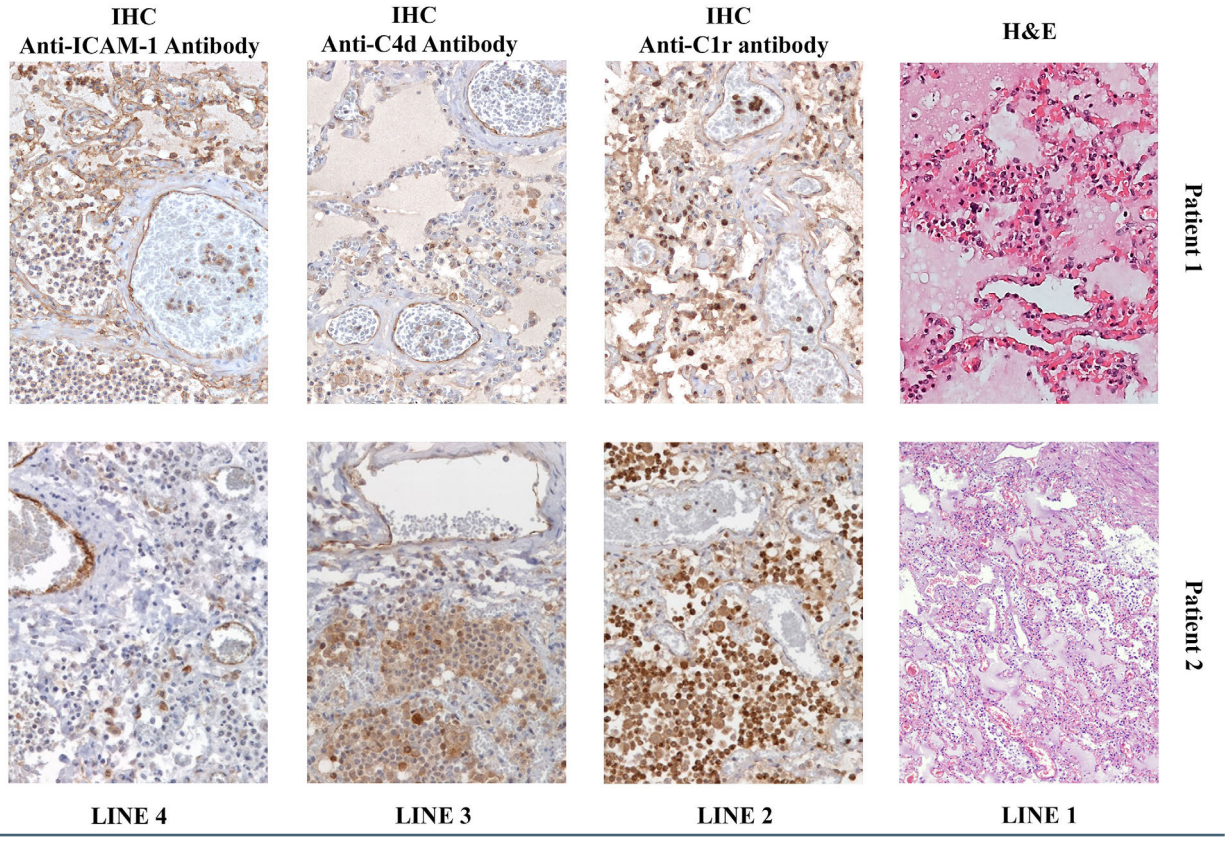

Figure 1. Microscopic investigation of lung tissue. (Line 1) Microscopic investigation of hematoxylin and eosin (H&E) stained lung tissue showed marked vascular congestion, blood extravasation and the presence of microthrombi and megakaryocytes in the interstitial spaces, magnification 20X. (Line 3) Immunohistochemical staining (IHC) revealed positivity for anti-C4d antibody and anti-ICAM-1 antibody, with the presence of inflammatory cells (especially leukocytes, both polymorphonucleates and monocytes/macrophages) and the deposition of pro-inflammatory molecules (C1r, C4d) on the endothelial surface , magnification 20X.

are similar to those recently described,[1-4] because in both cases complications occurred on average 10-15 days after vaccination and were accompanied by a very low platelet count, very high D-dimer and low fibrinogen with signs of consumption coagulopathy.[5] Both patients had detectable anti PF-4/polyanion antibodies unrelated to the use of heparin and positive results were confirmed by reactivity inhibition in the presence of excess heparin *in vitro*.[6] Patients tested negative for SARS-Cov-2 molecular assays and antibodies to the nucleocapsid and spike proteins, thus ruling out recent exposure to SARS-CoV-2 (Table 1). There was neither clinical and laboratory evidence of inherited or acquired thrombophilia nor of intake of prothrombotic medicines. Venous thrombosis was accompanied by severe intracranial bleeding, which was the final cause of death in both and developed after the administration of therapeutic doses of heparin in patient 1 but concomitantly with cerebral vein thrombosis and no anticoagulant in patient 2.

The peculiar features of these cases were the availability of macroscopic and microscopic autopsy findings. The main macroscopic finding was that venous thrombosis was much more widespread and catastrophic than diagnosed by imaging during life. Immunohistochemistry highlighted the expression of the adhesion molecule VICAM-1 (CD106) and of the complement components C1r and C4d on the vascular endothelial surface in the microcirculation of the heart, lung, liver, kidney and ileum. Diffuse endoluminal and peri-vascular immunoreactivity for IgM and IgG were additional findings in the microcirculation. CD61 revealed platelet aggregates diffusely lining the endothelial layer of small- and medium-size vessels and signs of platelet phagocytosis by myeloid elements in the vascular spaces. Scattered CD61-positive immunoreactive cells with morphological features of megakaryocytes were also detected in the lung microvasculature. The inflammation components were prominently represented by large CD163-positive monocytic/macrophagic elements that showed intra-vascular aggregates and variable monocytoid or epithelioid morphology, associated with C1r-positive medium-sized elements with granulocyte morphology.

All in all, this post-mortem examination of two typical cases of the novel vaccine-induced thrombotic thrombocytopenic syndrome (VITT) shows that the involvement of large venous vessels was much more extensive than appreciated by imaging during the brief clinical course of these fatal cases. Microscopic findings showed vascular thrombotic occlusions occurring in the microcirculation of multiple organs and increased inflammatory infiltrates. Immunohistochemical analyses highlighted the vascular and peri-vascular expression of adhesion molecules such as VICAM1, as well as the presence of $CD66b^+$, $CD163^+$ and $CD61^+$ activated inflammatory cells, also expressing C1r. These findings indicate that the activation of the innate immune system and complement pathway promote the inflammatory process leading to the microvascular damage of multiple organs.

Cristoforo Pomara,[1] Francesco Sessa,[2] Marcello Ciaccio,[3,4] Francesco Dieli,[5] Massimiliano Esposito,[1] Sebastiano Fabio Garozzo,[6] Antonino Giarratano,[7,8] Daniele Prati,[9] Francesca Rappa,[10] Monica Salerno,[1] Claudio Tripodo,[11] Paolo Zamboni[12] and Pier Mannuccio Mannucci[9]

[1]Department of Medical, Surgical and Advanced Technologies G.F. Ingrassia, University of Catania, Catania; [2]Department of Clinical and Experimental Medicine, University of Foggia, Foggia; [3]Institute of Clinical Biochemistry, Clinical Molecular Medicine and Laboratory Medicine, Department of Biomedicine, Neuroscience and Advanced Diagnostics, University of Palermo, Palermo; [4]Department of Laboratory Medicine, AOUP "P. Giaccone", Palermo; [5]Central Laboratory of Advanced Diagnosis and Biomedical Research (CLADIBIOR), University of Palermo, Palermo; [6]Clinical Pathology Unit, Garibaldi Centro Hospital, ARNAS Garibaldi, Catania; [7]Department of Surgical, Oncological and Oral Science (Di.Chir.On.S.), University of Palermo, Palermo; [8]Department of Anesthesia, Intensive Care and Emergency, Policlinico Paolo Giaccone, Palermo; [9]Fondazione IRCCS Ca' Granda Ospedale Maggiore Policlinico, Angelo Bianchi Bonomi Hemophilia and Thrombosis Center and Blood Transfusion Center, Milan; [10]Department of Biomedicine, Neuroscience and Advanced Diagnostics, University of Palermo, Palermo; [11]Tumor Immunology Unit, Department of Health Sciences, University School of Medicine of Palermo, Palermo and [12]Vascular Diseases Center, Mini-invasive Venous Surgery Unit, University of Ferrara, Ferrara, Italy

Correspondence: PIER MANNUCCIO MANNUCCI - piermannuccio.mannucci@policlinico.mi.it

doi:10.3324/haematol.2021.279075

Received: April 23, 2021.

Accepted: May 13, 2021.

Pre-published: May 20, 2021.

Disclosures: no conflicts of interest to disclose.

Contributions: all authors equally contributed to the preparation of the case report.

Acknowledgments: we thank the staff of the public prosecutor office of Catania and Gela and the Department of Health of the Sicily Region for help and assistance during the post-mortem examination.

References

1. Greinacher A, Thiele T, Warkentin TE, Weisser K, Kyrle PA, Eichinger S. Thrombotic thrombocytopenia after ChAdOx1 nCov-19 vaccination. N Engl J Med. 2021;384(22):2092-2101.
2. Schultz NH, Sørvoll IH, Michelsen AE, et al. Thrombosis and thrombocytopenia after ChAdOx1 nCoV-19 vaccination. N Engl J Med. 2021;384(22):2124-2130.
3. Scully M, Singh D, Lown R, et al. Pathologic antibodies to platelet factor 4 after ChAdOx1 nCoV-19 vaccination. N Engl J Med. 2021;384(23):2202-2211.
4. See I, Su JR, Lale A, et al. US case reports of cerebral venous sinus thrombosis with thrombocytopenia after Ad26.COV2.S vaccination, March 2 to April 21, 2021. JAMA. 2021;325(24):2448-2456.
5. Gresele P, Marietta M, Ageno W, et al. Management of cerebral and splanchnic vein thrombosis associated with thrombocytopenia in subjects previously vaccinated with Vaxzevria (AstraZeneca): a position statement from the Italian Society for the Study of Haemostasis and Thrombosis (SISET). Blood Transfus. 2021 Apr 15. [Epub ahead of print]
6. Whitlatch NL, Kong DF, Metjian AD, Arepally GM, Ortel TL. Validation of the high-dose heparin confirmatory step for the diagnosis of heparin-induced thrombocytopenia. Blood. 2010; 116(10):1761-1766.

Inhibitors of poly ADP-ribose polymerase (PARP) induce apoptosis of myeloid leukemic cells: potential for therapy of myeloid leukemia and myelodysplastic syndromes

Terry J Gaymes, Sydney Shall, Lee J Macpherson, Natalie A Twine, Nicholas C Lea, Farzin Farzaneh and Ghulam J Mufti

Department of Haematological Medicine, King's College London, Leukemia Sciences Laboratories, The Rayne Institute, Denmark Hill campus, London, UK

doi:10.3324/haematol.2020.262857

In the original article, there was a mistake in Figure 3D as published. In this instance, the annexin V fluorescence-activated cell sorting (FACS) image for Figure 1B (top right) had been unintentionally duplicated and substituted for the annexin V FACS image in Figure 3D (top left). As it is an untreated drug control rather than drug test additions, no scientific benefit or advantage interpretation could be made by duplicating the data here. The authors apologize for this error and state that this does not change the scientific conclusions of the article in any way. The amended Figure 3 is attached.

An incorrect version of Figure 3 appared in the May 2009 Issue on page 644. The correct version of Figure 3 is published on this page.

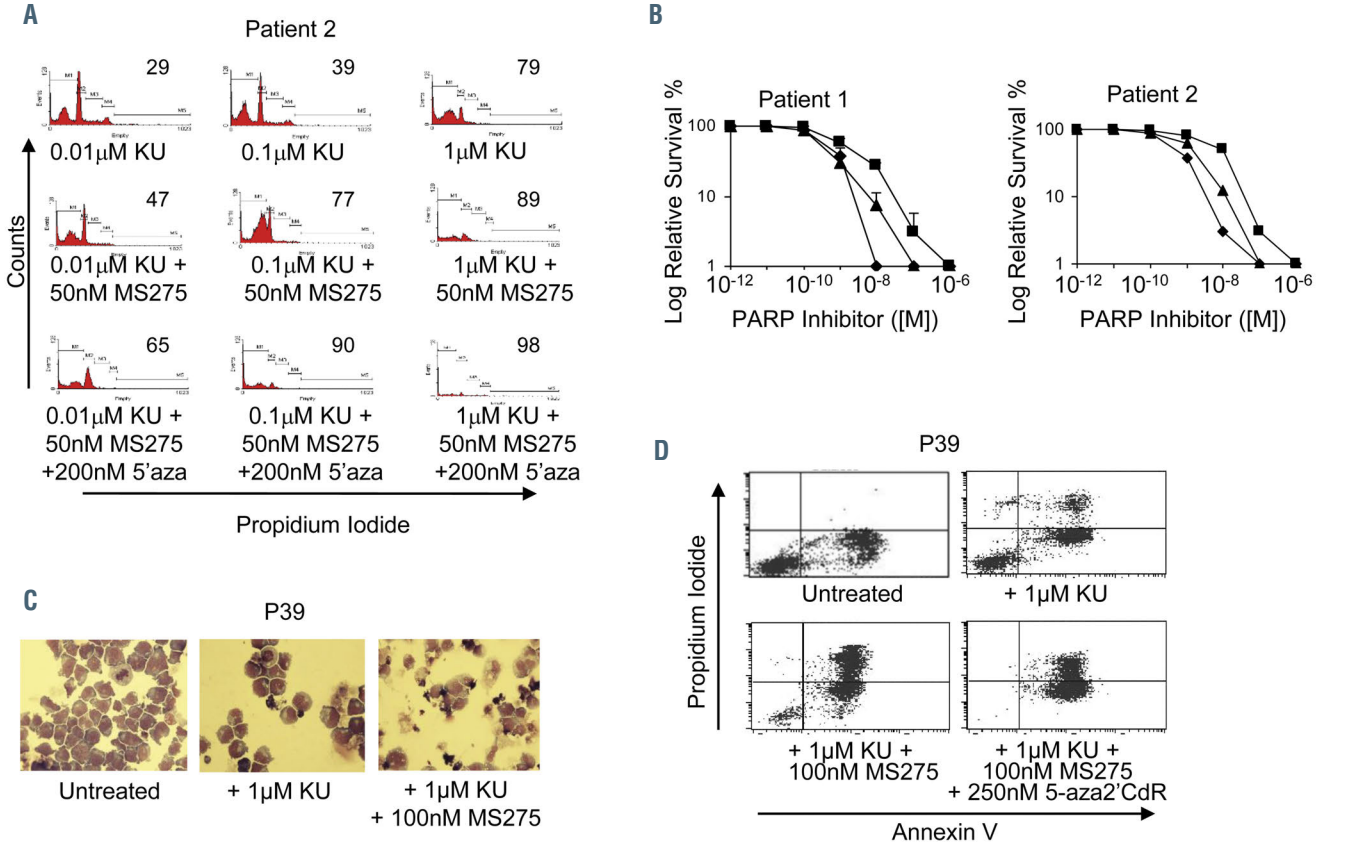

Figure 3. The effect on leukemic cells of the PARP inhibitor, KU in combination with non-cytotoxic concentrations of 5'-aza-2'-dCR and/or HDAC inhibitor. (A) The effect on primary acute myeloid leukemia (AML) cells of the PARP inhibitor, KU in combination with the HDAC inhibitor, MS275 and with 5'-aza-2'-dCR. KU was added at variable concentrations to Patient 2 continuously for 5 days with 50 nM MS275 and 200 nM 5'-aza-2'-dCR or KU alone and then analyzed by flow cytometry. The apoptotic index (Sub-G1population as a fraction of sub-G1+ G1 populations is shown in the right inset). (B) Trypan blue exclusion assays were used to determine cell survival in primary AML cells of Patient 2 exposed to KU, MS275 and 5'-aza-2'-dCR. Exposure to 50 nM MS275 and 200 nM 5'-aza-2'-dCR with varying concentrations of KU was continuous for 5 days in AML cells of Patient 1 and AML cells of Patient 2 cells. KU + MS275 (triangles), 5'-aza-2'-dCR + KU + MS275 (diamonds), KU alone (squares). (C) P39 cells were cultured in 1 μM KU, 1 μM KU + 100 nM MS275 or left untreated for 7 days. At 7 days cells were cytospun onto slides and stained with May-Grumwald stain. Images were taken at 40X magnification. (D) 1 μM KU, 100 nM MS275 and 250 nM 5'-aza-2'-CdR were added as indicated to P39 for 7 days before being treated with annexin V-FITC (FL-1, X-axis) and propidium iodide (FL-2, Y-axis). The figures show the percentage of early and late apoptotic cells in the population.

Impact of cytogenetic abnormalities on outcomes of adult Philadelphia-negative acute lymphoblastic leukemia after allogeneic hematopoietic stem cell transplantation: a study by the Acute Leukemia Working Committee of the Center for International Blood and Marrow Transplant Research

Aleksandr Lazaryan,[1] Michelle Dolan,[2] Mei-Jie Zhang,[3,4] Hai-Lin Wang,[3] Mohamed A. Kharfan-Dabaja,[5] David I. Marks,[6] Nelli Bejanyan,[7] Edward Copelan,[8] Navneet S. Majhail,[9] Edmund K. Waller,[10] Nelson Chao,[11] Tim Prestidge,[12] Taiga Nishihori,[13] Partow Kebriaei,[14] Yoshihiro Inamoto,[15] Betty Hamilton,[16] Shahrukh K. Hashmi,[17,18] Rammurti T. Kamble,[19] Ulrike Bacher,[20] Gerhard C. Hildebrandt,[21] Patrick J. Stiff,[22] Joseph McGuirk,[23] Ibrahim Aldoss,[24] Amer M. Beitinjaneh,[25] Lori Muffly,[26] Ravi Vij,[27] Richard F. Olsson[28,29], Michael Byrne,[30] Kirk R. Schultz,[31] Mahmoud Aljurf,[18] Matthew Seftel,[32] Mary Lynn Savoie,[33] Bipin N. Savani,[34] Leo F. Verdonck,[35] Mitchell S. Cairo,[36] Nasheed Hossain,[37] Vijaya Raj Bhatt,[38] Haydar A. Frangoul,[39] Hisham Abdel-Azim,[40] Monzr Al Malki,[24] Reinhold Munker,[41] David Rizzieri,[42] Nandita Khera,[43] Ryotaro Nakamura,[44] Olle Ringdén,[45] Marjolein van der Poel,[46] Hemant S. Murthy,[47] Hongtao Liu,[48] Shahram Mori,[49] Satiro De Oliveira,[50] Javier Bolaños-Meade,[51] Mahmoud Elsawy,[52] Pere Barba,[53] Sunita Nathan,[54] Biju George,[55] Attaphol Pawarode,[56] Michael Grunwald,[57] Vaibhav Agrawal,[58] Youjin Wang,[59] Amer Assal,[60] Paul Castillo Caro,[61] Yachiyo Kuwatsuka,[62] Sachiko Seo, [63]Celalettin Ustun,[64] Ioannis Politikos,[65] Hillard M. Lazarus,[66] Wael Saber,[3] Brenda M. Sandmaier,[67] Marcos De Lima,[68] Mark Litzow,[69] Veronika Bachanova[70] and Daniel Weisdorf,[71] Acute Leukemia Committee of the CIBMTR[3]

[1]H. Lee Moffitt Cancer Center and Research Institute, Tampa, FL, USA; [2]University of Minnesota Medical Center, Minneapolis, MN, USA; [3]CIBMTR (Center for International Blood and Marrow Transplant Research), Department of Medicine, Medical College of Wisconsin, Milwaukee, WI, USA; [4]Division of Biostatistics, Institute for Health and Equity, Medical College of Wisconsin, Milwaukee, WI, USA; [5]Division of Hematology-Oncology, Blood and Marrow Transplantation Program, Mayo Clinic, Jacksonville, FL, USA; [6]Adult Bone Marrow Transplant, University Hospitals Bristol NHS Trust, Bristol, UK; [7]Department of Blood and Marrow Transplant and Cellular Immunotherapy, Moffitt Cancer Center, Tampa, FL, USA; [8]Levine Cancer Institute, Atrium Health, Carolinas HealthCare System, Charlotte, NC, USA; [9]Blood & Marrow Transplant Program, Cleveland Clinic Taussig Cancer Institute, Cleveland, OH, USA; [10]Department of Hematology and Medical Oncology, Winship Cancer Institute, Emory University, Atlanta, GA, USA; [11]Division of Cell Therapy and Hematology, Department of Medicine, Duke University Medical Center, Durham, NC, USA; [12]Blood and Cancer Centre, Starship Children's Hospital, Auckland, New Zealand; [13]Department of Blood and Marrow Transplantation, H. Lee Moffitt Cancer Center and Research Institute, Tampa, FL, USA; [14]Department of Stem Cell Transplantation, Division of Cancer Medicine, The University of Texas MD Anderson Cancer Center, TX, USA; [15]Division of Hematopoietic Stem Cell Transplantation, National Cancer Center Hospital, Tokyo, Japan; [16]Blood & Marrow Transplant Program, Cleveland Clinic Taussig Cancer Institute, Cleveland, OH, USA; [17]Department of Internal Medicine, Mayo Clinic, MN, USA; [18]Oncology Center, King Faisal Specialist Hospital and Research Center, Riyadh, Saudi Arabia; [19]Division of Hematology and Oncology, Center for Cell and Gene Therapy, Baylor College of Medicine, Houston, TX, USA; [20]Department of Hematology, Inselspital, Bern University Hospital, Switzerland; [21]Markey Cancer Center, University of Kentucky, Lexington, KY, USA; [22]Loyola University Medical Center, Maywood, IL, USA; [23]University of Kansas Medical Center, Westwood, KS, USA; [24]City of Hope Comprehensive Cancer Center, Duarte, CA, USA; [25]University of Miami, Miami, FL, USA; [26]Division of Blood and Marrow Transplantation, Stanford University, Stanford, CA, USA; [27]Division of Hematology and Oncology, Washington University School of Medicine, St. Louis, MO, USA; [28]Department of Laboratory Medicine, Karolinska Institutet, Stockholm, Sweden; [29]Centre for Clinical Research Sormland, Uppsala University, Uppsala, Sweden; [30]Vanderbilt University Medical Center, Nashville, TN, USA; [31]Department of Pediatric Hematology, Oncology and Bone Marrow Transplant, British Columbia's Children's Hospital, The University of British Columbia, Vancouver, British Columbia, Canada; [32]Department of Medical Oncology and Hematology, CancerCare Manitoba, Winnipeg, Manitoba, Canada; [33]Tom Baker Cancer Centre, Calgary, Alberta, Canada; [34]Division of Hematology/Oncology, Department of Medicine, Vanderbilt University Medical Center, Nashville, TN, USA; [35]Department of Hematology/Oncology, Isala Clinic, Zwolle, the Netherlands; [36]Division of Pediatric Hematology, Oncology and Stem Cell Transplantation, Department of Pediatrics, New York Medical College, Valhalla, NY, USA; [37]Loyola University Chicago Stritch School of Medicine, Maywood, IL, USA; [38]The Fred and Pamela Buffett Cancer Center, University of Nebraska Medical Center, Omaha, NE, USA; [39]The Children's Hospital at TriStar Centennial and Sarah Cannon Research Institute, Nashville, TN, USA; [40]Division of Hematology, Oncology and Blood & Marrow Transplantation, Children's Hospital Los Angeles, University of Southern California Keck School of Medicine, Los Angeles, CA, USA; [41]Section of Hematology/Oncology, Department of Internal Medicine, Louisiana State University Health Shreveport, Shreveport, LA, USA; [42]Division of Hematologic Malignancies and Cellular Therapy, Duke University, Durham, NC, USA; [43]Department of Hematology/Oncology, Mayo Clinic, Phoenix, AZ, USA; [44]Department of Hematology & Hematopoietic Cell Transplantation, City of Hope, Duarte, CA, USA; [45]Translational Cell Therapy Group, CLINTEC (Clinical Science, Intervention and Technology), Karolinska Institutet, Stockholm Sweden; [46]Academische Ziekenhuis Maastricht, Maastricht, the Netherlands; [47]Mayo Clinic Florida, Jacksonville, FL, USA; [48]University of Chicago Medicine, Chicago, IL, USA; [49]Blood & Marrow Transplant Center, Florida Hospital Medical Group, Orlando, FL, USA; [50]UCLA Medical Center, Los Angeles, CA, USA; [51]The Sidney Kimmel Comprehensive Cancer Center at Johns Hopkins, Baltimore, MD, USA; [52]QE II Health Sciences Centre, Dalhousie University, Halifax, Nova Scotia, Canada; [53]Hospital Vall d'Hebron, Barcelona, Spain; [54]Rush University Medical Center, Chicago, IL, USA; [55]Christian Medical College, Vellore, India; [56]Blood and Marrow Transplantation Program, Division of Hematology/Oncology, Department of Internal Medicine, The University of Michigan Medical School, Ann Arbor, MI, USA; [57]Department of Hematologic Oncology and Blood Disorders, Levine Cancer Institute, Atrium Health, Charlotte, NC, USA; [58]Division of Hematology-Oncology, Indiana University School of Medicine, Indianapolis, IN, USA; [59]National Cancer Institute (NCI), Rockville, MD, USA; [60]New York Presbyterian Hospital/Columbia University Medical Center, New York, NY, USA; [61]UF Health Shands Children's Hospital, Gainesville, FL, USA; [62]Department of Advanced Medicine, Nagoya University Hospital, Nagoya, Japan; [63]Department of Hematology and Oncology, Dokkyo Medical University, Tochigi, Japan; [64]Division of Hematology/Oncology/Cell Therapy, Rush University, Chicago, IL, USA; [65]Memorial Sloan Kettering Cancer Center, New York, NY, USA; [66]Case Western Reserve University, Cleveland, OH, USA; [67]Division of Medical Oncology, University of Washington and Clinical Research Division, Fred Hutchinson Cancer Research Center, Seattle, WA, USA; [68]Department of Medicine, Seidman Cancer Center, University Hospitals Case Medical Center, Cleveland, OH, USA; [69]Division of

Hematology and Transplant Center, Mayo Clinic Rochester, Rochester, MN, USA; [70]Blood and Marrow Transplant Program, University of Minnesota Medical Center, Minneapolis, MN, USA and [71]Division of Hematology, Oncology and Transplantation, Department of Medicine, University of Minnesota Medical Center, Minneapolis, MN, USA.

Published in Haematologica 2020;105(5):1329-1338

doi:10.3324/haematol.2021.279046

The authors inadvertently included grant numbers OT3HL147741 & U24CA233032, which are grant-specific. This was an oversight on the authors' part as these grants did not support the research in this publication. .

An incorrect version of "acknowledgments" appeared in the May 2020 issue on page 1337.

Acknowledgments

*The CIBMTR is supported primarily by a public health service grant/cooperative agreement U24CA076518 from the National Cancer Institute (NCI), the National Heart, Lung and Blood Institute (NHLBI) and the National Institute of Allergy and Infectious Diseases (NIAID); grant/cooperative agreement U24HL138660 from the NHLBI and NCI; grant U24CA233032 from the NCI; grants OT3HL147741, R21HL140314 and U01HL128568 from the NHLBI; a contract HHSH250201700006C with Health Resources and Services Administration (HRSA/DHHS); grants N00014-18-1-2888 and N00014-17-1-2850 from the Office of Naval Research; and grants from *Actinium Pharmaceuticals, Inc.; Adaptive Biotechnologies; *Amgen, Inc.; Anonymous donation to the Medical College of Wisconsin; *Anthem, Inc.; Astellas Pharma US; Atara Biotherapeutics, Inc.; Be the Match Foundation; *bluebird bio, Inc.; Boston Children's Hospital; *Bristol Myers Squibb Co.; *Celgene Corp.; Children's Hospital of Los Angeles; *Chimerix, Inc.; *CSL Behring; *CytoSen Therapeutics, Inc.; Dana Farber Cancer Institute; *Daiichi Sankyo Co., Ltd.; Fred Hutchinson Cancer Research Center; *Gamida-Cell, Ltd.; Gilead Sciences, Inc.; *GlaxoSmithKline (GSK); HistoGenetics, Inc.; Immucor; Incyte Corporation; Janssen Biotech, Inc.; *Janssen Pharmaceuticals, Inc.; Janssen Scientific Affairs, LLC; *Jazz Pharmaceuticals, Inc.; Karius, Inc.; Karyopharm Therapeutics, Inc.; *Kite, a Gilead Company; *Magenta Therapeutics; Medac GmbH; The Medical College of Wisconsin; Mediware; Merck & Company, Inc.; *Mesoblast; MesoScale Diagnostics, Inc.; Millennium, the Takeda Oncology Co.; *Miltenyi Biotec, Inc.; Mundipharma EDO; National Marrow Donor Program; Novartis Oncology; Novartis Pharmaceuticals Corporation; *Omeros Corporation; *Oncoimmune, Inc.; PCORI; *Pfizer, Inc.; *Phamacyclics, LLC; PIRCHE AG; *Regeneron Pharmaceuticals, Inc.; REGiMMUNE Corp.; *Sanofi Genzyme; *Seattle Genetics; *Shire; Sobi, Inc.; Spectrum Pharmaceuticals, Inc.; St. Baldrick's Foundation; Swedish Orphan Biovitrum, Inc.; *Takeda Oncology; University of Minnesota; University of Pittsburgh; University of Texas-MD Anderson; University of Wisconsin – Madison and Viracor Eurofins. The views expressed in this article do not reflect the official policy or position of the National Institute of Health, the Department of the Navy, the Department of Defense, Health Resources and Services Administration (HRSA) or any other agency of the U.S. Government. *Corporate Members.*

The correct version of "acknowledgments" is published on this page.

Acknowledgments

*The CIBMTR is supported primarily by a public health service grant/cooperative agreement U24CA076518 from the National Cancer Institute (NCI), the National Heart, Lung and Blood Institute (NHLBI) and the National Institute of Allergy and Infectious Diseases (NIAID); grant/cooperative agreement U24HL138660 from the NHLBI and NCI; grants R21HL140314 and U01HL128568 from the NHLBI; a contract HHSH250201700006C with Health Resources and Services Administration (HRSA/DHHS); grants N00014-18-1-2888 and N00014-17-1-2850 from the Office of Naval Research; and grants from *Actinium Pharmaceuticals, Inc.; Adaptive Biotechnologies; *Amgen, Inc.; Anonymous donation to the Medical College of Wisconsin; *Anthem, Inc.; Astellas Pharma US; Atara Biotherapeutics, Inc.; Be the Match Foundation; *bluebird bio, Inc.; Boston Children's Hospital; *Bristol Myers Squibb Co.; *Celgene Corp.; Children's Hospital of Los Angeles; *Chimerix, Inc.; *CSL Behring; *CytoSen Therapeutics, Inc.; Dana Farber Cancer Institute; *Daiichi Sankyo Co., Ltd.; Fred Hutchinson Cancer Research Center; *Gamida-Cell, Ltd.; Gilead Sciences, Inc.; *GlaxoSmithKline (GSK); HistoGenetics, Inc.; Immucor; Incyte Corporation; Janssen Biotech, Inc.; *Janssen Pharmaceuticals, Inc.; Janssen Scientific Affairs, LLC; *Jazz Pharmaceuticals, Inc.; Karius, Inc.; Karyopharm Therapeutics, Inc.; *Kite, a Gilead Company; *Magenta Therapeutics; Medac GmbH; The Medical College of Wisconsin; Mediware; Merck & Company, Inc.; *Mesoblast; MesoScale Diagnostics, Inc.; Millennium, the Takeda Oncology Co.; *Miltenyi Biotec, Inc.; Mundipharma EDO; National Marrow Donor Program; Novartis Oncology; Novartis Pharmaceuticals Corporation; *Omeros Corporation; *Oncoimmune, Inc.; PCORI; *Pfizer, Inc.; *Phamacyclics, LLC; PIRCHE AG; *Regeneron Pharmaceuticals, Inc.; REGiMMUNE Corp.; *Sanofi Genzyme; *Seattle Genetics; *Shire; Sobi, Inc.; Spectrum Pharmaceuticals, Inc.; St. Baldrick's Foundation; Swedish Orphan Biovitrum, Inc.; *Takeda Oncology; University of Minnesota; University of Pittsburgh; University of Texas-MD Anderson; University of Wisconsin – Madison and Viracor Eurofins. The views expressed in this article do not reflect the official policy or position of the National Institute of Health, the Department of the Navy, the Department of Defense, Health Resources and Services Administration (HRSA) or any other agency of the U.S. Government. *Corporate Members.*

RESEARCH, READ & CONNECT

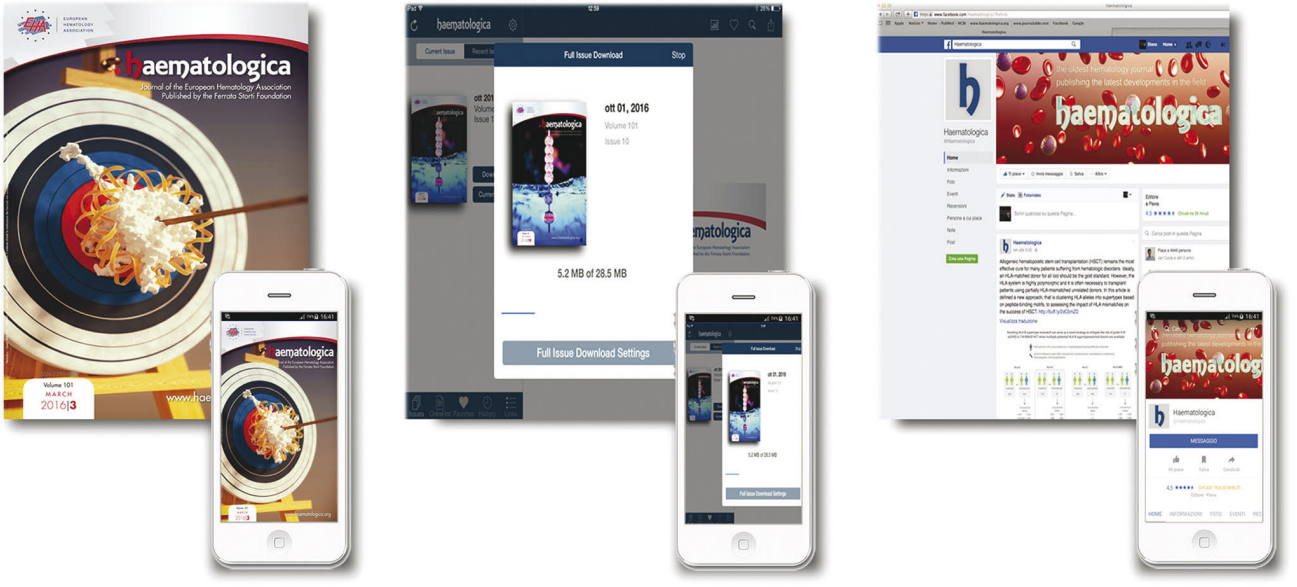

We reach more than
7 hundred thousand readers each year

The first Hematology Journal in Europe

Impressions YTD

14,606,781

Digital Readers

18,964

Total Audience

775,798

Worldwide rank	Impact factor	Total citations
8th	9.94	23,612

haematologica

Journal of the Ferrata Storti Foundation

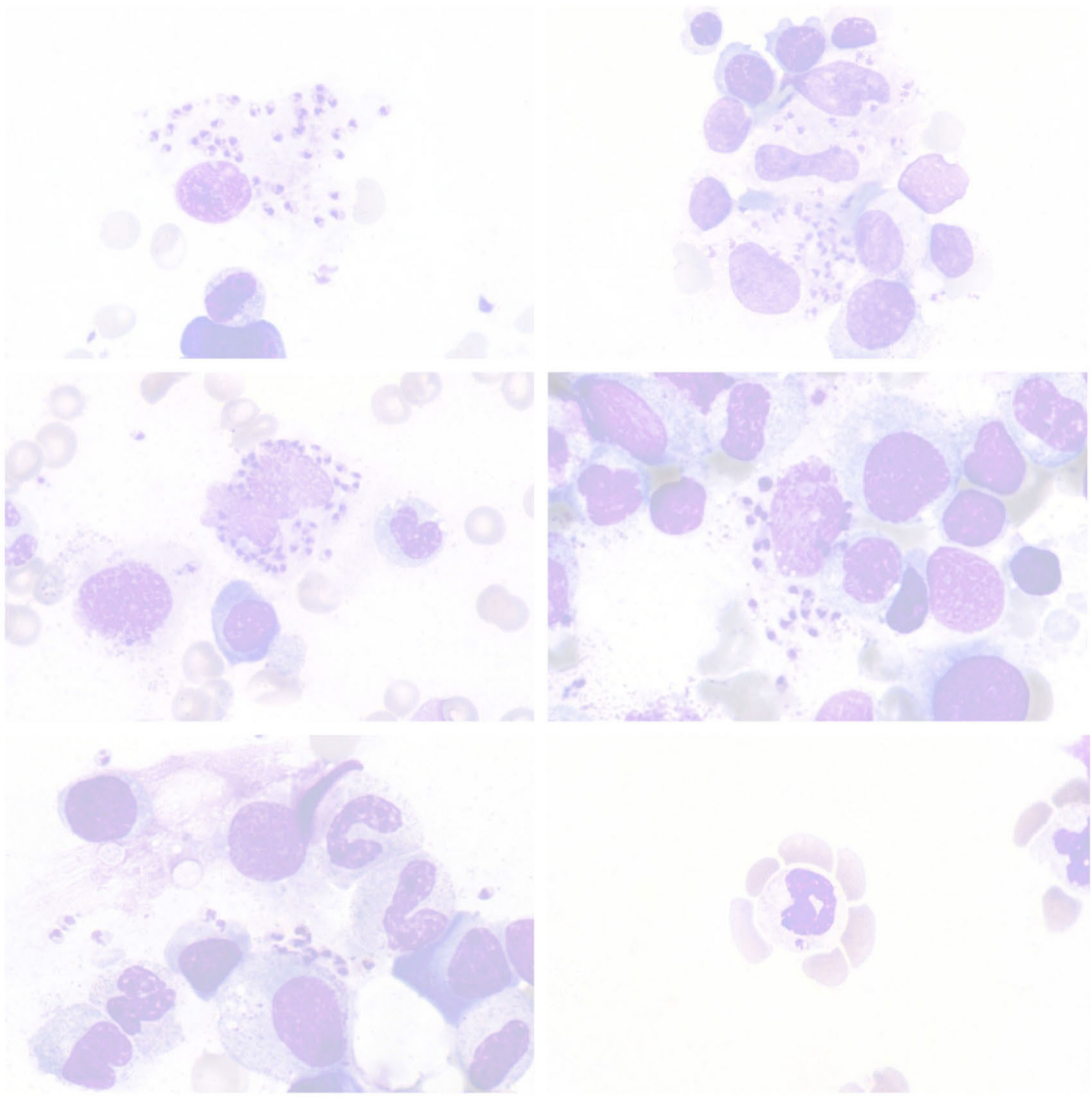

haematologica — Vol. 106 n. 8 — August 2021 — 2037-2296